UNIVERSITY OF SOUTHAMPTON

FACULTY OF SOCIAL, HUMAN AND MATHEMATICAL SCIENCES

GEOGRAPHY AND ENVIRONMENT

Volume 1 of 1

Static or dynamic: reconstructing past movement of the South Pacific Convergence Zone

by

Jonathan David Hassall

Thesis for the degree of Doctor of Philosophy

April 2017

UNIVERSITY OF SOUTHAMPTON

ABSTRACT

FACULTY OF SOCIAL, HUMAN AND MATHEMATICAL SCIENCES

Geography and Environment

Thesis for the degree of Doctor of Philosophy

STATIC OR DYNAMIC: RECONSTRUCTING PAST MOVEMENT OF THE SOUTH PACIFIC CONVERGENCE ZONE

Jonathan David Hassall

The largest climate system in the world exists over the Pacific Ocean. The behaviour of this system, which comprises El Nino/La Nina events and the South Pacific Convergence Zone (SPCZ), influences climate across the globe. Despite its importance, and because the region comprises archipelagos of sparsely populated islands, our understanding of the movement of the SPCZ is limited over the Holocene. This study addresses the lack of long, continuous records from this region to reconstruct movement of the SPCZ over millennial timescales.

Using a variety of geochemical proxies (compound-specific $\delta^{13}C$ and $\delta^{2}H$ analyses on *n*-alkanoic acids, total organic carbon $\delta^{13}C$, C/N, Itrax and magnetic susceptibility) from two sites (Lake Teroto, Atiu, Cook Islands, and Lake Lanoto'o, Samoa) this study has developed two palaeoclimatic reconstructions from which clear changes in SPCZ movement have been identified. A clear expansion and/or migration southeast is determined in the mid-Holocene (ca. 5,600-2,700 cal yr BP). Using the known relationship between SPCZ movement and prevailing climate states in the Pacific, specifically ENSO and IPO, inferences have been made on changes in these climate phenomena over the Holocene. When using a network of ENSO records from the tropical Pacific it is apparent that there are three distinct periods where a flavour of El Niño dominates: an early Holocene (ca. 9,500-6,800 cal yr BP) dominated by east Pacific El Niños; a transition period from ca. 6,800-5,600 cal yr BP before central Pacific El Niños dominate from ca. 5,600-2,700 cal yr BP; and a dominance of east Pacific El Niños from 2,700 cal yr BP to present. The first evidence for the 8.2 ka event is presented from the southwest tropical Pacific.

Table of Contents

List of Tables

List of Figures

DECLARATION OF AUTHORSHIP

I, Jonathan David Hassall, declare that this thesis and the work presented in it are my own and has been generated by me as the result of my own original research.

STATIC OR DYNAMIC: RECONSTRUCTING PAST MOVEMENT OF THE SOUTH PACIFIC CONVERGENCE ZONE.

I confirm that:

1. This work was done wholly or mainly while in candidature for a research degree at this University;
2. Where any part of this thesis has previously been submitted for a degree or any other qualification at this University or any other institution, this has been clearly stated;
3. Where I have consulted the published work of others, this is always clearly attributed;
4. Where I have quoted from the work of others, the source is always given. With the exception of such quotations, this thesis is entirely my own work;
5. I have acknowledged all main sources of help;
6. Where the thesis is based on work done by myself jointly with others, I have made clear exactly what was done by others and what I have contributed myself;
7. None of this work has been published before submission.

Signed:.....

Date: 19/04/2017

Acknowledgements

First I would like to express my sincerest gratitude to my supervisors Prof. David Sear, Prof. Pete Langdon and Prof. Ian Croudace. David and Pete: your enthusiasm and encouragement throughout this project has pushed me to do things I never imagined I would do in my lifetime. I am grateful for the opportunities you have encouraged me to take, even when at the time I didn't think I wanted to and was particularly vocal about it. Ian: I am indebted to your continuing help and for your generosity with time. Without your guidance and assistance crucial aspects of this thesis would not have been possible. You have all inspired me, and I will be forever indebted to you for this experience. Who would have thought I'd have been to the South Pacific (twice!), lived in Seattle for two months, and visited Japan at the start of this? I certainly didn't.

There are various people who have been a massive contribution towards this PhD. My sincerest thanks go to Prof. Julian Sachs and Dr Emma Pearson who allowed me to use their laboratories. Emma: once again I am sorry for dropping those samples and leaving a permanent stain in the laboratory; I hope you think of it as a pleasant reminder of my visit. I would also like to express my wholehearted thanks to (future Dr) Ashley Maloney. You have gone above and beyond with your help to this PhD both during my time in Seattle and afterwards. Without your help a vital dataset for this thesis would not have been produced. I would also like to thank Prof. Melanie Leng, Dr Charlotte Bryant, Dr Malu Cisneros-Dozal, Dr Ian Bull, and Dr Suzanne Maclachlan who helped with various aspects of data collection in this PhD. I would like to thank Peter Morgan, Dr Tom Bishop and Hayley Goodes for their support in Southampton's geography laboratories: too often your help is overlooked yet without you research wouldn't go anywhere near as smoothly as it does. Dr Cath Langdon: thank you for providing reassuring words for the last four years. It was all ok!

It would be remiss of me not to express my thanks to NERC, the RGS (with IBG), the Explorers' Club, and the Nantwich and Acton Grammar School Foundation. Your collective financial contributions meant that not only was fieldwork to a remote part of the world possible, but the analysis on the samples collected was possible too. I would also like to thank Vicky Lambert: you may never read this but you helped me through a particularly difficult time and I cannot thank you enough.

Throughout a PhD you go through highs and lows, the extent of which I didn't think were possible before starting this journey. Doing this on your own without support is, I think, an impossible task. To that end there are some very important people that need to be thanked. David Sutherland: you were one of the first people I met in Southampton and have become one of my closest friends. Living with you for two years was a real high point during my time here, and our conversations have never ceased to provide me with inappropriate entertainment. A particular taxi ride and text to the Christian Union always puts a smile on my face. Rob Collier and Laura Crossley: through thick and thin you've been with me on this. You've helped celebrate my highs and supported me during my lows – thank you for being there throughout, especially for those nights you can't fully remember. Charlotte Clarke: you insisted on being in these acknowledgements for reasons I just can't fathom. You have been nothing but a welcome distraction throughout this PhD and have become one of my closest friends. Alongside Dr Alan Smith, you two have ensured that this PhD was not completed much sooner. I'm still not sure how we didn't get ill after falling over in Jesters. Future doctors Olivia Cooke and Vix Franks: you've been there with me since our time in Aberystwyth. Who knew that we'd end up where we have? Thank you both for always being available to talk and making me laugh about anything and everything. Bella Ataç: your kind heart and generosity throughout has never gone unnoticed. To all of you: you've listened to my inane ramblings when even I wasn't sure I was making sense, and have been patient with me throughout the most stressful times. Don't ever underestimate the value your friendship has to me.

Finally, and most importantly, I want to thank my family for all of your support and encouragement. Mum, Dad, Ceri: thank you for always being there and helping in any way that you could. Your love has kept me afloat all of these years, and you have supported me during the hardest of times. I could not have gotten here without you. Thank you for keeping me on track, for making me listen when nobody else may have been able to, and most importantly ensuring I have a bed to come back to. Bet you're glad this is over now!

Thank you all. None of this would have been possible without any of you.

Jon Hassall, April 2017

University of Southampton

For Mum, Dad, and Ceri

"I suppose I better do some work now…"

(Jon Hassall, 2013-2017)

Definitions and Abbreviations

δ	delta
^{13}C	Carbon-13 (radioisotope)
^{14}C	Carbon-14 (radioisotope)
^{210}Pb	Lead-210 (radioisotope)
^{137}Cs	Caesium-137 (radioisotope)
^{219}Rn	Radon-219 (radioisotope)
^{220}Rn	Radon-220 (radioisotope)
^{222}Rn	Radon-222 (radioisotope)
^{238}U	Uranium-238 (radioisotope)
$\delta^{13}C_{TOC}$	Total organic carbon $\delta^{13}C$
$\delta^{13}C_{C16}$	C_{16} alkanoic acid $\delta^{13}C$
$\delta^{13}C_{C18}$	C_{18} alkanoic acid $\delta^{13}C$
$\delta^{13}C_{C26}$	C_{26} alkanoic acid $\delta^{13}C$
$\delta^{2}H_{bot}$	Botryococcene $\delta^{2}H$
$\delta^{2}H_{C16}$	C_{16} alkanoic acid $\delta^{2}H$
$\delta^{2}H_{C18}$	C_{18} alkanoic acid $\delta^{2}H$
$\delta^{2}H_{C26}$	C_{26} alkanoic acid $\delta^{2}H$
$\delta^{2}H_{dino}$	Dinosterol $\delta^{2}H$
$\delta^{2}H_{lw}$	Leaf water $\delta^{2}H$
$\delta^{18}O_{cal}$	Oxygen isotope ratios of authigenic calcite
$\delta^{18}O_{seawater}$	Oxygen isotope ratios of seawater
µS	Micro siemens
^{14}C yr BP	Radiocarbon year before present
AD	Anno Domini
AI	Aridity index
AMOC	Atlantic meridional overturning circulation
BDO	Bidecadal oscillation
Bot conc	Botryococcene concentration
ca.	*circa*
cal yr BP	Calibrated year before present
CESM	Community earth system model

CMIP3	Coupled model intercomparison project phase 3
CMIP5	Coupled model intercomparison project phase 3
C/N	Carbon/nitrogen ratio
CIC	Constant initial concentration
CPE	Central Pacific El Niño
CPL	Central Pacific La Niña
CRS	Constant rate of supply
DIC	Dissolved inorganic carbon
ENSO	El Niño-southern oscillation
EPE	Eastern Pacific El Niño
EPL	Eastern Pacific La Niña
ITCZ	Intertropical convergence zone
IPO	Interdecadal Pacific Oscillation
IPO TPI	Interdecadal Pacific Oscillation tripole index
LF mag susc	Low frequency magnetic suscpetibility
LIA	Little Ice Age
LEL	Local evaporation line
LOESS	Locally weighted smoothing
LOI	Loss-on-ignition
LOI_{550}	Loss-on-ignition at 550 °C
LOI_{950}	Loss-on-ignition at 950 °C
m.a.s.l.	Metres above sea level
MCA	Medieval Climate Anomaly
OLR	Outgoing longwave radiation
PCA	Principal components analysis
PDO	Pacific decadal oscillation
PMIP2	Palaeoclimate modelling intercomparison project phase 2
PMIP3	Palaeoclimate modelling intercomparison project phase 3
ppm	Parts per million
ppt	Parts per trillion
PPO	Pacific Pentadecadal oscillation
r^2	Linear regression
r	Linear correlation coefficient

SOI	Southern oscillation index
SPCZ	South Pacific Convergence Zone
SPCZI	South Pacific Convergence Zone index
SHPDO	Southern hemisphere Pacific decadal oscillation
SPDO	South Pacific decadal oscillation
SLP	Sea level pressure
SSS	Sea surface salinity
SST	Sea surface temperature
TDIC	Total dissolved inorganic carbon
WPWP	West Pacific Warm Pool
XRF	X-ray fluorescence
µXRF	Micro X-ray fluorescence
VPDB	Vienna Pee Dee Belemnite
VSMOW	Vienna standard mean ocean water
zSPCZ	zonal SPCZ events

Chapter 1: Introduction

1.1 Tropical Pacific palaeoclimate

In the late 1990s Cane (1998) argued that as the tropics cover half of the Earth's surface they have had a major contribution on the characteristics of palaeoclimate, with a potentially significant role in producing millennial-scale climate cycles. Arguably as a result of the significant effect the El Niño-Southern Oscillation (ENSO) has on global climate – especially the AD 1982/83 and 1997/98 El Niño which were two of the strongest on record – ENSO has been the focus of tropical Pacific palaeoclimate reconstructions, with much research directed on understanding ENSO variability throughout the Holocene (Cobb *et al*., 2013; Karamperidou *et al*., 2015; Emile-Geay *et al*., 2016). These reconstructions have primarily been undertaken in the south-eastern and central Pacific – likely due to these locales experiencing the largest changes in sea surface temperature (SST) during ENSO – leading to a paucity of palaeoclimatic reconstructions from the southwestern Pacific. Consequently this has led to an incomplete understanding of not only past changes in ENSO activity, but of Pacific palaeoclimate as a whole.

1.2 South Pacific Convergence Zone

The south-western Pacific is of great interest due to the presence of the South Pacific Convergence Zone (SPCZ). Extending ca. 10,000 km from Papua New Guinea towards French Polynesia in a NW-SE orientation, it is the most extensive rain band in the Southern Hemisphere (Cai *et al*., 2012). Covering most of Polynesia and Melanesia, the SPCZ has great importance for small island nations in the South Pacific as it provides potable water to circa 10 million people on these islands (Widlansky *et al*., 2013). Furthermore, the size of the SPCZ means it has global significance as the latent heat that the SPCZ releases leads to an important dynamical response through the excitation of Rossby Waves that influences climate on a global scale (Matthews, 2012). Despite the size and importance of the SPCZ not only regionally but globally, the IPCC state that the future rainfall outlook in this region is uncertain (IPCC, 2014). This is, in part, a result of a lack of millennial scale reconstructions on SPCZ movement that could provide a framework to assess how it will behave in the future.

The Interdecadal Pacific Oscillation (IPO) is suggested to represent the reddened ENSO component (this meaning each year's ENSO state being correlated with the previous year's state), driven by both interannual and decadal ENSO variability (Di Lorenzo *et al.,* 2015): essentially the IPO phase (positive/negative) is the interdecadal representation of its corresponding ENSO state (El Niño/La Niña) principally reflecting changes in sea surface temperature (SST). The position of the SPCZ is associated with both of these pan-Pacific climate phenomena (Vincent, 1994; Folland *et al*., 2002). On interannual timescales an El Niño (La Niña) is associated with the SPCZ taking a more zonal orientation and/or contracting (extend SE and/or expand) due to decreased (increased) zonal SST asymmetry and a weakened (strengthened) subtropical anticyclone in the east Pacific transporting moisture equatorward (southwestward) (Trenberth, 1976; Folland *et al*., 2002; van der Wiel *et al*., 2016a). At interdecadal timescales positive-phase IPO (negative-phase IPO) is associated with the SPCZ taking a more zonal orientation (extending SE and/or expanding) (Trenberth, 1976; Folland *et al*., 2002). This association between the SPCZ and pan-Pacific climate phenomena permits qualitative assessments of Pacific climate conditions, i.e. a record that indicates the SPCZ has taken a zonal orientation over interdecadal timescales indicates positive-phase IPO conditions, which in turn suggests an increase in El Niño activity. Long-term records of these patterns enhance our understanding of the IPO and ENSO as past changes in these phenomena are otherwise poorly understood. For example a variety of records indicate a reduction in ENSO in the mid-Holocene between ca. 6,000-3,000 cal yr BP; however the precise timing and nature of this reduction is still unknown (Riedinger *et al*., 2002; McGregor and Gagan, 2004; Rein *et al*., 2005; Conroy *et al*., 2008; McGregor *et al*., 2013a; Carré *et al*., 2014; Zhang *et al*., 2014; Emile-Geay *et al*., 2016; Chen *et al*., 2016). Both ENSO and the IPO have global impacts: for instance the AD 1997/98 El Niño caused an estimated US$35-45 billion in damage and claimed 23,000 human lives (Sponberg, 1999), and the shift ca. AD 1998/1999 from positive- to negative-phase IPO was determined to be a major cause in the recent slowdown of global warming (Dai *et al*., 2015). Understanding past changes in the IPO and ENSO are therefore vital to better contextualise climate models projecting future changes in these phenomena.

Movement of the SPCZ has a significant impact on the precipitation amount, and by extension the availability of potable water resources, experienced by small island nations

in this region. For example, during the AD 1997/1998 El Niño, when the SPCZ took a zonal orientation and merged with the ITCZ (termed zonal SPCZ (zSPCZ)) (Borlace *et al*., 2014), precipitation to Rarotonga, Cook Islands (1,091 mm in AD 1998) was reduced by 43% in comparison to the AD 1899-2012 average (1,931 mm/year) (Klatt, 2013). Additionally during the AD 1997-1998 El Niño sea level dropped 30 cm in Samoa causing the heads of shallow corals to die (Widlansky *et al*., 2014). During zSPCZ events the location of tropical cyclone genesis shifts towards the central Pacific, thus negatively affecting countries in this region such as French Polynesia (Vincent *et al*., 2011). Natural disasters and extreme events in this region, occurring during positive IPO phases associated with the SPCZ contracting and/or migrating NW (Folland *et al*., 2002), are estimated to have cost in excess of US $1 billion (FAO, 2008), affected more than 3.4 million people and caused over 1,700 reported fatalities since AD 1950 (excluding Papua New Guinea; World Bank, 2006). The position of the SPCZ therefore has a major impact on countries and people in the South Pacific, with its movement during El Niños causing significant reductions in precipitation amount and increasing the likelihood of tropical cyclones in the central Pacific (Vincent *et al*., 2011; Borlace *et al.*, 2014).

Due to the paucity of terrestrial sites in this region, most work reconstructing the position of the SPCZ in the past has been restricted to coral records that cover centennial timescales (Linsley *et al*., 2006). The phase of ENSO and the IPO has a significant impact on ocean currents in the Pacific; consequently, disentangling what is affecting the palaeo-marine record – whether it is local effects, ENSO, or the SPCZ – is fraught with difficulties. With this in mind, longer terrestrial records are vital for understanding where the SPCZ has moved in the past and what the possible drivers of this movement are: for example the IPO/ENSO, or zonal and/or meridional SST gradients (Trenberth, 1976; Folland *et al*., 2002; Saint-Lu *et al*., 2015; van der Wiel *et al*., 2016a). Terrestrial records from the SW Pacific often have poor chronologies (for example Stevenson *et al*., 2010) characterised by reworking materials and/or a lack of precision, and those records that are available are restricted to locations such as New Caledonia and Vanuatu. Further, there is often a reliance on one proxy – specifically pollen – which hampers comparisons with other palaeo-records from the region. With the current poor chronologies and general paucity of terrestrial palaeo-records, there is a need to develop improved palaeoclimatic reconstructions to provide a millennial-scale reconstruction of SPCZ movement.

Climate simulations suggest that with future global warming zonal SPCZ (zSPCZ) events will increase in frequency, leading to increased likelihood of extreme events such as droughts and cyclones, affecting island nations in the Pacific (Cai *et al*., 2012). However, this forecast only incorporates knowledge on SPCZ movement in the instrumental period. From a set of mid-Holocene (ca. 6,000 and 4,000 cal yr BP) modelling experiments (PMIP2), it has been suggested that the SPCZ expanded southeast and appeared to have more shifts per century of larger amplitude at ca. 6,000 cal yr BP (Braconnot *et al*., 2007; Mantsis *et al*., 2013; Saint-Lu *et al*., 2015). However, at present (AD 2017) there are no records covering this period that could support or refute the model outputs. Toomey *et al*. (2016) suggested using a sedimentary record from French Polynesia that the SPCZ intensified or migrated SE since ca. 3,000 cal yr BP, leading to wetter conditions in French Polynesia. Further, Partin *et al*. (2013) suggested, based on a speleothem record in Vanuatu, that changes in SPCZ position were larger over the last 446 years than that seen in the instrumental period. Without millennial-scale records that reconstruct SPCZ movement spanning much of the Holocene, there is no long-term context for SPCZ activity over the last ca. 3,000 cal yr BP, and thus no test of whether this aforementioned SPCZ movement is representative of a long-term trend. A corollary of this is historical analogues of how the SPCZ could behave in the future (as a result of global warming) are lacking. Long geological records are vital not only for contextualising climate models to incorporate longer term behaviour and for testing the validity of palaeo-simulations, but also for providing important practical information needed for water resource management in the South Pacific. This is especially pertinent when considering that the frequency of zonal SPCZ (zSPCZ) events are expected to increase which lead to dramatic decreases in precipitation amounts in countries dependent on the SPCZ for potable water (Cai *et al*., 2012).

1.3 The focus of this study

The aim of this study is to reconstruct the SPCZ's movement on millennial timescales – specifically the last ca. 10,000 years. This period covers the reduction in ENSO variability from ca. 6,000-3,000 cal yr BP, and the greatest ENSO variability ca. 2,000 cal yr BP indicated in various palaeo-records – for instance Conroy *et al*. (2008), Zhang *et al*. (2014), Koutavas and Joanides (2012), and Emile-Geay *et al*. (2016). Additionally, using the known

association between SPCZ location and IPO/ENSO phase, this study will explore potential changes in IPO/ENSO over the last ca. 10,000 cal yr BP by comparing records obtained in this study to other records in the Pacific basin. It utilises a multi-proxy approach incorporating both organic and inorganic geochemical proxies. Proxies to reconstruct lake and catchment productivity are employed, alongside compound-specific isotope measurements to provide semi-quantitative values for the amount of precipitation, semi-quantitative analysis of element composition in the bulk sediment, as well as magnetic analysis of bulk sediment. This study explicitly used an approach (compound-specific isotope measurements) that would provide information regarding changes in the amount of precipitation to avoid ambiguity associated with proxies such as pollen and diatoms that can be influenced by both climatic changes and anthropogenic activity.

1.4 Aims and Objectives

With the paucity of terrestrial palaeoenvironmental and palaeoclimatic records in the southwest Pacific, our understanding of this region is greatly lacking. Further it is hindering our knowledge on SPCZ behaviour on centennial and millennial timescales, which is vital to fully comprehend its potential movement. Consequently this study has the following aims:

1. Determine the feasibility of reconstructing long-term climate records from terrestrial/limnic proxies in the southwest Pacific; and
2. Dependent upon 1) assess the precipitation history in light of the SPCZ and broader patterns of internal variability in the Pacific basin over millennial timescales.

1.4.1 Past climatic changes in the Pacific region

In section 1.2 it was highlighted that at present (AD 2017) there is contention in regards to past climatic changes in the Pacific region: for example on the potential millennial-scale behaviour of the SPCZ, and the nature and timing of changes in the IPO and ENSO over the Holocene. This is, in part, not only due to a lack of records from the southwest Pacific but also due to there being no literature review for the Pacific region at present (AD 2017) that attempts to collate and examine changes in the various Pacific climate phenomena. It is therefore necessary in order to understand the regional palaeoclimatic record to

determine where research gaps lie and to identify areas of contested interpretation. Once understood, the palaeoclimatic records produced in this study can be compared and contextualised with regional Holocene climatic changes. Consequently to address the first aim outlined in section 1.4, the following objectives will be undertaken:

- Using published literature, develop a regional palaeoclimatic record for the southwest Pacific covering the Holocene, or as far back as the literature permits; and
- Determine research gaps and areas of contested interpretation in the literature to highlight future areas of research.

1.4.2 Recent climate change and SPCZ movement

It is known that the SPCZ has moved in the instrumental period, with various indices created to reconstruct this based on different environmental parameters. Determining the impact of SPCZ movement on precipitation in the study sites chosen needs to be evaluated. To address the first aim of section 1.4 the following objectives will be undertaken:

- Determine the relationship, if any, of the SPCZI – a movement index for the SPCZ (Salinger *et al*., 2014) – with precipitation in the study sites to determine if SPCZ movement can be reconstructed from the palaeorecord;
- Obtain and analyse modern catchment and lake geochemical data to aid interpretation of proxy data;
- Analyse lake cores using inorganic and organic proxies for palaeoenvironment and palaeoclimate reconstruction; and
- Evaluate whether proxies used are applicable to reconstruct SPCZ movement.

1.4.3 Palaeoclimatic records

Determining palaeoclimatic changes from lake records is complicated by lakes recording both regional changes but also changes at the catchment scale. Resolving the catchment processes against a regional climatic signal from lake sediments requires a multiproxy approach. Compound-specific isotope ratio analysis enables a regional precipitation signal to be determined making this an ideal analysis to determine semi-quantitative changes in

precipitation. Further, when combined with other proxies such as Itrax and C/N ratios, catchment processes can be determined with greater confidence. To determine the precipitation history in light of the SPCZ and other internal Pacific processes, the second aim of section 1.4, the following objectives will be undertaken:

- Apply proxies to the dated lake cores to determine long-term environmental and climatic changes in study sites chosen; and
- Compare results with other long-term climatic records in the Pacific to determine regional changes in Pacific palaeoclimate, and evaluate similarities and disparities between records.

1.5 Thesis structure

Following this chapter, Chapter 2 provides a literature review of the climate phenomena of the Pacific, followed by an overview of Holocene climate change in the tropical Pacific. Chapter 3 goes on to cover the study sites, and in Chapter 4 the methods used in this study are outlined. The age models used in this study are discussed in Chapter 5, after which the results of modern data and the short cores from both sites are interpreted and discussed (Chapter 6). In Chapters 7 and 8 the long core Lake Teroto and Lake Lanoto'o results are respectively interpreted. Chapter 9 provides a discussion of the data in regard to other sites in the Pacific in the context of SPCZ movement and changes in ENSO, followed by a brief examination of human colonisation in Samoa and Atiu. Finally, Chapter 10 outlines the main conclusions from this thesis and delineates future work that can be undertaken.

Chapter 2: Literature Review

2.1 Climate phenomena and climate systems in the Pacific

A number of climatic phenomena operate in the Pacific basin, each having a separate timescale (Figure 2.1). They have an impact that is not only felt in the Pacific basin but globally through climatic teleconnections: for instance two regions in both Africa and the Indian subcontinent were identified as having precipitation that was related to ENSO (Ropelewski and Halpert, 1987). Whilst their thermodynamics are not pertinent for this research, their expression in the atmosphere and the ocean is fundamental for understanding how they impact on climate systems in the Pacific basin – specifically the SPCZ.

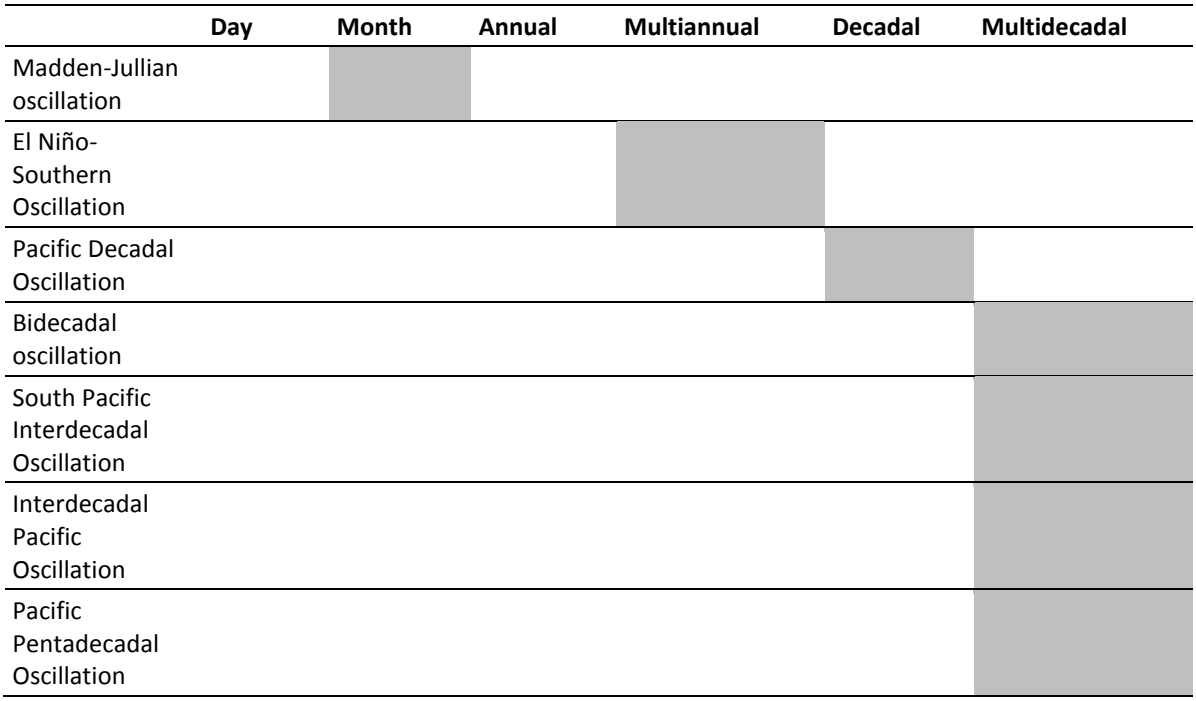

Figure 2.1: Timescales of different climatic phenomena that operate in the Pacific basin (Cane and Zebiak, 1985; Mantua *et al*., 1997; Minobe *et al*., 1997; Power *et al*., 1999; Hsu and Chen, 2011; Matthews, 2012).

2.1.1 The El Niño-Southern Oscillation

The El Niño-Southern Oscillation, referred to as ENSO, is one of Earth's most significant sources of year-to-year natural climatic variability (McPhaden *et* al., 2006, 2011; Collins *et al*, 2010; Borlace *et al*., 2013). Oscillating on a two- to seven-year timescale, it is a fluctuation between unusually warm (El Niño) and cold (La Niña) SST conditions in the

tropical Pacific. Whilst intimately related, El Niño and the Southern Oscillation reflect different aspects of climate: the former defined as the sea surface temperature (SST) anomaly between 90°W-150°W, 5°S-5°N (Niño3 region; Table 2.1 and Figure 2.2), and the latter the normalised sea level pressure (SLP) difference between Darwin, Australia, and Tahiti – the so-called Southern Oscillation Index (Bjerknes, 1969; Cane, 2005). It should be noted that at present there is no specific region or quantified amount of warming that is used to define an El Niño (Cane, 2005); however Trenberth (1997) suggested that a quantitative definition of El Niño should be a five-month running mean of SST anomalies in the Niño-3.4 region (Table 2.1 and Figure 2.2) that exceed 0.4 °C for six months or more.

Changes across the globe have been associated with ENSO, with Sun *et al*. (2016) finding that the evolution of ENSO was related to dry/wet conditions over ca. 38% of global land surface (excluding Antarctica). As would be expected with the Pacific being the principal centre of ENSO action, precipitation and temperature anomalies in this region are strongly influenced by ENSO on interannual timescales (Chen and Chung, 2015). In the Sahel region of Africa below average precipitation occurs during El Niños, whereas positive precipitation anomalies have been determined north of 20°N a year after an El Niño event (Bradley *et al*., 1987). The AD 1997/98 El Niño caused an estimated US$35-45 billion in damage and claimed 23,000 human lives (Sponberg, 1999). Further, El Niño can cause a drop in sea level of up to 30cm around Samoa, causing the heads of shallow corals to die (Widlansky *et al*., 2014). Ward *et al*. (2014) determined that across the globe (excluding Greenland and Antarctica) 34% of Earth's land surface experience significant flood anomalies in El Niño years and 38% during La Niña years. The AD 1998/1999 La Niña event caused flash flooding in Venezuela killing between 25,000-50,000 people (Takahashi *et al*., 1999), flooding in China that displaced over 200 million people (Jonkman, 2005), whereas drought in the U.S.A. in AD 1988 has been linked to the coeval La Niña.

The influence of ENSO on global records is not restricted to the instrumental period and has been determined in various past climatic records: for example the Lake Challa record, East Africa, where reduced ENSO variability has been reconstructed between ca. 19,000-21,000 cal yr BP (Wolff *et al*., 2011) and potentially indicates that La Niña conditions dominated. Deltaic modification of the Nile has been concluded to have been mediated

Index	Definition

Niño1+2	The region is bounded by equator-10°S, 90°W-80°W; the area averaged sea surface temperature anomaly (SSTA) over this region is known as the Niño1+2 index
Niño3	The region is bounded by 5°N-5°S, 150°W-90°W; the area averaged sea surface temperature anomaly (SSTA) over this region is known as the Niño3 index, which is a well-known ENSO index
Niño3.4	The region is bounded by 5°N-5°S, 170°W-120°W; the area-averaged sea surface temperature anomaly (SSTA) over this region is known as Niño3.4 index
Niño4	The region is bounded by 5°N-5°S, 160°E-150°W; the area-averaged sea surface temperature anomaly (SSTA) over this region is known as Niño4 index
EMI	The El Niño Modoki Index (EMI) is calculated using the following equation: $EMI = (SSTA)_A - 0.5*(SSTA)_B - 0.5*(SSTA)_C$ The brackets in the equation represent the area-averaged sea surface temperature anomaly (SSTA) over region A (165°E–140°W, 10°S–10°N), B (110°W–70°W, 15°S–5°N), and C (125°E–145°E, 10°S–20°N), respectively.
SOI	The normalised sea level pressure difference between Darwin, Australia, and Tahiti, French Polynesia (Cane, 2005).

Table 2.1: Definitions of different regions/sea surface temperature anomaly-based indices relating to the El Niño-Southern Oscillation (adapted from Ashok *et al.*, 2007). See Figure 2.2 for a map of the regions defined.

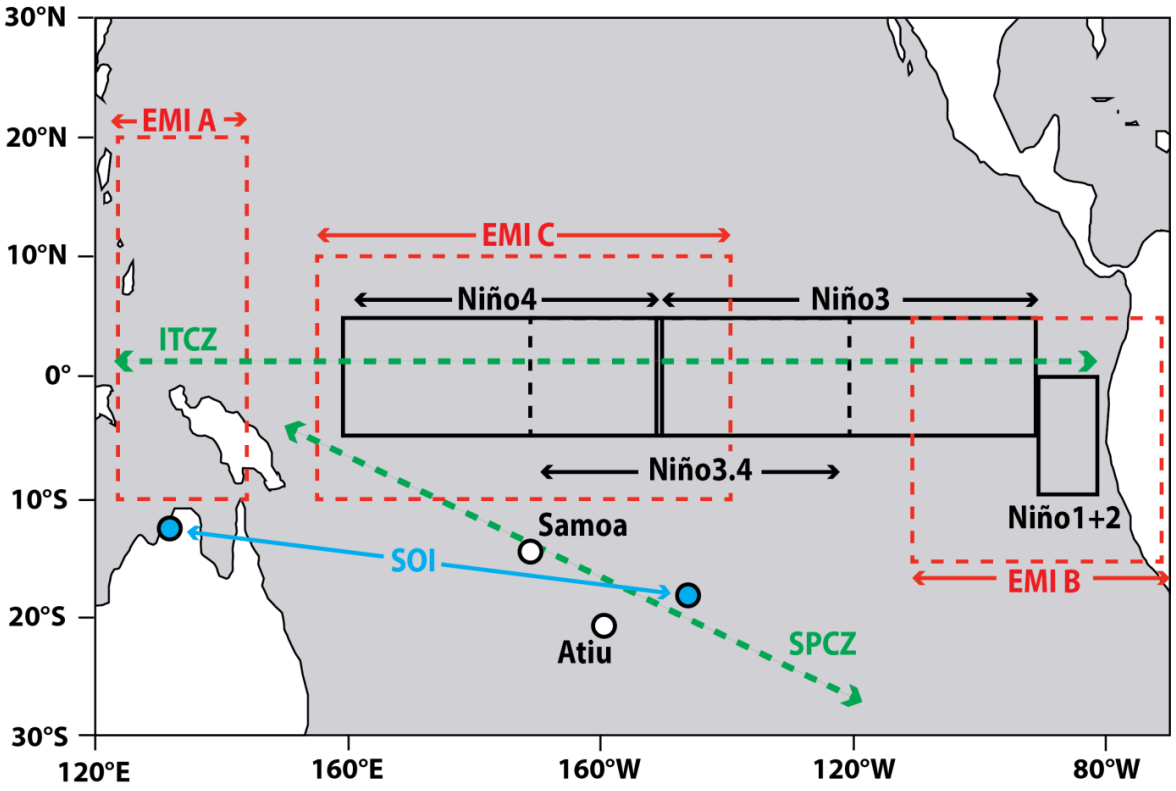

Figure 2.2: The regions used for indices relating to the El Niño-Southern Oscillation are illustrated. EMI: El Niño Modoki Index (adapted from Kao and Yu, 2009). Sites used in this thesis, specifically Samoa and Atiu, are highlighted.

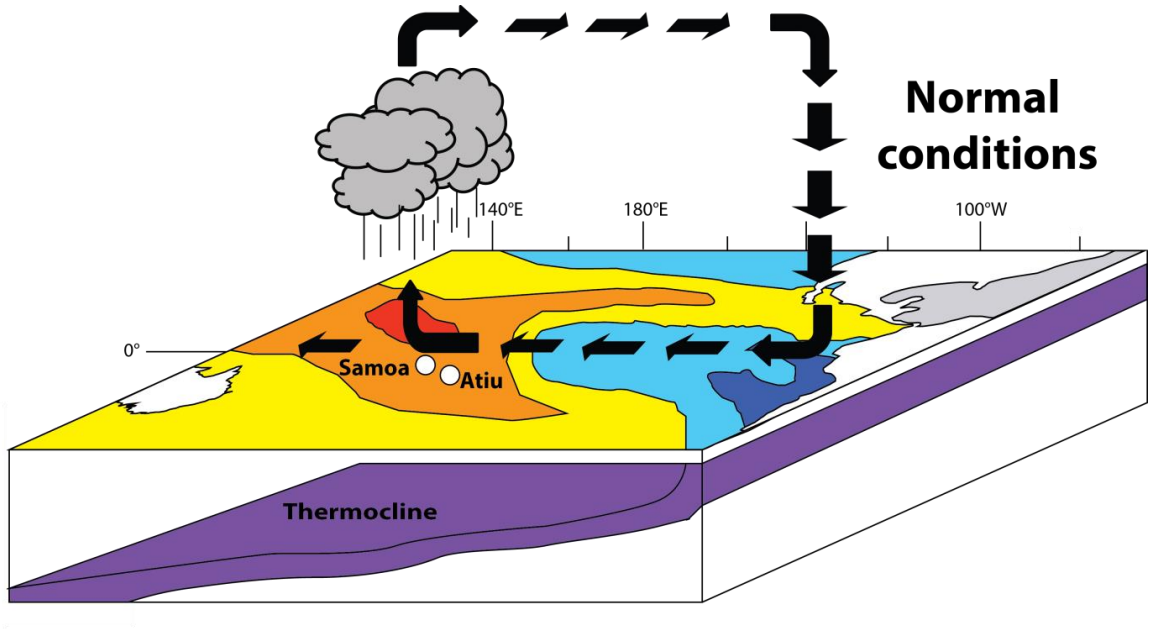

Figure 2.3: A simplified diagram of normal sea surface temperatures and atmospheric circulation in the equatorial Pacific. Red contours indicate warmer sea surface temperatures; dark blue indicates colder sea surface temperatures. The black arrows indicate wind direction (adapted from Cane, 2005).

by climate events linked to ENSO over the past ca. 8,000 cal yr BP (Marriner *et al*., 2012), albeit using the Laguna Pallcacohca record that has recently been highlighted as likely representing local responses to deglacial climate forcings rather than ENSO changes (Moy *et al*., 2002; Liu *et al*., 2014). Nevertheless, given the global effect of ENSO, understanding it in both the past and present is vital for assessing future changes generated by climate models used to simulated future global warming.

2.1.1.1 La Niña

La Niña is an exaggeration of normal conditions (Figure 2.3) in the Pacific basin, exemplified by colder than normal SST conditions in the eastern equatorial Pacific creating a zonally asymmetric SST distribution (Philander, 1985). This is due to trade winds that are stronger than normal pushing warm upper ocean waters towards the west thus causing the thermocline to shallow. It is both less frequent – La Niña occurred 23% whereas El Niño has occurred 31% of the time since AD 1950 (Trenberth, 1997) – and not symmetrical in expression to El Niño (Hoerling *et al.*, 1997; An and Jin, 2004; Larkin and Harrison, 2005). It was mooted that there are two types of La Niña (referred to as flavours in the literature): one operating in the eastern Pacific, termed eastern Pacific La Niña (EPL), for example AD 2007/2008; and one operating in the central Pacific, termed central

Form of ENSO	Definition
Central Pacific El Niño	A Central Pacific El Niño event (CPE) occurs when a positive SST departure from normal in the Niño4 region greater than 0.5 °C averaged over three consecutive months (NOAA; Kug *et al*., 2009; Kao and Yu *et al*., 2009). Kug *et al*. (2009) suggested CPE is driven more by wind-forced zonal SST advection. Can also be referred to as El Niño Modoki (Ashok *et al*., 2007), Warm Pool El Niño (Kug *et al*., 2009), and Date Line El Niño (Larkin and Harrison, 2005).
Eastern Pacific El Niño	An Eastern Pacific El Niño event (EPE) occurs when a positive SST departure from normal in the Niño3 region greater than 0.5 °C averaged over three consecutive months (NOAA; Kug *et al*., 2009; Kao and Yu *et al*., 2009). Kug *et al*. (2009) suggested EPE is characterised by thermocline variations. Can also be referred to as Cold Tongue El Niño and Canonical El Niño (Kug *et al*., 2009)
Mixed El Niño	A Mixed El Niño event occurs when a positive SST departure from normal in the Niño3.4 region greater than 0.5 °C averaged over three consecutive months (NOAA; Kug *et al*., 2009).
Central Pacific La Niña	A La Niña event occurs when either the Niño3 or Niño4 index is below -0.5°C and persists for a minimum of five months. To be classed as a Central Pacific La Niña the absolute value of Niño4 is larger than Niño3 (Yuan and Yan 2013). The Central Pacific La Niña (CPL) can also be referred to as La Niña Modoki in the literature (for example Cai and Cowan, 2009).
Eastern Pacific La Niña	A La Niña event occurs when either the Niño3 or Niño4 index is below -0.5 °C and persists for a minimum of five months. To be classed as an Eastern Pacific La Niña (EPL) the absolute value of Niño3 is larger than Niño4 (Yuan and Yan 2013).

Table 2.2: Definitions of the different forms of ENSO.

Pacific La Niña (CPL), for example AD 1988/1989 (Table 2.2) (Ashok *et al*., 2007; Kao and Yu, 2009; Cai and Cowan, 2009; Capotondi *et al*., 2015). La Niña events are different linear combinations of these flavours, which result from different balances of physical processes (Capotondi *et al*., 2015). As suggested by their names, EPL have the greatest anomalously cold SST in the eastern Pacific influencing precipitation mainly in northeastern Australia and south Australia, and CPL in the central Pacific influencing precipitation as far west as the Murray-Darling region in Australia (Cai and Cowen, 2009). Strong La Niñas, these having temperature anomalies greater than one standard deviation away from the mean, are of the CPL type (Yu *et al*., 2011). Figure 2.4 and Figure 2.5 show the SST and circulation patterns accompanying EPL and CPL respectively. Cai *et al*. (2015) determined in the Coupled Model Intercomparison Project phase 5 (CMIP5) that with future global warming CPL, referred to as extreme La Niña events by the authors, will increase in frequency from once in every 23 years to once in every 13 years.

2.1.1.2 El Niño

The initiation of El Niño can be found in the tropical Pacific through coupled interactions of the ocean and the atmosphere (McPhaden *et al*., 2011). This oscillation is the development of higher-than-normal pressure in the west Pacific and lower pressure over

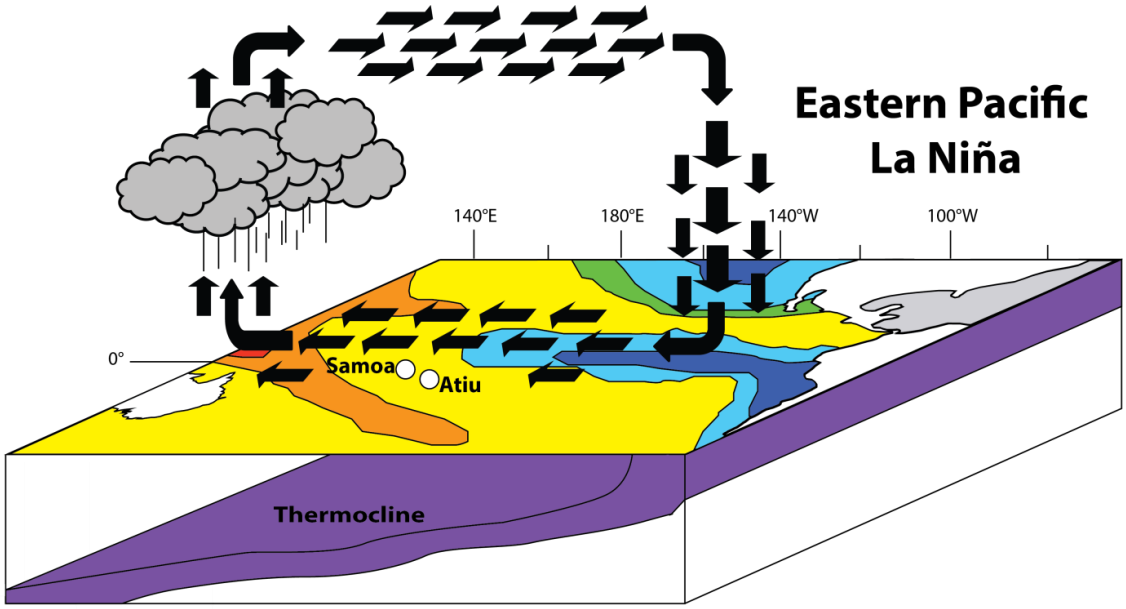

Figure 2.4: A simplified diagram of sea surface temperatures and atmospheric circulation in the equatorial Pacific during an Eastern Pacific La Niña. Red contours indicate warmer sea surface temperatures, dark blue indicates colder sea surface temperatures. The black arrows indicate wind direction with stronger winds indicated by multiple arrows in direction of wind travel (adapted from Cane, 2005).

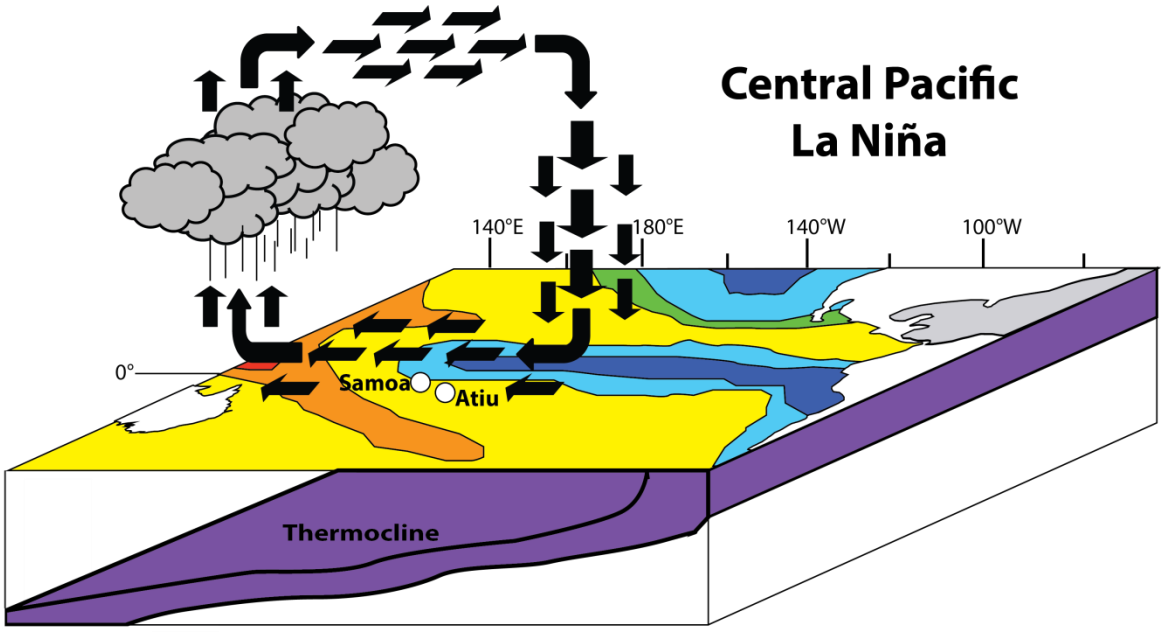

Figure 2.5: A simplified diagram of sea surface temperatures and atmospheric circulation in the equatorial Pacific during Central Pacific La Niña. Red contours indicate warmer sea surface temperatures, dark blue indicates colder sea surface temperatures. The black arrows indicate wind direction with stronger winds indicated by multiple arrows in direction of wind travel (adapted from Cane, 2005).

the eastern Pacific causing trade winds to weaken or even be replaced with west-to-east winds (Bjerknes, 1966) – simply put a switch of the normal conditions aforementioned. This alteration of the trade winds is followed by the expansion of warm waters from the west Pacific causing positive sea surface temperature (SST) anomalies that extend across the entire equatorial Pacific eastward of 170°E creating a more zonally symmetric SST distribution (Deser and Wallace, 1990). A further characteristic is the reduction of upwelling in the east Pacific. A consequence of these changes in the Pacific is that positive precipitation anomalies occur east of the dateline (Hoerling *et al*., 1997).

Until recently the paradigm for El Niño was that it only operates in the eastern half of the Pacific Ocean (Philander, 1985; Cane and Zebiak, 1985; Cane, 2005). Using observational data Ashok *et al*. (2007) argued that some El Niños had different SST anomalies to 'stereotypical' El Niño (see Table 2.2 for definitions). Terming this 'El Niño Modoki', they demonstrated that anomalous warming occurred in the central equatorial Pacific and not in the eastern equatorial Pacific (Ashok *et al*., 2007). Kug *et al*. (2009) and Kao and Yu (2009) indicated that El Niño has two clear types: the eastern Pacific El Niño (EPE) (Figure 2.6) with largest SST anomalies in the Niño3 region such as the AD 1997/1998 El Niño, and the central Pacific El Niño (CPE) (Figure 2.7) with greatest SST anomalies in the Niño4 region such as the AD 2004/2005 El Niño. The instrumental record suggests that CPE dominance is associated with increased La Niña activity (Kao and Yu, 2009; Carré *et al*., 2014). Yu *et al*. (2011) determined that strong El Niño events, these being events with anomalies greater than 1 standard deviation of the mean, are always of the EPE type and have a quasi-quadrennial periodicity between AD 1968 and 2001. It has been suggested that El Niño may exist in a spectrum, having different linear combinations of flavours, with a Mixed El Niño operating in the Niño3.4 region (Kug *et al*., 2009). As aforementioned Capotondi *et al*. (2015) stated that El Niño and La Niña events are different linear combinations of ENSO flavours, which would lend further support to ENSO being a spectrum rather than being classed as discrete types.

Using precipitation data, Murphy *et al*. (2014) argue that EPE – termed cold tongue El Niño in the study – has the strongest SST and wind anomalies of any El Niño type. The ramification of this for global climate is important as EPE greatly reduces the west Pacific warm pool, a fundamental component of Earth's climate system (Picaut *et al*., 1996).

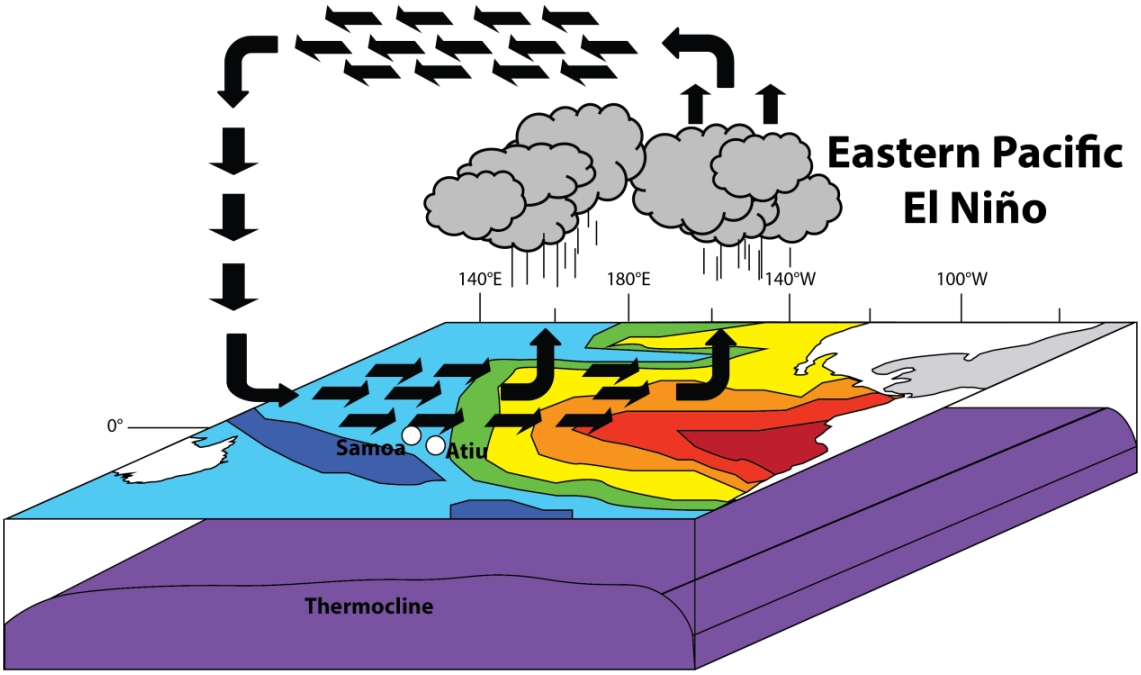

Figure 2.6: A simplified diagram of sea surface temperatures and atmospheric circulation in the equatorial Pacific during Eastern Pacific El Niño. Red contours indicate warmer sea surface temperatures, dark blue indicates colder sea surface temperatures. The black arrows indicate wind direction with stronger winds indicated by multiple arrows in direction of wind travel (adapted from Cane, 2005).

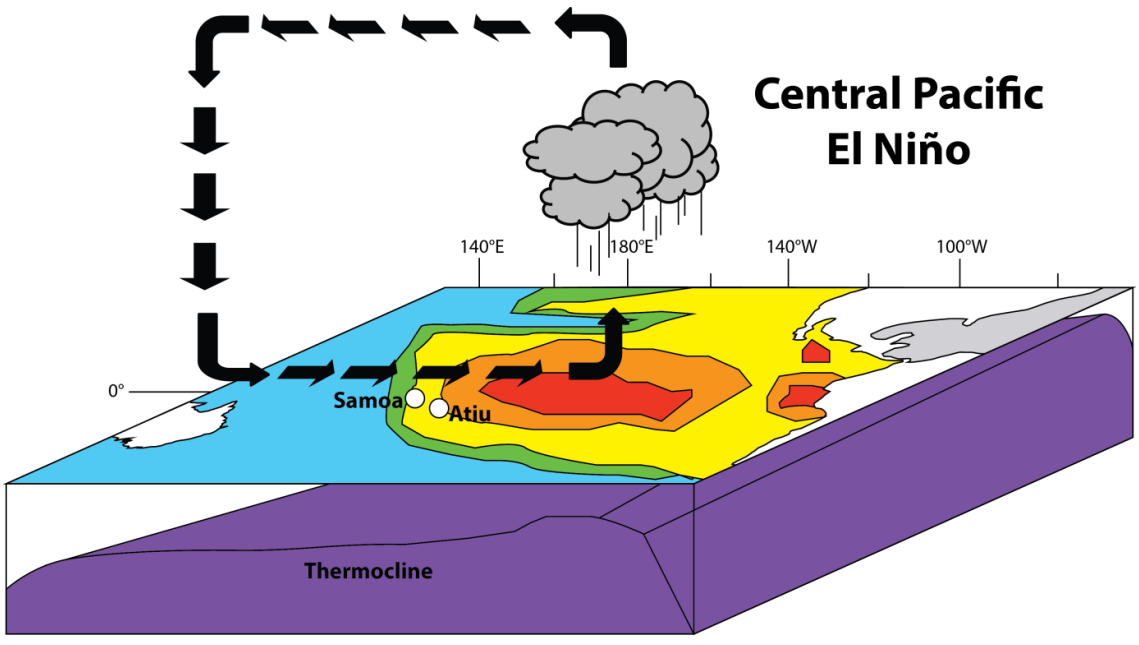

Figure 2.7: A simplified diagram of sea surface temperatures and atmospheric circulation in the equatorial Pacific during Central Pacific El Niño. Red contours indicate warmer sea surface temperatures, dark blue indicates colder sea surface temperatures. The black arrows indicate wind direction (adapted from Cane, 2005).

models in the Coupled Model Intercomparison Project phases 3 (CMIP3) and 5, Cai *et al*. (2014) show that whilst the total number of El Niño events decreases slightly as a result of projected global warming, the number of CPE increases having a frequency of one CPE every ten years. Furthermore, Ham and Kug (2016) concluded from CMIP5 that ENSO amplitude would increase under global warming.

2.1.1.3 Long-term ENSO records

At present (AD 2017) long-term ENSO records are inherently problematic. No continuous annually laminated lacustrine records from the equatorial Pacific are currently available, thus each centimetre in a lacustrine records spans greater than 10 years meaning that changes in ENSO variability with its 2-7-year periodicity cannot be interpreted. This has been overcome in some studies utilising organic geochemicals produced explicitly during El Niños allowing for qualitative interpretations: for example Atwood *et al*. (2014) and Zhang *et al*. (2014). Furthermore some long, continuous records positing to record ENSO are located in the circum-Pacific outside the ENSO centre of action, for instance Laguna Pallcacocha (Robdell *et al*. 1999; Moy *et al*., 2002), and likely represent local responses to deglacial climate forcings rather than ENSO (Liu *et al*., 2014). Marine records typically have interdecadal or centennial resolution and sediments are subject to bioturbation – for example, Koutavas and Joanides (2012) state 1 cm covers ca. 80 years in core V21-30. Consequently changes in ENSO cannot be readily interpreted from marine records. Moreover studies such as those by Koutavas and Joanides (2012) and Sadekov *et al*. (2013) use foraminifera to reconstruct ENSO variability, stating that the relative short lifespan of foraminifera (ca. 2-4 weeks) and employing population statistical approaches on individual foraminifera permit an interpretation of ENSO variability. This has been called into question by Thirumalai *et al*. (2013) who concluded that ENSO frequency cannot be determined from population statistics on foraminifera; additionally Liu *et al*. (2014) consider that changes in ENSO interpreted from foraminifera in Koutavas and Joanides (2012) probably reflect total SST variability rather than ENSO. Whilst coral records have subannual chronological resolution allowing for changes in ENSO to be interpreted, they are not continuous, providing only snapshots of conditions potentially causing erroneous interpretations. This is evidenced by Cobb *et al*. (2013) who stated no change in ENSO variance over the past 7,000 years based on discontinuous coral records, and later

refuted by Emile-Geay *et al*. (2016) who concluded from coral records a 64% reduction in ENSO variance between ca. 5,000-3,000 cal yr BP.

Despite these caveats there are noteworthy aspects of ENSO that have been deduced from a range of palaeorecords. Using archaeological evidence it was originally argued that ENSO initiated was ca. 5,000 yr BP (ca. 5,688 cal yr BP, Sandweiss *et al*., 1996); later work however indicated that ENSO has operated throughout the Holocene with differing levels of activity (Conroy *et al*., 2008). Moreover, analysis of *Porites* corals from Papua New Guinea suggest that ENSO was operating ca. 130,000 years ago during an interglacial period, and ca. 112,000 years ago in a glacial period (Tudhope *et al*., 2001). Many records have indicated that ENSO variance reduced in the mid-Holocene between ca. 6,000-3,000 cal yr BP (Riedinger *et al*., 2002; McGregor and Gagan, 2004; Rein *et al*., 2005; Conroy *et al*., 2008; McGregor *et al*., 2013a; Carré *et al*., 2014; Zhang *et al*., 2014; Emile-Geay *et al*., 2016; Chen *et al*., 2016). The precise timing of this change in ENSO varies between records, and may be a function of the flavour of El Niño that is recorded in the palaeo archive and the dominance of that flavour during the mid-Holocene (Karamperidou *et al*., 2015). An and Choi (2014) determined that in the palaeoclimate intercomparison project phase 2 and 3 (PMIP2 and PMIP3 respectively) 6,000 cal yr BP simulations there is evidence of a reduced number of EPE events (referred to as canonical El Niño in the study), and CPE events intensified. There is evidence for increased frequency of strong El Niño events beginning ca. 4000 cal yr BP, peaking at ca. 2000 cal yr BP, and decreasing in frequency towards present day (Conroy *et al*., 2008; Zhang *et al*., 2014). As strong El Niños appear to be of the EPE type predominantly (Yu *et al*., 2011), it is suggested here that there is increased frequency of EPE from ca. 4,000 cal yr BP

Climate models indicate the change in the mid-Holocene to have been a gradual change whereas proxies indicate it to have been abrupt (Donders *et al*., 2008; Chiang *et al*., 2009). This change in ENSO during the mid-Holocene has largely been attributed to orbital forcing, specifically due to precession (Luan *et al*., 2012; Lewis *et al*., 2014; Liu *et al*., 2014; Erb *et al*., 2015). Whilst orbital forcing is one factor for changing aspects of ENSO, it has been postulated that changes in the Atlantic – such as meltwater fluxes altering the Atlantic Meridional Overturning Circulation (AMOC) – also influence ENSO through teleconnections (Timmermann *et al*., 2007; McGregor *et al*., 2014). Moreover, Li *et al*. (2013) found that ENSO can also be impacted by large eruptions (VEI>4).

A number of ENSO proxies have been developed that cover several centuries to several millennia (for example Yan *et al*., 2011; McGregor *et al*., 2010; McGregor *et al*., 2013b). These proxies mostly utilise records that capitalise on the dichotomous precipitation response to El Niño and La Niña in the east and west equatorial Pacific: during El Niño the east (west) has positive (negative) precipitation anomalies, whereas during La Niña the east (west) has negative (positive) precipitation anomalies. The SOI_{pr} developed by Yan *et al*. (2011) covers the last 2000 years (Figure 2.8) using records from the Indo-Pacific and Galápagos. Positive Z-score values indicate La Niña-like conditions and negative Z-score values indicate El Niño-like conditions in the Pacific. However, it is likely that the SOI_{pr} will not fully represent ENSO changes in the southwest Pacific. Yamoah *et al*. (2016a) has shown that during strong El Niños, such as EPE, the Indo-Pacific has positive, not negative, precipitation anomalies which would appear as La Niña-like conditions in precipitation reconstructions. Consequently the SOI_{pr}, and records determined to have an ENSO record in the Indo-Pacific, need to be considered carefully in relation to proxy records from other Pacific regions. It is necessary to use, where possible, records from across the Pacific region that indicate the strength or flavour of ENSO to correctly disentangle what palaeorecords are representing. Moreover it highlights the need for continuous, multimillenial proxy records from the southwest Pacific to improve our understanding of ENSO changes throughout the Holocene.

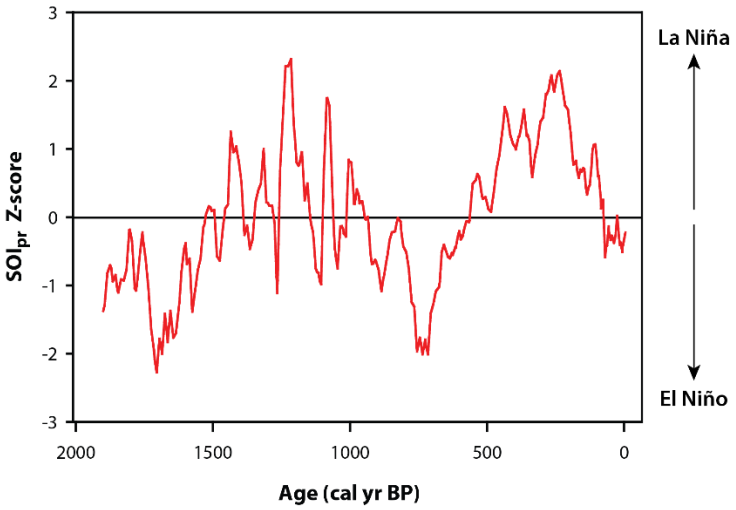

Figure 2.8: The SOI_{pr} (Yan *et al*., 2011). The index calculates the difference between reconstructed precipitation records from Indonesia, western equatorial Pacific, and the Galápagos, eastern equatorial Pacific, over the past 2,000 years. Values were standardised to Z-scores before the difference was calculated.

2.1.2 Interdecadal Pacific Oscillation

As well as ENSO a variety of climate oscillations operate in the Pacific basin. They have decadal to interdecadal frequencies, collectively referred to as Pacific Decadal Variability (PDV). In the literature it is not only the frequency of these oscillations that has been used to identify them, but also their geographic location (Figure 2.9). To date the following have been identified:

- The Pacific Decadal Oscillation (PDO) refers to the monthly SST anomalies over the North Pacific (north of 20°N) from which globally-averaged SST anomalies have been subtracted and is closely linked to fluctuations in the strength of the wintertime Aleutian Low (Mantua *et al*., 1997);
- The Interdecadal Pacific Oscillation (IPO) defined as a coherent pattern of SST variability on interdecadal timescales over the entire Pacific basin, having substantial amplitude in the tropical and southern Pacific (Power *et al*., 1999; Parker *et al*., 2007). It is argued to be the reddened response to ENSO (Di Lorenzo *et al*., 2015);
- The Bidecadal Oscillation (BDO) which is globally distributed but has the largest amplitude in the North Pacific associated with the Aleutian Low (Minobe *et al*., 2002);
- The Pacific Pentadecadal Oscillation (PPO) being a 50-70-year oscillation similar to the BDO in expression in the North Pacific but viewed as a different phenomenon due to its different seasonality in sea level pressure and land air surface temperature (Minobe, 1999). Interestingly, the superposition of the BDO and the PPO produce the observed PDO (Minobe, 1999);
- More recently the South Pacific (inter) Decadal Oscillation (SPDO) which is described as a SST pattern in the South Pacific with a frequency of 10-20 years (Hsu and Chen 2011).

Dong *et al*. (2014) stated that Pacific Decadal Variability (PDV) is one of the most important climate phenomena and a key element in regional and global climate change predictability. In general PDV more specifically refers to either the IPO or PDO. It has been suggested that the PDO and SPDO are the northern and southern expressions of the IPO

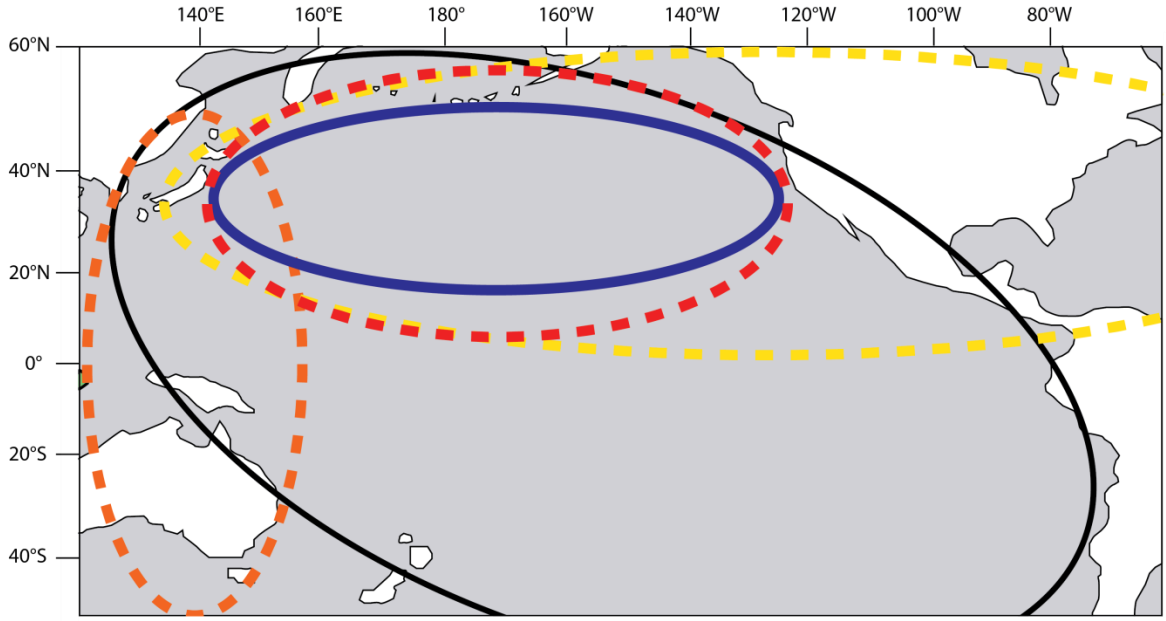

Figure 2.9: Approximate locations of climate oscillations that operate in the Pacific basin. The solid black line indicates the Interdecadal Pacific Oscillation; the red dashed line indicates the Pacific Decadal Oscillation; the yellow dashed line indicates the Bidecadal Oscillation; the solid blue line indicates the Pacific Pentadecadal Oscillation; and the orange dashed line indicates the South Pacific Decadal Oscillation.

respectively – the PDO and IPO are highly correlated (IPCC, 2014), and when the PDO, SPDO and IPO are compared they exhibit great similarity but are not identical (Chen and Wallace, 2015) (Figure 2.10). Newman *et al*. (2016) stated that differences between the PDO and IPO are a consequence of internal North Pacific processes; it is likely differences between the SPDO and IPO are due to internal South Pacific processes.

The PDO was first illustrated by Mantua *et al*. (1997), who showed that the annual Alaskan salmon catch had oscillated on interdecadal scales since the AD 1920s. Increased abundances relate to warmer than average SSTs in the eastern north Pacific – a consequence of a deepened and southward-shifted Aleutian Low (Mantua *et al*., 1997; Miller and Schneider, 2000). This anomalous Aleutian Low is a distinguishing feature of a positive phase PDO, with the associated SST anomalies north of 20°N characteristic of positive phase IPO. By becoming strengthened, warm, moist southerly winds increase in the eastern North Pacific reducing heat loss (Cayan *et al*., 1995). In the central North Pacific, westerly winds increase causing SST to cool (Miller and Schneider, 2000).

Modelling studies – such as those conducted by Blackmon *et al*. (1983) and Alexander

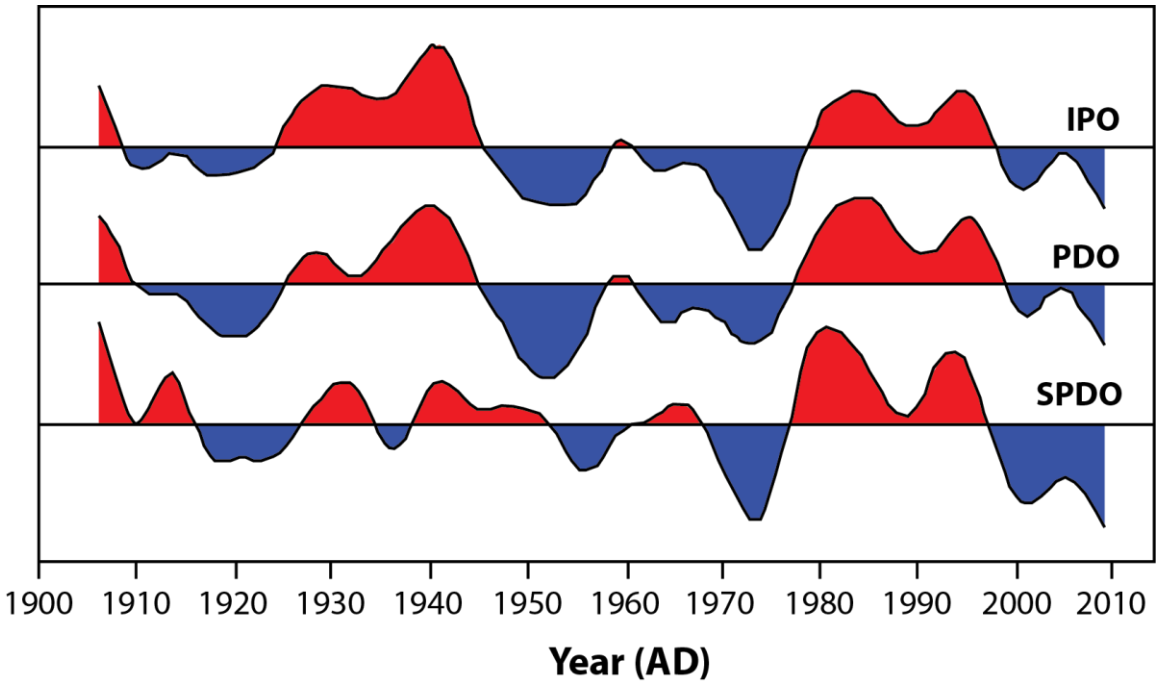

Figure 2.10: Comparison of the Interdecadal Pacific Oscillation (IPO) index, Pacific Decadal Oscillation (PDO) index, and South Pacific Decadal Oscillation (SPDO) index. Red indicates positive phases, blue indicates negative phases. The scaling is arbitrary (redrawn from Chen and Wallace, 2015).

(1992) – have demonstrated that El Niño conditions establish a deepened Aleutian Low, i.e. a positive PDO, through teleconnections (Trenberth and Hurrell, 1994). Further work has supported the argument that the PDO originates in the tropics (Garreaud and Battisti, 1999; Evans *et al*., 2001). That being said, attributing origins of the PDO is difficult as recent research indicates that that the PDO is not a single phenomenon but rather a combination of three groups of processes: 1) changes in ocean surface heat fluxes and Ekman transport related to the Aleutian low, a consequence of local unpredictable weather noise and remote tropical forcing for example from ENSO (Alexander *et al*., 2002; Alexander and Scott, 2008; Alexander, 2010; Yim *et al*., 2015; Zhang and Delworth, 2015); 2) ocean memory (Newman *et al*., 2003); and 3) decadal changes in the Kuroshio-Oyashio system (Qiu, 2003). Due to this mixture of causal processes care has to be taken when attributing the PDO as driving changes in proxy records (Newman *et al*., 2016). Further it may go some way to explaining the lack of coherence in PDO reconstructions due to instability of climatic responses to the PDO and the instability of the PDO through time (McAfee, 2014; Wise, 2015).

As the PDO is in the north Pacific, driven in part by tropical Pacific processes, the IPO should be the PDV considered for the southwest Pacific. The IPO is argued to represent

the reddened component of ENSO, this meaning each year's ENSO state being correlated with the previous year's state (Di Lorenzo *et al*., 2015). The IPO is driven by both interannual and decadal ENSO variability that is coherent across the north and south Pacific (Di Lorenzo *et al*., 2015; Newman *et al*., 2016). This could go some way in explaining the increase in El Niño and La Niña events during positive and negative phase IPO respectively (Verdon and Franks, 2006; Delcroix *et al*., 2007; Figure 2.11). Moreover, during negative-phase IPO there seems to be an increase in CPL and CPE frequency, and during positive-phase IPO an increase in EPE and EPL as well as more sustained CPE (Kao and Yu, 2009). These relationships allow for tentative qualitative statements on El Niño/La Niña frequency and flavours during these phases. Positive-phase IPO has a horse-shoe-like SSTA pattern with warm SSTs in the central and eastern equatorial Pacific and cooling in a horse-shoe-like pattern away from the equator (Mantua *et al*., 1997; Mantua and Hare, 2002; Cravatte *et al*., 2009) (Figure 2.12). The ocean and atmospheric features of negative phase IPO are the opposite of those in a positive phase IPO (Figure 2.13). The duration of IPO phases is multidecadal, with positive-phase IPO identified between AD 1896-1910, 1924-1944 and 1977-1999, negative-phase IPO between AD 1871-1895, 1945-1976, and 1999-2012, and a neutral phase between AD 1911-1923 (Henley *et al*., 2015).

The nature of phase changes this – defined as the transition from one state to another occurs within a period shorter than the length of each individual climatic state – has

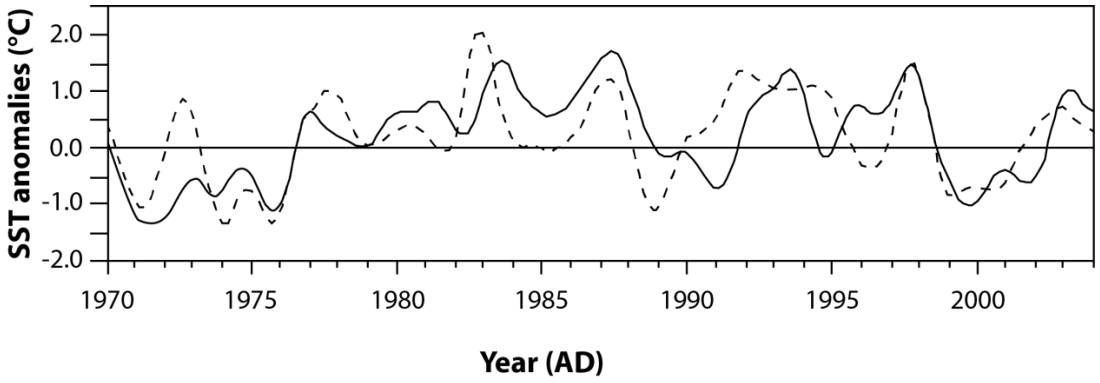

Figure 2.11: The time series for a 25-month Hanning filtered PDO (solid line) and reversed SOI (dashed line) for the AD 1970-2003 period. Positive values indicate warm phases of the PDO, negative values indicate the negative phase of the PDO. It should be noted that the PDO is derived as the leading empirical orthogonal function of monthly SST anomalies in the North Pacific Ocean poleward of 20°N (Delcroix *et al*., 2007).

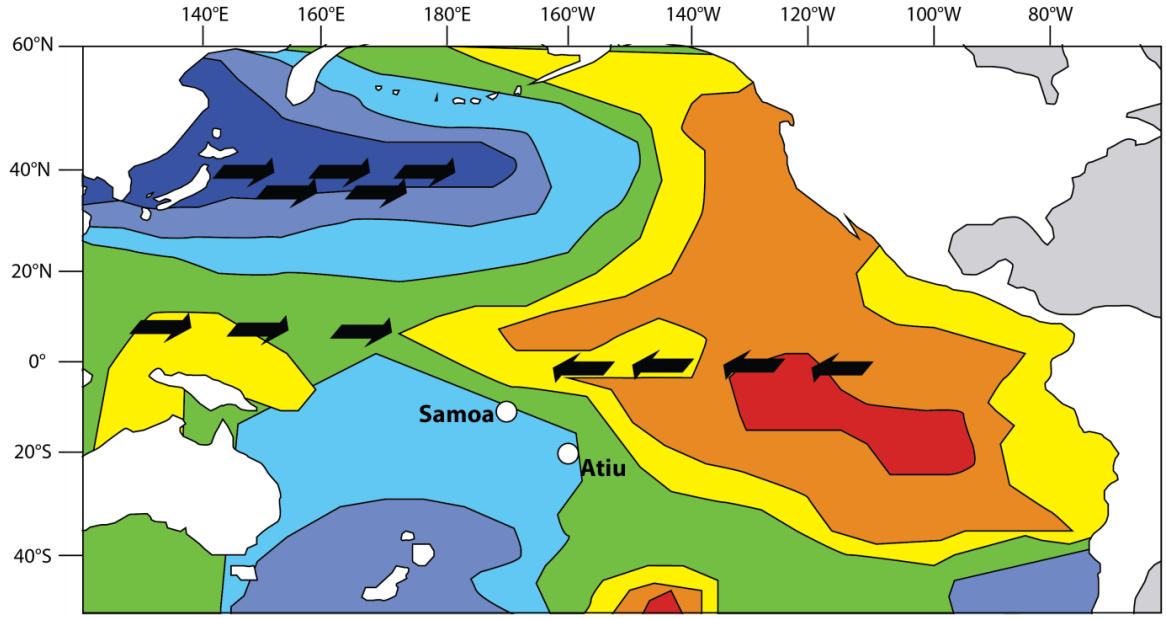

Figure 2.12: A simplified diagram of sea surface temperatures in the Pacific Ocean during positive phase IPO. A generalised positive phase PDO SSTA pattern can be observed north of 20°N. Red contours indicate warmer sea surface temperatures, dark blue indicates colder sea surface temperatures. The black arrows indicate wind direction with stronger winds indicated by multiple arrows in direction of wind travel (adapted from Power *et al*., 1999).

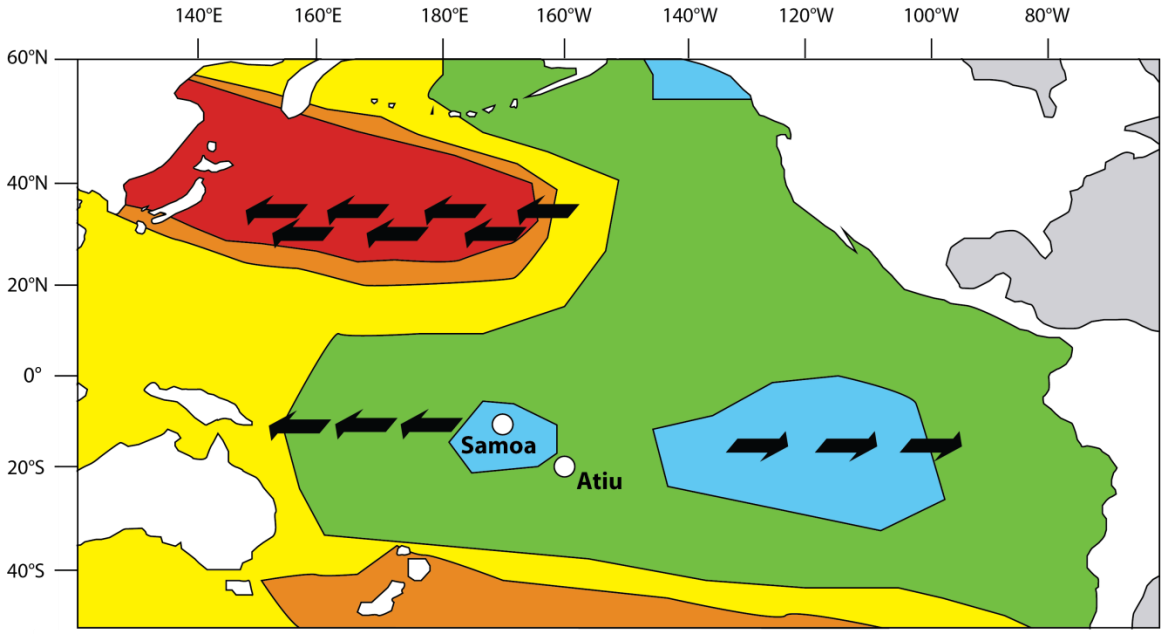

Figure 2.13: A simplified diagram of sea surface temperatures in the Pacific Ocean during negative phase IPO. Red contours indicate warmer sea surface temperatures, dark blue indicates colder sea surface temperatures. The black arrows indicate wind direction with stronger winds indicated by multiple arrows in direction of wind travel (adapted from Power *et al*., 1999).

meant that they have been termed climate "regime shifts" (Nitta and Yamada, 1989; Trenberth, 1990; Minobe, 1999; Chen *et al*., 2008). The phase shift around AD 1998/1999 to negative-phase IPO is determined to be a major cause of the recent slowdown in global warming rate (Kosaka and Zie, 2013; England *et al*., 2014; Dai *et al*., 2015), thus demonstrating the global importance of the IPO. This is further evidenced by the links between the IPO and interdecadal changes in surface temperature, precipitation and atmospheric circulation patterns across the globe: for example southern Africa (Reason and Rouault, 2002); the Indian monsoon region (Meehl and Hu, 2006); and eastern Australia (Henley *et al*., 2013). However Dong and Dai (2015) highlight that the North Atlantic may also have a major role in modulating global temperatures.

Vance *et al*. (2015) reconstructed the IPO over the last millennium based on a significant correlation between eastern Australian rainfall and the Law Dome ice core, Antarctica, during positive phase IPO, determining that the IPO has been predominantly neutral or positive for this time and has led to megadroughts (>5 year duration) in Australia. Using eight CMIP5 models, Dong *et al*. (2014) found that whilst IPO (referenced as PDV in the study) phase changes are dominated by internal variability, external factors such greenhouse gases and anthropogenic aerosols also force IPO phase changes. Dong *et al*. (2014) conclude that within the 20th Century the combined effect of greenhouse gases and anthropogenic aerosols favours a positive-phase IPO. This corroborates the IPO index (IPO Tripole Index) developed by Henley *et al*. (2015), who used SSTA in the central equatorial, northwest and southwest Pacific, that showed a dominance of positive phase IPO since AD 1890 to present. However, Smith *et al*. (2016) contradict this showing that the negative-phase PDO (essentially synonymous with negative-phase IPO) from AD 1998-2012 was driven by an increase in anthropogenic aerosols from China and a reduction from the USA. Smith *et al*. (2016) conclude that anthropogenic aerosols modulate the PDO rather than it being modulated by globally averaged forcing. It is apparent that understanding of PDV, be this PDO or IPO, is still evolving.

2.1.3 South Pacific Convergence Zone

The climate oscillations operating in the Pacific basin affect not only global climate but also climate systems that exist in the south Pacific – specifically the South Pacific Convergence Zone (SPCZ). Distinguished by a belt of low-level convergence, it extends

east-south-east from the West Pacific Warm Pool (WPWP) in Papua New Guinea towards French Polynesia 30°S, 120°W (Vincent, 1994; Folland *et al*., 2002) (Figure 2.14). Its diagonal (zonal) orientation is a consequence of a zonal SST asymmetry (symmetry), typical of La Niña (El Niño) events and normal conditions, which generates (weakens) a subtropical anticyclone over the SE Pacific (van der Wiel *et al*., 2016a). This anticyclone transports moisture SW into the SPCZ region (defined as 0°, 155°E to 20°S, 140°W in van der Wiel *et al*. (2016a)), with dynamical forcing from equatorward Rossby waves causing convection to be in a NW-SE oriented band (van der Wiel *et al*., 2016a) (Figure 2.15). With its location spanning most of Polynesia and Melanesia, approximately 10 million people are dependent on the SPCZ for potable water (Power *et al*., 2011). Convective events in the SPCZ have significant impacts on Pacific mean climate affecting upper-tropospheric climate in the south Pacific by hindering Rossby wave propagation in the region (van der Wiel *et al*., 2016b). As aforementioned, the SPCZ has global influences as its size causes a large release of latent heat that excites Rossby waves (Matthews, 2012) (Section 1.2). Moreover, the SPCZ region is the main location of tropical cyclogenesis (Revell and Goulter, 1986; Vincent *et al*., 2011; Dowdy *et al*., 2012). Consequently understanding the SPCZ has not only local importance but global importance (Brown *et al*., 2013).

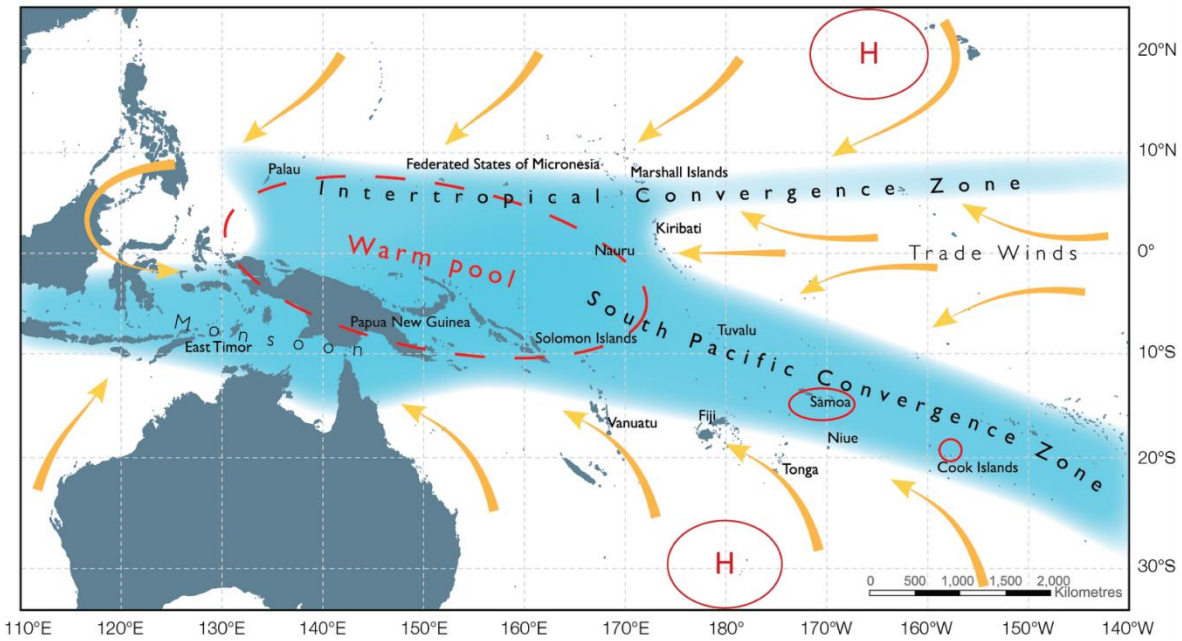

Figure 2.14: The South Pacific Convergence Zone is highlighted in the blue shaded area, with Samoa and Atiu, Cook Islands, indicated by the red circles. The yellow arrows indicate the predominant wind direction, with the red 'H' showing the location of anticyclones (ABOM CSIRO, 2011).

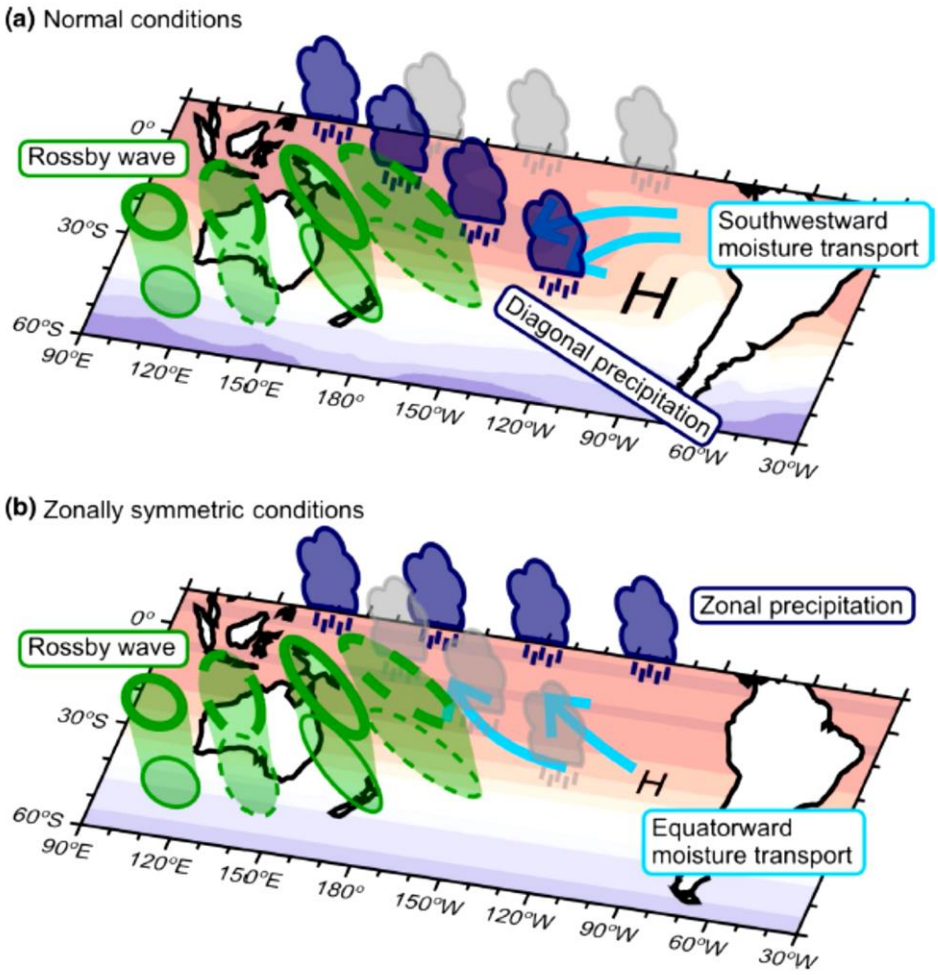

Figure 2.15: (A) A diagonal SPCZ orientation is first a consequence of an asymmetric SST distribution (typical of La Niñas and normal conditions) that produces a subtropical anticyclone over the SE Pacific which transports moisture on its western flank SW into the SPCZ region. Equatorward-propagating Rossby waves cause dynamical forcing that trigger convection in a NW-SE orientated band; (B) same as (A) but with zonally symmetric SST conditions (typical of El Niños). A weaker subtropical anticyclone leads to equatorward moisture transport. Whilst having similar diagonally orientated dynamical forcing, precipitation forms in a zonal band along the equator (van der Wiel *et al.*, 2016a).

No formal definition of the average location of the SPCZ currently exists. Defining its location is problematic as various indices position it differently (Figure 2.16). Figure 2.16 reveals that maxima in rainfall, 500 hPa vertical motion and low-level convergence broadly have the same average location over the AD 1958-1998 period. Consequently the average position of these three indices in Figure 2.16 will be utilised. This encompasses its movement between the austral summer and winter (Folland *et al*. 2002; Widlanksy *et al*., 2011; Lorrey *et al*., 2012).

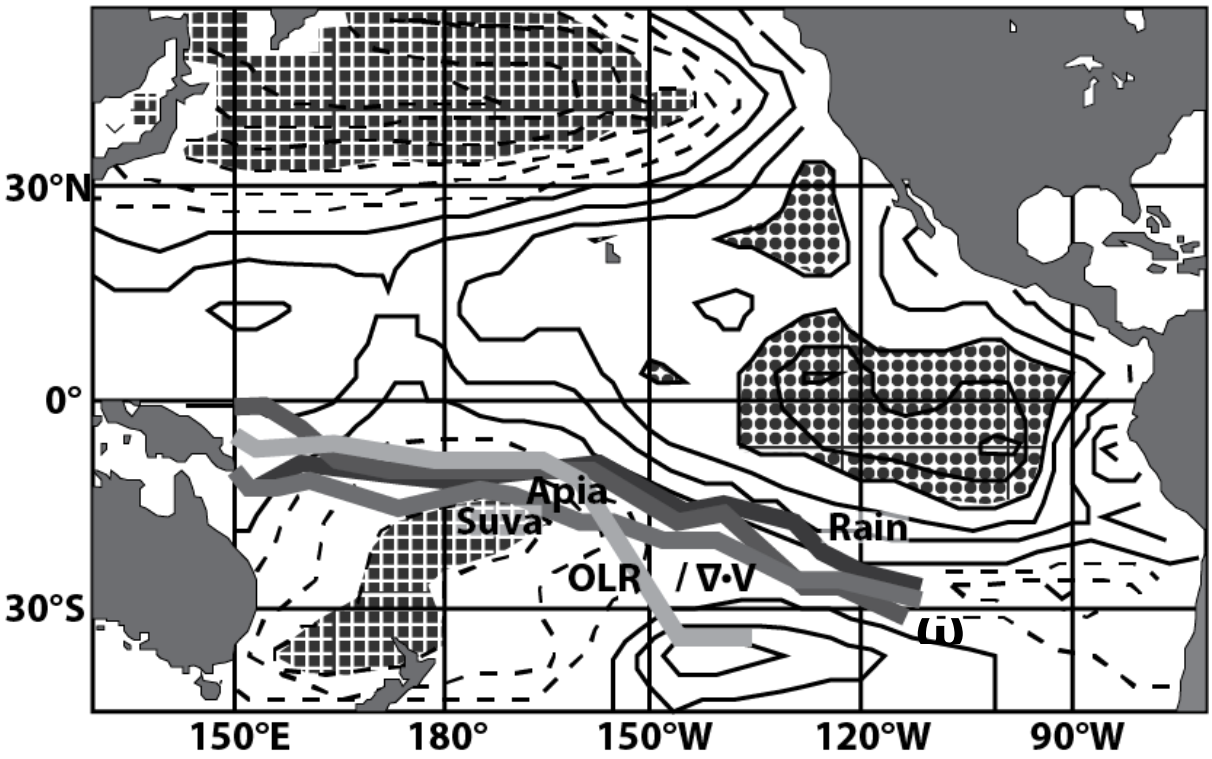

Figure 2.16: The mean November-April location for the SPCZ during the 1958-1998 AD period is indicated by four indices: maxima in rainfall (Rain), maxima in low level convergence (.V), maxima in 500 hPa vertical motion (w) and minima in outgoing long-wave radiation (OLR). The background contours indicate the IPO as a covariance map of the 3rd empirical orthogonal function of low-pass filtered SST anomalies for 1911-1995, with the contour interval being 0.04°C and negative contours being dashed. Values <-0.12°C have square stippling, and those >+0.12°C have circle stippling (Folland et al., 2002).

Results from satellite images taken every three hours from AD 1980 to 2012 reveal that the SPCZ has two distinct portions:

1. The tropical (zonal) portion in the west near the equator (0°, 130°E to 10°S, 170°W) that is orientated zonally and merges with the Intertropical Convergence Zone (ITCZ) (Vincent, 1994). This portion is present more often in the austral winter (JJAS) – the active season for the SPCZ (Haffke and Magnusdottir, 2013). The tropical portion is related to strong boundary layer convergence and located along high SST gradients due to low-level moisture convergence in the West Pacific Warm Pool (WPWP) (Lindzen and Nigam, 1987; Vincent, 1994; Lintner and Neelin, 2008; Widlansky *et al*., 2011; Haffke and Magnusdottir, 2013);

2. The subtropical portion (10°S, 170°W to 30°S, 110°W) is more diagonally orientated as a result of a zonal SST asymmetry which generates a subtropical anticyclone over the SE Pacific that transports moisture SW into this region, with dynamical forcing from equatorward Rossby waves causing convection to be in a NW-SE oriented band (Kiladis *et al*., 1989; Takahashi and Battisti, 2007; van der Wiel *et al*., 2016a). This portion of the SPCZ is more spatially variable on annual timescales (Haffke and Magnusdottir, 2013).

Analysis of satellite images over the AD 1980-2012 period indicate the SPCZ is often fragmented, consisting of several separate sections that are unconnected but cover the length of the SPCZ domain (Haffke and Magnusdottir, 2013). Nevertheless there are periods when the SPCZ is one complete connected feature covering the tropics and subtropics – such as in November AD 2006 (Haffke and Magnusdottir, 2013). Despite this fragmentation the SPCZ is present all year in the South Pacific, with the SPCZ being viewed as a sum of diagonal bands of precipitation (van der Wiel *et al*., 2015). The diagonal orientation of the SPCZ is dependent on zonally asymmetric SSTs – climate models (Intermediate Global Circulation Model version 4) indicate that a diagonal SPCZ is present with increases in absolute SST up to 6°C (van der Wiel *et al*., 2016a).

2.1.3.1 SPCZ movement

Shifts in the position of the SPCZ occur on a variety of timescales. On intraseasonal timescales the Madden-Julian Oscillation reflects changes in the location of the SPCZ: during the wet (dry) phase the SPCZ has expanded and/or migrated SE (contracted and/or migrated NW) (Vincent, 1994; Matthews and Li, 2005). Of more interest to this project are climate phenomena that cause shifts in the location of the SPCZ on interannual and interdecadal timescales. On interannual timescales the stae of ENSO strongly influences the location of the SPCZ, with El Niño being associated with a distinct northeast shift and/or contraction in the SPCZ and La Niña being associated with a shift southwest and/or expansion (Trenberth, 1976; Folland *et al*., 2002; Juillet-Leclerc *et al*., 2006; Vincent *et al*., 2009; Widlansky *et al*., 2011) (Figure 2.17). During El Niño and almost coevally with the movement of the SPCZ, the West Pacific Warm Pool (WPWP) extends eastward causing low salinity and warm waters to expand into the central Pacific creating a zonally symmetric SST gradient, whilst the sea surface salinity (SSS) front in the

Southwestern Tropical Pacific moves toward the northwest carrying salty and cold waters into the southwestern tropical Pacific (Gouriou and Delcroix, 2002). During La Niña the opposite trend occurs. Like El Niño, positive-phase IPO also causes the SPCZ to swing to a northeast position and/or contract; correspondingly negative-phase IPO causes the SPCZ to shift southwest and/or expand (Folland *et al*., 2002; Salinger *et al*., 2001). The main SPCZ precipitation axis tends to be furthest northeast, i.e. toward Samoa, during El Niño periods with a positive IPO, and furthest southwest, i.e. toward Fiji, during La Niña episodes with a negative IPO (Folland *et al*., 2002; Lorrey *et al*., 2012) (Figure 2.17 and Figure 2.18).

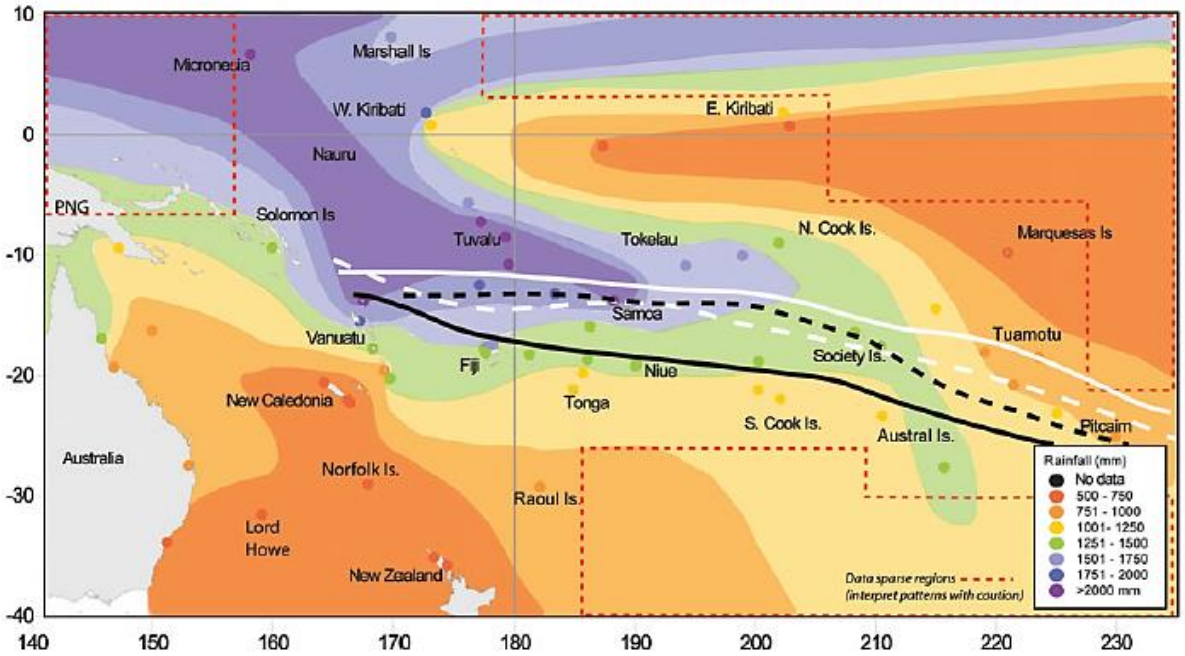

Figure 2.17: The average November-April rainfall in mm based on South Pacific island station data for the AD 1961-1990 period. The lines indicate the position of the SPCZ during the austral summer for conjoint IPO and ENSO phases based on the 10-m wind (after Folland *et al*., 2002). Solid white line: -SOI/+IPO; dashed white line: -SOI/-IPO; solid black line: +SOI/-IPO; and dashed black line: +SOI/+IPO (Lorrey *et al*., 2012).

Salinger *et al*. (2014) developed an index for the movement of the SPCZ using the difference in mean sea level pressure (MSLP) between Suva, Fiji, and Apia, Samoa, terming it the South Pacific Convergence Zone Index (SPCZI). Fiji is typically west of the SPCZ and Samoa east of it, thus capturing the variations in the position of the SPCZ. Positive values indicate when the SPCZ is northeast of its mean position, as occurs during El Niño or positive phase IPO; negative values indicate when the SPCZ is southwest of its mean position, as occurs during La Niña or negative phase IPO (Salinger *et al*., 2014).

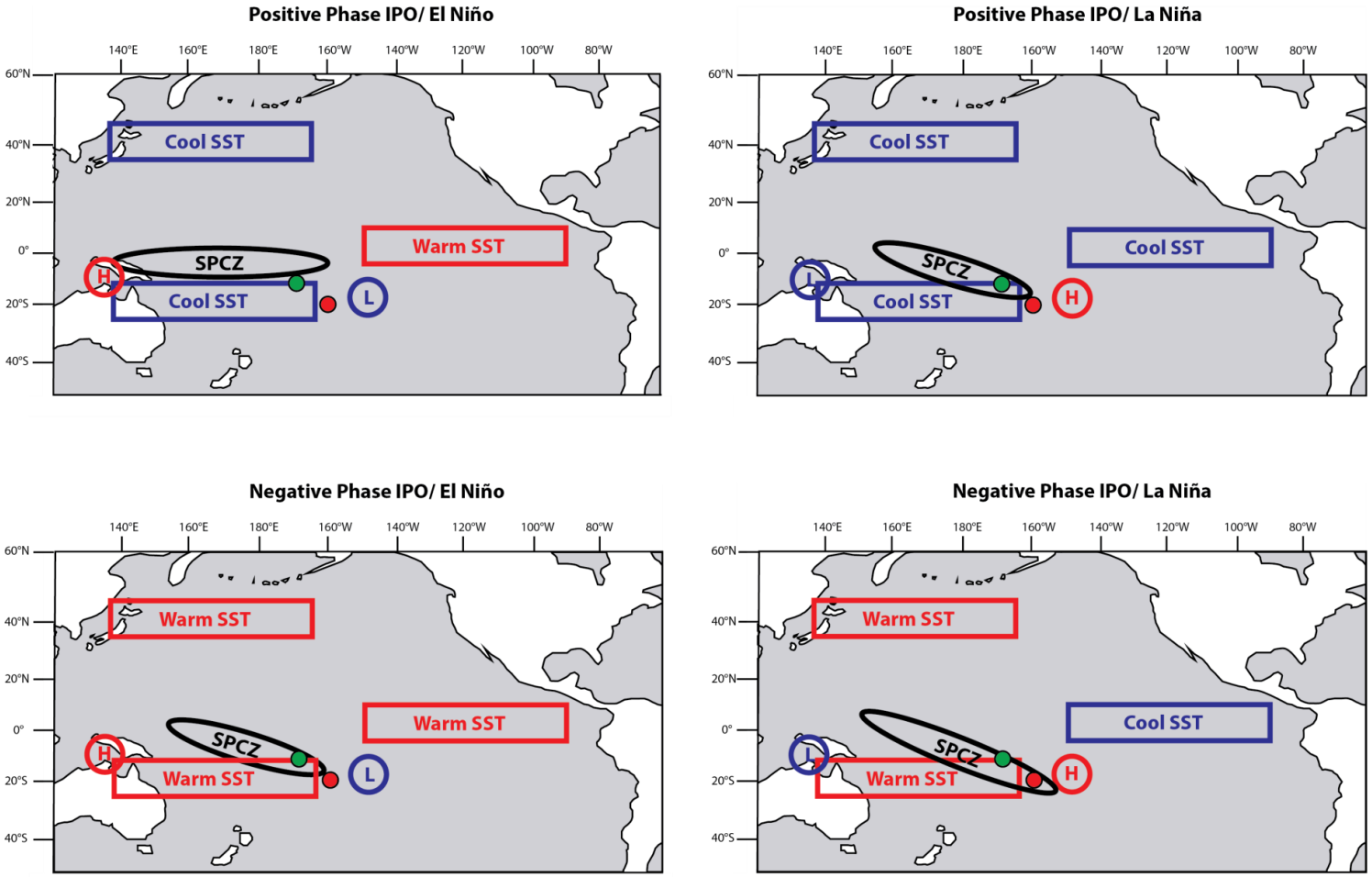

Figure 2.18: Overview of conditions in the Pacific and their relationship to the SPCZ during different climate oscillations. Samoa (green circle) and Atiu, Cook Islands (red circle) are highlighted. When the SPCZ is zonal (positive-phase IPO/El Niño) Samoa and Atiu are drier, during other phases (positive-phase IPO/La Niña, negative-phase IPO/ El Niño, and negative-phase IPO/La Niña) Samoa and Atiu are wet so changes in precipitation, and consequently SPCZ position, are harder to disentangle. High pressure (H) and low pressure (L) areas are highlighted.

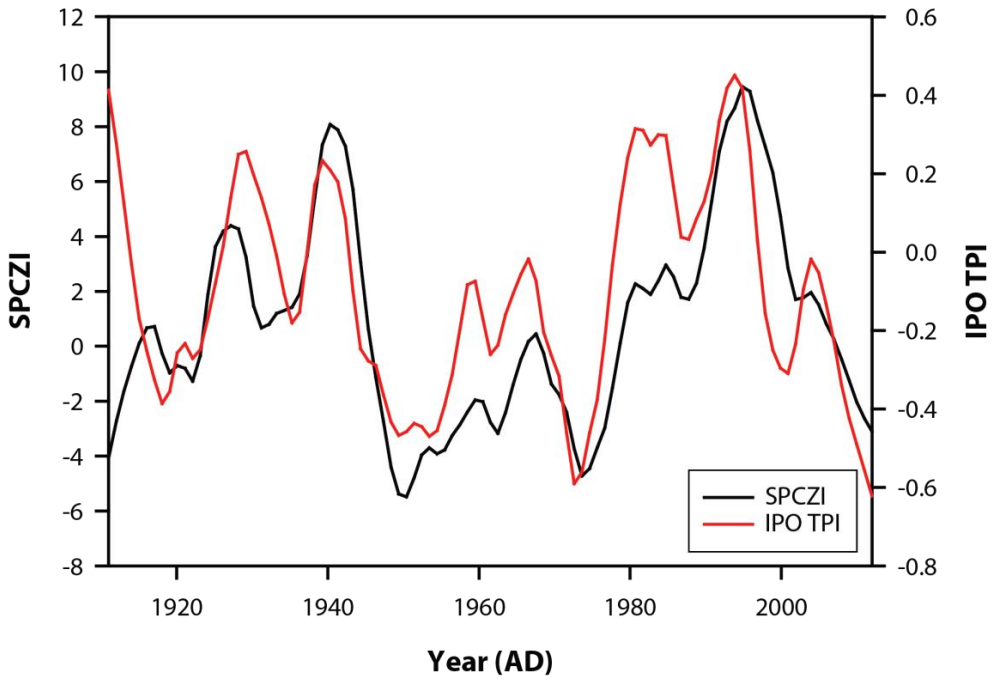

Figure 2.19: The SPCZI and IPO TPI smoothed with a LOESS smoothing function (0.1 sampling interval, polynomial degree of 1) (Salinger *et al*., 2014; Henley *et al*., 2015).

Upon analysis of the SPCZI (Figure 2.19) it can be observed that there are periods where it is predominantly positive and predominantly negative for several decades. Comparing a LOESS-smoothed SPCZI and IPO tripole index (IPO TPI) there is a significant correlation ($r = 0.48$, $p<0.0001$) (Salinger *et al*., 2014; Henley *et al*., 2015).

It has been observed in three El Niño events (AD 1982/1983, 1991/1992, and 1997/1998) that the SPCZ swung equatorward to such an extent it became zonal in orientation – termed zonal SPCZ events (zSPCZ) (Borlace *et al*., 2014) – and merged with the ITCZ (Salinger *et al*., 2014). This causing a relative precipitation anomaly of ca.-6mm/day between 0-30 °S, 160 °E-80 °W in the HadCM3 coupled global climate model used (Borlace *et al*., 2014). Associated with zSPCZ is a zonal shape of the WPWP, which moves southward in the west and eastward at the equator as a consequence of equatorial upwelling disappearing in the central part of the Pacific basin (Vincent *et al*., 2011). Kidwell *et al*. (2016) determined that zSPCZ events, and pronounced negative precipitation anomalies in Polynesia, occur during strong El Niño events (such as AD 1982/93, 1991/92 and 1997/98) which they consider are different to EPE, whereas during weak El Niños and CPE the SPCZ is the same size but lower magnitude. Whilst Kidwell *et al*. (2016) consider strong El Niño events to be different to EPE, the authors' note that the spatial structure of the SPCZ in both cases is near identical. Combining this with Yu *et al*.

(2011) surmising that from AD 1958-2001 a strong El Niño is associated with an EPE and not CPE, it is suggested here that strong El Niños and EPE are essentially the same in the historical record, and most likely in the palaeo record. Moreover, strong El Niño events, and by extension EPE, appear to occur in positive-phase IPO and not negative-phase IPO (Kao and Yu, 2009; Yu *et al*., 2011; Henley *et al*., 2015). As strong El Niños and EPE cause zSPCZ, it is suggested that their effect on the SPCZ over interdecadal timescales and longer will be indistinguishable. Combining this with the significant relationship between SPCZI and IPO TPI, it is put forward that if a record suggests that the SPCZ has taken a zonal orientation over interdecadal timescales it indicates positive-phase IPO, which in turn suggests increased EPE frequency and more sustained CPE (Kao and Yu, 2009).

2.1.3.2 Past and future SPCZ behaviour

During the mid-Holocene (ca. 6,000 and 4,000 cal yr BP) modelling experiments (PMIP2) suggest that the SPCZ was expanded southeast and appears to have had more shifts in SPCZ position per century of larger amplitude in the 6,000 cal yr BP run (Braconnot *et al*., 2007; Mantsis *et al*., 2013; Saint-Lu *et al*., 2015). Further, Saint-Lu *et al*. (2015) show that in the 6,000 and 4,000 cal yr BP runs the more southerly SPCZ position and its increased variability is due to an increased meridional SST gradient and/or reduced ENSO activity. Toomey *et al*. (2016) argue that the sedimentary record from Apu Bay, Tahaa, French Polynesia, suggests wetter conditions since ca. 3,000 cal yr BP as a result of the SPCZ intensifying or migrating which they attribute to precessional forcing due to the gradual intensification of background precipitation observed across French Polynesia. Linsley *et al*. (2006), Partin *et al*. (2013), and Maupin *et al*. (2014) indicate that the SPCZ has expanded southwest since AD 1800 suggesting La Niña-like or negative-phase IPO conditions in the Pacific. In these studies PDV – considered here to be IPO – is evident, with large abrupt shifts recorded in rainfall amount or salinity caused by PDV influencing the SPCZ position. Partin *et al*. (2013) in particular highlight that changes in PDV phases over the last 446 years have caused precipitation changes, as a result of SPCZ changing position, larger than that seen in the instrumental period. With the SPCZ being the major source of potable water in the South Pacific this has major implications for water resource management in this region, and potentially provide context for Polynesian colonisation history.

It is highly likely that the SPCZ will alter in the future as a result of anthropogenic warming. Model simulations performed by Cai *et al*. (2012) and Borlace *et al*. (2014) suggest that under projected future warming there would be an increase in zSPCZ, with 8 CMIP3 coupled general circulation models forecasting an 81% increase in frequency of zSCPCZ. With tropical warming of 1-2 °C, Widlansky *et al*. (2013) estimated a 6% decrease in SPCZ rainfall with a multi-model uncertainty exceeding ±20%, and Brown *et al*. (2013) concluded in 26 CMPI5 models that under the RCP8.5 emission scenario (CO_2-equivalent concentration of 1,370 ppm) there will be decreased precipitation at the eastern edge of the SPCZ. Drying in the eastern part of the SPCZ is corroborated by Chung and Power (2016) using a CMIP3 model. Under 4xCO_2 (1120 ppm) warming Saint-Lu *et al*. (2015) determined that the SPCZ will be shifted northward as a result of a reduced meridional SST gradient, leading to an increased frequency of SPCZ shifts. However Brown *et al*. (2015) highlighted that changes in SST gradients can lead to discrepancies in rainfall projections of the order of 60%, thus casting uncertainty as to exactly how the SPCZ will respond to future anthropogenic warming (Brown *et al*., 2013; Widlansky *et al*., 2013). Nevertheless it is apparent that the SPCZ behaviour will likely change. Consequently determining how it has altered in the past is vital to understand how it will potentially change in the future and provide important information needed for water resource management in the South Pacific.

2.2 Pacific palaeo-records

To be able to interpret the potential changes in the position of the SPCZ in the past it is first necessary to delineate a standard location. As a result of the SPCZ moving seasonally (Vincent, 1994) the 'average' position of the SPCZ aforementioned (Figure 3.16) will be utilised which encompasses its movement between the austral summer and winter (Folland *et al*., 2002; Widlanksy *et al*., 2011; Lorrey *et al*., 2012). The following regions that will be used to discuss palaeo-records from the Pacific cover the Niño 1, 2, 3, 3.4, 4, SOI, SPCZ and EMI region, and are as follows:

- Pacific Basin: includes the circum-Pacific (relevant records from the North Pacific and South America), Galápagos Islands, Easter Island, Ecuador, and Hawaii;
- The SPCZ region: lies northwest to southeast across the southwest Pacific and incorporates the tropical and subtropical SPCZ portions (Haffke and Magnusdottir,

2013). Localities included are Papua New Guinea, Solomon Islands, Samoa, Southern Cook Islands, Fiji, Tonga, and French Polynesia;

- North of the SPCZ: localities included are Palau, Guam, Kiribati, and Marquesas Islands;
- South of the SPCZ: localities included are Australia, Vanuatu, New Caledonia, and North Island of New Zealand.

A map showing the locations of records and their type is presented in Figure 2.20, with the lengths of these records in Figure 2.21 and Figure 2.22. Sites, with their corresponding codes, are listed in Appendix A. These regions will be reviewed in regards to the early Holocene (ca. 11,600-6,000 cal yr BP), mid-Holocene (ca. 6,000-3000 cal yr BP), and late Holocene (ca. 3,000 cal yr BP to present). This different subdivision of the Holocene compared to that proposed by Walker *et al*. (2012) reflects the subdivisions typically referenced in PMIP ENSO reconstructions such as Braconnot *et al*. (2007, 2012). Various studies discuss changes in ENSO, be this variability, frequency or strength, but they do not necessarily have annual or subannual chronological resolution to be able to discuss this interannual phenomenon. Some studies, such as Atwood and Sachs (2014), refer to ENSO activity and define it as a change in the frequency and/or intensity of El Niño events, and may be indicative of EPE and CPE frequency. Thus following an outline of a study's interpretation of ENSO, changes in ENSO will be put into context of the IPO in this review to facilitate comparison at the interdecadal, and greater, timescale and incorporate the various changes in ENSO proposed.

2.2.1 Pacific basin records

2.2.1.1 Early Holocene

Records from the Pacific basin provide contrasting conditions in the Pacific from the beginning of the Holocene up to ca. 6,000 cal yr BP. A speleothem record from Borneo indicates that ENSO was quite active in the early Holocene and also indicates reduced ENSO activity ca. 8,200 cal yr BP (Chen *et al*., 2016). This corroborates the El Junco, Galápagos, record which suggests medium ENSO activity in the early Holocene and also suggests reduced ENSO frequency at ca. 8,200 cal yr BP (Conroy *et al*., 2008; Zhang *et al*., 2014). Koutavas and Joanides (2012) conclude from a marine core in the Galápagos that

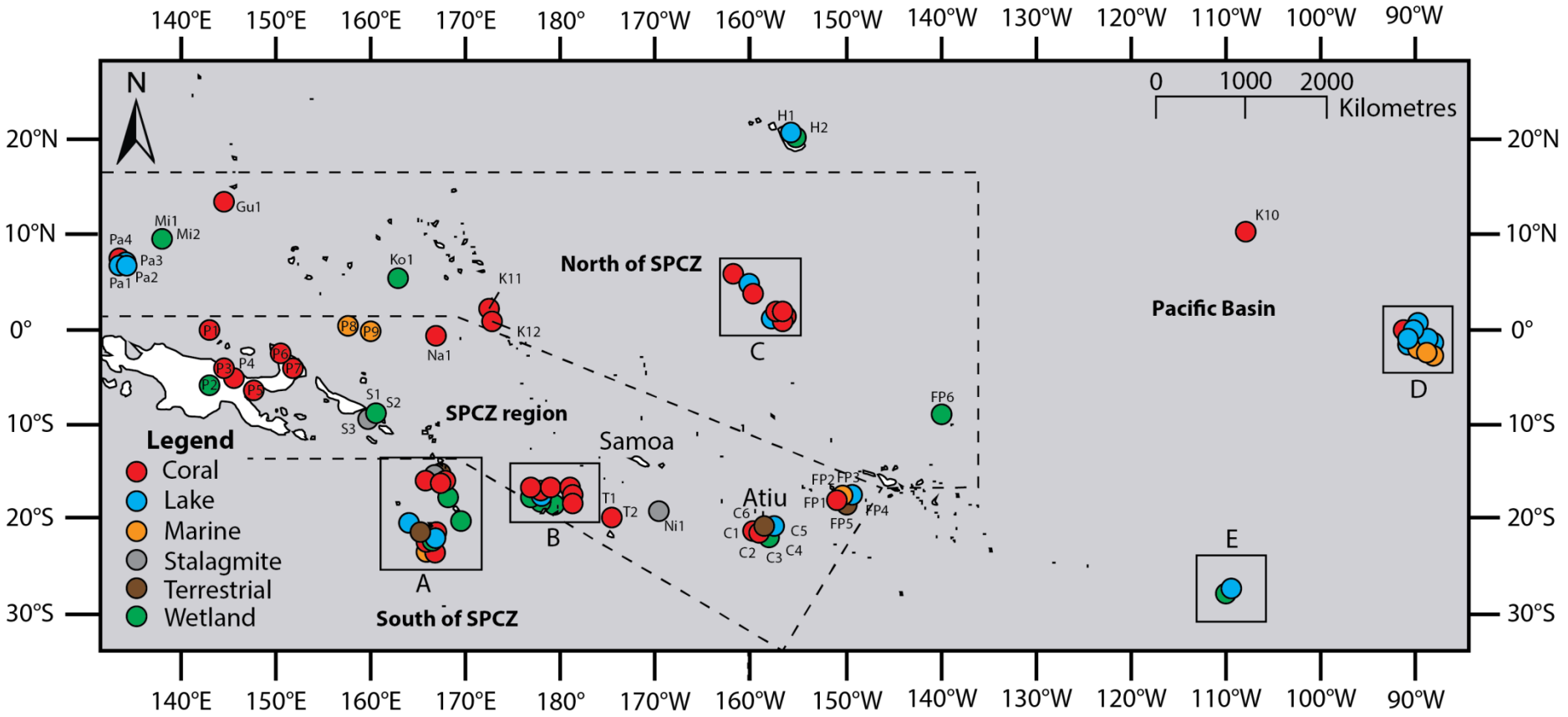

Figure 2.20: Locations of palaeo records in the Pacific basin. On the following page are (A) New Caledonia and Vanuatu; (B) Fiji; (C) Kiribati; (D) Galápagos; and (E) Easter Island. Dashed lines demarcate regions that are being discussed. Samoa and Atiu, Cook Islands are also highlighted.

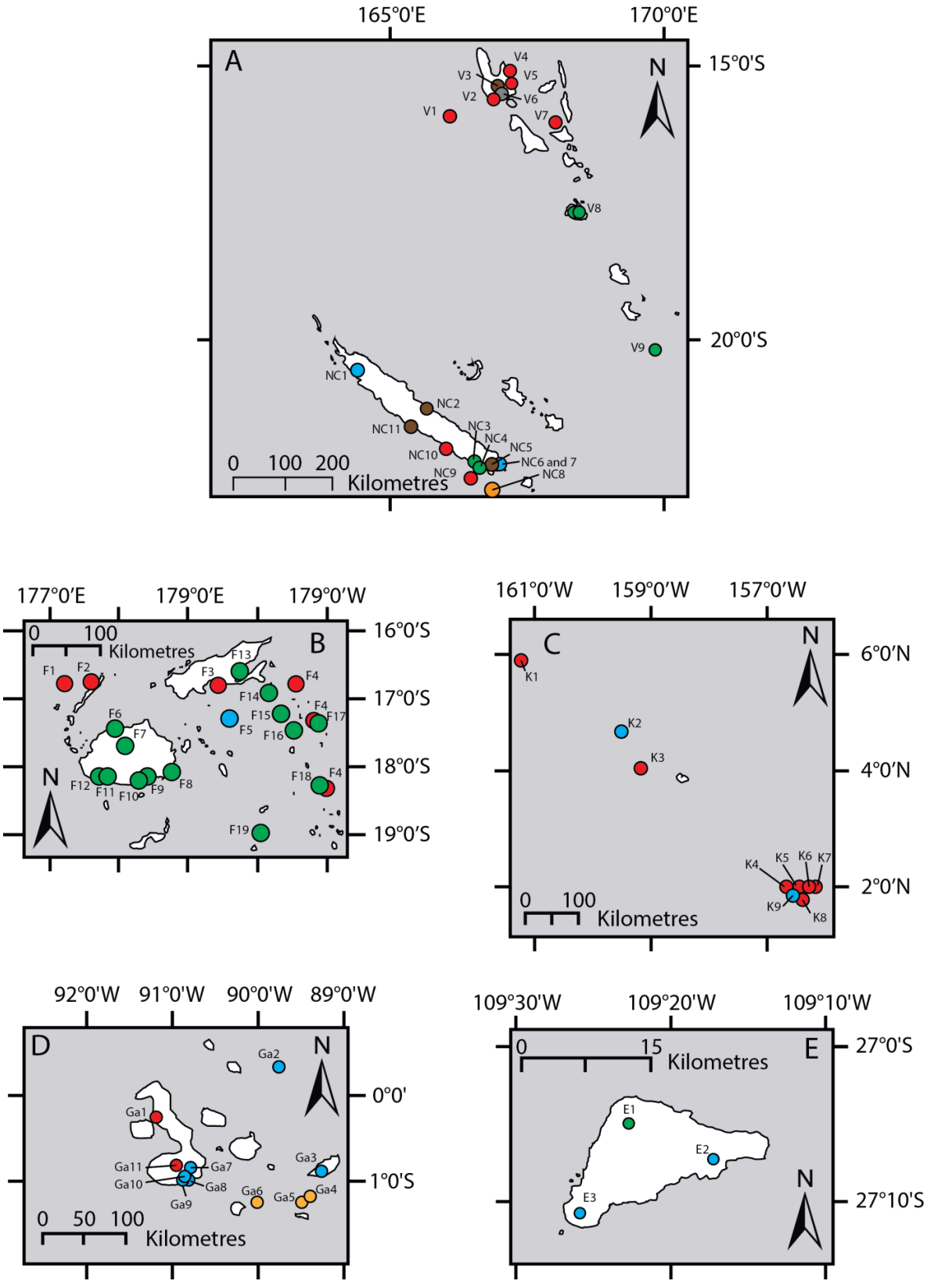

Figure 3.20 continued. A) New Caledonia and Vanuatu; (B) Fiji; (C) Kiribati; (D) Galápagos; and (E) Easter Island.

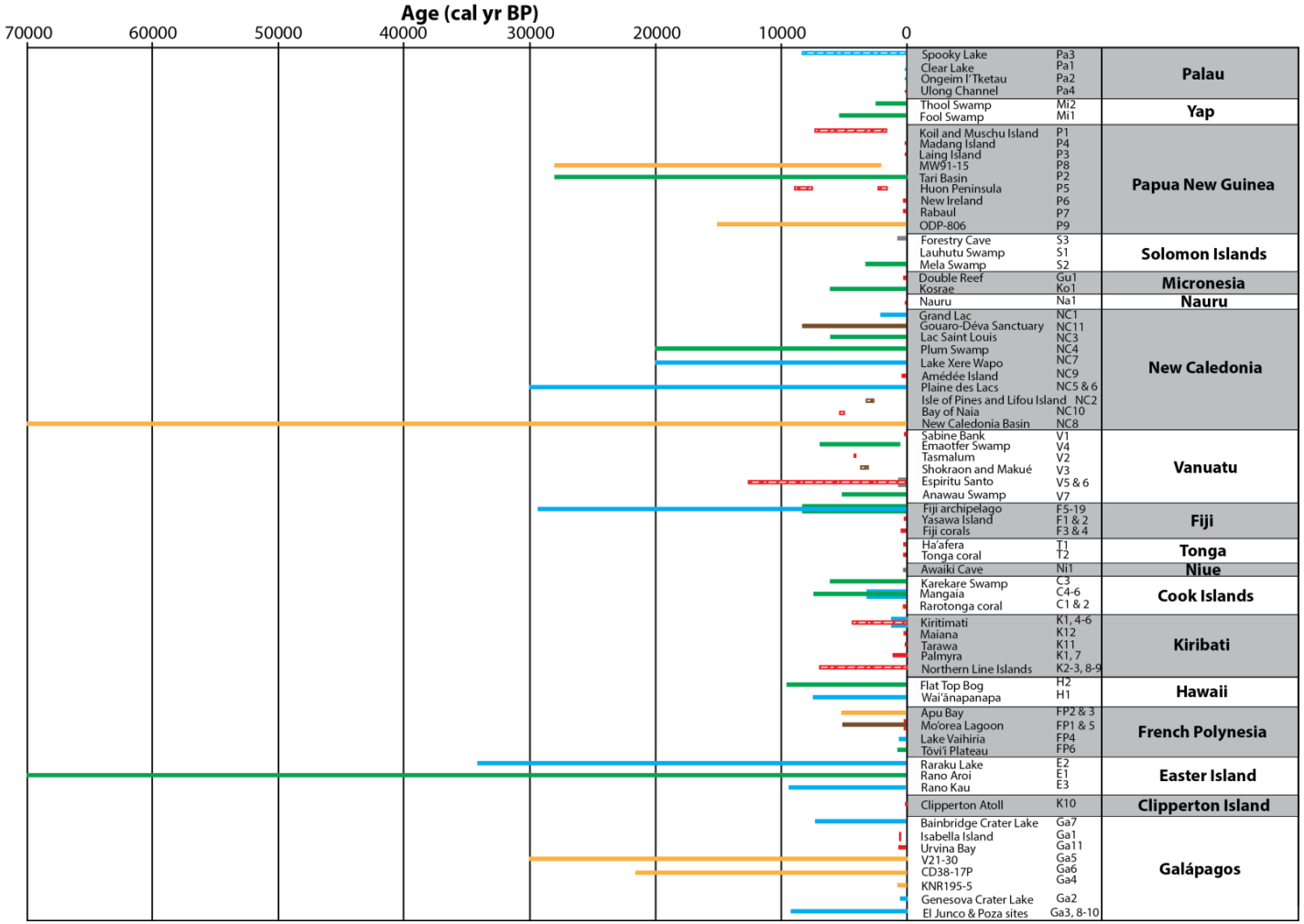

Figure 2.21: Length of palaeorecords in the Pacific basin. Blue indicates a lake record, red is coral, green is wetland, brown is terrestrial, yellow is marine, and grey is stalagmite. Hatching indicates a discontinuous record, with the length indicating the oldest age published.

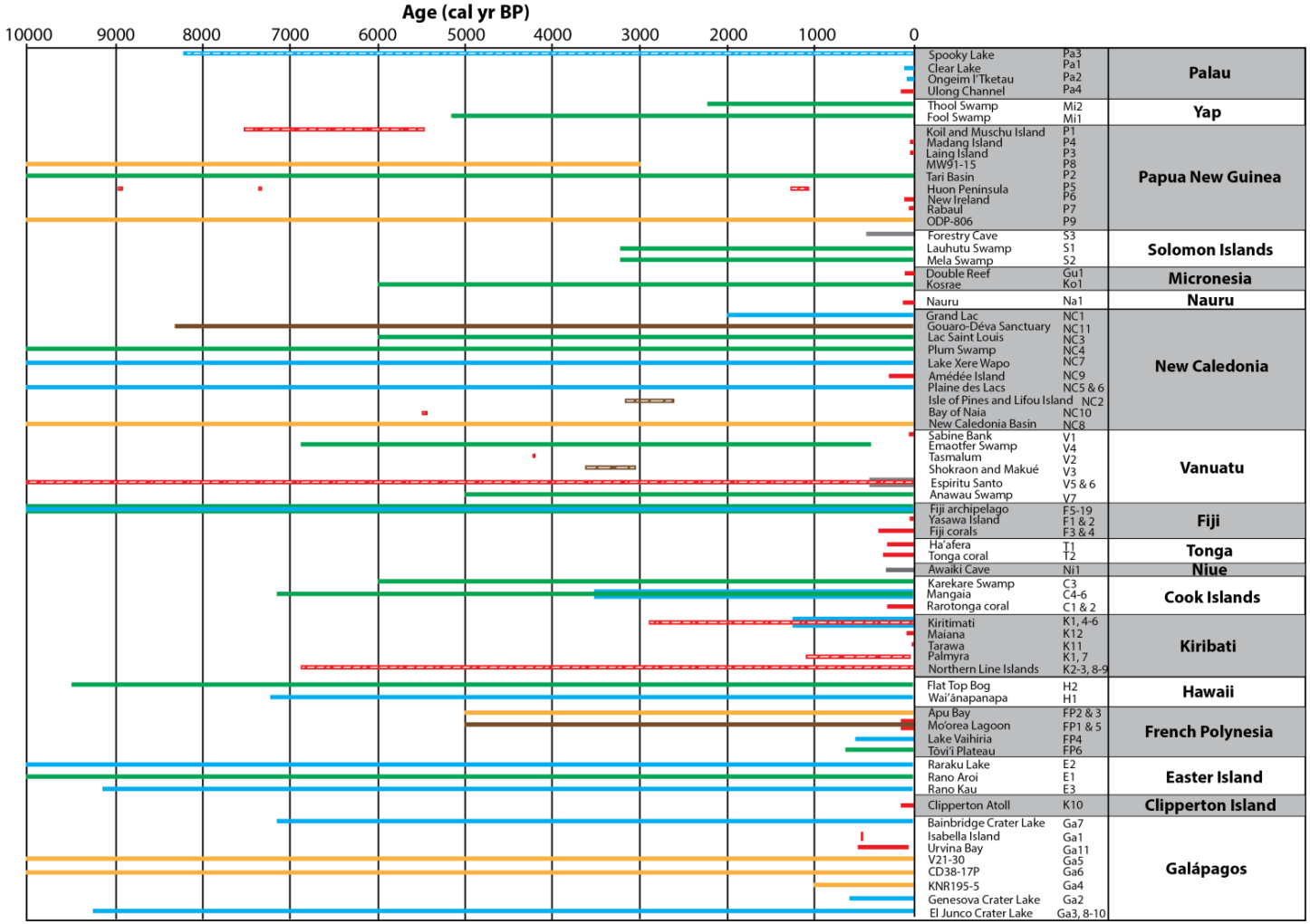

Figure 2.22: Length of palaeorecords in the Pacific basin with focus on the last 10,000 cal yr BP. Blue indicates a lake record, red is coral, green is wetland, brown is terrestrial, yellow is marine, and grey is stalagmite. Hatching indicates a discontinuous record, with the length indicating the oldest age published.

there is medium ENSO activity from the beginning of the Holocene until ca. 6,000 cal yr BP, supporting the El Junco lake record (Conroy *et al*., 2008; Zhang *et al*., 2014).

Weak to moderate ENSO activity is inferred from flood records from Peru and Ecuador (Robdell *et al*., 1999; Moy *et al*., 2002; Rein *et al*., 2005); however these records could significantly bias ENSO estimates (Emile-Geay and Tingley, 2016) and in fact be a record of soil erosion and glaciation in the case of Laguna Pallcacocha (Robdell *et al*., 2008) casting doubt on their efficacy as an ENSO record. Mollusc $\delta^{18}O$ records from the Peru coast are interpreted to show that EPE dominates prior to ca. 8,000 cal yr BP, and CPE dominates from ca. 7,500-6,700 cal yr BP with similar variability to when EPE dominates (Carré *et al*., 2014). Wetter conditions occurred in southern California prior to ca. 8,000 cal yr BP (Kirby *et al*., 2007) , and stable lake conditions with increased terrestrial input are interpreted in Rano Raraku, Easter Island (Cañellas-Bolta *et al*., 2012) which suggest wetter conditions. Wetter conditions in southern California and Easter Island are consistent with El Niño conditions in the Pacific and at the interdecadal scale suggest that the Pacific was in a predominantly positive-phase IPO throughout the early Holocene.

However, a synthesis of north American records is interpreted by Barron and Anderson (2011) (and references therein) to indicate negative-phase PDO from 8,000-6,000 cal yr BP, with this being corroborated by warm SST in the South China Sea (Kienast *et al*. 2001), which are characteristic of negative-phase PDO (Power *et al*., 1999). Negative-phase PDO in the North Pacific suggests that at the Pacific basin scale negative-phase IPO is operating, due to the aforementioned similarity between the two (Chen and Wallace, 2015). However Newman *et al*. (2016) highlight the difficulty in interpreting PDO conditions due to the PDO being an amalgamation of processes with different expressions, thus calling into question Barron and Anderson's (2011) interpretation. Interestingly other studies from Easter Island, specifically Rano Aroi and Rano Raraku, suggest drier conditions in the early Holocene (Sáez *et al*., 2009; Margalef *et al*., 2013, 2014; Cañellas-Bolta *et al*. 2016), possibly associated with negative-phase IPO (Power *et al*., 1999). A drier early Holocene interpreted from Rano Aroi is questionable due to this being solely derived from carbon isotopic and carbon/nitrogen ratio measurements on bulk sediment without supporting evidence of reduced terrestrial in-wash such as Ti measurements (Margalef *et al*., 2013). Moreover, Sáez *et al*. (2009) interpreted a lower lake level in Rano Raraku in the early Holocene to indicate more arid conditions. In the context of the Holocene only, where

there is a sedimentary hiatus in the Rano Raraku record in the mid-Holocene that is attributed to prolonged aridity suggested here to be a consequence of negative-phase IPO, the early Holocene could be reinterpreted as a period where there is enough precipitation to be conducive in maintaining a shallow lake. This would be consistent with positive-phase IPO conditions in the Pacific in the early Holocene over interdecadal, and greater, timescales. With these highlighted caveats it is postulated that early Holocene Pacific basin records indicate medium-strength ENSO, and positive-phase IPO dominated conditions, potentially indicating no particular dominance in EPE or CPE frequency throughout the suggested positive-phase IPO early Holocene conditions.

2.2.1.2 Mid Holocene

The Buki Assam Cave record, Borneo, indicates reduced ENSO variability in the mid-Holocene between ca. 5,500-3,500 cal yr BP (Chen *et al*., 2016), corroborating a reduction in ENSO variability determined from molluscs on the Peruvian coast between ca. 5,000-4,000 cal yr BP (Carré *et al*., 2014), a reduction in foraminifera $\delta^{18}O$ variability between ca. 6,000-3,000 cal yr BP in a marine core from the Galápagos (Koutavas and Joanides, 2012), and weak ENSO activity between ca. 5,600-3,400 cal yr BP determined from botryococcene concentration and $\delta^{2}H$ measurements on El Junco, Galápagos, sediments (Zhang *et al*., 2014). Moreover reduced ENSO activity is determined from Bainbridge Crater Lake, Galápagos, from ca. 6,100-3,000 ^{14}C yr BP (ca. 6,900-3,100 cal yr BP) (Riedenger *et al*., 2002; Bryksina and Last, 2005).

Deposition of sediment in Rano Raraku was interrupted by a sedimentary hiatus beginning ca. 4,200 cal yr BP, with this being interpreted to be a consequence of arid conditions drying out the lake and erosion removing the deposited sediments (Mann *et al*., 2008; Sáez *et al*., 2009; Cañellas-Boltà *et al*., 2012, 2016). Furthermore Rano Aroi, a peatland on Easter Island, indicates very low accumulation rates (0.06 mm/yr) from ca. 5,500-2,500 cal yr BP with this being construed as a result of dry conditions throughout this period (Margalef *et al*., 2013, 2014). These arid conditions are consistent with negative-phase IPO conditions in the Pacific, which are associated with reduced ENSO variability and weak ENSO activity (Di Lorenzo *et al*., 2015). Despite the unreliability of Laguna Pallcacocha as an ENSO record it too indicates a reduction in sedimentation rate at ca. 4,000 cal yr BP, interpreted by Moy *et al*. (2002) as a reduction in ENSO variability. Oxygen isotope ratios of authigenic calcite ($\delta^{18}O_{cal}$) obtained from Laguna Pumacocha,

Peru, suggest drier conditions prevailed from 7000-5000 cal yr BP as a result of reduced rainfall from the South American summer monsoon (Bird *et al*., 2011).

Whilst it has been stated that the reliability of PDO records is questionable due to the mixture of causal processes (Newman *et al*., 2016), it is interesting to note there is coherency with the records from Borneo, the Galápagos, Easter Island, and the North Pacific. Records from the eastern North Pacific basin suggest that from ca. 6000-4000 cal yr BP negative-phase PDO dominated, and by extension negative-phase IPO (Newman *et al*., 2016), causing wetter conditions in the northwest Pacific and drier conditions in the southwest US (Barron and Anderson, 2011, and references therein). Increased ENSO and PDO variability, suggested here to indicate a shift to positive-phase IPO dominated conditions (Di Lorenzo *et al*., 2015), is interpreted to begin at different times in the North Pacific, beginning at ca. 4,000 cal yr BP and ca. 3,400 cal yr BP in southern and northern California respectively, and ca. 2,000 cal yr BP in southwestern Yukon (Barron and Anderson, 2011). The differences in these timings may reflect a dominance of El Niño types at different times. As EPE have larger effects across the Pacific basin, it could be argued that the time transgressive nature of increased ENSO and PDO variability highlighted by Barron and Anderson (2011) in fact represents a change from CPE dominated conditions at ca. 4,000 cal yr BP to EPE dominated conditions at ca. 3,400-2000 cal yr BP. However without isochronous markers connecting these sites the suggested progressive nature of this change is questionable.

2.2.1.3 Late Holocene

A variety of records indicate that ENSO activity/variability increased from ca. 3,000 cal yr BP to present, including El Junco (Conroy *et al*., 2008; Zhang *et al*., 2014; Atwood and Sachs, 2014), Bainbridge Crater Lake (Riedinger *et al*., 2002; Bryksina and Last, 2005), the Galápagos marine cores CD38-179P (Sadekov *et al*., 2013) and V21-30 (Koutavas and Joanides, 2012), and speleothems from Borneo (Chen *et al*., 2016). Wetter conditions are also interpreted from Easter Island in the late Holocene (Sáez *et al*., 2009; Cañellas-Bolta *et al*., 2012, 2016; Margalef *et al*., 2013; Rull *et al*., 2015). Collectively this suggests that the Pacific has been in a predominantly positive-phase IPO state from ca. 3,000 cal yr BP to present.

In the late Holocene there is some periodicity in ENSO activity, having stronger activity (El Niño/positive-phase IPO dominated) from ca. 3,000-1,500 cal yr BP, after there appears to be a ca. 500-year oscillation between stronger (El Niño/positive-phase IPO dominated) and weaker activity (La Niña/negative-phase IPO dominated) ENSO activity (Atwood and Sachs, 2014; Nelson and Sachs, 2016). Yamoah *et al*. (2016a) determined a broad agreement with the El Junco ENSO record over the last 2,000 cal yr BP; however there is a disparity between their record in Thailand and records in the western Pacific on centennial timescales. Yamoah *et al*. (2016a) suggested that on centennial timescales strong El Niño events cause the Indo-Pacific to have an inverse relationship with the tropical west and southwest Pacific, and a positive correlation with the central and eastern Pacific. Simply: during strong El Niños – typically EPE (Yu *et al*., 2011) – the Indo-Pacific and central-eastern Pacific indicates wetter conditions, suggesting La Niña- and El Niño-like conditions respectively, whilst the western and southwestern Pacific indicates drier (El Niño-like) conditions. Decreased ENSO activity (La Niña/negative-phase IPO dominated) associated with a strong zonal SST gradient across the equatorial Pacific is determined from ca. 1,000-450 cal yr BP, after which increased ENSO activity (El Niño/positive-phase IPO dominated) and a weak zonal equatorial Pacific SST gradient is argued to occur (Conroy *et al*., 2010; Rustic *et al*., 2015). Evidence that the Medieval Climate Anomaly (MCA) (AD 800-1300, 1,150-650 cal yr BP) was dominated by La Niña conditions (negative-phase IPO), and the Little Ice Age (LIA) (AD 1500-1850, 450-100 cal yr BP) was dominated by El Niño conditions (positive-phase IPO) can be found in Borneo (Khider *et al*., 2011), the Galápagos (Conroy *et al*., 2009; Restropo *et al*. 2012; Rustic *et al*., 2015), and Easter Island (Dunbar *et al*., 1994).

2.2.1.4 Overview of Pacific Basin Records

From the beginning of the Holocene to ca. 6,000 cal yr BP the Pacific had increased ENSO activity (El Niño/positive-phase IPO dominated), with a reduction in ENSO activity (La Niña/negative-phase IPO dominated) at ca. 8,200 cal yr BP. The mid-Holocene (ca. 6,000-3,000 cal yr BP) was characterised by reduced ENSO activity (La Niña/negative-phase IPO dominated), seen across a variety of records in Borneo, Peru coast, and Galápagos definitively, Easter Island and the North Pacific tentatively. The late Holocene (ca. 3,000 cal yr BP to present) had increased ENSO activity (El Niño/positive-phase IPO dominated) prevail, albeit with some centennial-scale periodicity apparent in the last ca. 2,000 cal yr

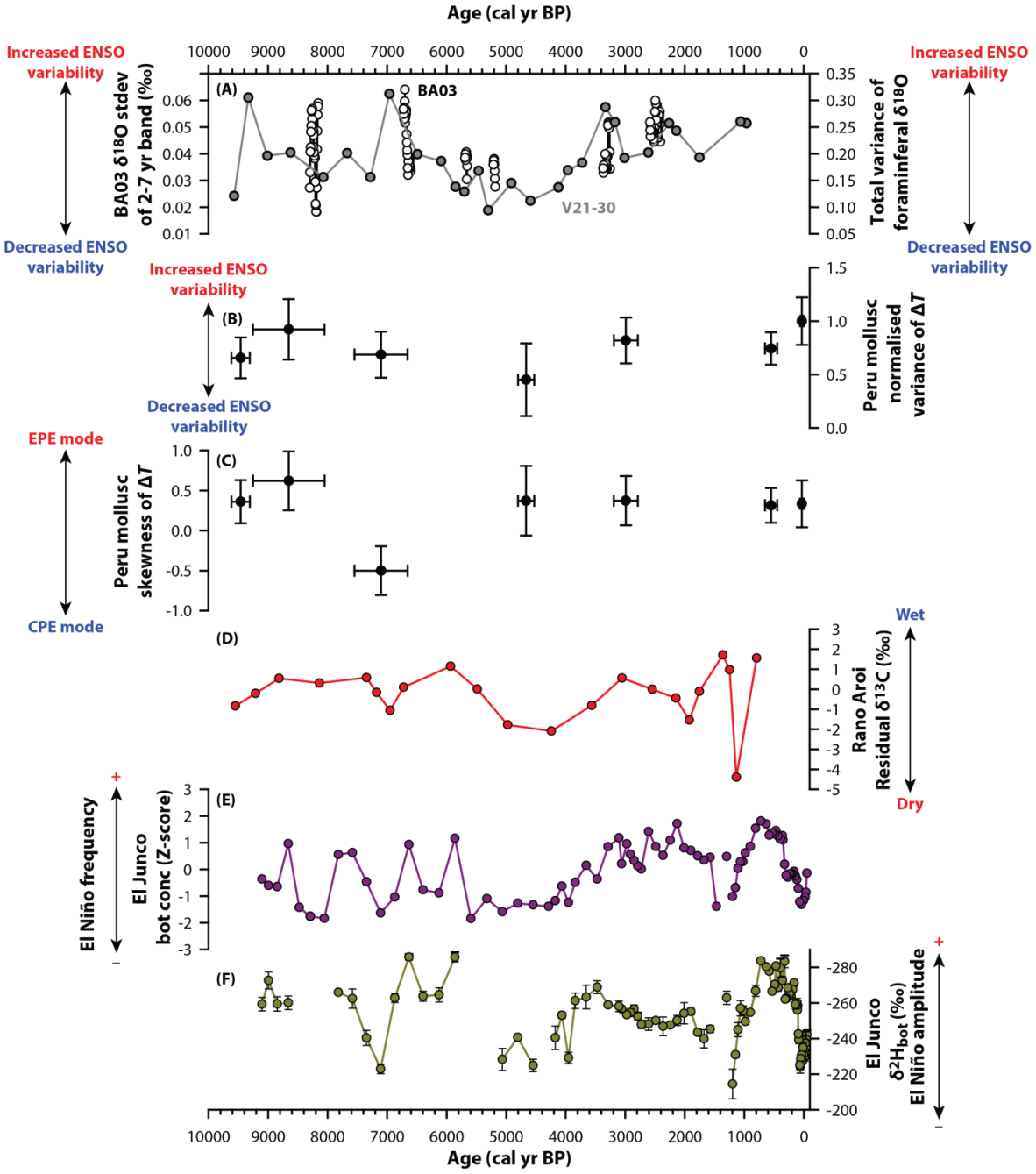

Figure 2.23: Comparison of Holocene ENSO records from the Pacific basin. (A) ENSO variability estimates from speleothem BA03, Borneo, (white circles) and foraminifera (grey circles) from V21-30, Galápagos (Koutavas and Joanides, 2012; Chen *et al.*, 2016). BA03 $\delta^{18}O$ estimates are based on the standard deviation (st dev) of the 2-7 year band in overlapping 30-year windows (5-year step) (Chen et al., 2016); foraminferal $\delta^{18}O$ variance is determined using the $\delta^{18}O$ of single tests in each 1-cm stratum (Koutavas and Joanides, 2012). The seasonal SST range variance (B) (as % difference from modern (0-60 yr BP) and skewness (C) with 1σ uncertainty on the Peruvian coast calculated from monthly molluscan shell $\delta^{18}O$ measurements (Carré et al., 2014). Variance is determined to be ENSO-driven and skewness to indicate the relative contribution of Central Pacific El Niños (CPE) and Eastern Pacific El Niños

(Carré *et al*., 2014). (D) Residual $\delta^{13}C$ values from Rano Aroi, Easter Island, which are caused by changes in humidity and determined not to relate to long-term C_4-C_3 vegetation changes (Margalef *et al*., 2013); El Junco, Galápagos, botryococcene concentration (bot conc) (E) and δ^2H (δ^2H_{bot}) (F), the former interpreted to indicate El Niño frequency and the latter to indicate the El Niño amplitude (Atwood and Sachs, 2014; Zhang *et al*., 2014). This figure is modified from Chen *et al*. (2016).

BP (Atwood and Sachs, 2014; Nelson and Sachs, 2016). The MCA and LIA are dominated by La Niña (negative-phase IPO) and El Niño (positive-phase IPO) conditions respectively. A comparison of Holocene ENSO records from the Pacific basin is presented in Figure 2.23, highlighting the broad agreement between different records spanning the Pacific basin and indicating that ENSO, and by extension the IPO, is the principal driver of variability.

2.2.2 The SPCZ region

2.2.2.1 Early Holocene

There is a paucity of records spanning the early Holocene from the SPCZ region. The discontinuous Lake Lanoto'o, Samoa, record indicates between ca. 9,000-6,000 cal yr BP stable conditions with high organic content, reduced Ti and low frequency magnetic susceptibility (Parkes, 1994). Collectively this suggests a reduced terrestrial catchment input into Lake Lanoto'o (Parkes, 1994). Lake Teroto, Atiu, Cook Islands also indicates reduced terrestrial catchment input between ca. 10,000-6,000 cal yr BP (Parkes, 1994). A reduced terrestrial catchment input suggests reduced precipitation. As both Samoa and Atiu receive their precipitation from the SPCZ (Thompson, 1986; Folland *et al*., 2002), a reduction in precipitation would indicate that the SPCZ has contracted and/or moved northwest which in turn suggests El Niño conditions at the interannual scale, and positive-phase IPO conditions at the interdecadal scale (Trenberth, 1976; Folland *et al*., 2002). Further, a pollen record from the Veitatei basin, Mangaia, Cook Islands, indicates the catchment was poorly forested between ca. 7,000-6,000 cal yr BP which Kirch *et al*. (1992) interpret to indicate drier conditions. As Mangaia also primarily receives its precipitation from the SPCZ (Thompson, 1986) this suggests the SPCZ has contracted and/or moved NW, and in turn positive-phase IPO conditions at the interdecadal scale (Folland *et al*., 2002). Coral records from Muschu Island, Papua New Guinea, indicate a reduced El Niño frequency between ca. 7,600-7,100 cal yr BP, having 12 events/century compared to 23

events/century in the AD 1950-1997 period (McGregor and Gagan, 2004). Further the El Niño amplitude at Mushu Island is reduced to 85% of the AD 1950-1997 average at ca. 7,600-7,100 cal yr BP (McGregor and Gagan, 2004). Despite this reduction in ENSO activity it is still active, suggesting that at the interdecadal scale positive-phase IPO is dominating ca. 7,000 cal yr BP. Huon Peninsula coral records dated at ca. 8,920 and 7370 cal yr BP indicate SST ca. 2-3 °C cooler than present (McCulloch *et al*., 1996); however this may be indicative of a cooler early Holocene rather than representative of ENSO conditions.

2.2.2.2 Mid-Holocene

Few continuous mid-Holocene records exist in the SPCZ region. Both the Lake Lanoto'o and Lake Teroto records show an increase in Ti and magnetic susceptibility in the mid-Holocene (ca. 6,000-3,000 cal yr BP), indicating an increase in terrestrial catchment input (Parkes, 1994). This indicates an increase in precipitation from the SPCZ, which in turn suggests La Niña-like conditions at the interannual scale and negative-phase IPO at the interdecadal scale (Trenberth, 1976; Folland *et al*., 2002). The Lake Tiriara record and various swamp records from Mangaia, Cook Islands, suggest an increase in wetland species at ca. 4,500 cal yr BP which tentatively suggest wetter conditions associated with SPCZ being positioned further southeast and/or expanded, and by extension a negative-phase IPO dominated Pacific (Ellison, 1994). Additional support for negative-phase IPO conditions in the mid-Holocene is provided by pollen records in the Tari Basin, Papua New Guinea, which reveal that a montane forest was supported throughout this time (Haberle, 1998). Montane forests require stable climatic conditions, thus suggesting that ENSO was dampened throughout the mid-Holocene. The wetter conditions during this time would be expected as negative-phase IPO would shift the SPCZ to a more southwest position and/or be expanded (see Figure 2.17). McGregor and Gagan (2004) determine that corals between ca. 6,000-5,400 cal yr BP from Papua New Guinea record eight El Niño events/century, compared to the 19 events/century between AD 1950-1997, that are 80% of the modern amplitude. A reduction in El Niño frequency and strength corresponds to negative-phase IPO (Kao and Yu, 2009).

2.2.2.3 Late Holocene

Coral records from Papua New Guinea indicate stronger and more frequent El Niños from ca. 3,000-1,700 cal yr BP (Tudhope *et al*., 2001; McGregor and Gagan, 2004), which is

consistent with positive-phase IPO conditions (Kao and Yu, 2009). In the Guadalcanal pollen record, Solomon Islands, a parsimonious explanation of human activity causing forest composition to constantly change ca. 3000 cal yr BP was applied to the observed changes in pollen record (Haberle, 1996). The Lake Tiriara, Mangaia, Cook Islands, record is argued to indicate drier conditions between ca. 2,900-2,000 cal yr BP (Chagué-Goff *et al*., 2016), likely indicating the SPCZ being in a more northwest position and/or contracted as a corollary of positive-phase IPO conditions in the Pacific (Folland *et al*., 2002). This is supported by higher organic content is determined from Lake Lanoto'o, Samoa, for the late Holocene which is consistent with drier conditions associated with positive-phase IPO causing zSPCZ and a reduction in terrestrial inwash (Folland *et al*., 2002). However, determining climatic conditions for the last ca. 1,000 cal yr BP in Atiu and Mangaia is difficult due to human activity having a notable impact on their respective lake catchments (Ellison, 1994; Parkes 1994; Chagué-Goff *et al*., 2016) – a problem also apparent with pollen records from Papua New Guinea and the Solomon Islands (Haberle 1996, 1998). A runoff record from Apu bay, French Polynesia, indicates reduced runoff, as a result of SPCZ being in a northwest position and/or contracted, between ca. 3,000-1,000 cal yr BP, and enhanced runoff from ca. 1,000-400 cal yr BP as a result of SPCZ being further southeast and/or expanded (Toomey *et al*., 2016). A northwest SPCZ from ca. 3,000-1,000 cal yr BP and a southeast SPCZ from ca. 1,000-400 cal yr BP (coincident with the MCA) is consistent with positive-phase IPO and negative-phase IPO conditions respectively determined from other records such as El Junco, Galápagos (Zhang *et al*., 2014).

Stalagmite records from Guadalcanal, Solomon Islands, exhibit interdecadal variability from ca. 500 cal yr BP (AD 1450) to present respectively (Maupin *et al*., 2014). These high temporal resolution records display oscillations that appear to be strongly correlated to Biondi *et al*.'s (2001) IPO index, with negative IPO phases correlating to increased precipitation in the stalagmite records associated with southeast movement of the SPCZ. Various coral records from the SPCZ region exhibit interannual variability that matches ENSO and interdecadal variability that appears to correlate to a degree with the IPO. Coral records from Rabaul and Madang, Papua New Guinea, display clear oscillations that are near-coeval with oscillations in the IPO index (Quinn *et al*., 2006; Tudhope *et al*., 1995), thus reflecting changes in the position of the SPCZ. Changes in the SPCZ position,

as a result of changes in IPO state, is also seen in Rarotonga, Cook Islands, and Fiji coral records that collectively span ca. 333 cal yr BP (AD 1617) to present (Le Bec *et al*., 2000; Ren *et al*., 2002; Bagnato *et al*., 2005; Linsley *et al*., 2000, 2004, 2006; Juillet-Leclerc *et al*., 2006; Dassié *et al*., 2014) and the Moorea coral record, French Polynesia (Boiseau *et al*., 1998) that spans the last 137 years (AD 1853-1989).

2.2.2.4 Overview of the SPCZ region

Early Holocene records from the SPCZ region tentatively indicate positive-phase IPO conditions in the Pacific, with conditions switching to negative-phase IPO dominated conditions at some interval in the mid-Holocene between ca. 6,000-3,000 cal yr BP. The late Holocene (ca. 3,000 cal yr BP to present) is suggested to be predominantly positive-phase IPO, with a negative-phase IPO period between ca. 1,000-400 cal yr BP indicated in French Polynesia (Toomey *et al*., 2016).

2.2.3 North of the SPCZ region

2.2.3.1 Early Holocene

Reconstructions of precipitation in lakes from Palau using δ^2H of dinosterol (δ^2H_{dino}), a dinoflagellate biomarker, suggests that from ca. 8000-7000 cal yr BP ENSO operated and that El Niño conditions (positive-phase IPO at the interdecadal timescale) dominated. (Smittenberg *et al*., 2011). However, Smittenberg *et al*. (2011) highlight that the Palau δ^2H_{dino} in the early Holocene is likely a reflection of millennial scale hydrological and water mass changes on a global scale. Coral records from Kiribati indicate that ENSO was operating between ca. 7,000-6,000 cal yr BP but was weaker than at present (Cobb *et al*., 2013); Emile-Geay *et al*. (2016) went further and showed that both ENSO variance and the annual cycle were reduced relative to modern day corals between ca. 7,000-6,000 cal yr BP.

2.2.3.2 Mid-Holocene

Coral records from Kiribati indicate that ENSO had reduced variance in the mid-Holocene. Whilst Cobb *et al*. (2013) posited that there was no change in ENSO variance at this time, Emile-Geay *et al*. (2016) analysed a coral dated to ca. 4,000 cal yr BP (a time slice missing from the Cobb *et al*. (2013) study) and found that there is unequivocal evidence of

reduced ENSO variance and annual cycle amplitude. This is in agreement with McGregor *et al*. (2013) who determined using a coral record from Christmas Island, Northern Line Islands, that ENSO variance was reduced over a 180-year period ca. 4300 cal yr BP. Emile-Geay *et al*. (2016) concluded that the reduction in ENSO variability spanned ca. 5,000-3,000 cal yr BP.

2.2.3.3 Late Holocene

ENSO variability in Kiribati coral records increases from ca. 3,000 cal yr BP (Cobb *et al*., 2013; Emile-Geay *et al*., 2016). Whilst overall the late Holocene appears to be dominated by positive-phase IPO, at ca. 1000 cal yr BP (approximate to the MCA) cool and/or dry conditions are interpreted in the Palmyra coral record typical of a negative IPO-like state (Power *et al*., 1999; Cobb *et al*., 2003). Wetter conditions are inferred for the LIA (400 cal yr BP) from the Palmyra coral record (Cobb *et al*., 2003) and pollen records from the Marquesas Islands (Allen *et al*., 2011). Wetter conditions in this region are determined to be a result of increased ENSO activity, suggested here to be a consequence of positive-phase IPO at the interdecadal scale (Di Lorenzo *et al*., 2015). Increased ENSO activity causes drying in Palau, thus it would be expected that during the Little Ace Age decreased precipitation amount would occur. The Palau lake records suggest this (Sachs *et al*. 2009; Richey and Sachs, 2016), indicating that the Little Ice Age is dominated by increased ENSO activity most likely a consequence of prolonged positive-phase IPO conditions (Newman *et al*., 2016)

Coral records from Double Reef, Guam (Asami *et al*., 2005), Maiana Atoll, Kiribati (Urban *et al*., 2000), Palau (Osborne *et al*., 2014), and Tarawa Atoll, Kiribati (Cole and Faribanks, 1990) all show strong correlation with ENSO. Moreover, the Guam record reveals interdecadal oscillation from AD 1787-2000 with the timing of this oscillation preceding known changes in the IPO by 3-5 years (Asami *et al*., 2005; Minobe, 2000). Whilst the IPO is not as conspicuous in the Maiana or Tarawa records, clear shifts in coral $\delta^{18}O$ can be observed at the time of known regime shifts in the IPO during the 20th Century (Urban *et al*., 2000; Cole and Fairbanks, 1990). An overall trend in IPO state in this period is difficult to determine, but records from Palau do indicate a long-term warming trend (Osborne *et al*., 2014).

2.2.3.4 Overview of north of the SPCZ region

Positive-phase IPO is suggested for the early Holocene from the few records in this region. The mid-Holocene shows conclusive evidence for reduced ENSO variance in a suite of coral records analysed by Emile-Geay *et al*. (2016) interpreted here to reflect negative-phase IPO conditions dominating during the mid-Holocene. Records covering the late Holocene suggest a prevalence of positive-phase IPO conditions, as indicated by an increase in ENSO variability (Cobb *et al*., 2013; Emile-Geay *et al*., 2016). There is evidence that the MCA and LIA is characterised by negative-phase IPO and positive-phase IPO conditions respectively (Cobb *et al*., 2003; Allen *et al*., 2011; Richey and Sachs, 2016).

2.2.4 South of the SPCZ region

2.2.4.1 Early Holocene

During the Younger Dryas and the early Holocene, coral records from Espiritu Santo, Vanuatu, indicate colder temperatures – similar to what was found in Papua New Guinea (Beck *et al*., 1992, 1997; Corrège *et al*., 2004). Corrège *et al*. (2004) noted that at Vanuatu at present both $\delta^{18}O_{sea\ water}$ and SSS decrease as SST rises during the austral summer intensification of the SPCZ which delivers ^{18}O-depeleted precipitation, whereas during the Younger Dryas SST and $\delta^{18}O_{sea\ water}$ were positively correlated. Consequently Corrège *et al*. (2004) concluded that during the Younger Dryas the SPCZ did not exist, or that it had merged with the ITCZ as has been observed during some El Niño events (i.e. zSPCZ). However, this conclusion should be treated with caution as Corrège *et al*. (2004) do not have SSS data to support the $\delta^{18}O_{sea\ water}$ and SST reconstructions. A more stable environment is suggested in Plum Swamp, New Caledonia, at ca. 9,000 cal yr BP; however Stevenson *et al*. (2001) highlight that assigning ages to this period is difficult thus any conclusions should be treated cautiously. Coral records from Vanuatu indicate that the SPCZ has likely shifted north from ca. 6,700-6,500 cal yr BP (Deng and Wei, 2015), interpreted here to be the result of positive-phase IPO conditions (Folland *et al*., 2002).

2.2.4.2 Mid-Holocene

Palaeo records from New Caledonia have proven particularly difficult to interpret due to sediment mixing and lack of suitable material to obtain ages from (Méon and Pannetier,

1994; Hope and Pask, 1998; Stevenson, 2004; Stevenson and Hope, 2005; Wirrman *et al*., 2006; Stevenson *et al*., 2010). One record that does cover the mid-Holocene – that from Plum Swamp, New Caledonia – suggests that from around ca. 6,000-4,000 cal yr BP climate was wetter (Stevenson *et al*., 2001). Further, peat accumulation occurs from ca. 6,200-3,700 cal yr BP in Lac Saint Louis, New Caledonia, suggesting that wetter conditions prevailed in New Caledonia (Stevenson, 2004). Wetter conditions are also suggested from Emaotfer Swamp, Vanuatu, ca. 6,000-3,000 cal yr BP based on the dominant pollen types being mangrove and rainforest (Wirrmann *et al*., 2011a). A coral record from New Caledonia dated to ca. 5,500 cal yr BP indicates conditions akin to that seen during La Niñas, but this record only spans 20 years thus inferring long-term trends is problematic (Lazareth *et al*., 2013). Overall these records suggest negative-phase IPO conditions in the mid-Holocene, as indicated in other parts of the Pacific basin.

Following this wetter period, the Plum Swamp record contains a 25 cm band of sandy clay dated to ca. 4,000 cal yr BP attributed to an extreme event, such as a cyclone (Stevenson *et al*., 2001). An extreme cold event – the cause of which is unknown – is also recorded in corals from Espiritu Santo, Vanuatu, 4,166 ± 15 cal yr BP (Beck *et al*., 1997). Average SSTs reconstructed from the Espiritu Santo record are slightly cooler than present ca. 4,100 cal yr BP and could suggest positive IPO or an El Niño-like state in the Pacific basin (Beck *et al*., 1997). Increased storminess ca. 4000 yr is also deduced from sediment records in eastern North Island, New Zealand, and attributed to the establishment of the contemporary ENSO-dominated climatic regime (Gomez *et al*., 2004, 2013). However, the reliability of records of runoff in relation to ENSO activity has been called into question by Emile-Geay and Tingley (2016), suggesting that the Gomez *et al*. (2004, 2013) record should be treated cautiously.

2.2.4.3 Late Holocene

Some of the records available for this time are difficult to interpret due to human alteration of the landscape (Stevenson, 2004). Drier conditions in Gouaro-Déva, New Caledonia, are interpreted from ca. 2,640 cal yr BP with these likely associated with positive-phase IPO conditions (Wirrmann *et al*., 2011b). A peak in microcharcoal at ca. 1,500 cal yr BP has been attributed to prolonged El Niño events, suggested here to be a dominance of positive-phase IPO (Folland *et al*., 2002), in Emaotfer Swamp, Vanuatu

(Combettes *et al*., 2015). There is a sharp increase in very coarse deposits ca. 1070-960 cal yr BP in Grand Lac, New Caledonia, possibly caused by a severe La Niña event (Wirrmann *et al*., 2006). This is unlikely to be the result of human activity due to the volume of sediment mobilised across the basin.

An Australian speleothem record indicates a dominance of La Niña conditions (negative-phase IPO) from the 9th-15th century (950-350 cal yr BP) and El Niño conditions (positive-phase IPO) from the 16th-19th century (250-50 cal yr BP): these timings are broadly synchronous with the MCA and the LIA respectively (Denniston *et al*., 2015). Drier conditions, associated with northward shift of the SPCZ and/or contractions likely associated with positive-phase IPO (Folland *et al*., 2002), are also observed in a Vanuatu speleothem record for the LIA (Partin *et al*., 2013). A number of records from Australia (Druffel and Griffin, 1993; Hendy *et al*., 2002; Rodriquez-Ramirez *et al*., 2014), Vanuatu (Quinn *et al*., 1993; 1996; Kilbourne *et al*., 2004; Gorman *et al*., 2012; Partin *et al*., 2013), and New Caledonia (Delong *et al*., 2007; 2012), that span 400 cal yr BP to present indicate interannual and interdecadal oscillations. Whilst most of these records conclude that ENSO causes interannual variability and the IPO causes the interdecadal variability; DeLong *et al*. (2012) suggest that it is the South Pacific Decadal Oscillation that cause the interdecadal variability in a coral from New Caledonia. Comparison of the IPO with DeLong *et al*.'s (2012) Sr/Ca coral record reveal that the trends match relatively well. Furthermore, The SHPDO is the southern hemisphere's manifestation of the IPO and thus has broadly the same oscillations as the IPO (Shakun and Shaman, 2009; Chen and Wallace, 2015).

2.2.4.4 Overview of south of the SPCZ region

The early Holocene is tentatively associated with prolonged El Niño conditions (positive-phase IPO), however there is limited evidence for this. The mid-Holocene in this region is suggested to be dominated by La Niña conditions (negative-phase IPO), and the late Holocene is suggested to be dominated by El Niño conditions (positive-phase IPO). There is some evidence that the Medieval Warm Period and Little Ice Age are characterized by La Niña (negative-phase IPO) and El Niño (positive-phase IPO) conditions respectively.

2.3 Summary

Climate across the Pacific is strongly influenced by ENSO on interannual timescales. Recent work has demonstrated that ENSO exists across a spectrum with El Niño having two principal types, or flavours, that operate: EPE and CPE (Ashok *et al*., 2007; Kao and Yu, 2009; Kug *et al*., 2009; Capotondi *et al*., 2015). At the interdecadal scale the IPO, this being the reddened ENSO component (Di Lorenzo *et al*., 2015), influences Pacific climate with the IPO phase (positive/negative) essentially being the interdecadal representation of its corresponding ENSO state (El Niño/La Niña). The position of the SPCZ is affected by these phenomena, with El Niño (positive-phase IPO) causing the SPCZ to migrate NW and/or contract and La Niña (negative-phase IPO) causing it to shift SE and/or expand (Trenberth, 1976; Folland *et al*., 2002). With this relationship in mind the position of the SPCZ can be used to make qualitative interpretations of the dominant state in the Pacific. Whilst some studies have shown SPCZ movement over centennial timescales, for example Linsley *et al*. (2006), Partin *et al*. (2013) and Maupin *et al*. (2014), and potentially over millennial timescales (Toomey *et al*., 2016) to date (AD 2017) this has not been undertaken for the Holocene as a whole.

The synthesis of records undertaken here have shown that whilst many continuous Holocene-length records exist in the Pacific basin, there is a paucity of continuous Holocene-length records from the SPCZ region, North of the SPCZ region and South of the SPCZ region. This has likely led to an incomplete understanding of Pacific climate throughout the Holocene. In the literature much work has focussed on changes in ENSO highlighting a reduction in ENSO variability/activity in the mid-Holocene between ca. 5,000-3,000 cal yr BP (Conroy *et al*., 2008; Koutavas and Joanides, 2012; McGregor *et al*., 2013; Carré *et al*., 2014; Zhang *et al*., 2014; Emile-Geay *et al*., 2016; Chen *et al*., 2016). Whilst there has been some suggestion of which El Niño type may have been operated at different times over the Holocene by Carré *et al*. (2014), no continuous Holocene records currently exist (AD 2017) that could disentangle the timings of when each type of El Niño principally operated, if a type did at all. Further the timings of the reduction in Holocene ENSO variability proposed by Emile-Geay *et al*. (2016) are based on discontinuous coral records and are thus may not an accurate representation of when this reduction occurred.

Even though it is apparent there is a paucity of palaeo-data from the southwest Pacific, for the subdivisions of the Holocene used in this review inferences have been made on the IPO phase that is dominating based on the evidence available. At multi-millennial timescales the early Holocene (ca. 11,600-6,000 cal yr BP) is suggested to be dominated by positive-phase IPO, the mid-Holocene (ca. 6,000-3000 cal yr BP) by negative-phase IPO, and the late Holocene (ca. 3,000 cal yr BP to present) by positive-phase IPO (Figure 2.24, Figure 2.25 and Figure 2.26 respectively). Using the relationship between the IPO and the SPCZ (Folland *et al*., 2002), hypotheses can be put forward to the likely changes in the SPCZ position over the Holocene. These are presented in Table 2.3 for the Holocene at the millennial scale and for climate events – specifically the 8.2 ka event, the MCA and the LIA.

Time (cal yr BP)	Phase of IPO (Positive/ Negative)	Position of SPCZ (Northwest of average/Southeast of average)	Samoa more precipitation/less precipitation?	Atiu, Cook Islands more precipitation/less precipitation?
11,600	Positive	Northwest of average	Less precipitation	Less precipitation
10,000	Positive	Northwest of average	Less precipitation	Less precipitation
9,000	Positive	Northwest of average	Less precipitation	Less precipitation
?8.2 ka event?	Negative	Southeast of average	More precipitation	More precipitation
8,000	Positive	Northwest of average	Less precipitation	Less precipitation
7,000	Positive	Northwest of average	Less precipitation	Less precipitation
6,000	Negative	Southeast of average	More precipitation	More precipitation
5,000	Negative	Southeast of average	More precipitation	More precipitation
4,000	Negative	Southeast of average	More precipitation	More precipitation
3,000	Positive	Northwest of average	Less precipitation	Less precipitation
2,000	Positive	Northwest of average	Less precipitation	Less precipitation
1,150-650 (MCA)	Negative	Southeast of average	More precipitation	More precipitation
450-150 (LIA)	Positive	Northwest of average	Less precipitation	Less precipitation

Table 2.3: Inferred phase of the IPO, position of the SPCZ and hydroclimatic conditions in Samoa and Atiu, Cook Islands, over the Holocene.

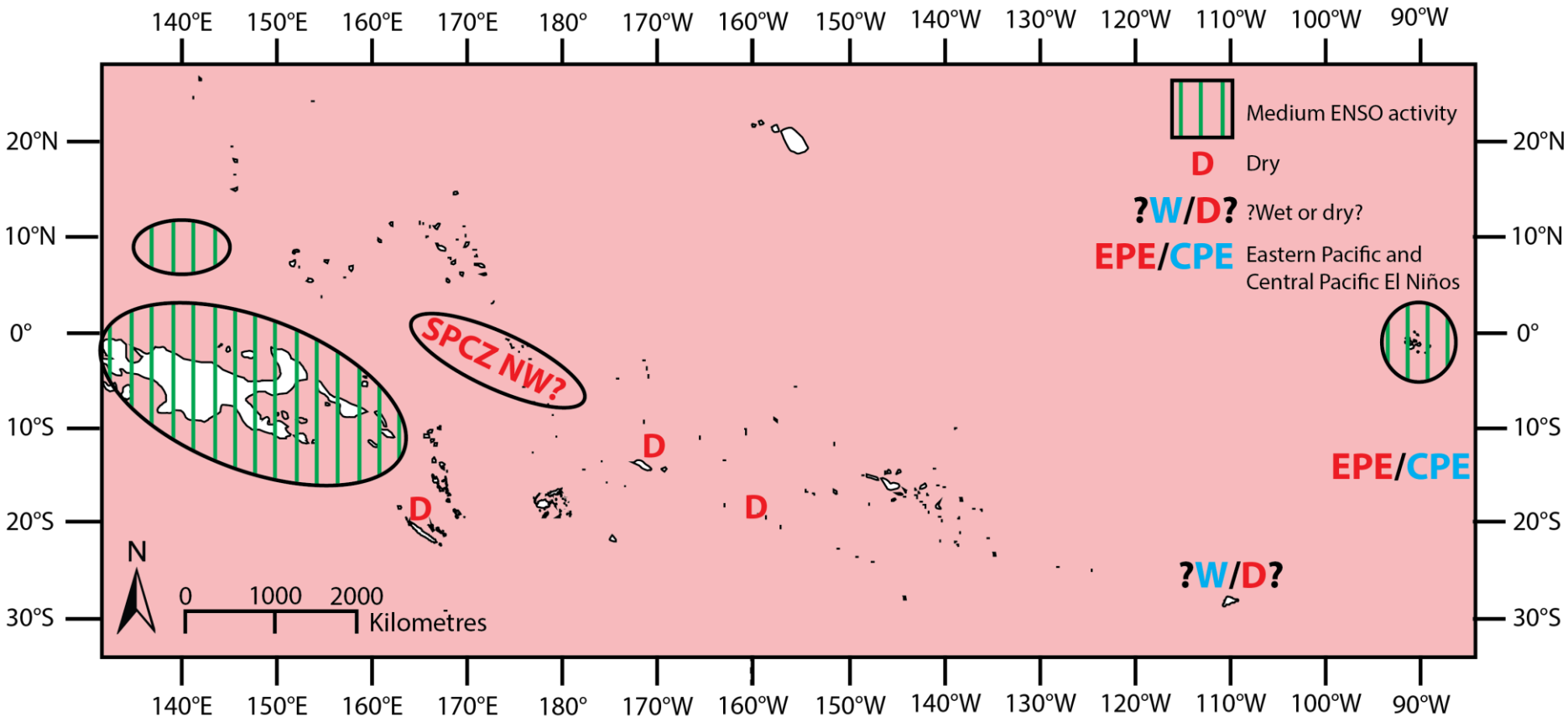

Figure 2.24: Summary of climate conditions for the early Holocene (ca. 11,600-6,000 cal yr BP) in the Pacific from published sources, with specific focus on the southwest Pacific. The pink background indicates positive-phase IPO conditions dominating at the multi-millennial scale. ENSO activity is defined as the frequency and/or intensity of El Niño events at the greater than decadal temporal scale (Atwood and Sachs, 2014).

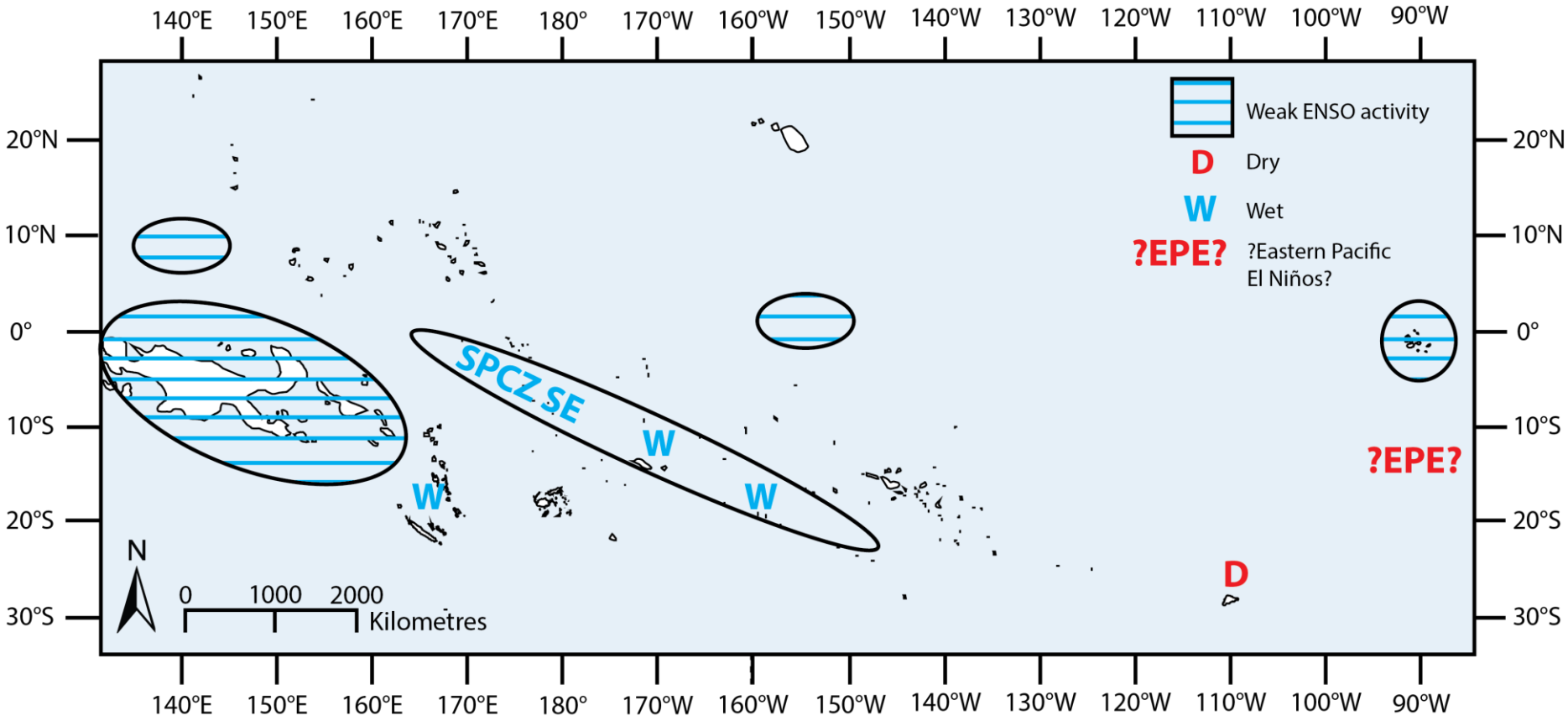

Figure 2.25: Summary of climate conditions for the mid-Holocene (ca. 6,000-3,000 cal yr BP) in the Pacific from published sources, with specific focus on the southwest Pacific. The blue background indicates negative-phase IPO conditions dominating at the multi-millennial scale. ENSO activity is defined as the frequency and/or intensity of El Niño events at the greater than decadal temporal scale (Atwood and Sachs, 2014). The '?EPE?' (Eastern Pacific El Niños) indicates the uncertainty on this as only one sample exists in the Carré *et al*. (2014) study for the mid-Holocene period.

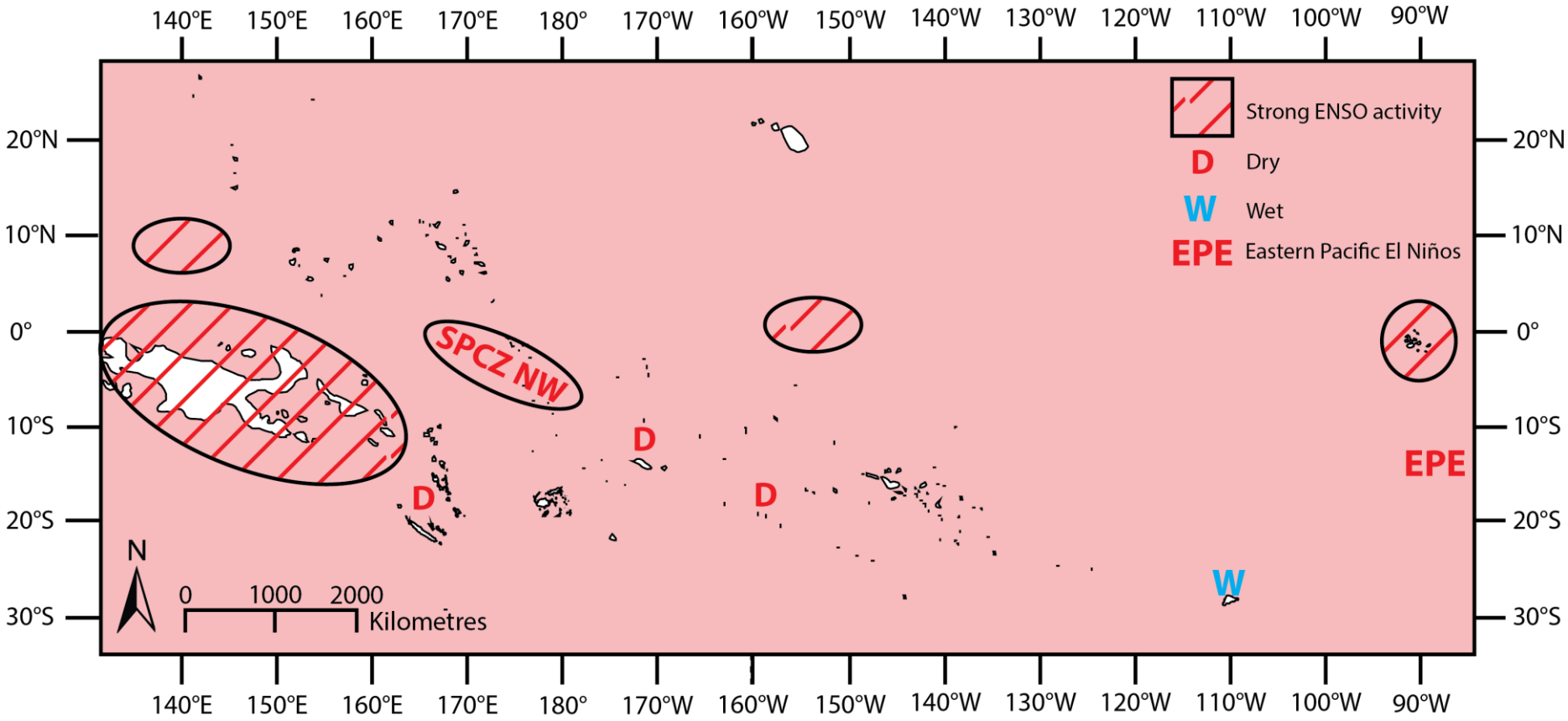

Figure 2.26: Summary of climate conditions for the mid-Holocene (ca. 3,000 cal yr BP to present) in the Pacific from published sources, with specific focus on the southwest Pacific. The pink background indicates positive-phase IPO conditions dominating at the multi-millennial scale. ENSO activity is defined as the frequency and/or intensity of El Niño events at the greater than decadal temporal scale (Atwood and Sachs, 2014).

Chapter 3: Site Descriptions

3.1 Introduction

This chapter describes the sites studied providing an overview of their respective countries' geography, climate, geology and soils, vegetation, and colonisation history. Whilst a full treatise on the colonisation of Polynesia is not relevant for this study, the timings of colonisation to Samoa and the Southern Cook Islands are relevant to provide an approximation of when human activity may have impacted on the Lake Lanoto'o and Lake Teroto records. Finally, each lake and its respective catchment are described in detail.

3.2 Lake Teroto

3.2.1 Geography of Atiu, Cook Islands

Atiu is one of fifteen islands that comprise the Cook Islands (Figure 3.1), being classed as part of the Southern Cook Islands. Overall the Cook Islands cover a spatial area of ocean equalling 2,200,000 km^2 and have a population of 14,974 in the 2011 census; Atiu specifically has an area of 26.9 km^2 and a population of 480 (Ministry of Finance and Economic Management, 2012). The island is located at 19° 59'S , 158° 07'W, has a maximum elevation of 76 m.a.s.l., and can be viewed as having three geographical regions: the volcanic interior; the raised coral rim – known locally as makatea; and the swampy lowlands (Figure 3.2 and Figure 3.3). Deep weathering of the interior has led to the formation of a red clay with limonitic nodules and black manganiferous veins (Wood and Hay, 1970); erosion has also led to a number of terraces on the volcanic slopes in the interior. Whilst these are thought to represent changes in sea level, it is not known what they actually represent (Stoddart *et al*., 1990). The makatea surrounds the volcanics and are thought to be Cenozoic in age – substantiated by the presence of fresh basalt fragments in the limestone suggesting that reef growth happened during volcanism (Campbell *et al*., 1979). The makatea is highest in the northwest and east, reaching a maximum height of 23 m. Between the makatea and the volcanic interior is swamp, one

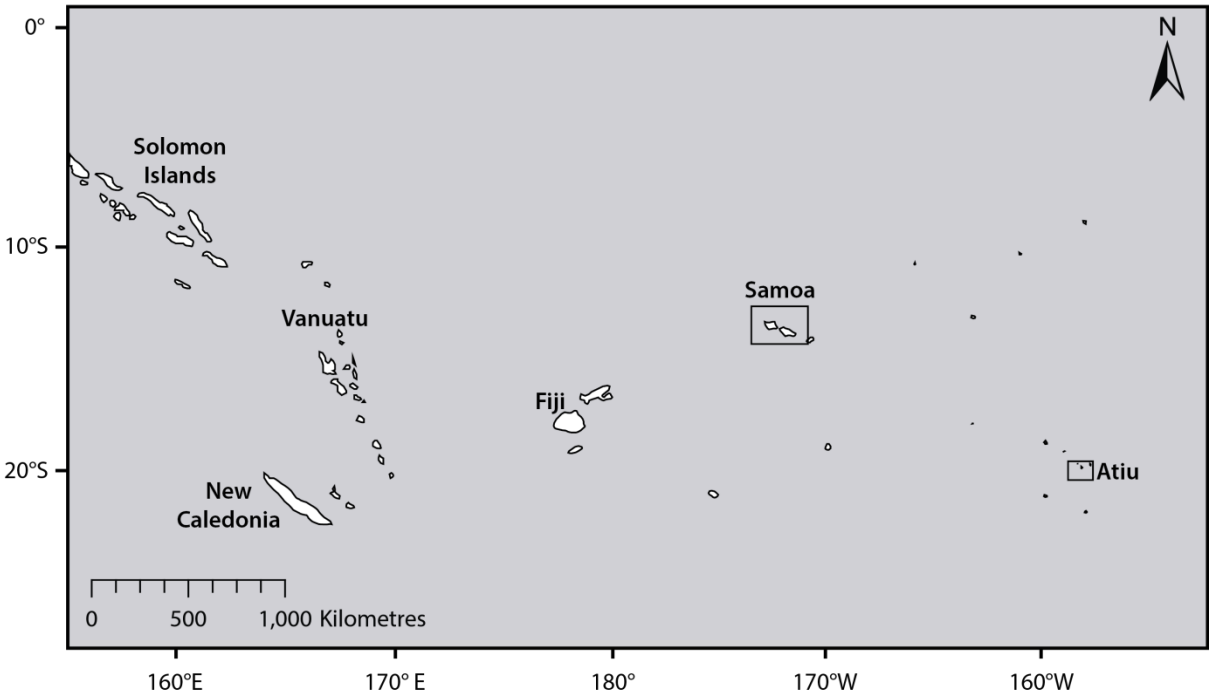

Figure 3.1: Map of southwest Pacific with Samoa and Atiu highlighted.

marsh of which has an extent of 3.5 km in the northeast (Stoddart *et al*., 1990). Some areas of swamp have been converted to taro cultivation.

3.2.2 Climate of Atiu

The climate of Atiu is controlled by the location of the SPCZ, with the principal impact SPCZ location has being on precipitation amount on Atiu (Thompson, 1986). Precipitation data from Atiu are available from AD 1983-2015 (R. Malcom, personal communication, September 2016), and when compared to Rarotonga (222 km southwest of Atiu) precipitation is very similar ($r = 0.68$, $p<0.0001$ and $r^2 = 0.46$, $p<0.0001$) (Figure 3.4). Thus it is considered the use of Rarotonga precipitation data (covering AD 1899-2012, Figure 3.5) to draw conclusions from is valid. Thompson (1986) presented precipitation data for Atiu covering AD 1958-1982. During the November to April wet season precipitation averages at 1336 mm (68% of the total annual precipitation) whereas during the May to October dry season precipitation averages at 634 mm (32% of the total annual precipitation) (Thompson, 1986). The high precipitation during the wet season is a consequence of the SPCZ expanding southeast, whereas the low precipitation in the dry season is due to the SPCZ shrinking northwest and the dry southeast trades over Atiu.

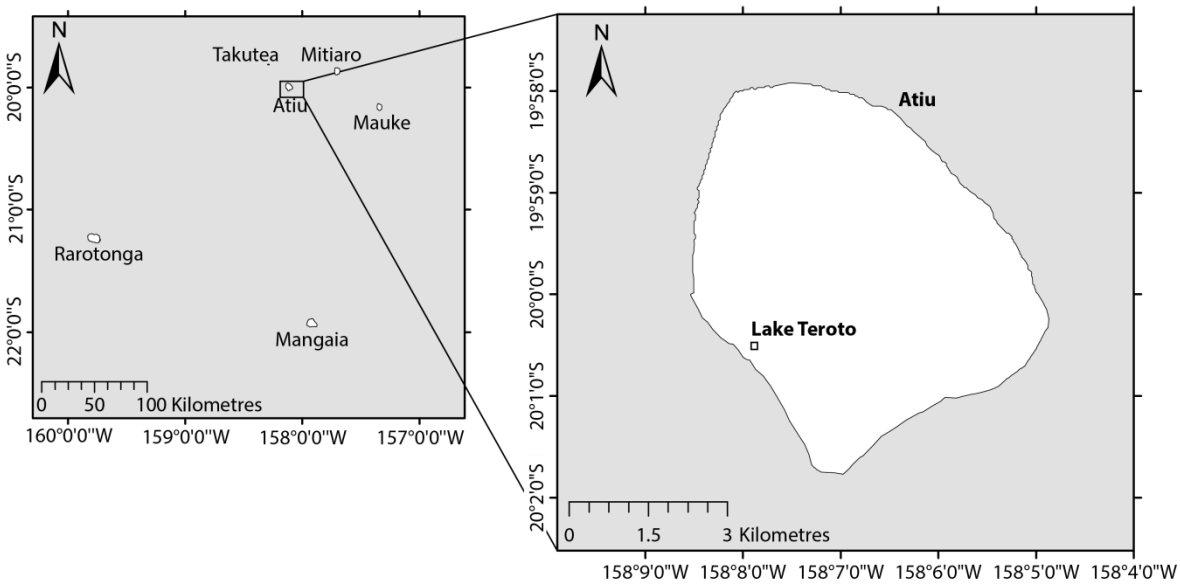

Figure 3.2: Atiu, Cook Islands. The location of Lake Teroto is highlighted with the square box.

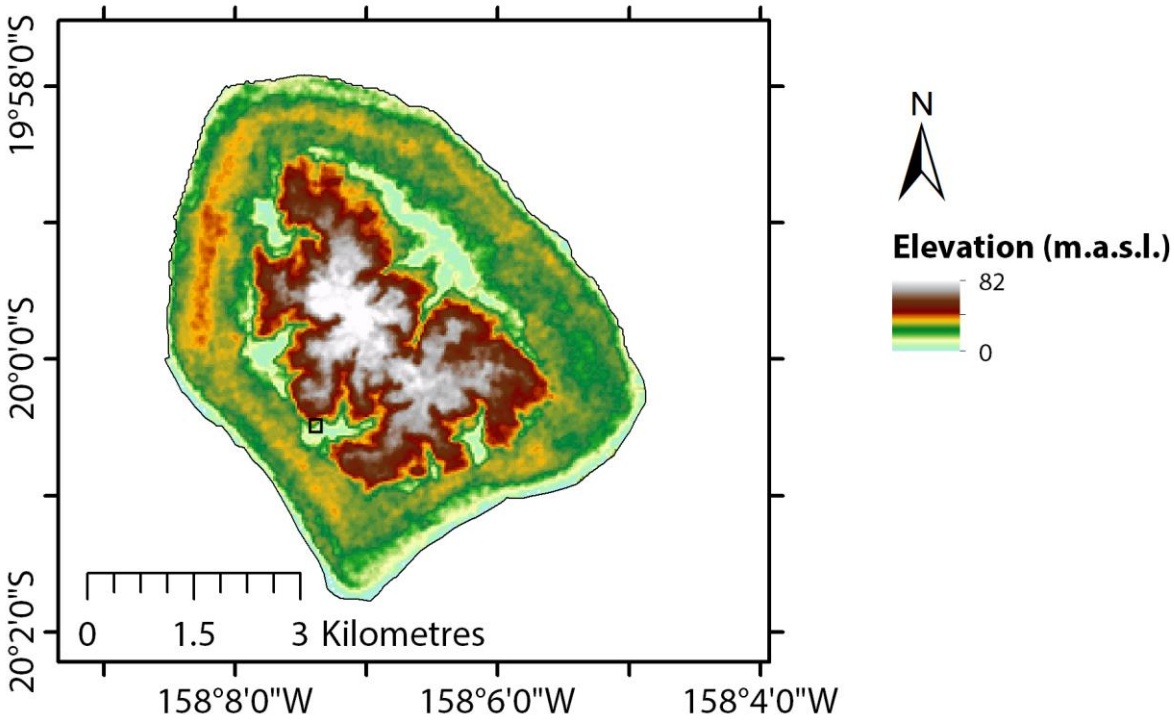

Figure 3.3: Elevation map of Atiu, Cook Islands – note the difference in elevation compared to Upolu, Samoa. The black box indicates the location of Lake Teroto (USGS, 2012).

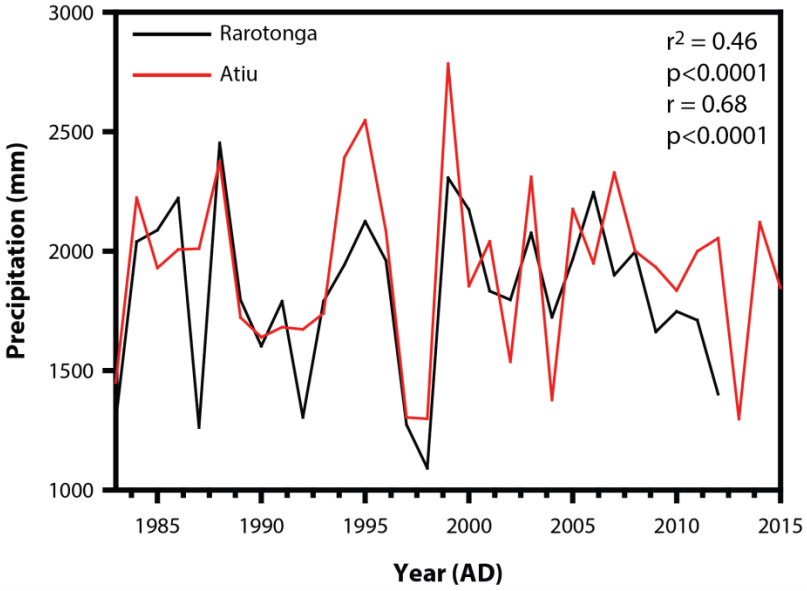

Figure 3.4: Rarotonga precipitation (black line) and Atiu precipitation (red line) covering AD 1983-2015 (R. Malcom, personal communication, September 2016).

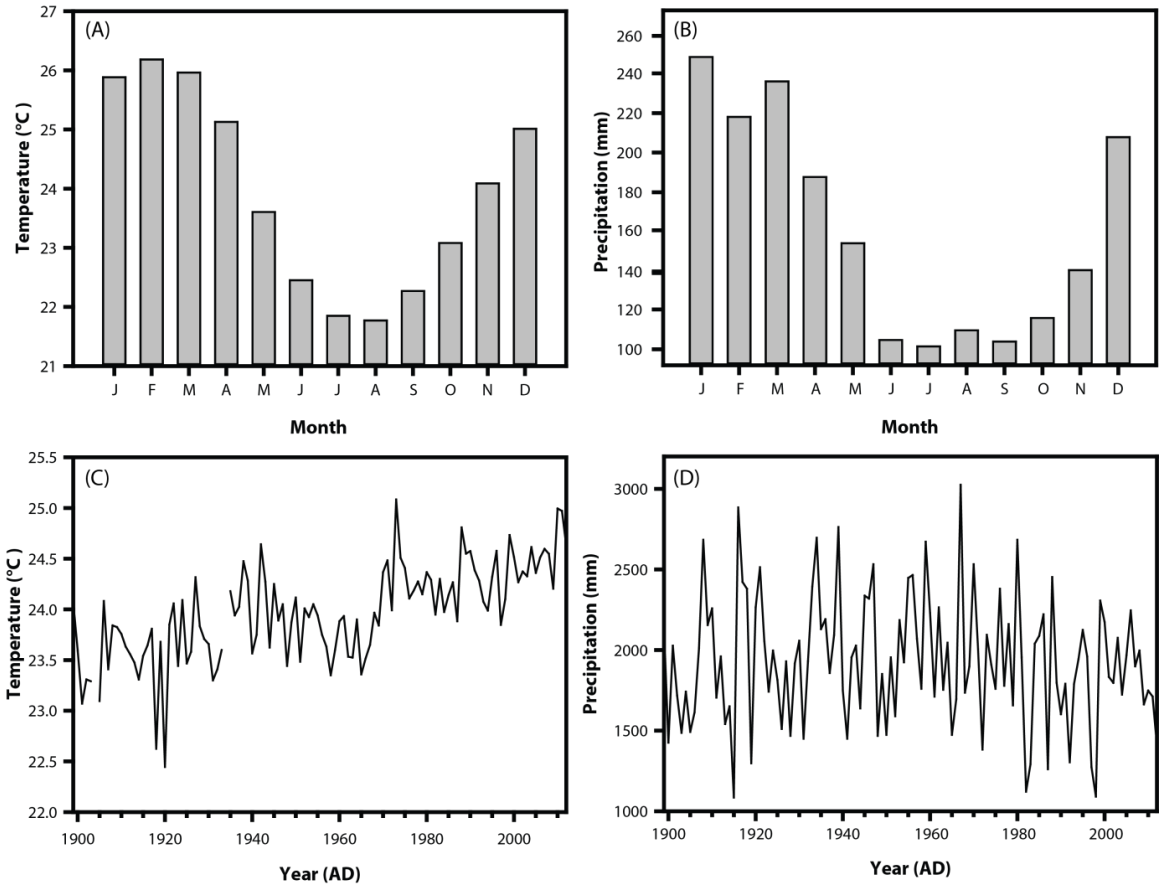

Figure 3.5: The average monthly temperature (A) and precipitation (B), and the average annual temperature (C) and precipitation (D) for the period AD 1899-2012 for Rarotonga, Cook Islands (Klatt, 2013; Berkeley Earth, 2016). Gaps in (C) indicate a lack of data.

Annual temperatures in the region are between 24-26 °C. Thompson (1986) details that Mauke (83 km southeast of Atiu) has a recorded temperature maximum of 34.8 °C and minimum of 13.1 °C, suggesting that similar temperature maxima and minima occur on Atiu. On average the Southern Cook Islands experience one tropical cyclone per year which originates from the SPCZ – the location of tropical cyclone genesis (Thompson, 1986; Stoddart *et al*., 1990).

3.2.3 Geology and soils of Atiu

Located on the southwest part of the Pacific Plate, the island is on the summit of a subconical, asymmetric volcano (Stoddart *et al*., 1990). Nakamura and Tatsumoto (1988) argue that isotopic evidence shows that the volcanic cone formed from heterogeneous mantle plumes, with K-Ar dating indicating that it formed in two periods of volcanism at 9-10 Ma and 8-8.4 Ma (Turner and Jarrard, 1982).

The geology of Atiu is relatively simple having two principal groups: these being the inner volcanic cone and the surrounding makatea (Figure 3.6). The volcanic rock is primarily basaltic breccia, olivine basalt and tuff (Wood, 1967). Wood (1978) further classed the volcanic rocks as moderately undersaturated, sodic basalt-basanite, spanning from alkali picrite to olivine-poor, aphyric basalt. Where the volcanic rock is weathered red clay has been identified that contains limonitic nodules and black manganiferous veins (Wood, 1967). In regards to the makatea, Marshall (1930) details that its seaward edge is composed of aragonite, also noting that some cavities in the makatea are infilled with secondary aragonite. Moreover, it was determined that calcite appears to replace primary aragonite over time and that dolomitisation has occurred in places on Atiu (Marshall, 1930). There are five soil-forming deposits that have been identified on Atiu: the volcanic rocks; the raised coral limestone; swamp deposits; storm beach deposits; and alluvial deposits (Campbell *et al*., 1982). The soils on Atiu are described in Table 3.1.

3.2.4 Vegetation of Atiu

The native vegetation of Atiu is typically situated in the makatea areas of the island where the rugged topography has made cultivation unpractical (Sykes, 1976). It transitions from littoral strand to coastal scrub communities, going on to the taller forest of the upland makatea (Parkes, 1994). Franklin and Merlin (1992) identified a littoral forest dominated

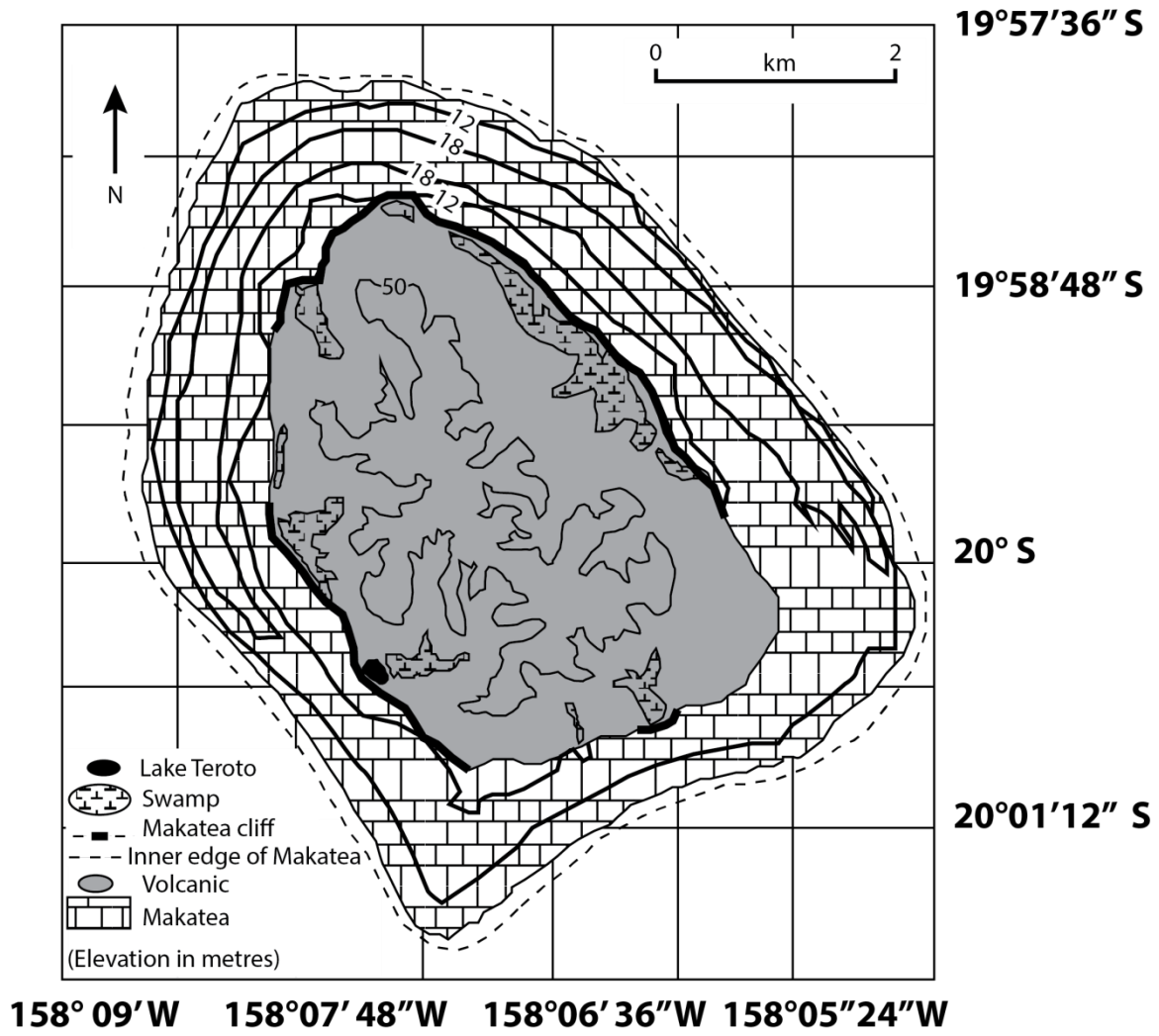

Figure 3.6: Geological map of Atiu, redrawn from Stoddart et al. (1990).

by *Hernandia nymphaeifolia*, and a makatea forest dominated by *Hernandia moerenhoutiana* and *Elaeocarpus tonganus*. Parkes (1994) determined that from ca. 6700-5000 yr BP (ca. 7535-5710 cal yr BP) vegetation was dominated by indigenous forest taxa such as *Calphyllum*, *Trema*, and *Elaeocarpus tonganus*. From ca. 5000-1420 yr BP (ca. 5710-1283 cal yr BP) saline tolerant plants such as coconut and *Acrostichum* were the principal vegetation; after ca. 1420 yr BP to present (ca. 1283 cal yr BP to present) human activity is suggested to have altered vegetation to an extent that coconut trees decrease significantly while grasses and ferns increased (see Section 3.2.5 for further information) (Parkes, 1994).

Soil type	Description
Omutu soils	Soils are developed on the outer edge of the makatea. Parent material is weakly consolidated, coarse textured, stony to gravelly coralline sand. It is an excessively drained soil.
Makatea soils	Developed on the outer slopes of the coral platform. Profiles consist of a small accumulation of litter amongst coral stones and boulders. Deep profiles do not develop as weathering products pass into solution.
Mokoera soils	Located on the inner margins of the makatea. Parent material is fine textured basaltic alluvium overlying coral.
Mokoera soils, shallow phase	Located on the seaward side of Mokoera soils, between 15-20 m.a.s.l. Parent material is basaltic alluvium. Profiles are shallower than Mokoera soils and has no transition zone of weathered limestone.
Tamarua soils	Occurs in low-lying swampy areas between the volcanic cone and the makatea. Due to being 1-2 m.a.s.l. soil has poor drainage with a water table near the surface. Can have a high organic matter accumulation in the A horizon.
Kurakei soils	Found mainly on the northeast side of the island. Parent material is a fine-textured strongly weathered basalt alluvium. Is moderately well drained. Has medium to very high soluble phosphorus and calcium and magnesium values.
Teenui soils	Mainly found in the north and northeast of the island and formed from weathered basaltic alluvium. Well-drained soil that supports a number of crops. Quite strongly leached.
Tetoa soils	Found on uppermost terrace surface and has physical properties that make it highly suitable for agricultural use. Similar to Teenui soils except browner soil colour, firmer consistency. Not strongly leached.
Ngatiarua hill soils	Located on steeper surface in the lowermost parts of valleys and on terrace scarps. Parent material is moderately to strongly weather basalt. Less erosion due to a coarser, more strongly developed soil structure.
Te Kapi hill soils	Formed from strongly weathered basalt. Has a lot of variability in soil profiles and is well drained. Highly susceptible to erosion and has low nutrient status.
Te Autua soils	Parent material is strongly weathered basalt and has deep profiles. A well-drained soil that can experience channel erosion.
Te Autua soils, rolling phase	Very similar to Te Autua soils but has a shallower A horizon and contains more weathered basalt. Susceptible to sheet erosion.

Table 3.1: Description of soils on Atiu as detailed by Campbell *et al*. (1982).

3.2.5 Colonisation of the Southern Cook Islands

The current earliest accepted evidence of human colonisation in the Southern Cook Islands is from the Ureia site, Aitutaki Island, dating to AD 1225-1430 (725-520 cal yr BP) (Allen and Wallace, 2007). Wilmhurst *et al*. (2011) estimated colonisation of the Southern Cook Islands to have occurred between AD 1250-1281 (ca. 700-670 cal yr BP) from a meta-analysis of radiocarbon dates in this region. Possible much earlier evidence of anthropogenic activity in the Southern Cook Islands has been found in pollen cores from Mangaia where there is a significant decline in native forest taxa and coeval increase in charcoal and altered sediment geochemistry dating to ca. 2495±41 yr BP (ca. 2536±171

cal yr BP) (Kirch and Ellison, 1994). This was later refined by Chagué-Goff *et al*. (2016) to ca. 2,017-1,552 cal yr BP. The chronology and interpreted anthropogenic activity in Mangaia is contested by Anderson (1995); however Parkes (1994) suggested in the Lake Teroto record at ca. 1,420 yr BP (ca. 1,283 cal yr BP) similar vegetation and geochemical patterns to those determined in Mangaia by Kirch and Ellison (1994) occurred. This suggests that the dates proposed by Kirch and Ellison (1994) and refined by Chagué-Goff *et al*. (2016) are valid. Parkes (1994) highlight the dramatic decrease in coconut trees, corresponding increase in aboriginal taxa, grasses, sedges and fern alongside significant increases in charcoal and low frequency magnetic susceptibility that occurred on both Mangaia and Atiu. Parkes (1994) suggested that this was the first signs of human colonisation of Atiu; however Lake Teroto's chronology is questionable due to the use of bulk sediment spanning 5-10 cm in the record. With this in mind it is suggested that human activity may impact the Lake Teroto record from ca. 1283 cal yr BP.

3.2.6 Lake Teroto

Lake Teroto – also known as Lake Roto, Lake Tiroto and Lake Tiriroto (Figure 3.7 and Figure 3.8) – is located in the southwest of Atiu at 20° 00.545 S, 158° 07.410 W. The aridity index (AI) for the site is 1.38 indicating the site is humid (Trabucco and Zomer, 2009). It is a small elliptical lake, with an area equalling 0.03 km^2 and a catchment totalling 0.3 km^2 at an elevation of 0.9 m.a.s.l. It is an open lake, with an inlet that passes through the nearby taro plantation and a sub-makatea tunnel that connects the lake to the Pacific Ocean. A maximum depth of 8.0 m was recorded in this study; however Parkes (1994) recorded a maximum depth of 8.4 m supporting Kautai'i *et al*.'s (1984) conclusion that the lake level fluctuates. A photo of the lake taken in AD 2016 during a rainstorm show pronounced sediment inwash to the lake (Figure 3.9; P. G. Langdon, personal communication, September 2016).

The lake lies within a volcanic cone and is surrounded on the west by makatea cliff. A taro plantation to the east of the lake is planted in a former swamp, as detailed by Stoddart *et al*. (1990). The wall of the makatea cliff is deeply notched, with a horizontal notch roof at 1-1.5 m above the swamp surface (Stoddart *et al*., 1990) – Parkes (1994) considered this to represent a higher than present water level. Lake Teroto has four soils in its catchment: Mokoera soils to the southwest; Tamarua soils in the taro plantation; and Ngatiarua hill

soils and Kurakei soils in the hills that feed into its catchment (Campbell *et al*., 1982). The Mokoera soils have 5.5% carbon, a C/N ratio of 11, and a total phosphorus of 900 mg in the A horizon; the Tamarua soils have 5.1% carbon, C/N equal to 13, and 368 mg total phosphorus in the A horizon; the Ngatiarua soils have 4.5% carbon, C/N ratio of 13 and a total phosphorus of 1253 mg in the A horizon; and the Kurakei soils have 6% carbon, C/N ratio of 13, and a total phosphorus of 458 mg in the A horizon (Campbell, *et al*., 1982). Parkes (1994) identified *Pandanus tectorius*, *Hibiscus tileaceus* and groves of coconut palms as the main vegetation around the lake, with reeds and aquatic sedges growing around the lake margins. Grasslands and fern scrub are located on the plateau slopes to the north.

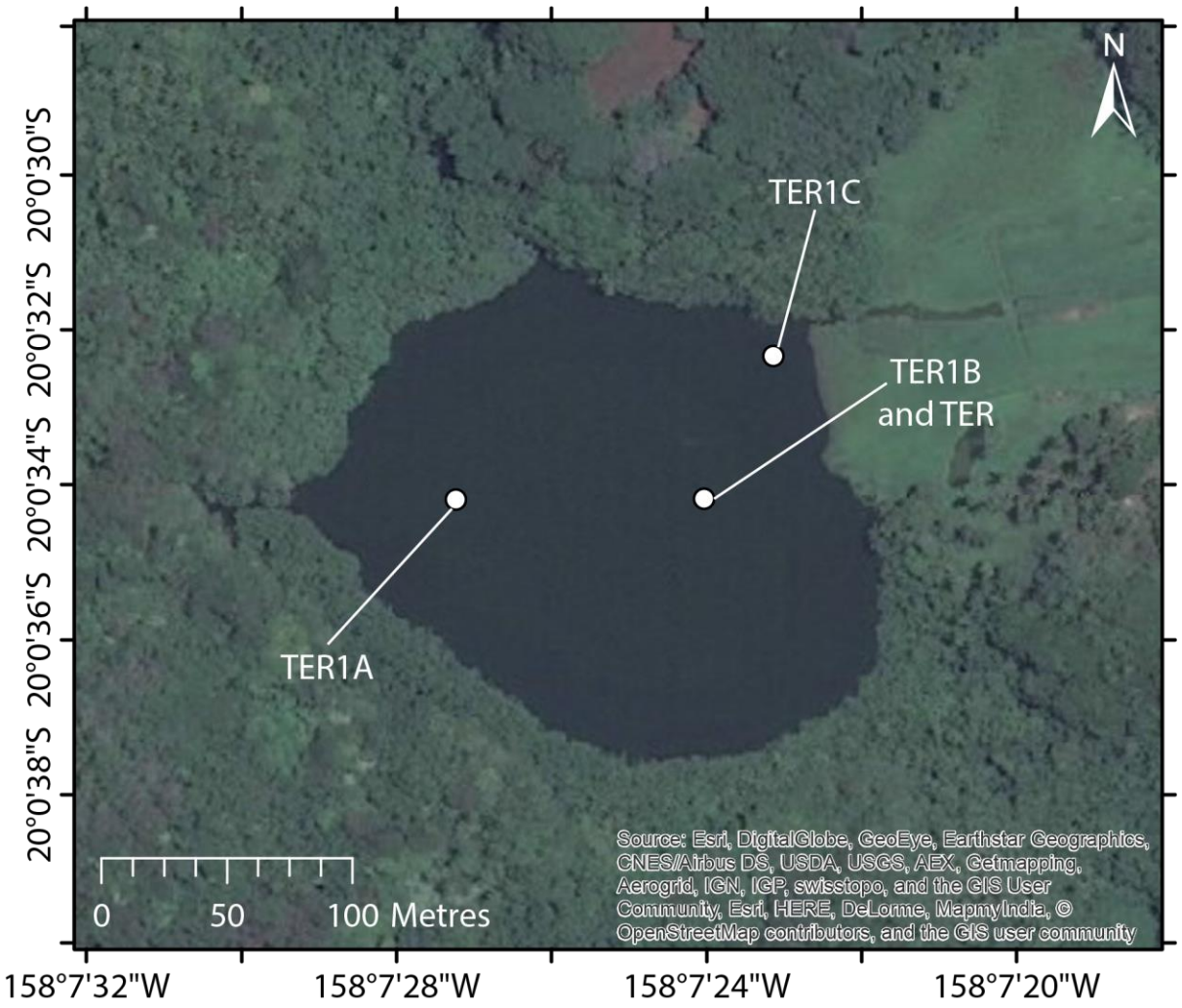

Figure 3.7: Aerial view of Lake Teroto, Atiu (Google Earth, 2015). The coring location (TER) and locations of measurements obtained with the YSI Sonde (TER1A, TER1B and TER1C) are highlighted.

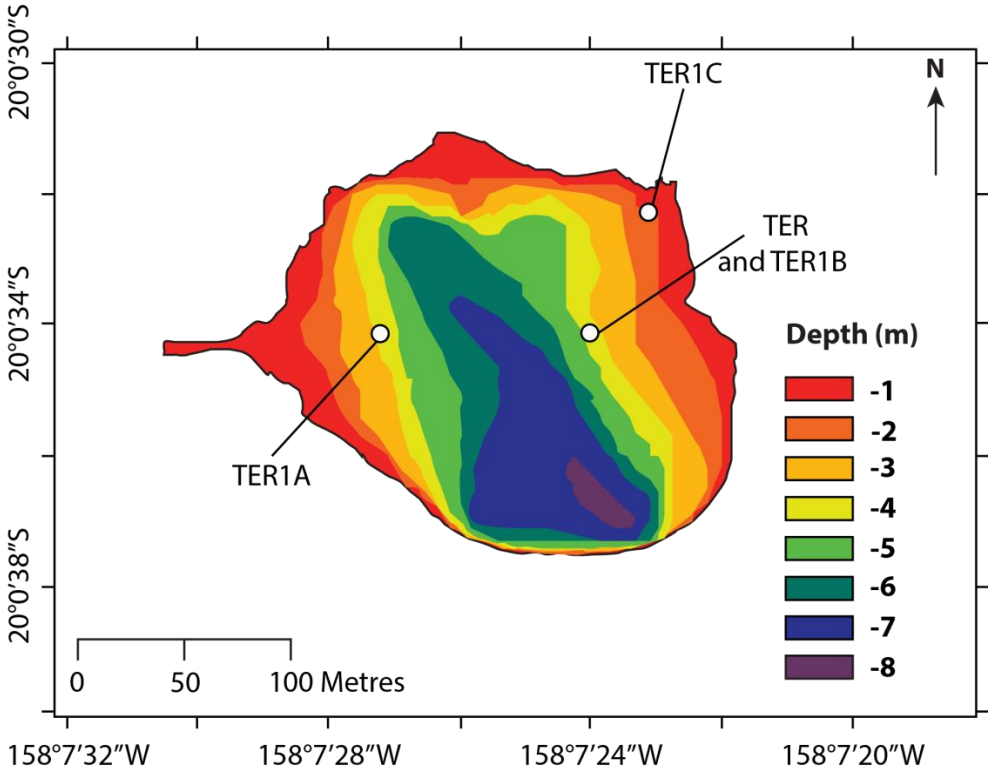

Figure 3.8: Bathymetry of Lake Teroto, Atiu, inferred from Parkes (1994) thus may not reflect the actual bathymetry of the lake. The coring location (TER) and locations of measurements obtained with the YSI Sonde (TER1A, TER1B and TER1C) are highlighted. Differences in depths stated in text and in the bathymetry are a result of a paucity of depth points obtained by Parkes (1994) that were used to develop this map.

Figure 3.9: Photo of Lake Teroto looking east taken during a rainstorm showing sediment inwash to the lake from the surrounding catchment (P. G. Langdon, personal communication, September 2016).

3.3 Lake Lanoto'o

3.3.1 Geography of Samoa

Samoa is located 13°15'S, 171°45'W in the southwest Pacific (Figure 3.1). Formally known as the Independent State of Samoa, the country is comprised of two main islands – these being Savai'i and Upolu – and eight islets that in total cover a surface area of 2842 km^2. Most of the country's 187,820 population is located on Upolu (United Nations, 2014), with Samoa's capital Apia being the most populous settlement in the country.

Savai'i is the only island still volcanically active in the archipelago, with the last eruption in AD 1911 from Mt. Matavanu. Like most islands in the southwest Pacific the archipelago is orientated northwest to southeast (Kear and Wood, 1959). Upolu specifically is elliptical in shape (Figure 3.10), with an area of 1125 km^2, having a spine of extinct volcanic cones running northwest to southeast that rise to a maximum height of 1142 m (Kear and Wood, 1959) (Figure 3.11).

3.3.2 Climate of Samoa

The climate of Samoa is principally controlled by the SPCZ and its location, of which the most noticeable effect is on precipitation. Seasonality is characterised by the difference in precipitation on Samoa as a consequence of SPCZ expansion and contraction: a wet austral summer where the SPCZ has expanded and winds oscillating between west to north; and a dry austral winter where the SPCZ has contracted and cooling southeast trade winds (Kear and Wood, 1959; Matthews and Li, 2005). Whilst temperature does change with the seasons, these changes are small with annual temperatures approximately 26.5 °C between AD 1957-2013 (Bureau of Meteorology, 2015) (Figure 3.12).

Annual precipitation in Samoa is typically never below 2000 mm (Figure 3.12). This is a consequence of the northwest-southeast alignment of Upolu's mountain ridge reducing the rainshadow effect. Nevertheless, the southwest of Upolu does receive more rainfall than the northeast as a result of the southeast trade winds (Ministry of Natural Resources and the Environment, 2015) for example Lotofaga on the southeast receives an annual

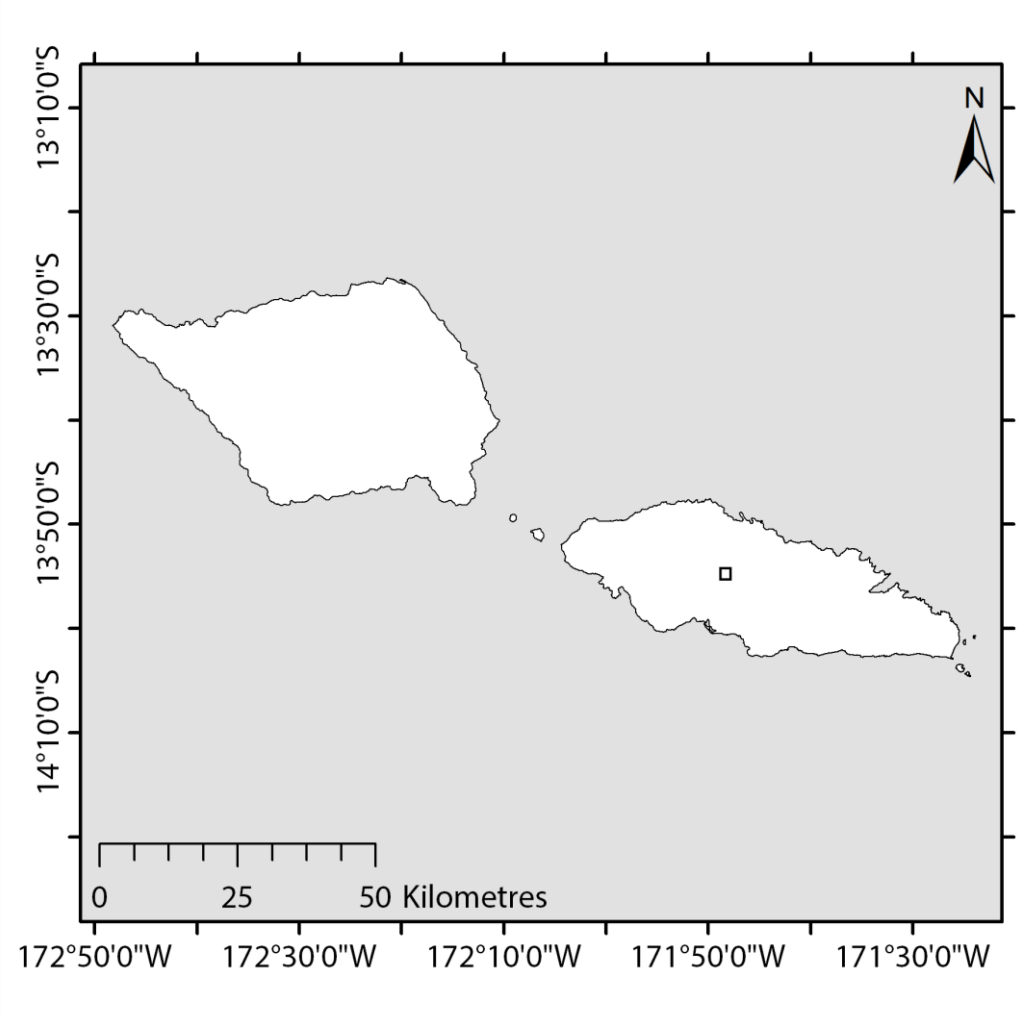

Figure 3.10: Map of Samoa. The square box indicates the location of Lake Lanoto'o.

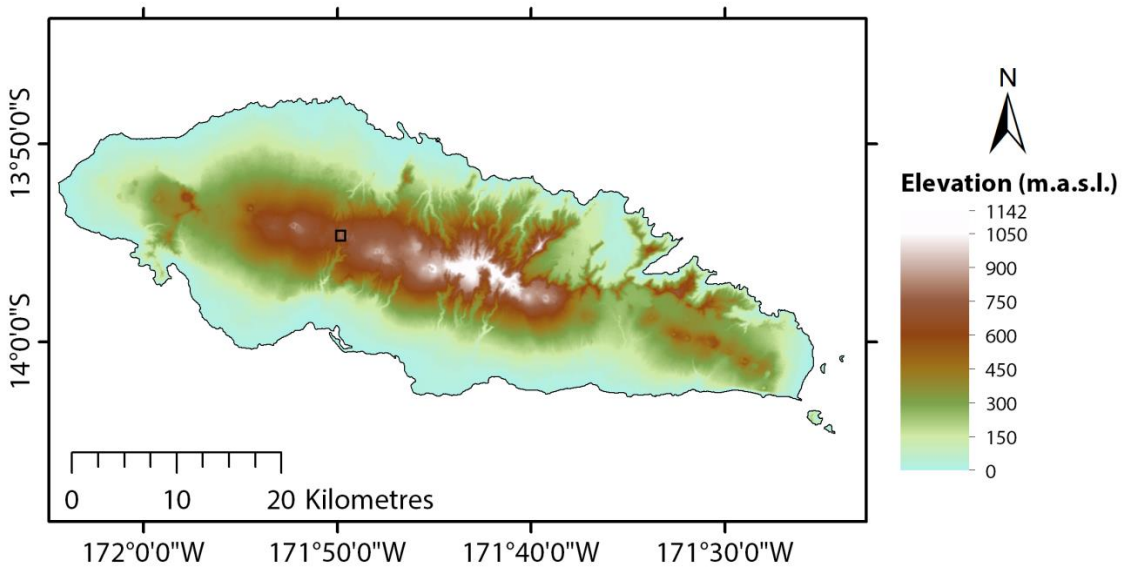

Figure 3.11: Elevation map of Upolu, Samoa – note the difference in elevation in comparison to Atiu, Cook Islands. The black box indicates the location of Lake Lanoto'o (USGS, 2012).

precipitation amount of 4000 mm, whereas Mulifanua on the northwest receives 2200 mm (Parkes, 1994). With the wetter austral summer there is also increased numbers of tropical cyclones hitting Samoa with these having a significant impact on the country: for instance on the archipelago's forests where up to 53% tree mortality can occur after a cyclone (Elmqvist *et al*., 1994). During El Niño years Samoa experiences more tropical cyclones due to the centre for tropical cyclone genesis shifting northwest with the SPCZ; conversely during La Niña years Samoa has less tropical cyclones as tropical cyclone genesis has shifted southeast with the SPCZ (Dowdy *et al*., 2012). It has been argued – albeit unsupported with data – by Angenheister (in Wright 1963) that with every 100 m increase in elevation there was a corresponding increase in precipitation amount between 21-29%. Whilst unsubstantiated, instrumental records of annual precipitation from Afiamalu at 780 m.a.s.l. never fall below 3000 mm between AD 1948-2012, whereas those from Apia at 2 m.a.s.l. elevation can be as low as 1000 mm between AD 1890-2013 (Bureau of Meteorology, 2015).

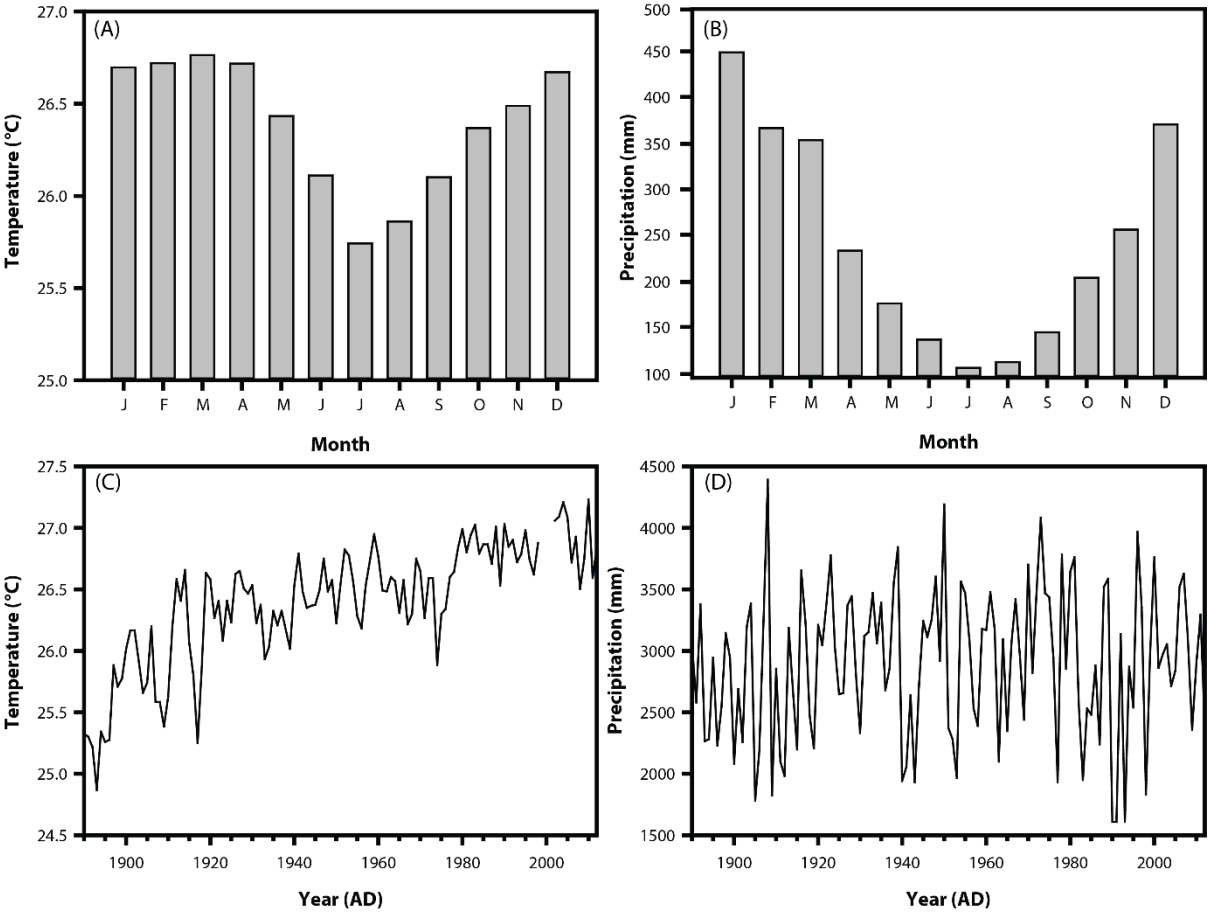

Figure 3.12: The average monthly temperature (A) and precipitation (B), and the average annual temperature (C) and precipitation (D) for the period AD 1890-2012 for Apia, Samoa (Klatt, 2013; Berkeley Earth, 2016). Gaps in (C) indicate a lack of data.

3.3.3 Geology and soils of Samoa

The Samoan archipelago is volcanic in origin and located on the southwest part of the Pacific plate. Koppers *et al*. (2008) date a submarine portion of the island to 5.0 Ma, asserting that this alongside other dates generated shows Savai'i began volcanic construction as early as ca. 5.0 Ma. Moreover, Koppers *et al*. (2008) suggest that the Samoan archipelago is a consequence of a primary hotspot trail, with the archipelago moving in a southeast-northwest direction and Upolu in the southeast being younger (ca. 2.0 Ma, Hart *et al*., (2004)) than Savai'i in the northwest (ca. 5.0 Ma).

The geology of Upolu is dominated by basalts, with a few minor andesites that are present in certain localities (Kear, 1967). These volcanic rocks are principally comprised of limburgite, olivine basalt, olivine basalt-porphyrite, trachydolerite, and nepheline basanite (Thomson, 1921). As a consequence of the dominance of basalt on Uplou the six major volcanic formations, excluding the Vini Tuff, are all similar (Table 3.2; Figure 3.13). The formations are differentiated by the relative proportion of massive lava, the presence of dikes, the effects of compaction, the infilling of cavities, and the depth of weathering which in turn controls the depth of overlying soil (Kear and Wood, 1959; Kear, 1967). The oldest of these is deemed to be the Fagaloa Volcanics in the north-eastern and central district of Upolu; however empirical dates for this are not presented (Kear and Wood, 1959). The Mulifanua, Lefaga, Salani and Puapua Volcanics – the four most widely distributed volcanic groups – rest unconformably on and fill valleys eroded in the Fagaloa rocks (Kear and Wood, 1959). Thus Upolu's general structure is concluded to be that of a deeply eroded Pliocene or early Pleistocene volcanic terrain, flanked and largely buried by more recent volcanic formations.

The deepest soils typically overlie volcanic formations that Kear and Wood (1959) conclude to be the oldest – these being the Fagaloa and Salani volcanics. Wright (1963) determined that the soils of Uplou have thin A horizons over reddish or red deeply weathered material which is low in silica but contain particularly high amounts of TiO_2 (7.8-12.6%). Soils were concluded to have varying fertility, with fertility most likely affected by the deficiency of potash and/or phosphate (Hamilton and Grange, 1938). A list of the main soil sets are presented in Table 3.3.

Volcanic formation	Description
Fagaloa Volcanics	Consists of basaltic lava flows of aa and pahoehoe, with associated dykes, tuffs and cone deposites. Characteristically form steep-sided mountains with slopes of 25°-50°. Can have a poor cover of vegetation, but typically very thick soils. Olivine nodules are common.
Vini Tuff	Forms dissected and partly dismembered tuff cones that consist of principally vitric-lithic tuff. Mollusc shells and coral fragments can be found up to 100 m above sea level.
Salani Volcanics	Characterised by deep soil and weathered, with evidence of pre-Mulifanua canyon-cutting. Determined to have a 'normal' cover of vegetation, with very weathered rounded boulders on the uneven land. Olivine nodules are present in this formation.
Mulifanua Volcanics	Most important feature is existence offshore of the widest barrier reefs and presence of only shallow stream channels. Soil is of intermediate thickness. Has a 'normal' cover of vegetation, with weathered boulders on uneven land. Olivine nodules are uncommon.
Lefaga Volcanics	Has a lack of dissection and presence of only a narrow fringing reef offshore. Soil is of intermediate thickness. Has a 'normal' cover of vegetation, boulders are very common on uneven land, and olivine nodules rare in the formation.
Puapua Volcanics	Lavas flowed over the wide reefs to form rocky iron-bound coasts. Soil is very thin. Has a 'normal' cover of vegetation, boulders are very common on uneven land, and olivine nodules rare in the formation.
Aopo Volcanics	These volcanic were all erupted within the last 200 years and only occur in northern Savai'i. No soil present. Has a 'poor' cover of vegetation, boulders are very common on uneven land, and olivine nodules rare in the formation.

Table 3.2: Description of main volcanic formations in Samoa, after Kear and Wood (1959).

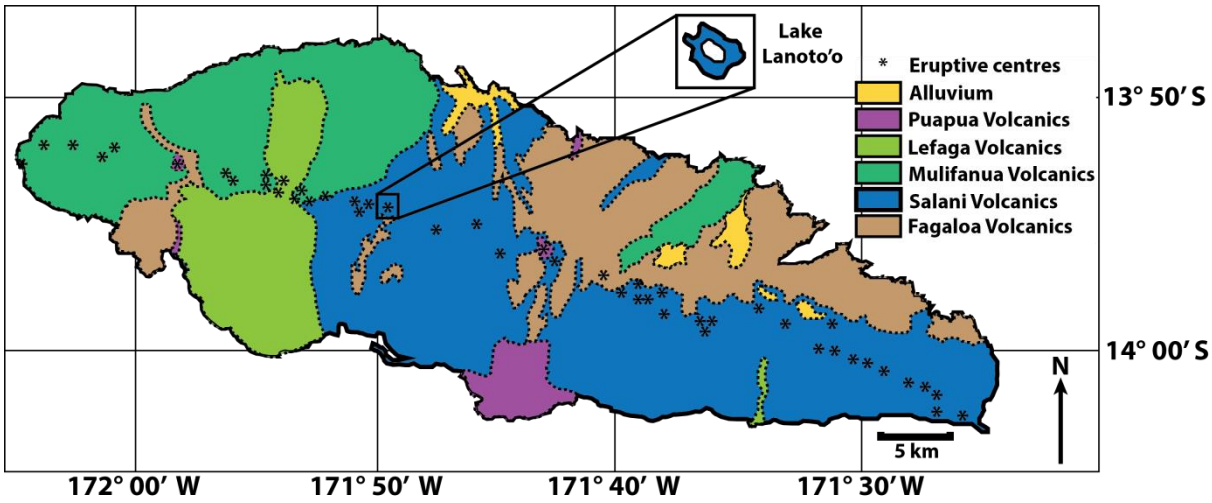

Figure 3.13: Geological map of Samoa, redrawn from Kear and Wood (1959).

Soil set	Description
Sasina and related soils	Shallow, dark brown silty clay loam. Occasional boulders present. Rest on pahoehoe lava that have a weakly weathered surface.
Vaisala and related soils	Usually dark brown to very dark grey very stony silty clay loams grading to reddish-brown, yellowish-brown, or dark brown very stony and boulder silty clay. Typically underlain by a mass of slightly to moderately weathered aa, sociara, or vesicular pahoehoe.
Magia and related soils	Dark brown to dark reddish brown stony clay loams and clays. Parent material is aa and pahoehoe lava that to is moderately to slightly moderately weathered. Soils in this group can be classed as well-drained.
Togitogiga and related soils	Developed on land with easy relief, are usually very dark brown to dark grey silty clays or loams. Quite shallow soils, typically very rich in organic matter and moderately to strongly acidic.
Lefaga and related soils	Includes latosolic soils that mainly come from aa and scoria. Usually stony and boulder clays and silty clays, with dark reddish brown or very dark brown topsoils, and dark brown or dark yellowish brown subsoils. Soils are usually well drained.
Tafatafa and related soils	Soils are mainly derived from pahoehoe and aa. Dark reddish brown stony and boulder clay loams and loams. Quite shallow as a group and can be very boulder. Soils are well drained.
Papauta and related soils	Underlying rocks and boulders are very weathered. Soils are often quite stony and boulder patches are common, also can be very deep and stone free. Moderately to very well drained soils. Topsoils are clays, reddish brown to brown, have strongly developed fine, firm blocky aggregates. Subsoils are reddish to dark yellowish brown silty clays and have a friable consistency.
Atua and related soils	Mainly stony or boulder soils developed on pahoehoe, aa, and scoria. Moderately to well-drained soils. Soil surface is usually somewhat peaty overlying a strongly peat-stained, very dark brown to very dusky red silty clay loam or heavy silt loam. Subsoils are dark greyish brown to very dark yellowish brown, and usually silty clay to silty clay lam in texture.
Etemuli and related soils	Mainly a deep soil developed on pahoehoe and scoria. Volcanic ash has likely contributed a lot to composition. Soils surface typically covered with a thin mantle of strongly acid forest litter and soil below is peat stained as a consequence. Topsoil colour dusky red to dark reddish brown, subsoil dark brown to reddish yellow. Soil is moderately well drained, but in locally can be poorly drained.
Papaloa and related soils	Soils are dark reddish brown that are usually deep. Soils are moderately fertile.
Lata and related soils	Soils are usually found on steepland associated with landscapes rich in dyke rocks. Mainly dark drown stony clay laoms, and can be very bouldery locally. Can have nutty aggregates.
Aopo and related soils	Restricted to Savai'i. Soils are derived from olivine basalt flows and are typically shallow. Texture ranges from sand to gravel. Due to recent nature of soils there is little differentiation.
Sauniatu and related soils	Developed in valley bottoms and flood plains. Range in texture from silt loams to loamy gravels and gravelly sandy clays. Topsoil colour ranges from dark greyish brown to pale yellowish brown, subsoils are dark reddish brown to yellowish brown. Are very fertile soils.
Maugamoa and related soils	Developed on rolling to strongly rolling land and are locally very boulder-rich. Have a dark reddish brown to very dusky red peaty silt loam topsoils; subsoils dark yellowish brown to yellowish red silty clay loam to gravelly loam subsoils. Soils are moderately to strongly acidic.
Tiavi and related soils	Soils are moderately deep brown silt loams and silty clay loams derived mainly from pahoehoe flow rocks or colluvial material overlying an impervious basalt sheet. Soil fertility is low and soils have poor drainage. Moderately to strongly acidic.

Table 3.3: Samoan soil set descriptions from Wright (1963)

3.3.4 Vegetation of Samoa

Whilst studies have been undertaken in Samoa, they have occurred on Savai'i and other islets in the country but not on Upolu. Therefore any statements in regards to the vegetation of Upolu typically concern the vegetation on Savai'i; however vegetation groups will largely be similar for the two islands.

Samoa is part of the Fijian floristic region that extends from the Santa Cruz Islands and Vanuatu to Niue (Takhtajan, 1969). The country has ca. 30% endemism, with ca. 550 angiosperm species and 215 pteridophyte species (Whistler, 1992). The vegetation in Samoa has been categorised into six vegetation groups (Whistler, 1992), detailed in Table 3.4.

Vegetation type	Description
Littoral vegetation	Comprised of three communities: herbaceous strand; littoral shrubland; and *Pandanus* scrub. The herbaceous strand community is typically found on the shore, and the species present are predominantly heliophytes. The littoral shrubland community is shrubby vegetation occurring on rocky or sandy seashores, mainly dominated by the shrubs *Wollastonia biflora* and/or *Scaevola taccada* (Whistler, 1980). The *Pandanus* shrub community is dominated by the screwpine *Pandanus tectorius.*
Wetland vegetation	Six wetland communities comprise this category: coastal marsh, montane marsh, montane bog, mangrove scrub, mangrove forest, and swamp forest. The coastal marsh community is found in low-lying coastal basing separated from the sea by a sand barrier and lack a stream outlet with characteristic species being *Eleocharis dulcis* and *Cyclosorus interruptus*. Montane marsh mainly occurs on the fringe of crater lakes at 500-1000 m elevation (Ollier *et al*., 1979) and is typified by *Eleocharis dulcis*. The montane bog community on Upolu is dominated by the indigenous sedge *Carex maculata*. The mangrove scrub community is located in coastal areas and along the margins of mangrove forest. The mangrove forest community is dominated by *Bruguiera gymnorrhiza* (Whistler 1976, 1980) and occurs along coastal areas. Swamp forest community is found in soils saturated with freshwater inland, such as in inland basins or craters with poor drainage.
Rainforest vegetation	Four main types found on Samoa: coastal forest, lowland forest, montane forest, and cloud forest. Coastal forest is a medium stature forest located inland on steep slopes or on tuff-cone craters. The lowland forest community is the most extensive and complex type of rainforest. Montane forest is found at high elevatons – typically >550m – and is dominated by *Dysoxylum huntii* (Ollier, *et al*., 1979). It is very wet and cooler than the lowland forest. Cloud forest community is found on the highest elevations of Savai'i.
Upland scrub vegetation	Two main types: summit scrub community, found on American Samoa only; and montane scrub found in old volcanic cores that have highly weathered soil. Characteristic species includes the tree *Pandanus reineckei*, and the fern *Dicranopteris linearis*.
Volcanic vegetation	Subcategorised into lowland volcanic scrub and upland volcanic scrub. Both only found on Savai'i.
Disturbed vegetation	Caused by anthropogenic activity and includes managed land, secondary scrub community, secondary forest community, and fernland community.

Table 3.4: Vegetation types found in Savai'i, Samoa (Whistler, 1992).

3.3.5 Colonisation of Samoa

For a detailed review of Samoan archaeology the reader is directed to Rieth and Hunt (2008). Briefly, the earliest evidence of human colonisation to Samoa is from the Mulifanua site that dates to ca. 2,900-2,700 cal yr BP (Green *et al*., 1974; Burley and Clark, 2003; Rieth and Hunt, 2008). This deposit predates the next earliest evidence at To'aga, Ofu Island, and Utumea, Tutuila Island by ca. 300 cal yr BP (Rieth and Hunt, 2008). The analysis of radiocarbon dates undertaken by Rieth and Hunt (2008) suggests that by ca. 2,100 cal yr BP settlements have appeared throughout the Samoan archipelago. There is a so-called "Dark Ages" in Samoa with an apparent lack of abundant archaeological evidence (Davidson, 1979) between ca. 1,500-1,000 cal yr BP. The reason for this Dark Age is unclear; especially whether its cause relates to some catastrophic event in Samoan prehistory or just that no archaeological site has been found that dates to this period. Following the Dark Ages, there is abundant evidence of human activity: specifically monumental architecture and expansive settlements along the coasts and into valleys (Rieth and Hunt, 2008). In regards to human activity in the Lake Lanoto'o catchment, Parkes (1994) suggested there was a decline in primary forest taxa at ca. 2,500 yr BP (ca. 2,540 cal yr BP) that corresponded to increases in secondary taxa argued to be associated with human activity. It is suggested that human activity may impact the Lake Lanoto'o record from ca. 2,900 cal yr BP.

3.3.6 Lake Lanoto'o

Lake Lanoto'o (13° 54.653 S, 171° 49.641 W) (Figure 3.14) is located at 760 m.a.s.l. in a volcanic crater on Upolu. The AI for the site is 3.96, indicting the site is humid (Trabucco and Zomer, 2009). The crater lake is 0.11 km^2 in size, having a catchment 0.23 km^2 in size and at present appears to be a closed-basin. Satellite imagery of the site suggests a possible outflow channel may have existed in the past to the north of the lake. It was observed that there is a submerged shoreline in the lake. Reaching a maximum depth of 17 m, bathymetry suggests that the lake bed has steeper sides on the east and west shores and a gentler dip on the north and south shores (Figure 3.15). The lake is surrounded by very steep inner slops which have an average elevation of 770 m.a.s.l and reach a maximum of 790 m in the west.

The volcanic rocks that the lake is located in are the Salani Volcanics (Kear and Wood, 1959). Akin to the description of Kear and Wood (1959), the red lateritic clay soils are deep. Parkes (1994) determined that the lake is surrounded by a relatively undisturbed cover of *Dysoxylum huntii* moist montane forest – detailed further in Whistler (1992). The catchment soils are Lanuto'o steepland soils that are classed as a silty clay loam that are friable, have a fine nutty structure that breaks to granular and crumb structure. It has a low organic carbon between 2-6% (Wright, 1963). Whilst it would be expected for trees such as *Syzygium* spp., *Elaeocarpus tonganus*, *Palaquium stehlinii*, *Myristica* spp., and *Alphitonia zizyphoides* to dominate, Parkes (1994) noted an abundance of tree ferns that typify secondary forests (Whistler, 1980). The corollary of this being that recent local catchment disturbance may have occurred. The trees and ground have a near-complete coverage of epiphytic ferns. On the lake margins *Pandanus* spp. are the principal vegetation, with aquatic sedges also noted (Parkes, 1994). At some point in the recent past coconut and banana trees have also been planted around the crater rim.

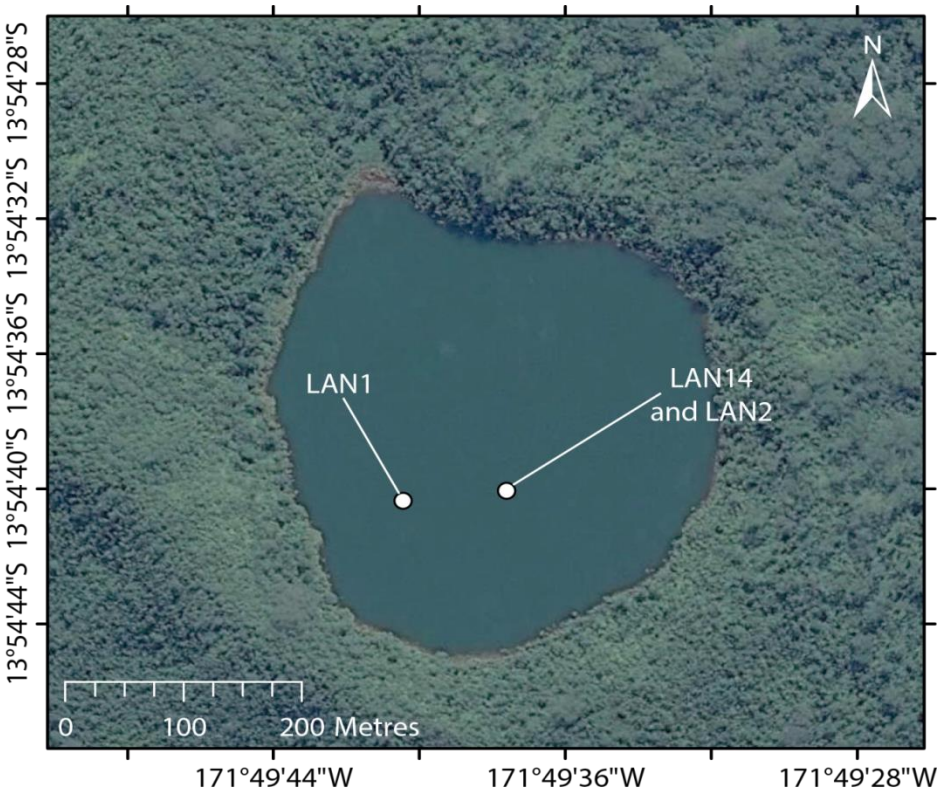

Figure 3.14: Aerial view of Lake Lanoto'o, Samoa (Google Earth, 2015). The coring location (LAN14) and locations of measurements obtained with the YSI Sonde (LAN1 and LAN2) are highlighted.

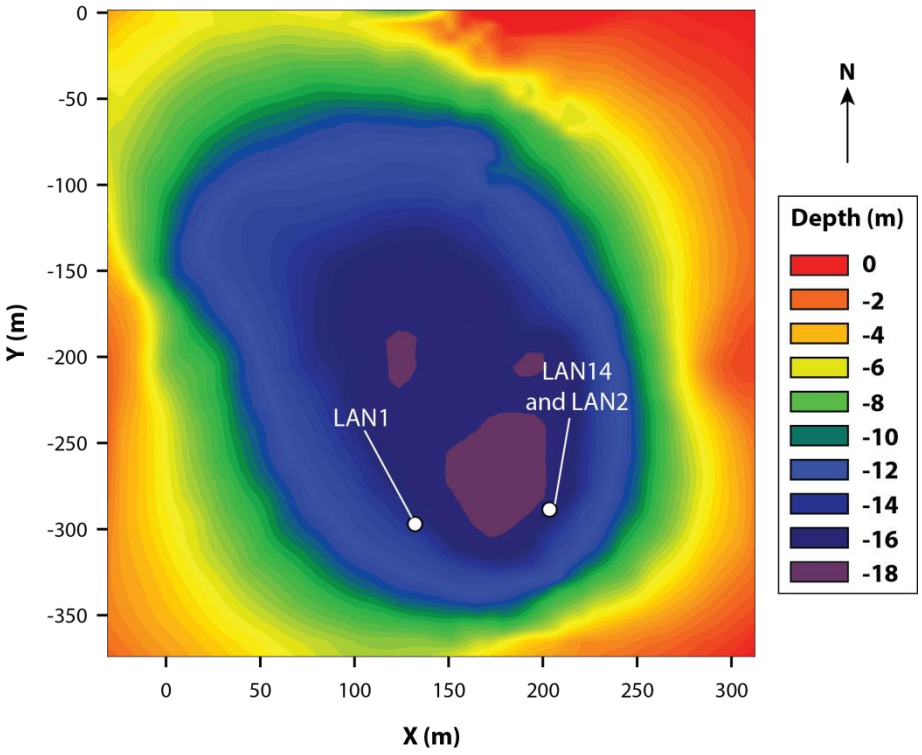

Figure 3.15: Bathymetry of Lake Lanoto'o (MNRE, personal communication, 2014). The approximate coring location (LAN14) and locations of measurements obtained with the YSI Sonde (LAN1 and LAN2) are highlighted.

Chapter 4: Methods

4.1 Introduction

This chapter delineates the methods used in subsequent chapters, with the first section addressing site methods, the second section detailing dating methods, the third section detailing inorganic geochemical methods used, and the fourth section dealing with organic geochemical methods used. The backgrounds to the methods used are explained alongside their use for addressing the aims.

4.2 Site methods

4.2.1 Coring

4.2.1.1 Short cores

A UWITEC gravity-type corer with core catcher and a barrel length of 60 cm was used in order to capture the sediment-water interface and most recent sediments (UWITEC, 2016). Sediment loss was avoided with the core catcher that seals the bottom of the core in situ before withdrawal through the water column. Cores were kept intact and stored in an airtight tube during transport and when placed in cold storage (+4 °C). The cores were split longitudinally and underwent low-frequency magnetic susceptibility analysis (Section 4.4.1) and micro X-ray fluorescence (µXRF) (Section 4.4.2) analysis before being subsampled at contiguous 1 cm intervals.

4.2.1.2 Long cores

A 120 cm-long Livingstone-type corer – GEOCORE (GeoCore, 2016) – was employed with both 5 cm and 3 cm core diameters to retrieve overlapping cores. Cores were kept intact inside the airtight aluminium sediment tubes during transport and then placed in cold storage (+4 °C). Each core was extruded in the laboratory into PVC guttering and covered with cling film. Cores were logged and underwent low frequency magnetic susceptibility analysis, then split longitudinally and U-channels taken for µXRF analysis. Subsamples were taken for subsequent proxy analysis.

4.2.2 Physicochemical characterisation

4.2.2.1 Overview

Understanding the physical and chemical characteristics of a lake is important for properly interpreting lake sedimentary deposits (Cohen, 2003). Physiochemical depth profiles in lakes provide a contemporary context that can be used to infer whether the lake has remained in a similar state in the past, for instance meromictic, or has changed state over time. At present there are very few studies that have undertaken depth-specific physicochemical profiling of lakes in the Pacific region, with these being in Vanuatu, Tonga, Fiji, Hawai'i, and Wallis and Futuna (Baker, 1929; Maciolek and Yamada, 1981; Southern *et al*., 1986; Donachie *et al*., 1999; Sichrowsky *et al*., 2014). This physicochemical information for each site will provide a framework from which the proxy data can be better interpreted.

Site	Sample ID	Coordinates	Depth (m)	Additional notes	Physicochemical parameters measured
Lake Lanoto'o	LAN1	13°54.659 S, 171°49.686 W	17.1	Sampled east of coring location	Dissolved oxygen (as % saturated); pH; temperature; conductivity
Lake Lanoto'o	LAN2	13°54.655 S, 171°49.637 W	16.4	Sampled near coring location	
Lake Teroto	TER1A	20°00.577 S, 158°07.456 W	3.6	Sampled near connection to sea	
Lake Teroto	TER1B	20°00.572 S, 158°07.412 W	7.2	Sampled near coring location	Dissolved oxygen (as % saturated); pH; temperature
Lake Teroto	TER1C	20°00.546 S, 158°07.389 W	2.3	Sampled near inflow	

Table 4.1: Sampling details and physico-chemical parameters measured in Lake Lanoto'o and Lake Teroto.

4.2.2.2 Analytical procedure

Sampling of Lake Lanoto'o and Lake Teroto was conducted between 19th September to 1st October 2014. Parameters measured for each site are listed in Table 4.1. Conductivity was not measured at Lake Teroto due to the failure to calibrate the conductivity probe – likely a result of the high salinity (>4000 µS/cm, (Schabetsberger *et al*., 2009); 6 ppt (A. Maloney, personal communication, 2015)) of this lake. The depth of samples was automatically collected by the submersible multi-parameter YSI Sonde 650 for Lake Lanoto'o; however

sampling depth was not automatically measured for Lake Teroto. Depth profiles for each sampling location in Lake Teroto have been assumed based on water depth at the sampling point and that measurements were obtained at uniform depth intervals. Consequently results should be treated with caution. Three profiles were taken in Lake Teroto (Figure 3.7) and two profiles were taken in Lake Lanoto'o (Figure 3.14).

4.3 Dating methods

4.3.1 ^{210}Pb and ^{137}Cs age-depth models

4.3.1.1 ^{210}Pb age-depth models

The ^{210}Pb dating method is widely applied for the dating of lake surface sediments and has been used in a variety of environmental settings (Abril, 2004). The method utilises the radioactive ^{210}Pb isotope that occurs as part of the ^{238}U decay series. In the decay sequence, the heavy metal isotopes ^{222}Rn, ^{220}Rn and ^{219}Rn diffuse into the atmosphere where, due to their mass, they become quickly attached to natural aerosols (Robbins, 1978). Over time the longer-lived decay products – especially ^{210}Pb – return to earth through atmospheric processes including rainfall (Robbins, 1978). In lakes the ^{210}Pb that falls into them is scavenged from the water column and deposited in the lake's surface sediments (Appleby, 2001).

The half-life of ^{210}Pb is 22.3 years, permitting the dating of sediments over the last 130-150 years (Appleby, 2001). Dating with ^{210}Pb is problematical due to the concentration of ^{210}Pb at the sediment-water interface being a function of both ^{210}Pb supplied to sediment from atmospheric and terrestrial inputs, as well as being produced in situ through the decay of naturally occurring ^{226}Ra. To overcome this issue a number of models have been developed – listed in Table 4.2– that calculate the sediment age from ^{210}Pb activity data. The most commonly applied models are the constant initial concentration (CIC) model and the constant rate of supply (CRS) model (Appleby and Oldfield, 1978), with the choice between using these depending on the assumption of a constant rate of ^{210}Pb delivery and/or constant sedimentation rate. The latter of these two assumptions may not be valid in this study due to the changes in precipitation amount that are known to occur due to SPCZ movement. This will cause a change in the sedimentation rate due to increased catchment input consequently diluting the concentration of ^{210}Pb. Moreover,

changes in precipitation could cause changes in the rate of supply og ^{210}Pb as the isotope is primarily derived from rainfall. Studies in other sites in the Pacific that also experience high variability in rainfall have not encountered changes in ^{210}Pb supply rate – for example El Junco, Galápagos (Conroy *et al*., 2008) and Spooky Lake, Palau (Sachs *et al*., 2009) – suggesting that this is unlikely to be a significant limitation. Consequently a constant rate of supply of ^{210}Pb into Lake Lanoto'o and Lake Teroto is assumed, meaning the CIC and CRS models are considered appropriate.

Model	Description	Reference
CFCS	Constant Flux Constant Sedimentation: based on the assumption that the rate of deposition of atmospheric ^{210}Pb is constant, and that the sedimentation rate is constant.	Krishnaswamy *et al*. (1971)
CIC	Constant Initial Concentration: assumes a constant rate of ^{210}Pb supply and that the sedimentation rate is constant.	Appleby and Oldfield (1978)
CRS	Constant Rate of Supply: assumes constant ^{210}Pb supply but allows for a changing sedimentation rate.	Appleby and Oldfield (1978)
IMZ	Incomplete Mixing Zone: assumes that the sediment contains a mobile radionuclide fraction.	Abril *et al*. (1992)
SIT	Sediment Isotope Tomography: used independent age markers to constrain the model rather than validate it. This model has no assumptions, allowing for sediment mixing, and changes in supply of ^{210}Pb and sedimentation rate.	Carroll and Lerche (2003)

Table 4.2: Overview of main ^{210}Pb age-depth models applied to date sediments.

4.3.1.2 ^{137}Cs age-depth models

To ensure that ^{210}Pb age-depth models are valid Smith (2001) proposed that any ^{210}Pb age-depth model must be validated with at least one independent tracer that can provide an unambiguous time-stratigraphic horizon. The main approach that has been taken is using ^{137}Cs introduced into the biosphere from atmospheric nuclear tests (Abril *et al*., 1992). Abril (2004) argued that ^{137}Cs cannot be used to support CRS or sediment isotope tomography (SIT) models (Carroll and Lerche, 2003), suggesting that the incomplete mixing zone (IMZ) model is the only viable alternative; however this is mainly applicable to sediments that indicate mixing. Terry *et al*. (2006) concluded that appreciable fallout levels of ^{137}Cs in the atmosphere first occurred AD 1954 and the ^{137}Cs fallout peak for the South Pacific – specifically Samoa – was in AD 1964, whereas Conroy *et al*. (2008) applied an AD 1963 ^{137}Cs bomb-spike for the Galápagos. This study accepts the first appreciable fallout levels of ^{137}Cs occurred at AD 1954±1 and a ^{137}Cs fallout peak of AD 1964±1.

4.3.1.3 Analytical procedure

Caesium-137 and lead-210 were measured using Canberra well-type HPGe gamma-ray spectrometers (Canbeera UK Ltd., Didcot – now Mirion Technologies). The gamma ray spectra were acquired for 100,000 s for each sample (contiguous 1 cm samples for Lake Teroto, contiguous 0.5 cm samples for Lake Lanoto'o) and processed using Fitzpeaks gamma deconvolving software (JF Computing, Stanford-in-the-Vale, UK). All measurements were undertaken at the Geosciences Advisory Unit (GAU) Laboratories based at the National Oceanography Centre, University of Southampton (UK).

4.3.2 ^{14}C age models

4.3.2.1 Overview

As a result of cosmic ray interactions with the Earth's atmosphere ^{14}N is converted to the radioactive isotope ^{14}C through neutron emission (Bowman, 1995). Carbon-14 is rapidly oxidised to CO_2 alongside other isotopes of carbon – specifically ^{13}C and ^{12}C – which gets mixed throughout the atmosphere and subsequently stored in various global reservoirs (Lowe and Walker, 2015). While an organism lives, their absorbed CO_2 is broadly in equilibrium with atmospheric CO_2; however when the organism dies the absorbed ^{14}C will continue to decay without being replenished (Bowman, 1995; Lowe and Walker, 2015). Consequently knowing the decay rate of ^{14}C and the residual ^{14}C activity the date of an organism's death can be calculated.

Over time the amount of ^{14}C produced has not been uniform leading to a need to calibrate radiocarbon ages to calendar ages. It has been determined that calibration in the Southern Hemisphere is different to that in the Northern Hemisphere, with relatively older ages in the Southern Hemisphere attributed to a higher sea-air $^{14}CO_2$ flux from the larger expanse of Southern Hemisphere oceans (Rodgers *et al*., 2011). Calibration curves have used a mix of different sources – including speleothems, marine records and tree rings – which all suffer from inherent problems. With the publication of the varved Lake Suigetsu record spanning the last 70,000 years (Nakagawa *et al*., 2012), this being longer than the radiocarbon age limit of ca. 50,000 years (Bronk Ramsey *et al*., 2012), a terrestrial calibration curve has been developed that covers the entire radiocarbon age limit and which does not suffer from the various problems associated with previous

calibration curves (Bronk Ramsey *et al*., 2012). Hogg *et al*. (2013) were able to determine the Southern Hemisphere offset over the last 2000 years from tree rings sourced in the Southern Hemisphere, and consequently applied a 43-year adjustment to their SHCal13 calibration curve that is largely derived from the IntCal13 calibration curve (Reimer *et al*., 2013).

The choice of material used for radiocarbon dating is an important one. Ideally short-lived terrestrial macrofossils such as leaves should be dated as these will have likely been in equilibrium with atmospheric CO_2 and not sourcing ^{14}C from carbon reservoirs that can give rise to erroneous ages. However obtaining terrestrial macrofossils in a lake sediment record can be difficult and compromises often have to be made using bulk sediment – thus leading to the TOC being dated (Grimm *et al*., 2009). As bulk sediment receives carbon from various provenances the ages produced may not be accurate. Therefore ^{14}C dates derived from bulk sediment should be viewed with caution and considered an approximate age. If a known age marker is present, such as a tephra, any age offset between a bulk age and the known age marker can be checked. In the Pacific ^{14}C dates have largely been produced from bulk sediment (for example: Conroy *et al*., 2008; Sachs *et al*., 2009; Wirrmann *et al*., 2006, 2011b). New Caledonia has been particularly problematic to obtain relaible ^{14}C ages– for example Wirrmann *et al*. (2006, 2011b) and Stevenson *et al*. (2001, 2010). Nevertheless terrestrial macrofossils have been dated and used to construct radiocarbon age-depth models from sites in Palau, Micronesia (Smittenberg *et al*., 2011), and some sites in the Galápagos (Nelson and Sachs, 2016). This study endeavours to use terrestrial macrofossils wherever possible, and bulk sediment when these cannot be found, to obtain radiocarbon dates.

4.3.2.2 Analytical procedure

Radiocarbon samples were prepared and measured at the Scottish Universities Environmental Research Centre and at Beta Analytic (Miami, USA). Sample pre-treatment followed the acid-alkali-acid method – specifically involving samples being digested in 2M HCl (80 °C for 8 hours) – washed with deionised water, then digested in 1M KOH (80 °C for 2 hours). Digestion was repeated using deionised water until no further humics were extracted. Remaining residue was rinsed free of alkali, digested in 2M HCl (80 °C for 5 hours), rinsed free of acid, dried and homogenised. The total carbon in a known weight of the pre-treated sample was recovered as CO_2 by combustion with CuO in a sealed quartz

tube, with the gas converted to graphite by Fe/Zn reduction. All dates were reported in conventional ^{14}C years before AD 1950, with analytical confidence expressed at the ±1σ interval. Radiocarbon dates were calibrated to calendar ages using BACON v2.2 (Blaauw and Christen, 2011) utilising SHCal13 for southern-hemisphere-specific calibration data (Hogg *et al*., 2013). All dates presented in this study are calibrated to calendar years before present (cal yr BP).

4.4 Inorganic geochemical methods

4.4.1 Magnetic susceptibility

4.4.1.1 Overview

Magnetic susceptibility measures how magnetisable a material is (Dearing, 1994). Therefore in the natural environment magnetic susceptibility tells us about the minerals present in sediment. In lake sediments there are five generally accepted origins of magnetic minerals:

- Allogenic: (1) atmospheric particles and (2) fluvially borne detrital minerals;
- Authigenic: (3) bacterial magnetosomes, (4) authigenic iron sulphides, and (5) reductive diagenesis (Dearing, 1999).

The input of these minerals is controlled principally by climate (rainfall, seasonality, temperature), and also by atmospheric deposition and human activity (Dearing, 1999). Magnetic susceptibility is measured using a small probe that produces a small magnetic field, and the magnetisation measured is the total magnetic force in the material while it is in this field (Dearing, 1994).

Both Lake Lanoto'o and Lake Teroto lake sediment have been previously analysed for their magnetic susceptibility; however measurements on the former were discontinuous (Parkes, 1994). The high magnetic susceptibility measured in Lake Lanoto'o and Lake Teroto was determined to be due to in-wash of catchment clays (Parkes, 1994). Stevenson (2004) determined that a decrease in magnetic values reflect less clay mineral deposition from fluvial sources in Lac Saint Louis, New Caledonia, and a transition to a closed lake. The use of magnetic susceptibility in this study has the principal application of determining the timings of terrigenous inputs into the lakes.

4.4.1.2 Analytical procedure

Whole cores were measured for volume-specific low frequency magnetic susceptibility using a Bartington Instruments MS2K sensor at contiguous 1 cm intervals. The magnetic susceptibility was measured against a background of ambient magnetism that was used to correct the sample measurement (Dearing, 1994).

4.4.2 Scanning micro-XRF

4.4.2.1 Overview

Obtaining the sediment properties of lacustrine sediment sequences are fundamental for inferring environmental, sedimentological and diagenetic changes (Croudace *et al*., 2006). Moreover they allow for the quality of the archive to be assessed and inform on sampling strategies for discrete samples (Richter *et al*., 2006). One method for obtaining the composition of sediments is X-ray fluorescence (XRF) (Jenkins and De Vries, 1970; Ramsey *et al*., 1995; Jenkins, 1999). XRF follows the principle that under the influence of X-ray radiation, an atom will eject an electron from an inner shell leaving a hole that is filled by an electron falling from an outer shell (Richter *et al*., 2006). The energy difference between the two shells is emitted as X-rays, with the emitted X-ray wavelength being characteristic for each element. The intensity of the emitted X-rays, i.e. the amplitude, are used to determine the concentration of the elements present. Whilst being able to analyse a large number of elements, XRF cannot analyse elements lighter than sodium (atomic number = 11) (Rollinson, 1993). Typically XRF measurements use one of two sample preparation methods (Croudace *et al*, 2006):

1. The fusion method: dissolving ca. 0.5 g of a sample in a lithium borate flux, producing a glass bead which permits the determination of major and some trace elements;
2. The pelletization method: uses a minimum 3 g of ground sample, pressed into a briquette at 15-20 tonnes. Permits both major and trace elements to be determined.

Whilst these methods produce quantified results, the primary drawbacks are that the preparation and analytical process for a 1 m core samples at 1 cm resolution will take up

to two weeks, and the fusion method is destructive (Croudace *et al*., 2006). Core scanners that incorporate XRF analysis are non-destructive, rapid, and allow continuous high-resolution analysis of sediment cores (Jansen *et al*., 1998; Rothwell *et al*., 2006; Croudace *et al*., 2006). One such core scanner is the Itrax (Figure 4.1) which obtains optical and micro-radiographic images, as well as µXRF elemental profiles for the core section at a high resolution – such as 200 µm intervals (Croudace *et al*., 2006). Unlike the aforementioned XRF analytical methods, the µXRF data produced by the Itrax is semi-quantitative and measured as counts per unit time per unit area (Croudace *et al*., 2006; Chawchai *et al*., 2014).

Analyses of marine and lacustrine sediment cores are increasingly using µXRF core scanners as a standard analytical procedure. At present most studies using µXRF have been undertaken on marine cores; however there has been an exponential increase in recent years of studies using µXRF on lacustrine cores (Rothwell and Croudace, 2015). Unlike marine cores, lacustrine cores have significant changes in water and organic content that necessitate careful interpretation of µXRF data (Davies *et al*., 2015). Micro-XRF core scanners are generally unable to detect elements lighter than Al, compounding the problem of varying water and organic matter content in lacustrine cores due to organic matter being principally composed of oxygen, hydrogen, nitrogen and carbon. Thus increases in these elements, in other words organic matter, will cause a decrease in the absolute counts detected for all measured elements. This effect is well known and is referred to as the 'closed-sum' effect (Rollinson, 1993). As a consequence of the closed-sum effect various normalisation approaches have been applied: for example to the incoherent scatter, total scatter (incoherent plus coherent), or by the total counts at each depth interval (Kylander *et al*., 2011; Cuven *et al*., 2011; Berntsson *et al*., 2014). Löwemark *et al*. (2011) suggested normalising against Al; however due to this being on the limit of µXRF core scanning capability Al often has low counts which can make it unreliable to use (Löwemark *et al*., 2011).

As well as changes in organic content, changes in sediment porosity and water content give rise to data artefacts in µXRF data (Ge *et al*., 2005; Kido *et al*., 2006; Böning *et al*., 2007; Tjallingii *et al*., 2007; Hennekam and de Lange, 2012; Weltje *et al*., 2015). Weltje and Tjallingii (2008) suggested that µXRF data should be plotted as logarithmic ratios of element intensities to overcome these problems. Boyle *et al*. (2015) outlined using the

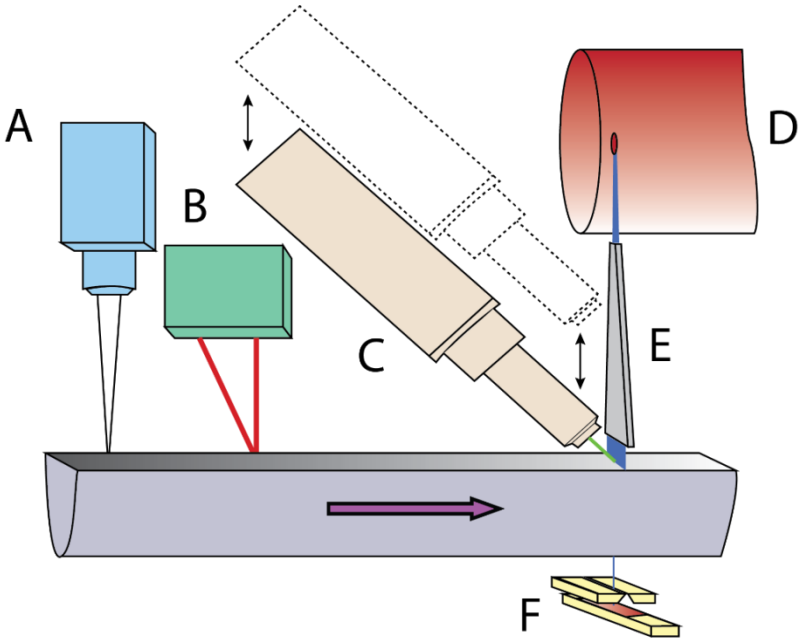

Figure 4.1: Overview of the Itrax system. The optical-line camera (A), laser triangulation system (B); motorised XRF SDD (Si-drift detector) (C); 3 kW X-ray tube (D); flat-beam X-ray waveguide and the X-ray line camera and slit system for the radiographic line camera (F) are displayed. The purple horizontal arrow indicates the direction of a core movement in the system, and the vertical arrows indicate the movement directions of the XRF detector (Croudace *et al*., 2006).

coherent/incoherent ratio to correct for water content changes – the authors utilise the principle that incoherent scatter is positively correlated with water content and determine that this approach is applicable when water content in the sediment varies systematically. It is also suggested that the aforementioned conventional XRF methods are used in tandem with µXRF core scanning data to quantify the µXRF core scanning data: for example in Marshall *et al*., (2011). Conventional XRF analysis is not affected by the data artefacts which µXRF core scanning is susceptible to as it reduces mineral and particle-size effects by creating dry, powdered and homogenised samples (Potts, 1987). All these approaches are taken with the aim to convert semi-quantitative µXRF data to quantitative results. If the focus of the study is relative changes downcore or initial sediment characterisation then quantification may not be necessary (Davies *et al*., 2015).

Itrax µXRF data can be analysed using a simple correlation analysis to reveal which elements are associated with lithogenic elements – such as Ti, Fe and Mn – and which are more closely associated with organic units. Moreover, ratios of elements can be used to determine periods where elements are produced autochthonously or are a consequence

of allochthonous input. Davies *et al*. (2015) detailed all elements and element ratios and their associated interpretation that have so far been used – some of those more commonly applied are listed in Table 4.3. Element ratios have to be applied carefully and are often site-specific. For example Ca/Ti was used to indicate lake level flucutations in Laguna Potrok Aike (Haberzettl *et al*., 2009); but it was later found that micropumice present in the lake record lowered Ti values thus impacting on the validity of the ratio for reconstructing hydrological variability (Jouve *et al*., 2013). It can also be possible to identify the presence of tephra and cryptotephra by using the relationship of certain elements. For instance Balascio *et al*. (2015) suggested that high values of Ti, Mn, Fe and Cu in the same horizon are indicative of basaltic tephra. Moreover Balascio *et al*. (2015) suggested that using a ratio to K for these elements showed the greatest difference between tephra layers and background counts.

At present (2017) only Lake Tiriara, Mangaia, Cook Islands has been analysed using µXRF. Therefore the use of µXRF analysis in this study will add much-needed information on the geochemical characteristics of lacustrine records in the Pacific region. It will indicate the key elements in the lakes' sedimentary records and assist in the palaeoenvironmental interpretation of the study sites.

4.4.2.2 Analytical procedure

Whole cores were subsampled into U-channels in the laboratory and subsequently stored and sealed in cold storage (+4 °C) prior to scanning. Analysis of U-channels was undertaken using an Itrax core scanner (Cox Analytical Systems, Goethenburg, Sweden) at the National Oceanography Centre, University of Southampton. Both a photographic and X-radiographic image were obtained at high resolution prior to each core's XRF scan. The chosen resolution of the XRF scans was determined by visual inspection of the cores' stratigraphy for fine laminations. Full analytical conditions are detailed in Table 4.4.

4.4.3 Modern water isotopes

4.4.3.1 Overview

A variety of studies have indicated that the covariation in the oxygen and hydrogen isotope composition of precipitation defines a global meteoric water line (GMWL) (Craig,

Element or ratio	Environmental interpretation
Br	Increased organic content due to Br being strongly covalently bonded to organic compounds.
Ca	Increased calcite precipitation/evaporative concentration. If increases in S at same time as Ca possible indicator of gypsum deposition.
Fe, Ti, Mn	All can be indicative of soil erosion (tropical weathering of basaltic/andesitic rocks) inputs from the catchment
Fe/Mn	An increase is often interpreted as anoxic conditions at the sediment-water interface.
Sr/Ca	Enhanced Sr may indicate the presence of high-Sr aragonite which requires a shallow water source.
Inc/Coh	X-ray scatter parameters – higher values are often interpreted as indicative of higher organic content.
Zr	Where zircon is present as a heavy accessory mineral it can be used an indicator of grain size, typically coarse sand and silt.
All	Correlation matrices allow a determination of elements association with allochthonous input and autochthonous productivity, which further allows for the identification of units.

Table 4.3: Elements or ratios considered informative for analysing sediments and their typical environmental interpretation (Croudace *et al*., 2006; Rothwell *et al*., 2006; Bishop, 2015; Davies *et al*., 2015).

Lake Lanoto'o		Lake Teroto	
Parameter	**Setting**	**Parameter**	**Setting**
Tube	Mo	Tube	Mo
Voltage	30 kV	Voltage	30 kV
Current	30 mA	Current	30 mA
Exposure time	30 s	Exposure time	30 s
Step size	500 µm (except LAN14-U2 and LAN14-2-2 which were both measured at 200µm)	Step size	200 µm

Table 4.4: Summary of measurement parameters in Itrax XRF analysis.

1961). Isotopic composition of rainfall is a ratio of $^{18}O/^{16}O$ and $^{2}H/^{1}H$ – presented as $\delta^{18}O$ and $\delta^{2}H$ respectively – with higher δ values indicating a higher abundance of the heavier isotope (^{18}O or ^{2}H) and vice versa. Typically the tropics have high δ values, whereas cold regions have low δ values. Lake waters that plot on or close to the GMWL are isotopically the same as precipitation. Often lakes plots off the GMWL onto a local evaporation line (LEL), thus indicating that they have undergone kinetic fractionation (Leng *et al*., 2006). This is a result of fractionation, as $^{1}H_2{}^{16}O$ is more diffusive than $^{2}H^{1}H^{16}O$ and $^{1}H_2{}^{18}O$. A lake that is groundwater-fed and open should, in general, have a $\delta^{18}O$ and $\delta^{2}H$ composition similar to mean weighted values for precipitation and fall on a meteoric water line (Leng

and Marshall, 2004); lakes that evaporate will have $\delta^{18}O$ and $\delta^{2}H$ values which lie on a LEL with a slope determined by local climate (Clark and Fritz, 1997). These data will aid in the interpretation of the proxy data and help determine the characteristics of each site.

4.4.3.2 Analytical procedure

Modern waters were collected in the 2013 and 2014 field campaigns from Lake Lanoto'o, and in the 2014 field campaign from Lake Teroto. Surface waters were obtained in both campaigns, whilst in the 2014 campaign abyssal waters were obtained from the water captured at the top of a UWITEC sampler. All samples were stored in double-sealed plastic containers and stored at +4 °C before analysis at the Natural Environmental Research Council Isotope Geosciences Facility. Samples were analysed using a GV Isoprime with Multiprep and EuroPyrOH and reported as $\delta^{18}O_{VSMOW}$ and $\delta^{2}H_{VSMOW}$ (relative to Vienna Standard Mean Ocean Water) with reference to in-house standards.

4.5 Organic geochemical methods

Analyses of bulk organic matter have been widely applied in palaeolimnological investigations on a variety of continents (Leng and Marshall, 2004). However to date (2017) they have not been widely applied in the Pacific region – for instance in El Junco, Galápagos, and Emaotfer Swamp where C/N ratios and total organic carbon (TOC) have been applied (Conroy *et al*., 2008; Wirrmann *et al*., 2011a). Moreover they have not been applied in Samoa and the Cook Islands. Thus their use in this study would make this the first application of TOC, carbon/nitrogen ratios (C/N ratios), and carbon isotope analysis on total organic matter ($\delta^{13}C_{TOC}$) for these countries. These techniques will provide key information to undertake palaeoenvironmental and palaeoclimatic reconstructions for each site. Whilst extensive reviews about organic carbon geochemical analysis have been produced by various authors – specifically Boutton (1991), Meyers and Teranes (2001), Leng and Marshall (2004) and Leng *et al*. (2006) – an overview of the techniques and the information they provide will be detailed in sections 4.5.1 and 4.5.24.5.1.

4.5.1 Loss-on-ignition and total organic carbon

4.5.1.1 Overview

Ball (1964) determined that the organic matter content of a sediment sample can be estimated by igniting a sample in a muffle furnace at high temperature (ca. 500 °C), with an assumption being made that element C to organic matter is constant. At higher temperatures (900-1000 °C) a secondary reaction occurs where CO_2 is evolved from carbonate, thus allowing an estimation of carbonate content to be made (Dean, 1974). The primary advantage of loss-on-ignition is that it provides a rapid and inexpensive means of estimating the percentage of organic matter and carbonate present within a sample (Dean, 1974). However, there are caveats to the method – for example depending on ignition temperature a sediment sample can also lose volatile salts and structural water in clays giving rise to erroneous results (Bengtsson and Enell, 1986). Heiri *et al*. (2001) highlighted that due to laboratories using different methods for loss-on-ignition (LOI) the range of values for a given sample was very large, thus a standard method was required. Lamb (2004) produced a standardised method to determine the organic and carbonate content of sediments from LOI.

Due to the caveats with LOI, a measure of the total organic carbon (TOC) is preferred to approximate the amount of organic matter present (Meyers and Teranes, 2001). As it is a measure of all organic carbon present in sediment it incorporates the different origins of organic matter, delivery routes, depositional processes, and the degree of preservation. The amount of TOC can be diluted due to the input of minerogenic components (Dean, 1999), which can also lead to changes in TOC values within a lake basin. For example it is more likely that coarse-grained sediment is deposited in the littoral zone than in the deepest part of a lake basin when fine-grained sediment slowly settles, causing lower TOC values due to comparatively rapid sediment accumulation in the littoral zone than in the deepest part of the lake basin (Meyers and Teranes, 2001). With this in mind it can be useful to present TOC data in mass accumulation rates (MARs) rather than as percentages as it provides an improved measure of the delivery and preservation of organic matter (Meyers and Teranes, 2001). Whilst an important measure of organic matter, TOC only provides general information on organic matter – other analyses are required to identify

their sources such as C/N. Total organic carbon measurements have been obtained in Vanuatu and New Caledonia (Wirrmann, *et* al., 2006, 2011a, b).

4.5.1.2 Analytical procedure

The method detailed in Lamb (2004) was applied in this study on contiguous 1 cm subsamples for each site. Briefly, samples were dried in a convection oven overnight at 105 °C to estimate water content, followed by ignition at 550 °C (LOI_{550}) for two hours to estimate organic content, and finally ignited at 950 °C (LOI_{950}) for four hours to estimate carbonate content. Total organic carbon (TOC) was obtained as part of C/N analysis (detailed in full in Section 4.5.2). A direct comparison between LOI_{550} and TOC was taken that validated the method, and a conversion factor between LOI_{550} and TOC values is displayed in Figure 4.2.

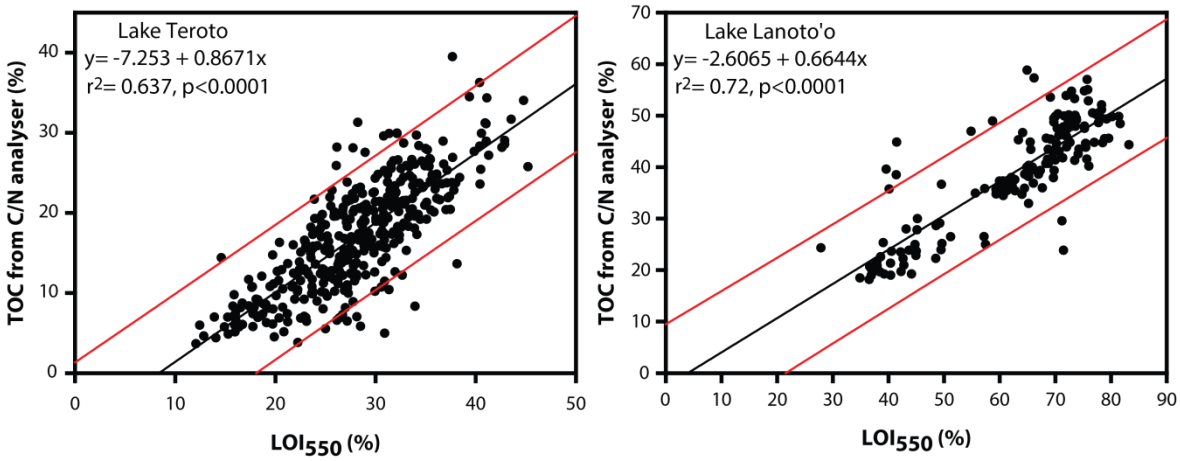

Figure 4.2: Comparison between loss-on-ignition at 550°C (LOI_{550}) and total organic carbon, derived from the element analyser, displaying the conversion factor for both sites. The black line is the linear line of best fit and the red lines are the 95% prediction bands

4.5.2 C/N and total organic carbon isotopes

4.5.2.1 C/N ratios

Using µXRF analysis can help determine increased terrestrial inputs from sediments – for example increased amounts of Ti is often interpreted as indicative of catchment inputs that are derived from the weathering of volcanic rocks (basalts and andesites) (Metcalfe *et al.*, 2010) – but does not indicate the source of organic matter. Increased terrestrial

inputs does not necessarily equate to increased inputs of terrestrially-derived organic matter. A relatively simple analysis that can be used to determine organic matter sources is carbon/nitrogen rations (C/N ratios) which indicate the relative proportions of autochthonous and allochthonous lacustrine organic matter sources (Talbot and Lærdal, 2000). In general terrestrial plants have high amounts of lignin and cellulose – both containing large amounts of carbon – whereas aquatic plants have higher amounts of protein and thus higher amounts of nitrogen (Meyers, 1994). Terrestrial vegetation produce C/N ratios >20 whilst aquatic plants have ratios between 4-10 – values between 10-20 are often interpreted as indicating mixed sources (Meyers and Teranes, 2001).

There are complications with interpreting C/N ratios. In sample preparation inorganic carbon is removed, whereas inorganic nitrogen is not. This is not typically considered a significant issue with C/N ratios because the inorganic nitrogen component is small (Meyers and Teranes, 2001). More noteworthy interpretation problems result from the presence of riparian and emergent aquatic plants that can have C/N ratios similar to terrestrial plants (Lamb *et al*., 2004). Additionally, green algae like *Botryococcus braunii* have particularly high C/N ratios that are similar to terrestrial vegetation (Lamb *et al*., 2004). These highlight that caution is needed when interpreting C/N ratios; nevertheless it can provide important information on changing plant types and productivity (Langdon *et al*., 2010). In El Junco, Galápagos, Conroy *et al*. (2008) interpret higher C/N values and greater C/N variance to indicate a shallower, more ephemeral lake with a greater influx of terrestrial organic matter to the basin floor, whereas lower C/N values suggest a larger algal input due to a more consistently deep lake. Whilst this interpretation is supported by grain-size data, no carbon isotope analyses were undertaken that would have further elucidated the processes operating in the site's carbon cycle.

4.5.2.2 Carbon isotopes of organic matter

Analysis of carbon isotopes in organic matter, specifically carbon isotope analysis of total organic carbon ($\delta^{13}C_{TOC}$), reflects the isotopic signal of the source material. Therefore it is necessary to obtain $\delta^{13}C_{TOC}$ with C/N ratios to determine if the signal is aquatic or terrestrial to fully understand changes in $\delta^{13}C_{TOC}$ values.

4.5.2.2.1 Aquatic-sourced $\delta^{13}C_{TOC}$

If it can be determined that there is low terrestrial input into a lake the $\delta^{13}C_{TOC}$ can indicate within-lake processes associated with aquatic plants and algae. Algae take up carbon from lake water as dissolved CO_2 or HCO_3^- (both referred generally as total dissolved inorganic carbon (TDIC)). If a lake is open and has inflowing water this can alter the TDIC which can be recorded in the $\delta^{13}C_{TOC}$: for example marine TDIC has $\delta^{13}C$ values that are +1 to +3‰ thus increasing the $\delta^{13}C_{TOC}$ value (Boutton, 1991). Further the TDIC isotopic value can also vary due to: 1) the extent in which atmospheric CO_2 is in equilibrium with the water mass; 2) seasonal rates of photosynthesis and respiration; and 3) input of CO_2 from decomposition of ^{13}C-depleted terrestrial detritus (Boutton, 1991).

Most aquatic plants use the C_3 photosynthetic pathway which preferentially takes up ^{12}C causing aquatic plants to have more negative $\delta^{13}C$ values compared to TDIC $\delta^{13}C$. During period of increased productivity the TDIC $\delta^{13}C$ becomes increasingly enriched, which in turn causes the aquatic plants to have more positive $\delta^{13}C$ values over time. Increased productivity can also lead to dissolved CO_2 being limited and aquatic plants using dissolved HCO_3^- which is more positive ($\delta^{13}C$ = 1‰), again leading to increased $\delta^{13}C$ values in the aquatic plants (Meyers and Teranes, 2001). Consequently, when an aquatic source for $\delta^{13}C_{TOC}$ can be determined it can be used to reconstruct past changes in productivity.

4.5.2.2.2 Terrestrial-sourced $\delta^{13}C_{TOC}$

When C/N ratios indicate that carbon is sourced from terrestrial material the values reflect the composition of the surrounding catchment vegetation. Vegetation can be split based on its photosynthetic pathway: most plants and aquatic algae use the C_3 pathway, whereas some grasses in lowland arid regions can use the C_4 pathway. These have distinct kinetic effects on carbon thus producing different $\delta^{13}C$ values. C_3 plants produce $\delta^{13}C$ values of -27‰ on average and C_4 plants produce -13‰ (Meyers and Teranes, 2001). A third photosynthetic pathway exists – Crassulacean acid metabolism (CAM) – that produces $\delta^{13}C$ values ranging from -4 to -20‰ (O'Leary, 1988) however it is unlikely CAM photosynthesisers are present in the tropical Pacific as these are typically found in arid environments. In Figure 4.3 the carbon isotope values of major carbon isotope sources are outlined incorporating an idealized carbon cycle. Also presented in Figure 4.4 is a

diagnostic matrix for determining the source of $\delta^{13}C_{TOC}$ combining C/N ratios and $\delta^{13}C_{TOC}$ values for a sample. Whilst these provide a general overview and diagnostic tool, due to the mixed inputs that are recorded in $\delta^{13}C_{TOC}$ it is necessary to use more specific sources to determine what is driving changes in the $\delta^{13}C_{TOC}$ record.

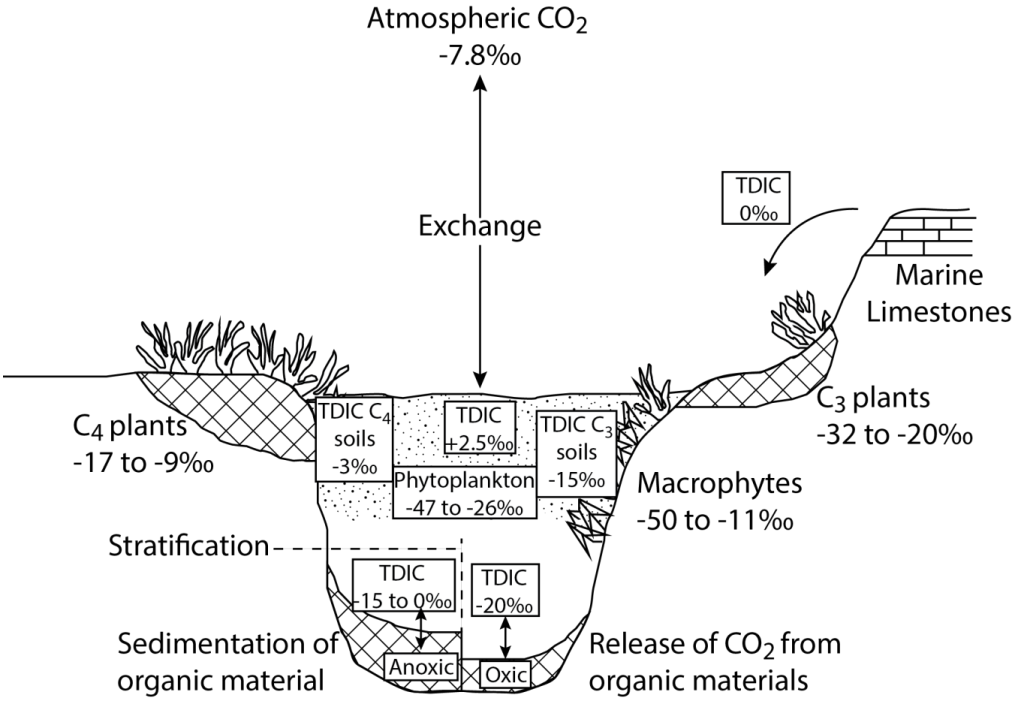

Figure 4.3: Carbon isotope values for principal sources of carbon into lakes, and $\delta^{13}C_{TDIC}$ values that can result from these inputs (Leng *et al*., 2006).

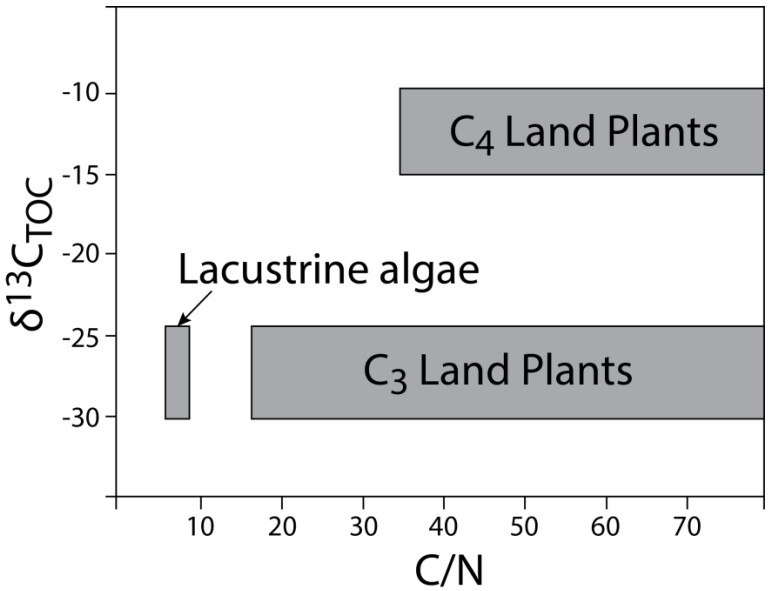

Figure 4.4: Elemental and carbon isotopic values of organic matter from C_3 plants, C_4 plants and lacustrine algae that use CO_2 as their carbon source in photosynthesis (Meyers and Teranes, 2001).

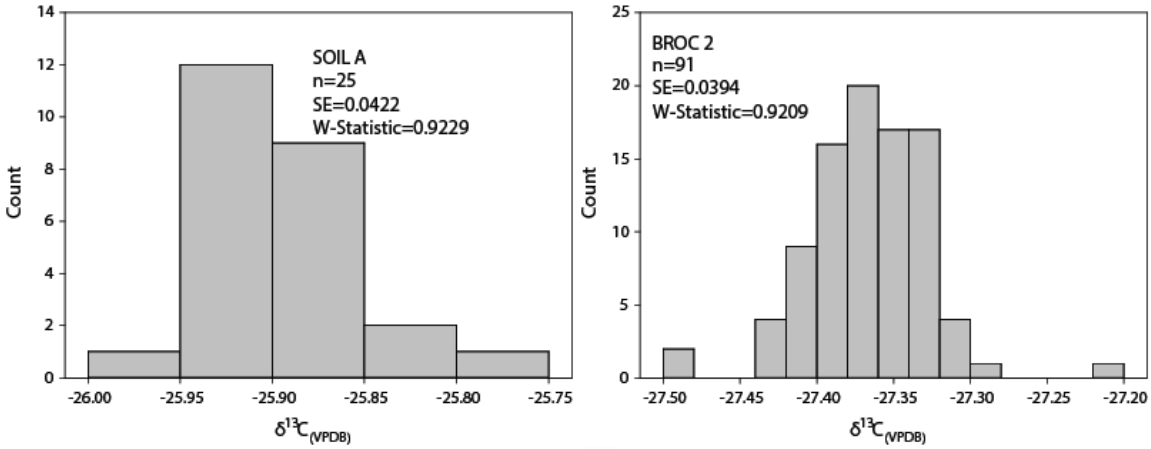

Figure 4.5: $\delta^{13}C$ measurements on internal laboratory standards SOIL A and BROC2, including standard deviations for both standards. Normality is assumed for both due to the sample size.

4.5.2.2.3 Analytical procedure

Sediment cores from the two sites were sub-sampled at 2 cm resolution using a 1 cm^3 sub-sampler and treated with 5% HCl for 12 hours to remove any carbonate present. Samples were placed into containers, filled with 400 ml of deionised water, and spun in a centrifuge at 3000 rpm for 3 minutes, and the supernatant decanted out. This was repeated four times; following this samples were placed in a convection oven at 40 °C overnight until dry. Analyses were performed at the Natural Environmental Research Council Isotope Geosciences Facility. Samples were ground in a pestle and mortar, and sub-samples of powdered samples were placed into tin capsules and weighed before combustion. Carbon/nitrogen analysis was undertaken using a Thermo Finnegan Delta +XL followed by $^{13}C/^{12}C$ analysis using a VG optimate with Carlo Erda NA1500. In-house standards were used throughout and the values corrected to $\delta^{13}C_{VPDB}$ (Vienna Pee Dee Belemnite) standard. No errors are reported as analysis of standards throughout analysis show very low analytical error (Figure 4.5).

4.5.3 Compound-specific isotope analysis

4.5.3.1 Overview

Biological markers, or biomarkers, are compounds or compound classes that originated in living organisms and can be attributed to a particular source (Peters *et al*., 2005; Castañeda and Shouten, 2011). Typically biomarkers are lipids that occur in distinctive distributions in different organic matter sources, and have the foremost advantage over bulk geochemical methods of permitting the separation and concurrent analysis of aquatic, sedimentary and terrestrial constituents (Bianchi and Canuel, 2011). Combining this advantage with lake records that commonly have a range of lipid compounds sourced from autochthonous and allochthonous sources, conditions in both the water column and the catchment can be determined – this cannot always transpire due to a lack of preservation of non-siliceous algae or carbonate (Pearson *et al*., 2007). Moreover, lipid biomarkers can exist in the sedimentary record over millions of years and are largely resistant to diagenetic alteration due to the hydrogen atoms being covalently bonded to carbon atoms which are not easily exchanged at temperatures below 100 °C (Sauer *et al*., 2001; Sessions *et al*., 2004). At present biomarkers are largely used as a semi-quantitative tool for reconstructing environmental conditions. This is due to the fractionation that occurs in biosynthesis between the isotope source and produced biomarker not being fully understood, but also due to it varying between different plant types: for example angiosperms and gymnosperms (Chikaraishi and Naraoka, 2003). Thus the values recorded indicate relative changes in environmental conditions and cannot be used to reconstruct source water δ^2H or inorganic $\delta^{13}C$.

In most organisms the most abundant lipids are fatty acids, often referred to in the literature as *n*-alkanoic acids (Volkman *et al*., 1998) (Figure 4.6). The *n*-alkanoic acids are straight-chain hydrocarbons, with the main chain length, carbon number distributions and isotopic composition dependent on the source organism (Castañeda and Schouten, 2011). Specifically, *n*-alkanoic acids are dominated by even-numbered chain lengths, with the short-chain *n*-alkanoic acids (C_{16} and $C_{18)}$ often attributed to an aquatic algal source, mid-chain lengths (C_{20} to C_{24}) attributed to aquatic macrophytes (Ficken *et al*., 2000), and long-chain *n*-alkanoic acids (C_{26} and longer) from higher terrestrial plants (Eglinton and Hamilton, 1967). However, exceptions do exists: for instance birch leaves have been

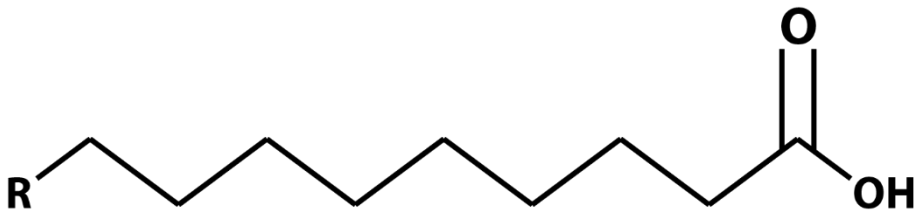

Figure 4.6: Chemical structure of *n*-alkanoic acids.

found to contain significant concentrations of C_{23} *n*-alkane (Sachse *et al*., 2006), and C_{27} and C_{29} *n*-alkane have been noted from immersed aquatic macrophytes and *Botryococcus braunii* (Lichtfouse *et al*., 1994; Aichner *et al*., 2010). Whilst not the same biomarker, *n*-alkanoic acids and *n*-alkanes are produced in the same biosynthetic mechanism thus these observations are pertinent for interpreting *n*-alkanoic acid results. Both *n*-alkanoic acids and *n*-alkanes are synthesised in photosynthesis, ultimately produced through elongation and decarboxylation of *n*-alkyl compounds (Chikaraishi and Naraoka, 2007).

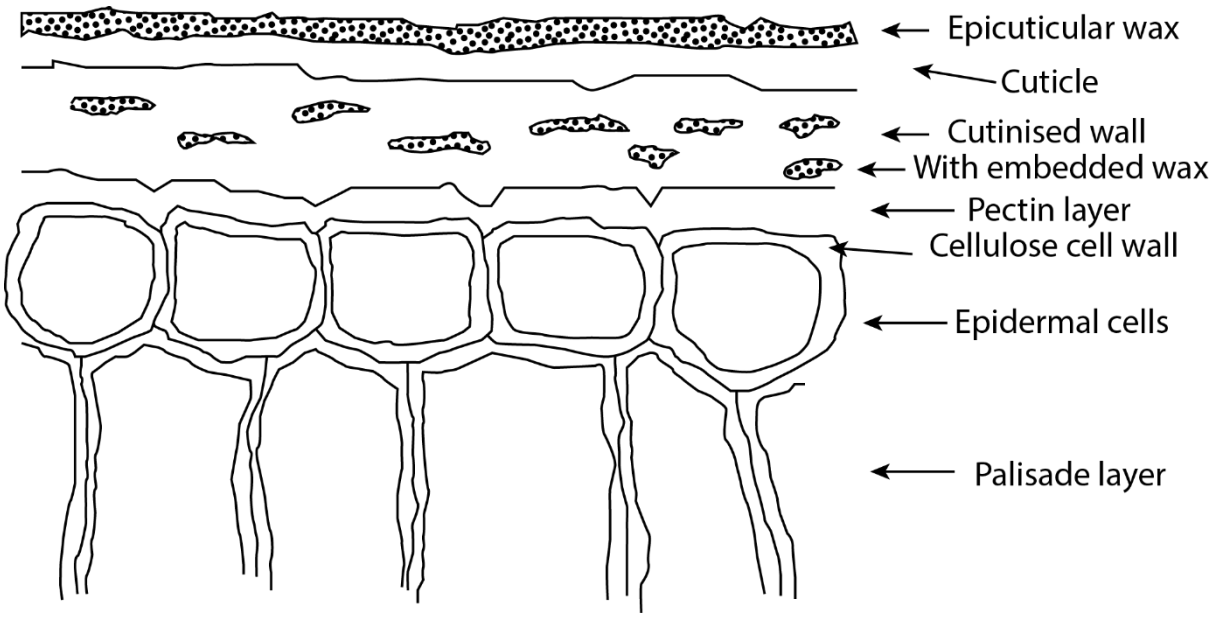

Figure 4.7: Structure of a plant's epicuticle (Eglinton and Hamilton, 1967).

Long-chain *n*-alkanoic acids are the main components of epicuticular leaf waxes of higher plants, being part of the cutin to which the waxes are bound (Eglinton and Hamilton, 1967) (Figure 4.7). Eglinton and Hamilton (1967) noted that leaf waxes, and by extension *n*-alkanoic acids, are present in substantial amounts in soils – Huang *et al*. (2004) went further and determined that *n*-alkanoic acids are a significant constituent of lake sediments. Their transport into lake sediments is considered to be via surface run-off or wind erosion (Casataneda and Schouten, 2011). As is common with lipid biomarkers, *n*-alkanoic acids are resistant to biodegradation in sediments (Cranwell, 1981).

4.5.3.2 Compound-specific carbon isotope analysis

In section 4.5.2.2, it was outlined that the $\delta^{13}C_{TOC}$ is used to determine changes in aquatic productivity or, where a dominant terrestrial source can be established, changes in C_3 and C_4 vegetation. However, examining the $\delta^{13}C_{TOC}$ can cause erroneous interpretations due to the signal being an amalgamation of aquatic, bacterial and terrestrial sources. Examining the $\delta^{13}C$ of biomarkers can provide more detailed and specific information in relation to the $\delta^{13}C$ of source organisms. For *n*-alkanoic acids the $\delta^{13}C$ of short-chain *n*-alkanoic acids delineates changes in the $\delta^{13}C$ of aquatic sources, whereas the $\delta^{13}C$ of long-chain *n*-alkanoic acids is related to the $\delta^{13}C$ of terrestrial sources. Combining the $\delta^{13}C$ of aquatic- and terrestrial-sourced biomarkers with $\delta^{13}C_{TOC}$ allows for drivers of $\delta^{13}C_{TOC}$ to be determined.

4.5.3.2.1 Primary productivity and short-chain *n*-alkanoic acids

Aquatic communities have the ability to utilise different carbon sources depending on CO_2 availability in the lake: when CO_2 is freely available dissolved CO_2 is assimilated, and when CO_2 [CO_2(aq)] is limited to assimilation of bicarbonate (HCO_3^-) (Allen and Spence, 1981; Prins and Elzenga, 1989). If CO_2 demand exceeds supply, for instance during algal blooms, then isotopic discrimination against ^{13}C decreases causing increased assimilation of ^{13}C and a consequent increase of $\delta^{13}C$ of the consuming organism (Papadimitrou *et al*., 2005). An increase in $\delta^{13}C$ of short-chain alkanoic acids, where an aquatic source can be concluded, can be construed in relation to carbon-limitation in the lake (Aichner *et al*., 2010). This can be caused by low partial pressure of atmospheric CO_2 (unlikely to be a factor in the Holocene where it has remained relatively constant compared to changes over glacial-interglacial timescales (Indermühle *et al*., 1999; Monnin *et al*., 2001)) and side effects of aridity including high water temperatures, pH or salinity; physical barriers to diffusion such as oil films produced by *Botryococcus braunii*; and high aquatic productivity due to enhanced nutrient supply (Street-Perrot *et al*., 1998, 2004). Productivity can be inferred by determining the mean accumulation rates of aquatic biomarkers which can also assist in understanding shifts in $\delta^{13}C$ (Castañeda *et al*., 2009a). It is salient to note that whilst short-chain *n*-alkanoic acids are more source-specific than bulk organic matter they are likely to be sourced from multiple organisms making interpretation of their $\delta^{13}C$ record complicated (Castañeda and Schouten, 2011).

4.5.3.2.2 C_3 vs. C_4 vegetation and long-chain *n*-alkanoic acids

As mentioned in section 4.5.2.2.2 C_3 and C_4 plants can be differentiated by their carbon isotopic composition due to utilising distinct photosynthetic pathways. Specifically, C_3 plants generally use a Calvin-Benson cycle that is typified by using ribulose bisphosphate carboxylase oxidase, whereas C_4 plants use a Hatch-Slack cycle characterised by phoenol-pyruvate carboxylase (Castañeda and Schouten, 2011). These different pathways have varying kinetic effects on carbon isotopes between bulk plant tissue and CO_2 as previously mentioned.

The $\delta^{13}C$ values of *n*-alkyl compounds sourced from terrestrial higher plants are recognised to be ca. -35 ± 5‰ for C_3 plants and ca. -20 ± 5‰ for C_4 plants (Collister *et al*., 1994; Chikaraishi and Naraoka, 2007). However there is considerable variation between plant groups. For instance, Chikaraishi and Naraoka (2003) established that angiosperms have more negative $\delta^{13}C$ values for *n*-alkyl compounds relative to gymnosperms. This difference in values could be due to: 1) molecular flux among *n*-alkyl compounds; 2) leaf growth rate; 3) water-efficiency; and 4) kinetic isotope effects of key biochemical reactions (Chikaraishi *et al*., 2004a). The results of Chikaraishi and Naraoka (2003) were further substantiated by Diefendorf *et al*. (2010) who noted that a large range of leaf $\delta^{13}C$ values occur in C_3 plants that they conclude are the result of plant functional types and mean annual precipitation. Nonetheless, general trends in more negative (less negative) $\delta^{13}C$ for *n*-alkyl compounds – including *n*-alkanoic acids – suggest decreased (increased) inputs from C_4 plants in the sedimentary record. This is of primary interest in Africa where changes in aridity cause large shifts in C_3 and C_4 plants (for instance Castañeda *et al*., 2007, 2009a, 2009b). Whilst vegetation changes are known to have occurred due to changes in aridity in the South Pacific (Parkes, 1994) it is currently unknown whether these are restricted to changes in C_3 vegetation or shifts to C_4 vegetation from C_3. Moreover no $\delta^{13}C_{TOC}$ analyses or $\delta^{13}C$ analyses on biomarkers have been undertaken at present in the Pacific region (AD 2017). Consequently a thorough understanding of the carbon cycle in Pacific sites is lacking in comparison to other regions.

It is apparent that understanding $\delta^{13}C$ records from biomarkers is particularly difficult because of the variety of factors affecting their values, and has led to uncertain interpretations of the results (for example Castañeda *et al*., 2009a). Nevertheless, by

using both aquatic and terrestrial-sourced $\delta^{13}C$ biomarker records an improved understanding of changes in carbon source and primary productivity can be obtained. This is vital for understanding the biomarker δ^2H record as C_3 and C_4 plants fractionate meteoric water differently leading to changes in biomarker δ^2H values (Smith and Freeman, 2006).

4.5.3.3 Compound-specific hydrogen isotope analysis

The hydrogen isotopic composition of plant leaf waxes (δ^2H_{lw}) – including the long-chain *n*-alkyl compounds that comprise the waxes – is largely controlled by the hydrogen isotopic composition of a plant's source water (δ^2H) (Sauer *et al*., 2001). For detailed reviews on hydrogen isotope analysis on biomarkers the reader is directed to Sachse *et al*. (2012) and Castañeda and Schouten (2011).

4.5.3.3.1 Environmental controls on source water δ^2H

The δ^2H of precipitation varies both spatially and temporally and can be largely explained by Rayleigh processes during condensation and evaporation (Gat, 1996). Precipitation is depleted in ^2H relative to seawater due to the lighter ^1H evaporating faster than ^2H. When precipitation falls, it is enriched in ^2H compared to the air mass it is sourced from resulting in the air mass's vapour being depleted in ^2H (Dansgaard, 1964). In the seminal work of Dansgaard (1964) three primary environmental factors that control precipitation δ^2H were identified:

1. Continental effect: the precipitation δ^2H values are increasingly negative as an air mass progresses inland over a continent due to the preferential loss of ^2H;
2. Temperature effect: in areas with large temperature variability the precipitation δ^2H is strongly correlated with temperature;
3. Amount effect: typically the main control on δ^2H in the tropics. When there is little temperature variation but strong seasonality rainfall the δ^2H of precipitation is related to the amount of rainfall. With high precipitation the δ^2H is more negative.

In the South Pacific all land masses are islands, thus the continental effect is not a control on precipitation δ^2H. Similarly, temperature changes are small – further detailed in Chapter 3 – consequently the temperature effect is not a control on δ^2H in the South

Pacific. Precipitation seasonality occurs in this region due to the contraction and expansion of the SPCZ causing large differences in the amount of rainfall: therefore the amount effect is likely the primary control on precipitation δ^2H in this region. This is further explored in Chapter 6.

4.5.3.3.2 Controls on short-chain *n*-alkanoic acid δ^2H

Short-chain *n*-alkanoic acids produced by algae are theoretically ideal to reconstruct the δ^2H of lake water as all hydrogen is sourced from the lake water and algae do not transpire, the latter of which reduces the complication of kinetic isotope effects on the short-chain *n*-alkanoic acid δ^2H value (Zhang and Sachs, 2007). Various studies have demonstrated the ability of algal lipid δ^2H with water δ^2H ($R^2 > 0.99$) (for example Zhang and Sachs, 2007), and core top sediments also having positive correlations with the δ^2H of the lake source water (Sauer *et al*., 2001; Huang *et al*., 2004; Sachse *et al*., 2004; Hou *et al*., 2007; Zhang and Sachs, 2007; Henderson *et al*., 2010).

Nevertheless, Zhang and Sachs (2007) found large differences in the hydrogen isotopic fractionation of an individual lipid between families of green algae, and comparatively small difference in the hydrogen isotopic fractionation between different species of green algae. The corollary of this it that changes in short-chain *n*-alkanoic acid δ^2H values may be due to changes in the algae producing them rather than due to changes in lake water δ^2H. Despite this, it can be the case in some lakes – such as Blood Pond, Massachusetts – that a singular source can be the principal producer of short-chain *n*-alkanoic acids making them suitable to reconstruct lake water δ^2H (Gao *et al*., 2011). With this in mind combining $\delta^{13}C$ analysis on short-chain *n*-alkanoic acid with δ^2H analysis would help determine whether changes in carbon source, and by extension source organism, are resulting in changes in δ^2H values rather than changes in lake water δ^2H. Further, if trends in short-chain and long-chain *n*-alkanoic acid δ^2H values are similar it would suggest a similar principal control due to the different organisms, specifically aquatic and terrestrial, that primarily produce them.

As well as changes in source organism affecting short-chain *n*-alkanoic acid δ^2H values, environmental factors such as temperature, salinity, growth rate and nutrient availability can also influence $^2H/^1H$ fractionation (Castañeda and Schouten, 2011). Zhang *et al*. (2009) determined that growth rate likely does not influence $^2H/^1H$ fractionation in the

lipids synthesised through acetogenic synthesis, i.e. *n*-alkanoic acids. Temperature does affect hydrogen fractionation, with this considered being due, in part, to enzymes that synthesise lipids in different organisms having different responses to temperature (Zhang *et al*., 2009; Garcin *et al*., 2012). Further increases in salinity cause increased in δ^2H values for lipids which would need to be accounted for (Schouten *et al*., 2006; Sachse and Sachs, 2008; Sachs and Schwab, 2011). With Lake Teroto's connection to the sea the effect of salinity will need to be considered. Parkes (1994) produced a diatom record for Lake Teroto which can assist in understanding when changes in salinity are affecting the short-chain *n*-alkanoic δ^2H values. By combining the various lines of evidence – such as $\delta^{13}C$ analysis on the short-chain *n*-alkanoic acids, comparing the trends in δ^2H values for the short-chain and long-chain *n*-alkanoic acids, and using other proxy evidence – a palaeoenvironmental and palaeoclimatic signal could be disentangled form environmental factors influencing the short-chain *n*-alkanoic δ^2H values.

4.5.3.3.3 Controls on long-chain *n*-alkanoic acid δ^2H

The main source of water for terrestrial plants – and consequently for *n*-alkanoic acids – is soil water, which in turn is sourced from precipitation. Therefore it is expected that the δ^2H of soil water should be the same as the δ^2H of precipitation; however in open, arid environments evaporative enrichment can alter the values of δ^2H (Riley *et al*., 2002; Polissar and Freeman, 2010). Despite this many studies have shown that the δ^2H of terrestrial *n*-alkyl lipids tracks the δ^2H of precipitation (for example Sauer *et al*., 2001; Sachse *et al*., 2004; Hou *et al*., 2008).

It is important to understand the possible sources of fractionation that occur in the biosynthesis of *n*-alkanoic acids from precipitation. Most studies indicate that fractionation occurs in leaf water as a result of transpiration (Hou *et al*., 2008); nevertheless this has been questioned by McInerney *et al*. (2011) who suggested that soil evaporation appeared more important than transpiration in determining the δ^2H for a taxa's *n*-alkane δ^2H value – and by extension *n*-alkanoic acid δ^2H value. This difference in sources of hydrogen is important due to how the hydrogen is incorporated into *n*-alkyl lipids in biosynthesis and the fractionation that occurs from source water to *n*-alkyl lipid synthesis (Figure 4.8).

Akin to carbon, hydrogen is incorporated into *n*-alkyl lipids when they are synthesised along the acetogenic pathway (Chikaraishi and Naraoka, 2003, 2004a, 2004b; Chikaraishi *et al*., 2007). Consequently there are differences in the fractionation of hydrogen between different plant types. C_4 plants were found to produce more positive δ^2H values than C_3 plants (Smith and Freeman, 2006), with Liu *et al*. (2006) and Chikaraishi *et al*. (2007) finding that shrubs, trees, herbs and grasses also record different δ^2H for *n*-alkyl lipids even on the same site. Kahman *et al*. (2013a) suggested that differences between angiosperm plants in the δ^2H values of *n*-alkyl lipids was due to differences in leaf growth and development. However Liu *et al*. (2006) and Liu and Yang (2008), whilst agreeing with findings of Kahman *et al*. (2013a), argue that differences in *n*-alkyl δ^2H values in plants is a result of different water acquisition systems. Specifically that woody plants have longer and deeper roots thus utilising water from deeper soil horizons that contain water with less negative δ^2H compared to shallower soil horizons (Dawson and Ehleringer, 1991; Liu and Yang, 2008).

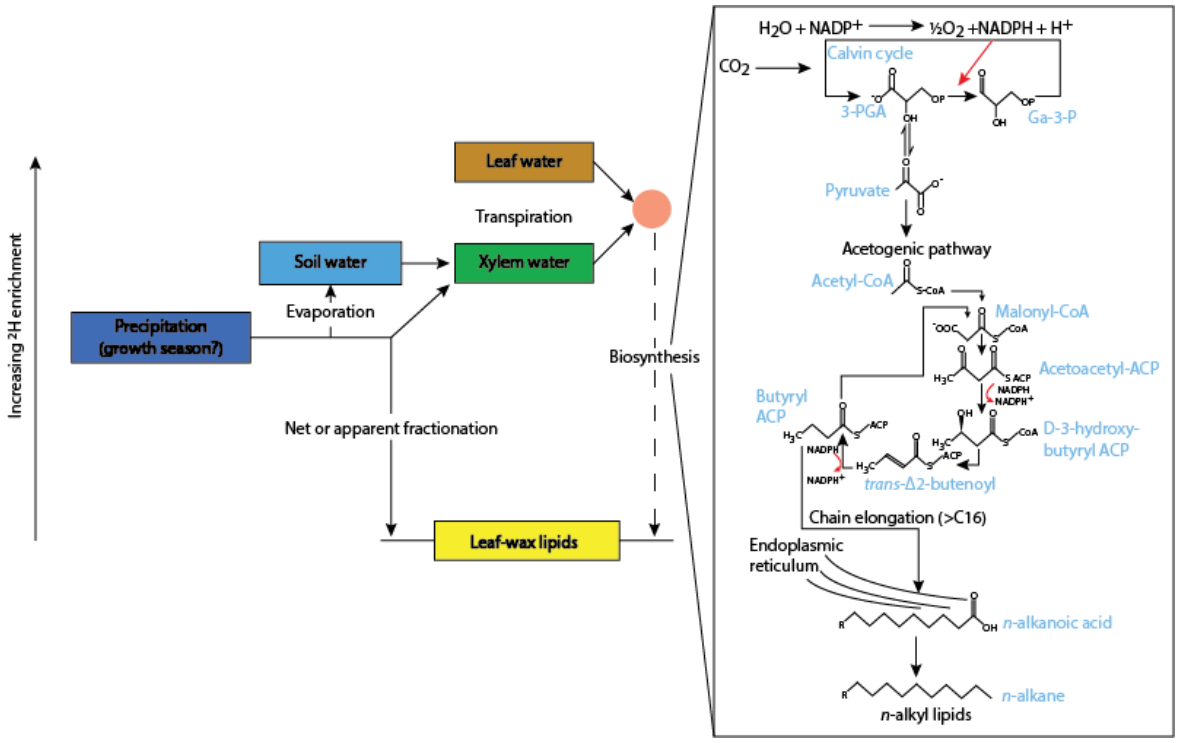

Figure 4.8: Overview of the acetogenic pathway for lipid biosynthesis in photosynthesising organisms. This pathway has been simplified to focus on *n*-alkyl biosynthesis that leads to the production of *n*-alkanoic acids. The red dot indicates the biosynthetic water pool – a potential mixture of different water pools within the leaf and the ultimate source of hydrogen for lipid biosynthesis (adapted from Sachse *et al*. (2012)).

Despite these differences in δ^2H values recorded in *n*-alkyl lipids Liu and Yang (2008) and Kahman *et al*. (2013b) concluded that the δ^2H recorded in sedimentary leaf wax *n*-alkanes – and by extension *n*-alkanoic acids – reflect qualitative hydrological information that is primarily controlled by precipitation δ^2H values. Garcin *et al*. (2012) recommend that combining both δ^2H and $\delta^{13}C$ of biomarkers is necessary to differentiate between photosynthetic pathway for plants and therefore the source of hydrogen used during lipid biosynthesis. With the results of Liu and Yang (2008) in mind, shifts in δ^2H values should also be interpreted alongside a pollen record where possible so that changes in δ^2H values can be determined to be the result of changes in precipitation δ^2H values and not the result of shifts in the dominant vegetation producing the *n*-alkyl lipids.

Douglas *et al*. (2012) found that there was no relationship between the δ^2H of precipitation and the δ^2H of *n*-alkanoic acids, but a weak significant relationship between aridity and δ^2H of *n*-alkanoic acids exists. Whilst important to consider for Lake Lanoto'o and Lake Teroto, the effect of aridity on fractionation is the same as the of the amount effect – i.e. when more arid δ^2H becomes less negative and vice versa, similarly with less precipitation amount δ^2H becomes less negative and vice versa. As the trends are the same, overall interpretations on what the δ^2H of *n*-alkanoic acids indicate climatically will still relate to whether there is an increase or decrease in precipitation amount. Furthermore the AI, calculated as mean annual precipitation/mean annual potential evapotranspiration, for both sites indicates they are both humid over the period AD 1950-2000 (Trabbuco and Zomer, 2009) (sections 3.2.6 and 3.3.6). This suggests that aridity has a minimal impact on these sites in modern times. With this in mind an assumption is made in this study that palaeoclimatic reconstructions using δ^2H of *n*-alkanoic acids can be relied upon to infer changes in the amount of precipitaiton.

Douglas *et al*. (2014) outlined that long-term soil storage of plant waxes can input pre-aged plant waxes into sedimentary records, complicating interpretations of δ^2H from *n*-alkanoic acids for samples taken at a high temporal resolution (e.g. decadal). However, sediment cores obtained from lakes with small catchments – like Lake Teroto and Lake Lanoto'o – which receive most of their terrigenous organic carbon from fresh vegetation, and are fed by surface runoff, will all reduce the amount of pre-aged plant waxes entering the sediment record (Parkes, 1994; Douglas *et al*., 2014). With Lake Teroto and Lake Lanoto'o both having small catchments, and no evidence of groundwater input (sections

3.2.6 and 3.3.6), it is considered that the effect of pre-aged plant waxes is minimal. Nevertheless this cannot be completely discounted from impacting the plant wax records from the two sites.

Studies in the Pacific region have primarily focussed on obtaining δ^2H using aquatic biomarkers – for example Sachs *et al*. (2009), Smittenberg *et al.* (2011), Atwood and Sachs (2014), Zhang *et al*. (2014), and Nelson and Sachs (2016). Therefore at present (2017) there have been no palaeoclimatic reconstructions undertaken in the Pacific region using terrestrial higher plant biomarkers, making this study the first to use a terrestrial higher plant biomarker to obtain a δ^2H record in the Southwest Pacific region.

4.5.3.4 Analytical procedure

4.5.3.4.1 Lake Teroto samples

Sub-samples were taken from cores and freeze-dried. Isolation of TLEs was done using 15 ml of DCM:MeOH in a 9:1 ratio and a MARS 5 microwaves assisted solvent extraction system (CEM Microwave Technology Ltd., UK). A temperature programme that heated to 70 °C in 2min and held at 70 °C for 5 min was applied. Total lipid extracts were dried down using a rotary evaporator and nitrogen stream, after which the sample TLE was saponified with 6% KOH. Neutral compounds were separated from the sample using hexane. The remaining sample was acidified with HCl and the acid fraction subsequently removed using hexane. The acid fraction was esterified using BF_3/MeOH to convert *n*-acids into fatty acid methyl esters (FAMEs) – FAMEs were removed using hexane and dried down under N_2 gas. All sample preparations for Lake Teroto were undertaken at Newcastle University.

Analyses of acid extracted FAMEs were performed using an Agilent 6980 gas chromatograph, equipped with an autosampler. The flame ionisation detector (FID) used to monitor column effluent was constantly heated at a temperature of 300 °C. FAMEs were introduced to the system *via* split-splitless injection injection (1 µL) operating in splitless mode with a splitless time of 2 minutes. The analytical column was a 50 m x 0.32 mm fused silica capillary column coated (0.17 µm) with a 100% dimethylpolysiloxane non-polar stationary phase (Rtx-1, Restek). The GC temperature programme was set to hold at 50 °C for 1 min, followed by a temperature ramp to 170 °C at 10 °C/min and then to

300 °C at 3 °C/min before a final isothermal hold at 300 °C for 10 min. Helium, set to constant flow of 2.0 mL/min, was used as the carrier gas. Data was acquired using DataApex Clarity (version 2.6.2.226).

GC-MS analyses of FAME aliquots were performed using a ThermoScientific Trace 1300 gas chromatograph couple to an ISQ single quadrupole mass spectrometer. Samples (1 µL) were introduced via a programmable temperature vaporising (PTV) injector, set to splitless mode with a splitless time of 2 minutes, onto a 50 m x 0.32 mm fused silica capillary column coated (0.17 µm) with an 100% dimethylpolysiloxane stationary phase (Rtx-1, Restek) for non-polar analyses. The GC temperature programme was set to hold at 50°C for 1 min, followed by a temperature ramp to 170 °C at 10 °C/min and then to 300 °C at 3 °C/min before a final isothermal hold at 300 °C for 10 min. Helium, set to a constant flow of 2 mL/min, was used as the carrier gas. The MS was operated in electron ionisation (EI) mode operating with an electron energy of 70 eV, a GC interface temperature of 300 °C and a source temperature of 300 °C. The emission current was set to 150 µA and the MS was set to acquire in the range of *m/z* 50-650 at 2 scans/s in full scan mode. The data acquisition and processing were carried out using XCalibur software, version 3.0. Compounds were identified by comparison with authentic standards or the NIST mass spectra library (version 2.0) and other reference to external sources such as The Lipid Library (www.lipidlibrary.aocs.org).

Compound specific $\delta^{13}C$ determinations on C_{16}, C_{18} and C_{26} alkanoic acids were performed using an Agilent Technologies 7890A gas chromatograph coupled to an IsoPrime 100 mass spectrometer *via* a GC5 interface (IsoPrime). Samples (1 µL) were introduced via a split/splitless injector, operating in splitless mode with a splitless time of 2 minutes, onto a 50 m x 0.32 mm fused silica capillary column coated (0.17 µm) with a 10 % dimethylpolysiloxane stationary phase (HP-1, Agilent Technologies). The GC temperature programme was set to hold at 50 °C for 1 min, followed by a temperature ramp to 170 °C at 10 °C/min and then to 300 °C at 3 °C/min before a final isothermal hold at 300 °C for 10 min. Helium was used as a carrier gas and maintained at a constant flow of 2 mL/min. The combustion reactor consisted of a quartz tube filled with copper oxide pellets and was maintained at a temperature of 850 °C. Instrument accuracy was monitored and precision determined using an external FAME standard mixture (C_{11}, C_{13}, C_{16}, C_{21} and C_{23}) of known isotopic composition. Samples were run in duplicate and an average taken. The

$\delta^{13}C$ values are the ratios $^{13}C/^{12}C$ expressed relative to the Vienna Pee Dee Belemnite (VPDB), calibrated using a quaternary CO_2 reference gas of known isotopic composition. Precision was determined to be ±0.3‰. Data processing was carried out using Ion Vantage software (version 1.5.6.0, IsoPrime). As the $\delta^{13}C$ for the esterification agent was not obtained a correction for the addition of one C added during methylation to the C_{16}, C_{18}, and C_{26} *n*-acid $\delta^{13}C$ value has not been undertaken for this site. As the trends will be the same a qualitative interpretation on changes in the $\delta^{13}C$ values is sufficient to determine palaeoenvironmental changes. The mean values and standard deviations are reported for each sample.

For $\delta^{2}H$ determinations each sample was first dissolved in a solution of hexane which contained sacrificial compounds ethyldecanoate and pentadecane at ca. 0.3 mg/cm^3. Compound-specific $\delta^{2}H$ determinations were performed using a ThermoScientific Trace 2000 gas chromatograph coupled to an ThermoScientific Delta V *via* a GCIsolink and Conflow IV interface. Samples (1 µl) were introduced via a programmable temperature vaporising (PTV) injector, set to splitless mode with a splitless time of 2 minutes, onto a 30 m x 0.25 mm fused silica capillary column coated (0.25 µm) with an 100% dimethylpolysiloxane stationary phase (ZB-1, Phenomenx) for non-polar analyses. The GC temperature programme was set to hold at 50 °C for 1 min, followed by a temperature ramp to 120 °C at 80 °C/min and then to 300 °C at 3°C/min before a final isothermal hold at 300 °C for 10 min. Helium was used as a carrier gas and maintained at a constant flow of 2 mL/min. The thermal conversion reactor comprised an empty ceramic tube maintained at a temperature of 1450 °C. All analyses were conducted in duplicate. The instrument performance was evaluated and a H_3^+ factor calculated on a daily basis using H_2 reference gas (stable and <2 ppm/mV) (Sessions *et al*., 2001). Data were initially calibrated to two H_2 reference peaks injected directly into the ion source, before being normalized using the equation of a line from a plot of measured versus known $\delta^{2}H$ values for a standard suite of 15 *n*-alkanes (C_{16}-C_{30}; Mixture B3, Arndt Schimmelmann, University of Indiana) which was injected prior to every two sample runs. Peak heights <50 mV identified on the GC-IRMS were below the cutoff and not considered to avoid size-dependent $\delta^{2}H$ effects (Polissar *et al*., 2009). Instrument error was typically less than 5‰, calculated using the same *n*-alkane standard. As the $\delta^{2}H$ for the esterification agent was not obtained a correction for the addition of three Hs added during methylation to the C_{16},

C_{18}, and C_{26} *n*-acid δ^2H value has not been undertaken for this site. As the trends will be the same a qualitative interpretation on changes in the δ^2H values is sufficient to determine palaeoenvironmental and palaeoclimatic changes. All $\delta^{13}C$ and δ^2H analyses for Lake Teroto were undertaken at the Organic Geochemistry Unit, Bristol.

4.5.3.4.2 Lake Lanoto'o samples

Sub-samples were taken from cores and freeze-dried. A standard was added to the freeze-dried sediment (50 µl of C_{36} *n*-alkane) prior to isolation of the total lipid extracts (TLEs) using a Dionex ASE 200 accelerated solved extractor with three cycles of dichloromethane (DCM) and methanol (MeOH) in a 9:1 ratio at 100 °C and 1500 psi. Total lipid extracts were collected in 60ml ASE vials and dried under N_2 using a Turbo-vap system (Caliper, Hopkinton, USA). The resultant TLE was saponified using 1N KOH. Saponified TLE was separated into neutral and acid fractions using column chromatography over 5% aminopropyl silica gel (500 mg) with 8 ml DCM:isopropyl alcohol (3:1) (neutral fraction), followed by 6 ml 4% acetic acid in diethyl ether (acid fraction), followed by elution of the polar fraction with 6ml MeOH. The acid fraction was then methylated using a 10:1 acetyl chloride:MeOH, with the MeOH being gas chromatography grade and having a known isotopic composition. The methyl chloride fraction, containing the FAMEs was dried under N_2 gas and redissolved in toluene prior to analysis.

FAMEs were assigned using an Agilent 6890N GC instrument coupled to an Agilent 5975 Mass Selective Detector (Samples were injected in splitless mode at 300 °C using helium carrier gas at 1.5 mL/min) and quantified using an Agilent 6890N GC-FID instrument. The oven temperature programme began at 110 °C for 3 min after sample injection, then increased to 170 °C at 15 °C/min, then to 325 °C at 5 °C/min where it was held for 24 min. Sample dilution required for isotope analysis was determined by quantification estimates based on the relative areas of unknown peaks to that of a 5α-cholestane internal standard of known concentration that was added to each sample prior to GC-MS analysis.

The $\delta^{13}C$ composition of C_{16}, C_{18} and C_{26} *n*-alkanoic acids (as FAMEs) was determined using an Agilent Technologies 7890A gas chromatograph coupled to an IsoPrime 100 mass spectrometer via a GC5 interface (IsoPrime). Samples (1 µL) were introduced *via* a split/splitless injector, operating in splitless mode with a splitless time of 2 minutes, onto a 50 m x 0.32 mm fused silica capillary column coated (0.17 µm) with a 100%

dimethylpolysiloxane stationary phase (HP-1, Agilent Technologies). The GC temperature programme was set to hold at 50 °C for 1 min, followed by a temperature ramp to 170°C at 10 °C/min and then to 300 °C at 3 °C/min before a final isothermal hold at 300 °C for 10 min. Helium was used as a carrier gas and maintained at a constant flow of 2 mL/min. The combustion reactor consisted of a quartz tube filled with copper oxide pellets and was maintained at a temperature of 850 °C. Instrument accuracy was monitored and precision determined using an external FAME standard mixture (C_{11}, C_{13}, C_{16}, C_{21} and C_{23}) of known isotopic composition. Samples were run in duplicate and an average taken. The $\delta^{13}C$ values are the ratios $^{13}C/^{12}C$ expressed relative to the Vienna Pee Dee Belemnite (VPDB), calibrated using a quaternary CO_2 reference gas of known isotopic composition. Precision was determined to be ±0.3‰. Data processing was carried out using Ion Vantage software (version 1.5.6.0, IsoPrime). The C_{16}, C_{18} and C_{26} *n*-acid $\delta^{13}C$ values were corrected for the addition of one C (of known $\delta^{13}C$ value) during methylation using a mass balance calculation. The mean values and standard deviations are reported for each sample. All $\delta^{13}C$ analyses were undertaken at the Organic Geochemistry Unit, Bristol.

The hydrogen isotope composition of C_{26} *n*-acid (as a FAME) was determined using a Thermo Trace GC Ultra with an Agilent VF17 column (60m x 0.25mm x0 .25µm) and a pyrolysis reactor. The oven temperature programme began at 120°C at sample injection, then increased to 175 °C at 20 °C/min, then to 325 °C at 2.5 °C/min, followed by a 10 min hold at 325 °C. The GC instrument was coupled to a Finnigan Delta V Plus IRMS instrument. All analyses were performed in triplicate. Instrument performance was evaluated and a H_3^+ factor calculated on a daily basis using H_2 reference gas (stable and <5 ppm/mV) (Sessions *et al*., 2001), and a standard of *n*-alkanes (nC_{26}, nC_{32}, and nC_{36}) of known δ^2H values (standards from Arndt Schimmelmann at Indiana University). Peak areas <15 V·s were below the cutoff identified on the GC-IRMS were not considered to avoid size-dependent δ^2H effects (Polissar *et al*., 2009). All isotopic peaks were initially evaluated within the Isodat 2.0 software relative to a calibrated reference gas. Further corrections were undertaken based on the regression of Isodat-reported δ^2H values of *n*-alkane standards and their accepted values to maintain similar treatment of standards and samples. This also corrects for potential scale compression or stretching that can result from the one-point referencing to VSMOW performed by the Isodat software. The C_{26} *n*-acid δ^2H value was corrected for the addition of three Hs (of known δ^2H value)

during methylation using a mass balance calculation. The mean values and standard deviations are reported for each sample. All sample preparation and δ^2H for C_{26} *n*-acid analysis were undertaken at the University of Washington, Seattle.

Both C_{16} and C_{18} *n*-acid δ^2H were measured at the Organic Geochemistry Unit, Bristol. Each sample was first dissolved in a solution of hexane which contained sacrificial compounds ethyldecanoate and pentadecane at ca. 0.3 mg/cm^3. Compound-specific δ^2H determinations were performed using a ThermoScientific Trace 2000 gas chromatograph coupled to an ThermoScientific Delta V via a GCIsolink and Conflow IV interface. Samples (1 µl) were introduced *via* a programmable temperature vaporising (PTV) injector, set to splitless mode with a splitless time of 2 minutes, onto a 30 m x 0.25 mm fused silica capillary column coated (0.25 µm) with an 100% dimethylpolysiloxane stationary phase (ZB-1, Phenomenx) for non-polar analyses. The GC temperature programme was set to hold at 50 °C for 1 min, followed by a temperature ramp to 120 °C at 80 °C/min and then to 300 °C at 3 °C/min before a final isothermal hold at 300 °C for 10 min. Helium was used as a carrier gas and maintained at a constant flow of 2 mL/min. The thermal conversion reactor comprised an empty ceramic tube maintained at a temperature of 1450 °C. All analyses were conducted in duplicate. The instrument performance was evaluated and a H_3^+ factor calculated on a daily basis using H_2 reference gas (stable and <2ppm/mV) (Sessions *et al*., 2001). Data were initially calibrated to two H_2 reference peaks injected directly into the ion source, before being normalized using the equation of a line from a plot of measured *vs* known δ^2H values for a standard suite of 15 *n*-alkanes (C_{16}-C_{30}; Mixture B3, Arndt Schimmelmann, University of Indiana) which was injected prior to every two sample runs. Peak heights <50 mV identified on the GC-IRMS were below the cutoff and not considered to avoid size-dependent δ^2H effects (Polissar *et al*., 2009). Instrument error was typically less than 5‰, calculated using the same *n*-alkane standard. The addition of three Hs (of known δ^2H value) during methylation was corrected for using a mass balance calculation. The mean values and standard deviations are reported for each sample.

4.6 Summary

The methods outlined have not been widely employed in the southwest Pacific, with some methods applied in this study being their first use in this region. The methods

detailed will help address the aims outlined in Chapter 1, allowing for a paleoenvironmental and palaeoclimatic reconstruction from both Lake Teroto and Lake Lanoto'o.

Chapter 5: Chronology

5.1 Introduction

This chapter outlines the results of the Lake Teroto and Lake Lanoto'o stratigraphy, and presents and analyses the results of ^{210}Pb, ^{137}Cs, and ^{14}C data from the short and long cores. The age/depth models developed here are used in subsequent chapters for each site. The choice of ^{210}Pb model used is outlined, and causes for outliers in the age-depth models for both sites are discussed.

5.2 ^{210}Pb and ^{137}Cs dating using the CIC and CRS models

5.2.1 ^{210}Pb dating using the CIC and CRS models

Figure 5.1 shows the raw data and $^{210}Pb_{supported}$ value – this being the ^{210}Pb activity supported by in-situ decay from ^{226}Ra – used in both the CIC and CRS models for each site (see section 4.3.1.1 for details). The $^{210}Pb_{supported}$ value used was the lowest measured in both sites, but also due to the CRS model not permitting values of $^{210}Pb_{supported}$ being greater than $^{210}Pb_{unsupported}$ values. Unsupported ^{210}Pb is that which is in surplus of the $^{210}Pb_{supported}$ as a consequence of ^{222}Rn, ^{221}Rn and ^{220}Rn decay in the water column and the atmosphere (Robbins, 1978). Comparisons with values of $^{210}Pb_{supported}$ from other sites in the Pacific to determine if the $^{210}Pb_{supported}$ is indicative of regional values is not possible due to values not being published alongside the ^{210}Pb age/depth models (for example Conroy *et al*., 2008; Sachs *et al*., 2009).

Some samples had unexpectedly low ^{210}Pb values compared with surrounding samples. The cause of this is unknown as there is no evidence of mixing or tephra that may reduce ^{210}Pb activity. These sample points were not deleted as there is no valid explanation that can be provided for their removal. Results of the CIC model for both sites are presented in Figure 5.2. The CIC model for Lake Teroto produces an accumulation rate 0.004 yr/cm whereas Lake Lanoto'o produces an accumulation rate of 2.044 yr/cm. Errors are stated at the 1σ level, and incorporated analytical error, the CIC model's goodness-of-fit, and error propagation down-core. It is apparent that the Lake Teroto and Lanoto'o CIC models

completely misestimate the ages, likely a result of the increases in ^{210}Pb values most notably at 9 cm and 4.5cm below the sediment surface in Lake Teroto and Lanoto'o respectively. The lower values above these horizons may be a result of increased sediment input diluting the concentration of ^{210}Pb in the sediment – whether this is a result of increased precipitation and associated terrestrial inwash or human activity causing increased inwash remains to be determined. Overall for both sites it is considered that the CIC model does not perform well and that it does not account for changes in accumulation rate within the errors presented for each model. This is unsurprising considering that there are relatively significant increases in ^{210}Pb values with depth at certain horizons akin to what was determined in Lough Erne and Lake Ipea leading to the development of the CRS model (Appleby and Oldfield, 1978).

The CRS model was applied for both sites (Figure 5.3) as it accounts for variations in accumulation rate, with both models obtaining r^2 values >0.8. Average accumulation rates using this model for Lake Teroto was 3.67 yr/cm and Lake Lanoto'o was 9.92 yr/cm. Due to the aforesaid problems with the applied CIC model for both sites the CRS model is used. This model has been used in other sites in the Pacific: for example Palau (Smittenberg *et al*., 2011) and the Galápagos (Conroy *et al.*, 2014; Zhang *et al*., 2014).

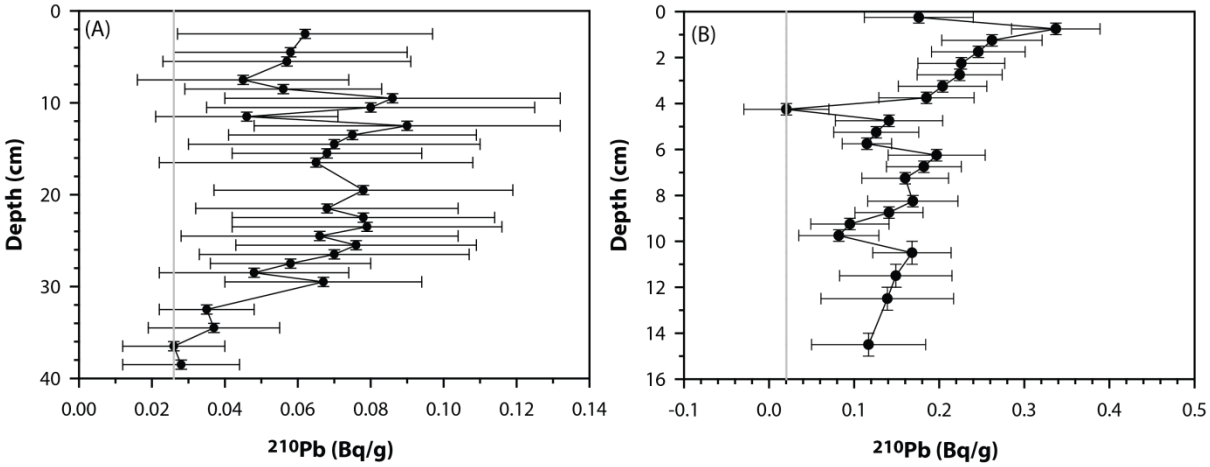

Figure 5.1: ^{210}Pb activity data are presented in black and the ^{210}Pb supported values used in the CRS and CIC models are presented in grey for (A) Lake Teroto, and (B) Lake Lanoto'o. Vertical error bars show sample depth range, horizontal error bars show analytical error.

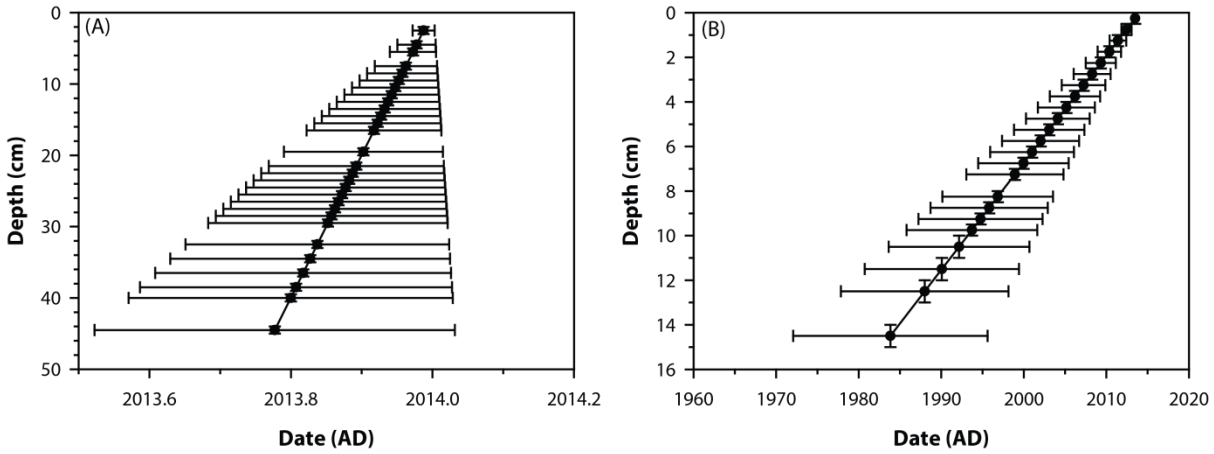

Figure 5.2: The CIC model results for (A) Lake Teroto and (B) Lake Lanoto'o. Vertical error bars show sample depth range, horizontal error bars show the propagated error

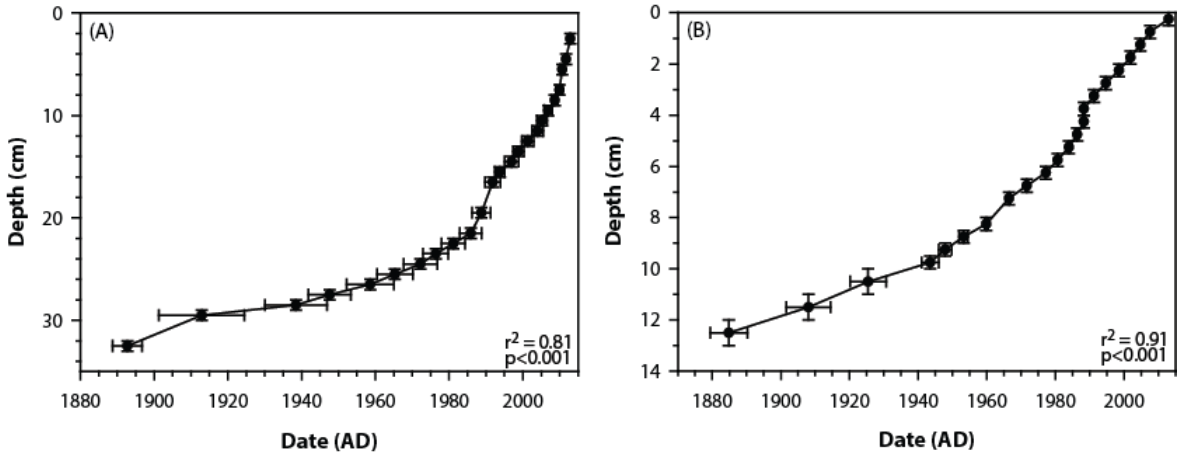

Figure 5.3: The CRS model results for (A) Lake Teroto and (B) Lake Lanoto'o. Vertical error bars show sample depth range, horizontal error bars show the propagated error.

5.2.2 ^{137}Cs dating

No ^{137}Cs activity was detected in Lake Teroto therefore independent verification of the CRS model for this site is not possible. The Lake Lanoto'o curve shows an initial rise at 9 cm and an initial peak in ^{137}Cs activity at 7 cm, and a decline at the top of the core (Figure 5.4). The initial rise in ^{137}Cs activity at 9 cm is ascribed to AD 1954±1 when appreciable fallout levels of ^{137}Cs in the atmosphere first occurred, and the peak determined at 7 cm is ascribed to the AD 1964±1 fallout peak (Terry *et al*., 2006). The CRS model for Lake Lanoto'o produces a date of AD 1953±1 at 9 cm and AD 1971±1 at 7 cm, the former agrees within errors with the timing of appreciable ^{137}Cs fallout from the atmosphere

(Terry *et al*., 2006). Whilst at 7 cm the CRS model produces an age outside the AD 1964±1 fallout peak at 7.5 cm the model produces an age of AD 1966±1: consequently within the depth range of the samples the AD 1964±1 fallout peak is in agreement with the CRS model. Consequently the ^{210}Pb age/depth model for Lake Lanoto'o can be used with confidence as it is supported by the independent ^{137}Cs ages. Without ^{137}Cs ages to verify the CRS model for Lake Teroto it is assumed that the model can be used, as has been the case in Palau (Smittenberg *et al*., 2011) and the Galápagos (Zhang *et al*., 2014) where no independent verification has been applied. Comparisons of the CIC and CRS (and^{137}Cs for Lake Lanoto'o) are presented for both sites in Figure 5.5 and Figure 5.6.

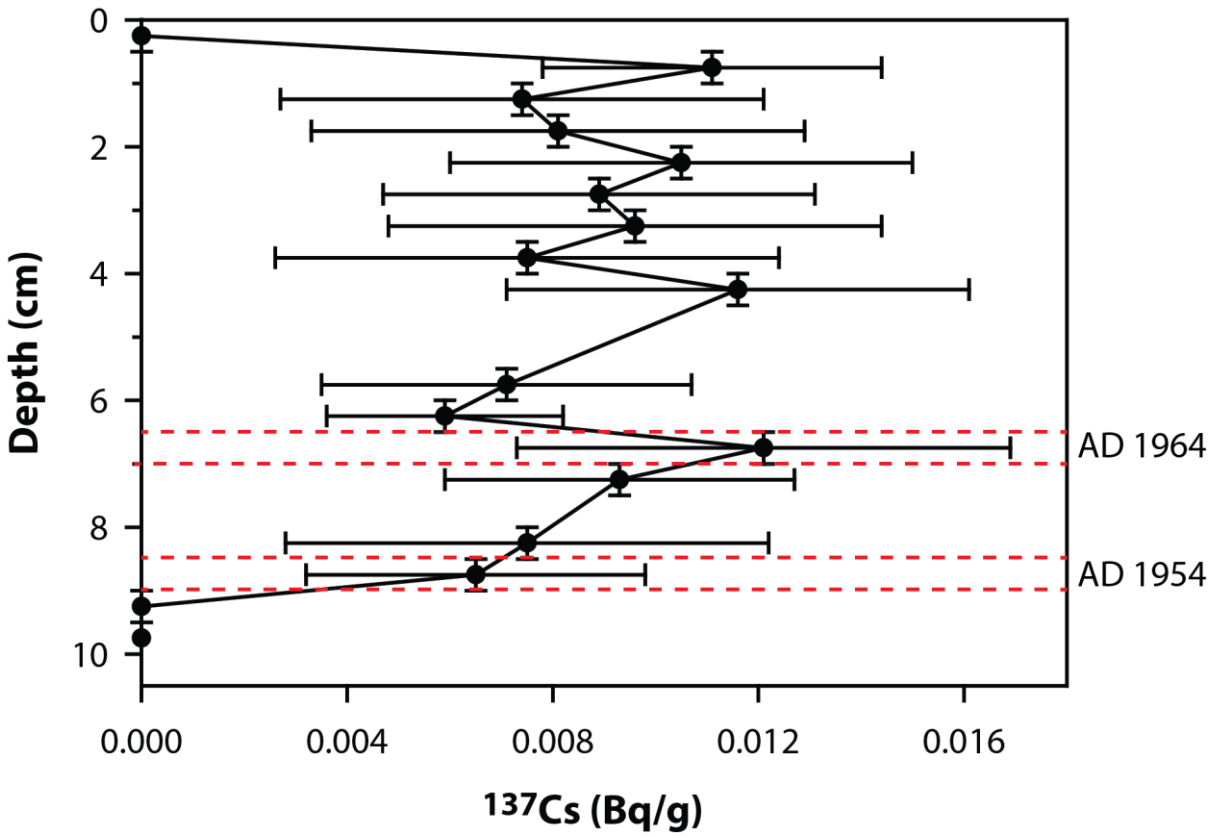

Figure 5.4: Raw ^{137}Cs profile for Lake Lanoto'o. The peak centred on AD 1954±1 and AD 1964±1 are highlighted with the red dashed lines. Vertical error bars show sample depth range, horizontal error bars show the propagated error.

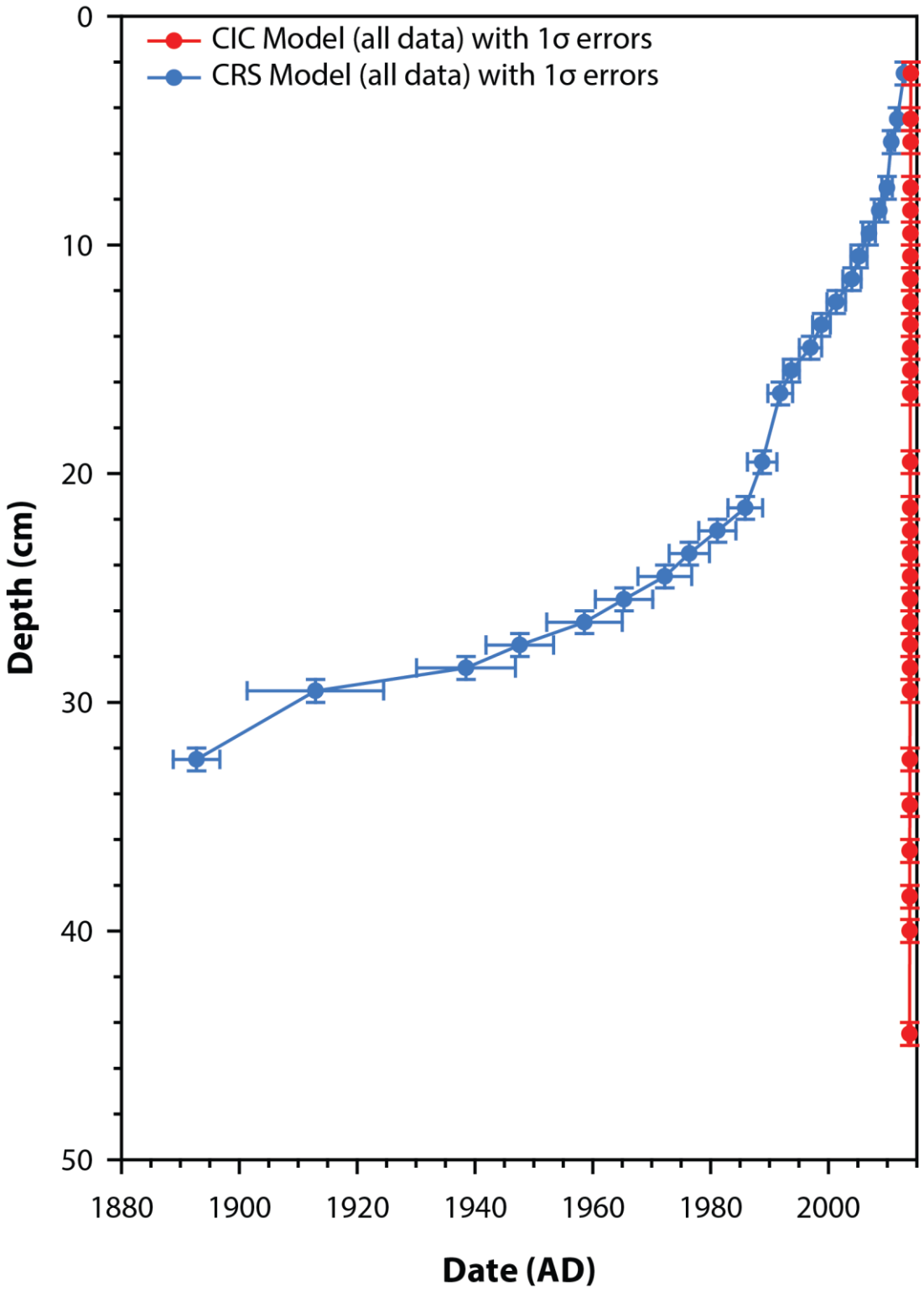

Figure 5.5: Comparison of the Lake Teroto age/depth models produced using the CIC (red) and CRS (blue) models. The CIC model clearly misestimates the ages for the sequence. The CRS model produces the most reasonable age model, albeit this cannot be validated with ^{137}Cs dating, and is the model used for the Lake Teroto sequence.

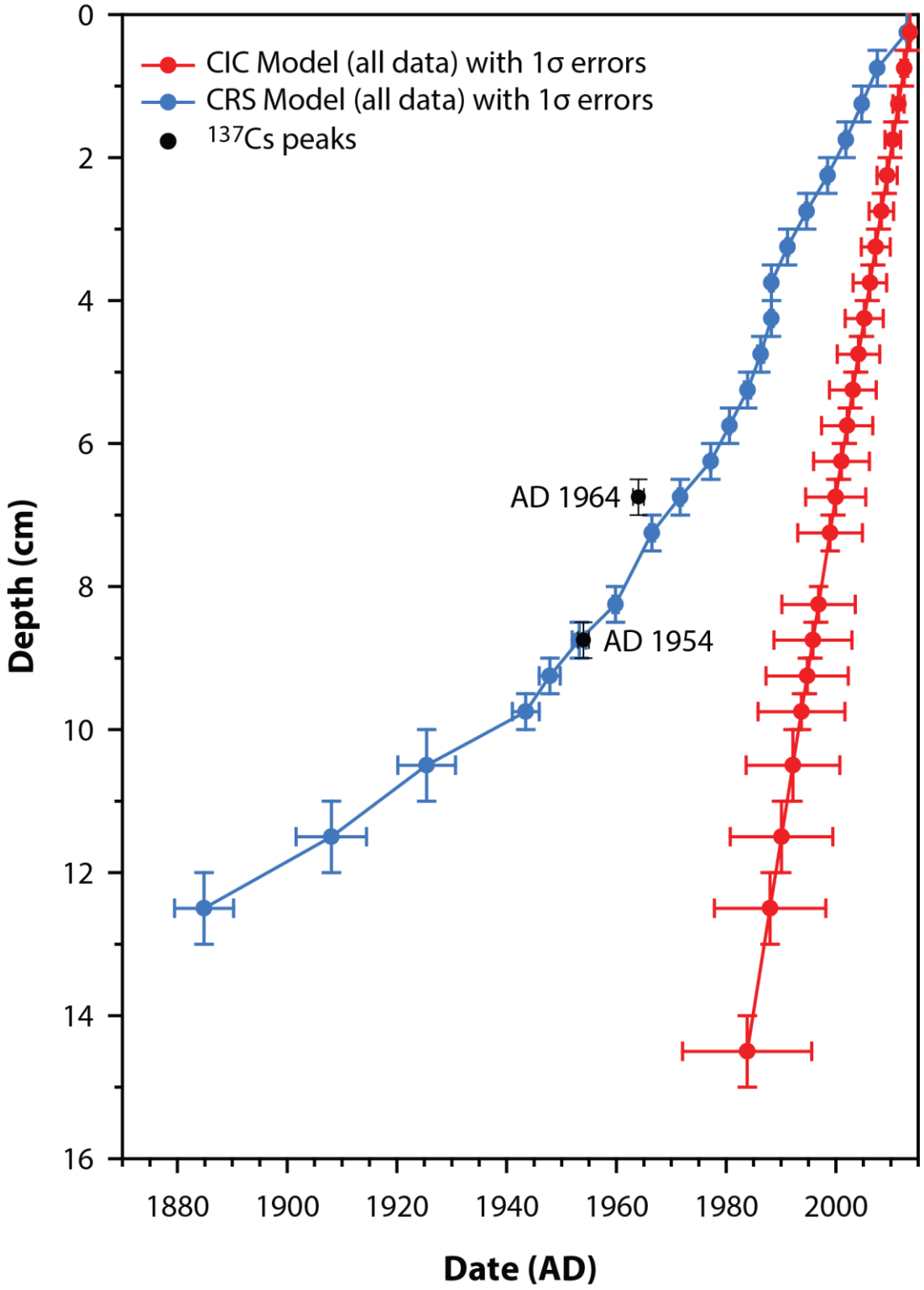

Figure 5.6: Comparison of the Lake Lanoto'o age/depth models produced using the CIC (red) and CRS (blue) models. The CRS model produces the most reasonable age model that is within errors of the ^{137}Cs independent age markers – although it is apparent that the CRS model is not completely in agreement with the AD 1964±1 bomb spike. The CRS model is the model used for the Lake Lanoto'o sequence.

5.3 ^{14}C dating

5.3.1 Lake Teroto

5.3.1.1 Core correlation and stratigraphy

A sequence of overlapping cores was obtained for Lake Teroto to an overall depth of 783 cm (Figure 5.7). Cores were correlated using LOI, magnetic and Itrax data, with core depths then re-mapped onto a single depth model that has been used for age/depth modelling. The sequence is laminated gyttja throughout, alternating between light grey (7/N) and black (2.5/N) lamina. From 0-105 cm the laminae are a different colour, alternating between light grey (7/2Y) and black (2.5/N).

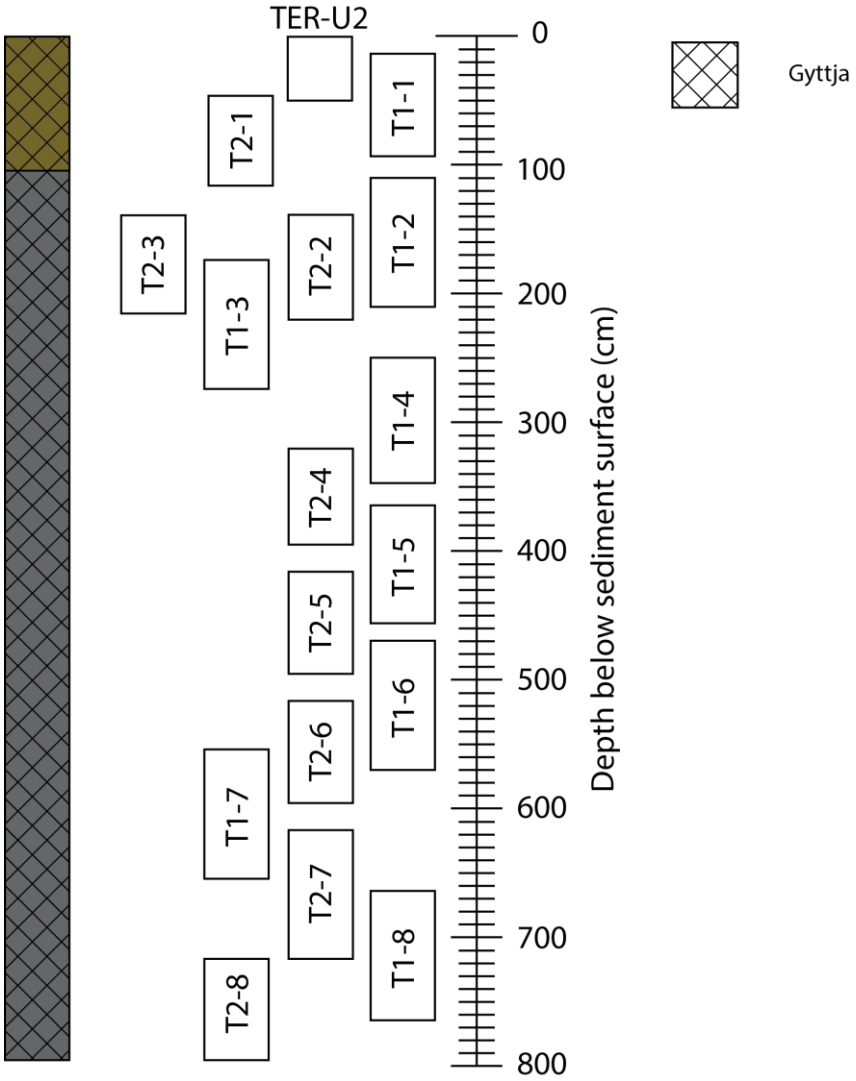

Figure 5.7: The core correlation for Lake Teroto, with individual core IDs presented. The olive brown indicates the change in laminae colour detailed in Section 5.3.1.1 from the rest of the sequence shown in dark grey

5.3.1.2 ^{14}C Chronology

A total of 14 bulk samples were analysed for ^{14}C measurements, presented in Table 5.1, which produced an age of ca. 6635 cal yr BP for the base of the sequence. Bulk samples were used due to the lack of terrestrial macrofossils found in the sequence. One sample (T1-1 72-73 cm) did not produce a ^{14}C age due to the presence of modern carbon in the sample (108.24% absolute ^{14}C enrichment).

Lab ID	Sample ID	Depth below sediment surface (cm)	Material	$\delta^{13}C_{VPDB}$ ‰)	^{14}C uncalibrated age (yr BP)
SUERC-68897	T1-1 72-73cm	83-84	Bulk	-29.4	N/A
SUERC-63973	T1-2 18-19cm	127-128	Bulk	-28.1	427±37
SUERC-68901	T1-2 94-95cm	202-203	Bulk	-25.5	846±37
UCIAMS-179839	T1-2 94-95cm	202-203	Wood	-28.1	105±15
SUERC-68902	T1-3 68-69cm	238-239	Bulk	-33.1	1664±35
SUERC-63974	T1-3 91-92cm	262-263	Bulk	-33.4	2023±37
SUERC-68903	T1-4 74-75cm	319-320	Bulk	-27.6	3211±37
SUERC-68904	T2-4 63-64cm	379-380	Bulk	-33.2	2259±37
SUERC-68905	T1-5 58-59cm	418-419	Bulk	-26.2	3568±38
SUERC-68906	T2-5 59-60cm	473-474	Bulk	-25.9	3390±37
SUERC-68907	T1-6 60-61cm	528-529	Bulk	-27.3	4140±35
SUERC-63975	T1-6 69-70cm	539-539	Bulk	-28.7	4304±36
SUERC-68911	T1-7 53-54cm	604-605	Bulk	-25.6	5167±37
SUERC-68912	T2-7 50-51cm	664-665	Bulk	-27.0	3918±37
SUERC-63976	T2-8 67-69cm	781-783	Bulk	-24.2	5780±37

Table 5.1: ^{14}C ages obtained from Lake Teroto, presented as ^{14}C years before AD 1950. The δ^{13}C is expressed as relative to the VPDB standard ($\delta^{13}C_{VPDB}$).

The Bayesian model produced from BACON v2.2 is presented in Figure 5.8. There are a number of samples that BACON determines to be outliers as a result of being too young

or too old, falling outside the weighted mean calibrated ages**.** The younger than expected ages could be the result of bioturbation causing the downward movement of younger sediments, the infiltration of younger humic acids through older horizons, root penetration through an older soil that is washed into the lake, or contamination of samples by modern carbon. As the Lake Teroto sequence is laminated throughout bioturbation is discounted as a cause of younger-than-expected ages. Consequently either infiltration of younger humic acids, root penetration into older horizons that are subsequently washed in, modern carbon contamination or a mixture of all three are attributed as causes for the younger-than-expected ages.

The older-than-expected ages could be a result of inwash of older inorganic carbon, or a result of hard-water error (Lowe and Walker, 2015). Contamination from fossil makatea is possible as the lake is surrounded on the west by a makatea cliff (Section 3.2.6), which would lead to an introduction of older inorganic carbon. Sample T2-4 63-64 cm has a more negative $\delta^{13}C$ value in comparison to the other samples dated in the sequence. This may be an indicator of high humus content in the sample, suggesting the cause for the younger-than-expected age is the result of younger humic acid infiltration (Stuiver and Polach, 1977). Of note is the T1-2 94-95cm wood sample compared to the bulk. The BACON model shows the wood sample to be an outlier, whereas the bulk sample is not. One possible explanation for the large difference in ages is that the wood sample was caught at the bottom of the corer and dragged down during coring, thus explaining its location at the bottom of the core and the large difference in ages. Alternatively, were the wood sample age to be accepted as terrestrial macrofossils are considered more reliable ages in comparison to bulk (Lowe and Walker, 2015), it implies a sedimentation rate ca. 1cm/yr. Using the simplest explanation it is considered that the wood sample has most likely been dragged down by the corer and is thus not reliable to use.

Throughout the sequence the accumulation rate is largely constant at ca. 9 yr/cm; however it slows at ca. 1,600 cal yr BP to ca. 15 yr/cm (Figure 5.9). The average accumulation rate is greater than the 2-7 year ENSO periodicity, thus meaning that changes in ENSO cannot be examined. As the accumulation rate is less than the 20-30 year IPO periodicity, any climatic interpretation should be put into context of the IPO. Comparisons with other palaeorecords can be undertaken at the interdecadal scale.

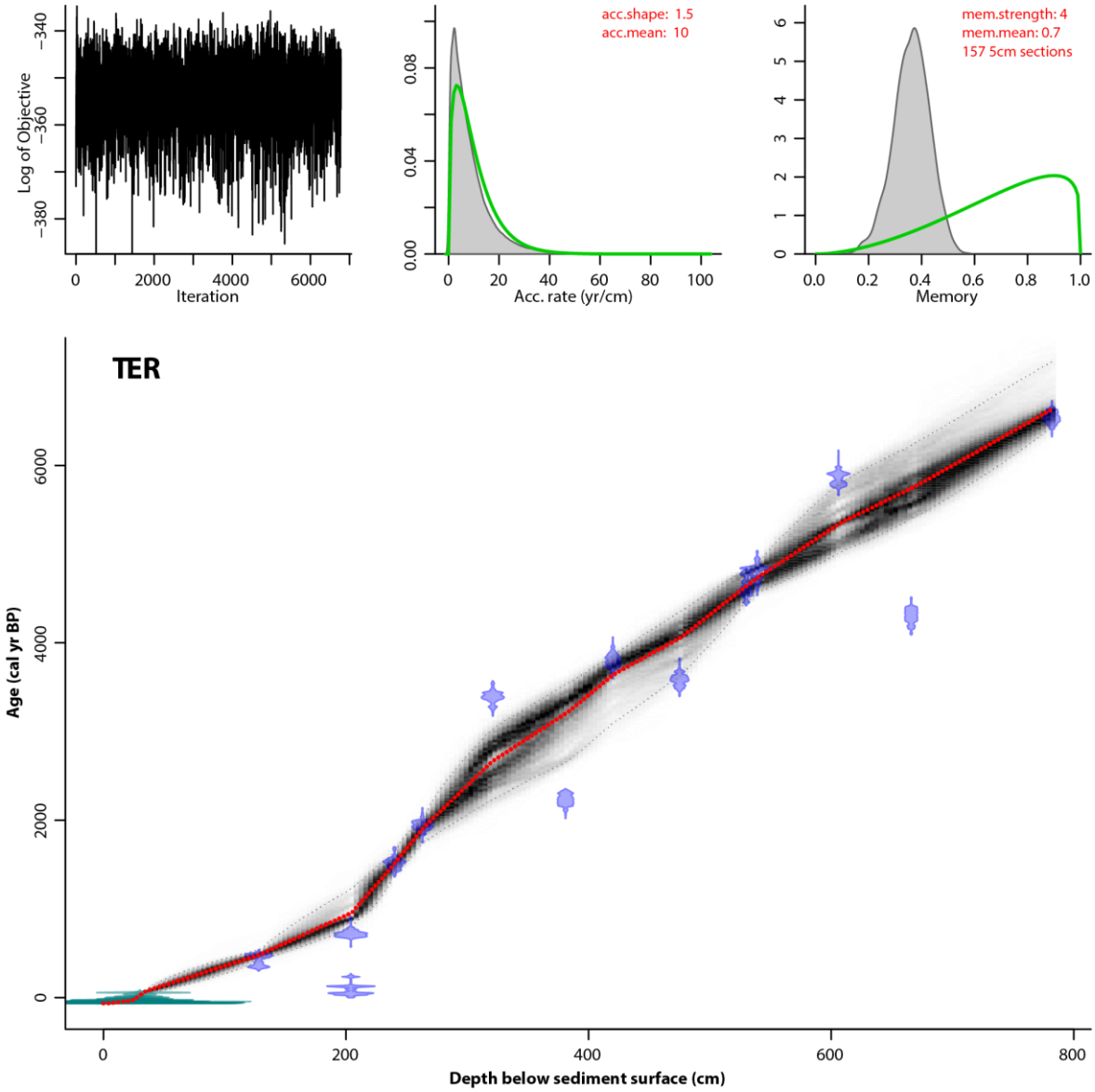

Figure 5.8: Bayesian age-depth model for Lake Teroto. The ^{210}Pb ages (determined from the CRS model), and lake sediment surface, are represented by the transparent green markers. Calibrated ^{14}C dates are indicated by transparent blue markers. The darker grey lines represent the most likely ages in the age-depth model; grey stippled lines indicate the 95% confidence intervals; and the red line shows the 'best' model based on the weighted mean age for each depth.

5.3.2 Lake Lanoto'o

5.3.2.1 Core correlation and stratigraphy

A sequence of overlapping cores was obtained for Lake Lanoto'o to an overall depth of 302 cm (Figure 5.10). Cores were correlated using LOI, magnetic and Itrax data, with core depths then re-mapped onto a single depth model that has been used for age/depth

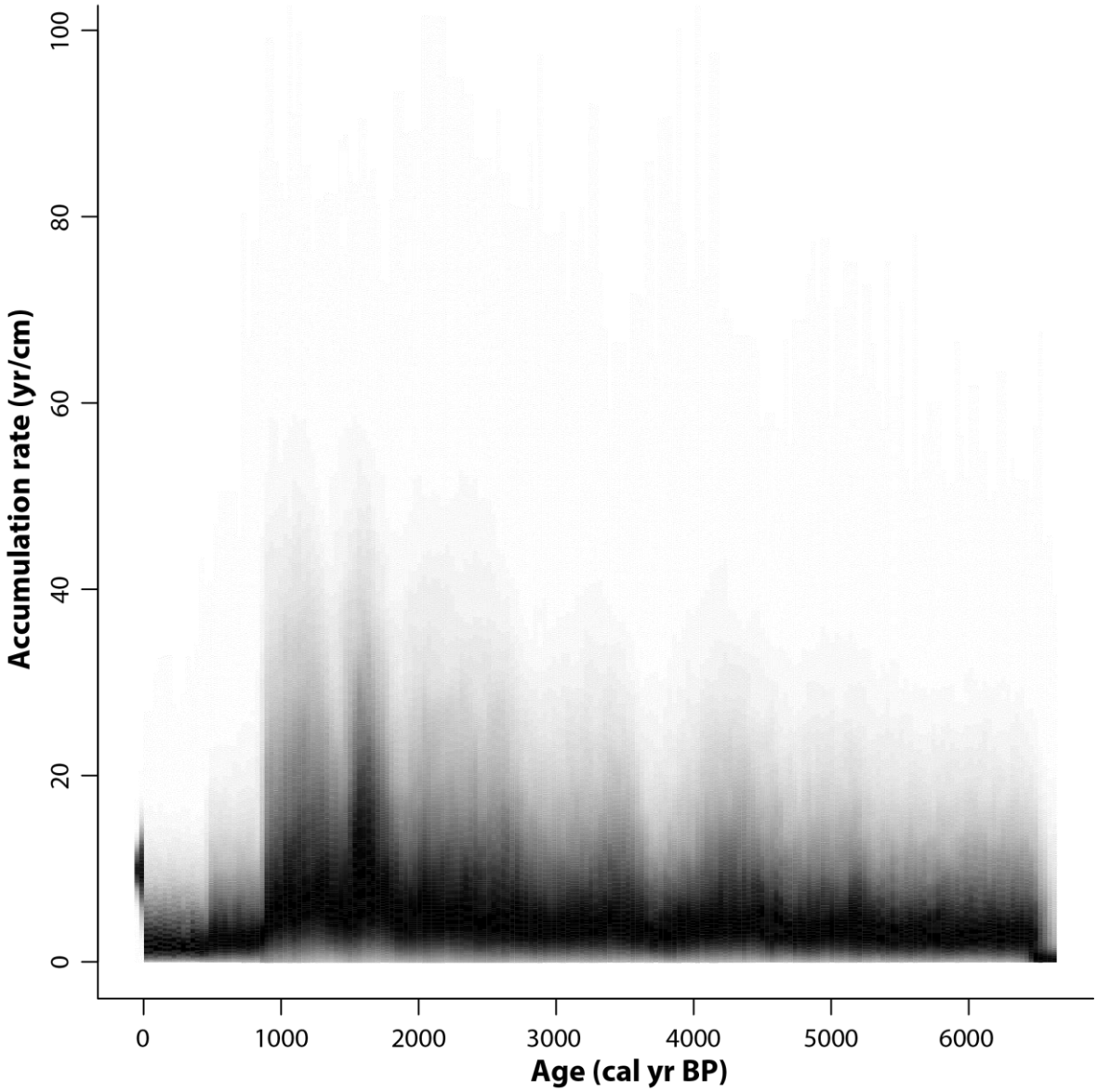

Figure 5.9: The accumulation rate for the Lake Teroto sequence produced using BACON v2.2 and the weighted mean age for each depth. The darker grey lines represent the most likely accumulation rate for the sequence, and the grey stippled lines indicate the 95% confidence intervals.

modelling. There is some visual stratigraphic change throughout the sequence, primarily alternating between two units of very dark brown (7.5YR 2.5/2) gyttja and strong brown (7.5YR 5/6) silicilastic sediment. From 246-302 cm, whilst still gyttja, the unit is a strong brown (7.5YR 4/4); further at 294-297 cm a strong brown (7.5YR 4/6) sand-sized unit is observed.

5.3.2.2 ^{14}C Chronology

Few terrestrial macrofossils were found in the sequence, requiring that most ^{14}C

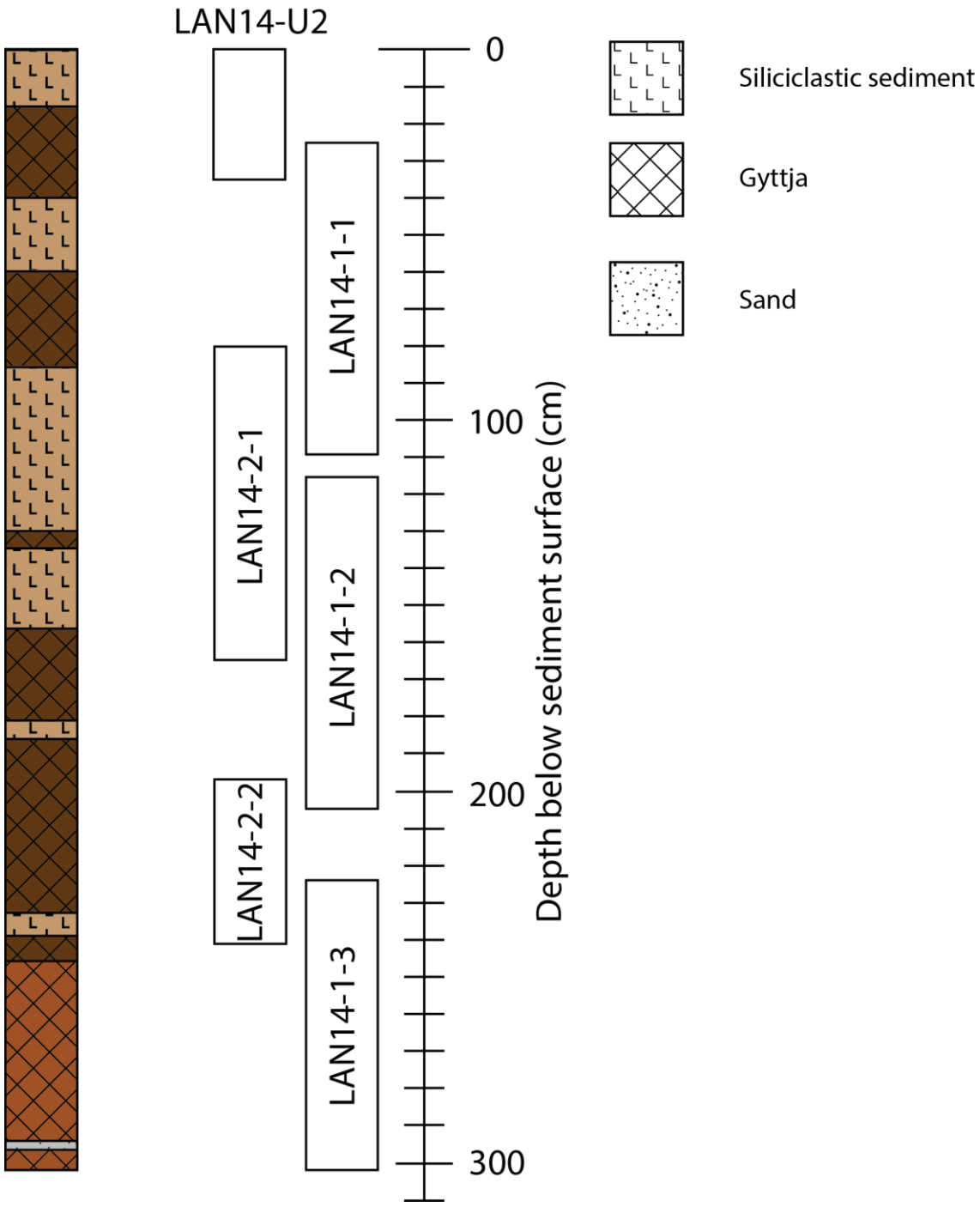

Figure 5.10: The core correlation for Lake Lanoto'o, with individual core IDs presented. The very dark brown and brown indicates gyttja, the latter of which is representative of the change in colour at the base. The light brown indicates siliciclastic units, and the grey indicates a sand (grain-size) layer.

measurements were sourced from bulk sediment. The methods used followed those delineated in section 4.3.2.2; all samples sent and the associated data are presented in Table 5.2. The Bayesian model produced from BACON v2.2 is shown in Figure 5.11.

Lab ID	Sample ID	Depth below sediment surface (cm)	Material	$\delta^{13}C_{VPDB}$ ‰)	^{14}C uncalibrated age (yr BP)
UCIAMS-179834	LAN14-U2 24-25cm	24-25	Plant macrofossil	-25.9	540±15
SUERC-63980	LAN14-1-1 20-22cm	45-46	Bulk	-22.6	1096±35
BETA-439599	LAN14-1-1 31-32cm	56-57	Wood	-26.8	1630±30
BETA-439600	LAN14-1-1 45-46cm	70-71	Plant	-26.7	2570±30
SUERC-63981	LAN14-1-1 54-55cm	79-80	Bulk	-24.8	2453±37
UCIAMS-179835	LAN14-1-1 61-62cm	86-87	Plant macrofossil	-26.86	2700±20
SUERC-68884	LAN14-2-1 30-31cm	108-109	Bulk	-25.9	3607±44
SUERC-68885	LAN14-2-1 60-61cm	138-139	Bulk	-27.3	4497±48
SUERC-63982	LAN14-1-2 13-14cm	128-129	Bulk	-24.2	4064±35
SUERC-63983	LAN14-1-2 35-36cm	150-151	Bulk	-25.6	4638±36
SUERC-68886	LAN14-1-2 43-44cm	157-158	Bulk	-25.2	5071±48
SUERC-63984	LAN14-1-2 57-58cm	172-173	Bulk	-24.0	5768±38
SUERC-68887	LAN14-1-2 69-70cm	183-184	Bulk	-23.4	6128±59
SUERC-68891	LAN14-2-2 11-12cm	208-209	Bulk	-23.6	8092±77
SUERC-68892	LAN14-1-3 17-18cm	238-239	Bulk	-24.5	5879±56
SUERC-68893	LAN14-1-3 33-34cm	254-255	Bulk	-24.2	7794±74
SUERC-68894	LAN14-1-3 68-59cm	279-280	Bulk	-25.7	8462±82
SUERC-63985	LAN14-1-3 77-78cm	299-300	Bulk	-22.8	9440±40

Table 5.2: ^{14}C ages obtained from Lake Lanoto'o, presented as ^{14}C years before AD 1950. The $\delta^{13}C$ is expressed as relative to the VPDB standard ($\delta^{13}C_{VPDB}$).

Whilst the majority of the dates are stratigraphically consistent throughout the sequence, BACON highlights two samples (LAN14-2-2 11-12cm and LAN14-1-3 17-18cm) that are outliers, the former being older than expected and the latter being younger than expected. The younger than expected age could be the result of bioturbation causing the downward movement of younger sediments, the infiltration of younger humic acids

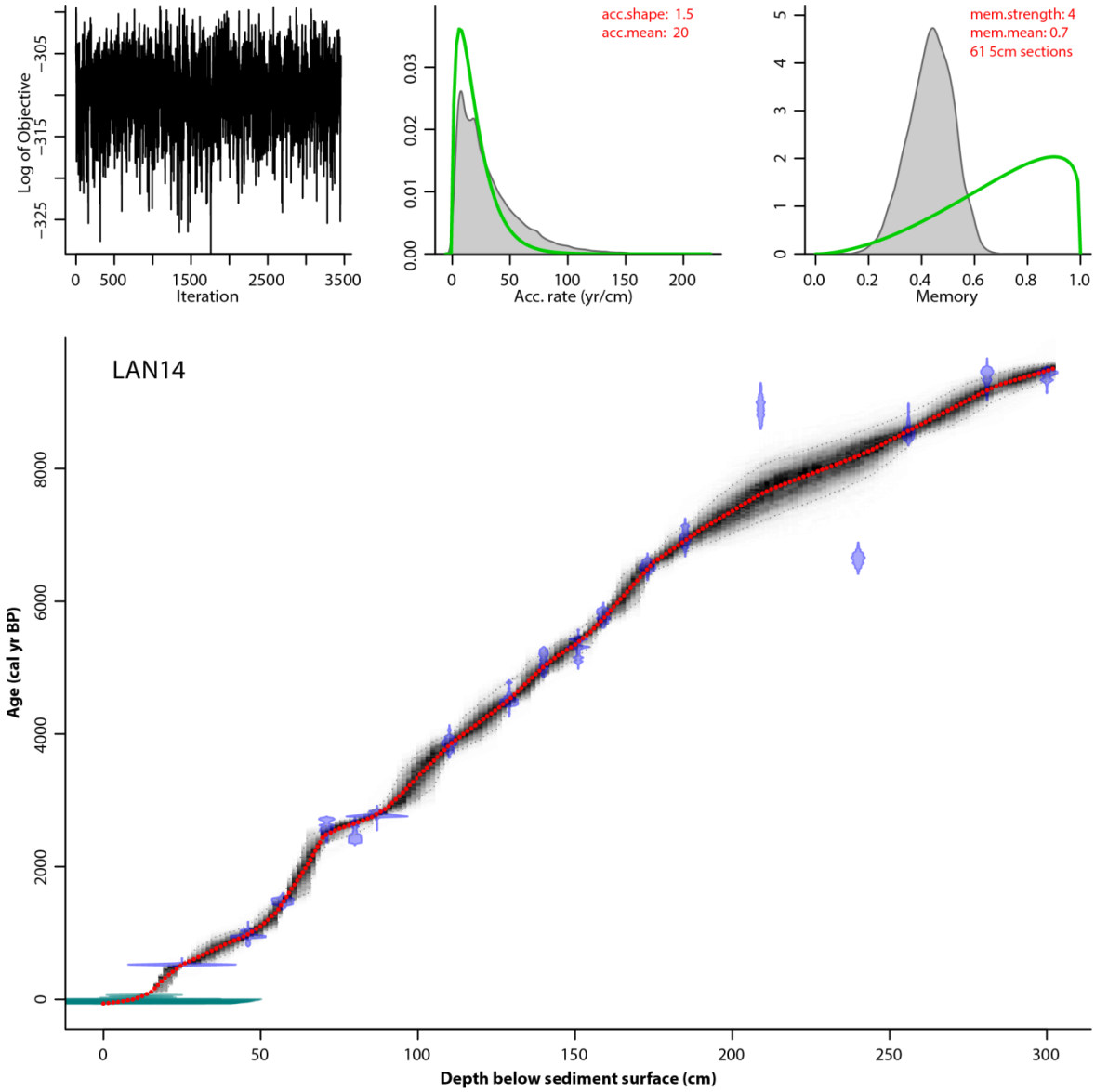

Figure 5.11: Bayesian age-depth model for Lake Lanoto'o. The ^{210}Pb ages (determined from the CRS model), and lake sediment surface, are represented by the transparent green markers. Calibrated ^{14}C dates are indicated by transparent blue markers. The darker grey lines represent the most likely ages in the age-depth model; grey stippled lines indicate the 95% confidence intervals; and the red line shows the 'best' model based on the weighted mean age for each depth.

through older horizons, root penetration through an older soil that is washed into the lake, or contamination of samples by modern carbon. There is no observable evidence of bioturbation in the Lake Lanoto'o sequence, so bioturbation is discounted as a cause of younger-than-expected ages. Consequently either infiltration of younger humic acids, root penetration into older horizons that are subsequently washed in, modern carbon contamination or a mixture of all three are attributed as causes for the younger-than-expected ages. The older-than-expected age could be a result of inwash of older inorganic

carbon, or a result of hard-water error (Lowe and Walker, 2015). Spot samples throughout the sequence indicated that calcium carbonate was not present, precluding this as a cause of the older-than expected age.

Overall the accumulation rate has remained relatively constant in Lake Lanoto'o, albeit there are two clear periods with a slower accumulation rate at ca. 6,000 cal yr BP equalling ca. 50 yr/cm, and 1,500 cal yr BP equalling 100 yr/cm (Figure 5.12). The average accumulation for the sequence is 32 yr/cm – less than El Junco, a crater lake in the Galápagos, which has an accumulation rate of 25 yr/cm. As the average accumulation is greater than ENSO's periodicity but within error of the 20-30 year IPO periodicity, any climatic interpretations made should be put into context of the IPO. Comparisons with other palaeorecords can be undertaken at the interdecadal scale.

5.4 Summary

This chapter has presented data that has been used to construct ^{210}Pb age/depth models, and verified with ^{137}Cs data, and ^{14}C age/depth models. The age/depth models developed will be applied to the proxy data presented and interpreted in subsequent chapters. The main conclusions are:

- Short cores from Lake Teroto and Lake Lanoto'o have been dated using ^{210}Pb and the CRS model, with only Lake Lanoto'o's ^{210}Pb age/depth model being verified with ^{137}Cs;
- No ^{137}Cs activity was determined for Lake Teroto. This is similar to other lacustrine records from the Pacific region, such as those from Palau and the Galápagos (Smittenberg *et al*., 2011; Zhang *et al*., 2014); and
- The Lake Teroto and Lake Lanoto'o sequences have been dated using ^{14}C.

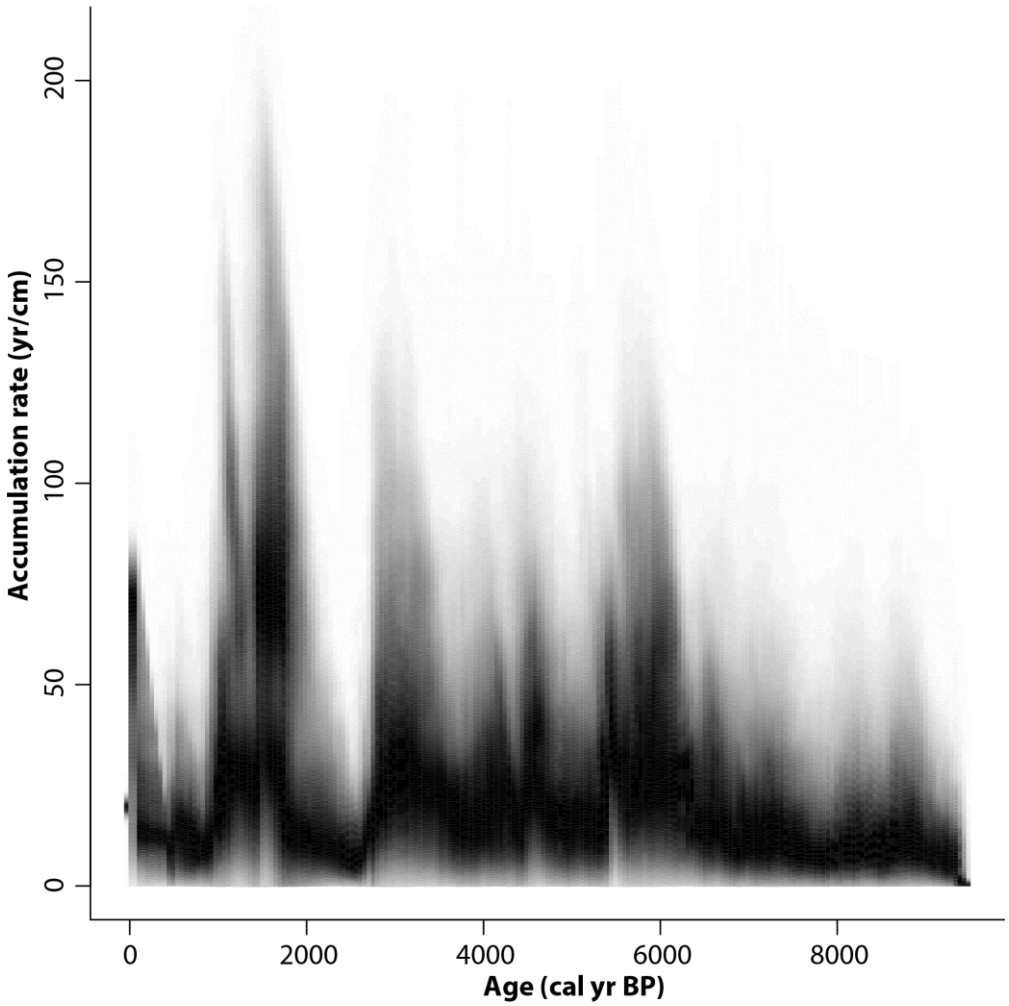

Figure 5.12: The accumulation rate for the Lake Lanoto'o sequence produced using BACON v2.2 and the weighted mean age for each depth. The darker grey lines represent the most likely accumulation rate for the sequence, and the grey stippled lines indicate the 95% confidence intervals.

Chapter 6: Modern samples and short cores: results and interpretation

6.1 Introduction

Data are presented for modern samples and short cores (UWITEC gravity cores) for both Lake Teroto and Lake Lanoto'o. The relationships between modern precipitation and climate indices for the two sites are explored to better understand controls on changes in precipitation. Following this modern precipitation and lake water isotope data are examined to determine catchment hydrology, after which the physicochemical characteristics of each site are presented and interpreted. Inorganic (low frequency magnetic susceptibility and Itrax) and organic (TOC, C/N and $\delta^{13}C_{TOC}$) chemistry results will be presented, with frameworks for interpreting the Itrax and carbon isotope data in regards to environmental and climatic controls delineated. Short cores obtained for both sites are subsequently analysed in context to the proposed frameworks and climatic data.

6.2 Modern precipitation and climate indices

6.2.1 Results

Annual precipitation data from Apia, Samoa, and Rarotonga, Cook Islands, spanning AD 1890-2012 and AD 1899-2012 (Klatt, 2013) respectively were compared with various climate indices detailed in Table 6.1. Long-term precipitation data are not available from Atiu, Cook Islands, hence using precipitation data from Rarotonga as this is the closest rainfall station. Figure 3.4 highlighted the strong, significant correlation between Rarotonga and Atiu precipitation between AD 1983-2012, and linear regression indicates a significant relationship for precipitation between the two islands revealing that precipitation values from Rarotonga can be used to predict precipitation for Atiu. Consequently it is assumed that trends and relationships of different climate indices with precipitation values for Rarotonga are broadly representative of those for precipitation to Atiu.

Climate index	Length of record (AD)	Source
SPCZI	1911-2012	Salinger *et al*. (2014)
IPO TPI	1870-2010	Henley *et al*. (2015)
PDO	1900-2016	NOAA (2016)
Niño1+2	1870-2016	NOAA (2016)
Niño3	1870-2016	NOAA (2016)
Niño3.4	1870-2016	NOAA (2016)
Niño4	1870-2016	NOAA (2016)
SOI	1866-2014	NOAA (2016)

Table 6.1: Climate indices used for comparison to instrumental precipitation data obtained from Apia, Samoa, and Rarotonga, Cook Islands.

Outlined in Table 6.2 are the correlation coefficients for the climate indices compared to precipitation for the two sites for the period AD 1911-2012 for which data exists for all indices. Linear correlation was undertaken on the SPCZI with precipitation for Rarotonga and Apia (Table 6.3; Figure 6.1) and indicated that the SPCZI has a significant negative relationship with the annual precipitation values. As positive SPCZI values indicate when the SPCZ has moved NW and/or contracted during El Niño events causing precipitation amount to decrease for these localities, this negative correlation is expected. The percentage difference between the annual and average precipitation from AD 1911-2012 indicated that years with SPCZI >11 (the SPCZI being an SPCZ movement index and values >11 being where positive-phase IPO and El Niño operate concurrently (Salinger *et*

	SPCZI	**IPO TPI**	**PDO**	**Niño1+2**	**Niño3**	**Niño3.4**	**Niño4**	**SOI**	**Apia ppt**	**Rarotonga ppt**
SPCZI		<0.01	<0.01	0.02	<0.01	<0.01	<0.01	<0.01	<0.01	<0.01
IPO TPI	0.48		<0.01	<0.01	<0.01	<0.01	<0.01	<0.01	<0.01	<0.01
PDO	0.58	**0.70**		<0.01	<0.01	<0.01	<0.01	<0.01	<0.01	<0.01
Niño1+2	0.23	**0.71**	0.39		<0.01	<0.01	<0.01	<0.01	<0.01	<0.01
Niño3	0.34	**0.89**	0.51	**0.89**		<0.01	<0.01	<0.01	<0.01	<0.01
Niño3.4	0.41	**0.93**	0.53	**0.72**	**0.94**		<0.01	<0.01	<0.01	<0.01
Niño4	0.48	**0.84**	0.53	0.50	**0.78**	**0.92**		<0.01	<0.01	<0.01
SOI	-0.38	**-0.83**	-0.51	-0.59	**-0.76**	-0.82	-0.79		<0.01	<0.01
Apia ppt	-0.30	-0.49	-0.28	-0.47	-0.52	-0.51	-0.45	0.53		<0.01
Rarotonga ppt	-0.39	-0.48	-0.20	-0.48	-0.56	-0.53	-0.41	0.43	0.38	

Table 6.2: Linear correlation matrix table for climate indices and precipitation (ppt) data from Rarotonga and Apia for AD 1911-2010, with correlation values below the diagonal and p values above it. In bold are correlations r≥0.7 and r≤-0.7. Highlighted in red are values that are not statistically significant below the 0.01 significance level.

	SPCZI	Apia ppt	Raro ppt
SPCZI		<0.01	<0.01
Apia ppt	-0.29243		<0.01
Raro ppt	-0.37139	0.37947	

Table 6.3: Linear correlation matrix table for precipitation from Rarotonga and Apia with the SPCZI spanning AD 1911-2012 (Salinger *et al*., 2014). Correlation values below the diagonal and p values above it.

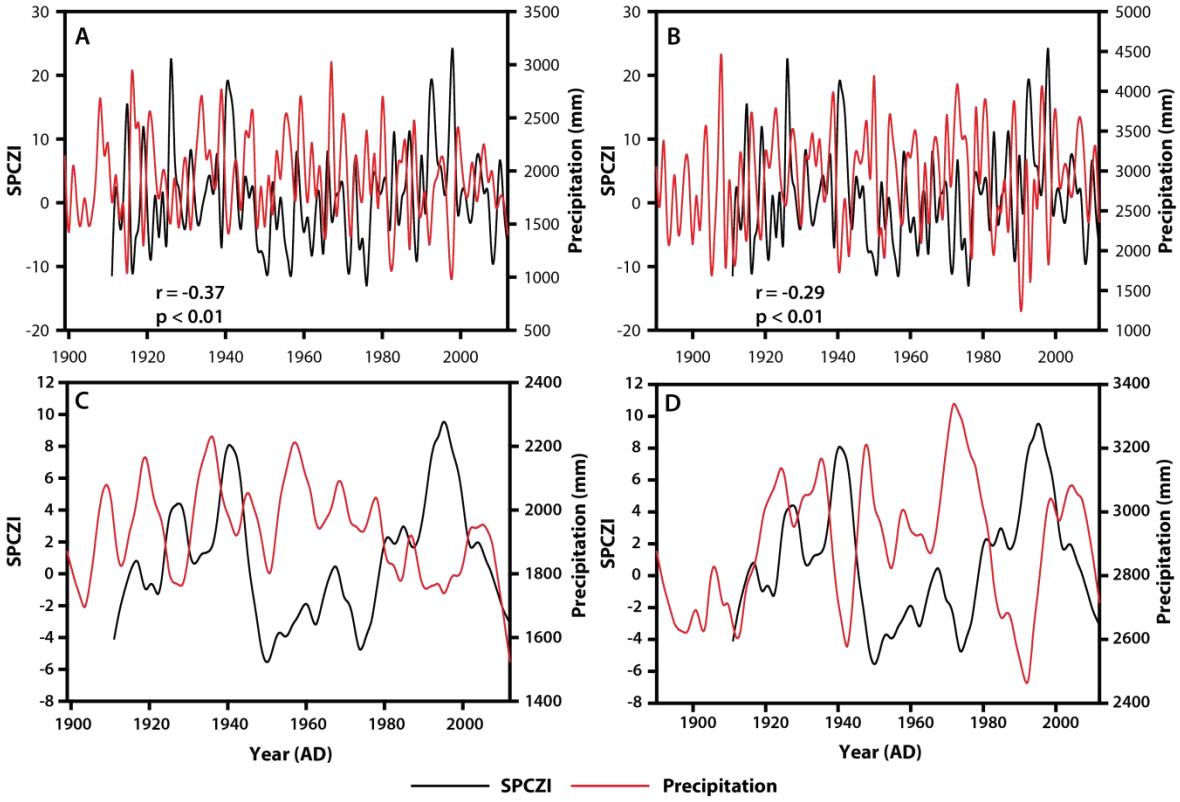

Figure 6.1: Comparison of the SPCZI (black line) (Salinger *et al*., 2014) with precipitation from Rarotonga and Apia (red lines) (Klatt, 2013). (A) and (B) are the annual values for precipitation and the SPCZI in Rarotonga and Apia respectively; (C) and (D) are the LOESS-smoothed (0.1 sampling resolution, polynomial degree of 1) SPCZI and precipitation data for Rarotonga and Apia respectively to highlight the negative correlation between the SPCZI and precipitation from both sites.

al. (2014)) have a predominantly negative precipitation difference from the average (Figure 6.2) and clearly delineates years with SPCZI values >11. Linear regression for years with SPCZI >11 and precipitation indicates a weak but significant relationship for both Rarotonga (r^2 = 0.0855, p<0.01) and Apia (r^2 = 0.1279, p<0.01).

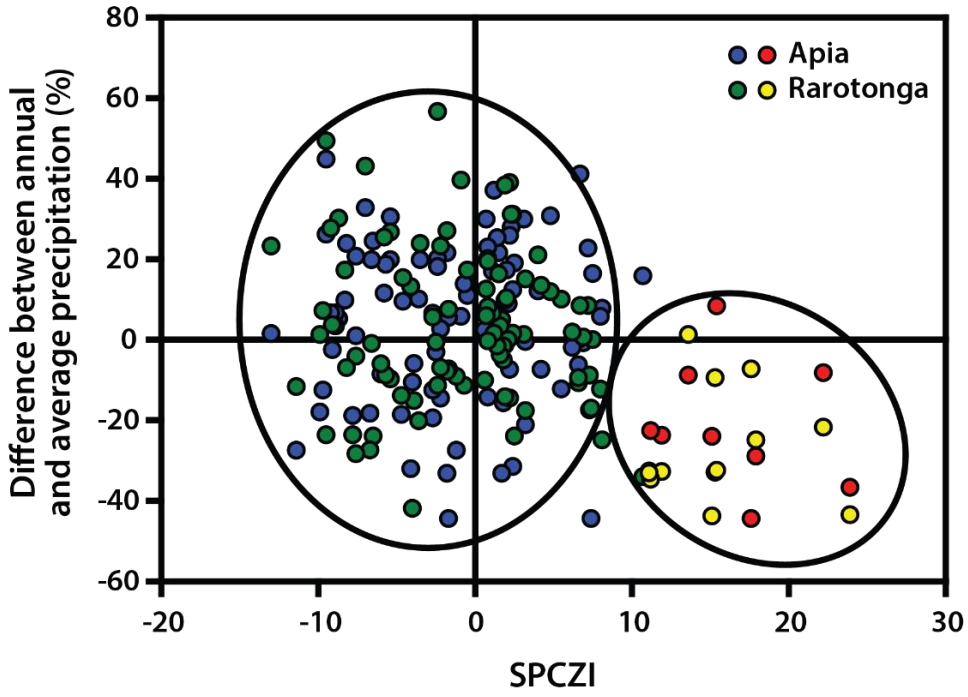

Figure 6.2: The percentage difference between annual and average precipitation for both Rarotonga and Apia are compared with their corresponding SPCZI value. Years where the SPCZI is >11 are highlighted in red for Apia and yellow for Rarotonga. Years where the SPCZI is <11 are shown in blue for Apia and green for Rarotonga.

To further disentangle the relationships between the data principal components analysis (PCA) was performed on all the variables (Figure 6.3). A total of eight climate indices (Table 6.1) and precipitation data from Apia and Rarotonga covering AD 1911-2010 were used in the PCA. Table 6.4 shows the eigenvalues for the first four principal components; axes 1 and 2 explained 73.4% of the climatic data, with PC1 having an eigenvalue (λ_1) of 6.276 and explaining 62.7% of the data and PC2 having an eigenvalue (λ_2) of 1.071 explaining 10.7% of the data.

In the PCA years where the SPCZI is >11 and <-1, these being average values for concurrent positive IPO and El Niño and concurrent negative IPO and La Niña respectively (Salinger *et al*., 2014), are highlighted. It can be seen that years with SPCZI values >11 and <-1 form two clusters: negative IPO and La Niña years form a more dispersive cluster

	PC1	PC2	PC3	PC4
Eigenvalue	6.276	1.071	0.821	0.645
Variance (%)	62.761	10.718	8.2137	6.4505

Table 6.4: Summary of eigenvalues from PCA of climate indices and rainfall data covering AD 1911-2010.

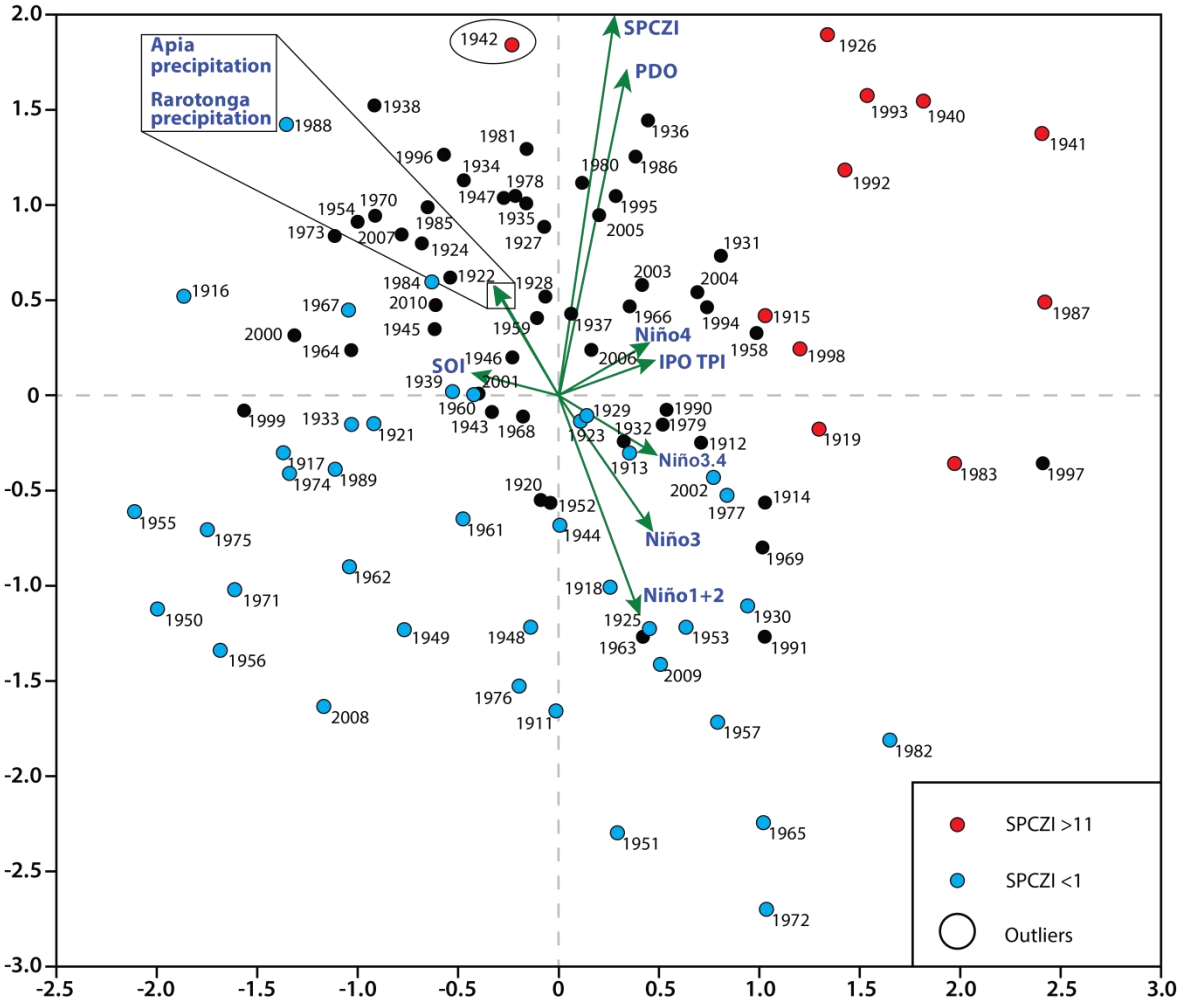

Figure 6.3: PCA of all climate variables and precipitation data for Ratonga and Apia, with SPCZI >11 and <1 highlighted in red and blue correspondingly.

compared to the positive IPO and El Niño years. It is noted that there are fewer concurrent positive IPO and El Niño years than concurrent negative IPO and La Niña during the instrumental period which may be biasing the output. The PCA results suggest that axis 1 is most closely correlated with the various ENSO indices (SOI, Niño1+2, Niño3, Niño3.4, and Niño4) and the IPO TPI. The SPCZI is correlated best with axis 2, and is closely associated with the PDO. Of note is AD 1942 which had the lowest axis 1 score for years where the SPCZI is >11.

6.2.2 Interpretation

The SPCZI has moderately positive significant ($p<0.05$) correlations with all ENSO and IPO climate indexes (Table 6.2). This is expected due to the known nature of the interaction between the SPCZ with both ENSO and the IPO (Trenberth, 1976; Folland *et al*., 2002), and was demonstrated in Salinger *et al*. (2014). The SPCZI produces positive (negative)

values during El Niño (La Niña) and positive-phase (negative-phase) IPO, reflecting contraction and/or movement NW (expansion and/or movement SE) of the SPCZ. Thus: positive SPCZI values indicate a decrease in precipitation for Apia and Rarotonga and negative SPCZI values an increase in precipitation hence the moderately negative correlation. Both Apia and Rarotonga precipitation have stronger, significant correlations with indices for ENSO (SOI, Niño1+2, Niño3, Niño3.4 and Niño4) than with the SPCZI, indicating that on annual timescales precipitation is influenced more by ENSO. Considering that the SPCZI is affected by both the IPO and ENSO, with ENSO being the dominant control on annual timescales (Salinger *et al*., 2014), it is unsurprising that precipitation on Apia and Rarotonga will have a stronger correlation to ENSO indices at annual temporal resolution.

A significant relationship between years with SPCZI values >11 – those being years when positive-phase IPO and El Niño operate concurrently – and precipitation on Apia and Rarotonga is present, but this relationship is weak. At first glance this suggests that the SPCZI is not a good predictor of precipitation for Apia and Rarotonga (and by extension Atiu) due to a variety of factors – specifically ENSO – having a substantial effect on precipitation. Nevertheless it can be determined that there is less precipitation during years where the SPCZI is >11; further corroborated by PCA of the climate indices and precipitation data (Figures 5.2 and 5.3). The PCA clearly shows that years with SPCZI >11 cluster together distinctly from those with SPCZI <-1, i.e. those years where negative-phase IPO and La Niña are operating coevally. One outlier, that being AD 1942, is determined for the SPCZI >11 years. It potentially relates to 1942 having a mixture of El Niño conditions at the beginning of the year (January-April), which would cause a reduction in precipitation amount, and La Niña conditions at the end of the year (July-December) lasting longer than the El Niño conditions, which would cause an increase in precipitation amount (Trenberth, 1976). The precipitation data is at annual resolution only, consequently this cannot be further explored (Klatt, 2013).

Using the instrumental data alone it is proposed that during the instrumental period only years with SPCZI values >11 have a significant impact on precipitation on Rarotonga and Apia. Essentially: during years when positive-phase IPO and El Niños operate in tandem the SPCZ contracts and/or moves NW, and in some years merges with the ITCZ (zSPCZ) (Borlace *et al*., 2014; Salinger *et al*., 2014), causing a significant decrease in precipitation

to Rarotonga – and by extension Atiu – and Apia. Using the precipitation data from the instrumental period alone and assuming the relationships stand for the palaeo-record, interpreting SPCZ movement from the Lake Teroto and Lake Lanoto'o palaeo records will be somewhat binary. When drier conditions are determined from the palaeo records it will indicate significant SPCZ contraction and/or movement NW during coeval positive-phase IPO and El Niño periods (Borlace *et al*., 2014); if the records indicate wetter conditions it will simply indicate that the SPCZ is in a position over these sites and could relate to either positive-phase IPO and La Niña, negative-phase IPO and El Niño, negative-phase IPO and La Niña (Trenberth, 1976; Folland *et al*., 2002). This interpretation of the instrumental precipitation data corroborates with Kidwell *et al*. (2016) who determined that only zSPCZ events – specifically those that occurred during AD 1982/83 and 1997/98 El Niños in a positive-phase IPO period and each of which have SPCZI values >11 – caused a pronounced reduction in SPCZ convergence and consequent decrease in precipitation amount. The relationship between precipitation and the geochemical record is further explored in section6.4.

6.3 Modern samples

6.3.1 δ^2H and $\delta^{18}O$ of modern water results

Stable H and O isotope analysis of modern water provides an understanding of the catchment hydrology. Further it indicates the evaporative conditions at each site. Monthly precipitation and $\delta^{18}O$ values from Rarotonga and Apia are compared indicating that as precipitation amount increases $\delta^{18}O$ values decrease (Figure 6.4). In this instance $\delta^{18}O$ values are used due to more $\delta^{18}O$ data in comparison to δ^2H data in the GNIP database for Rarotonga and Apia. Again data are not available for Atiu – hence using data from Rarotonga as the nearest site to Atiu – and the data from Apia and Rarotonga is sparse and discontinuous. Annual precipitation and $\delta^{18}O$ values are plotted on the monthly precipitation and $\delta^{18}O$ values, with positive SPCZI years highlighted in red and negative SPCZI years highlighted in blue. Data from Apia shows that negative SPCZI years produce less negative $\delta^{18}O$ values than positive SPCZI years, whereas there is no clear relationship in Rarotonga. Figure 6.5 indicates that there is seasonality in the precipitation amount and $\delta^{18}O$ values for both sites, with austral winter (JJA) having less negative $\delta^{18}O$

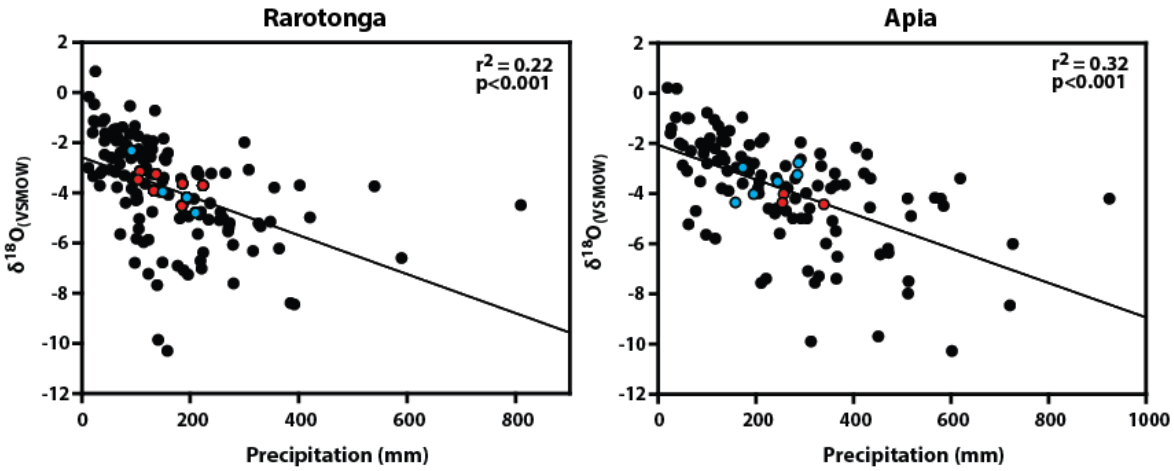

Figure 6.4: Monthly precipitation and $\delta^{18}O$ values are plotted for Rarotonga and Apia. Average annual precipitation and $\delta^{18}O$ values are overlain for years where >9 months of data are available – in blue are negative SPCZI years when the SPCZ has expanded and/or migrated SE, in red are positive SPCZI years when the SPCZ has contracted and/or migrated NW (Salinger *et al*., 2014; IAEA/WMO, 2016).

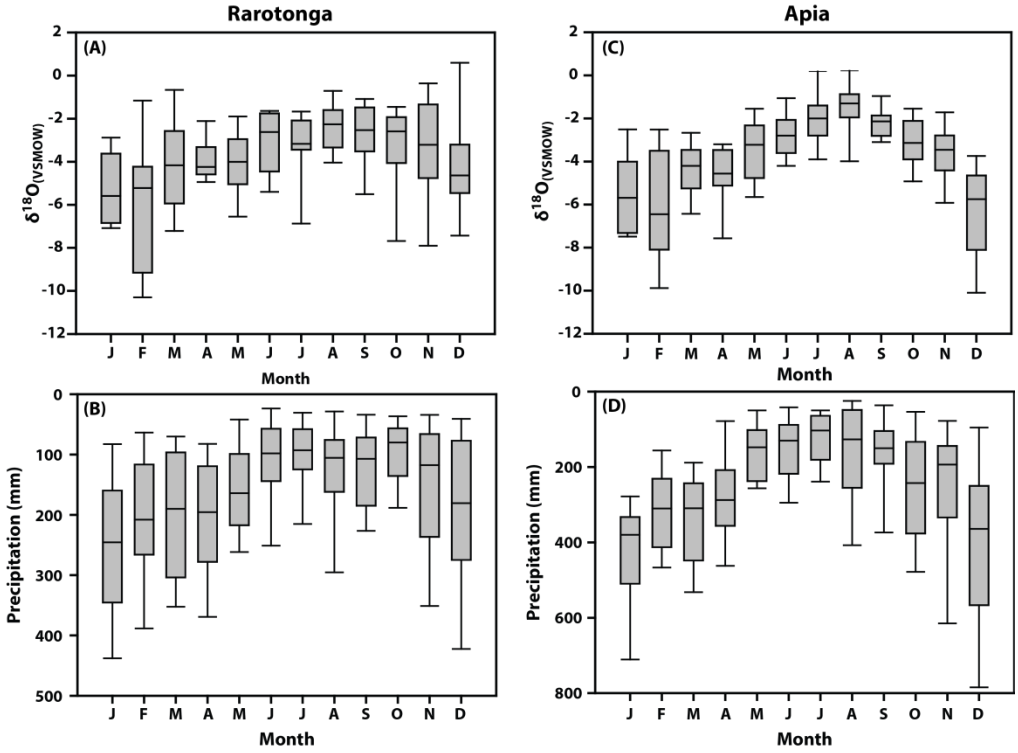

Figure 6.5: Monthly $\delta^{18}O$ values in precipitation and precipitation amount (mm) for Rarotonga (A and B) and Apia (C and D) respectively (IAEA/WMO, 2016).

values and less precipitation in comparison to austral summer $\delta^{18}O$ values (DJF) which has more negative $\delta^{18}O$ values with increased precipitation amount. Multidecadal isotope precipitation values at monthly resolution for Rarotonga and Apia are not available, thus limiting a thorough understanding of catchment hydrology in these locales. Interannual

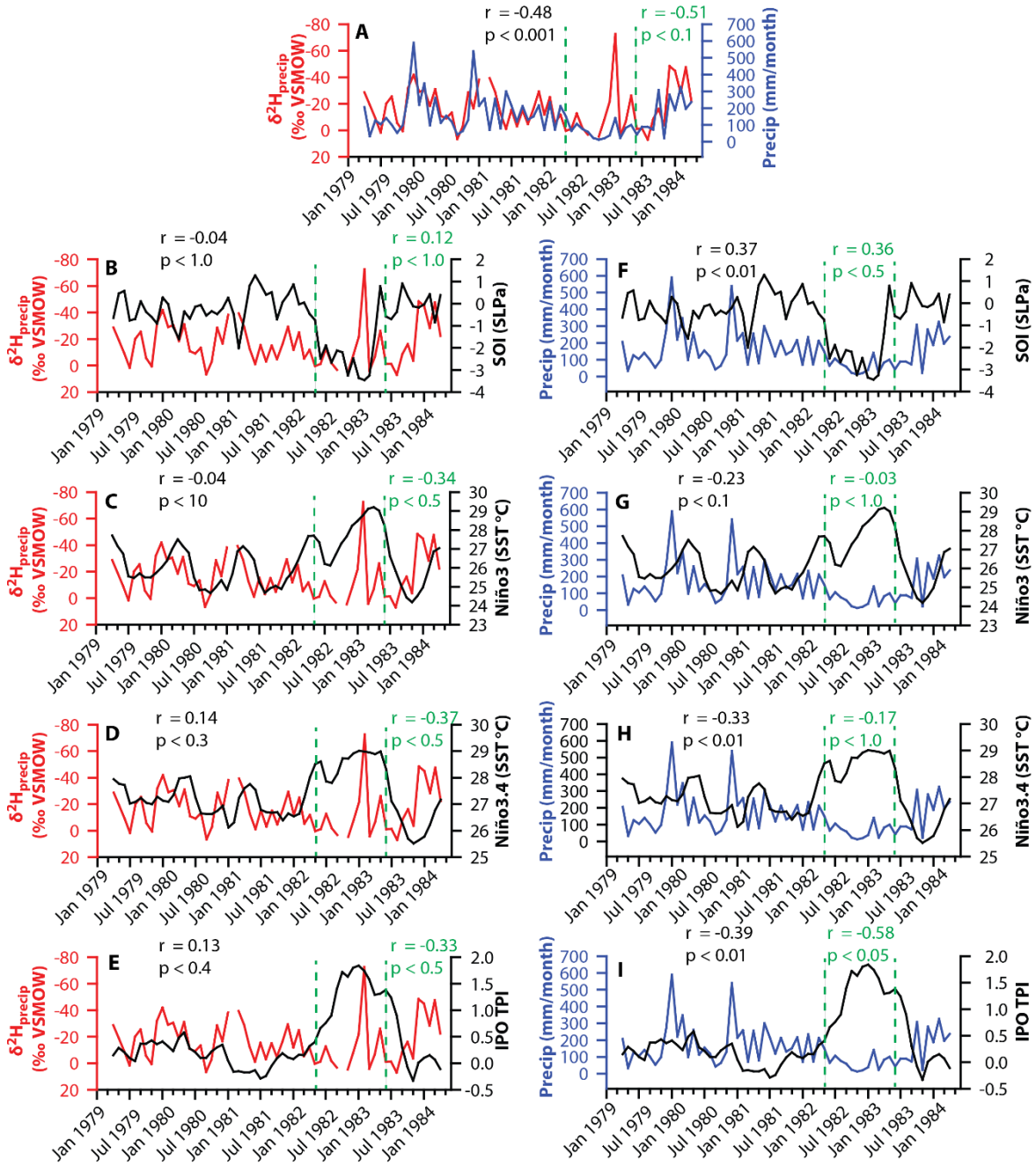

Figure 6.6: (A) Timeseries of monthly Rarotonga precipitation δ^2H and Rarotonga precipitation amount. (B-E) Correlation (r and p value in black for the duration of the timeseries) between (B) SOI, (C) Niño3, (D) Niño3.4, and (E) IPO TPI with Rarotonga precipitation δ^2H. (F-I) same as (B-E) but for monthly Rarotonga precipitation amount. Green lines delineate the AD 1982/1983 (EPE type) El Niño event as classified by Yu *et al*. (2011) with associated r and p value in green for the El Niño event. The axes for Rarotonga precipitation δ^2H are inverted. Precipitation isotope values and amount from IAEA/WMO (2016), Niño and SOI indices from NOAA (2016), and IPO TPI from Henley *et al*. (2015).

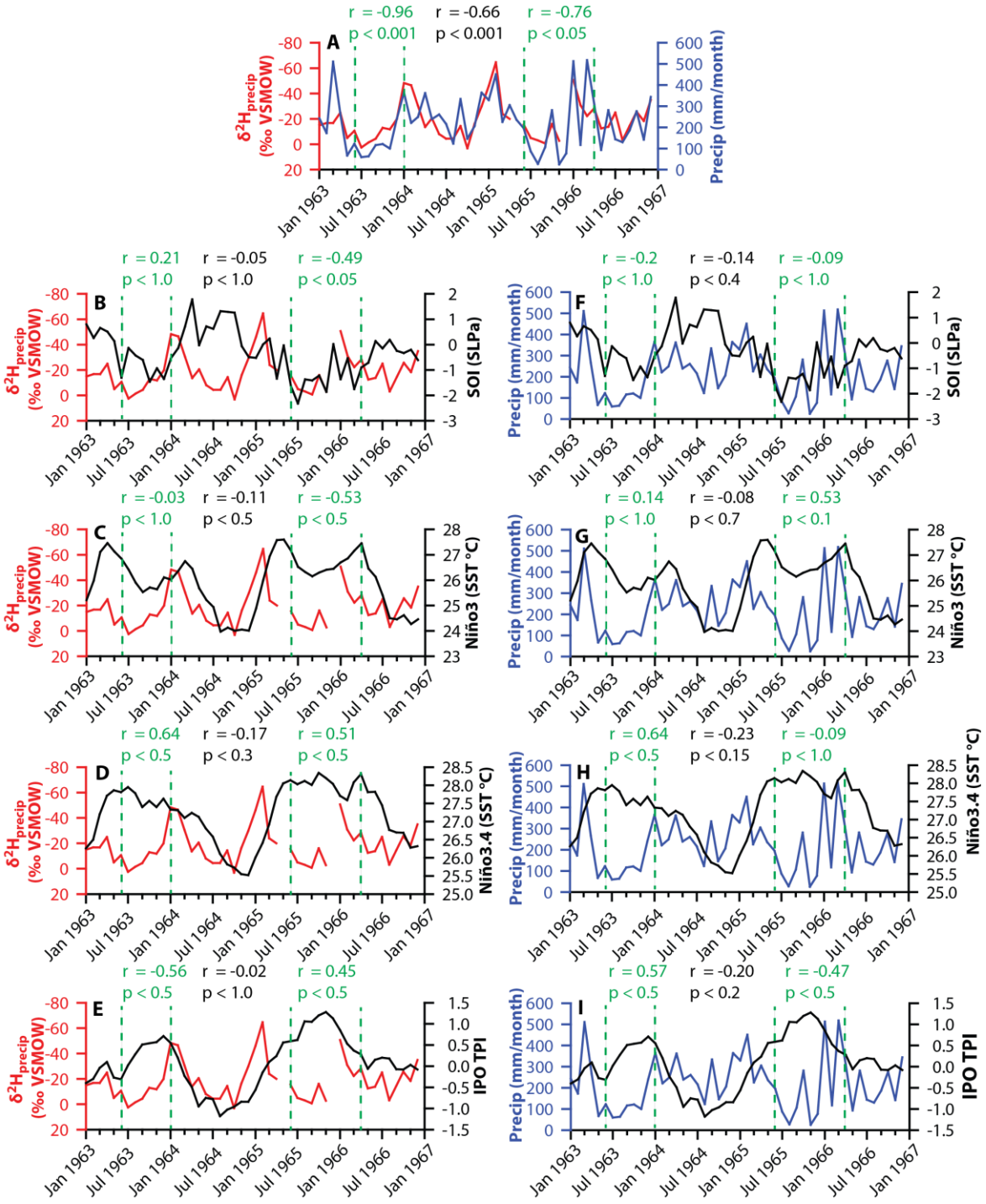

Figure 6.7: (A) Timeseries of monthly Apia precipitation δ^2H and Apia precipitation amount. (B-E) Correlation (r and p value in black for the duration of the timeseries) between (B) SOI, (C) Niño3, (D) Niño3.4, and (E) IPO TPI with Apia precipitation δ^2H. (F-I) same as (B-E) but for monthly Apia precipitation amount. Green lines delineate the AD 1963/64 (CPE type) and 65/66 (mixed type) El Niño events as classified by Yu *et al*. (2011) with associated r and p value in green for the El Niño event. The axes for Apia precipitation δ^2H are inverted. Precipitation isotope values and amount from IAEA/WMO (2016), Niño and SOI indices from NOAA (2016), and IPO TPI from Henley *et al*. (2015).

precipitation amount and isotope data spanning El Niño events, as defined by Yu *et al*. (2011) and classed according to El Niño type and flavour, is presented and compared to ENSO indices and the IPO TPI. The ENSO indices chosen – specifically SOI, Niño3 and Niño3.4 – have a correlation with precipitation in at least one site r≥0.5 or r≤ -0.5. As δ^2H data is available for the duration of the periods analysed it is used to enable more direct interpretations relevant to δ^2H analysed on long-chain alkanoic acids. In both sites a significant negative correlation between precipitation and δ^2H value is evident (Rarotonga r = -0.48, p<0.001; Apia = -0.66, p<0.001) (Figure 6.6 and Figure 6.7). Interannual precipitation amount and δ^2H have no significant correlation with the climate indices. However during El Niño events the correlation becomes stronger, albeit it is not significant.

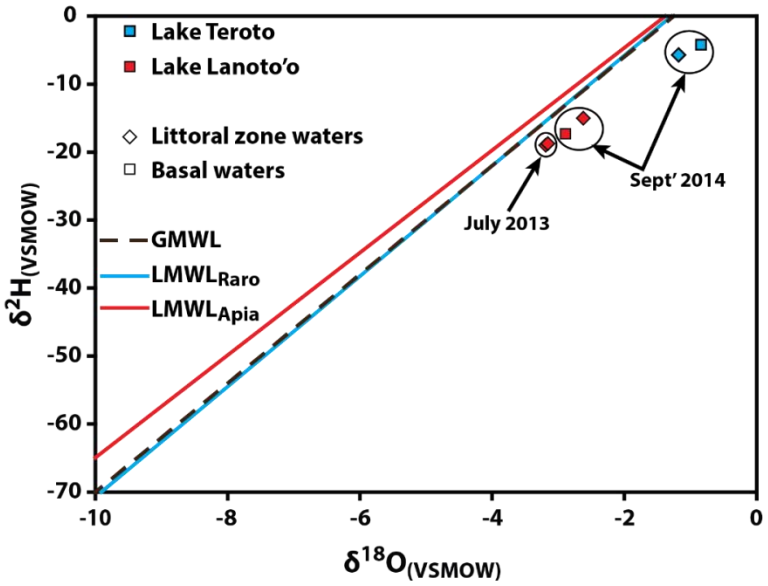

Figure 6.8: Lake water isotope values from Lake Teroto and Lake Lanoto'o plotted alongside local meteoric water lines for Rarotonga ($LMWL_{Raro}$), Apia ($LMWL_{Apia}$), and the global meteoric water line (GMWL) (IAEA/WMO, 2016).

Lake Lanoto'o water samples are more fractionated in comparison to Lake Teroto (Figure 6.8); moreover samples taken from the littoral and basal zones in Lake Teroto and Lake Lanoto'o show differences in their values. Both sites δ-values are offset in comparison to the local meteoric water lines (LMWL).

6.3.2 Interpretation

For both Rarotonga and Apia the amount effect, as delineated by Dansgaard (1964), has been previously determined by Rozanski *et al*. (1993) to be the primary control on

precipitation isotope values and is further demonstrated here (Figure 6.4, Figure 6.5, Figure 6.6 and Figure 6.7). It is expected that movement of the SPCZ would cause changes in the precipitation δ-values. Monthly precipitation δ-values for both Rarotonga and Apia indicate seasonality, with this being ascribed to seasonal movement of the SPCZ (Matthews, 2012). In the austral winter the SPCZ contracts, reducing the precipitation amount which is characterised with less negative δ-values; contrastingly in austral summer the SPCZ has expanded, increasing the precipitation amount which has more negative precipitation δ-values (Trenberth, 1976). Figure 6.4 shows that the SPCZI is not a good predictor of δ-values, with no clear relationship for Rarotonga. For Apia when the SPCZI is negative (SPCZ has expanded and/or moved SE) there is less precipitation and less negative precipitation δ-values, and vice versa. This is opposite to what is expected, that being when the SPCZI is negative (SPCZ has expanded and/or moved SE) that there is increased precipitation and more negative precipitation δ-values. However there are only a few years of data available, none of which have SCPZI values >11.

Figure 6.2 indicated that there is only a consistent decrease in precipitation amount for both Rarotonga and Apia when the SPCZI is >11 – this likely explains the lack of correlation between the SPCZI and $\delta^{18}O$ values. Moreover, since seasonal SPCZ movement is observed in δ-values (Figure 6.5), it follows that SPCZ movement on interannual and interdecadal timescales will likely be reflected in precipitation isotope values. This is because during austral winter (summer) the SPCZ contracts and/or moves NW (expands and/or moves SE) precipitation amount is reduced (increased) with coeval less negative (more negative) δ-values, showing that SPCZ location affects both precipitation amount and δ-values as expected. Whilst the correlation between climate indices with precipitation amount or precipitation isotope values is not strong or significant, the strength of the correlation does increase during El Niños (Figure 6.6 and Figure 6.7) – it is highlighted that these correlations are not significant. It is interesting to note that the direction of correlation is not consistent through El Niños, especially in Apia. Nevertheless visually it can be seen during El Niños for the Niño3, Niño3.4 and IPO TPI (SOI) when values increase (decrease) the precipitation amount decreases and isotope values are more positive. It suggests that although there are a number of controls on precipitation amount, during El Niños or positive-phase IPO precipitation amount is reduced due to the SPCZ contracting and/or migration NW with this being reflected in the

precipitation isotope values (Trenberth, 1976; Folland *et al*., 2002). This lends further support to the conclusions drawn in section 6.2.2**.**

Little research has been undertaken to determine air mass trajectories in the Pacific region, with changing air mass trajectories potentially causing changes in the precipitation isotope values that could be misinterpreted as changes in precipitation amount (Gat, 1996). van der Wiel *et al*. (2016b) suggested that during normal and La Niña (El Niño), and by extension negative-phase (positive-phase) IPO, conditions when the SPCZ is diagonal (zonal) moisture is transported southwestward (equatorward). This change in moisture source during an El Niño may account for the very low δ^2H values for a modest increase in precipitation amount in January AD 1983 during the AD 1982/83 El Niño. Conroy *et al*. (2013) highlighted that precipitation $\delta^{18}O$ in Palau, equatorial Pacific, is mainly controlled by vapour transport history and the degree of vapour parcel distillation. Further the precipitation $\delta^{18}O$ in Palau is more strongly correlated to basin-wide precipitation amount rather than local precipitation amount (Conroy *et al*., 2013). Whether this is the case for Rarotonga is difficult to evaluate; however the evidence does indicate the local amount effect is the primary control on precipitation isotope values (Figure 6.4, Figure 6.5 and Figure 6.6) (Rozanski *et al*., 1993). Moreover, local factors such as relative humidity and precipitation rate could have contributed to this very low δ^2H value (Risi *et al*. 2008).

Due to the paucity of knowledge on air mass trajectories in the southwest Pacific region an assumption has to be made in this study that the amount effect controls precipitation isotope values in the SPCZ region that will be reflected in δ^2H values of long-chain alkanoic acids. Long-chain alkanoic acid δ^2H values have a significant positive correlation with precipitation δ^2H values (Hou *et al.*, 2008) thus it is assumed that the long-chain alkanoic acid δ^2H values will reflect precipitation δ^2H in this region – potential controls on alkanoic acid δ^2H values will be further explored in sections 8.3.2 and 8.3.2. Further, due to the lack of multidecadal precipitation isotope data an assumption has to be made that over these timescales the IPO, and ENSO, will be reflected in precipitation isotope values due to their impact on SPCZ location and precipitation amount. Figure 6.6 and Figure 6.7 suggest that this is the case, and this is also grounded in theory: during positive-phase (negative-phase) IPO there is an increase in El Niños (La Niñas) (Delcroix *et al*., 2007; Kao and Yu, 2009) which cause the SPCZ to contract and/or shift NW (expand and/or shift SE) decreasing (increasing) precipitation amount and increasing (decreasing) isotope values

(Trenberth, 1976; Folland *et al*., 2002). Linear regression indicates a significant relationship between precipitation amount and precipitation isotope value in Rarotonga and Apia (Figure 6.4), and the correlation between precipitation amount, the SPCZI and the IPO TPI is also significant (Table 6.2) lending support to this assumption.

When examining Figure 6.8 the slopes of the LMWL for Rarotonga and Apia have a value of 8 and 7.5 respectively, this being outside the range of evaporative sites (Gibson *et al*., 2002) (Figure 6.8). Rarotonga's intercept is equivalent to the global meteoric water line (GMWL), and Apia's is very similar, suggesting that they are indicative of the first condensate from an undisturbed marine source (Dansgaard, 1964). Lake Teroto's δ^2H and $\delta^{18}O$ values are more positive and do not match the predicted isotope ranges produced from the Isomap project modelling: δ^2H = 0-15‰ and $\delta^{18}O$ = -2 to -3.9‰ (Bowen and Revenaugh, 2003). This is likely due to the lake's connection to the sea which can in some cases lead to positive isotope values (Rao *et al*., 1987). The δ^2H and $\delta^{18}O$ data for Lake Lanoto'o does match the aforesaid predicted isotope values from the Isomap project (Bowen and Revenaugh, 2003). Lake Lanoto'o water samples are more fractionated in comparison to Lake Teroto (Figure 6.8) which is to be expected with the difference in altitude between the two sites: Lake Lanoto'o is at 760 m.a.s.l., Lake Teroto is at 0.9 m.a.s.l. (Darling *et al*., 2005). Samples from Lake Lanoto'o indicate small shifts between seasons; however it is not possible to determine if this is part of a seasonal trend with the number of samples available.

6.3.3 Physicochemical characterisation of sites

6.3.3.1 Lake Teroto

The pH in all sampling profile shows a weak decreasing gradient from pH 8.3 to pH 7 (Figure 6.9). This occurs at 2 m depth in the shallower profiles, but at 3 m in the deeper profile. All temperature profiles show a small temperature increase to 28 °C, and decrease to a minimum of 26.5 °C after this. The temperature inversion occurs at 1 m in the shallower profiles, and 2m in the deeper profile. A similar profile to temperature can be observed for dissolved oxygen: values increase from 140% to 200% before dropping sharply to 6%. In TER1A this occurs at 2 m, whereas in TER1B it occurs at 3 m. This collective evidence is concluded to indicate a chemocline in Lake Teroto from 3 m in the deepest profile and 2 m in the profiles taken in the littoral parts of the lake. Differences in

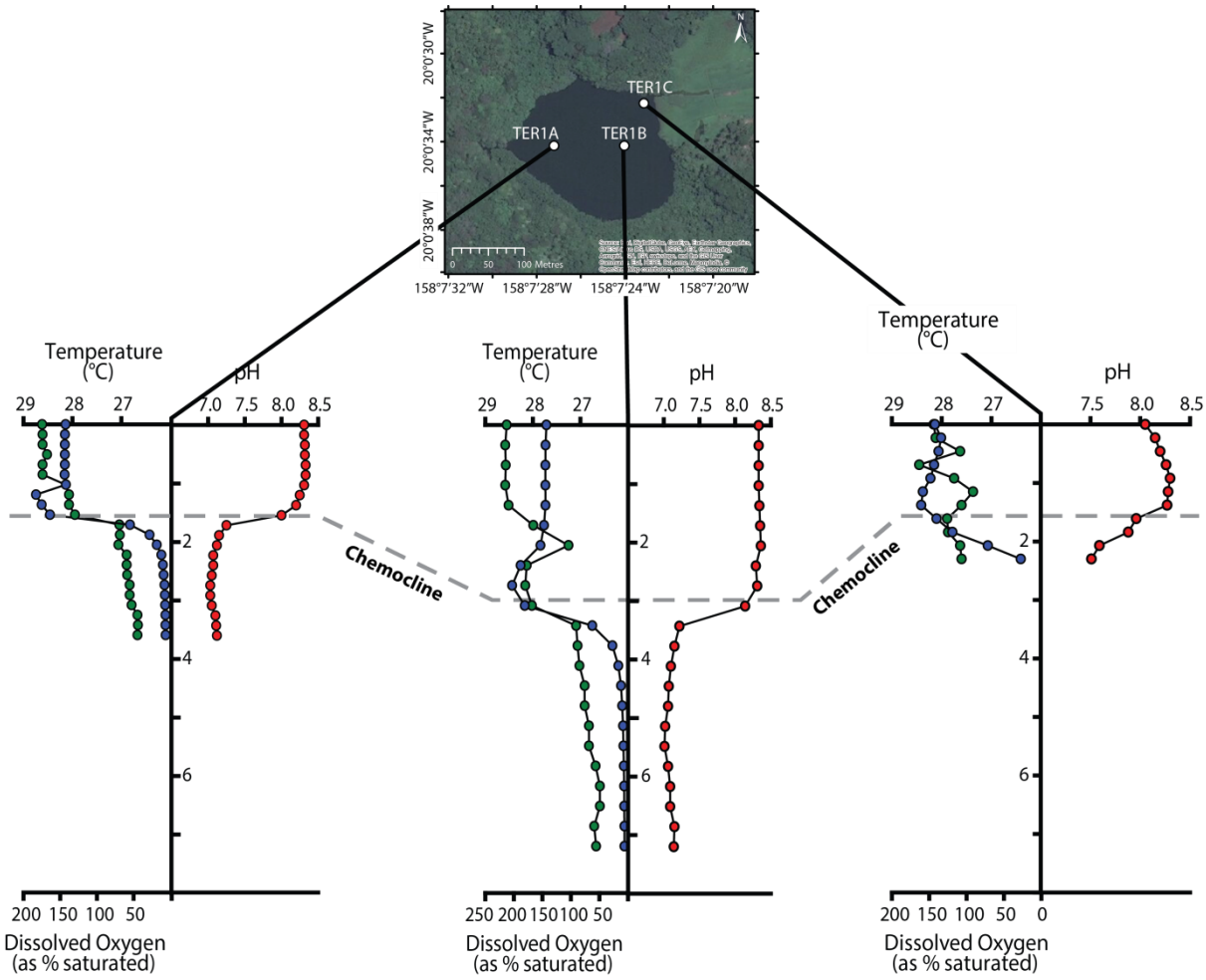

Figure 6.9: Physicochemical profiles for Lake Teroto. Red circles indicate pH; blue circles indicate dissolved oxygen (as % saturated); and green circles are temperature (°C). Due to depth not being automatically measured in this lake the depths are assumed based on water depth at the sampling point and that measurements were obtained at uniform depth intervals.

the depth of the chemocline between the deepest and littoral profiles is most likely a result of inferring depths as previously stated in Section 4.2.2.2. The suggested cause for the anoxic hypolimnion relates to the lake's connection to the sea. The intrusion of dense, saline water from the sea stratifies the lake, with the anoxia being caused by the reduced solubility of oxygen in saline waters (Wetzel, 2001). The near-positive δ-values – outside the range of those predicted with Isomap (Bowen and Revenaugh, 2003) – further suggest a marine input into the site, with the different δ-values between the littoral and basal zones also indicating that the lake is stratified. With this in mind it is suggested that the lake exhibits ectogenic meromixis; however without conductivity measurements and long-term monitoring this cannot be substantiated. The more positive δ-values in basal waters of Lake Teroto compared to littoral waters are suggested to be a result of the

lake's connection to the sea. The intrusion of dense highly saline sea water, with more positive δ-values, would sink into the hypolimnion and lead to more positive δ-values as is observed. The temperature and dissolved oxygen inversion observed between 2 and 3 m is indicative of a positive heterograde profile, suggesting that there is aquatic productivity in the thermocline increasing the saturation of dissolved oxygen in the water.

A littoral water sample from the lake had a salinity of 6 ppt (A. Maloney, personal communication, 2015) indicating that the lake is brackish: this corroborates Lake Teroto's connection to the sea and that it is open. Consequently interpretation of hydrological change from the lake will be more complex. It has been previously concluded by Kautai'i *et al*. (1984) that the lake level fluctuates, and further supported by differences in lake depth recorded in this study and Parkes (1994) (Section 3.2.6). Lake level could lower as a result of: 1) increased temperatures; 2) reduced precipitation due to SPCZ contraction and/or movement NW; or 3) sea level lowering reducing the volume of sea water supplied to the lake. Contrary to this, lake level could raise as a consequence of: 1) decreased temperatures; 2) increased precipitation due to SPCZ expansion and/or movement SE; or 3) a sea level rise increasing marine input to the lake.

6.3.3.2 Lake Lanoto'o

In both profiles pH increases at 1.9 m below the water surface, staying stable at pH 7 until 9 m before sharply decreasing to pH 4 or less (Figure 6.10). Both conductivity profiles show a small decrease in conductivity at 2.9 m from 15 µS/cm to 14 µS/cm. Conductivity increases from 9 m with a stepwise progression to maximum values at 14.5 m of 21 µS/cm. The temperature profiles both a steady decrease in temperature from ca. 27 °C to 23 °C at 14.5 m; there is a notable temperature decrease occurs between 1 and 2 m depth from 27 °C to 26 °C. Oxygen dropped from 105% at 9.5 m to 10% at 12 m. The combined physicochemical changes that occur at 10 m are inferred to represent a chemocline in the lake and it having an anoxic hypolimnion. When considering that the lake has strong physicochemical gradients, and that the lake is sheltered from storms in the volcanic crater, it is highly likely that the lake is meromictic. This is further supported by the different δ-values from the littoral and basal zones of the lake that indicate the lake is stratified. The less negative δ-values in littoral water of Lake Lanoto'o in contrast to

the basal waters is possibly a consequence of a recent precipitation event with a high amount

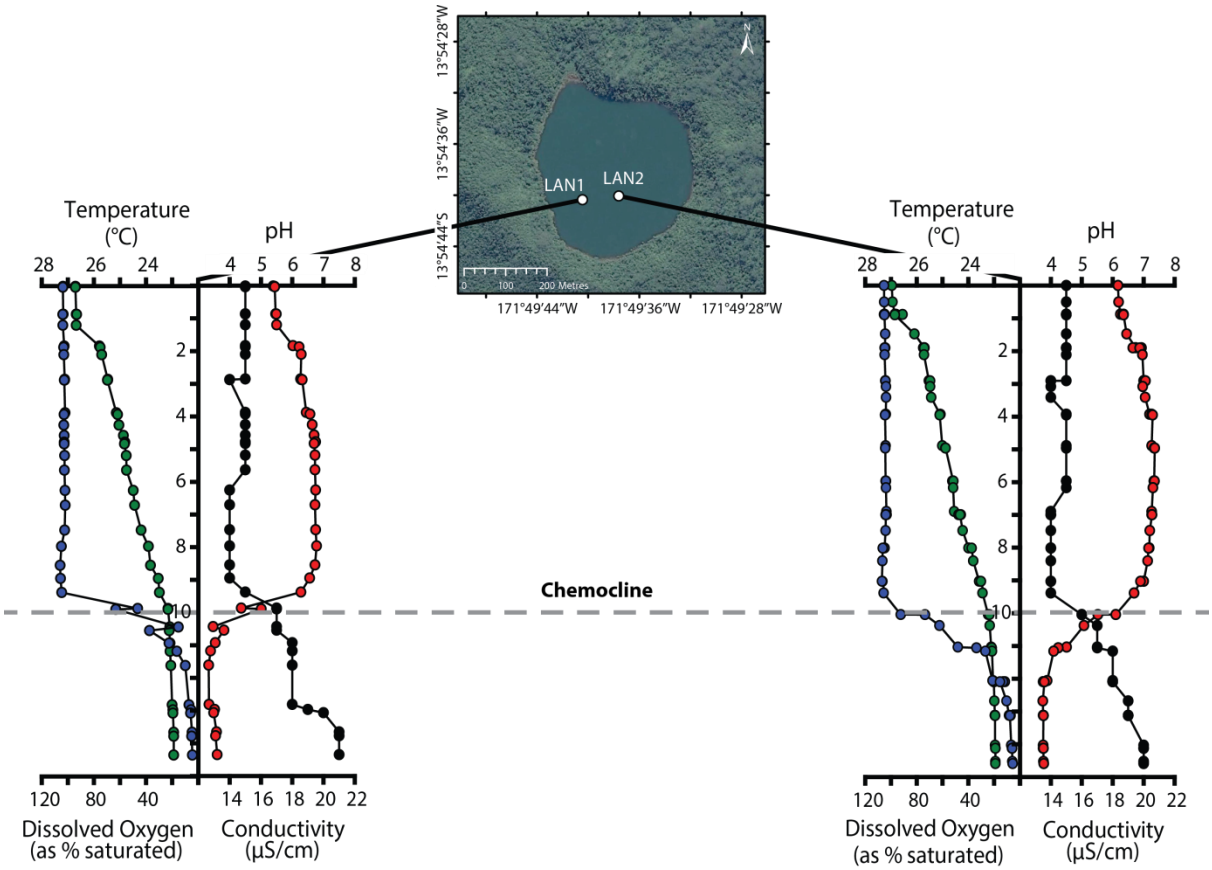

Figure 6.10: Physicochemical profiles for Lake Lanoto'o. Red circles indicate pH; black circles indicate conductivity (µS/cm); blue circles indicate dissolved oxygen (as % saturated); and green circles are temperature (°C).

of precipitation and resultant more negative δ-values. The dissolved oxygen curve represents a clinograde profile which suggests the lake is productive (Wetzel, 2001). It is inferred that the pH increases in the hypolimnion due to microbial decomposition of organic matter and CO_2 outgassing related to this (Wetzel, 2001).

In regards to interpreting hydrological change of the long-core data from Lake Lanoto'o, the lake is a fresh, closed system at present. Any changes in lake level will either be a consequence of increased temperature causing increased evaporation and lowering of lake level, or an increase (decrease) in the amount of precipitation causing a correspondent increase (decrease) in lake level. Based on known climatology it is put forward that lake level is primarily controlled by the amount of precipitation it receives as a result of SPCZ movement. Any prolonged contraction and/or movement of the SPCZ NW will likely cause a decrease in precipitation to the lake and the lake level lowering.

Observations of the lake indicated that there is submerged lake shoreline, suggesting prolonged lowering of lake level in the past that may relate to SPCZ contraction and/or movement NW resulting in a precipitation amount decrease.

6.4 Lake sediment sources

6.4.1 Overview

Lakes have two sources of sediment: autochthonous – sediment produced by within-lake processes – and allochthonous – sediment transported into the lake from the surrounding catchment. Micro-XRF (Itrax) analysis can assist in disentangling the two sediment sources; however to be confident with the interpretation it is best combined with low frequency magnetic susceptibility. This is due to most magnetic susceptibility being allogenic, i.e. produced in the catchment, thus those elements that correlate well with low frequency magnetic susceptibility are likely allochthonous in their source (Dearing, 1999). Itrax measurements were obtained at contiguous 200 µm intervals on the short cores and following analysis has been standardised to the incoherent scatter to reduce the effects of organic matter and water content (Marshall *et al*., 2011; Kylander *et al*., 2011). For each site the elements that showed the greatest variability are presented. Data was averaged to 1 cm resolution to facilitate comparison with other proxy data, specifically magnetic susceptibility and TOC. Measurements for low frequency magnetic susceptibility were undertaken at contiguous 1 cm resolution on the short cores for both sites. To further understand the sources of sediments in the lakes correlation matrices and PCA were undertaken on the Itrax data to determine the relationship of elements to each other, and in the case of the correlation matrices quantify the strength of association between pairs of elements in each unit identified in both lakes' short cores. For PCA and the correlation matrices the 200 µm Itrax data for both sites were used to better determine the relationships in the data. Each unit had a separate correlation matrix created due to the lithostratigraphy in both lakes' short cores indicating significant variability. Comparison of Ti, Br and TOC with precipitation was undertaken to see if changes in precipitation result in changes in the geochemical record.

6.4.2 Lake Teroto

The short core is laminated throughout, alternating between black and grey laminae (Section 5.3.1.1). Two units were identified based on the lithostratigraphy (Figure 6.11). Whilst Ti, Fe, Mn and Si show similar variation throughout the short core, Ti shows greater variability. Br shows little variability, only increasing towards present and peaking when Ti values are low. Ca values decrease from ca. 150 cal yr BP to present. Sulphur increases from ca.150 cal yr BP to present, whilst Sr shows little variability except for in Unit 2. Magnetic susceptibility values decreased until ca. 80 cal yr BP, then increased to their highest values (0.00046) at ca. 14 cal yr BP. Values decreased until present, having a much smaller range of variability from 10 cal yr BP to present (Figure 6.11). Ratios of various elements to Ti are presented in Figure 6.12– Ca/Ti and S/Ti show similar trends throughout both units and have a significant relationship ($r^2 = 0.3838$, $p<0.0001$).

Principal components analysis of the entire core, with Unit 1 and 2 highlighted (Figure 6.13), indicates that the first two axes explaining 53% of the data, and $\lambda_1 = 7.20$ and $\lambda_2 = 2.94$. Three groups can be observed in the PCA: the first cluster relates to Unit 2 and is associated with Br, which in turn is related to component 1. The other two groups are not related to each other, one being more closely related to Ca, S, Cl, Mn, K and Fe, the other more closely related with Si, Ti, Al, Zr, Sr and Zn.

The correlation matrix for the two units (Table 6.5 and Table 6.6) identified in the short core indicates that there is a coupling and decoupling of elements. In Lake Teroto, only Si, Ti, Cr, V and Fe remain strongly and significantly correlated in all units. The similar trend between these elements and magnetic susceptibility suggests that they are allochthonous in origin (Figure 6.11). The strong correlation between Si and Ti throughout the short core suggests that Si is principally derived from allochthonous silicate sources. Whilst biogenic sources cannot be discounted, specifically diatom frustules (Peinerud, 2000), it is considered unlikely to be a significant component of the Si signal as a result of the strong, significant correlation.

Both the Itrax stratigraphy and correlation matrices reveal that Fe and Mn are not related, indicating that redox processes are not controlling Fe and Mn. As Fe is closely associated with Ti and Si it is likely a detrital input. Bromine only shows a negative correlation with

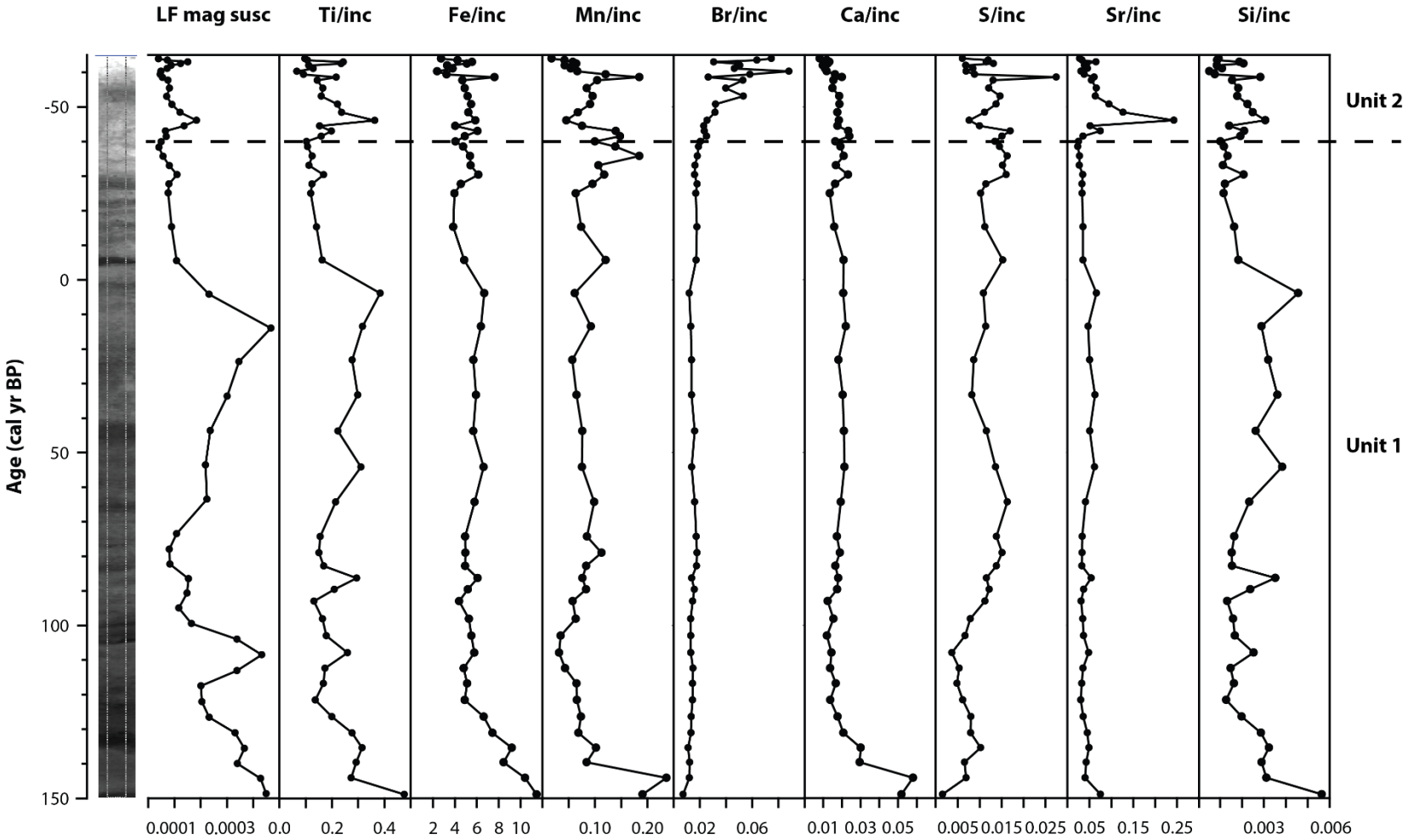

Figure 6.11: Itrax profile for the short core from Lake Teroto. LF mag susc is low frequency magnetic susceptibility. The core's radiograph is also presented: the darker layers indicate denser core material and vice versa.

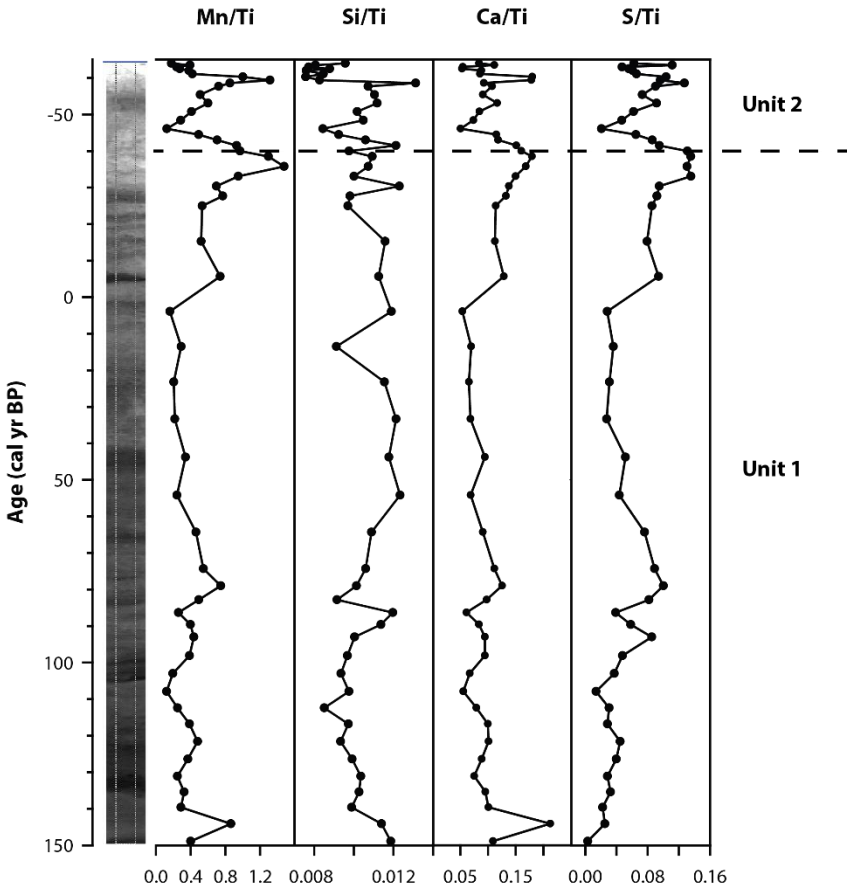

Figure 6.12: Element ratios for the Lake Teroto short core. The core's radiograph is also presented: the darker layers indicate denser core material and vice versa.

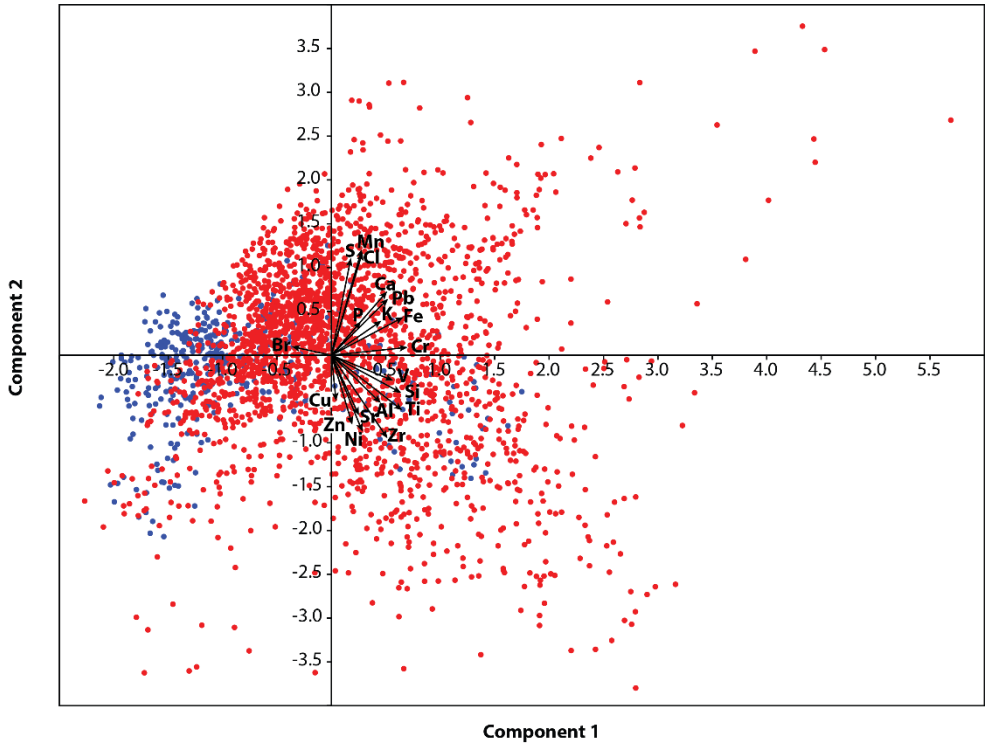

Figure 6.13: PCA of the short core Itrax data from Lake Teroto. Red circles indicate Unit 1, blue circles indicate Unit 2.

Fe in Unit 1, suggesting that it is not allochthonous in origin. Considering that Br is associated with organic compounds (Davies *et al*., 2015) it is suggested Br is indicative of autochthonous productivity. The PCA (Figure 6.13) indicates that there are two distinct clusters of elements that are not related to each other: Si, Ti, Al, Sr, and Zr form one cluster, Fe, K, Ca, Cl, S, and Mn form another. The lack of association between Fe and Ti is not reflected in the Itrax stratigraphy or the correlation matrices for the units, both of which suggest that the two are correlated. The correlation matrix indicates that Ca and Fe have a stronger correlation than Fe and Ti in Unit 2, likely contributing to the apparent lack of association in the PCA between Ti and Fe.

Silicon, Ti, Al and Sr covary throughout the short core and correspond to grey laminae – these being clay laminae comprised of kaolinite as shown by XRD analysis (Appendix B) – whereas the black laminae are associated with K, Ca, Cl, S, and Mn. It is suggested that grey laminae form when precipitation causes in-wash of soil into the lake. Due to the brackish lake water, this causes this material to flocculate into clays. Strontium is strongly adsorbed onto clays (Wahlberg *et al*., 1965) thus likely explaining the strong correlation between Sr and the clay laminae. The black laminae correspond to peaks in S, Cl and Ca. X-ray diffraction analysis has indicated the presence of gypsum ($CaSO_4$) and halite (NaCl) in the black laminae throughout the record (Appendix B) – this explains the peaks in Ca, S and Cl in these laminae. Calcium carbonate was not present in spot samples sent from across the entire record (M. J. Leng, personal communication, January 2015). In the short core, the sample analysed was taken from a clay layer thus explaining the lack of gypsum in this particular sample (Appendix B). Black laminae could be indicative of relatively drier conditions which cause the lake level to lower, consequently increasing the concentration of gypsum and halite and causing them to precipitate out into the lake sediment. A conceptual diagram of these lake sediment formation processes is presented in Figure 6.14.

Titanium is abundant, is not biologically important and has a conservative nature during weathering and transport making it a suitable candidate for examining ratios with other process-indicative elements (Kylander *et al*., 2011). Moreover having established that Ti is allochthonous in its source it follows that by standardising to Ti will allow autochthonous sources of elements to be disentangled: specifically Ca and Si. Peaks in Ca/Ti would

	Al/inc	Si/inc	P/inc	S/inc	Cl/inc	K/inc	Ca/inc	Ti/inc	V/inc	Cr/inc	Mn/inc	Fe/inc	Ni/inc	Cu/inc	Zn/inc	Br/inc	Sr/inc	Zr/inc	Pb/inc
Al/inc		<0.01	<0.01	0.01	0.08	<0.01	<0.01	<0.01	<0.01	<0.01	0.08	<0.01	<0.01	<0.01	<0.01	<0.01	<0.01	<0.01	<0.01
Si/inc	0.64		<0.01	0.01	<0.01	<0.01	<0.01	<0.01	<0.01	<0.01	<0.01	<0.01	<0.01	<0.01	<0.01	<0.01	<0.01	<0.01	<0.01
P/inc	0.25	0.29		<0.01	<0.01	<0.01	<0.01	<0.01	<0.01	<0.01	<0.01	<0.01	0.32	<0.01	0.97	0.48	<0.01	<0.01	<0.01
S/inc	-0.05	0.06	0.29		<0.01	<0.01	<0.01	<0.01	<0.01	<0.01	<0.01	<0.01	0.07	<0.01	<0.01	<0.01	<0.01	<0.01	<0.01
Cl/inc	-0.04	0.16	0.32	0.51		<0.01	<0.01	<0.01	<0.01	<0.01	<0.01	<0.01	<0.01	0.37	<0.01	<0.01	<0.01	<0.01	<0.01
K/inc	0.21	0.56	0.32	0.36	0.61		<0.01	<0.01	<0.01	<0.01	<0.01	<0.01	<0.01	<0.01	<0.01	0.06	0.88	<0.01	<0.01
Ca/inc	0.28	0.41	0.15	0.13	0.40	0.36		<0.01	<0.01	<0.01	<0.01	<0.01	0.52	0.06	<0.01	<0.01	0.14	<0.01	<0.01
Ti/inc	0.59	**0.87**	0.19	-0.09	0.13	0.51	0.40		<0.01	<0.01	0.44	<0.01	<0.01	<0.01	<0.01	<0.01	<0.01	<0.01	<0.01
V/inc	0.43	0.60	0.14	-0.11	0.16	0.35	0.45	**0.70**		<0.01	<0.01	<0.01	<0.01	0.03	<0.01	<0.01	<0.01	<0.01	<0.01
Cr/inc	0.49	**0.80**	0.27	0.14	0.45	0.63	0.63	**0.84**	0.68		<0.01	<0.01	<0.01	<0.01	<0.01	<0.01	<0.01	<0.01	<0.01
Mn/inc	0.04	0.08	0.14	0.48	0.42	0.22	**0.73**	-0.02	0.11	0.28		<0.01	<0.01	<0.01	0.27	<0.01	<0.01	<0.01	<0.01
Fe/inc	0.43	0.64	0.25	0.17	0.46	0.48	**0.76**	0.67	0.67	**0.89**	0.45		0.40	<0.01	<0.01	<0.01	<0.01	<0.01	<0.01
Ni/inc	0.32	0.46	0.02	-0.04	-0.17	0.25	0.01	0.44	0.20	0.26	-0.11	0.02		<0.01	<0.01	<0.01	<0.01	<0.01	0.26
Cu/inc	0.08	0.18	0.06	-0.08	0.02	0.19	-0.04	0.19	0.05	0.10	-0.12	-0.08	0.44		<0.01	<0.01	0.06	<0.01	<0.01
Zn/inc	0.28	0.34	0.00	-0.19	-0.13	0.13	0.15	0.44	0.31	0.29	-0.02	0.20	0.35	0.14		<0.01	<0.01	<0.01	<0.01
Br/inc	-0.16	-0.21	0.02	0.25	0.19	-0.04	-0.12	-0.25	-0.26	-0.26	0.09	-0.26	-0.16	-0.10	-0.18		<0.01	<0.01	<0.01
Sr/inc	0.32	0.35	0.10	-0.06	-0.09	0.00	0.03	0.47	0.29	0.24	-0.12	0.14	0.15	0.04	0.10	0.20		<0.01	0.41
Zr/inc	0.50	0.67	0.06	-0.28	-0.14	0.26	0.21	**0.79**	0.59	0.59	-0.14	0.45	0.43	0.20	0.46	-0.29	0.43		<0.01
Pb/inc	0.27	0.42	0.18	0.19	0.39	0.35	0.68	0.41	0.45	0.65	0.46	0.78	-0.02	-0.09	0.12	-0.20	-0.02	0.24	

Table 6.5: Lake Teroto correlation matrix of Itrax data for Unit 1. In bold are correlations r≥0.7 and r≤-0.7. Highlighted in red are values that are not statistically significant below the 0.01 significance level.

	Al/inc	Si/inc	P/inc	S/inc	Cl/inc	K/inc	Ca/inc	Ti/inc	V/inc	Cr/inc	Mn/inc	Fe/inc	Ni/inc	Cu/inc	Zn/inc	Br/inc	Sr/inc	Zr/inc	Pb/inc
Al/inc		<0.01	<0.01	<0.01	0.96	<0.01	<0.01	<0.01	<0.01	<0.01	0.71	<0.01	<0.01	<0.01	0.06	<0.01	<0.01	<0.01	<0.01
Si/inc	0.64		<0.01	<0.01	0.38	<0.01	<0.01	<0.01	<0.01	<0.01	0.33	<0.01	<0.01	<0.01	<0.01	<0.01	<0.01	<0.01	<0.01
P/inc	0.42	0.42		<0.01	<0.01	<0.01	<0.01	<0.01	<0.01	<0.01	0.01	<0.01	0.14	0.01	0.06	<0.01	<0.01	<0.01	<0.01
S/inc	0.44	0.64	0.41		<0.01	<0.01	<0.01	<0.01	<0.01	<0.01	<0.01	<0.01	<0.01	<0.01	0.95	<0.01	<0.01	<0.01	<0.01
Cl/inc	0.00	0.04	0.25	0.25		<0.01	<0.01	<0.01	<0.01	<0.01	0.00	<0.01	0.01	<0.01	<0.01	<0.01	<0.01	<0.01	<0.01
K/inc	0.30	0.53	0.35	0.52	0.60		<0.01	<0.01	<0.01	<0.01	<0.01	<0.01	<0.01	0.04	0.94	<0.01	<0.01	<0.01	<0.01
Ca/inc	0.27	0.39	0.27	0.49	0.41	0.55		<0.01	<0.01	<0.01	<0.01	<0.01	<0.01	0.18	0.00	<0.01	<0.01	<0.01	<0.01
Ti/inc	0.59	**0.90**	0.38	0.69	0.19	0.65	0.45		<0.01	<0.01	0.02	<0.01	<0.01	<0.01	<0.01	<0.01	<0.01	<0.01	<0.01
V/inc	0.44	0.68	0.33	0.61	0.25	0.57	0.31	**0.80**		<0.01	0.26	<0.01	<0.01	<0.01	<0.01	<0.01	<0.01	<0.01	<0.01
Cr/inc	0.52	**0.81**	0.40	**0.74**	0.39	**0.73**	0.56	**0.93**	**0.76**		<0.01	<0.01	<0.01	<0.01	0.03	<0.01	<0.01	<0.01	<0.01
Mn/inc	0.02	0.05	0.14	0.20	0.42	0.27	**0.70**	0.12	0.06	0.23		<0.01	0.01	0.34	<0.01	0.09	<0.01	0.02	<0.01
Fe/inc	0.50	**0.77**	0.41	**0.85**	0.35	0.67	0.49	**0.89**	**0.78**	**0.93**	0.17		<0.01	<0.01	0.10	<0.01	<0.01	<0.01	<0.01
Ni/inc	0.24	0.38	0.07	0.15	0.13	0.36	0.26	0.44	0.34	0.43	0.14	0.28		<0.01	<0.01	<0.01	<0.01	<0.01	<0.01
Cu/inc	-0.28	-0.38	-0.14	-0.39	0.15	-0.11	-0.07	-0.37	-0.31	-0.31	0.05	-0.43	0.19		0.65	<0.01	<0.01	<0.01	<0.01
Zn/inc	0.10	0.20	-0.10	0.00	-0.32	0.00	-0.21	0.20	0.19	0.11	-0.33	0.09	0.29	-0.02		0.62	0.26	0.01	0.28
Br/inc	-0.33	-0.52	-0.28	-0.40	-0.44	-0.53	-0.29	-0.67	-0.63	**-0.71**	-0.09	**-0.73**	-0.25	0.30	-0.03		<0.01	<0.01	<0.01
Sr/inc	0.41	0.64	0.34	0.48	0.54	**0.71**	0.45	**0.79**	0.69	**0.85**	0.20	**0.78**	0.44	-0.20	0.06	**-0.83**		<0.01	<0.01
Zr/inc	0.39	0.62	0.34	0.52	0.45	0.65	0.36	**0.79**	**0.73**	**0.80**	0.11	**0.78**	0.40	-0.22	0.14	**-0.74**	**0.88**		<0.01
Pb/inc	0.36	0.50	0.26	0.61	0.29	0.46	0.40	0.59	0.56	0.62	0.20	0.67	0.20	-0.21	0.06	-0.41	0.49	0.50	

Table 6.6: Lake Teroto correlation matrix of Itrax data for Unit 2. In bold are correlations r≥0.7 and r≤-0.7. Highlighted in red are values that are not statistically significant below the 0.01 significance level.

indicate increased precipitation of calcium, likely to be gypsum. This can be corroborated with S/Ti: Ca/Ti and S/Ti have a significant, positive correlation ($r = 0.74$, $p<0.01$) hypothesised to indicate gypsum precipitation as revealed by XRD analysis (Appendix B). Peaks in Si/Ti are suggested to indicate autochthonous Si; whether this is a biogenic in origin is not possible to determine with the data available. Nevertheless, Parkes (1994) produced a diatom record for Lake Teroto, thus changes in Si/Ti can be related to this to determine the contribution diatoms have to autochthonous Si. As there is not a suitably strong correlation between Fe and Mn standardising Fe to Mn would not provide an indicator of anoxia in bottom waters (Kylander *et al*., 2011); however standardising Mn to Ti can provide an indicator of oxygenated bottom waters. Manganese has a very weak correlation to Ti in both units in the Lake Teroto short core, indicating it is not allochthonous in origin, thus changes in its abundance relate to autochthonous processes. As Mn precipitates as an insoluble oxide in oxygenated waters, standardising to Ti would provide an indicator of enhanced Mn precipitation that is suggested to be a consequence of oxygenated bottom waters (Kylander *et al*., 2011).

As Ti is allochthonous in source it has been compared to the precipitation record from Rarotonga to further examine how precipitation relates to the Lake Teroto record. The Lake Teroto Ca/Ti record has also been compared to the Rarotonga precipitation record to determine its relationship to precipication. Both Ca/Ti and Ti show relatively similar trends to Rarotonga precipitation from AD 1899-2012 (Figure 6.15): with increases in Ca/Ti (decreses in Ti) when Rarotonga precipitation amount is lower (higher). This supports that peaks Ca/Ti likely relate to gypsum precipitation during periods with reduced precipitation amount. The peaks in Ti corresponding to peaks in precipitation amount indicates that Ti, and the aforementioned elements that covary with it, are washed into the lake from catchment soils as a result of precipitation. From AD 1982-2012 reductions in precipitation associated with SPCZI values >11 correspond to increases in Ca/Ti and decreases in Ti – albeit these are small reductions. This indicates that with reduced precipitation amount as a result of the SPCZ contracting and/or moving NW (Trenberth, 1976; Folland *et al*., 2002), less catchment soil is washed into the lake with this being reflected in a corresponding decrease in Ti, and Ca/Ti increases as gypsum has precipitated out of the water column. It is hypothesised that during these periods the δ^2H values of long-chain alkanoic acids will be less negative as a result of the decreased

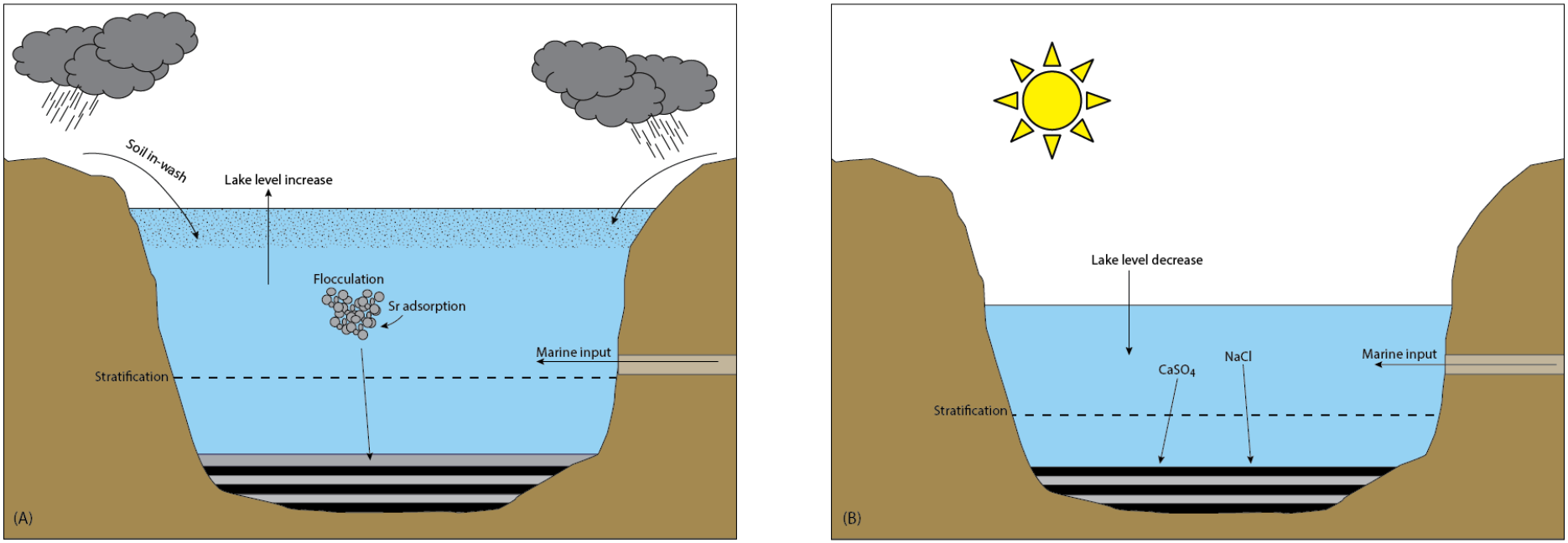

Figure 6.14: Conceptual diagram for laminae formation in Lake Teroto. (A) Precipitation causes in-wash of soils and increase in lake level; the brackish lake water causes the soil material to flocculate and Sr to be adsorbed to the flocculated sediment; sediment is deposited as a grey lamina characterised with high Ti, Al, Si and Sr. (B) Drier period causes lake level to decrease; gypsum ($CaSO_4$) and halite (NaCl) increase in concentration in lake waters and precipitate out; sediment is deposited in black lamina characterised with high Ca/Ti and S/Ti.

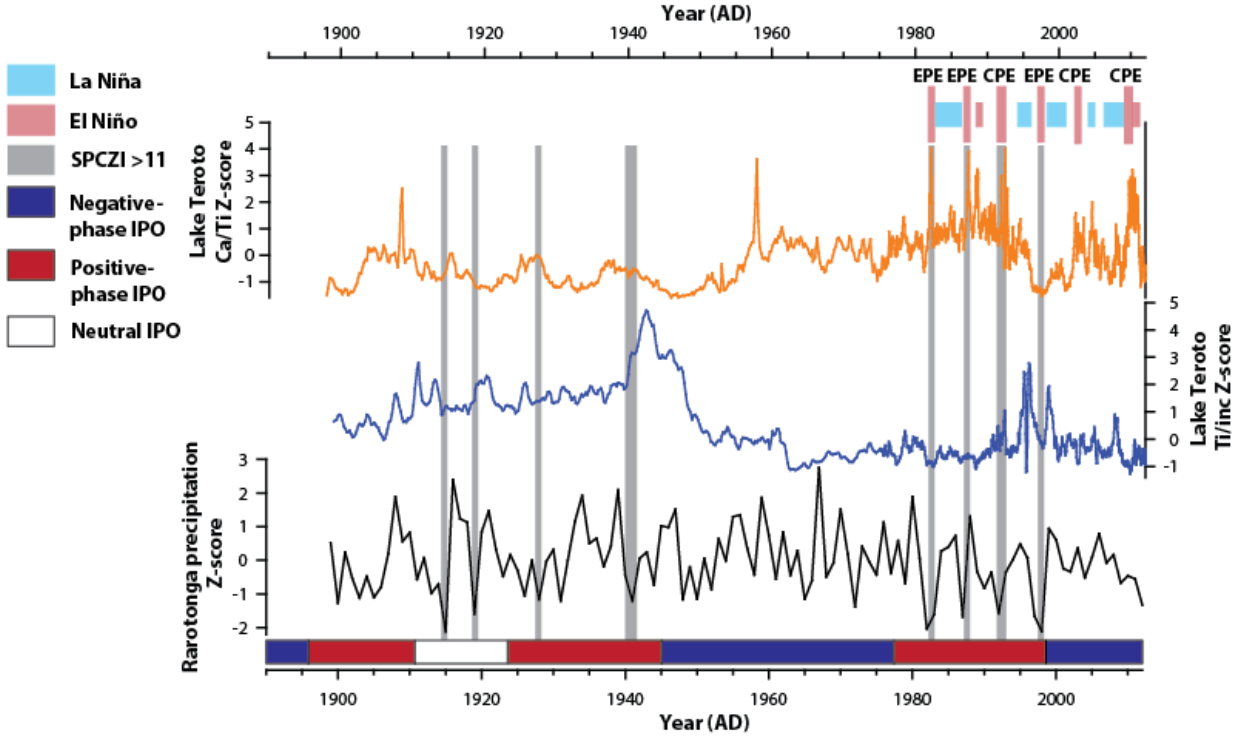

Figure 6.15: Comparison of Lake Teroto Ca/Ti and Ti/inc with Rarotonga precipitation from AD 1899-2012. Phases of IPO are highlighted (Henley *et al*., 2015), and blue shaded bars at the top of the plot indicate La Niña events, whereas red-shaded bars indicate El Niño events. Moderate to strong El Niño events are indicated by longer-length bars. El Niño and La Niña events are defined by 3-month running mean Niño 3.4 SSTAs where El Niño (La Niña) events are defined as SSTAs ≥0.5 °C (≤−0.5 °C) and moderate-to-strong El Niño events are defined as SSTAs ≥1.0 °C for three or more consecutive months (Atwood and Sachs, 2014). SST data was obtained from NOAA ERSST v3b. ENSO Events have been determined from AD 1982 to 2011 to correlate with Eastern Pacific El Niño (EPE) and Central Pacific El Niño (CPE) designations from Kidwell *et al*. (2014). Years with SPCZI values >11 are highlighted with full-length grey bars (Salinger *et al*., 2014).

precipitation amount as determined in section 6.3.2. When examining El Niño types with Ca/Ti and Ti, the most pronounced increases (decreases) in Ca/Ti (Ti) during this period correlates with both EPE and CPE. CPE do relate to reductions in Ti but not to the same degree, notably the AD 1991/1992 El Niño which causes smaller reductions in Ti. Interestingly there is no apparent increase in Ca/Ti during the AD 1997/98 EPE, with a peak occurring between AD 1998/99. This may be due to an increase in precipitation amount in November and December AD 1997 (R. Malcom, personal communication, September 2016), decreasing the concentration of gypsum in the water column thus meaning gypsum did not precipitate out. Overall the Ca/Ti (Ti) in the Lake Teroto record show increases (decreases) with all El Niño types over the AD 1982-2012 period, with EPE during positive-phase IPO causing the largest increases (decreases) in Ca/Ti (Ti).

Increases in precipitation relate to La Niña events during this period, which also relate to higher Ti values indicating that with increased precipitation during a La Niña, as a result of the SPCZ expanding and/or moving SE (Trenberth, 1976; Folland *et al*., 2002), more catchment soil is washed in to the lake causing increases in Ti. It is hypothesised that during these periods the δ^2H values of long-chain alkanoic acids will be more negative as a result of the increased precipitation amount as concluded in section 6.3.2. Prior to AD 1982 reductions in precipitation amount relate to reductions in Ti, and years with SPCZI >11 occur there is a reduction in Ti. The reduced Ti value in AD 1941 (an SPCZI >11 year) is not as pronounced; nevertheless there is a small reduction. Whilst it is likely that there are multiple factors influencing Ti in the Lake Teroto record, it can be inferred that precipitation amount, related to SPCZ position, does affect Ti values in an expected way: i.e. with decreased precipitation amount, such as during years when the SPCZI value is >11, Ti decreases as a result of reduced catchment soil input. Overall it indicates that the geochemical record can be used to interpret qualitative changes in precipitation amount, which in turn can be related to SPCZ position. However it should be noted that over centennial, and greater, timescales interpretations of wet or dry conditions should be related to IPO phases as a result of the chronological resolution in Lake Teroto being greater than ENSO's periodicity (Section 5.3.1.2).

6.4.3 Lake Lanoto'o

The Itrax data were separated into two units based on the lithostratigraphy. Bromine shows higher values in Unit 1, whereas Ti, Fe, Mn, Ca and Si are higher in Unit 2 (Figure 6.16). Low frequency magnetic susceptibility values decrease from ca. 640 cal yr BP, reaching their lowest at ca. 370 cal yr BP, then increasing until present, matching the trends in Ti, Fe and Mn. Ratios of various elements to Ti are shown in Figure 6.17. PCA of the entire short core shows two distinct groups that clearly related to the two units identified from the lithostratigraphy, with 58% of the variance explained by the first two components and $\lambda_1 = 6.85$ and $\lambda_2 = 1.31$ (Figure 6.18). Chromium, Ca, Fe, Mn, Ni and Br are all associated with axis 1; however Br has an inverse correlation with these elements. Correlation tables for elements in each unit are presented in Table 6.7 and Table 6.8.

The correlation matrices for the two Itrax units suggest that Fe and Mn are coupled in Unit 2 and decoupled in Unit 1; however in Unit 1 the correlation is strong (0.64): it is suggested that Fe and Mn are coupled throughout the short core. Consequently it is inferred that redox processes control Fe and Mn, thus standardising Fe to Mn can indicate bottom water anoxia in Lake Lanoto'o. Silicon and Ti are not correlated, suggesting that standardising Si to Ti would provide an indicator of autochthonous Si. As with Lake Teroto it is not possible with the data available to determine if this is biogenic in origin. Calcium follows a similar trend to Ti/Fe/Mn in the Itrax stratigraphy, and is closely associated in the PCA of for both units. However the correlation matrices indicate this is not a strong relationship. Despite this it is suggested that the Ca source is allogenic (erosion); therefore standardising Ca to Ti would indicate authigenic Ca (within lake precipitation) (Cohen, 2003).

The Itrax stratigraphy indicates an inverse relationship between Ti/Fe/Mn with Br, supported by PCA (Figure 6.18). Bromine is indicative of organic matter in lakes (Davies et al., 2015) – the Lake Lanoto'o Br has a positive, significant correlation with Lake Lanoto'o TOC ($r = 0.43$, $p<0.05$). With trends in Ti/Fe/Mn matching the low frequency magnetic susceptibility, it indicates that these elements are allochthonous in source. It is hypothesised that the negative correlation between Br and Ti/Fe/Mn is a consequence of catchment inputs diluting the Br signal, and by extension organic matter content in the lake. Lake Lanoto'o appears to be a relatively simple system: precipitation causes in-wash

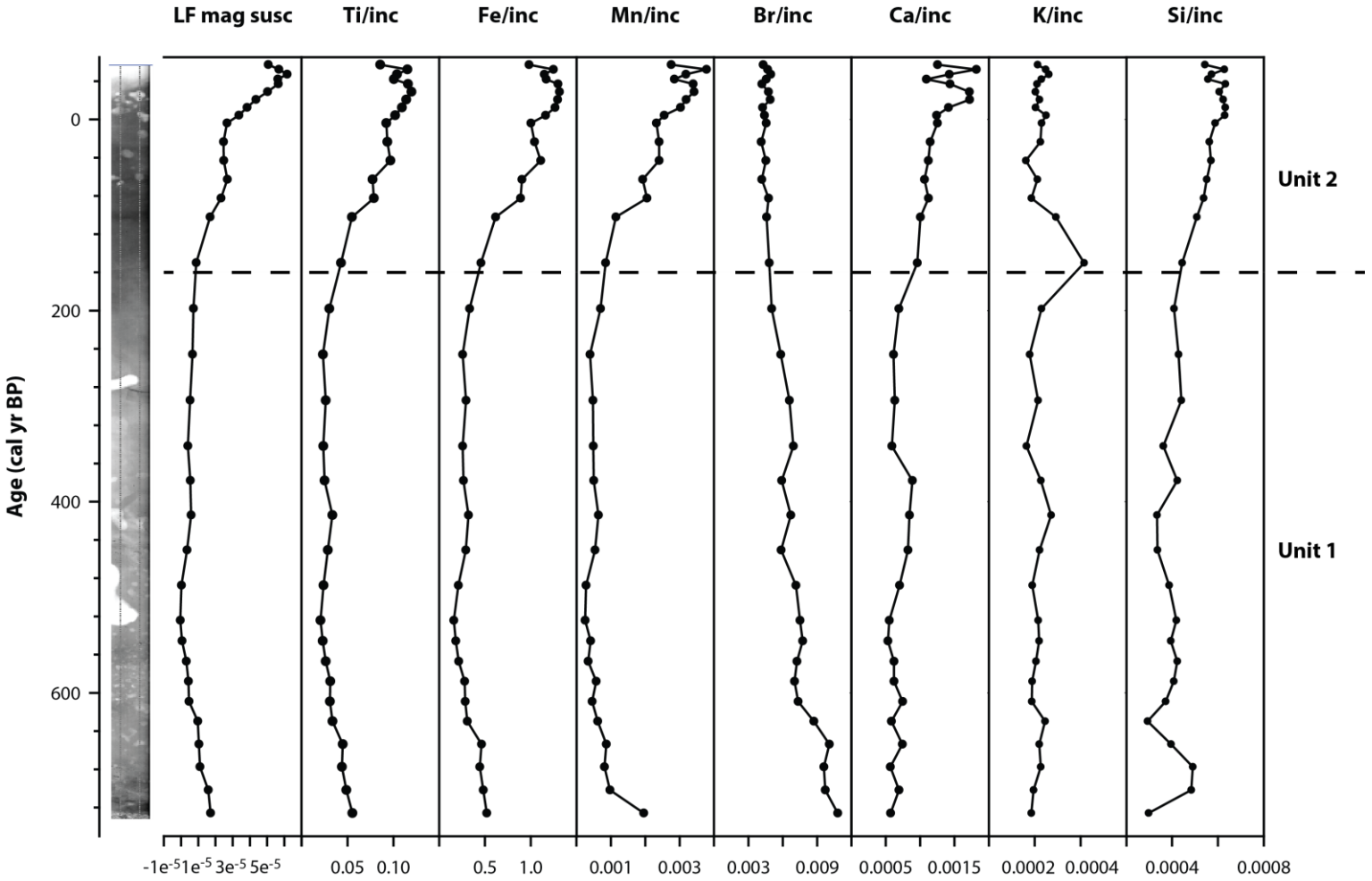

Figure 6.16: Itrax profile for the Lake Lanoto'o short core. LF mag susc is low frequency magnetic susceptibility. The core's radiograph is also presented: the darker layers indicate denser core material and vice versa.

of catchment soils (increasing Ti/Fe/Mn) diluting organic matter deposited in the lake sediment (decreasing Br). During drier periods catchment soils are not washed into the lake (decreasing Ti/Fe/Mn) thus organic matter is not diluted and increases in relative concentration in the lake sediment (increased Br and TOC). A conceptual diagram of lake sediment formation processes is presented in Figure 6.19.

Bromine and Ti, the latter determined to be allochthonous in source, were compared to the Apia precipitation record to examine their respective relationships to it (Figure 6.20). From AD 1982-2012 reductions in precipitation that occur during years with SPCZI values >11, i.e. when the SPCZ has contracted and/or moved NW, relate to increases (decreases) in Br (Ti). A notable exception is AD 1992 where precipitation amount is high and Ti is higher. This indicates that with a reduced precipitation amount as a result of the SPCZ contracting and/or moving NW (Trenberth, 1976; Folland *et al*., 2002), less catchment soil is washed into the lake with this being reflected in a corresponding decrease in Ti and increase in Br. It is postulated that during these periods the δ^2H values of long-chain alkanoic acids will be less negative as a result of the decreased precipitation amount – this is supported by the conclusions drawn in section 6.3.2. All EPE events in this period correspond with reductions in precipitation amount and clear increases (decreases) in Br (Ti), whereas CPE events do not always cause reductions (increases) in precipitation or Ti (Br) such as AD 1991/92 and 2002/03. This corroborates with Kidwell *et al*. (2016) who showed that EPE events caused the SPCZ to take a zonal orientation (zSPCZ), reducing precipitation amount whereas CPE events have varying impacts and can relate to both increases and decreases in precipitation. Consequently this indicates that for the AD 1982-2012 period Lake Lanoto'o shows increases (decreases) in Br (Ti) with EPE. During the AD 1982-2012 period La Niña events relate to increases in precipitation amount, due to SCPZ expansion and/or movement SE (Trenberth, 1976; Folland *et al*., 2002), and increases (decreases) in Ti (Br) in the Lanoto'o record. It is put forward that during these periods the δ^2H values of long-chain alkanoic acids will be more negative as a result of the increased precipitation amount; section 6.3.2 substantiates this.

Prior to AD 1982 SPCZI years >11 relate to increases (decreases) in (Br) Ti, suggesting this relationship holds further back in time. Further increases in Ti correspond with increases in precipitation amount for this period. Overall it indicates that the geochemical record

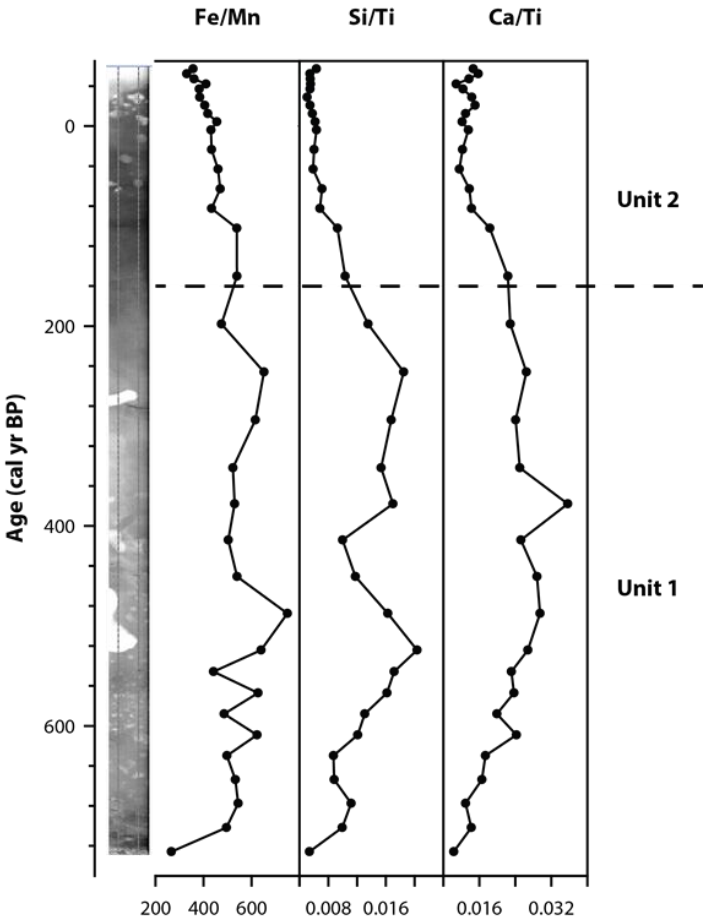

Figure 6.17: Element ratios for the Lake Lanoto'o short core. The core's radiograph is also presented: the darker layers indicate denser core material and vice versa.

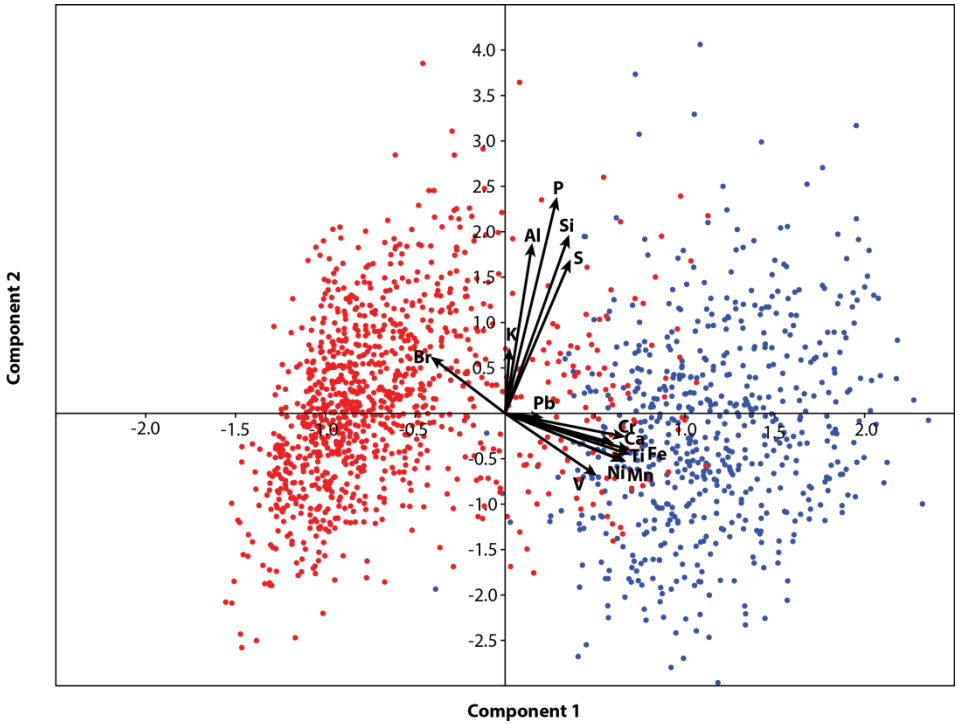

Figure 6.18: PCA of the short core from Lake Lanoto'o. Red circles indicate Unit 1, blue circles indicate Unit 2.

	Al/inc	Si/inc	P/inc	S/inc	K/inc	Ca/inc	Ti/inc	V/inc	Cr/inc	Mn/inc	Fe/inc	Ni/inc	Br/inc	Pb/inc
Al/inc		<0.01	<0.01	0.17	0.44	<0.01	0.02	0.01	0.49	0.05	0.03	0.23	0.60	0.86
Si/inc	0.21		<0.01	<0.01	0.96	<0.01	<0.01	<0.01	<0.01	<0.01	<0.01	<0.01	<0.01	0.42
P/inc	0.11	0.28		<0.01	0.03	<0.01	<0.01	<0.01	<0.01	<0.01	<0.01	<0.01	0.06	0.15
S/inc	0.04	0.30	0.38		<0.01	<0.01	<0.01	<0.01	<0.01	<0.01	<0.01	<0.01	0.31	0.03
K/inc	-0.02	0.00	0.07	0.12		<0.01	0.49	0.25	0.30	0.21	0.37	0.81	<0.01	0.38
Ca/inc	0.11	0.15	0.13	0.26	0.13		<0.01	<0.01	<0.01	<0.01	<0.01	<0.01	<0.01	0.05
Ti/inc	0.07	0.25	0.23	0.37	0.02	0.50		<0.01	<0.01	<0.01	<0.01	<0.01	<0.01	<0.01
V/inc	0.08	0.10	0.15	0.15	0.04	0.26	0.51		<0.01	<0.01	<0.01	<0.01	<0.01	0.15
Cr/inc	0.02	0.25	0.26	0.43	0.03	0.39	**0.82**	0.37		<0.01	<0.01	<0.01	0.02	<0.01
Mn/inc	0.06	0.20	0.20	0.30	0.04	0.46	**0.80**	0.47	0.63		<0.01	<0.01	<0.01	<0.01
Fe/inc	0.07	0.25	0.22	0.33	0.03	0.53	**0.98**	0.53	**0.78**	**0.80**		<0.01	<0.01	<0.01
Ni/inc	0.04	0.20	0.18	0.32	0.01	0.43	**0.77**	0.42	**0.73**	0.67	**0.75**		<0.01	0.04
Br/inc	-0.02	-0.10	-0.06	0.03	-0.09	-0.33	-0.20	-0.22	-0.07	-0.23	-0.28	-0.17		0.69
Pb/inc	-0.01	0.02	0.04	0.07	0.03	0.06	0.12	0.04	0.10	0.10	0.12	0.06	0.01	

Table 6.7: Correlaton matrix for elements from Lake Lanoto'o Unit 1. In bold are correlations r≥0.7 and r≤-0.7. Highlighted in red are values that are not statistically significant below the 0.01 significance level.

	Al/inc	Si/inc	P/inc	S/inc	K/inc	Ca/inc	Ti/inc	V/inc	Cr/inc	Mn/inc	Fe/inc	Ni/inc	Br/inc	Pb/inc
Al/inc		<0.01	<0.01	0.11	0.32	0.93	0.62	0.38	0.87	0.59	0.96	0.99	0.41	0.46
Si/inc	0.27		<0.01	<0.01	0.16	0.04	<0.01	0.75	0.01	0.22	<0.01	0.55	0.53	0.94
P/inc	0.18	0.31		<0.01	0.12	<0.01	<0.01	0.30	<0.01	0.34	<0.01	0.99	0.61	0.24
S/inc	0.07	0.14	0.27		0.01	<0.01	<0.01	0.71	<0.01	<0.01	<0.01	<0.01	0.78	0.02
K/inc	-0.04	0.06	0.06	0.11		0.14	0.84	0.50	0.49	0.22	0.68	0.37	0.53	0.08
Ca/inc	0.00	0.09	0.12	0.25	0.06		<0.01	<0.01	<0.01	<0.01	<0.01	<0.01	0.04	0.19
Ti/inc	0.02	0.16	0.15	0.32	0.01	0.62		<0.01	<0.01	<0.01	<0.01	<0.01	0.07	0.07
V/inc	0.04	0.01	-0.04	-0.02	0.03	0.15	0.19		0.01	<0.01	<0.01	<0.01	0.54	0.35
Cr/inc	0.01	0.11	0.15	0.25	0.03	0.51	**0.74**	0.11		<0.01	<0.01	<0.01	0.03	0.03
Mn/inc	0.02	0.05	0.04	0.13	0.05	0.55	0.67	0.25	0.56		<0.01	<0.01	0.16	0.27
Fe/inc	0.00	0.15	0.13	0.29	-0.02	0.55	**0.95**	0.21	**0.70**	0.64		<0.01	0.19	0.18
Ni/inc	0.00	0.02	0.00	0.12	-0.04	0.39	0.63	0.16	0.57	0.56	0.63		0.46	0.54
Br/inc	0.03	-0.03	-0.02	-0.01	0.03	0.09	0.08	-0.02	0.09	0.06	0.05	0.03		0.19
Pb/inc	-0.03	0.00	0.05	0.10	0.07	0.05	0.07	-0.04	0.09	0.05	0.05	0.03	0.05	

Table 6.8: Correlaton matrix for elements from Lake Lanoto'o Unit 2. In bold are correlations r≥0.7 and r≤-0.7. Highlighted in red are values that are not statistically significant below the 0.01 significance level

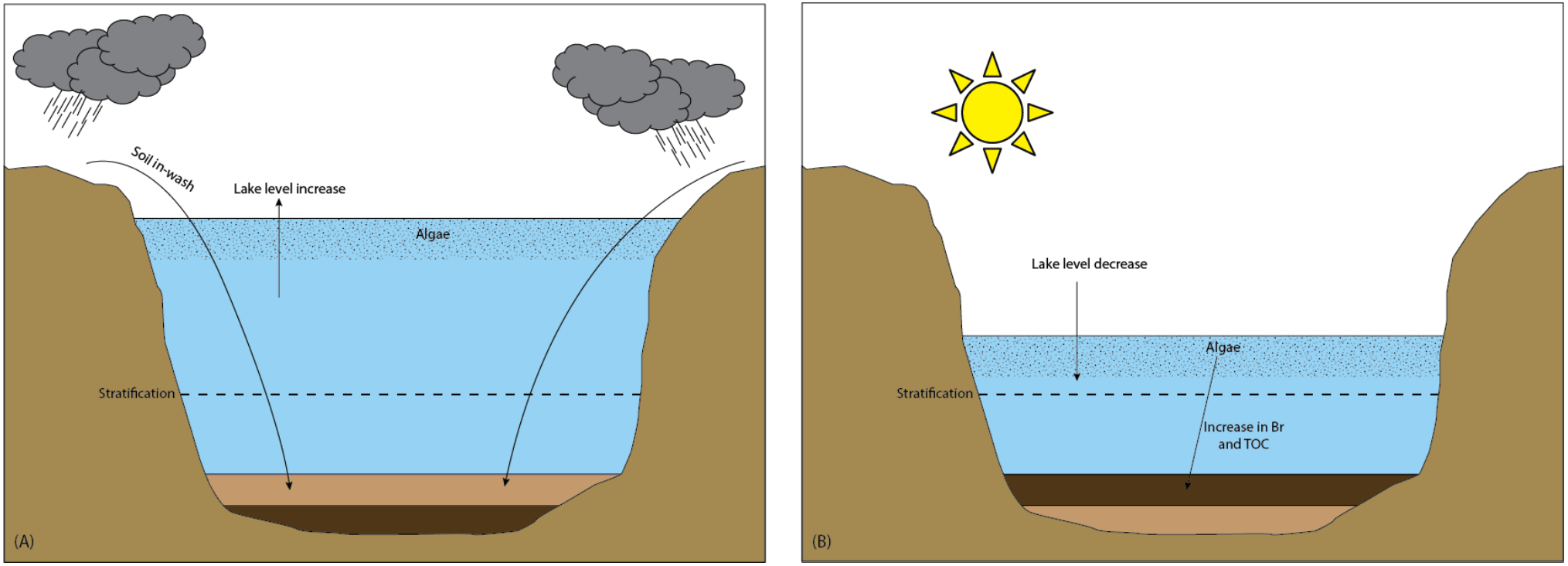

Figure 6.19: Conceptual diagram for sediment deposition in Lake Lanoto'o. (A) Precipitation causes soil in-wash and lake level increase; sediment is deposited as a light brown unit characterised by high Ti, Fe, and Mn; and (B) drier conditions cause a lake level decrease and reduced soil in-wash; Br and total organic carbon (TOC) increases due to soil in-wash no longer diluting the organic matter component.

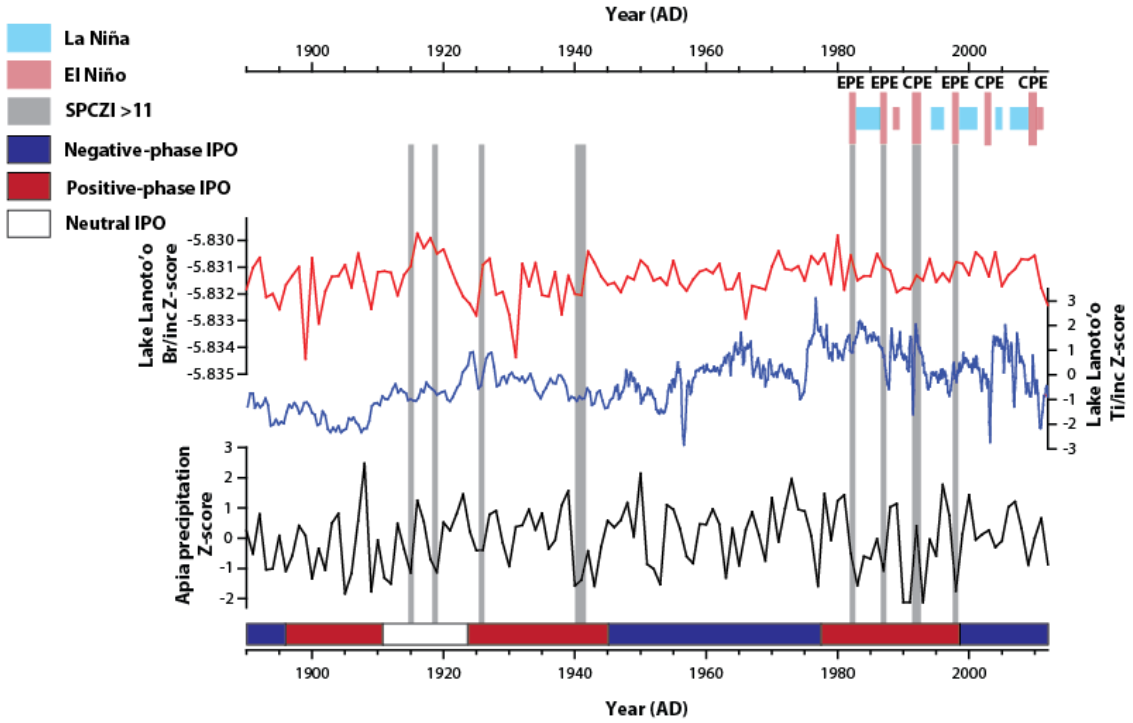

Figure 6.20: Comparison of Lake Lanoto'o Br/inc and Ti/inc with Apia precipitation from AD 1890-2012. Phases of IPO are highlighted (Henley *et al*., 2015), and blue shaded bars at the top of the plot indicate La Niña events, whereas red-shaded bars indicate El Niño events. Moderate to strong El Niño events are indicated by longer-length bars. El Niño and La Niña events are defined by 3-month running mean Niño 3.4 SSTAs where El Niño (La Niña) events are defined as SSTAs ≥0.5 °C (≤−0.5 °C) and moderate-to-strong El Niño events are defined as SSTAs ≥1.0 °C for three or more consecutive months (Atwood and Sachs, 2014). SST data was obtained from NOAA ERSST v3b. ENSO Events have been determined from AD 1982 to 2011 to correlate with Eastern Pacific El Niño (EPE) and Central Pacific El Niño (CPE) designations from Kidwell *et al*. (2014). Years with SPCZI values >11 are highlighted with full-length grey bars (Salinger *et al*., 2014).

can be used to interpret qualitative changes in precipitation amount, which in turn can be related to SPCZ position. The aforesaid significant, positive correlation between Br and TOC indicates that TOC can be used to infer reductions in precipitation amount for the long core record – TOC is more approximate of organic matter than Br and thus appropriate to apply (Meyers and Teranes, 2001; Davies *et al*., 2015). It should be noted that over centennial, and greater, timescales interpretations of wet or dry periods from the geochemical record should be related to IPO phases as a result of chronological resolution (section 5.3.2.2).

6.4.4 Summary interpretation

The relationships outlined present a framework from which climatic interpretations can be drawn from the geochemical proxy data in Lake Teroto and Lake Lanoto'o. This is presented in Figure 6.21. As previously stated due to the paucity of data in this region some assumptions, whilst grounded with data presented in this study, have to be made. Specifically:

1. The amount effect controls precipitation isotope values in these sites; and
2. Long-chain *n*-alkanoic δ^2H values will reflect precipitation isotope values.

Climatic interpretations, specifically of the IPO phase, are linked to known relationships to SPCZ position as delineated by Folland *et al*. (2002) (Section 2.1.3.1). Whilst qualitative statements could be made on ENSO flavours – this being the potential increase in CPL (EPL) and CPE (EPE) frequency in negative-phase (positive-phase) IPO (Kao and Yu, 2009; Carré *et al*., 2014) (Section 2.1.2) – it is more appropriate to evaluate potential changes in the dominance of these ENSO flavours using the Lake Teroto and Lake Lanoto'o records in comparison to a network of sites in the Pacific region that record ENSO (section 9.4).

6.5 Modern and lake sediment carbon

6.5.1 Source carbon in the study catchments

The C/N vs. $\delta^{13}C_{TOC}$ biplots indicate that the plants and soils follow known relationships, specifically terrestrial C_3 plants have high C/N and lower $\delta^{13}C$ (Figure 6.22). Grasses in Lake Teroto plot towards generalised C_4 terrestrial plant values, indicating that grasses in

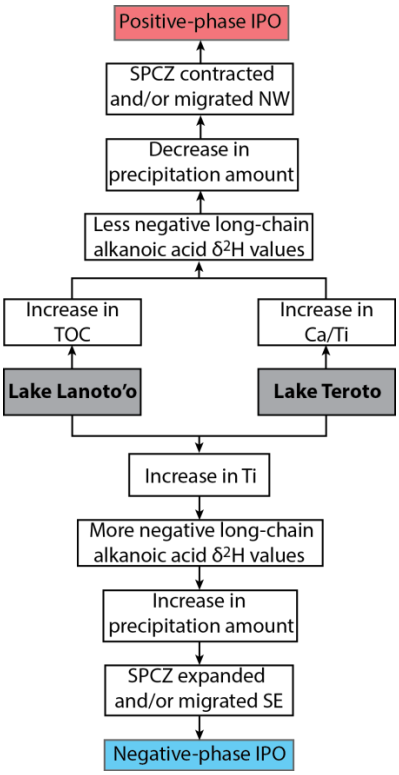

Figure 6.21: The geochemical evidence for both Lake Lanoto'o and Lake Teroto to infer climatic conditions in the southwest Pacific. The inferred IPO phases are based on known associations between the SPCZ location and the IPO during the instrumental period (Trenberth, 1976; Folland *et al*., 2002).

this catchment utilise the C_4 photosynthetic pathway (Meyers and Teranes, 2001). Shrubs plot outside the generalised values for C_3 terrestrial plants and close to aquatic plant values suggesting that were their contribution to lake sediment carbon significant, disentangling their contribution from aquatic plants would be difficult. The Lake Teroto sediment does not plot near C_4 plants indicating that C_3 plants and aquatics likely have the dominating influence on $\delta^{13}C_{TOC}$ values. The short core results indicate that C/N values and TOC increase from 150 cal yr BP to present, whilst $\delta^{13}C_{TOC}$ values become more negative (Figure 6.23). The highest variability in the short core is observed at the top of the core.

For Lake Lanoto'o the limited data available means that a full understanding of carbon sources in the lake's catchment is not possible. Soils cluster together close to generalised C_3 terrestrial plant values suggesting catchment soil inputs more closely relate to C_3 terrestrial plants than C_4 terrestrial plants. The short core samples cluster in C_3 plants and with the soils, suggesting that soils and C_3 plants comprise the $\delta^{13}C_{TOC}$. From the base of

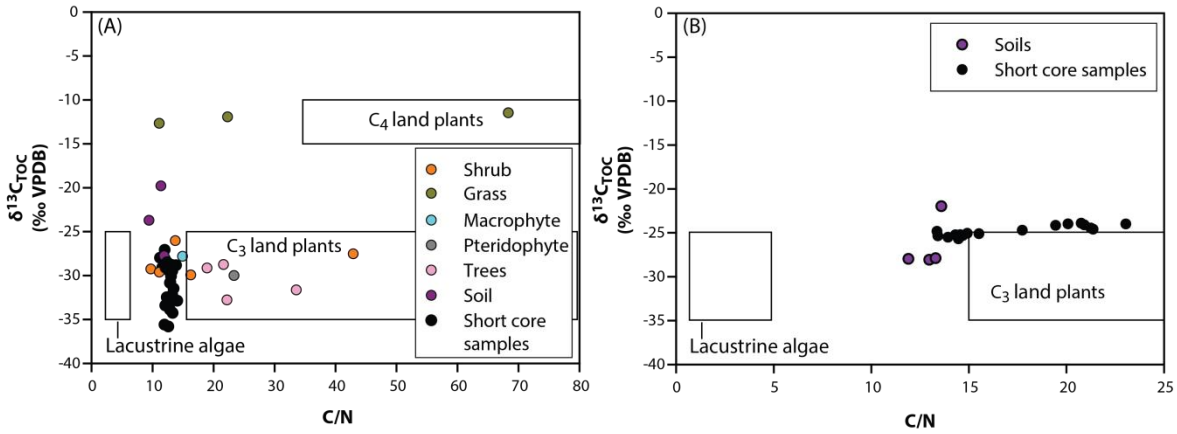

Figure 6.22: $\delta^{13}C_{TOC}$ and C/N ratio for samples collected in: (A) Lake Teroto and its catchment; and (B) Lake Lanoto'o and its catchment. Colours indicate different vegetation types and soil samples, and the generalised values for plants with different photosynthetic pathways are shown in rectangles (Meyers and Teranes, 2001).

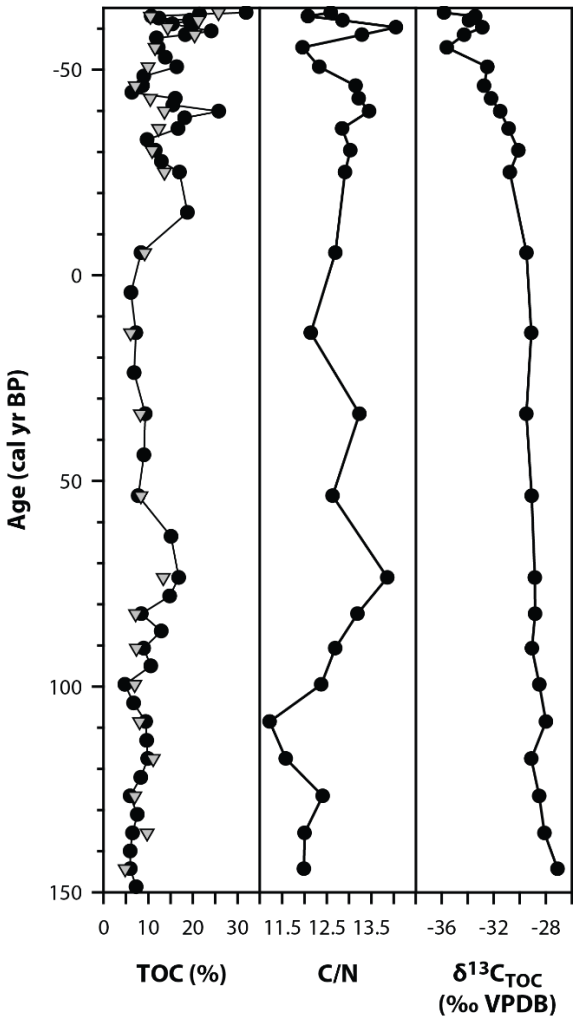

Figure 6.23: The %TOC, $\delta^{13}C_{TOC}$ and C/N for the Lake Teroto short core. In the %TOC column triangles represent element analyser data, and the circles represent adjusted loss-on-ignition data.

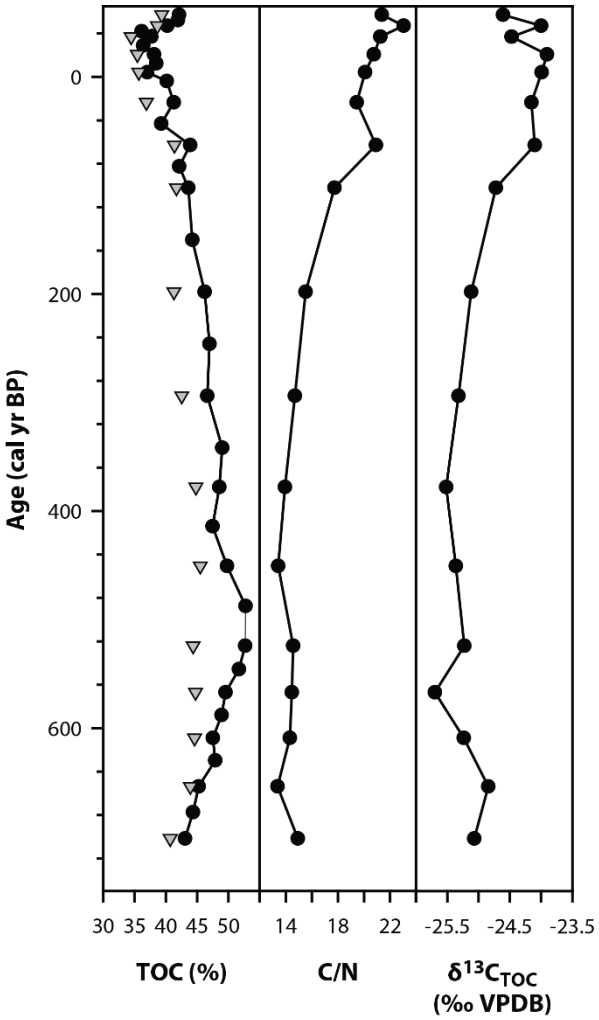

Figure 6.24: The %TOC, $\delta^{13}C_{TOC}$ and C/N for the Lake Lanoto'o short core. In the %TOC column triangles represent element analyser data, and the circles represent adjusted loss-on-ignition data.

the short core TOC values decrease by a small amount, whilst C/N and $\delta^{13}C_{TOC}$ increase (Figure 6.24).

6.5.2 Potential pathways of change in lake sediment $\delta^{13}C_{TOC}$ and C/N

Factors that affect $\delta^{13}C_{TOC}$ and C/N have been reviewed in section 4.5.2. However because both lakes are likely meromictic, diagenetic effects on $\delta^{13}C_{TOC}$ and C/N are likely to play a factor (Best *et al*., 1990; Lehmann *et al*., 2002). More specifically, with anoxia $\delta^{13}C_{TOC}$ is more negative due to the selective preservation of less reactive compounds that are depleted in ^{13}C (Lehmann *et al*., 2002). The conceptual model previously presented (Figure 4.3; Leng *et al*., 2006) has been redrawn to reflect the observed data and factors likely affecting $\delta^{13}C_{TOc}$ values for both sites (Figure 6.25 and Figure 6.26 for Lake Teroto and Lake Lanoto'o respectively).

6.5.2.1 Lake Teroto

Figure 6.25 indicates that that the short core sediment from Lake Teroto likely has mixed algal and terrestrial sources making interpretation of the $\delta^{13}C_{TOC}$ values difficult (Leng *et al*., 2004). The possible pathways of change in $\delta^{13}C_{TOC}$ and C/N for Lake Teroto using the data presented in Figure 6.25 are:

1. An increase in the volume of terrestrially-derived material leading to increasing C/N values and a decrease in $\delta^{13}C_{TOC}$ values;
2. An increased input of C_4 terrestrial plants increasing both C/N and $\delta^{13}C_{TOC}$ values;
3. A decrease in terrestrially derived material and an increase in algal productivity decreasing C/N values and increasing $\delta^{13}C_{TOC}$. This is due to ^{12}C is being removed from the lake system and the dissolved inorganic carbon pool being enriched in ^{13}C;
4. The lake no longer being stratified, causing an increase in sediment $\delta^{13}C_{TOC}$ values as more compounds are degraded;
5. An increased marine input, increasing the $\delta^{13}C_{TOC}$ value of the TDIC pool to near positive values (Boutton, 1991).

When the carbon source is allochthonous pathways 1 and 2 will indicate changes in source carbon; when carbon source is autochthonous pathways 3, 4, and 5 will indicate changes in the TDIC pool or productivity.

6.5.2.2 Lake Lanoto'o

The Lake Lanoto'o short core sediment indicates terrestrially-sourced carbon (Figure 6.26). Possible pathways of change in $\delta^{13}C_{TOC}$ and C/N for Lake Lanoto'o using the data presented in Figure 6.26 are:

1. An increase in the volume of terrestrially-derived material leading to increasing C/N values and a decrease in $\delta^{13}C_{TOC}$ values;
2. A decrease in terrestrially derived material and an increase in algal productivity decreasing C/N values and increasing $\delta^{13}C_{TOC}$. This is due to ^{12}C is being removed from the lake system and the dissolved inorganic carbon pool being enriched in $\delta^{13}C_{TOC}$;

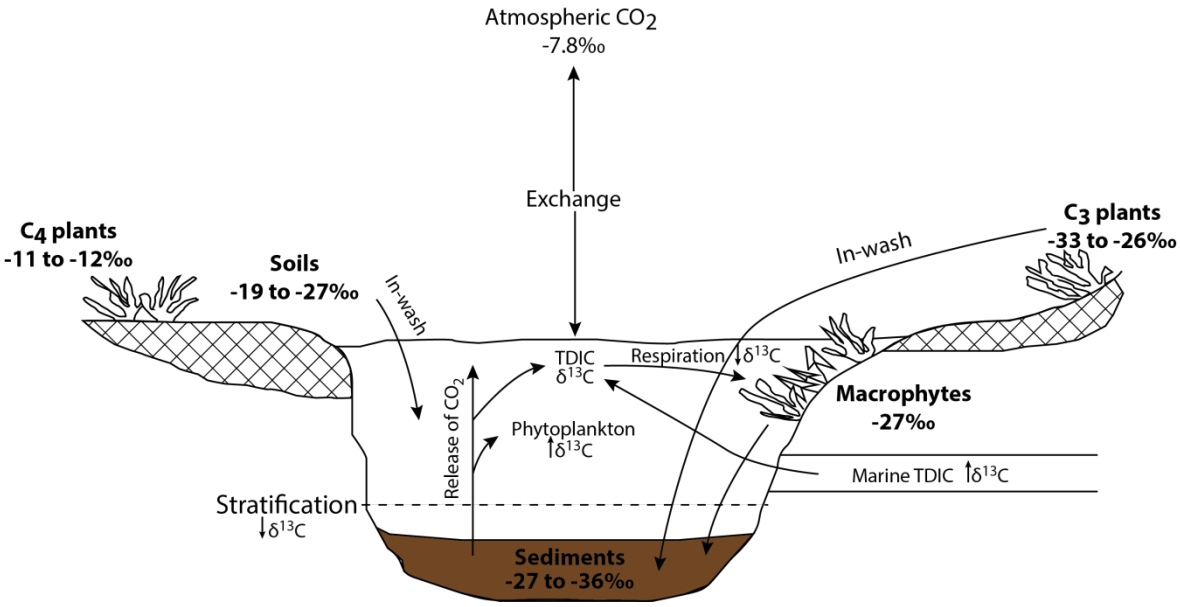

Figure 6.25: Conceptual diagram of carbon cycling in Lake Teroto, after Leng *et al*. (2006). Values in bold are observed data. Short vertical arrows next to carbon sources indicate effect on TDIC $\delta^{13}C$ values.

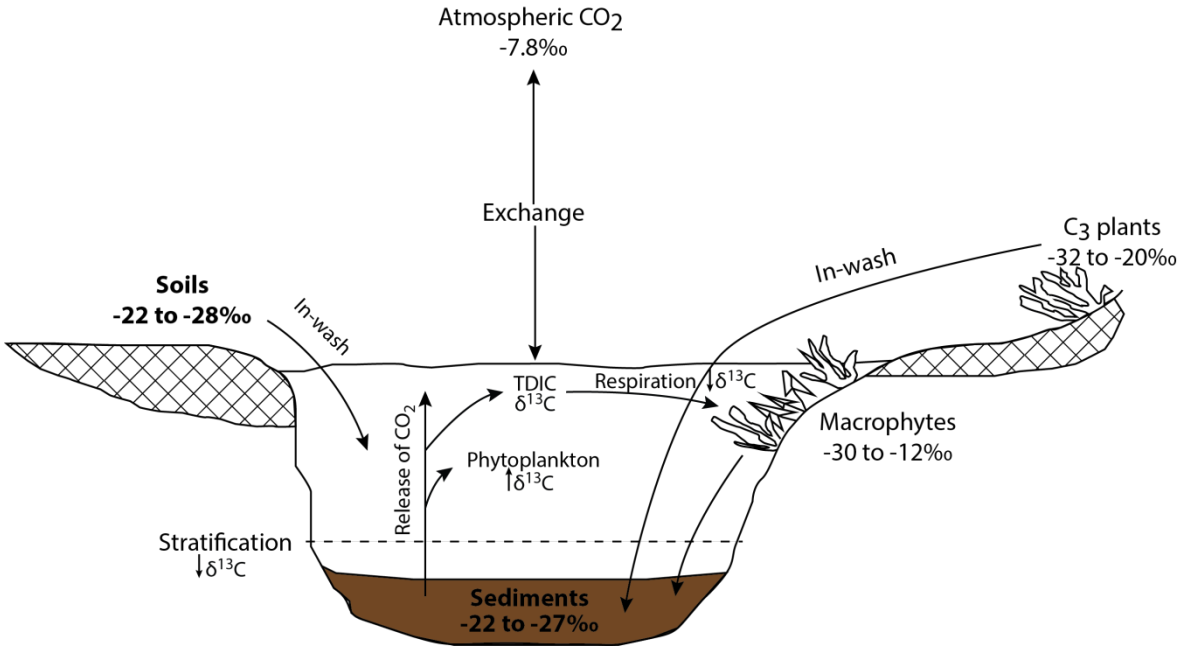

Figure 6.26: Conceptual diagram of carbon cycling in Lake Lanoto'o, after Leng *et al*. (2006). Values in bold are observed data. Short vertical arrows next to carbon sources indicate effect on TDIC $\delta^{13}C$ values.

3. The lake no longer being stratified, causing an increase in sediment $\delta^{13}C_{TOC}$ values as more compounds are degraded.

When the carbon source is allochthonous pathway 1 will indicate changes in source carbon; when carbon source is autochthonous pathways 2 and 3 will indicate changes in productivity.

6.6 Palaeoenvironmental interpretation

With the geochemical frameworks for Itrax and carbon delineated a palaeoenvironmental and palaeoclimatic interpretation can be undertaken for both sites.

6.6.1 Lake Teroto

6.6.1.1 Unit 1 150 cal yr BP to -40 cal yr BP

Throughout the unit low frequency magnetic susceptibility correlates with Ti, the former of which has high values, indicating a large terrestrial input (Figure 6.11). This is most likely a consequence of precipitation; however human activity causing disturbance in the catchment cannot be discounted especially when accounting for the taro plantation near the lake. The high Ti suggests that the SPCZ has expanded and increased precipitation and inwash into the lake, which in turn would suggest prolonged La Niña and/or negative-phase IPO conditions (Trenberth, 1976; Folland *et al*., 2002). Peaks in the Si/Ti ratio correlate with peaks in Ti, suggesting that increased authigenic Si production occurs following terrestrial input (Figure 6.12). Whether this relates to increased diatom productivity cannot be determined with the data available, nevertheless it is speculated that this is the cause of peaks in the Si/Ti ratio. The Mn/Ti, Ca/Ti and S/Ti all correlate, but appear to be in antiphase with Si/Ti. This suggests that during periods of decreased terrestrial input due to reduced precipitation, gypsum ($CaSO_4$, as determined from XRD (Appendix B)) increased in concentration and precipitates out of lake waters. The higher Mn/Ti suggests relatively less anoxic bottom waters, interpreted to be a result of lower lake levels caused by a drier climate.

The average C/N in Lake Teroto is 12 with a maximum value of 14 and minimum of 11 (Figure 6.23). This range of values are considered to indicate algal origin, nonetheless a

definitive algal source has C/N <10 indicating a terrestrial contribution. The C/N correlates with Ti, suggesting that C/N increases are a result of an increased terrestrial input. Shrub and soil C/N are all low (10-15) and cluster with the short core samples (Figure 6.22) – this suggests that the carbon source for the short core may be entirely terrestrial. Throughout the unit $\delta^{13}C_{TOC}$ values progressively decrease, showing no correlation with TOC or C/N. Pollen evidence from Lake Teroto indicates ca. 60% of pollen is sourced from pteridophytes (Parkes, 1994). A modern pteridophyte sample had $\delta^{13}C_{TOC}$ = -30‰ and C/N 23.3 – with the short core's average C/N = 12 this is not considered a causal factor for the increasingly negative $\delta^{13}C_{TOC}$ values. Langdon *et al*. (2010) determined that decreasing $\delta^{13}C$ values, in conjunction with higher C/N, were a result of increasing terrestrial plant contribution suggesting soil developing in the catchments that were being progressively washed into lakes. The decay of terrestrial organic matter in soil releases isotopically light CO_2 and enters soil waters (Leng and Marshall, 2004). Whilst Ti and low frequency magnetic susceptibility show a decreasing trend, values are high indicating high terrestrial input. Furthermore, considering soils and shrubs have low C/N values that cluster with the short core samples it is suggested that a continued influx of soil-derived CO_2, be this the result of increased precipitation or human activity in the catchment, would progressively lower the $\delta^{13}C_{TOC}$ due to the more negative $\delta^{13}C_{TOC}$ in soil waters lowering the $\delta^{13}C_{TOC}$ values in the DIC pool (Leng *et al*., 2006).

6.6.1.2 Unit 2 -40 cal yr BP to present

The highest Br and TOC values occur in this unit, with Ti and low frequency magnetic susceptibility decreasing, suggesting a reduced terrestrial input (Figure 6.11). The concomitant increase in Si/Ti with the increase in Br indicates that there was increased authigenic Si production, which may be a consequence of an algal bloom (Figure 6.12). The increase in $\delta^{13}C_{TOC}$ could be due to increased aquatic productivity removing ^{12}C from the lacustrine TDIC pool; however C/N ratios increase with $\delta^{13}C_{TOC}$ suggesting a change in carbon source. A distinct drier period can be inferred from the peak in Ca/Ti and S/Ti at ca. -60 cal yr BP which is followed by a peak in Mn/Ti. This could be a result of a drier period causing lower lake levels and a deeper chemocline causing bottom waters to become relatively less anoxic (Naeher *et al*., 2013). The elevated Ca/Ti and S/Ti, and lower Ti, would suggest reduced precipitation. By extension, knowing that SPCZ movement is the primary control on precipitation with reductions in precipitation relating to reductions in

Ti, this suggests SPCZ contraction and/or movement NW due to positive-phase IPO conditions (Trenberth, 1876; Folland *et al*., 2002).

6.6.2 Lake Lanoto'o

6.6.2.1 Unit 1 640 cal yr BP to 180 cal yr BP

Bromine and TOC are high throughout the unit, but do show a decreasing trend, whilst Ti/Fe/Mn and low frequency magnetic susceptibility are low but in turn showing an increasing trend (Figure 6.16). The C/N values (14) do not indicate a purely aquatic source according to known associations and suggest some terrestrial contribution (Meyers and Teranes, 2001) (Figure 6.24). Little change occurs with $\delta^{13}C_{TOC}$ throughout most of the unit, but with the increasing trend that is concomitant with C/N it further suggests a change in carbon source. Parkes (1994) interpreted an increase in aquatic vegetation around this time, and with the higher Si/Ti ratio indicating increased authigenic Si (Figure 6.17), it is suggested that the change in carbon source for this period is due to an increased aquatic input from diatoms (Peinerud, 2000). With the low Ti, likely to be related to precipitation and sourced from the catchment, it is suggested that it was drier throughout this time. This is likely a result of SPCZ contraction and/or movement NW, which in turn would indicate positive-phase IPO conditions are dominating (Trenberth, 1976; Folland *et al*., 2002).

The high Fe/Mn throughout the unit indicates that the lake stayed stratified and the hypolimnion anoxic. Moreover, the high Si/Ti and Ca/Ti values indicate elevated authigenic Si and Ca production. Considering the TOC is high throughout the unit it is speculated this is due to increased algal production; nevertheless this cannot be verified with the data available. Authigenic Si production peaks at ca. 360 cal yr BP, before dropping at ca. 280 cal yr BP – a concomitant rise in $\delta^{13}C_{TOC}$ suggests that, were the Si/Ti indicative of aquatic productivity, that the TDIC pool was becoming progressively enriched as algae preferentially remove ^{12}C (Leng and Marshall, 2004). The drop in Si/Ti and $\delta^{13}C_{TOC}$ values at ca. 280 cal yr BP, coeval with an increase in Ti, suggests that a period of terrestrial inwash reduced authigenic Si production and introduced more negative $\delta^{13}C$ into the lake. The source of the authigenic Ca, as indicated from Ca/Ti, is difficult to determine. It may be biogenic or a result of lower lake levels increasing the concentration of Ca minerals enough for them to precipitate out of the water column. In this instance it

appears to reflect drier conditions, so it is tentatively suggested elevated Ca/Ti is a consequence of increased concentration of Ca minerals precipitating out.

6.6.2.2 Unit 2 180 cal yr BP to present

The high Ti and Fe, increasing throughout the unit and mirrored in the low frequency magnetic susceptibility, indicate increased terrestrial input which is corroborated by the high C/N values (>20) that indicate a terrestrial vegetation source for organic carbon. This enhanced terrestrial input is most likely a result of SPCZ expansion due to prolonged La Niña and/or negative-phase IPO (Trenberth, 1976; Folland *et al*., 2002). The associated increase in $\delta^{13}C_{TOC}$ values indicates a change in carbon source to terrestrial C_3 vegetation. The reduced TOC, and Br which is indicative of organic compounds (Davies *et al*., 2015), is considered not to indicate reduced productivity but rather a dilution effect as a consequence of enhanced siliciclastic input.

With the increased terrestrial inwash there is a reduction in authigenic Si and Ca production, as indicated by low Si/Ti and Ca/Ti respectively. The reduced authigenic Si production could again be a result of the enhanced siliciclastic input diluting any autocthonous Si. A reduction in authigenic Ca production throughout this unit likely reflects a decrease in concentration of Ca in the water column as a result of increased precipitation. The Fe/Mn shows a declining trend possibly indicating oxic bottom waters; however it is put forward that this is unlikely considering modern limnology indicates the lake is stratified and rather this is indicative of a deeper chemocline.

6.7 Conclusions

The aim of studying modern samples and the short cores from Lake Lanoto'o and Lake Teroto was to better discern controls on precipitation for these sites, and to understand the modern catchments and sediment sources to better enable an interpretation of long core data from these lakes. In summary the following conclusions can be drawn from the data discussed and the short core palaeoenvironmental interpretation:

- Based on modern climate data alone it is determined that both sites will only conclusively show SPCZ movement when the IPO is in a positive phase and El Niño is operating at the same time;

- Both lakes are currently stratified and proposed to be meromictic;
- In both sites Ti is allochthonous in source and is transported into the lakes due to precipitation. Since the SPCZ is the precipitation source changes in Ti will indicate SPCZ contraction and expansion. Drier conditions can be determined in both sites: in Lake Teroto by concurrent high Ca/Ti and S/Ti, and in Lanoto'o by high TOC and Br values;
- Comparison of the Lake Teroto Ca/Ti and Ti to Rarotonga precipitation indicates that Lake Teroto is sensitive to both CPE and EPE, recording both El Niño types with high (low) Ca/Ti (Ti). In addition, comparison of Lake Lanoto'o Br and Ti to Apia precipitation inidicates that Lake Lanoto'o is sensitive to EPE. Combined these observations will indicate SPCZ movement, which in turn will provide an indirect indication of prevailing climatic conditions in the Pacific due to the relationship between ENSO/IPO and the SPCZ;
- The C/N and $\delta^{13}C_{TOC}$ reveal that Lake Lanoto'o and Lake Teroto have distinctly different carbon sources that relate to climate or within-lake processes.

With the relationships determined in this chapter, climate-lake geochemistry relationships can be outlined for each lake (Table 6.9). In the long records for each lake changes in the amount of precipitation (less precipitation in drier periods, more precipitation in wetter periods) will be further examined using compound-specific hydrogen analyses on *n*-alkanoic acids to verify interpretations drawn from the geochemical record.

IPO phase	Positive	Positive	Negative	Negative
El Niño/La Niña	El Niño	La Niña	El Niño	La Niña
SPCZI value	+11	-5	-4	-1
SPCZ location	Contracted and/or migrated NW	Contracted and/or migrated NW; Expanded and/or migrated SE	Contracted and/or migrated NW; Expanded and/or migrated SE	Contracted and/or migrated NW; Expanded and/or migrated SE
Precipitation and precipitation isotope response	Decreased amount and less negative δ^2H	Increased/decreased amount and less/more negative δ^2H respectively	Increased/decreased amount and less/more negative δ^2H respectively	Increased/decreased amount and less/more negative δ^2H respectively
Hypothesised long-chain *n*-alkanoic acid δ^2H response	Less negative δ^2H	Less/more negative δ^2H	Less/more negative δ^2H	Less/more negative δ^2H
Lake Lanoto'o geochemical response	Decrease in Ti; Increase in Br/TOC	Decrease/Increase in Ti; Increase/decrease in Br/TOC	Decrease/Increase in Ti; Increase/decrease in Br/TOC	Decrease/Increase in Ti; Increase/decrease in Br/TOC
Lake Teroto geochemical response	Decrease in Ti; Increase in Ca/Ti and S/Ti	Decrease/Increase in Ti; Increase/decrease in Ca/Ti and S/Ti	Decrease/Increase in Ti; Increase/decrease in Ca/Ti and S/Ti	Decrease/Increase in Ti; Increase/decrease in Ca/Ti and S/Ti

Table 6.9: Climate-lake geochemistry relationships for Lake Lanoto'o and Lake Teroto during an IPO phase and ENSO state with hypothesised long-chain *n*-alkanoic acid δ^2H response. SPCZI values use average values in Salinger *et al*. (2014).

Chapter 7: Lake Teroto long core results and proxy interpretation

7.1 Introduction

This chapter outlines the results for proxy data from Lake Teroto: specifically low frequency magnetic susceptibility, Itrax, TOC, C/N, $\delta^{13}C_{TOC}$, and *n*-alkanoic acid $\delta^{2}H$ and $\delta^{13}C$. The record spans from ca. 6,630 cal yr BP, with the proxy data covering this entire period. An interpretation of the data in both a palaeoenvironmental and palaeoclimatic perspective is provided, with changes determined to be the result of changing climatic conditions in the Pacific affecting the position of the SPCZ.

7.2 Results

7.2.1 Magnetic susceptibility

Low frequency magnetic susceptibility measurements were obtained at contiguous 1 cm intervals for all cores (Figure 7.1). Low values occur from ca. 6,635-1,000 cal yr BP, nevertheless relatively higher values can be determined throughout this period at ca. 6,200 cal yr BP, ca. 5,020-4,130 cal yr BP, ca. 3,430 cal yr BP, ca. 3150-2580 cal yr BP and ca. 1,740-1,080 cal yr BP. From ca. 1,000 cal yr BP the magnetic susceptibility values are several orders of magnitude higher, with two peaks at ca. 905 cal yr BP and ca. 296 cal yr BP, correlating with the different coloured laminae (light grey (7/N) and black (2.5/N)) at the top of the sequence.

7.2.2 Itrax

Whilst the sequence is laminated throughout, it is presently unknown whether these laminations are annually deposited. Consequently examining subdecadal climate phenomena, specifically ENSO, using the Itrax data acquired at 200 µm intervals would not be valid as the chronological resolution (ca. 9 yr/cm) is not sufficiently resolved to permit this. Therefore Itrax data was averaged to 1 cm resolution to facilitate comparison

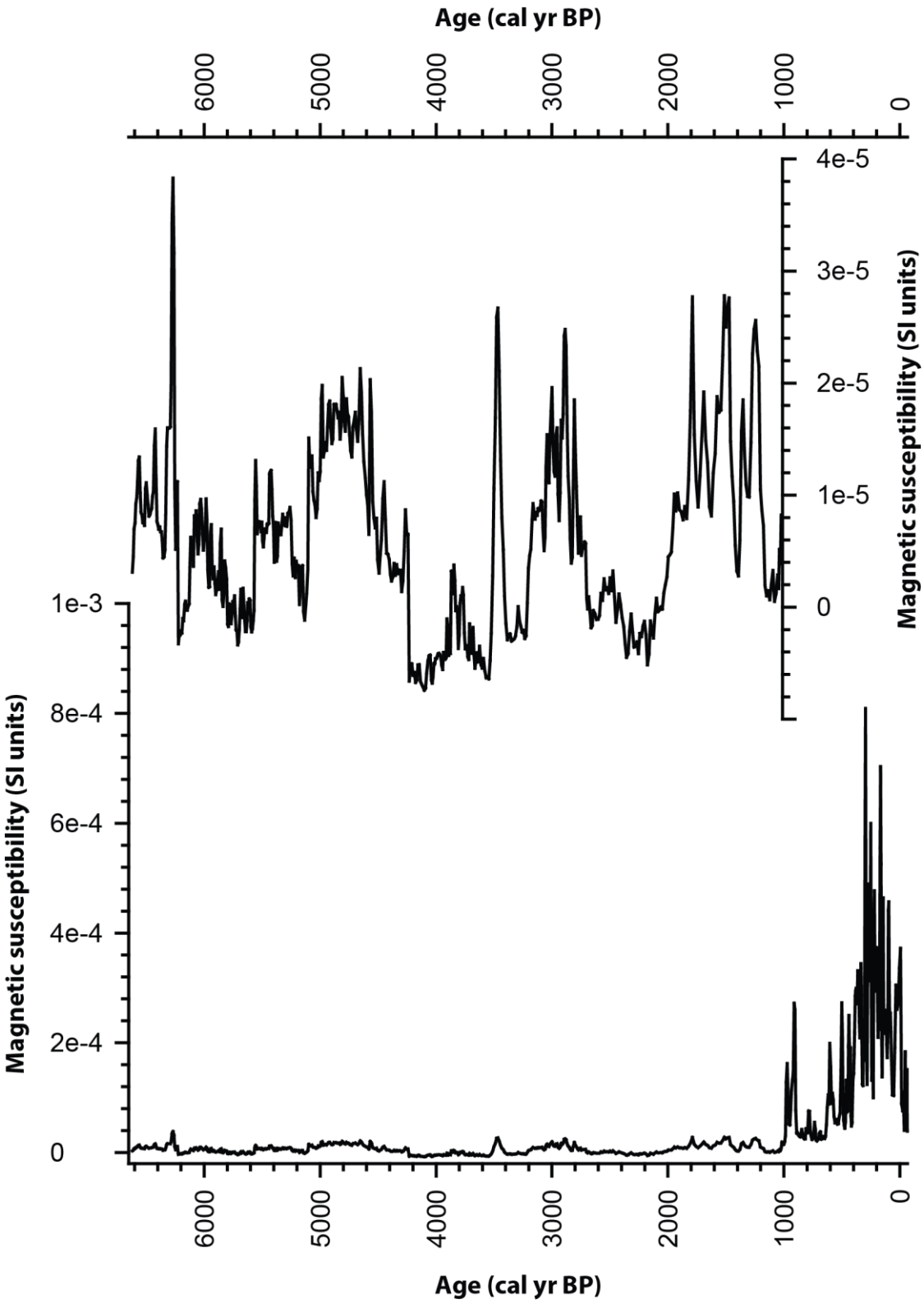

Figure 7.1: Lake Teroto low frequency magnetic susceptibility. The top graph focusses on ca. 6,630-1,000 cal yr BP to help delineate trends

with other proxy data collected at this interval, analogous to the short core data presented in Section 6.4.2; this permits an interpretation of climate and environmental changes at the interdecadal, and longer timescale. All Itrax data have been standardised

to the incoherent scatter to reduce the effects of organic matter and water content (Kylander *et al*., 2011; Marshall *et al*., 2011) (Figure 7.2). Elements presented show the largest variability through the sequence.

From ca. 6,630-4,580 cal yr BP element values remain relatively constant, with notable decreases at ca. 6,320-6,110 cal yr BP and ca. 5,880-5530 cal yr BP in Ti, Fe, Mn, Ca, S and Sr values. A pronounced decrease in Ti, Fe, Mn, S, and Si occurs at ca. 4,560 cal yr BP whereas Br increases. Low values persist until ca. 3,230 cal yr BP, interrupted by a peak in Ti, Fe, Ca, S and Si at ca. 3,770 cal yr BP. Titanium, Fe, Mn and Si increase in value and remain relatively constant, with a notable peak in Ti and Si at ca. 2,700 cal yr BP. Calcium and sulphur show more pronounced cyclicity, having relatively lower values from ca. 3,230-1,900 cal yr BP (with notable peaks at ca. 3,020, 2,800 and 2,100 cal yr BP) and relatively higher values from ca. 1,900-1,000 cal yr BP. All elements show a distinct change at ca. 1,090 cal yr BP: Ti, Fe, Mn and Si initially decrease before increasing steadily from ca. 625 cal yr BP to present; Br, Ca and S progressively decrease to present; and Sr progressively increases towards present day.

Ratios of Mn/Ti, Si/Ti, Ca/Ti and S/Ti have been undertaken to determine bottom water oxygenation (Mn/Ti), and autochthonous production of Si, Ca and S (Si/Ti, Ca/Ti and S/Ti respectively). The justification for these ratios are delineated in section 6.4.2**.** Ratios of Mn/Ti, Si/Ti, Ca/Ti and S/Ti are low at ca. 6,630-6,320 cal yr BP before increasing sharply to the highest values seen in the sequence (Figure 7.3). The Mn/Ti, Si/Ti and S/Ti ratios progressively decrease until ca. 5,700 cal yr BP after which values remain relatively constant whereas Ca/Ti remains relatively constant until ca. 4,000 cal yr BP. A pronounced decrease occurs at ca. 4,500 cal yr BP in the Si/Ti ratio after which values increase. All ratios show variability, but on average stay relatively constant until ca. 1,090 cal yr BP where all ratios decrease significantly until present.

The Itrax data can be zoned as follows:

Itrax Zone 1 6,635-4,580 cal yr BP: all elements show relatively high values, with a pronounced decreases at ca. 6,320-6,080 cal yr BP and ca. 5,880-5530 cal yr BP.

Itrax Zone 2 4,580-3,180 cal yr BP: low values of all elements characterise this zone. An increase in Ti, Fe, Mn, Ca, S and Sr is observed at ca. 3,770 cal yr BP.

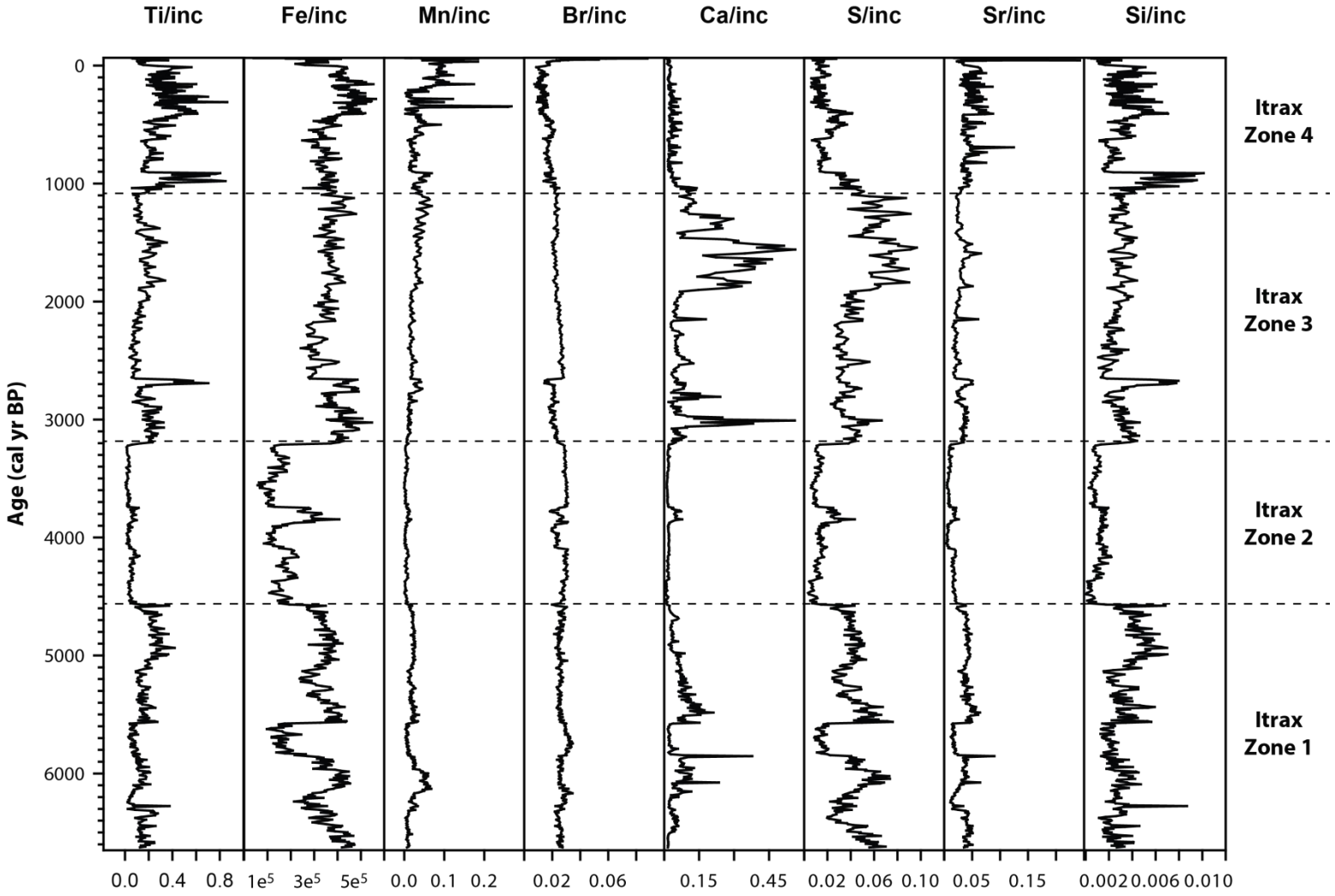

Figure 7.2: Itrax profile for Lake Teroto long core.

Itrax Zone 3 3,180-905 cal yr BP: Ti, Fe, Ca, S, Sr and Si increase sharply and remain relatively constant. Calcium shows variability, having relatively lower values from ca. 3,230-1,900 cal yr BP and relatively higher values from ca. 1,900-1,000 cal yr BP.

Itrax Zone 4 1,090 cal yr BP to present: Ti, Fe, Mn and Si decrease before increasing steadily from ca. 625 cal yr BP to present. Bromine, Ca and S all decrease and remain low, whereas Sr has higher values throughout – most notably at ca. 690 cal yr BP.

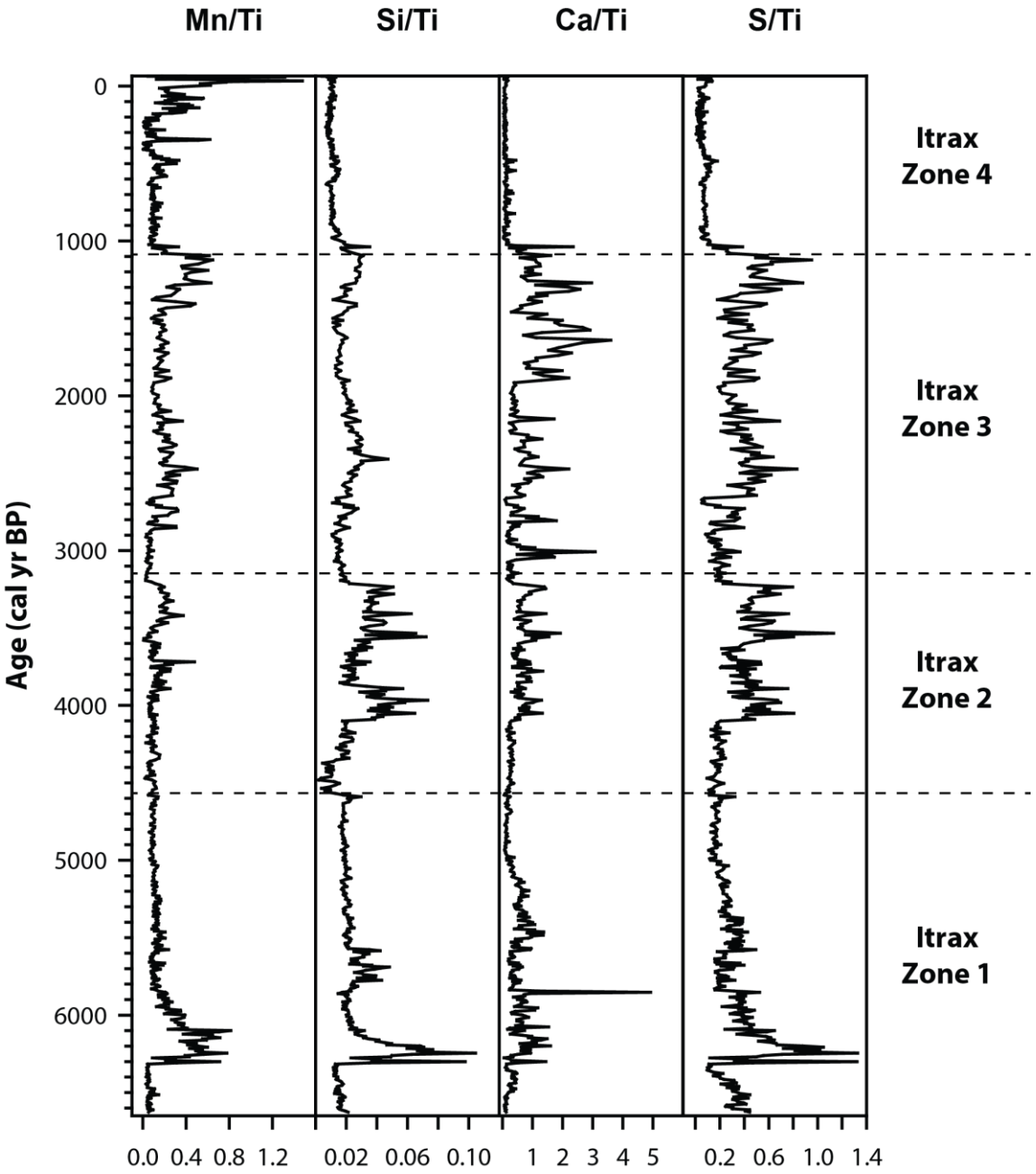

Figure 7.3: Itrax ratios of the Lake Teroto long core.

A correlation matrix and PCA is shown for the entire sequence to resolve the strength of association between elements in the sequence (Table 7.1). Like the short core, strong

correlations ($r \geq 0.7$ or $r \leq -0.7$) are highlighted. Calcium and sulphur have a significant positive correlation akin to the short core; Fe and Mn have a significant strong positive correlation which is not seen in the short core. Additionally P has a significant strong correlation with S that is not apparent in the short core. Titanium has significant positive correlations with Si, V, Fe, Sr and Zr. Bromine has a significant negative correlation with Fe and Ti.

The PCA of the Lake Teroto sequence indicates that Itrax Zone 1 and 3 are strongly associated with Ca, S, Fe, Mn and Si, whereas Itrax Zone 2 is strongly associated with Br and Itrax Zone 4 is strongly associated with Ti and Sr (Figure 7.4). The first two axes explain 59.2% of the data, and $\lambda_1 = 7.71$ and $\lambda_2 = 3.54$. Interestingly, most of Itrax Zone 4 plots separately from the other zones.

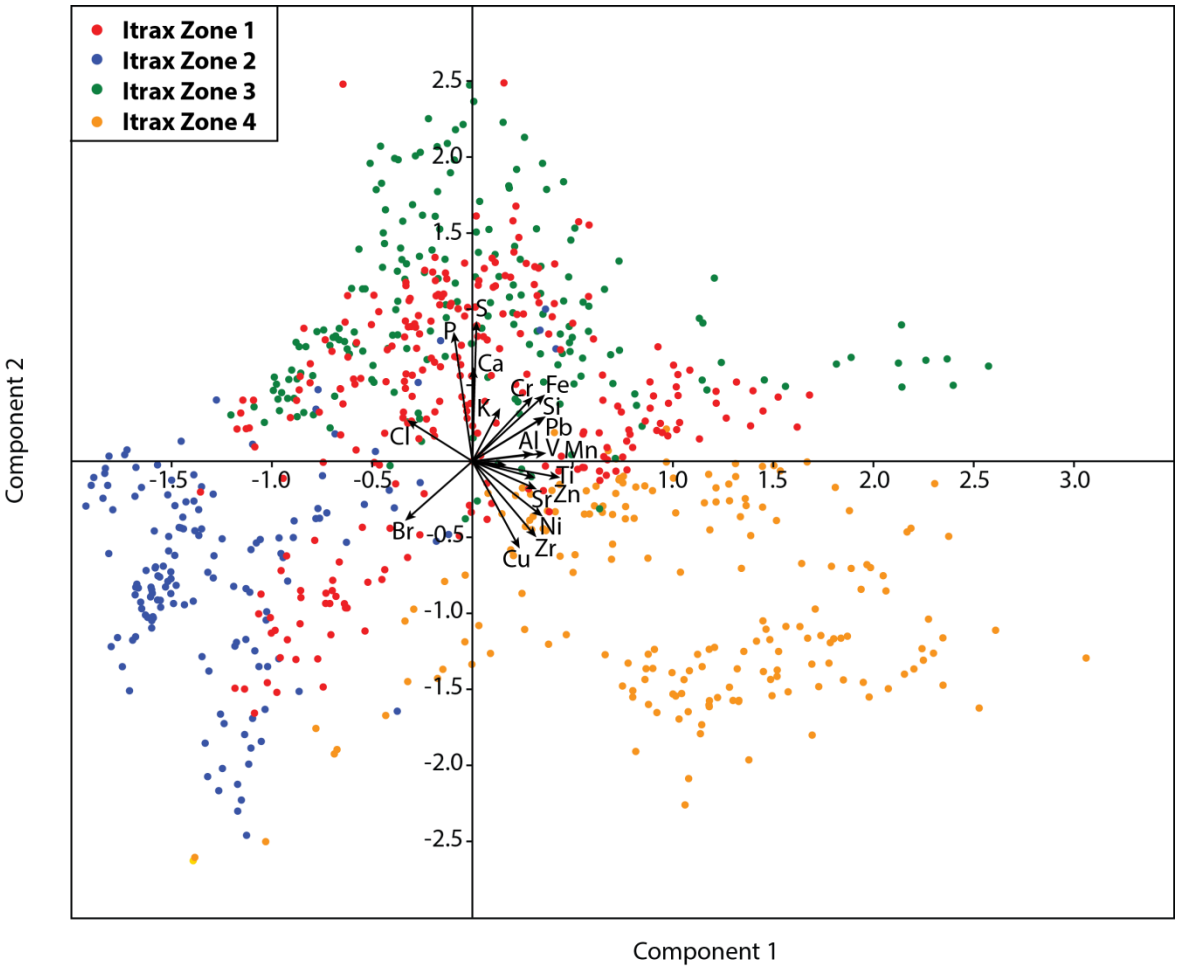

Figure 7.4: PCA of Itrax data from the Lake Teroto long core. Red indicates Zone 1, blue indicates Zone 2, green indicates Zone 3, and yellow indicates Zone 4.

	Al	Si	P	S	Cl	K	Ca	Ti	V	Cr	Mn	Fe	Ni	Cu	Zn	Br	Sr	Zr	Pb
Al		<0.01	0.04	0.36	<0.01	0.01	<0.01	<0.01	<0.01	<0.01	<0.01	<0.01	<0.01	<0.01	<0.01	<0.01	<0.01	<0.01	<0.01
Si	**0.73**		<0.01	<0.01	<0.01	<0.01	0.65	<0.01	<0.01	<0.01	<0.01	<0.01	<0.01	<0.01	<0.01	<0.01	<0.01	<0.01	<0.01
P	-0.07	0.16		<0.01	<0.01	<0.01	<0.01	<0.01	<0.01	<0.01	0.01	<0.01	<0.01	<0.01	<0.01	<0.01	<0.01	<0.01	<0.01
S	0.03	0.25	**0.74**		<0.01	<0.01	<0.01	<0.01	0.57	<0.01	0.01	<0.01	<0.01	<0.01	0.23	<0.01	0.03	<0.01	<0.01
Cl	-0.41	-0.33	0.47	0.19		0.00	0.87	<0.01	<0.01	<0.01	<0.01	<0.01	<0.01	<0.01	<0.01	<0.01	0.00	<0.01	<0.01
K	0.10	0.50	0.20	0.29	0.15		0.00	<0.01	<0.01	<0.01	<0.01	<0.01	<0.01	<0.01	<0.01	<0.01	0.57	<0.01	<0.01
Ca	-0.13	0.02	0.32	0.64	-0.01	0.33		0.09	0.06	0.01	0.47	<0.01	<0.01	<0.01	0.62	<0.01	0.29	<0.01	<0.01
Ti	0.63	**0.77**	-0.26	-0.12	-0.68	0.36	-0.06		<0.01	<0.01	<0.01	<0.01	<0.01	<0.01	<0.01	<0.01	<0.01	<0.01	<0.01
V	0.45	0.55	-0.20	0.02	-0.50	0.28	0.07	**0.71**		<0.01	<0.01	<0.01	<0.01	<0.01	<0.01	<0.01	<0.01	<0.01	<0.01
Cr	**0.72**	0.67	0.18	0.38	-0.28	0.25	0.10	0.55	0.55		<0.01	<0.01	<0.01	0.01	<0.01	<0.01	<0.01	<0.01	<0.01
Mn	0.30	0.17	-0.09	-0.10	-0.46	-0.27	-0.03	0.34	0.17	0.34		<0.01	<0.01	0.35	0.73	<0.01	<0.01	<0.01	<0.01
Fe	0.35	0.58	0.21	0.43	-0.52	0.19	0.22	0.65	0.66	0.60	0.36		<0.01	<0.01	<0.01	<0.01	<0.01	<0.01	<0.01
Ni	0.43	0.53	-0.35	-0.17	-0.45	0.18	-0.21	**0.71**	0.50	0.22	0.10	0.40		<0.01	<0.01	<0.01	<0.01	<0.01	<0.01
Cu	0.11	0.25	-0.48	-0.42	-0.32	0.14	-0.26	0.52	0.36	-0.10	0.03	0.17	**0.84**		<0.01	<0.01	<0.01	<0.01	<0.01
Zn	0.32	0.49	-0.20	-0.04	-0.37	0.41	-0.02	0.63	0.61	0.28	-0.01	0.43	0.65	0.45		<0.01	<0.01	<0.01	<0.01
Br	-0.37	-0.60	-0.14	-0.30	0.47	-0.27	-0.23	-0.66	-0.60	-0.49	-0.27	**-0.79**	-0.37	-0.14	-0.42		<0.01	<0.01	<0.01
Sr	0.45	0.37	-0.27	-0.08	-0.58	-0.02	0.04	0.62	0.47	0.43	0.33	0.46	0.55	0.35	0.41	-0.35		<0.01	<0.01
Zr	0.42	0.36	-0.57	-0.36	-0.64	0.16	-0.19	**0.71**	0.44	0.31	0.20	0.27	0.65	0.55	0.49	-0.22	0.63		<0.01
Pb	0.33	0.55	0.11	0.34	-0.53	0.16	0.14	0.66	0.62	0.48	0.35	**0.94**	0.54	0.35	0.42	**-0.74**	0.45	0.33	

Table 7.1: Linear correlation matrix for the Lake Teroto long core data, with correlation values below the diagonal and P values above it. In bold are correlations r≥0.7 and r≤-0.7. Highlighted in red are values that are not statistically significant below the 0.01 significance level.

7.2.3 %TOC, $\delta^{13}C$ and C/N

Loss-on-ignition measurements (LOI_{550}) calibrated against TOC were obtained at contiguous 1 cm intervals on all cores (including overlaps). Total organic carbon, C/N and $\delta^{13}C$ on total organic carbon ($\delta^{13}C_{TOC}$) were obtained at evenly spaced 2 cm intervals throughout the long core totalling 390 measurements. Measurement of $\delta^{13}C$ on C_{16}, C_{18} and C_{26} *n*-alkanoic acids ($\delta^{13}C_{C16}$, $\delta^{13}C_{C18}$ and $\delta^{13}C_{C26}$ respectively) were performed in duplicate on samples taken throughout the long core at the Organic Geochemistry Unit, Bristol. The aquatic algal carbon source is represented by $\delta^{13}C_{C16}$ and $\delta^{13}C_{C18}$, and the terrestrial carbon source is represented by $\delta^{13}C_{C26}$ (Eglington and Hamilton, 1967; Ficken *et al*., 2000). Samples were taken at 16 cm intervals throughout most of the sequence, totalling 49 samples.

The distribution of *n*-alkanoic acids through the Lake Teroto record (Figure 7.5) shows that the long-chain *n*-alkanoic acid distribution – specifically C_{26} and C_{28} – had variability from ca. 6,500-4,000 cal yr BP before remaining relatively constant from ca. 4,000 cal yr BP to present. C_{30} *n*-alkanoic acid shows variability throughout the record. The short-chain *n*-alkanoic acids (C_{16} and C_{18}) show variability throughout.

From ca. 6,640-5,760 cal yr BP TOC, C/N, $\delta^{13}C_{TOC}$ and $\delta^{13}C_{C26}$ are in phase, i.e. when TOC and C/N decrease $\delta^{13}C_{TOC}$ and $\delta^{13}C_{C26}$ becomes more negative and vice versa (Figure 7.6). The $\delta^{13}C_{C16}$ record remains relatively constant, with a small decrease to -28.5‰ at ca. 6,300 cal yr BP, whereas $\delta^{13}C_{C18}$ shows more variability. A pronounced decrease in TOC and C/N occurs between ca. 5,760-5,540 cal yr BP whilst $\delta^{13}C_{TOC}$ and $\delta^{13}C_{C26}$ becomes slightly more negative at this time. The $\delta^{13}C_{C16}$ remains constant, whilst $\delta^{13}C_{C18}$ indicates increased variability with values ranging from -25.6‰ to -30.7‰ during this period. From ca. 5,540-5,000 cal yr BP C/N decreases, remaining relatively constant with values of 13-14 until ca. 2,610 cal yr BP. The $\delta^{13}C_{TOC}$ and $\delta^{13}C_{C26}$ records covary throughout this time – interestingly $\delta^{13}C_{TOC}$ becomes progressively more negative from ca. 3,450 cal yr BP (-24.8‰) to ca. 2,830 cal yr BP (-32.6‰). The least negative $\delta^{13}C_{C18}$ value (-24‰) for the sequence occurs at ca. 3,070 cal yr BP. A small increase in C/N (20) between ca. 2,690-2,160 cal yr BP occurs alongside less negative $\delta^{13}C_{TOC}$ and $\delta^{13}C_{C26}$ values, whereas $\delta^{13}C_{C16}$ and $\delta^{13}C_{C18}$ are relatively constant. At ca. 1,110 cal yr BP TOC decrease sharply, $\delta^{13}C_{TOC}$

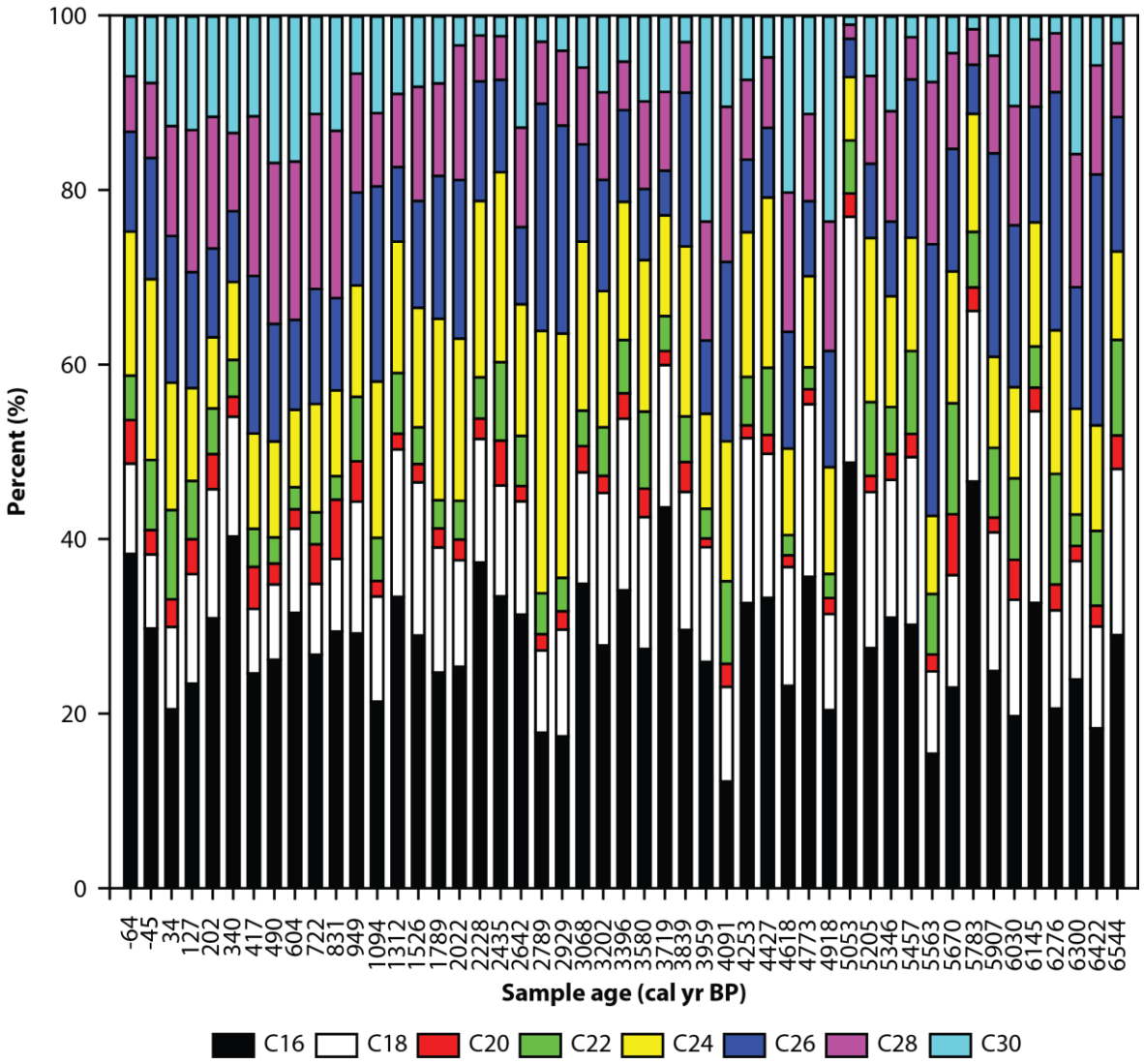

Figure 7.5: Even chain length *n*-alkanoic acids for Lake Teroto. The ratio of each compound against the total chain length *n*-alkanoic acids were calculated as a percentage.

has a pronounced increase to less negative values whereas C/N stays constant with values of 14. From ca. 1052 cal yr BP to present $\delta^{13}C_{TOC}$, $\delta^{13}C_{C16}$, $\delta^{13}C_{C18}$ and $\delta^{13}C_{C26}$ covary and all become progressively more negative from ca. 605 cal yr BP. In summary carbon can be zoned into:

Carbon Zone 1 6,640-5,760 cal yr BP: Total organic carbon, C/N, $\delta^{13}C_{TOC}$ and $\delta^{13}C_{C26}$ covary throughout the zone. Whilst $\delta^{13}C_{C16}$ is constant, $\delta^{13}C_{C18}$ becomes steadily less negative to -25.4‰ before decreasing sharply to -28.1‰.

Carbon Zone 2 5,760-3,450 cal yr BP: At the beginning of the zone C/N shows pronounced shifts in values, before remaining constant from ca. 5,000 cal yr BP with values between

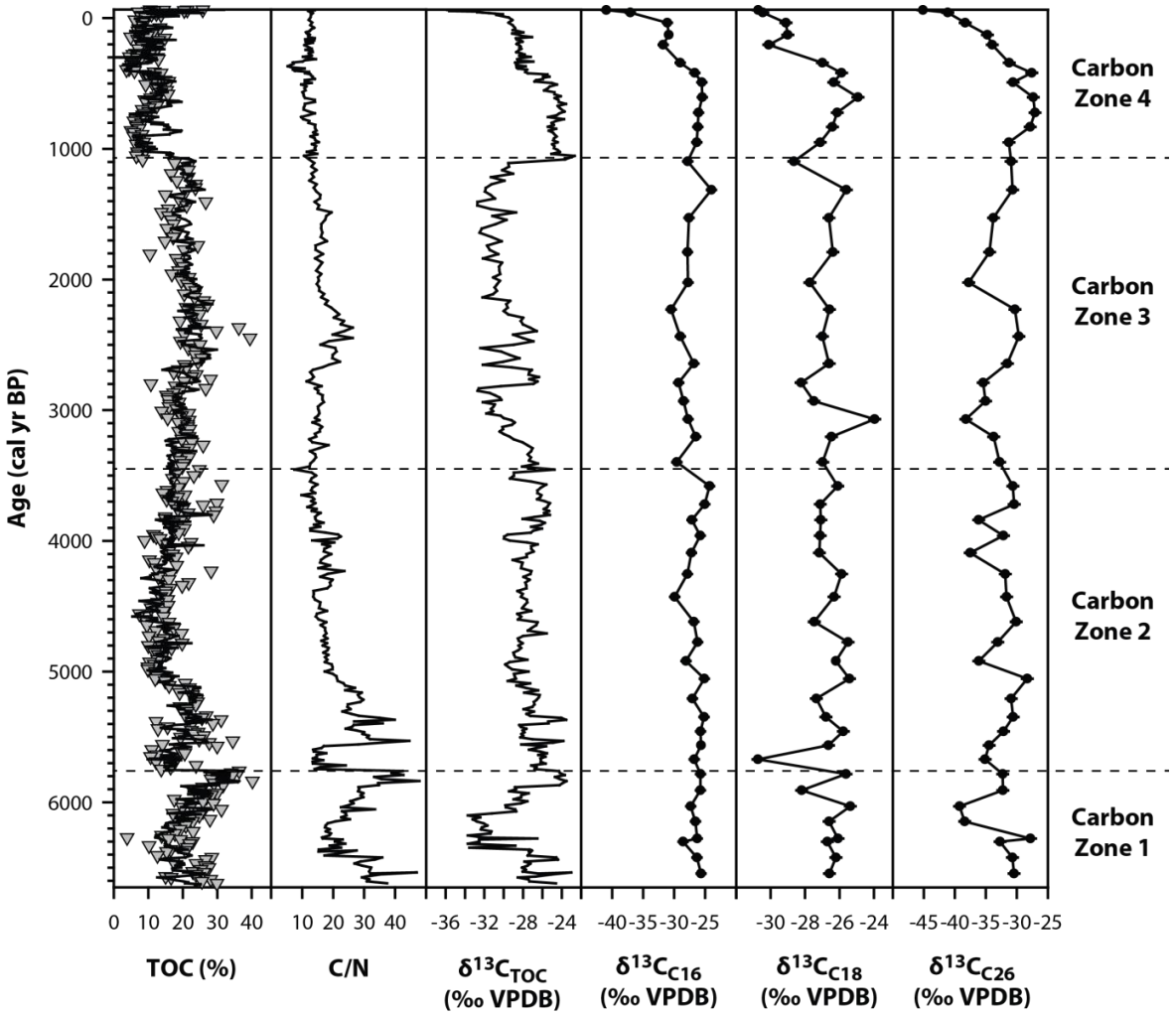

Figure 7.6: The %TOC, $\delta^{13}C_{TOC}$, C/N, $\delta^{13}C_{C16}$, $\delta^{13}C_{C18}$ and $\delta^{13}C_{C26}$ for the Lake Teroto long core. In the %TOC column triangles represent element analyser data.

13-14. Both $\delta^{13}C_{TOC}$ and $\delta^{13}C_{C26}$ covary throughout, and $\delta^{13}C_{C16}$ and $\delta^{13}C_{C18}$ show some variability.

Carbon Zone 3 3,450-1,050 cal yr BP: Increased variability in $\delta^{13}C_{TOC}$, whereas TOC, C/N and $\delta^{13}C_{C16}$ remain comparatively constant. Both $\delta^{13}C_{C18}$ and $\delta^{13}C_{C26}$ indicate variability.

Carbon Zone 4 1,100 cal yr BP to present: Whilst C/N remains constant, TOC shows a pronounced decrease. The $\delta^{13}C_{TOC}$, $\delta^{13}C_{C16}$, $\delta^{13}C_{C18}$ and $\delta^{13}C_{C26}$ records increase until ca. 500 cal yr BP. Following this $\delta^{13}C_{TOC}$, $\delta^{13}C_{C16}$, $\delta^{13}C_{C18}$ and $\delta^{13}C_{C26}$ all become progressively more negative, with all $\delta^{13}C$ records having the most negative values for the entire sequence in this zone.

Figure 7.7 indicates that the majority of Carbon Zone 1, 2 and 3 plot within generalised C_3 terrestrial plant values. Carbon Zone 4 plots outside of this, and appears to have values most similar to modern soil and shrub values.

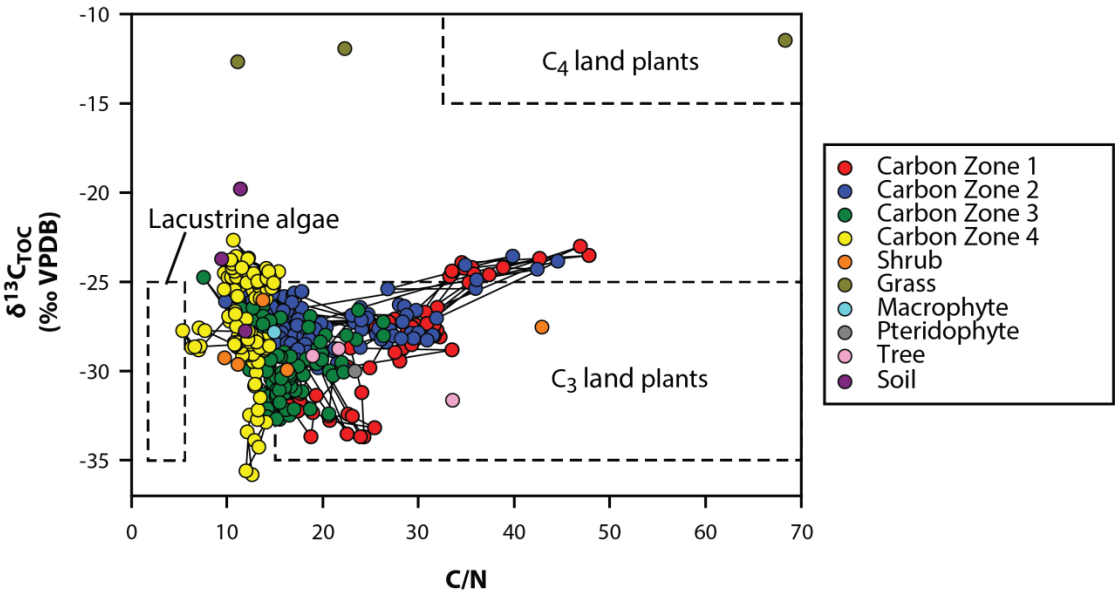

Figure 7.7: $\delta^{13}C_{TOC}$ and C/N ratio for Lake Teroto long core samples. Carbon zones are indicated with different colours (legend) and the solid line connects adjacent samples. The dashed line indicates generalised values for lacustrine algae, and C_3 and C_4 land plants (Meyers and Terranes, 2001). Modern soil and plant samples are also plotted (legend).

7.2.4 *n*-alkanoic acid δ^2H

Measurements of δ^2H on C_{16}, C_{18} and C_{26} *n*-alkanoic acid (δ^2H_{C16}, δ^2H_{C18} and δ^2H_{C26} respectively) were performed in duplicate at the Organic Geochemistry Unit (Bristol) on samples taken throughout the long core (Figure 7.8). The δ^2H_{C16}, δ^2H_{C18} and δ^2H_{C26} have similar trends throughout the record. From ca. 6,500-5,450 cal yr BP δ^2H values are less negative, after which values become more negative until ca. 3,840 cal yr BP. There is variability in the δ^2H values from ca. 3,840-2,680 cal yr BP; following this values are relatively stable before becoming variable from ca. 1,135 cal yr BP.

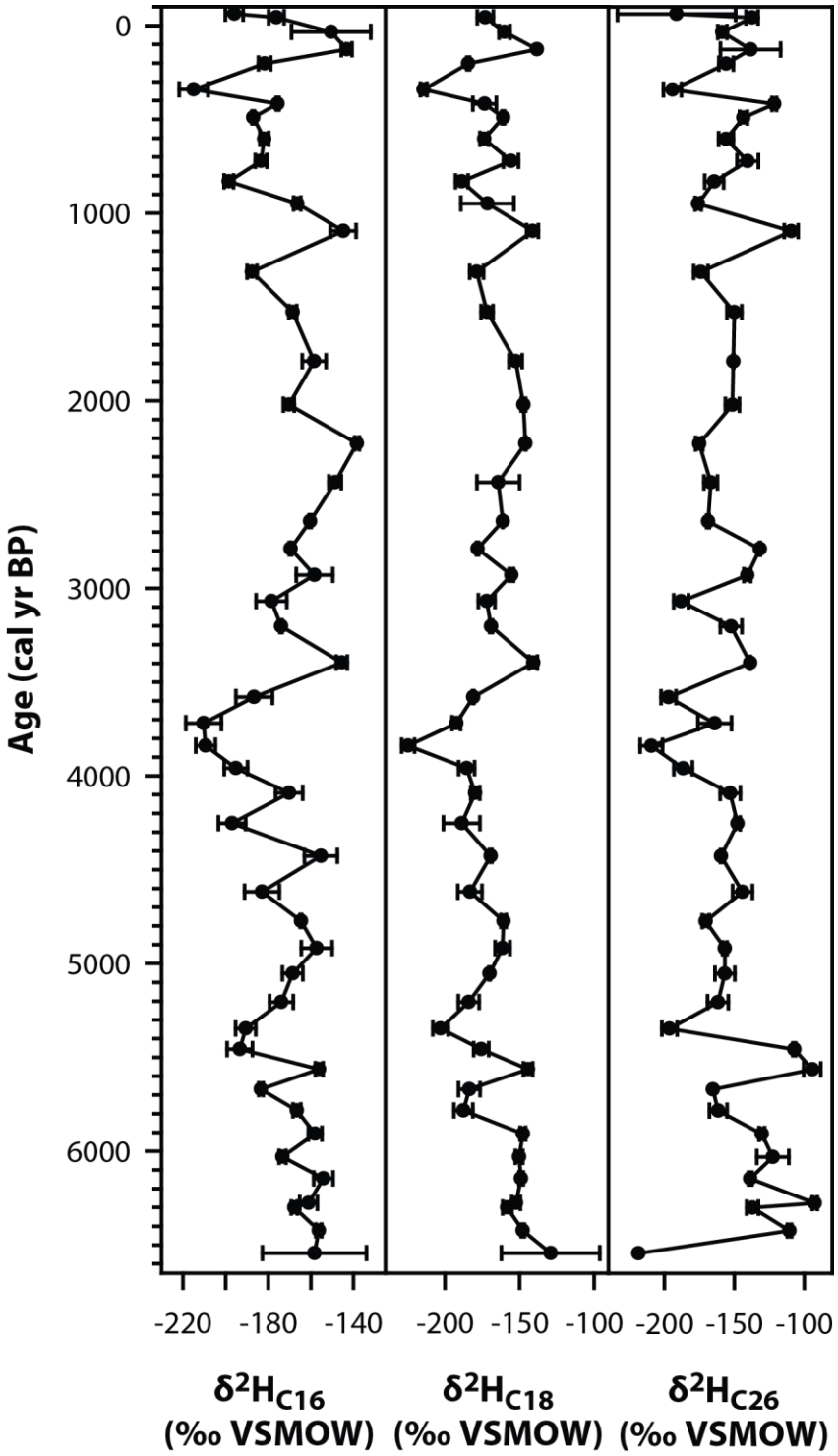

Figure 7.8: δ^2H measurements on C_{16}, C_{18} and C_{26} alkanoic acid (δ^2H_{C16}, δ^2H_{C18} and δ^2H_{C26} respectively) throughout the Lake Teroto long core.

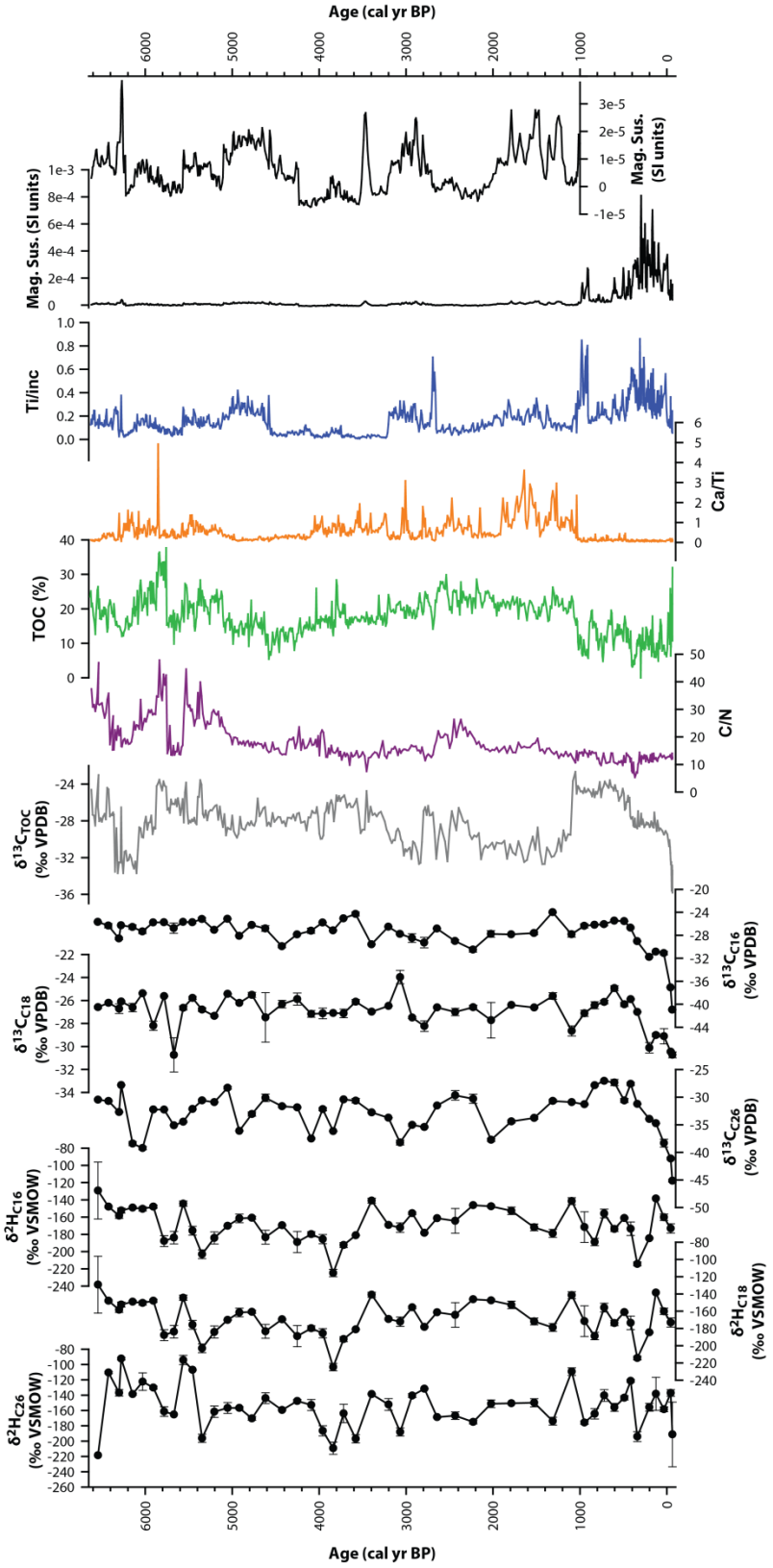

Figure 7.9: Summary of the data for the Lake Teroto long core. Presented are low frequency magnetic susceptibility; Ti; total organic carbon derived from adjusted LOI_{550} values (TOC); C/N; $\delta^{13}C$ of total organic carbon ($\delta^{13}C_{TOC}$); $\delta^{13}C$ of C_{16}, C_{18} and C_{26} alkanoic acids ($\delta^{13}C_{C16}$, $\delta^{13}C_{C18}$ and $\delta^{13}C_{C26}$ respectively); and $\delta^{2}H$ measurements on C_{16}, C_{18} and C_{26} alkanoic acids ($\delta^{2}H_{C16}$, $\delta^{2}H_{C18}$ and $\delta^{2}H_{C26}$ respectively).

7.3 Interpretation

7.3.1 Overview and general remarks

Figure 7.9 presents a summary of the Lake Teroto long core proxy data. With 1 cm equal to ca. 9 years the average accumulation rate is greater than ENSO's two- to seven-year periodicity – consequently changes in ENSO cannot be examined. As this is less than the 20-30 year IPO periodicity, all climatic interpretations will be put into context of IPO state.

Whilst Ca and S indicate the amount of each element in the sediment, by standardising it against Ti (this being allochthonous in source (section 6.4.2)) authigenic Ca and S production can be determined. Thus authigenic Ca and S production, determined to indicate gypsum (section 6.4.2), may appear high when overall amount of Ca and S is low. Carbon is likely coming from a mixed terrestrial and aquatic source throughout most of the record – with the exception of ca. 6,630-4,600 cal yr BP and ca. 2,600-2050 cal yr BP which indicate that carbon is terrestrially sourced. It is suggested that from ca. 4,450-3,200 cal yr BP there is a compositional change in the Lake Teroto sequence as shown by a change in the Itrax for most elements. Moreover, it is postulated that from ca. 1,100 cal yr BP to present human activity has greatly impacted the record by increasing terrestrial input into the lake.

7.3.2 Controls on *n*-alkanoic δ^2H

A correlation matrix of the $\delta^{13}C$ and δ^2H values for C_{16}, C_{18} and C_{26} alkanoic acids shows that there is no significant correlation between the $\delta^{13}C$ and δ^2H values for the aforesaid *n*-alkanoic acids (Table 7.2). This therefore suggests that changing carbon sources are not causing changes in the δ^2H values (Zhang and Sachs, 2007). The significant positive correlation between the $\delta^{13}C_{C16}$ and $\delta^{13}C_{C18}$ records likely represents a similar aquatic source. Taking into account Lake Teroto's connection to the sea, changes in $\delta^{13}C_{C16}$ and $\delta^{13}C_{C18}$ values could be due to: 1) changes in algal productivity; 2) an increase in marine input to the lake increasing the $\delta^{13}C$ values; or 3) changes in the dominant algal source producing C_{16} and C_{18} alkanoic acids (Zhang and Sachs, 2007). As the distribution of C_{18} *n*-alkanoic acid stays relatively stable throughout the Lake Teroto record, and with the significant positive correlation between $\delta^{13}C_{C16}$ and $\delta^{13}C_{C18}$ values, it is concluded that changes in the $\delta^{13}C_{C16}$ and $\delta^{13}C_{C18}$ values are principally the result of changing algal

productivity. Changes in marine input can be disentangled using the diatom record produced by Parkes (1994), and using the distribution of the *n*-alkanoic acids in Figure 7.5 it can be determined if $\delta^{13}C$ values are the result of a change in the amount of C_{16} or C_{18} *n*-alkanoic acid (Yamoah *et al*., 2016b).

	$\delta^{13}C_{C16}$	$\delta^{2}H_{C16}$	$\delta^{13}C_{C18}$	$\delta^{2}H_{C18}$	$\delta^{13}C_{C26}$	$\delta^{2}H_{C26}$
$\delta^{13}C_{C16}$		0.50	<0.01	0.47	<0.01	0.75
$\delta^{2}H_{C16}$	-0.10		0.83	<0.01	0.76	0.01
$\delta^{13}C_{C18}$	0.66	-0.03		0.97	<0.01	0.99
$\delta^{2}H_{C18}$	-0.11	**0.82**	0.00		0.58	<0.01
$\delta^{13}C_{C26}$	0.64	-0.04	0.47	-0.08		0.66
$\delta^{2}H_{C26}$	0.05	0.37	0.00	0.46	0.06	

Table 7.2: Linear correlation matrix for the Lake Teroto biomarker data, with correlation values below the diagonal and p values above it. In bold are correlations r≥0.7 and r≤-0.7. Highlighted in red are values that are not statistically significant below the 0.01 significance level.

Whilst there is some fluctuation in the proportion of C_{26} *n*-alkanoic acid, potentially indicative of changes in terrestrial carbon sources, a majority of the $\delta^{13}C_{TOC}$ plot within or near generalised C_3 terrestrial plant values, indicating that changes in $\delta^{2}H_{C26}$ are not a consequence of changes between C_3 and C_4 plants. With it being previously determined that changes in Ti in the Lake Teroto record are a result of changes in precipitation amount over the AD 1899-2012 period (section 6.4.2) and increased precipitation amount resulting in more negative precipitation $\delta^{2}H$ values (section 6.3.2), it is expected that increases in Ti in the record will be a consequence of increased precipitation amount which in turn would be reflected in more negative $\delta^{2}H_{C26}$ values. Further, having established that high values of Ca and S indicate gypsum deposition (an evaporite, section 6.4.2) indicating drier conditions, reduced precipitation amount will be reflected in less negative $\delta^{2}H_{C26}$ values. Whilst not a statistically significant relationship, over the ca. 6,630 cal yr BP record increases (decreases) in Ti largely correspond to decreases (increases) in $\delta^{2}H_{C26}$ values – thus changes in $\delta^{2}H_{C26}$ values are interpreted to relate to changes in precipitation amount.

The significant positive correlation between $\delta^{2}H_{C16}$ and $\delta^{2}H_{C18}$ (algal) with $\delta^{2}H_{C26}$ (terrestrial) (Eglington and Hamilton, 1967; Castañeda and Schouten, 2011) suggests that there is a similar principal control on their respective $\delta^{2}H$ values. Having concluded that changes in $\delta^{2}H_{C26}$ values are due to changes in precipitation amount, it is put forward that

changes in δ^2H_{C16} and δ^2H_{C18} values also reflect changes in precipitation amount due to their significant positive correlation with δ^2H_{C26}. It is important to note that with Lake Teroto's connection to the sea less negative δ^2H_{C16} and δ^2H_{C18} values may be a consequence of increased marine input. This can be disentangled by determining if an increase in δ^2H_{C16} and δ^2H_{C18} values are independent of an increase in δ^2H_{C26} values and using the diatom record produced by Parkes (1994).

7.3.3 Palaeoclimatic and palaeoenvironmental interpretation

7.3.3.1 Drier conditions ca. 6,630-5,400 cal yr BP

High low frequency magnetic susceptibility and Ti values from ca. 6,630-6,270 cal yr BP indicate an allogenic source. The high C/N values (>20) indicate a terrestrial carbon source (Meyers and Teranes, 2001; Leng *et al*., 2006). Despite this the Ca/Ti record steadily increases over this period, suggesting increased gypsum deposition, and thus drier conditions. This is supported by a shift from more negative δ^2H_{C26} value at ca. 6,540 cal yr BP, indicating increased precipitation amount, towards less negative δ^2H_{C26} values indicating reduced precipitation amount – this in turn suggests that the SPCZ has contracted and/or moved NW, indicating positive-phase IPO dominating at this time (Folland *et al*. 2002). Whilst the δ^2H_{C16} and δ^2H_{C18} values have similar trends after ca. 6,420 cal yr BP to δ^2H_{C26}, albeit with smaller changes, at ca. 6,540 cal yr BP the δ^2H_{C16} and δ^2H_{C18} values are less negative whereas δ^2H_{C26} is more negative. The diatom record indicates no increase in salinity at this time (Parkes, 1994), and the $\delta^{13}C_{C16}$ and $\delta^{13}C_{C18}$ values do not show pronounced less negative values – consequently an increase in marine input to the lake is unlikely to cause the less negative δ^2H_{C16} and δ^2H_{C18} values. However these is a shift from *Chaetoceros* and *Amphora* species to a significant increase in *Fragilaribrevistriata* and *Nitzschia* species at this time, thus the discrepancy between the δ^2H_{C16} and δ^2H_{C18} with δ^2H_{C26} at ca. 6,540 cal yr BP may be the result of a change in the dominant source organism producing the short-chain alkanoic acids (Zhang and Sachs, 2007) rather than due to more evaporative conditions within the lake.

The decreasing C/N values occur alongside decreasing TOC, and $\delta^{13}C_{TOC}$ and $\delta^{13}C_{C26}$ that become more negative throughout this period indicating a change in terrestrial carbon source. More negative $\delta^{13}C$ values are associated with most shrubs, trees and pteridophyte samples from the catchment, whereas less negative $\delta^{13}C_{TOC}$ values are

associated with soils (Figure 7.7). This suggests that a shift of $\delta^{13}C$ source from soils to either shrubs, trees, pteridophytes or a mixture of all plant types – this is corroborated by Parkes (1994) who shows an increase in trees and decrease in pteridophytes at this time (Appendix C, Figure C1). Both $\delta^{13}C_{C16}$ and $\delta^{13}C_{C18}$ are less negative from ca. 6,540-6,420 cal yr BP suggesting increased primary productivity (Leng *et al*., 2006), after which both become more negative at ca. 6,300 cal yr BP. The increase in Mn/Ti and Si/Ti values at ca. 6,300 cal yr BP suggests a relative decrease in anoxia and deeper chemocline, and increased authigenic Si production respectively. Laminations occur throughout this period thus indicating that the lake was still meromictic. It is proposed that this relative decrease in anoxia led to ^{13}C-depleted CO_2 from anaerobic respiration in the hypolimnion becoming incorporated into the epilimnion generating phytoplankton that are ^{13}C-depleted at ca. 6,270 cal yr BP during this period of increased productivity (Hollander and Smith, 2001), thus leading to more negative $\delta^{13}C_{C16}$ and $\delta^{13}C_{C18}$ values at this time.

The Ca/Ti and S/Ti ratio is consistently high from ca. 6,270-5,400 cal yr BP, whereas there is a pronounced decrease in Ca and S between ca. 5,800-5,600 cal yr BP which is not apparent in the Ca/Ti and S/Ti records. These discrepancies are suggested to relate to the amount of allogenic material entering the lake. Between ca. 5,800-5,600 cal yr BP there is reduced catchment inwash to the lake – indicated by Ti and low frequency magnetic susceptibility – suggesting decreased precipitation. Thus whilst the overall amount of Ca and S is lower at this time precipitation of gypsum remains comparatively unchanged. Whilst the high levels of Ca/Ti and S/Ti indicate drier conditions, the $\delta^{2}H$ values become more negative from ca. 6,270 to 5,600 cal yr BP indicating increased precipitation amount. Parkes (1994) records the development of indigenous forest taxa at this time, having the impact of reducing the allogenic input into the lake by stabilising the catchment. This therefore causes a decrease in Ti and low frequency magnetic susceptibility, appearing to indicate reduced allogenic input when the $\delta^{2}H$ record indicates an increase in precipitation amount. With the diatom record indicating an increase in salinity from ca. 6,270 to 5,600 cal yr BP it would be expected that the $\delta^{2}H_{C16}$ and $\delta^{2}H_{C18}$ values would become less negative (Schouten *et al*., 2006; Sachse and Sachs, 2008; Sachs and Schwab, 2011) – as $\delta^{2}H_{C16}$ and $\delta^{2}H_{C18}$ values have a similar trend to $\delta^{2}H_{C26}$ values and become more negative it is determined that precipitation $\delta^{2}H$ values is the primary control on the $\delta^{2}H_{C16}$ and $\delta^{2}H_{C18}$ values for this period. With the trend towards more negative $\delta^{2}H$ values it is

suggested that from ca. 6,270-5,600 cal yr BP the SPCZ has expanded and/or migrated SE increasing precipitation to Lake Teroto, with this indicating negative-phase IPO conditions at this time (Folland *et al*. 2002). From ca. 5,600-5400 cal yr BP the δ^2H record becomes less negative, and a corresponding increase in Ca/Ti and S/Ti values, indicating reduced precipitation amount. This suggests the SPCZ has contracted and/or migrated NW, indicative of positive-phase IPO.

From ca. 6,270-5,400 cal yr BP the C/N, $\delta^{13}C_{TOC}$, $\delta^{13}C_{C26}$, Ti and low frequency magnetic susceptibility records broadly agree indicating that $\delta^{13}C_{TOC}$ is predominantly sourced from terrestrial sources (Ficken *et al*., 2000; Meyers and Teranes, 2001), in agreement with the pollen record that indicates trees and pteridophytes are the primary vegetation types for this period (Parkes, 1994). Further Figure 7.7 indicates that the Carbon Zone 1 and 2 – spanning ca. 6,300-5,400 cal yr BP – mainly plot within generalised C_3 terrestrial plant values. This period is also characterised by less negative $\delta^{13}C_{C16}$ and $\delta^{13}C_{C18}$ indicating that aquatic plants have removed ^{12}C from the DIC pool and are using ^{13}C likely as a consequence of increased productivity (Meyers and Teranes, 2001; Leng *et al*., 2006). The similar trends in Ca/Ti and S/Ti with $\delta^{13}C_{C16}$ and $\delta^{13}C_{C18}$ over this time frame suggests that drier conditions are associated with increased aquatic productivity in this site, corroborated by the nutrient-rich conditions suggested from the diatom record (Parkes, 1994). It is also possible that the drier climate has lowered lake levels causing a reduction in dissolved CO_2 concentrations, leading to photosynthetic aquatic plants changing from CO_2^- to HCO_3^- metabolism (Smith and Walker, 1980; Lucas, 1983). This leads to aquatic plants becoming relatively enriched in ^{13}C, producing less negative $\delta^{13}C_{C16}$ and $\delta^{13}C_{C18}$ values (Smith and Walker, 1980). As diatoms indicate productive conditions it is postulated that the increase in $\delta^{13}C_{C16}$ and $\delta^{13}C_{C18}$ is due to increased productivity.

There are observable discrepancies from the aforesaid broad trends from ca. 6,270-5,400 cal yr BP. There is an observable decrease in C/N, $\delta^{13}C_{TOC}$ and $\delta^{13}C_{C26}$ values between ca. 6,300-5,800 cal yr BP; this occurs alongside a reduction in Ti and low frequency magnetic susceptibility at this time, suggesting a change in terrestrial C_3 carbon source. There is a decrease in tree pollen and increase in herb pollen at this time, supporting a change in carbon source (Parkes, 1994). A pronounced drop in C/N values (13) between ca. 5,700-5,500 cal yr BP is accompanied by a smaller decrease in $\delta^{13}C_{TOC}$ values that is also observed in the $\delta^{13}C_{C16,}$ $\delta^{13}C_{C18}$ and $\delta^{13}C_{C26}$ at ca. 5,670 cal yr BP. The correlation between

these *n*-alkanoic acids at this time suggests an overlap in plant types producing them (Yamoah *et al*., 2016b); combining this with the reduced C/N (13) and low frequency magnetic susceptibility values, indicative of reduced allogenic input, it is suggested that there is a mixed aquatic and terrestrial carbon source (Meyers and Teranes, 2001). The pollen record indicates an increase in coconut vegetation from 10 to 50% for this period alongside 5% aquatics (Appendix C, Figure C1). As diatoms indicate productive conditions for this period, which would corroborate the small increase in authigenic Si (high Si/Ti) that can indicate increased diatom productivity (Parkes, 1994; Peinerud, 2000), this lends support to a mixed carbon source.

7.3.3.2 Increase in precipitation amount ca. 5,400-4,000 cal yr BP

This period is characterised by Ca/Ti and S/Ti reducing from higher values at ca. 5,400 cal yr BP, reaching a minimum from ca. 4,000 cal yr BP, and higher values of Ti and low frequency magnetic susceptibility until ca. 4,200 cal yr BP. With the increased catchment input indicated by Ti and low frequency magnetic susceptibility it would be expected that C/N would record values >20 indicative of terrestrial plants (Meyers and Teranes, 2001). However C/N values for most of the ca. 5,400-4,000 cal yr BP period are <20 indicating that carbon had a mixed terrestrial and aquatic source. Figure 7.7 reveals that contemporary soil samples have C/N values between 9 and 12. Consequently, the low C/N values between ca. 5,400-4,000 cal yr BP are suggested to indicate a mixed carbon source that is dominated by soil inwash that resulted from increased precipitation associated with SPCZ expansion and/or migration SE. This is corroborated by the δ^2H values which are more negative overall, indicating increased precipitation amount, in comparison to ca. 6,630-5,400 cal yr BP suggesting prolonged millennial-scale negative-phase IPO conditions. Moreover, with δ^2H values staying relatively constant it indicates a more stable climate – more specifically that the SPCZ had expanded and/or migrated to a SE position throughout this time in comparison to ca. 6,630-5,400 cal yr BP.

The $\delta^{13}C_{TOC}$ and $\delta^{13}C_{C26}$ records are in broad agreement throughout, supporting the interpretation of a predominantly terrestrial carbon source, whereas $\delta^{13}C_{C16}$ and $\delta^{13}C_{C18}$ values are less negative indicating increased productivity (Leng *et al*., 2006). Fluctuations in the more negative $\delta^{13}C_{TOC}$ values between ca. 5,400-4,000 cal yr BP, matching the $\delta^{13}C_{C26}$ fluctuations, likely reflect changing terrestrial carbon sources. The diatom record

indicates increased salinity in the lake attributed by Parkes (1994) to indicate an increase in sea level, which would have the corollary of increasing the C_{16} and C_{18} alkanoic acid δ^2H as well as $\delta^{13}C$ values. As the δ^2H_{C16} and δ^2H_{C18} become more negative, and have similar trends to δ^2H_{C26} during this period, it is proposed that precipitation δ^2H is the primary control on aquatic δ^2H values. Therefore, the less negative $\delta^{13}C_{C16}$ and $\delta^{13}C_{C18}$ values can be interpreted as indicative of changes in aquatic productivity rather than a consequence of increased marine input. Nonetheless a marine influence on the $\delta^{13}C_{C16}$ and $\delta^{13}C_{C18}$ values cannot be completely discounted.

It is important to note that the Itrax profiles indicate a distinct change at ca. 4,450 cal yr BP, and reduced low frequency magnetic susceptibility values from ca. 4,200 cal yr BP (Figure 7.1 and Figure 7.2), lasting until ca. 3,200 cal yr BP. Due to Itrax and low frequency magnetic susceptibility changing at broadly the same time, and rather than it being a select few elements, it would suggest that there is a compositional change in the Lake Teroto sequence during this period. The δ^2H_{C26} record corresponds to the Ca/Ti record throughout this period suggesting the despite this compositional change the record can be used to reconstruct precipitation.

7.3.3.3 Variable precipitation amount ca. 4,000-2,700 cal yr BP

From ca. 4,000 cal yr BP the Ca/Ti and S/Ti increases, intimating that conditions in the lake were suitable for gypsum deposition. The δ^2H values showing increased variability with values becoming increasingly less negative, with less negative (more negative) δ^2H values corresponding to increases (decreases) in Ca/Ti and S/Ti. Combined this indicates that the SPCZ position is highly variable for this time, and with δ^2H values becoming less negative suggests that the SPCZ is contracting and/or migrating NW. In turn, this denotes a progressive shift from the negative-phase IPO conditions that dominated from ca. 5,400-4,000 cal yr BP to a dominance of positive-phase IPO conditions at ca. 2,700 cal yr BP (Folland *et al*., 2002). It is interesting to note that δ^2H values during this time frame are more negative than during ca. 5,400-4,000 cal yr BP suggesting that precipitation amount at certain times, for example ca. 3,900 cal yr BP, is higher than previous periods. It suggests that whilst the ca. 5,400-4,000 cal yr BP was wetter with an SPCZ in a SE position and/or expanded and prolonged negative-phase IPO conditions, the ca. 4,000-

2,700 cal yr BP period had far more variability in precipitation amount and SPCZ movement.

From 4,000-3,200 cal yr BP $\delta^{13}C_{TOC}$ values increase whilst C/N values decrease, suggesting an increased aquatic carbon input. This is corroborated by the increase in $\delta^{13}C_{C16}$ values which suggests increased aquatic productivity, substantiated by highly productive water conditions indicated by the diatom record (Parkes, 1994). Although the diatom species indicate saline conditions, hence a marine input that could be leading to an in $\delta^{13}C_{C16}$ values, the Si/Ti ratio is high throughout this period indicative of increased authigenic Si as would be expected during period of increased diatom productivity. This occurs during increased Ca/Ti and S/Ti, suggesting that during drier conditions aquatic plants are more productive, although a change from CO_2^- to HCO_3^- metabolism cannot be disregarded. Interestingly the $\delta^{13}C_{C18}$ record is increasingly negative from ca. 5,000-3,200 cal yr BP. Assuming an aquatic source for C_{18} alkanoic acid (Ficken *et al*., 2000) this indicates that the primary producers of C_{18} alkanoic acid are less productive throughout this period.

Between ca. 3,200-2,700 cal yr the C/N ratio indicates a mixed terrestrial and carbon carbon source, nevertheless values increase throughout the period suggesting an increasingly dominant terrestrial component. Parkes (1994) revealed that this period is characterised primarily by tree and pteridophyte vegetation (ca. 90%) with little evidence of aquatic vegetation (Appendix C, Figure C1), contrary to the C/N record. However, Parkes (1994) highlighted that diatom concentrations were the highest in the record during this period which suggests increased aquatic productivity, contrary to the $\delta^{13}C_{TOC}$, $\delta^{13}C_{C16}$ and $\delta^{13}C_{C18}$ which show increasingly negative values from ca. 3,200-2,700 cal yr BP intimating decreased productivity. This disparity between proxies could reflect a soil input into the lake, suggested by the elevated Ti and low frequency magnetic susceptibility values, bringing in depleted $\delta^{13}C$. This would cause the TDIC pool to have more negative $\delta^{13}C$ values, reflected in the aquatic-derived *n*-alkanoic acids despite increased productivity suggested by the diatom record (Parkes, 1994; Ficken *et al*., 2000; Leng *et al*., 2006). Whilst the $\delta^{2}H$ values suggest decreased precipitation amount overall, Parkes (1994) concluded that primary forest cover was reduced at this time hence the catchment may have been more susceptible to erosion from leading to an increased soil input.The $\delta^{13}C_{C26}$ record for this period increases, suggesting a change in terrestrial carbon source.

7.3.3.4 Drier conditions 2,700-1,100 cal yr BP

From ca. 2,700-2,200 cal yr BP δ^2H values are more negative, indicating increased precipitation amount and SPCZ expansion and/or migration SE, compared to ca. 2,200-1,100 cal yr BP where overall δ^2H values are less negative indicating decreased precipitation amount and SPCZ contraction and/or migration NW. This in turn suggests negative-phase IPO conditions from ca. 2,700-2,200 cal yr BP and positive-phase IPO conditions from ca. 2,200-1,100 cal yr BP. The Ca/Ti and S/Ti records are in agreement with this, having lower values between ca. 2,700-2,200 cal yr and higher values from ca. 2,200-1,100 cal yr BP. Whilst Ca/Ti and S/Ti is high suggesting drier conditions, and by extension reduced precipitation amount, the δ^2H values over this time frame compared with ca. 6,600-5,400 cal yr BP are more negative. This could be due to increasing SSTs in the SW Pacific causing an overall increase in the amount of precipitation from the SPCZ (van der Wiel *et al*., 2015).

The C/N values between ca. 2,700-2,000 cal yr BP are >20 indicating a terrestrial carbon source (Meyers and Teranes, 2001), which is supported by a small increase in low frequency magnetic susceptibility at this time indicating increased allogenic input. The increase in $\delta^{13}C_{TOC}$ and $\delta^{13}C_{C26}$ coincides with the C/N increase, indicating a change in terrestrial carbon source (Ficken *et al*., 2000). The C/N values for this time are similar to some of the contemporary tree sample values (Figure 7.7), suggesting that a change to a carbon source dominated by tree inputs caused the increase in $\delta^{13}C_{TOC}$ and $\delta^{13}C_{C26}$ – this is corroborated by pollen which indicates that trees were the primary vegetation for this period (Parkes, 1994; Appendix C, Figure C1). The $\delta^{13}C_{C16}$ and $\delta^{13}C_{C18}$ values decrease suggesting decreased aquatic productivity. With the diatom record indicating highly productive conditions (Parkes, 1994) and the high Si/Ti values indicating increased authigenic Si it would be expected that the $\delta^{13}C_{C16}$ and $\delta^{13}C_{C18}$ would show less negative values due to enhanced productivity removing ^{12}C from the TDIC pool and aquatic plants incorporating ^{13}C (Leng *et al*., 2006). However, $\delta^{13}C_{C16}$ and $\delta^{13}C_{C18}$ are slightly lower likely a result of increased allogenic catchment input adding more negative $\delta^{13}C$ soil-derived CO_2 to the TDIC pool which is subsequently incorporated by the aquatic plants (Leng *et al*, 2006). From ca. 1,800-1,100 cal yr BP a mixed terrestrial and aquatic carbon source is indicated from the C/N record (12-15). The $\delta^{13}C_{C16}$ and $\delta^{13}C_{C18}$ are relatively stable, although both increase at ca. 1,360 cal yr BP suggesting increased aquatic productivity

(Meyers and Teranes, 2001; Leng *et al*., 2006). An increasing trend is observed in $\delta^{13}C_{C26}$ that partially agrees with $\delta^{13}C_{TOC}$, suggesting a primarily terrestrial carbon source that is supported by increased low frequency magnetic susceptibility and Ti values both of which indicate an increased allogenic input.

7.3.3.5 Human impact 1,100 cal yr BP to present

This period is characterized by pronounced changes in Lake Teroto's geochemistry from ca. 1,100 cal yr BP to present. Most notable is a pronounced increased in low frequency magnetic susceptibility several orders of magnitude larger than any other part of the sequence indicating much higher allogenic input. The magnetic susceptibility indicates an initial peak at ca. 905 cal yr BP and a second, larger peak at ca. 300 cal yr BP. Coeval with this is an increase in Ti, Fe and Sr with decreases in Br, Ca, S, and Si; a decrease in TOC from 22% to 7%; a pronounced increase in $\delta^{13}C_{C16}$, $\delta^{13}C_{C18}$, $\delta^{13}C_{C26}$ and $\delta^{13}C_{TOC}$ with the later increasing from -29.5‰ to -22.7‰ followed by a progressive decrease in all $\delta^{13}C$ records. Of note is the lack of pronounced change in C/N values at this time with values around 11 to 12. Further, in Figure 7.4 the PCA analysis indicates this period is distinct from the rest of the sequence and more related to Ti, Zr and Sr, and in Figure 7.7 it plots away from generalised C_3 plant values indicating that the carbon source is mixed between aquatic and terrestrial. In addition, low values of Si/Ti indicate a decreased authigenic production of Si for this period, alongside reduced values for Ca/Ti and S/Ti which indicate a reduction in gypsum precipitation. Parkes (1994) also noted similar changes occurring with an increase in low frequency magnetic susceptibility, an increase in charcoal and pteridophytes (the latter of which increased from ca. 15% to ca. 70% (Appendix C), and decrease in coconut trees occurring at ca.1,160 cal yr BP (1,283 ^{14}C yr BP). Moreover, the diatom record indicates that the lake became highly productive (Parkes, 1994).

Parkes (1994) concluded that these distinct changes in the palaeo record were caused by human colonisation of Atiu. If this change in the Lake Teroto record was a consequence of human colonisation of Atiu, it occurs ca. 400 years earlier than the estimated colonisation of the Southern Cook Islands determined by Wilmshurst *et al*. (2011) to have occurred at 700 cal yr BP. Moreover, Kirch and Ellison (1994) and Kirch (1996) suggested that Mangaia, 215km south of Atiu, was colonised at ca. 2495±41 yr BP (ca. 2536±171 cal yr BP). Chagué-Goff *et al*. (2016) refined this to ca. 2,017-1,552 cal yr BP which would indicate

that Atiu wasn't colonised until ca. 1,000-500 years later. It should be highlighted that Anderson (1995) contests the date proposed by Kirch and Ellison (1994) for the colonisation of Mangaia. Considering the evidence obtained by Parkes (1994) and that obtained in this study, it is concluded that the pronounced changes in the Lake Teroto record occurring from ca. 1,100 cal yr BP fall outside of natural variability and are most likely the consequence of human colonisation of Atiu. The changes outlined are similar to those in Mangaia attributed to human colonisation, these being a substantial increase in allogenic input (as indicated by low frequency magnetic susceptibility), charcoal, and pteridophytes with a concomitant decrease in trees (Kirch, 1996). It is noted that the ages obtained in this study were on bulk sediments, therefore caution should be applied in stating human colonisation of Atiu occurred at ca. 1,100 cal yr BP. As previously mentioned low frequency magnetic susceptibility has two spikes occurring at ca. 905 and 300 cal yr BP. Following the initial peak at 905 cal yr BP, there is a reduction in low frequency magnetic susceptibility from ca. 810-630 cal yr BP before increasing from ca. 630 cal yr BP. At its simplest this indicates that there were two separate periods of increased allogenic input. Charcoal evidence indicates two separate peaks occurring at ca. 1,200 cal yr BP and 400 cal yr BP (Parkes, 1994), in broad agreement with the low frequency magnetic susceptibility record. It could be argued that this indicates two separate periods of colonisation of Atiu; however further evidence is required before this conclusion can be fully supported.

The large decrease in Ca/Ti and S/Ti suggests that the pronounced increase in terrestrial inwash created unfavourable conditions for gypsum precipitation by diluting the amount of Ca and S in the water column, consequently drier conditions would not cause Ca and S (as gypsum) to precipitate to the same degree as had previously occurred. With the distinct change from trees to pteridophytes changes in δ^2H_{C26} values may reflect this change in the main catchment vegetation rather than change in the amount of precipitation (Liu and Yang, 2008). When compared to Ti and Ca/Ti, the changes in δ^2H values for this period correspond to the changes in Ti and Ca/Ti as hypothesised – that being with high (low) Ti, indicating increased (decreased) allogenic input, δ^2H values are more (less) negative indicating increased (decreased) precipitation amount (Figure 7.10). As the $\delta^{13}C$ record does not match the δ^2H record, and there is no evidence of an increase

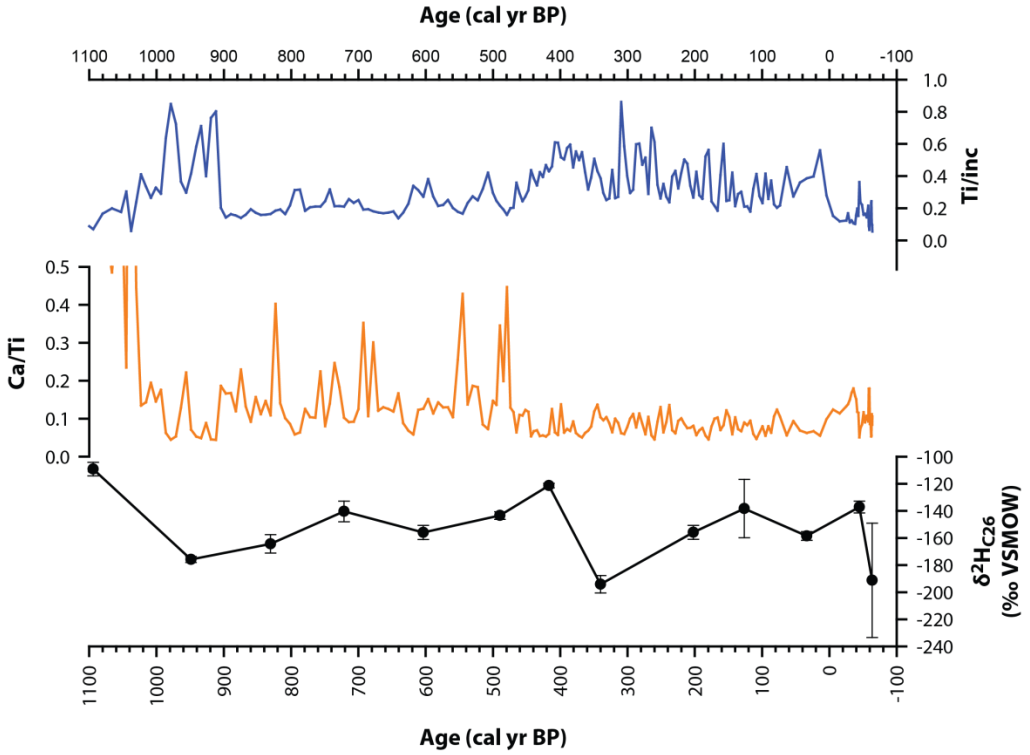

Figure 7.10: Comparison of Ti and Ca/Ti with δ^2H_{C26} over the last ca. 1,100 cal yr BP. Increases in Ti correspond to more negative δ^2H_{C26} values indicating that with increased allogenic input into the lake there is an increase in precipitation amount. Further, less negative δ^2H_{C26} correspond with increases in Ca/Ti, suggesting that with increased gypsum precipitation, indicative of drier conditions, there is reduced precipitation amount.

in marine input to the lake (Parkes, 1994), it is surmised that the δ^2H record represents changes in precipitation amount for this period akin to the rest of the sequence. A progressive shift from increased to decreased precipitation amount occurs from ca. 950-430 cal yr BP and ca. 430-130 cal yr BP, indicating the SPCZ went from being expanded and/or migrated SE to contracted and/or migrated NW. In turn this indicates a shift from negative-phase to positive-phase IPO conditions.

Whilst it is put forward that the pronounced changes in the Lake Teroto record from ca. 1,100 cal yr BP are due to human colonisation of Atiu, in itself it does not explain the distinct change observed in the $\delta^{13}C_{TOC}$, $\delta^{13}C_{C16}$, $\delta^{13}C_{C18}$ and $\delta^{13}C_{C26}$ records. This initial increase in $\delta^{13}C_{C16}$ and $\delta^{13}C_{C18}$ values could indicate an increase in aquatic productivity until ca. 500 cal yr BP, after which productivity decreases progressively with a brief increase in productivity occurring at ca. 130 cal yr BP. It is possible that the $\delta^{13}C_{C16}$ and $\delta^{13}C_{C18}$ records show a change from CO_2^- to HCO_3^- metabolism in aquatic

photosynthesisers due to drier conditions until ca. 500 cal yr BP, after which they switch back to CO_2^- metabolism (Leng *et al*., 2006). However δ^2H values suggest increased precipitation amount at this time discounting this suggestion. The increase in $\delta^{13}C_{C26}$ until ca. 420 cal yr BP and following decrease could indicate a changing terrestrial carbon source which would correspond to the large increase in pteridophytes (Parkes, 1994; Appendix C, Figure C1). With the covarying trends in $\delta^{13}C_{C16}$ and $\delta^{13}C_{C18}$ with $\delta^{13}C_{C26}$ it could be put forward that changes in $\delta^{13}C$ relate to changes in pteridophytes. However, Chikaraishi and Naraoka (2003) determined that for a Japanese pteridophyte the shortest *n*-alkane chain length was 23. With the obvious caveat that this is one sample in the study and not from the same site, the fact that *n*-alkanes and *n*-alkanoic acids are produced along the same acetogenic pathway (Sachse *et al*., 2012) it can be surmised that both C_{16} and C_{18} alkanoic acids are unlikely to be sourced from pteridophytes in the Lake Teroto catchment. Thus it is considered unlikely the changes in $\delta^{13}C$ records at this time are a result of a change in terrestrial vegetation.

Laminations occur throughout this period suggesting that the lake is still meromicitic and that DIC from the hypolimnion, often having more negative $\delta^{13}C$ due to respiration in this zone, has not entered the epilimnion and caused the negative $\delta^{13}C$ values observed. Another possibility for the initial increase in $\delta^{13}C$ values and subsequent decrease could relate to an increase in aquatic productivity following by oxidation of methane, the latter of which has been suggested to result in DIC $\delta^{13}C$ values ca. -60 to -80‰ (Jones and Grey, 2011; Finney *et al*., 2012). With the data presented it is difficult to accept or discount this mechanism; however the $\delta^{13}C$ values for TOC and *n*-alkanoic acids are within, or near, generalised values for C_3 plants indicating it is unlikely (Collister *et al*., 1994; Meyers and Teranes, 2001; Castañeda *et al*., 2009b).

With the change in $\delta^{13}C$ for TOC and *n*-alkanoic occurring alongside increases in low frequency magnetic susceptibility and Ti values it is considered that the change in carbon relates to increased terrestrial inwash. Contemporary soil C/N values and some shrub samples are similar to C/N values from ca. 1,100 cal yr BP to present, corroborating a terrestrial carbon source. With the aforementioned correlation between $\delta^{13}C$ of the *n*-alkanoic acids indicating an overlap in plant types producing them, it is proposed that the changes in the $\delta^{13}C$ records are instigated by the increased terrestrial inwash. The increased terrestrial inwash at ca. 1,100 cal yr BP inputted nutrients into the lake creating

pronounced highly productive conditions as indicated by the diatom record (Parkes, 1994). Whilst the data presented make it difficult to determine, it is suggested that both short- and long-chain *n*-alkanoic acids were aquatically sourced throughout this period due to their covarying nature (Yamoah *et al*., 2016b). The increased terrestrial input led to increased aquatic productivity, increasing $\delta^{13}C_{TOC}$ and *n*-alkanoic $\delta^{13}C$ values until ca. 490 cal yr BP. Following this low frequency susceptibility and Ti indicates a significant increase in terrestrial input with a concomitant decrease in $\delta^{13}C_{TOC}$ and *n*-alkanoic $\delta^{13}C$ values towards present. It is suggested that the large increase in terrestrial input caused the lakes DIC to be have more ^{12}C from a greater influx of soil-derived CO_2. This caused much lower $\delta^{13}C$ values in the DIC pool, lowering the $\delta^{13}C$ in aquatic sources observed in the $\delta^{13}C_{TOC}$ and *n*-alkanoic $\delta^{13}C$ values.

7.4 Summary

A summary of the proxy data from Lake Teroto is presented in Figure 7.11, and a summary of the proxy data interpretation is presented in Figure 7.9. There are five zones in the lake stratigraphy split at ca. 5,400, 4,000, 2,700 and 1,100 cal yr BP. From ca. 6,630-5,400 cal yr BP precipitation amount is interpreted to be decreased, with organic carbon concluded to be derived from C_3 terrestrial plants from ca. 6,630-6,270 cal yr BP. The ca. 6,270-5,400 cal yr BP period indicates aquatic productivity; however TOC is interpreted to be primarily terrestrially sourced. An increase in precipitation amount is determined from ca. 5,400-4,000 cal yr BP, after which SPCZ position appears highly variable from ca. 4,000-2,700 cal yr BP. The Ca/Ti and S/Ti record suggest that conditions suitable for gypsum deposition occur from ca. 4,000 cal yr BP that may indicate an increase in El Niño frequency. Aquatic productivity is suggested to increase over this period. From ca. 2,700-1,100 cal yr BP decreased precipitation amount is determined; however $\delta^{2}H$ values are more negative than the ca. 6,630-5,400 cal yr BP period possibly due to increased SSTs increasing overall precipitation amount from the SPCZ (van der Wiel *et al*., 2015). A pronounced change in the record occurs from ca. 1,100 cal yr BP to present suggested to be the result of human colonisation of Atiu causing increased catchment inwash into Lake Teroto. Comparison of this date with Lake Lanoto'o and the wider literature will be fully explored in section 9.5.

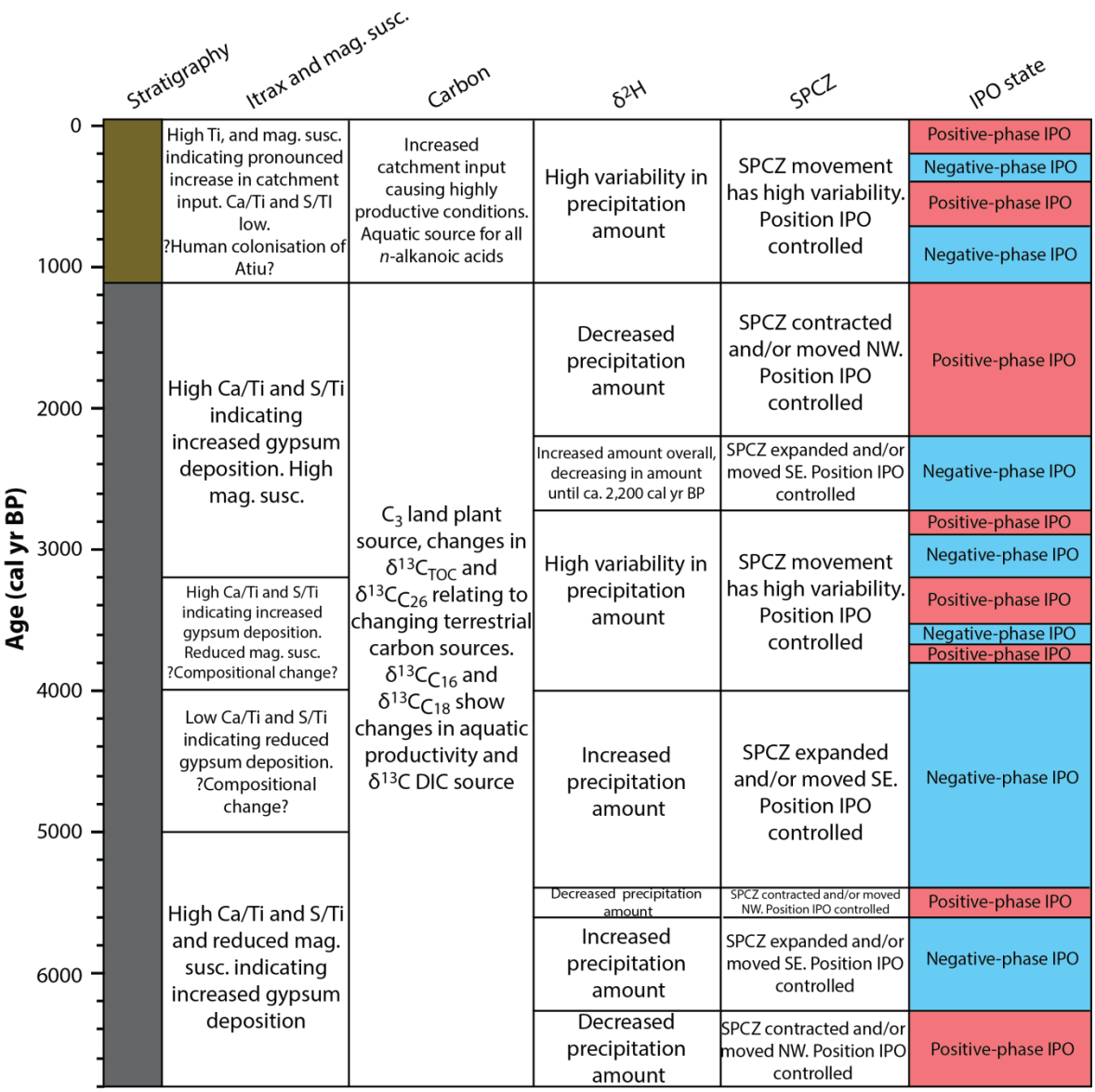

Figure 7.11: Summary interpretation of the proxy data, SPCZ location and controls, and IPO state from Lake Teroto.

Chapter 8: Lake Lanoto'o long core results and proxy interpretation

8.1 Introduction

This chapter outlines the results for proxy data from Lake Lanoto'o: specifically low frequency magnetic susceptibility, Itrax scanning-XRF, TOC, C/N, $\delta^{13}C_{TOC}$, and *n*-alkanoic acid $\delta^{2}H$ and $\delta^{13}C$. The stratigraphic record covers most of the Holocene (9,500 cal yr BP), with proxy data covering this entire period. An interpretation of the data in both a palaeoenvironmental and palaeoclimatic perspective is provided, with changes determined to be the result of changing climatic conditions in the Pacific affecting the position of the SPCZ. As Lake Lanoto'o is not annually laminated and has an average accumulation rate of 32 yr/cm (Section 5.3.2.2) changes in the SPCZ position are in context of the IPO and not ENSO, unless evidence suggests other casual factors could be responsible. This is due to the chronological resolution in Lake Lanoto'o being insufficient to examine changes in ENSO variability.

8.2 Results

8.2.1 Magnetic susceptibility

Measurements of low frequency magnetic susceptibility were obtained at 1 cm intervals for all cores (Figure 8.1). The highest values at the base of the core (ca. 9,390-9,220 cal yr BP) are an order of magnitude larger than any other part of the core, corresponding with the sand unit aforementioned in Section 5.3.2.1. Magnetic susceptibility values are consistently high from ca. 5,640-2,850 cal yr BP and correlate to strong brown units (7.5YR 5/6). Values increase steadily from ca. 1,800 cal yr BP, before sharply decreasing at ca. 800 cal yr BP).

8.2.2 Itrax

As with the short core data presented in section 6.4.3, Itrax data were averaged to 1 cm resolution to facilitate comparison with other proxy data. All Itrax data have been

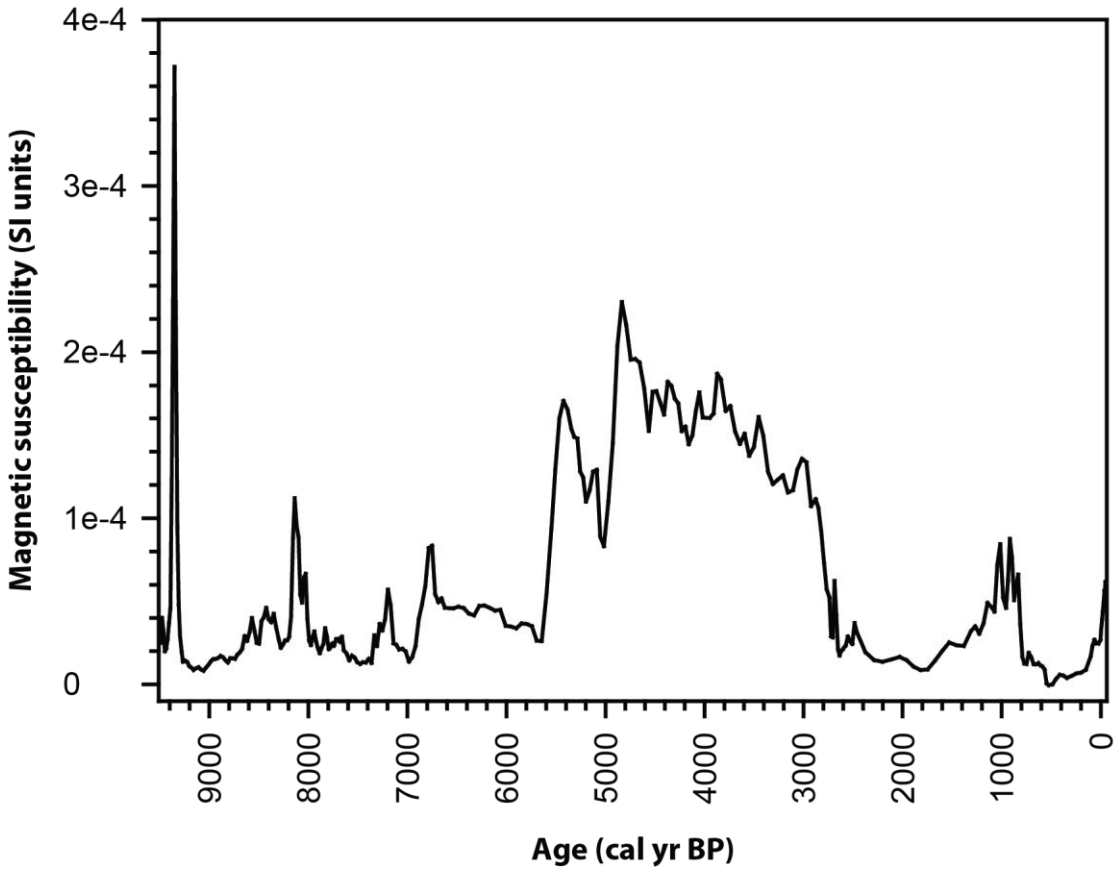

Figure 8.1: Low frequency magnetic susceptibility for Lake Lanoto'o.

standardised to the incoherent scatter to reduce the effects of organic matter and water content (Kylander *et al*., 2011; Marshall *et al*., 2011). The gap in the Mn data is a result of an analytical artefact producing zero values, thus the data have been removed (Figure 8.2). No other element data have been affected by this analytical artefact. The Fe/Mn ratio is used to indicate bottom water anoxia bottom waters, Si/Ti to indicate autochthonous Si, and Ca/Ti to indicate authigenic Ca.

From ca. 9,500-7,000 cal yr BP Br is high whilst Ti, Fe, Mn and Si are low, except for a brief increase in Ti/Fe/Si between ca. 8,200-8,000 cal yr BP with a concomitant decrease in Br for this period. Titanium, Fe, Mn and Si have high values from ca. 5,600-2,700 cal yr BP, whereas Br steadily decreases and shows high variability. From ca. 2,800 cal yr BP to present, Br is high, with lower values between ca. 1,600-800 cal yr BP when Ti/Fe/Si increase. Whilst Ca and K are low throughout the record there are notable peaks at ca. 9,400 cal yr BP, 8,280-7,340 cal yr BP, 1,070 cal yr BP and 940 cal yr BP. Silicon has much higher values from ca. 590 cal yr BP.

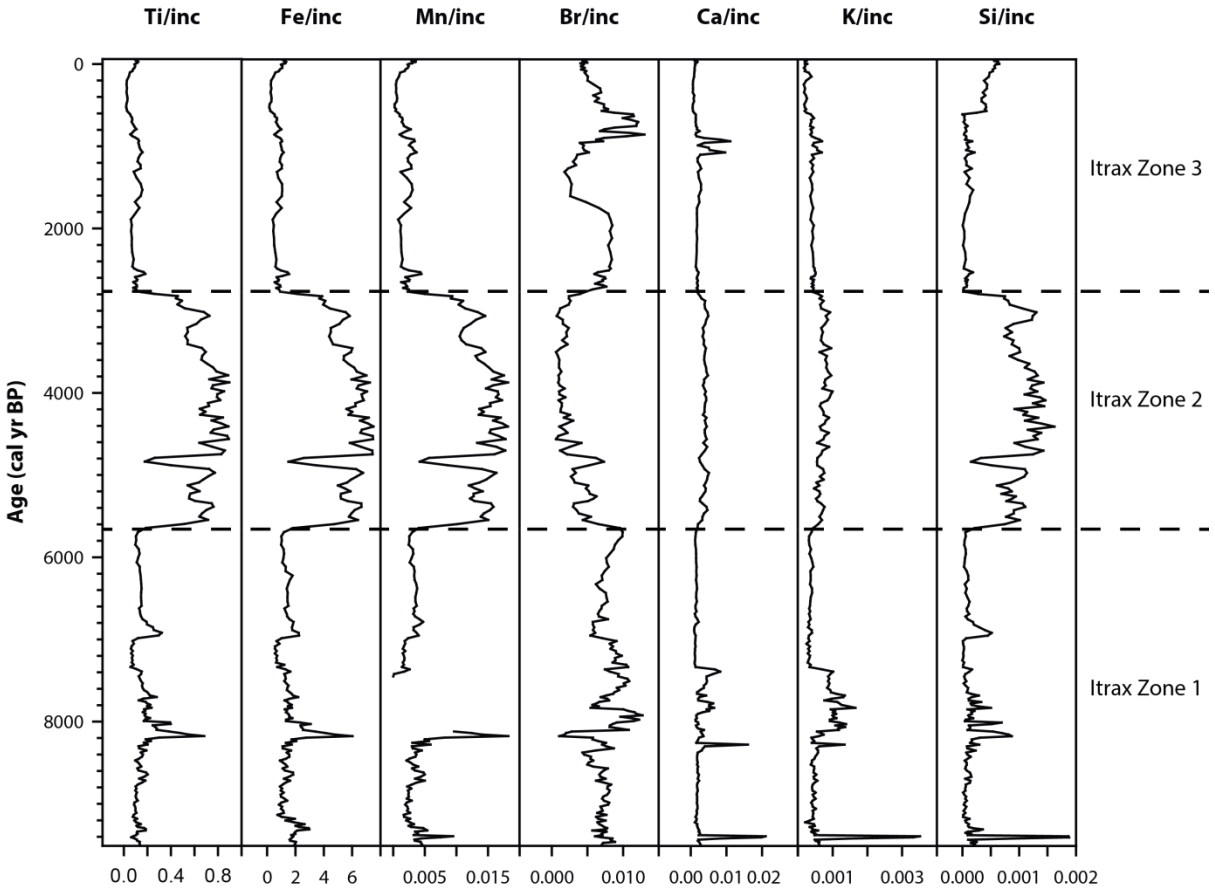

Figure 8.2: Itrax profile for Lake Lanoto'o long core. The gap in Mn is due to an analytical artefact producing zero values.

Ratios of Fe/Mn, Si/Ti and Ca/Ti were undertaken to determine bottom water anoxia, and autochthonous production of Si and Ca (Si/Ti and Ca/Ti respectively). Justification for applying these ratios is outlined in Section 6.3.3.2**.** Ratios of Fe/Mn, Si/Ti and Ca/Ti show little variation throughout the core (Figure 8.3). Fe/Mn peaks at ca. 9,250 cal yr BP and ca. 490 cal yr BP. Due to the aforesaid analytical artefact with Mn it cannot be determined if Fe/Mn is peaking for a section of the core; nevertheless it appears to be high ca. 7400 cal yr BP. High values for Si/Ti only occur at ca. 9,400 cal yr BP and ca. 590 cal yr BP to present, showing little variation throughout the record. Peaks in Ca/Ti occur at ca. 9,400 cal yr BP (coevally with a decrease in Fe/Mn), and at ca. 8,280 cal yr BP, 7,370 cal yr BP, 1,070 cal yr BP and 940 cal yr BP.

In summation the Itrax data can be zoned as follows:

Itrax Zone 1 9,500-5,690 cal yr BP: Bromine is high throughout the unit with low values of Ti/Fe/Mn/Si. A sharp decrease in Br, and concomitant increase in Ti/Fe occurs at ca. 8,200 cal yr BP.

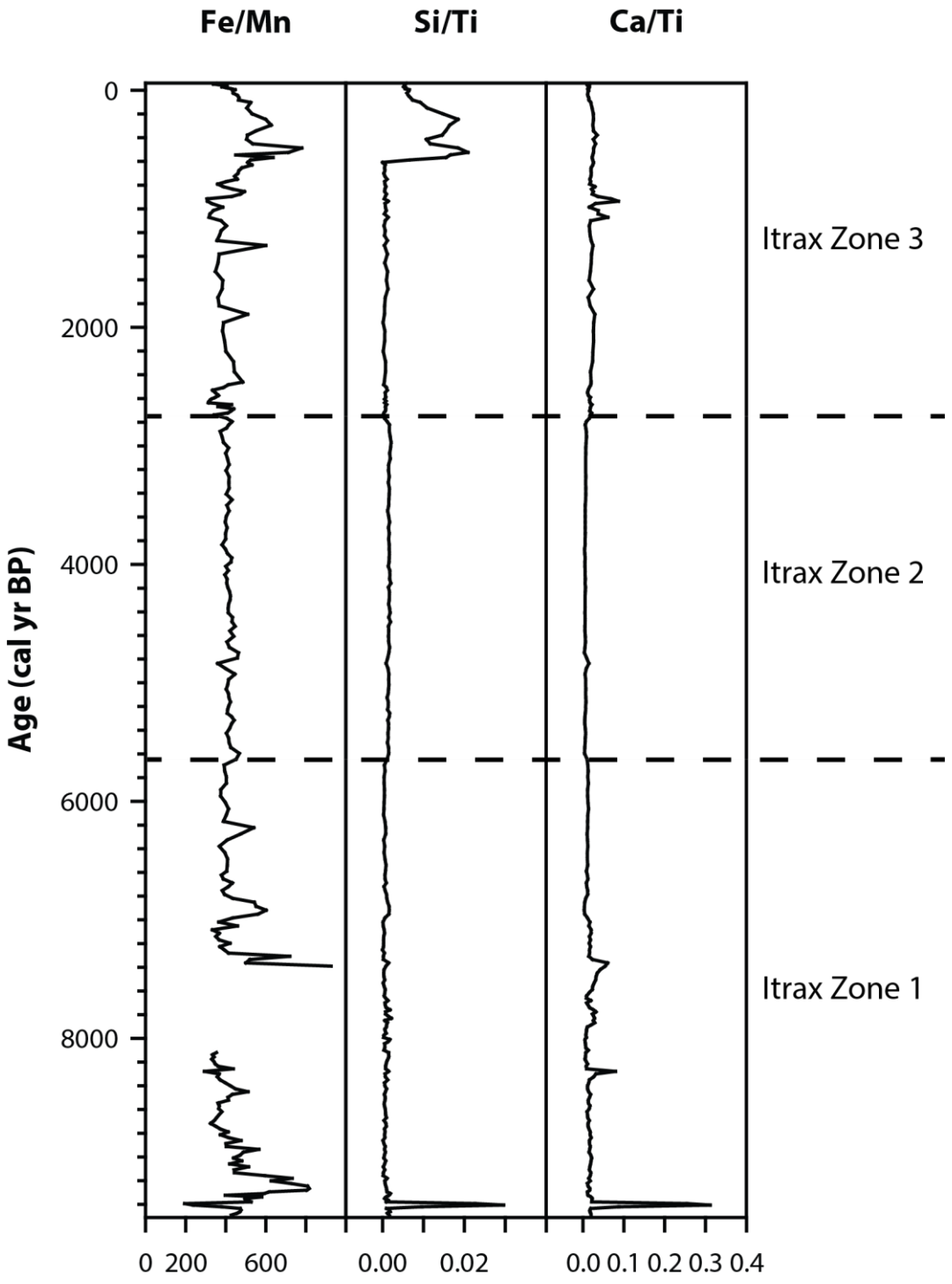

Figure 8.3: Itrax ratios of the Lake Lanoto'o long core. The gap in the Fe/Mn ratio is due to an analytical artefact.

Itrax Zone 2 5,690-2,700 cal yr BP: High values of Ti/Fe/Mn/Ca/K and Si, alongside low values of Br, characterise this unit. A sharp decrease in Ti/Fe/Mn/Si occurs at ca. 4,840 cal yr BP.

Itrax Zone 3 2,700 cal yr BP – present: Bromine is high throughout, with low values of Ti/Fe/Mn. Whilst Si shows a similar trend to Ti/Fe/Mn from ca. 2,700-600 cal yr BP, it increases sharply at 590 cal yr BP.

A correlation matrix and PCA is presented for the entire core sequence to determine the strength of association between pairs of elements in the dataset (Table 8.1). As the long core data indicate similar lithostratigraphy to the short core a correlation matrix was created for the overall core. Like the short core strong correlations ($r \geq 0.7$ or $r \leq -0.7$) are highlighted. Unlike the short core K and Ca are strongly and significantly correlated in the long core. Moreover Br has strong negative and significant correlation with Ti and elements associated with Ti – specifically Al, Si, V, Cr, Fe and Mn. Titanium has strong, positive and significant correlations with similar elements to Unit 1 in the short core: specifically Cr, Mn, Fe and Ni.

The PCA of the long core indicates that Zone 1 is strongly associated with Br and Zone 2 with Ti/Fe/Ni (Figure 8.4). The first two axes explain 81.8% of the data and and $\lambda_1 = 10.58$ and $\lambda_2 = 1.69$. Of interest is that Zones 1 and 3 plot together whereas Zone 2 plots completely separately along axis 1. Zones 1 and 3 are associated with Br, whereas Zone 2 is associated with Fe/Ti/Mn/Si. An outlier at ca. 9,400 cal yr BP is highlighted for Zone 1: examination of the data indicates this outlier is corresponds with the peaks in Ca, K and Si. Further the PCA clearly shows it is associated with Ca and K and has little relationship with Br, Fe, Mn, and Ti.

8.2.3 %TOC, $\delta^{13}C$ and C/N

Loss-on-ignition measurements (LOI_{550}) calibrated against TOC were obtained at contiguous 1 cm intervals on all cores (including overlaps). Total organic carbon, C/N and $\delta^{13}C$ on total organic carbon ($\delta^{13}C_{TOC}$) were obtained at evenly spaced 2 cm intervals throughout the long core, totalling 150 measurements. Measurement of $\delta^{13}C$ on C_{16}, C_{18} and C_{26} *n*-alkanoic acids ($\delta^{13}C_{C16}$, $\delta^{13}C_{C18}$ and $\delta^{13}C_{C26}$ respectively) were performed in duplicate on samples taken throughout the long core at the Organic Geochemistry Unit, Bristol. The aquatic algal carbon source is represented by $\delta^{13}C_{C16}$ and $\delta^{13}C_{C18}$, and the terrestrial carbon source is represented by $\delta^{13}C_{C26}$ (Eglington and Hamilton, 1967; Ficken *et al.*, 2000). Samples were taken at 8 cm intervals or discrete points of interest totalling

	Al/inc	Si/inc	P/inc	S/inc	K/inc	Ca/inc	Ti/inc	V/inc	Cr/inc	Mn/inc	Fe/inc	Ni/inc	Sr/inc	Br/inc	Pb/inc
Al/inc		<0.01	<0.01	0.07	<0.01	<0.01	<0.01	<0.01	<0.01	<0.01	<0.01	<0.01	<0.01	<0.01	<0.01
Si/inc	**0.88**		<0.01	0.02	<0.01	<0.01	<0.01	<0.01	<0.01	<0.01	<0.01	<0.01	<0.01	<0.01	<0.01
P/inc	0.66	**0.82**		0.01	<0.01	<0.01	<0.01	<0.01	<0.01	<0.01	<0.01	<0.01	<0.01	<0.01	<0.01
S/inc	0.10	0.13	0.16		<0.01	<0.01	0.01	0.02	0.01	0.12	<0.01	0.01	0.05	0.69	<0.01
K/inc	0.20	0.43	0.26	0.28		<0.01	<0.01	<0.01	<0.01	<0.01	<0.01	<0.01	<0.01	0.24	<0.01
Ca/inc	0.27	0.47	0.26	0.17	**0.79**		<0.01	<0.01	<0.01	<0.01	<0.01	<0.01	<0.01	<0.01	<0.01
Ti/inc	**0.93**	**0.86**	0.60	0.14	0.31	0.31		<0.01	<0.01	<0.01	<0.01	<0.01	<0.01	<0.01	<0.01
V/inc	**0.93**	**0.85**	0.57	0.14	0.28	0.30	**0.99**		<0.01	<0.01	<0.01	<0.01	<0.01	<0.01	<0.01
Cr/inc	**0.92**	**0.86**	0.59	0.15	0.30	0.32	**0.99**	**0.98**		<0.01	<0.01	<0.01	<0.01	<0.01	<0.01
Mn/inc	**0.94**	**0.88**	0.58	0.09	0.22	0.35	**0.95**	**0.96**	**0.96**		<0.01	<0.01	<0.01	<0.01	<0.01
Fe/inc	**0.93**	**0.87**	0.62	0.23	0.32	0.33	**0.99**	**0.99**	**0.98**	**0.96**		<0.01	<0.01	<0.01	<0.01
Ni/inc	**0.81**	**0.78**	0.57	0.16	0.39	0.29	**0.94**	**0.91**	**0.93**	**0.81**	**0.91**		<0.01	<0.01	<0.01
Sr/inc	**0.87**	**0.83**	0.52	0.11	0.40	0.48	**0.95**	**0.95**	**0.94**	**0.93**	**0.95**	**0.87**		<0.01	<0.01
Br/inc	**-0.72**	**-0.74**	-0.58	-0.02	-0.07	-0.24	**-0.72**	**-0.70**	**-0.75**	**-0.77**	**-0.70**	-0.64	-0.68		<0.01
Pb/inc	**0.95**	**0.87**	0.67	0.22	0.28	0.29	**0.96**	**0.96**	**0.95**	**0.93**	**0.97**	**0.87**	**0.90**	-0.68	

Table 8.1: Linear correlation matrix for the Lake Lanoto'o long core data, with correlation values below the diagonal and P values above it. In bold are correlations r≥0.7 and r≤-0.7. Highlighted in red are values that are not statistically significant below the 0.01 significance level.

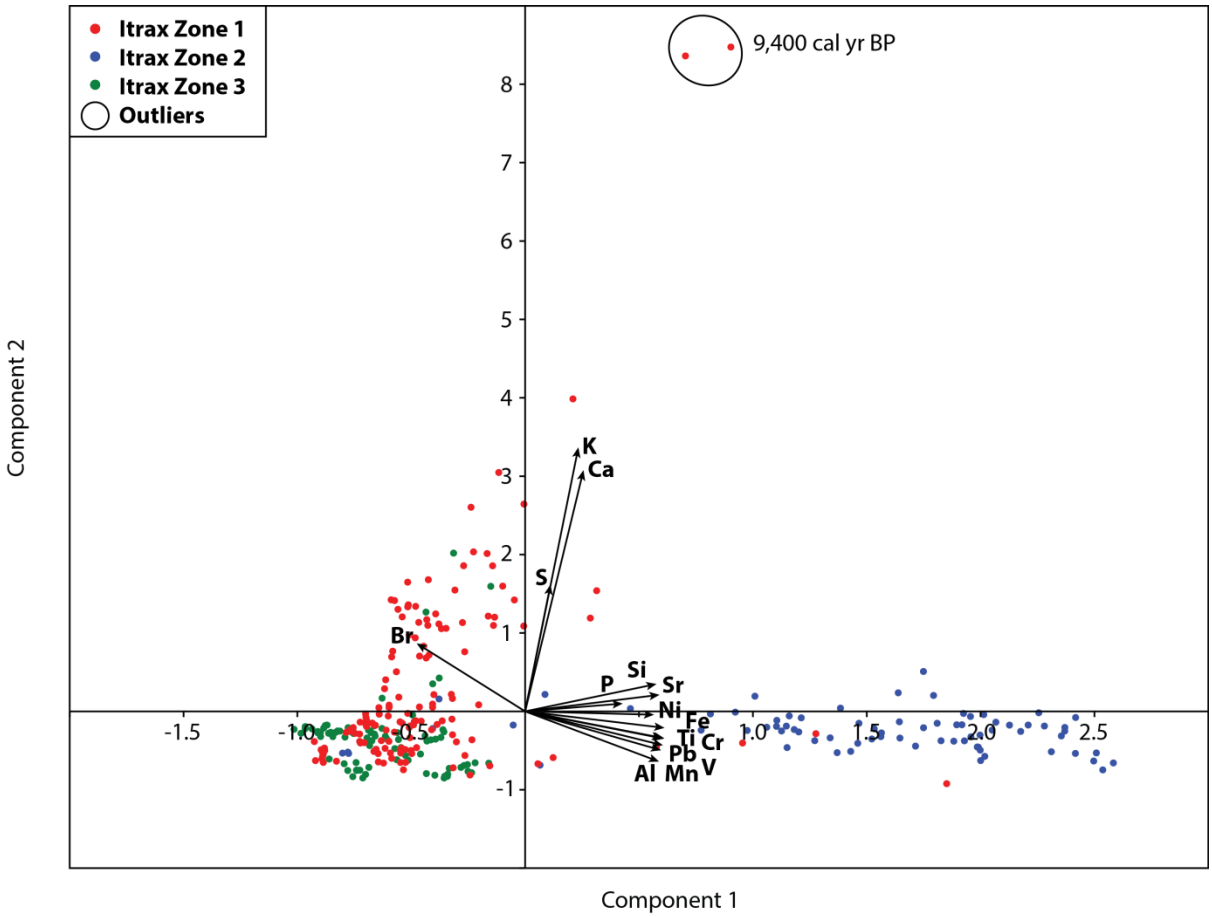

Figure 8.4: PCA of Itrax data from the Lake Lanoto'o long core. Red indicates Zone 1, blue indicates Zone 2, and green indicates Zone 3. The age of proposed outliers are also presented.

40 samples measured for δ^2H_{C26} at the University of Washington. Twenty-nine samples were analysed at the University of Bristol for $\delta^{13}C_{C16}$, $\delta^{13}C_{C18}$, $\delta^{13}C_{C26}$, δ^2H_{C16} and δ^2H_{C18} as these samples indicated no co-elution.

The relative distribution of *n*-alkanoic acids throughout the record (Figure 8.5) suggests that the distribution of long-chain *n*-alkanoic acids (C_{26} and C_{28}) has remained relatively constant, with a notable reduction at ca. 6,485 and 6,918 cal yr BP. However the short-chain *n*-alkanoic acids (C_{16} and C_{18}) has fluctuated with higher proportions between ca. 8,293-7,999 cal yr BP, 7,362-5,068 cal yr BP and 2,508 cal yr BP to present. The proportion of C_{30} *n*-alkanoic acid has reduced throughout the record, having the lowest proportion over the last ca. 3,000 cal yr BP.

From ca. 9,500-7,000 cal yr BP C/N and $\delta^{13}C_{TOC}$ oscillate and are in antiphase to each other, i.e. when C/N is high (>30) $\delta^{13}C_{TOC}$ is more negative (as low as -26‰) (Figure 8.6).

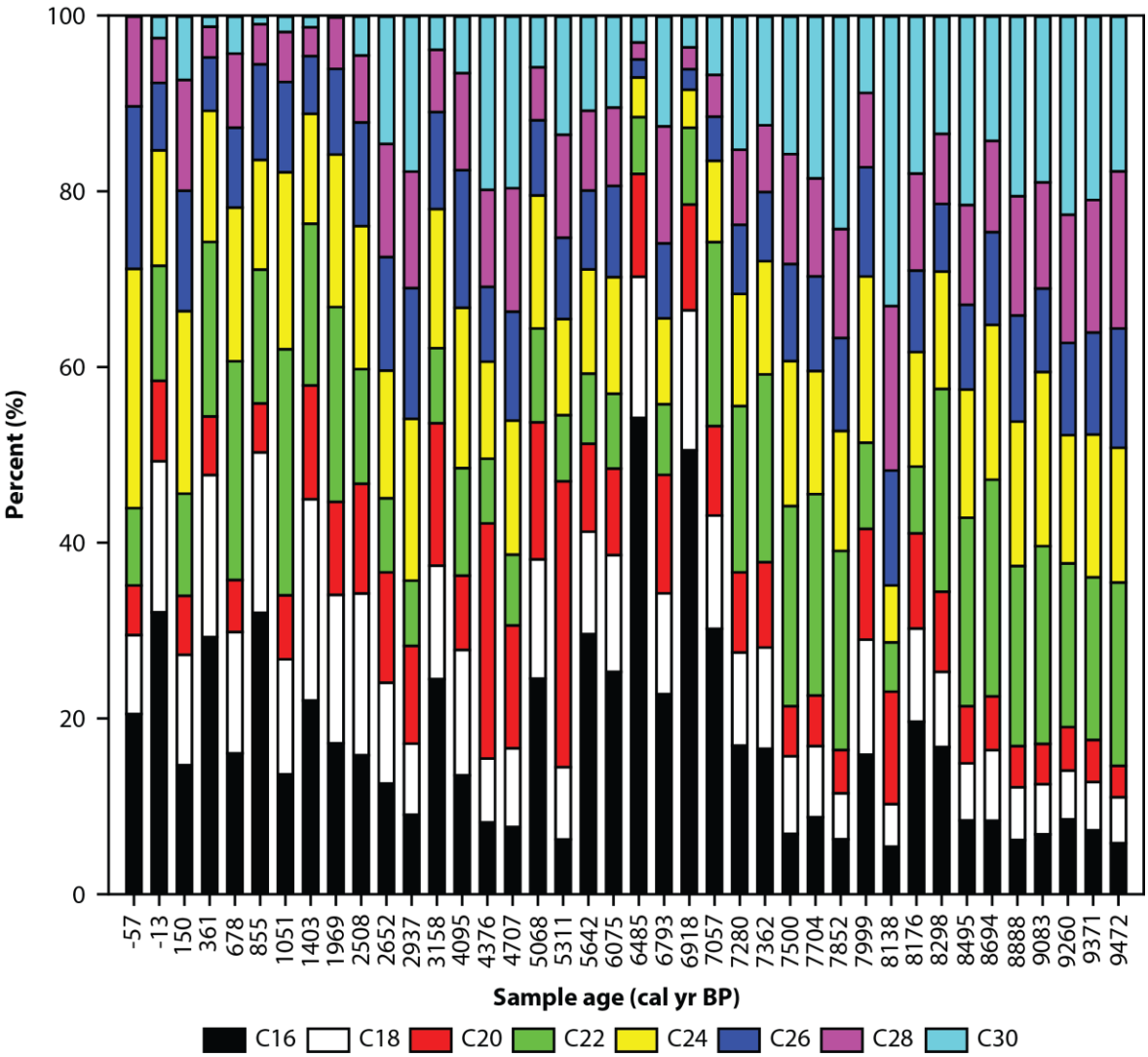

Figure 8.5: Even chain length *n*-alkanoic acids for Lake Lanoto'o. The ratio of each compound against the total even chain length *n*-alkanoic acids were calculated as a percentage.

Both $\delta^{13}C_{C16}$ and $\delta^{13}C_{C18}$ values show a pronounced decrease at ca. 9,370 cal yr BP after which values progressively increase overall until ca. 7,060 cal yr BP. The $\delta^{13}C_{C26}$ record from ca. 9,500-7,000 cal yr BP has similar trends to the $\delta^{13}C_{TOC}$ for this period. From ca. 7,000-5,000 cal yr BP $\delta^{13}C_{TOC}$ gets progressively more negative whilst C/N stays stable. The progressively more negative $\delta^{13}C_{TOC}$ values are not seen in the $\delta^{13}C_{C16}$, $\delta^{13}C_{C18}$ or $\delta^{13}C_{C26}$ records. High C/N values occur between ca. 5,000-2,700 cal yr BP, with $\delta^{13}C_{TOC}$ showing high variability throughout that is not reflected in the $\delta^{13}C_{C16}$, $\delta^{13}C_{C18}$ or $\delta^{13}C_{C26}$ records. This may be a consequence of the low sample resolution for this time frame. Following ca. 2,700 cal yr BP C/N values progressively decrease to as low as 14, whilst $\delta^{13}C_{TOC}$ oscillates between -22‰ to -25‰. Whilst $\delta^{13}C_{C16}$ values are increasingly more

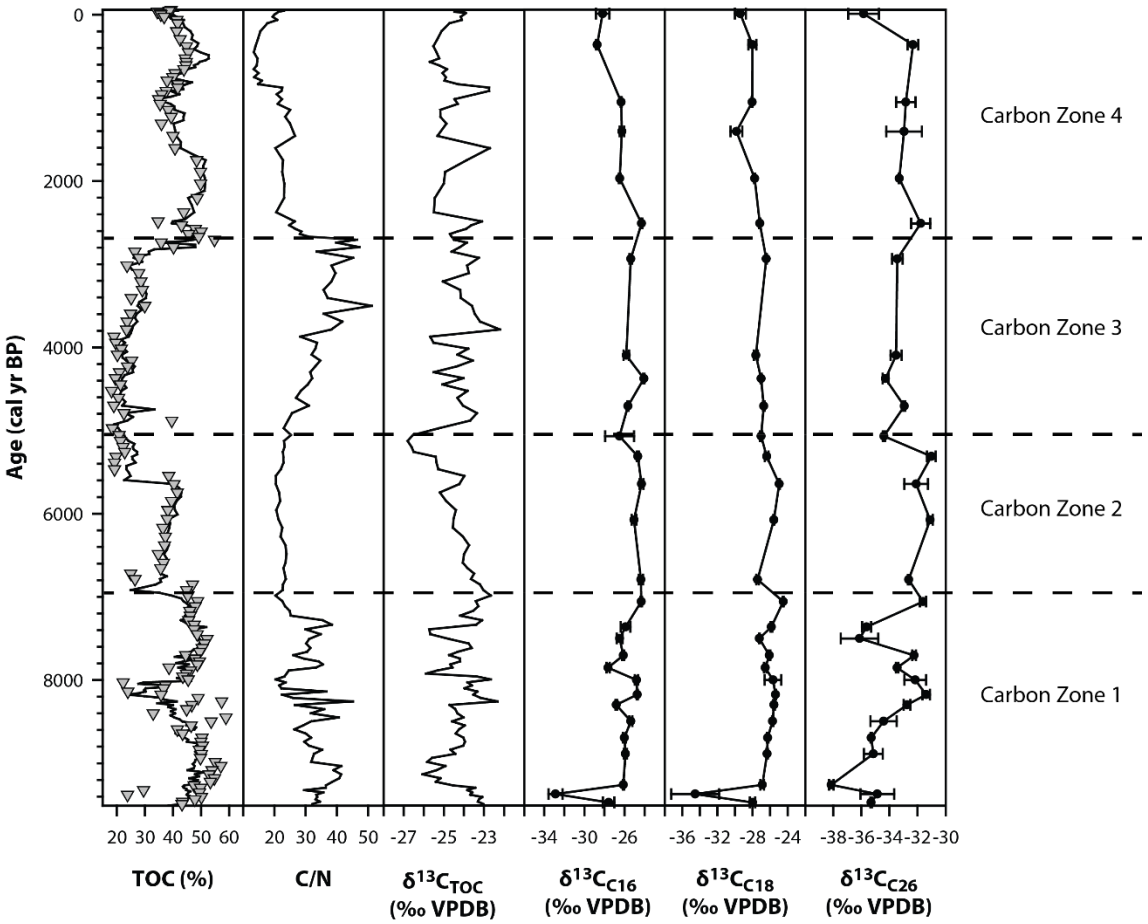

Figure 8.6: The %TOC, $\delta^{13}C_{TOC}$, C/N, $\delta^{13}C_{C16}$, $\delta^{13}C_{C18}$ and $\delta^{13}C_{C26}$ for the Lake Lanoto'o long core. In the %TOC column triangles represent element analyser data, and the solid black line indicates adjusted loss-on-ignition data.

negative, the $\delta^{13}C_{C18}$ record decreases until ca. 1,400 cal yr BP before increasing until ca. 360 cal yr BP after which the $\delta^{13}C_{C18}$ decreases. The $\delta^{13}C_{C26}$ record is relatively stable for this period until ca. 360 cal yr BP, after which values become more negative. This zonation can be summarised as follows:

Carbon Zone 1 9,500-7,000 cal yr BP: Both C/N and $\delta^{13}C_{TOC}$ is variable throughout, oscillating between 20 to 45 and -23‰ to -26‰ respectively. Total organic carbon is high (>40%) throughout, except between ca. 8,200-8,000 cal yr BP where element analyser TOC values are as low as 25%. Adjusted LOI values do not show any reduction at this time, whereas both $\delta^{13}C_{C16}$ and $\delta^{13}C_{C18}$ do. The $\delta^{13}C_{C26}$ record matches the $\delta^{13}C_{TOC}$ trends.

Carbon Zone 2 7,000-5,000 val yr BP: C/N are stable, with $\delta^{13}C_{TOC}$ becoming increasingly negative throughout. The TOC shows sharp decreases at ca. 6.900 and 5,600 cal yr BP.

Carbon Zone 3 5,000-2,700 cal yr BP: The $\delta^{13}C_{TOC}$ values are variable throughout, TOC progressively increases to 50%, and C/N increases to values as high as 50. Changes in $\delta^{13}C_{C16}$, $\delta^{13}C_{C18}$ or $\delta^{13}C_{C26}$ are not as variable as the $\delta^{13}C_{TOC}$ which may be a consequence of low sample resolution.

Carbon Zone 4 2,700 cal yr BP to present: C/N decreases to 14 whilst TOC remains high (>40%). The $\delta^{13}C_{TOC}$ values oscillate between -22‰ and -25‰. The $\delta^{13}C_{C16}$ and $\delta^{13}C_{C18}$ records show different trends, and the $\delta^{13}C_{C26}$ record is relatively stable for this period.

Figure 8.7 indicates that most of the long core samples plot outside, albeit near, generalised C_3 terrestrial plant values (Meyers and Teranes, 2001). The entire set of long core samples plot within the range of modern soil values. Carbon zones are highlighted and indicate that some of Carbon Zone 4 (ca. 800-200 cal yr BP) is distinct from the other carbon zones delineated.

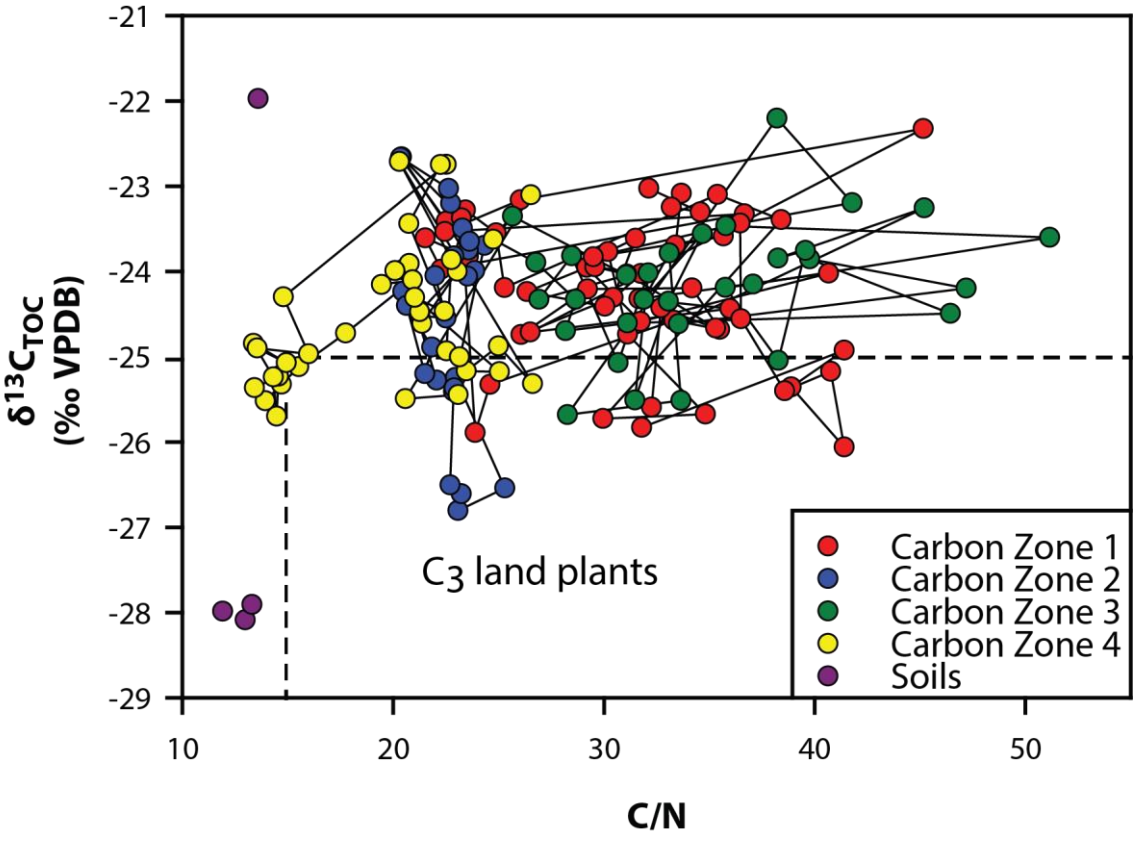

Figure 8.7: $\delta^{13}C_{TOC}$ and C/N ratio for Lake Lanoto'o long core samples. Carbon zones are indicated with different colours (legend) and the solid line connects adjacent samples. The dashed line indicates generalised values for C_3 land plants (Meyers and Teranes, 2001). Modern soil samples are also shown in purple.

8.2.4 *n*-alkanoic acid δ^2H

Measurements of δ^2H on C_{16}, C_{18} and C_{26} alkanoic acid (δ^2H_{C16}, δ^2H_{C18} and δ^2H_{C26} respectively) were performed on samples taken throughout the long core (Figure 8.8). Both C_{16} and C_{18} measurements were performed in duplicate at the Organic Geochemistry Unit (Bristol), and in triplicate for C_{26} at the University of Washington (Seattle). Of interest are the distinct negative δ^2H_{C26} values at ca. 8,000 cal yr BP which is not seen to the same extent in the δ^2H_{C16} and δ^2H_{C18} records. Progressively more negative values are observed from ca. 6,800-3,000 cal yr BP in the δ^2H_{C26} record that are not seen in the δ^2H_{C16} and δ^2H_{C18} records. An increase to less negative δ^2H_{C26} values occurs from ca. 3,000-1,400 cal yr BP, after which values become increasingly negative towards present. Contrary to this the δ^2H_{C16} and δ^2H_{C18} records become increasingly less negative from ca. 2,800 cal yr BP to present.

8.3 Interpretation

8.3.1 Overview and general remarks

A summary of the proxy data for the Lake Lanoto'o long core is presented in Figure 7.9. It is important to note that with 1 cm equal to ca. 32 years' temporal resolution in this site it is not sufficient to discuss ENSO, which has a two- to seven-year timescale. As the IPO has a ca. 20-30-year timescale, thus being within errors to the temporal resolution in this site, inferences on the prevailing Pacific climatic state should be in reference to IPO state rather than ENSO state (as previously discussed in Section 5.3.2.2). The δ^2H_{C26} values represent discrete points that aimed to corroborate climatic interpretations made from Ti and TOC trends independent of any potential human activity that may impact the Lake Lanoto'o record. Consequently interdecadal trends in precipitation amount from δ^2H_{C26} data, which relate to SPCZ location, cannot be deduced. Further, with the large errors in these samples any trends in precipitation amount should be interpreted with caution. However, by combining the δ^2H_{C26} data with Ti and TOC changes in the SPCZ location can be inferred and potentially provide additional information on SPCZ behaviour and hydrological changes over the Holocene.

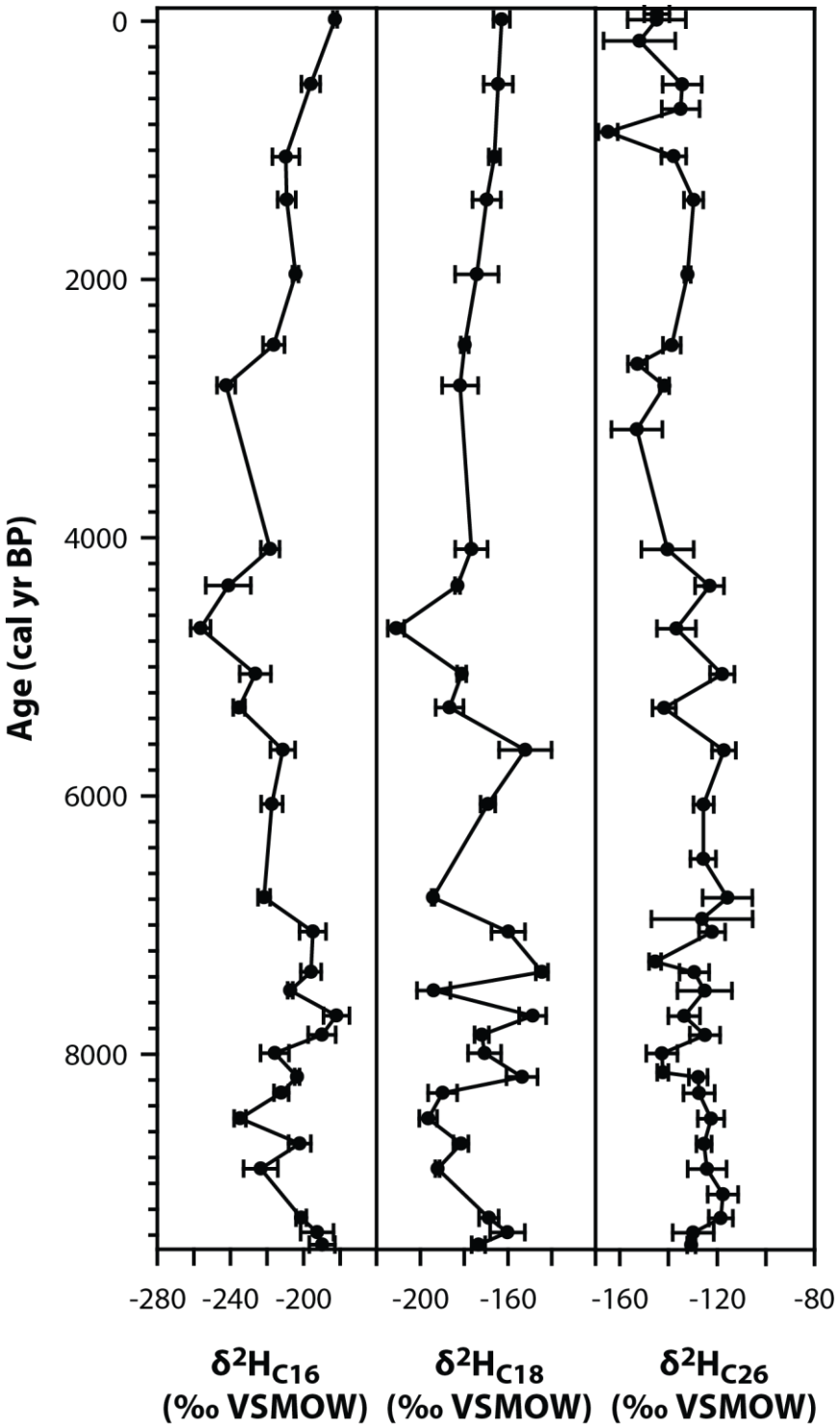

Figure 8.8: δ^2H measurements on C_{16}, C_{18} and C_{26} alkanoic acid (δ^2H_{C16}, δ^2H_{C18} and δ^2H_{C26} respectively) throughout the Lake Lanoto'o long core.

From ca. 9,500-450 cal yr BP carbon is interpreted to be derived from C_3 terrestrial plants (Meyers and Terranes, 2001). From ca. 450 cal yr BP to present C/N is 14: this combined with other evidence outlined is suggested to indicate a mixed aquatic and terrestrial carbon source. Changes in the $\delta^{13}C$ record are interpreted to be largely the result of changing terrestrial carbon sources with a small contribution from aquatic carbon

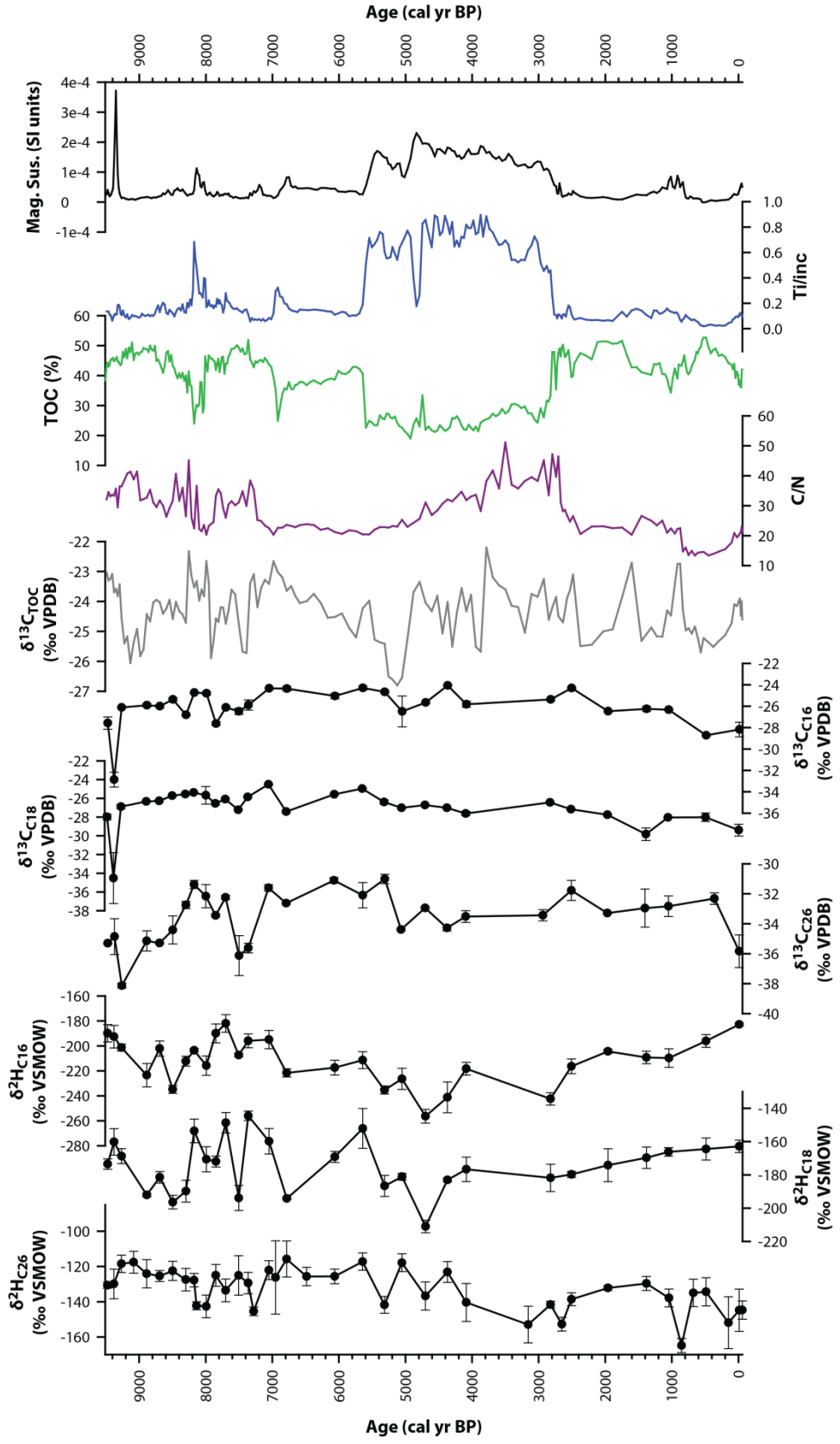

Figure 8.9: Summary of the data for the Lake Lanoto'o long core. Presented are low frequency magnetic susceptibility; Ti; total organic carbon derived from adjusted LOI_{550} values (TOC); C/N; $\delta^{13}C$ of total organic carbon ($\delta^{13}C_{TOC}$); $\delta^{13}C$ of C_{16}, C_{18} and C_{26} alkanoic acids ($\delta^{13}C_{C16}$, $\delta^{13}C_{C18}$ and $\delta^{13}C_{C26}$ respectively); and $\delta^{2}H$ measurements on C_{16}, C_{18} and C_{26} alkanoic acids ($\delta^{2}H_{C16}$, $\delta^{2}H_{C18}$ and $\delta^{2}H_{C26}$ respectively).

sources; the exact changes in source are not possible to determine with the data available. The most distinct change in the record, interpreted to relate to a change in IPO state, occurs between ca. 5,600-2,700 cal yr BP. Whilst human impact on the Lake Lanoto'o record from ca. 2,500 cal yr BP cannot be unequivocally discounted, it is concluded that climate is the primary control on changes in the geochemical record and thus it can be used with confidence to determine SPCZ movement.

8.3.2 Controls on *n*-alkanoic δ^2H

A correlation matrix comparing the $\delta^{13}C$ and δ^2H values for C_{16}, C_{18} and C_{26} alkanoic acids indicated that there is a significant negative correlation between C_{16} $\delta^{13}C$ and δ^2H values (r = -0.48, p<0.05) (Table 8.2). Further it reveals that the respective $\delta^{13}C$ and δ^2H values for C_{16} and C_{18} have a strong significant positive correlation ($\delta^{13}C$: r = 0.8, p<0.01; δ^2H: r = 0.72, p<0.01). Interestingly the correlation between C_{18} $\delta^{13}C$ and δ^2H values is not significant; this is also the case for C_{26} $\delta^{13}C$ and δ^2H values.

	$\delta^{13}C_{C16}$	δ^2H_{C16}	$\delta^{13}C_{C18}$	δ^2H_{C18}	$\delta^{13}C_{C26}$	δ^2H_{C26}
$\delta^{13}C_{C16}$		0.01	<0.01	0.34	0.04	0.48
δ^2H_{C16}	-0.48		0.21	<0.01	0.30	0.89
$\delta^{13}C_{C18}$	**0.80**	-0.24		0.74	0.11	0.26
δ^2H_{C18}	-0.19	**0.72**	-0.07		0.63	0.82
$\delta^{13}C_{C26}$	0.38	-0.20	0.30	0.09		0.24
δ^2H_{C26}	0.14	0.03	0.21	-0.04	-0.22	

Table 8.2: Linear correlation matrix for the Lake Lanoto'o biomarker data, with correlation values below the diagonal and p values above it. In bold are correlations r≥0.7 and r≤-0.7. Highlighted in red are values that are not statistically significant below the 0.01 significance level.

The significant negative correlation of $\delta^{13}C_{C16}$ and δ^2H_{C16} suggests that changes in carbon source are controlling changes in hydrogen, likely to be a result of changes in the principal source organism producing C_{16} alkanoic acid (Zhang and Sachs, 2007). Whilst there is not a significant correlation between $\delta^{13}C_{C18}$ and δ^2H_{C18}, the significant correlation between $\delta^{13}C_{C16}$ and $\delta^{13}C_{C18}$ as well as δ^2H_{C16} and δ^2H_{C18} indicates that they reflect the same carbon source and that changes δ^2H_{C18} are also controlled by changes in the source organism producing them. The significant changes in the proportion of C_{16} and C_{18} throughout the Lake Lanoto'o record further suggest changes in source organisms within the lake. With this in mind changes in $\delta^{13}C_{16}$ and $\delta^{13}C_{C18}$ values may not reflect changes in lake

productivity but rather changes in the principal organism producing them as a consequence of the differences in the biosynthetic pathways that produce C_{16} and C_{18} alkanoic acids (Zhang and Sachs, 2007).

With C_{26} alkanoic acid being terrestrially derived (Eglington and Hamilton, 1967), it would be expected to reflect changes in the δ^2H values of precipitation (Section 4.5.3.3.3). The lack of a significant correlation between δ^2H_{C26} and $\delta^{13}C_{C26}$ indicates that changes in carbon are not affecting the δ^2H_{C26} values; furthermore the relatively constant proportion of C_{26} alkanoic acid in the Lake Lanoto'o record suggests no large vegetation changes have occurred through time in regards to plant sources around the Lake Lanoto'o catchment (Yamoah *et al*., 2016b). Parkes (1994) concluded a shift from trees to pteridophytes being the dominant taxa at ca. 2,540 cal yr BP (Appendix C, Figure C2). No significant change in the δ^2H_{C26} values is apparent after this time suggesting that changes in δ^2H_{C26} reflect changes in precipitation δ^2H (Hou *et al*., 2008; Kahman *et al*., 2013b); albeit a full evaluation is hindered by sample resolution. Having previously established that precipitation amount is the primary control on precipitation isotope values (Section 6.3.2), and that changes in Ti and Br (and by extension TOC) in Lake Lanoto'o are a result of changes in catchment inwash that relate to changes in precipitation amount over the AD 1890-2012 period (Section 6.4.3), it is expected that increases (decreases) in Ti (TOC) in the Lake Lanoto'o record are a result of increased (decreased) precipitation amount which in turn would be reflected in more negative (less negative) δ^2H_{C26} values. Over the ca. 9,500 cal yr BP record, increases in Ti (TOC) largely correspond to more negative (less negative) δ^2H_{C26} values; however this relationship is not statistically significant. It is concluded that changes in δ^2H_{C26} values relate to changes in precipitation amount.

It can be seen that in some parts of the Lake Lanoto'o record changes in δ^2H_{C16} and δ^2H_{C18} values correspond to changes in δ^2H_{C26} values, for examples at ca. 8,000 cal yr BP and between ca. 6,000-4,000 cal yr BP. It is proposed that at these times the δ^2H_{C16} and δ^2H_{C18} values are reflecting the lake water δ^2H value, which in turn is being controlled by the precipitation δ^2H value that itself is determined by the amount of precipitation. Consequently it is possible to disentangle when precipitation δ^2H is controlling δ^2H_{C16} and δ^2H_{C18} values and when changes in algal carbon source are controlling δ^2H_{C16} and δ^2H_{C18} values.

8.3.3 Palaeoclimatic and palaeoenvironmental interpretation

8.3.3.1 Prolonged reduction in precipitation amount 9,500-8,200 cal yr BP

The high Ti and low frequency magnetic susceptibility values at the base of the sequence indicate an allogenic sediment source. Combined with C/N values greater than 20 – indicative of a terrestrial carbon source (Meyers and Terranes, 2001; Leng *et al*., 2006) – and more negative δ^2H_{C26} values suggests increased rainfall and catchment input from ca. 9,500-9,300 cal yr BP. Albeit this is difficult to determine at the base of the record given the absence of earlier dates. Based on relationships determined in Section 6.4.3 high values of Ti relate to increased rainfall amount which is indicative of SPCZ expansion and/or movement SE. This in turn would suggest that negative-phase IPO is the prevailing climate state in the Pacific at this time (Folland *et al*, 2002).

The pronounced and high low frequency magnetic susceptibility spike at ca. 9,300 cal yr BP is the highest value for the entire sequence. It occurs alongside spikes in Ca/Ti, Si/Ti and K, coincidentally the highest values for each of these in the entire record, and a reduction in Fe/Mn indicating a reduction in bottom water anoxia. Further there is a pronounced reduction in both $\delta^{13}C_{C16}$ and $\delta^{13}C_{C18}$ values with a small increase in $\delta^{13}C_{C26}$. As Ti does not increase, suggesting no increased allogenic input, an inwash event is discounted. Further there is a small decrease in C/N and $\delta^{13}C_{TOC}$, and pronounced decreases in TOC derived from the element analyser whilst LOI-adjusted TOC values appear stable at ca. 9,300 cal yr BP (Figure 8.7).The high Ca/Ti and Si/Ti would suggest increased authigenic Ca and Si production respectively, the latter of which may be due to increased diatom productivity (Peinerud, 2000). However with only a small change in C/N and $\delta^{13}C_{TOC}$, and a decrease in element analyser derived TOC this is discounted. This is because it would be expected that C/N values would decrease close to 10 indicative of mixed carbon sources (Meyers and Terranes, 2001), and $\delta^{13}C_{TOC}$ values would become more positive due to increase aquatic productivity (Leng *et al*., 2006). It is tentatively suggested that these distinct changes relate to a tephra deposit, supported by the high K and Ca at this horizon which is typical of alkali basalts (the dominant geology in the region, see Section 3.3); however with the data available this cannot be validated. With the reduction in Fe/Mn indicating a reduction in bottom water anoxia and the pronounced negative $\delta^{13}C_{C16}$ and $\delta^{13}C_{C18}$ values it is suggested that the lake overturned, bringing more

negative $\delta^{13}C$ from the hypolimnion that was incorporated by algae in the lake (Leng *et al*., 2006).

Whilst it is suggested that precipitation is higher and the SPCZ had expanded and/or migrated SE from ca. 9,500-9,300 cal yr BP, overall from ca. 9,500-8,200 cal yr BP TOC and Br are high (albeit with a decreasing trend). In Section 6.4.3 it was determined that high Br and TOC represented a reduced siliciclastic input into the lake from the catchment, suggesting reduced precipitation. This is corroborated by the less negative $\delta^{2}H_{C26}$ values throughout this time that are stable and suggest less precipitation amount. However, $\delta^{2}H_{C26}$ values become increasingly negative corresponding to the decreasing trend in TOC; it is suggested that precipitation amount is increasing over this time period. Climatically this indicates that from ca. 9,300-8,200 cal yr BP the SPCZ has contracted and/or migrated NE, reducing precipitation amount to the Lake Lanoto'o catchment. Apropos to this a contracted SPCZ indicates that positive-phase IPO conditions are prevalent in the Pacific (Folland *et al*., 2002). For this period a decreasing trend in $\delta^{2}H_{C16}$ and $\delta^{2}H_{C18}$ values corresponds to an increasing trend in their respective $\delta^{13}C$ values – consequently changes in the $\delta^{2}H_{C16}$ and $\delta^{2}H_{C18}$ and their respective $\delta^{13}C$ values for this period are interpreted to be a result of a change in algal source producing them. There are small increases in Ti throughout this time period, for examples at ca. 8,600 cal yr BP, suggesting that whilst overall positive-phase IPO conditions are the dominant climate regime, relatively short-lived switches to negative-phase IPO conditions (and consequent SPCZ expansion and/or movement SE) are occurring. This is similar to modern climatology, where La Niña (El Niño) events still occur during positive IPO (negative IPO) (Power *et al*., 1999).

In contrast to the small fluctuations in Ti and TOC, C/N and $\delta^{13}C$ values show relatively large variability. As aforementioned C/N values indicate terrestrial sources, with Figure 7.8 indicating that carbon is sourced from C_3 terrestrial plants – this is further supported by Parkes (1994) who determined most vegetation at this time is trees (ca. 40%) and pteridophytes (ca. 45%), with ca. 2% aquatics observed, and all of which show little variability (Appendix C, Figure C2). The high C/N values at 9,000 cal yr BP coincide with more negative $\delta^{13}C_{TOC}$ and $\delta^{13}C_{C26}$ values; considering the C_3 terrestrial plant source it is suggested that this change in $\delta^{13}C_{TOC}$ indicates a change in carbon source. This could be due an inwash event; however Ti and low frequency magnetic susceptibility does not increase at this time indicating there is no allogenic input in the lake. Consequently it

suggests a change in the composition of the carbon flux. With the data available the cause of the change is not possible to determine, but it could be related to an increase in tree input as trees typically have high C/N (>40) and more negative $\delta^{13}C$ values (Meyers and Terranes, 2001) – Parkes (1994) determines a small increase in tree pollen around this time from ca. 37 to 42% (Appendix C, Figure C2). A decrease in C/N values towards 30 precedes a shift to less negative $\delta^{13}C_{TOC}$ values: this again is interpreted as a change in the composition of the carbon source as both Ti and low frequency magnetic susceptibility values are low.

8.3.3.2 Abrupt climate change 8,200-7,900 cal yr BP

At ca. 8,200 cal yr BP both C/N increases and $\delta^{13}C_{TOC}$ becomes less negative suggesting a change in carbon source, which is likely a result of increased catchment inwash as shown by the rising Ti values. Two distinct spikes in allogenic input, indicated by spikes in Ti and low frequency magnetic susceptibility, occur at ca. 8,175 and ca. 8,010 cal yr BP. Contemporaneous with this is a reduction in TOC, considered to be a consequence of TOC being diluted by the increased siliciclastic input. Carbon/nitrogen ratios, $\delta^{13}C_{TOC}$ and $\delta^{13}C_{C26}$ change together throughout this period of increased allogenic input, suggesting a prolonged change in terrestrial carbon source. The high values of C/N (>30) are tentatively suggested to be a consequence of trees (Meyers and Terranes, 2001), which Parkes (1994) concluded were 50% of the vegetation in the Lake Lanoto'o record at this time (Appendix C, Figure C2). Pronouncd negative $\delta^{2}H_{C26}$ values occur at ca. 8,100 and 8,000 cal yr BP suggesting that this period of increased allogenic input relates to a significant increase in the precipitation amount to the lake's catchment. In addition, both $\delta^{2}H_{C16}$ and $\delta^{2}H_{C18}$ values become more negative at this time; with stable $\delta^{13}C_{C16}$ and $\delta^{13}C_{C18}$ values it is inferred that $\delta^{2}H_{C16}$ and $\delta^{2}H_{C18}$ reflect the lake water $\delta^{2}H$ that is more negative due to the increased precipitation amount inputted into the lake.

The proxy evidence indicates that from ca. 8,200-7,900 cal yr BP there was a period of increased catchment inwash due to increased precipitation amount. Whilst there are only two $\delta^{2}H_{C26}$ measurements for this period they supports an interpretation that this inwash was the result of an increase in precipitation amount as it is isotopically distinct from measurements obtained either side of this time period and occurs in a Ti spike. The Ti record indicates there are two well-defined inwash events, suggesting that whilst

precipitation was higher throughout there were two periods where precipitation amount was greater. A brief reduction in precipitation occurred at ca. 8,070 cal yr BP, indicated by the reduction in Ti and coeval increase in TOC. It would suggest that the SPCZ has expanded and/or moved SW throughout this time. In regards to prevailing Pacific climate, it would suggest that from 8,200-7,900 cal yr BP negative-phase IPO prevailed.

8.3.3.3 Return to prolonged reduction in precipitation amount 7,900-6,900 cal yr BP

Total organic carbon is high throughout this period, albeit punctuated by decreases that are contemporaneous with small increases in Ti and low frequency magnetic susceptibility. Climatically this suggests that the catchment is receiving less precipitation, with brief periods (ca. 200 years) of moderate increases in precipitation as shown by the small increases in Ti – for example ca. 7,800-7,700 cal yr BP. A reduction of precipitation amount to the catchment is substantiated by the less negative δ^2H_{C26} values. Whilst there is structure in the δ^2H_{C26} record suggesting a period of slightly increased precipitation amount, all measurements are within error of each other throughout this period. Consequently the only substantive interpretation that can be made is that there is less precipitation between ca. 7,900-6,900 cal yr BP than at at ca. 8,000 cal yr BP. The evidence suggests that with reduced precipitation amount that the SPCZ has contracted, indicating a positive-phase IPO state. Furthermore, Ca/Ti is high throughout this time suggesting increased authigenic Ca production. This could be a result of lake level lowering as a consequence of the SPCZ contracting and reduced precipitation amount to the lake, causing Ca concentration to increase enough for Ca to precipitate out of the water column.

Carbon is still likely sourced from C_3 terrestrial plants (Meyers and Terranes, 2001) for this time. Peaks in C/N correspond to peaks in Ti, suggesting increased allogenic input mobilises carbon from a different source to that which usually enters the lake. More negative $\delta^{13}C_{TOC}$ and $\delta^{13}C_{C26}$ occurs at ca. 7,800 cal yr BP following the abrupt shift from high Ti (increased precipitation) to high TOC (decreased precipitation), which would suggest that there is a corresponding change in terrestrial carbon source. Without contemporary plant samples it is difficult to contextualise what this change in carbon source could relate to. The more negative $\delta^{13}C_{C16}$ and $\delta^{13}C_{C18}$ at this time likely relates to a change in algal source – potentially this is due to decreased catchment inputs meaning

conditions are suitable for other algal species to dominate. From ca. 7,700-7,000 cal yr BP C/N, $\delta^{13}C_{TOC}$, $\delta^{13}C_{C16}$, $\delta^{13}C_{C18}$ and $\delta^{13}C_{C26}$ covary suggesting that terrestrial and aquatic carbon source is changing. Whilst this could be due to a terrestrial source being the dominant carbon source for all alkanoic acids, it is inferred that it is more likely that $\delta^{13}C_{C26}$ is reflecting changing terrestrial carbon sources and $\delta^{13}C_{C16}$ and $\delta^{13}C_{C18}$ changing carbon sources. With Ti being slightly elevated for this period, an increase in allogenic input may alter conditions within the lake to allow other algal species to dominate over another, thus resulting in a change in all $\delta^{13}C$ values. With $\delta^{2}H_{C16}$ and $\delta^{2}H_{C18}$ trends matching $\delta^{13}C_{C16}$ and $\delta^{13}C_{C18}$ respectively, this supports a change in aquatic carbon source. Furthermore $\delta^{2}H_{C16}$ and $\delta^{2}H_{C18}$ trends are different to $\delta^{2}H_{C26}$ for this time – were all alkanoic acids terrestrially sourced at this time it would be expected that they covary to reflect changes in precipitation $\delta^{2}H$ (Sauer *et al*., 2001; Sachse *et al*., 2004). At ca. 7,170 cal yr BP a peak in C/N and less negative $\delta^{13}C_{TOC}$ occurs with a small increase in low frequency magnetic susceptibility suggesting that in this instance changes in carbon are a consequence of increased allogenic input.

8.3.3.4 Two-stage shift to increased precipitation amount 6,900-2,700 cal yr BP

It is put forward that from ca. 6,900-2,700 cal yr BP a two-stage shift to negative-IPO conditions occurred. Beginning at ca. 6,900 cal yr BP where positive-phase IPO conditions are inferred, a full change to multimillenial negative IPO-conditions begins at ca. 5,600 cal yr BP lasting until ca. 2,700 cal yr BP.

A distinct spike in Ti and low frequency magnetic susceptibility, with a coeval decrease in TOC, occurs at ca. 6,900-6,800 cal yr BP alongside a more negative $\delta^{2}H_{C26}$ value (albeit with large errors). This indicates enhanced allogenic input as a consequence of increased precipitation with the SPCZ over the site in conjunction with a negative-phase IPO (Folland *et al*., 2002). Noteworthy is that following this ca. 100 cal yr increase in precipitation from ca. 6,900-5,600 cal yr BP TOC does not return to the high values determined in the periods ca. 9,500-8,200 and 7,900-6,900 cal yr BP. Both Ti and low frequency magnetic susceptibility are higher than in these aforementioned previous periods. It is suggested that whilst the high TOC suggests a reduced allogenic input – a consequence of reduced precipitation associated with SPCZ contraction and positive-phase IPO – the slightly elevated Ti and low frequency magnetic susceptibility in

comparison to previous units indicate that allogenic input has increased due to a moderate increase in precipitation. Supporting this interpretation is the δ^2H_{C26} value at ca. 6,485 and 6,060 cal yr BP which are more negative than that at ca. 6,780 suggesting an increased amount of precipitation; however these values are within error of each other making this interpretation tentative. Whilst there is a reduction in the amount of C_{26} *n*-acid at ca. 6,485 cal yr BP (2% in comparison to average of 10%) it is interpreted that this is not caused by a shift in terrestrial vegetation producing it due to having similar trends to TOC and Ti. Further, a similarly low amount of C_{26} *n*-acid occurred at ca. 6,918 cal yr BP. At this time a more negative δ^2H_{C26} value corresponds with less TOC and higher Ti, indicating an increase in precipitation amount and increased catchment input as a consequence. Thus it is determined that the δ^2H_{C26} values for these times are indicative of precipitation amount changes rather than changes in catchment vegetation. The δ^2H_{C16} and δ^2H_{C18} values from ca. 6,900-5,600 cal yr BP have similar trends to their respective $\delta^{13}C$ values – akin to previous periods it is determined that changes in δ^2H_{C16} and δ^2H_{C18} are a result of changes in the dominant algae producing them rather than indicative of lake water δ^2H.

The stable C/N ratio, still within generalised values for C_3 land plants (Meyers and Terranes, 2001), is in contrast to the increasingly negative $\delta^{13}C_{TOC}$ values from ca. 6,900-5,600 cal yr BP. During this period the trends in $\delta^{13}C_{C16}$, $\delta^{13}C_{C18}$ and $\delta^{13}C_{C26}$ do not correlate to $\delta^{13}C_{TOC}$; consequently what is driving the progressively negative $\delta^{13}C_{TOC}$ cannot be elucidated from these more source-specific compounds. It is likely that the $\delta^{13}C_{TOC}$ record for this period indicates changing terrestrial carbon sources that have similar C/N values but different $\delta^{13}C_{TOC}$ values. This is evidenced with contemporary soil samples (Figure 8.7) that have very similar C/N values, but $\delta^{13}C_{TOC}$ values that range from -21.9 to -28.1‰; nevertheless without contemporary plant samples from the catchment this cannot be explored further. A gap in the pollen record obtained by Parkes (1994) (Appendix C, Figure C2) for this period means that any changes in carbon source cannot be further elucidated.

A significant change in the lake sediment record is observed from ca. 5,600-2,700 cal yr BP, evidenced by the high Ti and magnetic susceptibility, concurrent low TOC, and clustering distinctly in the PCA of the Itrax data (Figure 8.4). Titanium remains relatively high and stable throughout, indicating a continuous increased allochthonous input due to

increased precipitation most likely a result of SPCZ expansion related to prolonged negative-phase IPO in the Pacific. Notable is a sharp decrease in Ti, and coeval increase in TOC, from ca. 4,850-4,630 cal yr BP, signifying a decrease in precipitation as a consequence of a contracted SPCZ due to positive-phase IPO Pacific conditions.

It would be expected that with the pronounced and sustained increase in Ti that δ^2H_{C26} values would be more negative indicating an increase in the amount of precipitation. What is observed is high variability in these values unlike that seen in prior periods. Of note is that both δ^2H_{C16} and δ^2H_{C18} trends match the δ^2H_{C26} indicating that precipitation δ^2H is controlling the δ^2H_{C16} and δ^2H_{C18} changes rather than changes in dominant algal source. Due to these being discrete points it could be argued that they represent discrete contraction and expansion of the SPCZ as a consequence of different IPO states and not indicative of an overall trend. Considering that from ca. 9,500-8,200 and 7,900-6,900 cal yr BP TOC and Ti suggest prolonged positive-phase IPO conditions and δ^2H_{C26} values show little variability in precipitation, this suggests little change in SPCZ position. Contrary to this the high variability in precipitation amount from ca. 5,600-4,100 cal yr BP indicated by the δ^2H_{C26} values during a period of inferred prolonged negative-phase IPO (as indicated by the high Ti) reveals pronounced changes in SPCZ position. This may relate to the SPCZ shifting more frequently in the mid-Holocene (Saint-Lu *et al*., 2015). Model simulations suggest that at 6,000 cal yr BP and at 4,000 cal yr BP the SPCZ is in a more southerly position SE due to a strengthened meridional SST gradient between 0-5 °S and 5-10 °S and/or reduced ENSO activity (Mantsis *et al*., 2013; Saint-Lu *et al*., 2015). Further model results indicate that at 6,000 cal yr BP there are more SPCZ shifts per century and of larger amplitude, and at ca. 4,000 cal yr BP there is also an increased frequency of SPCZ shifts per century (Saint-Lu *et al*., 2015). The change in SPCZ variability in the 6,000 and 4,000 cal yr BP model runs is attributed to an increased meridional SST gradient and/or reduced ENSO activity (more likely prolonged negative-phase IPO over centennial timescales); however these changes may have concurrent effects on the SPCZ spatial variability (Saint-Lu *et al*., 2015).The variable δ^2H_{C26} values from ca. 6,000-4,000 cal yr BP in Lake Lanoto'o appear to support these model results. Furthermore, the high Ti indicates wetter background conditions consistent with an SPCZ in a more southerly position lending support to the model results (Mantsis *et al*., 2013). It is nevertheless

stressed that higher temporal resolution δ^2H_{C26} measurements are required to support this hypothesis.

Interestingly C/N values start to increase following the reduction in allochthonous input at ca. 4,800 cal yr BP. Alongside this is increased variability in $\delta^{13}C_{TOC}$ that matches the changes in C/N. This indicates a change in carbon to the lake. With similar changes in $\delta^{13}C_{C26}$ value to the $\delta^{13}C_{TOC}$ values, and opposite trends in $\delta^{13}C_{C16}$ and $\delta^{13}C_{C18}$ values to the $\delta^{13}C_{TOC}$ values, it is inferred that the changes in carbon source are terrestrial in origin. The increase in C/N following a decrease in allochthonous input – an aforesaid consequence of decreased precipitation amount – may indicate instability in the catchment causing increased input of land plants with higher C/N values, possibly tree material which typically have higher C/N values (Meyers and Terranes, 2001).

8.3.3.5 Decrease in precipitation amount ca. 2,700 cal yr BP to present

The sharp increase in TOC at ca. 2,700 cal yr BP and the corresponding decrease in Ti and low frequency magnetic susceptibility indicates a decrease in allogenic input in the lake as a consequence of decreased precipitation. This would suggest that the SPCZ has contracted and/or moved NW, which in turn suggests positive-phase IPO conditions in the Pacific (Folland *et al*., 2002).

Unlike earlier parts of the Lake Lanoto'o record there appears to be cyclicity in the Ti and TOC records over this latter time span. Total organic carbon is high from ca. 2,700-1,700 cal yr BP indicating decreased precipitation; Ti is higher from ca. 1,700-720 cal yr BP indicating increased precipitation; TOC is high from ca. 720-200 cal yr BP indicating decreased precipitation; and Ti is high from 200 cal yr BP to present indicating increased precipitation amount. These inferred changes in precipitation are a consequence of previously established relationships between precipitation, the SPCZ, and the IPO. Of interest is that values of Ti from ca. 2,700 cal yr BP to present are below those seen at any other point in the record. This would suggest that there is a decrease of catchment material into the lake, which would be inferred to reflect a decrease in the amount of precipitation transporting catchment material. This decrease in Ti is evident at ca. 400 cal yr BP, with coeval high TOC values. The Si/Ti and Fe/Mn ratio is highest for the entire record at this time (Figure 8.3), indicating increased authigenic Si production and possibly a shallower hypolimnion respectively. Further, the Ca/Ti ratio is higher at ca. 1,070 and

940 cal yr BP suggesting increased authigenic Ca production at these times. Collectively this evidence indicates a decrease in precipitation amount.

The δ^2H_{C26} record disagrees with this, with values overall more negative than previous parts of the record thus suggesting an overall increase in precipitation. The trends in the δ^2H_{C26} record follow the trends observed in the Ti and TOC record. van der Wiel *et al*. (2015) indicated that increasing SSTs increase the amount of precipitation from the SPCZ. Thus it is suggested that following ca. 2,700 cal yr BP, SSTs in the southwest Pacific increased causing an overall increase in the amount of precipitation from the SPCZ. The similar relationship between δ^2H_{C26} and Ti/TOC suggests that the IPO is the principal control on SPCZ movement. Moreover, as these are discrete sample points they may only reflect a ca. 30-year average of conditions rather than be representative of a distinct trend in precipitation amount over the last ca. 2,700 cal yr BP that is contrary to that from other proxies. It is noted that the most negative δ^2H_{C26} value for the record occurs at ca. 855 cal yr BP, coinciding with an increase in pteridophytes from 50 to 60% (Parkes, 1994; Appendix C, Figure C2) which may be affecting the δ^2H_{C26} value (Liu and Yang, 2008). Titanium values are higher at this time suggesting an increased allchthonous input, corroborating an increase in precipitation amount as indicated by the δ^2H_{C26} value. Thus this δ^2H_{C26} value most likely reflects an increase in precipitation amount, but further qualitative interpretation in regards to the scale of precipitation amount increase should not be taken.

As discussed in section 3.3.5 human colonisation of Samoa occurred at ca. 2,900 cal yr BP (Rieth and Hunt, 2008), and possibly affecting catchment vegetation around Lake Lanoto'o from 2,500 yr BP (ca. 2,540 cal yr BP) (Parkes, 1994). It would be expected that if humans are affecting the catchment that Ti and low frequency magnetic susceptibility would increase due to the catchment becoming unstable. A small increase in both Ti and low frequency magnetic susceptibility occurred at ca. 2,500 cal yr BP suggesting there may be some human activity in the Lake Lanoto'o catchment evident in the geochemical record. Were this caused by human activity in the catchment the record indicates it lasted ca. 50 years and appears to not have had a significant impact on the palaeoenvironmental and palaeoclimatic record. With the data presented here it should be stressed that human activity cannot be unequivocally determined or excluded at this time; consequently it would be inappropriate to interpret this change in the geochemical

record in regards to climate. This raises the question as to whether the geochemical record can be used to interpret climate changes from ca. 2,700 cal yr BP to present. Trends in TOC and Ti correspond to trends in δ^2H_{C26} as previously established in section 8.3.2 indicating that changes in precipitation amount was the primary control on the geochemical record for this period. Thus it is put forward that the geochemical record from Lake Lanoto'o can be used with confidence in interpreting past climatic changes from 2,700 cal yr BP. This however does not solve the discrepancy between lower Ti, indicating reduced precipitation amount, and the overall more negative δ^2H_{C26} values for this period indicating increased precipitation amount. With the data available it is not possible to unravel this further.

Whilst $\delta^{13}C_{C16}$ and $\delta^{13}C_{C18}$ values decrease overall the δ^2H_{C16} and δ^2H_{C18} progressively increase. Interpreting the δ^2H_{C16} and δ^2H_{C18} alone it would suggest that conditions are warmer causing increased evaporation from the lake leading to lake water having less negative δ^2H values. With the decrease in $\delta^{13}C_{C16}$ and $\delta^{13}C_{C18}$ corresponding with the increase in δ^2H_{C16} and δ^2H_{C18} it suggests that a change in the dominant algal source for the short-chain alkanoic acids is causing the trend in δ^2H_{C16} and δ^2H_{C18} values. It is apparent that source-specific aquatic biomarkers, such as botryococcene that has been determined to be in the Lake Lanoto'o record (A. Maloney, personal communication, July 2015), would help unravel whether the changes in δ^2H_{C16} and δ^2H_{C18} are indicative of changes in lake water δ^2H.

The peaks in the $\delta^{13}C_{TOC}$ record appear to be related to changes in carbon sources, occurring with small peaks in C/N and low frequency magnetic susceptibility. Of note is the relatively low C/N (15) and $\delta^{13}C_{TOC}$ values at ca. 600 cal yr BP. With them changing together it indicates a distinct change in carbon source. This period plots distinctly in Figure 8.7 further supporting this hypothesised change of carbon source. The C/N values (14) would indicate a mixed contribution from terrestrial and aquatic sources (Meyers and Terranes, 2001); with the higher Si/Ti ratio at this time it is speculated that this increased aquatic input is from diatoms (Peinerud, 2000). Parkes (1994) interpreted an increase in aquatic vegetation around ca. 500 cal yr BP lending further support to a mixed carbon source. Silicon is higher than any other part of the record (Figure 8.2), adding further support to a possible increase in diatom input to the lake sediment record. There is an increase in the proportion of C_{16} and C_{18} alkanoic acid at this time, suggesting

increased aquatic contribution. Further, assuming the dominant algal source of short-chain alkanoic acids has not changed during this time, $\delta^{13}C_{C16}$ increases with $\delta^{13}C_{TOC}$ whereas $\delta^{13}C_{18}$ and $\delta^{13}C_{26}$ decrease suggesting an increase in aquatic productivity (Leng *et al*., 2006). Nevertheless, a change in dominant algal source cannot be discounted from causing the increase in $\delta^{13}C_{C16}$ values.

8.4 Summary

A summary of the proxy data from Lake Lanoto'o is presented in Figure 8.9, and a summary of the interpretation of that proxy data is presented in Figure 8.10 from the interpretation of the data presented in section 8.3.3. As changes in $\delta^{2}H_{C16}$ and $\delta^{2}H_{C18}$ have been inferred to be a consequence of changes in the dominant algae producing them rather than changes in lake water $\delta^{2}H$, Figure 8.10 focusses on interpretations from $\delta^{2}H_{C26}$. There are four distinct zones in the lake stratigraphy, separated at ca. 8,200 cal yr BP, 7,900 cal yr BP, 6,900 cal yr BP and 2,700 cal yr BP. From ca. 9,500-8,200 cal yr BP the record indicates reduced precipitation amount, and organic carbon is derived from C_3 terrestrial land plants. At ca. 8,200-7,900 cal yr BP a short-lived shift to increased precipitation amount is associated with an increased in allochthonous terrestrial material and allogenic organic matter. Reduced precipitation is interpreted from ca. 7,900-6,900 cal yr BP. Following this a two-stage shift to increased precipitation is inferred, beginning at ca. 6,900 cal yr BP and intensifying from ca. 5,600-2,700 cal yr BP. Organic carbon is still interpreted to be allogenic. The $\delta^{2}H_{C26}$ record suggests possible increased variability and strength in the SPCZ. From ca. 2,700 cal yr BP to present drier conditions are interpreted, albeit the $\delta^{2}H_{C26}$ record indicates that precipitation amount is higher overall. A distinct change in carbon source occurs at ca. 600 cal yr BP that indicates a mixed aquatic and terrestrial source, contrasting with the rest of the record that indicates all organic carbon is derived from C_3 terrestrial plants. The importance of these data is fully explored in relation to the wider literature in Chapter 9.

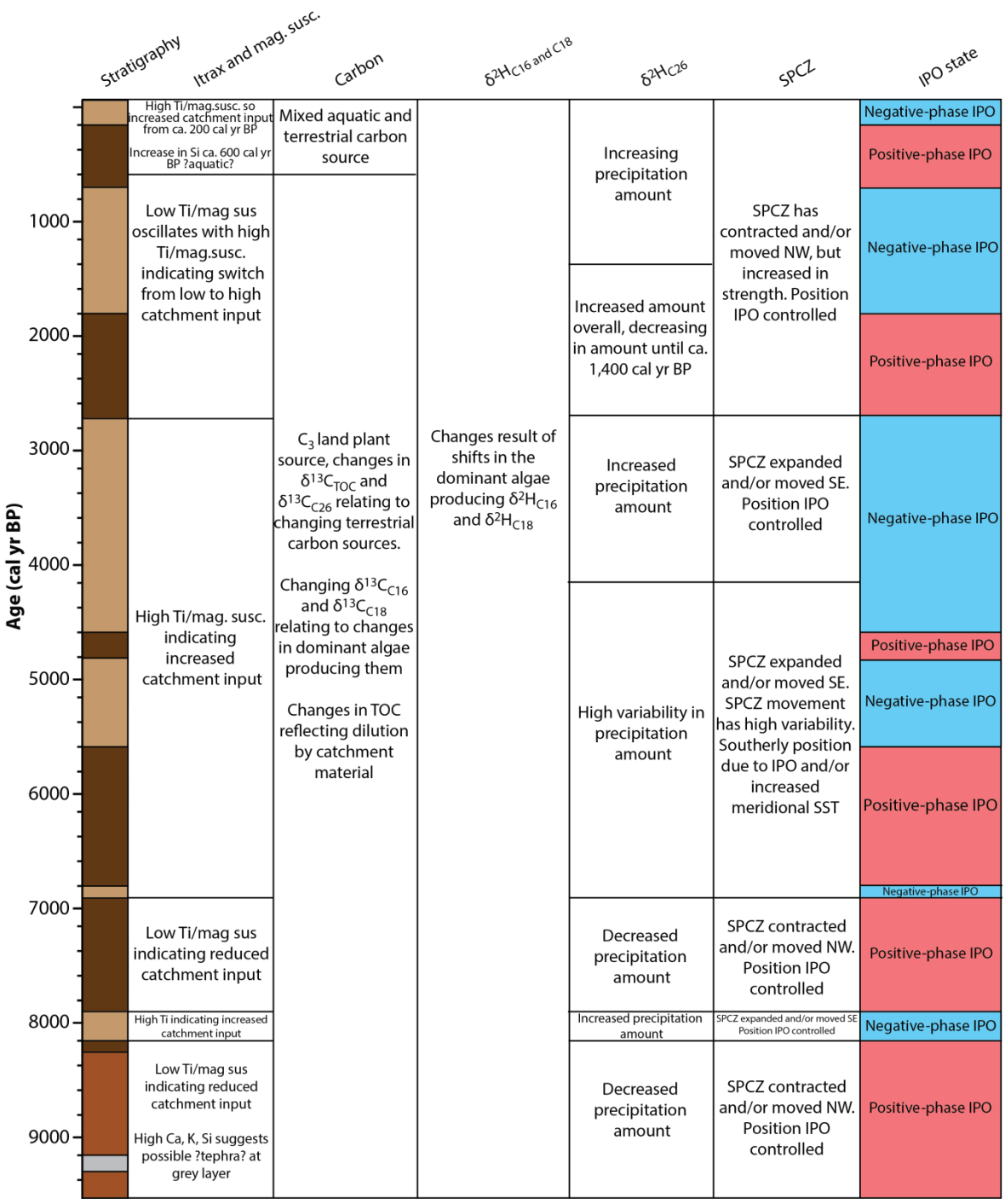

Figure 8.10: Summary interpretation of the proxy data, SPCZ location and controls, and IPO state from Lake Lanoto'o. The very dark brown and brown indicates gyttja, the latter of which is representative of the change in colour at the base. The light brown indicates siliciclastic units, and the grey indicates a sand (grain-size) layer.

Chapter 9: Discussion

9.1 Introduction

The aims of this thesis, as outlined in Chapter 1, were to:

1. Determine the feasibility of reconstructing long-term climate records from terrestrial/limnic proxies in the southwest Pacific; and
2. Dependent upon 1) assess the precipitation history in light of the SPCZ and broader patterns of internal variability in the Pacific basin over millennial timescales.

The data shown and discussed in Chapter 6, Chapter 7 and Chapter 8 have presented palaeoclimatic records for sites in the southwest Pacific along a NW-SE gradient, thus addressing the first aim. To further explore this aim this chapter will begin by comparing how climate is recorded geochemically in the two sites, and how this compares with other Pacific sites.

In order to address the second aim of this thesis the findings from all chapters will be used to reconstruct movement of the SPCZ over millennial timescales. van der Wiel *et al*. (2016a) demonstrated how the diagonal SPCZ orientation relates to zonally asymmetric SST gradients (section 2.1.3). Zonal SST gradient reconstructions for the equatorial Pacific spanning the Holocene have been developed (Conroy *et al*., 2010; Koutavas and Joanides, 2012; Rustic *et al*., 2015) and will be used to further investigate SPCZ movement over the last ca. 9,500 cal yr BP.

Knowing that SPCZ movement is principally related to both the IPO and ENSO, the records from Lake Teroto and Lake Lanoto'o will be compared with ENSO records from the Pacific region. This is first to determine if these sites have an ENSO signal, after which an examination of causes for similarities and differences (if any) will be undertaken to further address the second aim. Finally, Lake Teroto presented strong evidence of human impact overprinting the climatic signal recorded in some proxies. Human impact on the Lake Teroto and Lake Lanoto'o records, and how this relates to the timings of human colonisation of Samoa and Atiu, will be examined. Furthermore by using the palaeoclimatic records developed in this thesis, as well as those from the Pacific region,

the timings of human colonisation will be compared to investigate whether potential climatic forcings can be incited as possible/likely causes for Polynesian dispersal into the Pacific.

9.2 Lake Teroto and Lake Lanoto'o

9.2.1 Comparison between Lake Teroto and Lake Lanoto'o

The results outlined in Chapters 6 to 8 have shown that both Lake Teroto and Lake Lanoto'o respond to increases in precipitation in a similar manner – that being an increase in Ti as a result of increased catchment inwash. However, the respective responses of the lakes to reductions in precipitation are dissimilar. Lake Lanoto'o, arguably a simpler catchment-lake system, indicates a relative increase in TOC as a corollary of reduced siliciclastic inputs. Contrast this with Lake Teroto, where a decrease in precipitation and drier conditions causes gypsum ($CaSO_4$), an evaporite, to precipitate due to increasing the concentration of gypsum to the point of supersaturation within the lake water. It is interesting to note that the laminations in Lake Teroto, those being alternations between black and grey laminae, are not dissimilar to those recorded in the Dead Sea concluded to be evaporitic laminae (Heim *et al*., 1997) – although the verification of this requires further research.

Before comparing the records, the strengths and weaknesses of the records should be examined. In Lake Teroto the geochemical record is impacted by human activity after ca. 1,100 cal yr BP (section 9.5). The presence of $CaSO_4$, indicated by the Ca/Ti and S/Ti record, permits an interpretation of changes in climate – specifically when lake level lowers as a consequence of either increased temperature or a decrease in precipitation amount. As temperature is relatively constant throughout the year (Figure 3.5), changes in precipitation amount as a consequence of SPCZ movement is most likely the principal driver for changes in lake level. As Lake Teroto is further southeast in comparison to Lake Lanoto'o it is more sensitive to reductions in precipitation amount relating to SPCZ movement (Figure 6.15), with the site recording both CPE and EPE (Figure 6.15). This is expressed as decreases in Ti and increases in the Ca/Ti and S/Ti record. The Ca/Ti and S/Ti record in Lake Teroto is more sensitive to changes in precipitation amount than the Ti record in this site, akin to TOC in Lake Lanoto'o. In section 7.3.2 the controls on Lake

Teroto *n*-alkanoic acid δ^2H were examined. Both δ^2H_{C16} and δ^2H_{C18} could be influenced by changing algal sources and a marine input and are likely not a robust measure of changes in precipitation amount. Analysis in section 7.3.2 indicated that the δ^2H_{C26} record can be used as a proxy for changes in precipitation amount, with it being suggested that it is unlikely to have been influenced by changes in dominant terrestrial vegetation source. Any changes in precipitation amount inferred from δ^2H_{C26} are qualitative (Kahman *et al*., 2013b).

The Lake Lanoto'o record was determined to show no evidence of human impact affecting the geochemical proxies. Changes in precipitation amount have been inferred using Ti and TOC; however these are not independent of each other thus it may be that an increase in Ti caused by a forcing other than precipitation would lead to an erroneous climatic interpretation. There is no evidence in this study to indicate that other mechanisms are responsible for changes in Ti and TOC in Lake Lanoto'o, consequently it is concluded that changes in precipitation amount relating to SPCZ movement are the primary control on changes in Ti and TOC. Lake Lanoto'o TOC and Ti suggests it is sensitive to EPE only, and that CPE have varying effects on the geochemical record (Figure 6.20). The controls on Lake Lanoto'o *n*-alkanoic acid δ^2H were outlined in section 8.3.2: both δ^2H_{C16} and δ^2H_{C18} are determined to indicate changes in dominant algal source. Whilst it is possible that δ^2H_{C26} from Lake Lanoto'o may be influenced by changes in the dominant terrestrial vegetation source, due to there being gaps in the pollen record obtained by Parkes (1994) this cannot be fully investigated. Therefore an assumption has been made that δ^2H_{C26} represents qualitative changes in precipitation amount relating to SPCZ movement (Kahman *et al*., 2013b).

Figure 9.1 presents a comparison of Lake Teroto and Lake Lanoto'o over the last ca. 6,650 cal yr BP. Due to the significant positive correlation between Ca and S in Lake Teroto (Table 7.1), only the Ca/Ti record is presented. Over millennial timescales it can be seen that Ca/Ti in Lake Teroto both lags reductions in TOC and leads increases in TOC in Lake Lanoto'o. Specifically the low values in TOC in Lake Lanoto'o at ca. 5,600 cal yr BP is not seen in the Lake Teroto Ca/Ti until ca. 5,000 cal yr BP. Further, Ca/Ti increases from ca. 4,000 cal yr BP whereas high TOC values are not observed in Lake Lanoto'o until ca. 2,700 cal yr BP. Closer examination of the records indicates that changes in Lake Teroto Ca/Ti do correspond to changes in Lake Lanoto'o TOC: for example between ca. 5,600-5,000 cal yr

BP a further reduction in TOC to a minimum at ca. 5,000 cal yr BP parallels the reduction in Ca/Ti. It is suggested that this lends further support to Lake Teroto being more sensitive to changes in precipitation amount as a result of SPCZ movement compared to Lake Lanoto'o. From the instrumental record it was concluded that the two sites will only

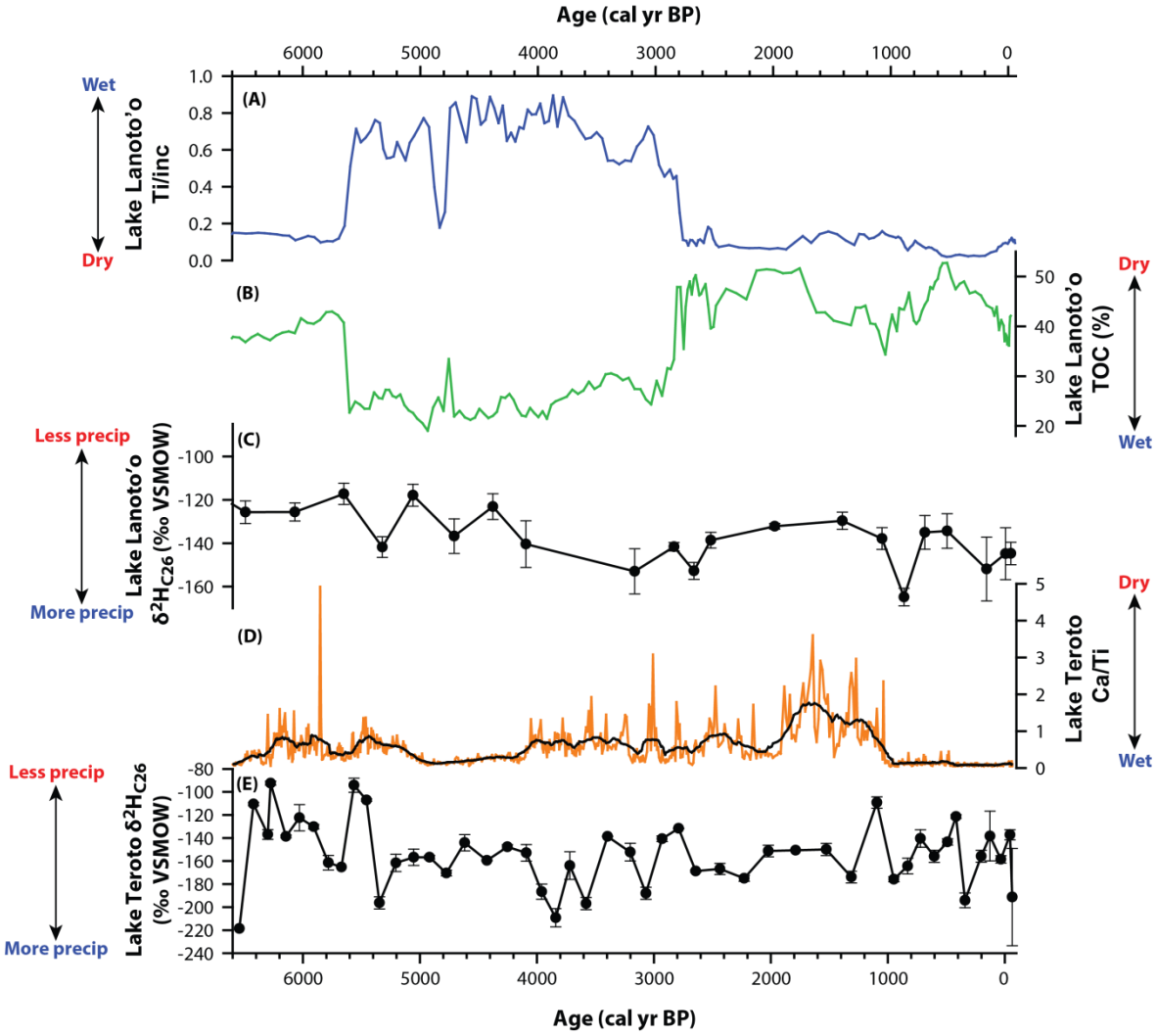

Figure 9.1: Comparison of Lake Lanoto'o Ti (A), TOC (B) and δ^2H_{C26} (C) with Lake Teroto Ca/Ti (D) and δ^2H_{C26} (E) over the last ca. 6,650 cal yr BP. In (C) the black line indicates LOESS smoothing of the Lake Teroto Ca/Ti values (sampling proportion 0.01, polynomial degree of 1).

definitively indicate SPCZ movement during coeval positive-phase IPO and EPE (Chapter 6). However, the geochemical record showed that Lake Teroto is sensitive to both CPE and EPE (as indicated by increases in Ca/Ti representative of gypsum deposition) whereas Lake Lanoto'o is sensitive to EPE only (indicated by increases in Br and TOC). Assuming that IPO and ENSO, and associated zonal SST gradients, are the principal controls on SPCZ movement over the Holocene, akin to the instrumental period (Trenberth, 1976; Folland

et al., 2002; Salinger *et al*., 2014), it is suggested that over millennial timescales Lake Teroto records SPCZ movement as a consequence of CPE and EPE during positive-phase IPO and Lake Lanoto'o records SPCZ movement due to EPE driving positive-phase IPO. This will be further explored in section 9.4 by comparing Lake Teroto and Lake Lanoto'o with other sites concluded to record changes in ENSO over the Holocene.

The δ^2H_{C26} records from the two sites appear to agree, although the lower sample resolution in Lake Lanoto'o in comparison to Lake Teroto precludes a more detailed investigation. The δ^2H_{C26} values from the two sites do not always agree with other proxies interpreted to be indicative of changes in precipitation amount. For example between ca. 4,000-2,700 cal yr BP the Lake Teroto δ^2H_{C26} record shows variability not seen in the Lake Lanoto'o record or the Ca/Ti record from Lake Teroto. Assuming that the δ^2H_{C26} records from the two sites primarily record changes in precipitation, it is suggested that the δ^2H_{C26} records indicate variability in any inferred NW/contracted or SE/expanded SPCZ position, whereas the Ca/Ti record from Lake Teroto and the TOC and Ti records from Lake Lanoto'o indicate the average SPCZ position over millennial timescales. Further work using source-specific biomarker records, such as botryococcene δ^2H, would substantiate this interpretation for the δ^2H_{C26} record and allow an appraisal on whether changes in dominant terrestrial vegetation source are influencing the δ^2H_{C26} values. SPCZ movement over the last ca. 9,500 cal yr BP will be investigated fully in section 9.3.

9.2.2 Comparison of Lake Teroto and Lake Lanoto'o record types with other Pacific lakes

9.2.2.1 Lake Teroto

Laminated lacustrine records from the south Pacific do exist, such as the discontinuous laminated record in Rano Raraku (Sáez *et al*. 2009), and the Bainbridge and Genovesa crater lake records, Galápagos (Riedenger *et al*., 2002; Conroy *et al*., 2014). The notable difference between these laminated records and the Lake Teroto laminated record is the sediment composition. The Genovesa record is dominated by $CaCO_3$, with Ca precipitation determined to be a result of evaporative enrichment, analogous to the hypothesised mechanism for $CaSO_4$ deposition in Lake Teroto (Conroy *et al*., 2014). Akin to Lake Teroto, Genovesa indicates a connection to the sea; however the lake does not exhibit a chemocline and Conroy *et al*. (2014) found evidence for mixing within the lake

during a warm/wet season. The cause for laminations is suggested to be related to prolonged dry conditions, nevertheless Conroy *et al*. (2014) do not full explore the genesis of the laminations. Whilst $CaSO_4$ is noted to occur in the Bainbridge Crater Lake record like Lake Teroto, the laminae present are either siliciclastic or carbonate in nature and no attempt is undertaken to determine their genesis (Riedenger *et al*., 2002). Riedenger *et al*. (2002) highlight that the lake is likely not chemically stratified – it is suggested here that the silicilastic laminations are likely a result of increased precipitation resulting in catchment inwash, and that the carbonate laminations are likely a result of prolonged dry conditions akin to the Genovesa record (Conroy *et al*., 2014). Laminations in Rano Raraku, Easter Island, are attributed in part to algal activity in some units and increased siliciclastic input in others (Sáez *et al*., 2009; Cañellas-Boltà *et al*., 2012). Only the Genovesa and Bainbridge crater lake records indicate continuous laminations akin to Lake Teroto (Riedenger *et al*., 2002; Conroy *et al*., 2014). At present it has not been determined if these laminated records are annually deposited for any of these sites.

As Lake Teroto is known to contain a continuously laminated Holocene record (Parkes, 1994), it has great potential as a climatic archive for the southwest Pacific. A relevant point to note is that a similar record may exist in Lake Tiriara, Mangaia, Cook Islands. Ellison (1994) noted that Lake Tiriara contains laminations suggesting they may be annually deposited – although Ellison (1994) presents no evidence to substantiate this. In regards to climate, Mangaia receives a similar amount of annual precipitation to Atiu (ranging from 1024-2983 mm in the AD 1914-1984 period (Thompson, 1986)), and like Atiu has a wet season from November to April and a dry season from May to October (see Section 3.2.2). The geology of Mangaia is similar to that of Atiu: a basaltic inner volcanic cone surrounded by makatea (Ellison, 1994). Further, Lake Tiriara has a connection to the sea akin to Lake Teroto: it can be hypothesised that the lake may demonstrate ectogenic meromixis as suggested for Lake Teroto. If Lake Tiriara was deep enough during the Holocene to not be mixed by wind activity lacustrine conditions may be such that laminae formation akin to that described for Lake Teroto could occur. Further work is required to determine firstly whether Lake Teroto preserves annual laminations, and secondly to investigate whether Lake Tiriara is also laminated and the nature of any laminations present.

9.2.2.2 Lake Lanoto'o

At present (AD 2017) the lacustrine record obtained from Lake Lanoto'o is unique for the southwest Pacific, being the only ca. 9,500 cal yr BP record of climate from a freshwater, meromictic lake. As a crater lake record in comparison to other crater lakes from the south Pacific its geochemical record of climate is also unique. Rano Raraku, a crater lake in Easter Island, indicates a reduction in Ti from ca. 9,500 cal yr BP with a shift towards a shallow swamp system and a sedimentary hiatus from ca. 5,000-800 cal yr BP (Sáéz *et al*., 2009), in contrast to Lake Lanoto'o which demonstrates a continuous lacustrine record throughout this period. The El Junco, Galápagos, record demonstrates C/N ratios that are predominantly terrestrial over the ca. 9,100 cal yr BP record, akin to Lake Lanoto'o (Conroy *et al*., 2008).

Perhaps the most salient comment on the Lake Lanoto'o record in comparison to other south Pacific lacustrine records is its potential temporal length. Currently the longest continuous records in the south Pacific are: the Rano Raraku record at ca. 34,000 cal yr BP old (Sáez *et al*., 2009), the Lake Suprin record, Plaine des Lacs, New Caledonia, at ca. 30,000 cal yr BP – albeit dating of lacustrine records from New Caledonia have demonstrated to be problematic thus casting potential doubt on the reliability of this site (Hope and Pask, 1998; Stevenson *et al*., 2010) – and the Lake Tagamaucia record, Fiji at ca. 27,000 cal yr BP (Hope *et al*., 2009). Whilst this study presents a ca. 9,500 cal yr BP record, it is unlikely that the base of the lake was reached. Further, when accounting for the geology of Upolu, Samoa, which is at a minimum ca. 2.0 Ma old, the Lake Lanoto'o record may extend through most of the Quaternary period and thus could provide a vital contribution to the understanding of Pacific Quaternary climate which, at present, is lacking in comparison to Atlantic records.

9.3 SPCZ movement over the Holocene

Using the relationships between TOC and Ti in Lake Lanoto'o and Ca/Ti and Ti in Lake Teroto combined with the δ^2H_{C26} records from both sites inferences on SPCZ movement over the last ca. 9,500 cal yr BP are presented in Figure 9.2. In Chapter 6 it was established that in Lake Lanoto'o high (low) TOC indicated a reduction (increase) in siliciclastic input from the catchment, as indicted by low (high) Ti, due to reduced

(increased) precipitation amount. With the SPCZ being the primary control on precipitation to Lake Lanoto'o, it was therefore determind that high TOC indicated that the SPCZ had contracted and/or shifted NW and high Ti indicated that the SPCZ had expanded and/or shifted SE. Furthermore it has been shown that high Ca/Ti in Lake Teroto indicates high gypsum precipitation as a consequence of reduced precipitation amount lowering lake levels. Similar to Lake Lanoto'o, the SPCZ is the primary control on precipitation to Lake Teroto thus it was concluded that high (low) Ca/Ti in Lake Teroto indicates that the SPCZ had contracted and/or shifted NW (expanded and/or shifted SE). In section 9.2.1 it was suggested that Ca/Ti in Lake Teroto and TOC and Ti in Lake Lanoto'o indicate average SPCZ position over millennial timescales; therefore combining these records it was determined that:

- High TOC in Lake Lanoto'o and high Ca/Ti in Lake Teroto indicate the SPCZ was in a more NW position and/or had contracted; and
- High Ti (low TOC) in Lake Lanoto'o and low Ca/Ti in Lake Teroto indicate the SPCZ was in a more SE position and/or had expanded.

In addition in section 9.2.1 it was suggested that the δ^2H_{C26} records indicate variability in SPCZ position in its inferred NW/contracted or SE/expanded position. The changes in precipitation amount in Figure 9.2 were inferred from comparing the δ^2H_{C26} records from the two sites. In section 2.1.3 it was outlined that the diagonal orientation of the SPCZ is a consequence of zonal SST asymmetry typical of most conditions in the Pacific (La Niña, CPE and normal conditions), and that zSPCZ events are a result of zonally symmetric SST conditions typical during EPE (Figure 2.15; van der Wiel *et al*., 2016a). Comprison with zonal SST gradient reconstructions over the last ca. 9,500 cal yr BP (Koutavas and Joanides, 2012) can corroborate inferences made on SPCZ position over this period – albeit the chronological resolution is at the millennial scale limiting a detailed examination. It is salient to note that the inferred position and shifts in SPCZ are not specific and that this study has undertaken a qualitative assessment.

9.3.1 SPCZ movement 9,500-6,900 cal yr BP and the 8.2 ka event

The high TOC in Lake Lanoto'o from ca. 9,500-6,900 cal yr BP suggests that the overall position of the SPCZ was in a more NW position and/or that the SPCZ had contracted over millennial timescales – the first time that this has been demonstrated. The zonal SST

gradient is reduced from ca. 9,600-8,200 cal yr BP and at ca. 7,210 cal yr BP (Koutavas and Joanides, 2012) which would contribute to the SPCZ being in a more zonal orientation (van der Wiel *et al*., 2016a), corroborating the contracted/NW SPCZ position inferred

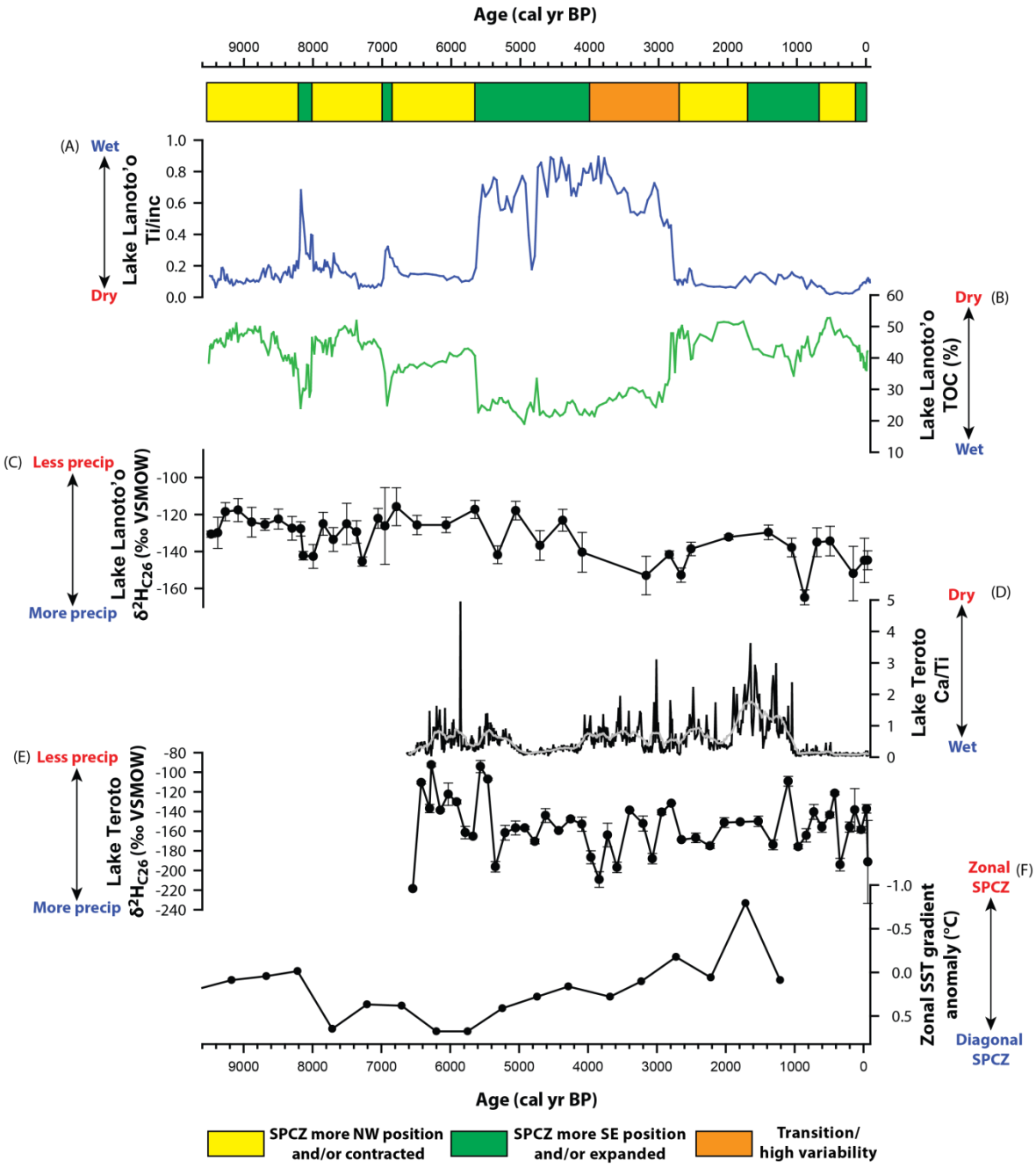

Figure 9.2: Comparison of the Lake Lanoto'o and Lake Teroto records from ca. 9,500 cal yr BP to present. Lake Lanoto'o Ti (A), TOC (B) and δ^2H_{C26} (C) shows similar changes to Lake Teroto Ca/Ti (D) and δ^2H_{C26} (E). The grey line on (D) indicates LOESS smoothing of the Lake Teroto Ca/Ti values (sampling proportion 0.01, polynomial degree of 1). (F) Zonal SST gradient anomaly using marine cores from the east and west equatorial Pacific – note the reversed y-axis (Koutavas and Joanides, 2012). Data in (F) is digitised from Koutavas and Joanides (2012). Red bars indicate less

precipitation amount and blue bars indicate more precipitation amount. The position and activity of the SPCZ is shown in yellow (more NW position and/or contracted), green (more SE position and/or expanded) and orange (transition/high variability in position).

from Lake Lanoto'o at this time. The δ^2H_{C26} record, in comparison to the rest of the δ^2H_{C26} record in Lake Lanoto'o, is relatively constant suggesting a reduction in precipitation amount that would concur with the inference made from TOC. There are periods where SPCZ expansion and/or migration SE are suggested at ca. 9,500-9,350, 8,600, 8,200-7,900, 7,700, 7,280 and 6,950 cal yr BP. Interestingly an increased zonal SST gradient is inferred at ca. 7,700 cal yr BP which would contribute to SPCZ expansion and/or migration SE and supports the Ti and δ^2H_{C26} value at this time (van der Wiel *et al*., 2016a). The small increases in Ti (excluding the 8,200-7,900 cal yr BP which is discussed in the next section) may reflect small SPCZ movement akin to that outlined by Lorrey *et al*. (2012) (Figure 3.17) during positive-phase IPO and La Niña/El Niño, with SPCZ movement from 9,500-6,800 cal yr BP causing only relatively modest increases in catchment input and precipitation amount to Lake Lanoto'o. Whilst some of these periods are isotopically distinct – specifically 8,200-7,900 and 7,280 cal yr BP – others fall within error of neighbouring samples but correspond to increases in Ti substantiating the interpretation of SPCZ expansion and/or movement SE.

At ca. 7,280 cal yr BP a small decrease in δ^2H_{C26} values would be expected to correspond to a small increase in Ti, and at ca. 6,900 cal yr BP a distinctly more negative δ^2H_{C26} value would be expected to correspond with the pronounced increase in Ti. For both of these points the opposite occurs: at ca. 7,280 cal yr BP the small increase in Ti corresponds to a pronounced negative δ^2H_{C26} value and at ca. 6,900 cal yr BP the high Ti corresponds to a relatively small decrease in δ^2H_{C26} value. It may be that at ca. 7,280 cal yr BP there was a large increase in precipitation amount that simply was not reflected in the Ti record – as may have potentially occurred in AD 1908 (Figure 6.20). Equally it is possible that a large increase in precipitation amount was not reflected in the δ^2H_{C26} value but was indicated with the pronounced increase in Ti. Alternatively it may represent a change in the dominant vegetation producing C_{26} alkanoic acid; however there is no pollen record for this period that could support or refute this (Parkes, 1994; Appendix C2)**.** Applying Occam's razor, the simplest explanation – that being a large increase in precipitation

amount not reflected in the δ^2H_{C26} record – is put forward due to the various factors that influence δ^2H_{C26} values (section 4.5.3.3.3). At 6,900 cal yr BP the disparity between δ^2H_{C26} value and Ti can be more easily explained by the large error associated with this δ^2H_{C26} value. Although the δ^2H_{C26} value and error could also suggest a decrease in precipitation amount, in conjunction with the increase in Ti it is considered more likely that it represents an increase in precipitation amount as a result of SPCZ expansion and/or migration SE.

9.3.1.1 The 8.2 ka event

The pronounced increase in Ti at Lake Lanoto'o, associated with an increase in precipitation amount, between ca. 8,200-7,900 cal yr BP is similar in timing to the 8.2 ka event determined from the Greenland ice cores (GICC05; Rasmussen *et al*., 2006) between 8,347-8,136 cal yr BP (Thomas *et al*., 2007) and from a composite of sediment cores in eastern Canada that dates it between ca. 8,490-8,040 cal yr BP centred at ca. 8,330 cal yr BP (Lewis *et al*., 2012). The 8.2 ka event is considered to be the boundary between the early and mid-Holocene, with its associated isotopic excursion in the Greenland ice core records proposed to be the global stratotype section and point (Walker *et al*., 2012). The Lake Lanoto'o record indicates that the SPCZ has expanded and/or shifted SE during this period. Further, the structure of the Ti for this time indicates an initial SPCZ expansion and/or shift SE at ca. 8,175 cal yr BP, a contraction and/or shift NW at ca. 8,070 cal yr BP, and a further expansion and/or shift SE at ca. 8,010 cal yr BP. The structure of the Lake Lanoto'o Ti is very similar to that in the GICC05 record (Figure 9.3). With the timing and structure of this event being similar to the 8.2 ka event in GICC05 it is postulated that the 8.2 ka event was expressed in the SW Pacific.

This study therefore presents the first evidence of the 8.2 ka event in the SW Pacific; however it has also been determined from the El Junco record, Galápagos (Atwood, 2015). Atwood (2015) interpreted the 8.2 ka event as being expressed by weak El Niño activity and an ITCZ that shifted equatorward in the equatorial east Pacific. Mechanistically Atwood (2015) used a a community earth system model (CESM) to propose that due to the weakened Atlantic Meridional overturning circulation (AMOC), hemispherical asymmetric changes in surface energy fluxes causes the ITCZ to shift southward in the equatorial east Pacific which in turn caused a strengthening (weakening) of the northern

hemisphere (southern hemisphere) Hadley cell. The Hadley circulation changes strengthen (weaken) the North Atlantic (South Atlantic) subtropical anticyclones, driving easterly trade winds in the tropical Atlantic communicated through the eastern and central tropical Pacific (Atwood, 2015). Collectively this results in a reduction in El Niño

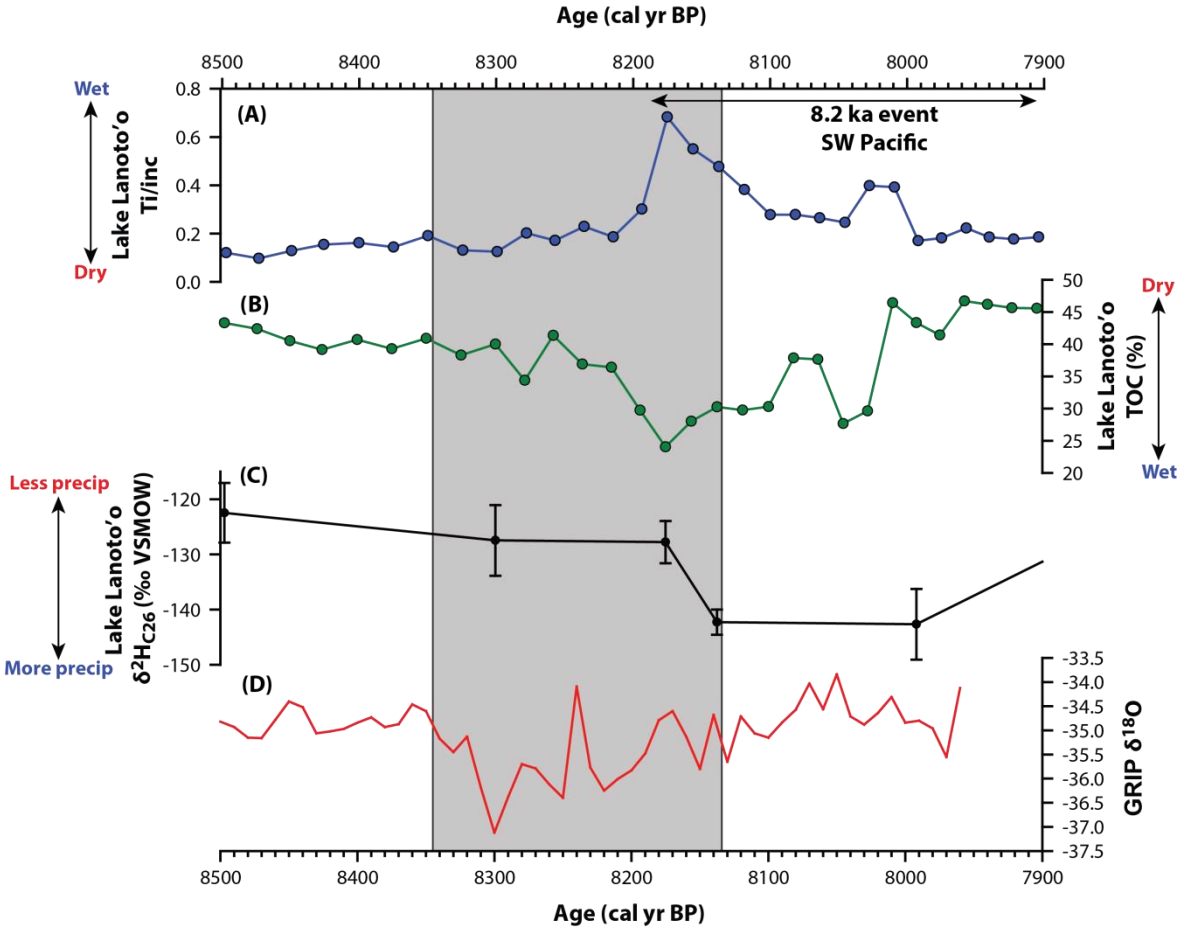

Figure 9.3: The proposed 8.2 ka event in Lake Lanoto'o Ti (A), TOC (B) and δ^2H_{C26} (C) compared to the GRIP $\delta^{18}O$ record (Rasmussen *et al*., 2006). The grey box indicates the 8.2 ka event as outlined by Thomas *et al*. (2007).

activity, with these Pacific conditions conducive for an SPCZ that expanded and/or shifted SE as interpreted from the Lake Lanoto'o record.

9.3.2 SPCZ movement 6,900-2,700 cal yr BP

Following a pronounced increase in Ti at ca. 6,900 cal yr BP in Lake Lanoto'o Ti values were slightly elevated, albeit decreasing, from ca. 6,900-5,700 cal yr BP in comparison to the previous part of the record. This suggests that the SPCZ had expanded and/or shifted to a SE position at 6,900 cal yr BP, after which the reduction in Ti indicates that the SPCZ was contracting and/or shifting NW. The elevated Ca/Ti values in Lake Teroto from ca. 6,600 cal yr BP indicates drier conditions in the lake, in line with an SPCZ that is contracted and/or shifted NW. This is in agreement with the δ^2H_{C26} values from both sites which overall indicate reduced precipitation amount from ca. 6,900-5,700 cal yr BP, and corroborates reduced precipitation from the SPCZ in PMIP2 and PMIP3 models at 6,000

cal yr BP (An and Choi, 2014). A notable increase in precipitation amount, indicating SPCZ expansion and/or migration SE, at ca. 5,800 cal yr BP is interpreted to indicate SPCZ movement akin to that outlined by Lorrey *et al*. (2012) (Figure 2.17) during a positive-phase IPO with La Niña/El Niño events.

The prominent increase in Ti at 5,700 cal yr BP indicates an increase in catchment input as a result of increased precipitation, which would suggest that the SPCZ has expanded and/or migrated SE. This is in further agreement with a southward shift in SPCZ location 6,000 cal yr BP modelled in PMIP2 (Mantsis *et al*., 2013). The Ca/Ti values are high in Lake Teroto until ca. 5,000 cal yr BP indicating lake conditions were conducive to gypsum precipitation. Combining the two lake lake records it is proposed that from 5,700-5,000 cal yr BP, whilst the SPCZ was in a more SE position, it was still contracting and/or migrating to a NW position, as a result of ENSO during an IPO phase (Trenberth, 1976; Folland *et* al., 2002; Matthews, 2012). This led to reduced precipitation to Atiu such that lake level lowers and gypsum precipitated out.

Between ca. 5,000-4,000 cal yr BP the highest values in Ti in Lake Lanoto'o correspond with the lowest values in Ca/Ti in Lake Teroto indicating wetter conditions. It would therefore be expected that the SPCZ has expanded and/or shifted SE, increasing precipitation amount that would be reflected in more negative δ^2H_{C26} values with low variability. Contrary to this the δ^2H_{C26} values reveal high variability. Mantsis *et al*. (2013) determined using a PMIP2 model that the SPCZ had shifted to a more southerly position ca. 6,000 cal yr BP, also found by Saint-Lu *et al*. (2015) – a more southerly SPCZ position would cause background precipitation to be higher in both Samoa and Atiu, thus providing a potential mechanism for the high Ti and low Ca/Ti in Lake Lanoto'o and Lake Teroto respectively. Additionally Saint-Lu *et al*. (2015) concluded using CMIP5 models that at 6,000 cal yr BP there were more SPCZ shifts per century of larger amplitude than in the pre-industrial period (AD 1860), and at 4,000 cal yr BP the SPCZ was in a more southerly position with a likewise increased frequency of SPCZ shifts per century but no change in amplitude compared to the pre-industrial period. The change in SPCZ variability in the ca. 6,000 and 4,000 cal yr BP model runs is attributed to an increased meridional SST gradient and/or reduced ENSO activity; however these changes may have concurrent effects on the SPCZ spatial variability (Saint-Lu *et al*., 2015). The variable δ^2H_{C26} values from both sites over the ca. 6,000-2,700 cal yr BP period appear to agree with an increased

frequency of SPCZ movement; however concluding a change in amplitude of SPCZ shifts is not possible. This is due to the recommendations of Kahman *et al*. (2013b) that δ^2H_{C26} should only be used to provide qualitative hydrological information. Moreover the high Ti values in Lake Lanoto'o and low Ca/Ti in Lake Teroto appear to agree with an SPCZ in a more southerly position – especially between ca. 5,000-4,000 cal yr BP. Determining meridional SST gradients in the SPCZ region is difficult due to the records available from the west Pacific not being located in this area (Stott *et al*., 2004; Koutavas and Joanides, 2012). Zonal SST gradients over this period indicate a trend towards zonal symmetry that would lead to the SPCZ being in a zonal orientation (Koutavas and Joanides, 2012; van der Wiel *et al*., 2016a), contrary to the inferred more southerly SPCZ position. However, SST anomalies are still positive over this period (Koutavas and Joanides, 2012), thus suggesting that the SPCZ was in a diagonal position and corroborating the more SE position inferred from Lake Teroto and Lake Lanoto'o.

From ca. 4,000-2,700 cal yr BP TOC steadily increased in Lake Lanto'o and Ca/Ti increased in Lake Teroto, both of which indicate a progressive shift to drier conditions that in turn would suggest the SPCZ was contracted and/or shifted NW. The high relative variability in δ^2H_{C26} values in Lake Teroto supports the increase in frequency in SPCZ shifts as determined from the ca. 4,000 cal yr BP CMIP5 simulation (Saint-Lu *et al*., 2015). Overall, the interpretation for SPCZ movement over the ca. 6,900-2,700 cal yr BP period are as follows:

- 6,900-5,600 cal yr BP: SPCZ in a NW position;
- 5,600-5,000 cal yr BP: SPCZ in a SE position, with increased frequency and amplitude of SPCZ shifts per century (Mantsis *et al*., 2013; Saint-Lu *et al*., 2015);
- 5,000-4,000 cal yr B: SPCZ in a SE position with increased frequency in SPCZ shifts per century (Saint-Lu *et al*., 2015);
- 4,000-2,700 cal yr BP: SPCZ transitioning to a NW position, with an increased frequency in SPCZ shifts per century (Saint-Lu *et al*., 2015).

9.3.3 SPCZ movement over the last 2,700 years

Despite the evidence for impact of human activity on the Lake Teroto Ca/Ti record, which was determined to not have affected the δ^2H_{C26} record from this site (Section 7.3.3.5), the δ^2H_{C26} record from Lake Teroto shows agreement with the Lake Lanoto'o record. Overall

the high TOC in the Lake Lanoto'o record suggests drier conditions, suggested here to be due to the SPCZ in a more northerly position. This is corroborated by zonally symettric SST conditions that would be conducive for a zonal SPCZ orientation (Koutavas and Joanides, 2012; van der Wiel *et al*., 2016a). There are broad trends in SPCZ movement over this period, specifically:

- ca. 2,700-1,700 indicates SPCZ contraction and/or migration NW;
- ca. 1,700-725 cal yr BP indicates SPCZ expansion and/or migration SE;
- ca. 725-150 cal yr BP indicates SPCZ contraction and/or migration NW; and
- ca. 150 cal yr BP to present indicates SPCZ expansion and/or migration SE.

Conroy *et al*. (2010) determined a reduced zonal SST gradient from 750 cal yr BP, which would lead to a zonal SPCZ orientation (van der Wiel *et al*., 2016a) and corroborates the contraction and/or migration NW inferred from Lake Teroto and Lake Lanoto'o. The Lake Lanoto'o δ^2H_{C26} values were overall more negative from ca. 2,700 cal yr BP which could indicate an overall increase in precipitation amount potentially as a consequence of increasing SSTs (van der Wiel *et al*., 2015). Toomey *et al*. (2016) suggested that from ca. 3,000 cal yr BP to present the Tahaa, French Polynesia, record shows a trend towards gradual intensification of background precipitation reflecting SPCZ migration and/or intensification forced by precession (Figure 9.4). Irrespective of the mechanism an intensification of background precipitation would lead to an increase in δ^2H_{C26} values as occurs in Lake Lanoto'o. The records presented in this thesis will allow modellers to test whether increasing SSTs and/or precession is the causal mechanism for an increase in precipitation from the SPCZ over this period.

The disparity between the Lake Lanoto'o TOC and the δ^2H_{C26} values could indicate that whilst the SPCZ is in a more northerly position leading to overall drier conditions, when expanded the amount of precipitation that fell was higher than that in preceding periods leading to δ^2H_{C26} values being more negative. More negative δ^2H_{C26} values are not seen in the Lake Teroto δ^2H_{C26} record to corroborate this. It may be that the decrease in precipitation amount, as indicated by the Lake Lanoto'o TOC, was not reflected in the Lake Lanoto'o δ^2H_{C26} record. Further, there are caveats to the Toomey *et al*. (2016) study:

1. There is no attempt to show that changes in precipitation amount are related to SPCZ movement; and

2. By using Ti/Ca as a ratio for increased terrestrial inputs it is prone to being affected by soils with Ca values higher than Ti, as is the case for some soils in the study. Thus were these soils to dominate the Tahaa record it may be interpreted to indicate a reduction in terrestrial input (Toomey *et al*., 2016).

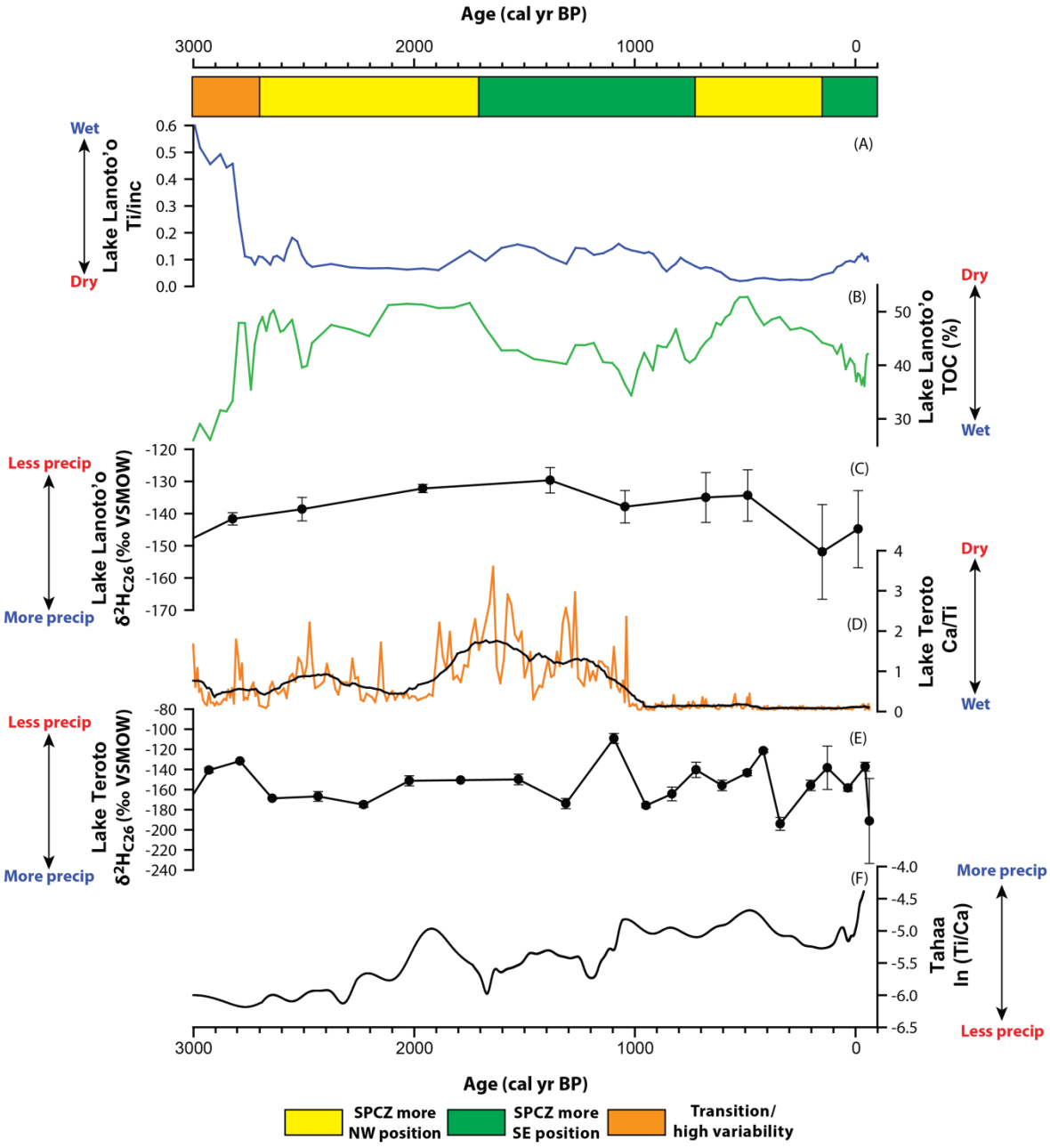

Figure 9.4: Comparison of Lake Lanoto'o (Ti (A), TOC (B) and δ^2H_{C26} (C)), Lake Teroto (Ca/Ti (D) and δ^2H_{C26} (E)) and the Tahaa, French Polynesia, records (F) (Toomey *et al*., (2016). The black line on (D) indicates LOESS smoothing of the Lake Teroto Ca/Ti values (sampling proportion 0.01, polynomial degree of 1).

Consequently further work is needed to determine if precipitation amount from the SPCZ has increased from ca. 2,700 cal yr BP as the results from this study are equivocal in

regards to this. Despite this, millennial-scale trends in SPCZ movement over this time frame have been determined

9.3.4 Overview of Holocene SPCZ movement

SPCZ movement from ca. 9,500 cal yr BP to present is displayed in Figure 9.2. From 9,500-5,700 cal yr BP the SPCZ was likely NW and/or contracted, with a notable expansion and/or migration SE between 8,200-7,900 cal yr BP interpreted to be a manifestation of the 8.2 ka event in the SW Pacific. Between 5,700-2,700 cal yr BP the SPCZ is likely in a more southerly position, in agreement with the Mantsis *et al*. (2013) model results, and with increased frequency of SPCZ shifts, in agreement with the Saint-Lu *et al*. (2015) model results. Whilst a trend in SPCZ precipitation amount, and causal mechanisms, cannot be unequivocally determined from ca. 2,700 cal yr BP to present, SPCZ movement appears to show centennial-scale shifts in location. The results of this study indicate that the SPCZ can shift position over centennial and millennial timescales – the first time this has been presented. Whilst the zonal SST gradient reconstruction is at low temporal resolution (Koutavas and Joanides, 2012), the broad trends support inferences on SPCZ location from Lake Teroto and Lake Lanoto'o over the last ca. 9,500 cal yr BP (van der Wiel *et al*., 2016a). It is salient to note that this is a qualitative assessment and determined shifts in SPCZ location are not specific. This study provides a framework upon which future research can test and refine the interpretations drawn.

9.4 ENSO and IPO over the Holocene

As the Lake Lanoto'o and Lake Teroto records are the first continuous Holocene records from the southwest Pacific, and with the known association between SPCZ movement and ENSO/IPO state, an understanding of millennial-scale changes in ENSO/IPO over the Holocene is possible. It is suggested that the Ca/Ti in Lake Teroto and the Ti and TOC in Lake Lanoto'o indicate the average SPCZ position over millennial timescales, and that the δ^2H_{C26} records from the two sites shows SPCZ variability in those positions. With this in mind when the SPCZ is inferred to be NW and/or contracted (SE and/or expanded) this indicates positive-phase IPO and/or El Niño (negative-phase IPO and/or La Niña) using known relationships between the SPCZ and the IPO/ENSO during the instrumental period (Trenberth, 1976; Folland *et al*., 2002). However, an assumption is being made in this

study that this relationship between the SPCZ and the IPO/ENSO extends through the Holocene. This can be challenged by the potential meridional SST gradient influence on SPCZ position at ca. 6,000 and 4,000 cal yr BP indicated from climate models (Mantsis *et al*., 2013; Saint-Lu *et al*., 2015). The results of this thesis cannot provide further insight on this, but can provide much needed context for climate models to test these controls on SPCZ movement and position over millennial timescales in further work. Comparing the Lake Teroto and Lake Lanoto'o records with other ENSO records from the Pacific will provide insight into whether the relationship between the SPCZ and the IPO/ENSO is maintained over the Holocene. Moreover this study, as a result of not providing evidence that the lacustrine records are annually laminated, has discussed changes in relation to IPO state rather than ENSO. Comparison with other records from the Pacific region could permit changes in ENSO to be disentangled.

9.4.1 ENSO over the last 3,000 cal yr BP

Unlike the SPCZ several indices for ENSO changes have been developed, covering a variety of timescales, which allow comparisons with the Lake Teroto and Lake Lanoto'o records to ascertain whether they contain a record of ENSO. Most indices that have been used to reconstruct ENSO only span a few centuries, such as that of McGregor *et al*. (2010). A notable exception is the SOI_{pr} is an ENSO-like proxy spanning the past 2,000 cal yr BP reconstructing the difference between precipitation in the east and west equatorial Pacific, having a significant positive correlation with the SOI between AD 1951-1997 ($r = 0.68$, $p<0.0001$) (Yan *et al*., 2011). Positive values indicate the Pacific is in a La Niña-like state with increased (decreased) precipitation in the west (east) equatorial Pacific, and vice versa for El Niño-like conditions (Yan *et al*., 2011). Further the El Junco, Galápagos, record has been interpreted to record changes in ENSO activity – specifically the site is susceptible to both CPE and EPE (Conroy *et al*., 2008; Atwood and Sachs, 2014; Zhang *et al*., 2014). In this record high concentrations of botryococcene and more negative botryococcene δ^2H (δ^2H_{bot}) indicate more frequent, stronger El Niños, and more negative dinosterol δ^2H (δ^2H_{dino}) is indicative of higher long-term mean precipitation (Atwood and Sachs, 2014; Zhang *et al*., 2014). As strong El Niños are mainly of the EPE type during the instrumental period, periods characterized by more frequent, stronger El Niños are interpreted to represent increased EPE frequency (Yu *et al*., 2011). Thus, by comparing

these records with the Lake Teroto and Lake Lanoto'o records it will be possible to determine if they record ENSO.

El Junco and Lake Teroto are sensitive to both CPE and EPE over the instrumental period (AD 1965-2011) (Atwood and Sachs, 2014), Lake Lanoto'o is sensitive to EPE over the instrumental period (Section 6.2.2). CPE have varying effects on SPCZ precipitation amount in Samoa over the instrumental period (Section 6.4) and it is thus difficult to disentangle from the effects of La Niña which cause the SPCZ to expand and/or migrate SE (Trenberth, 1976; Folland *et al*., 2002; Yu *et al*., 2011; Borlace *et al*., 2014; Salinger *et al*., 2014; Van der Wiel *et al*., 2015; Kidwell *et al*., 2016). As the instrumental record suggests that CPE dominance is associated with La Niña conditions (Kao and Yu, 2009; Carré *et al*., 2014) it is inferred that wetter conditions in Lake Lanoto'o are either caused by CPE dominance and/or increased La Niña activity. Accounting for the flavours of El Niño that affect El Junco, Lake Teroto and Lake Lanoto'o, the flavour of El Niño over decadal and greater timescales can potentially be determined (Karamperidou *et al*., 2015). As the Lake Teroto and Lake Lanoto'o age model uncertainty averages are ca. 9 years and 30 years respectively comparisons between sites is limited to decadal and centennial timescales and therefore larger than the interannual timescale associated with ENSO. Thus interpreted changes in ENSO will be framed in regards to dominance of a flavour, which is described as a period with an increase in one type of El Niño over another over centennial, and greater, timescales.

Over the last ca. 3,000 cal yr BP TOC has a significant correlation with El Junco botryococcene concentration (bot conc) and δ^2H value (δ^2H_{bot}) whereas Ti has no significant correlation (Table 9.1). No significant correlation occurs between the Lake Teroto record and Lake Lanoto'o or El Junco. Further, no significant correlation occurs between the SOI_{pr} and the proxies from Lake Teroto, Lake Lanoto'o and El Junco. Despite this, visual inspection between the datasets (which includes chronological uncertainties) does suggest some possible similarities. With the flavours of El Niño that El Junco, Lake Lanoto'o and Lake Teroto are sensitive to in mind it is postulated that:

- High TOC and less negative δ^2H_{C26} in Lake Lanoto'o, high Ca/Ti (prior to human impact at ca. 1,100 cal yr BP) and less negative δ^2H_{C26} in Lake Teroto, and high

botryococcene concentration (bot conc) with more negative δ^2H_{bot} in El Junco indicate EPE dominance; and

- High Ti (low TOC) in Lake Lanoto'o and more negative δ^2H_{C26}, low Ca/Ti (prior to human impact at ca. 1,100 cal yr BP) and more negative δ^2H_{C26} in Lake Teroto, and low botryococcene concentration with less negative δ^2H_{bot} in El Junco indicates CPE dominance.

	Bot conc	**δ^2H_{bot}**	**TOC**	**Ti**
Bot conc		<0.05	<0.05	0.61
δ^2H_{bot}	-0.62		<0.05	0.41
TOC	0.36	-0.36		<0.01
Ti	-0.08	0.12	**-0.74**	

Table 9.1: Linear correlation matrix for the Lake Lanoto'o TOC and Ti with El Junco botryococcene concentration (bot conc) and botryococcene δ^2H (δ^2H_{bot}), with correlation values below the diagonal and p values above it. In bold are correlations r≥0.7 and r≤-0.7. Highlighted in red are values that are not statistically significant below the 0.01 significance level. The botryococcene concentration and δ^2H correlation and significance value is from Atwood and Sachs (2014).

From ca. 3,000-2,800 cal yr BP the high Ti (low TOC) in Lake Lanoto'o and low Ca/Ti in Lake Teroto, combined with the high botryococcene concentration and less negative δ^2H values is suggested to indicate a transition towards EPE dominance that begins at ca. 2,800 cal yr BP (Figure 9.5). This is corroborated by the increased frequency and amplitudes of El Niño from ca. 2,800-1,500 cal yr BP in El Junco, the high TOC and less negative δ^2H_{C26} in Lake Lanoto'o, and increasing Ca/Ti and less negative δ^2H_{C26} in Lake Teroto that are inferred to show a dominance of EPE over this time frame. This would explain the higher mean precipitation indicated by dinosterol (δ^2H_{dino}) as the increased frequency and amplitude of El Niños would lead to wetter average conditions. The increasing Ca/Ti from Lake Teroto peaking at ca. 1,700 cal yr BP corresponds to strong ENSO – suggested here to be EPE dominance (Yu *et al*, 2011) – in the Galápagos (Zhang *et al*., 2014; Nelson and Sachs, 2016), and high ENSO variability indicated in other Pacific records for this time (Koutavas and Joanides, 2012; Emile-Geay *et al*., 2016; Chen *et al*., 2016). With a dominance of strong El Niños (EPE) it would be expected that the Indo-Pacific would indicate La Niña-like conditions and thus negative SOI_{pr} values, contrary to

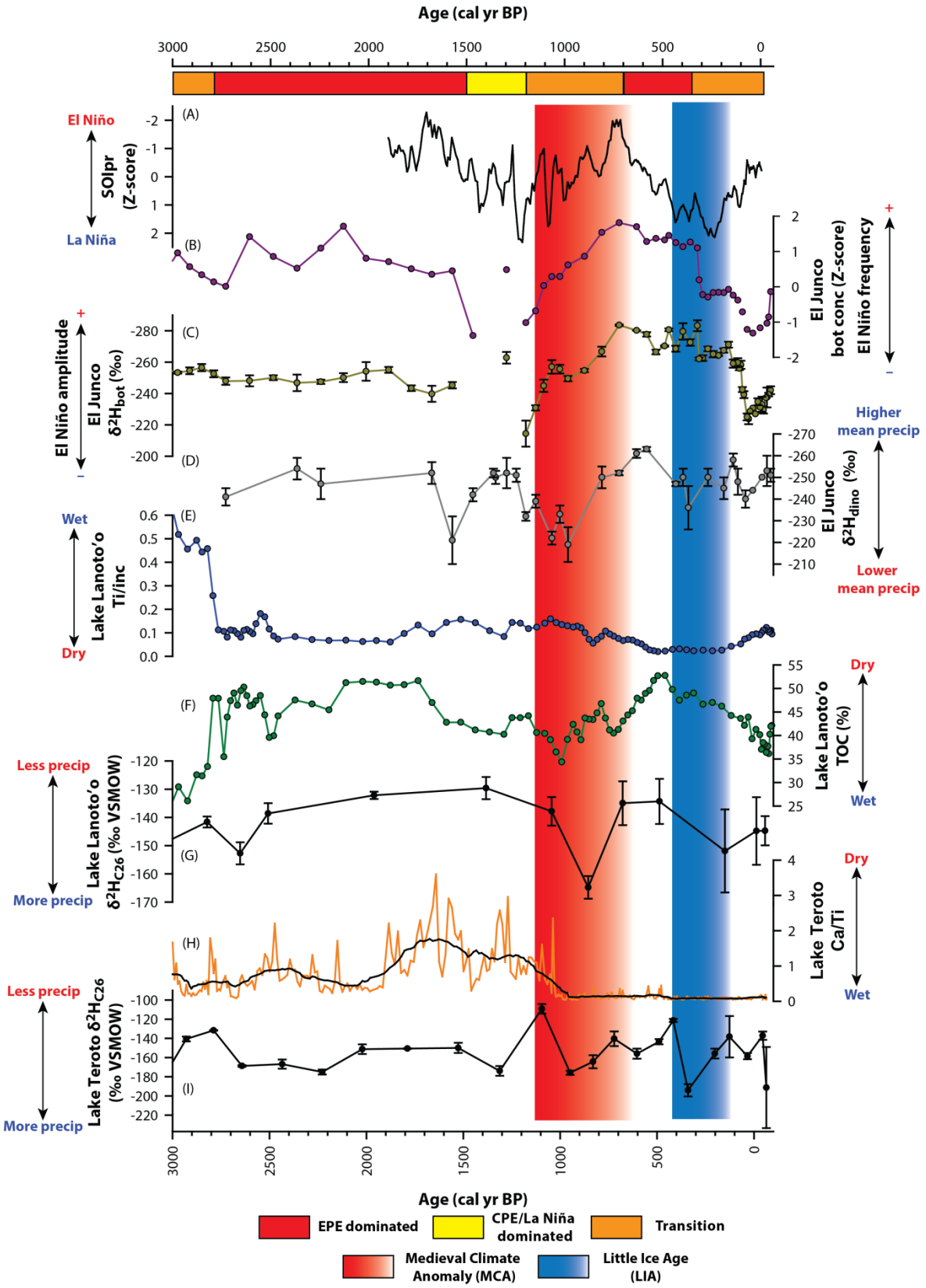

Figure 9.5: The SOI_{pr} (A) from Yan *et al*. (2011); (B) El Junco botryococcene concentration (bot conc), (C) botryococcene δ^2H (δ^2H_{bot}), and (D) dinosterol δ^2H (δ^2H_{dino}) (Atwood and Sachs, 2014); Lake Lanoto'o Ti (E), TOC (F), and C_{26} alkanoic acid δ^2H (δ^2H_{C26}) (G); and Lake Teroto Ca/Ti (H) and C_{26} alkanoic acid δ^2H (δ^2H_{C26}) (I). The black line on (H) indicates LOESS smoothing of the Lake Teroto Ca/Ti values (sampling

proportion 0.01, polynomial degree of 1). The Medieval Climate Anomaly (MCA) is highlighted in red and the Little Ice Age (LIA) is highlighted in blue. The timings of these are sourced from Nelson and Sachs (2016).

what is observed at this time (Yan *et al*., 2011; Yamoah *et al*., 2016a; Section 2.2.1.3). As the SOI_{pr} begins at ca. 1,900 cal yr BP it is difficult to further explore this.

Between ca. 1,500-1,200 cal yr BP CPE is inferred to dominate with the low values in El Junco bot conc and δ^2H_{bot}, the low TOC values in Lake Lanoto'o, and decrasing trend in Ca/Ti values in Lake Teroto. The SOI_{pr} indicates La Niña-like conditions in the Pacific, which would corroborate with an increase in CPE (Kao and Yu, 2009). Of interest is that the Ca/Ti in Lake Teroto has high values during this period indicating lower lake levels and drier conditions due to SPCZ contraction and/or migration NW (Trenberth, 1976; Folland *et al*., 2002). It would be expected that during CPE dominated conditions that there would be a decrease in Ca/Ti due to SPCZ expansion and/or migration SW – this is determined in Lake Lanoto'o where Ti has increased and TOC has decreased. This lends further support that Lake Teroto is sensitive to both flavours of El Niño (Section 6.4.2).This can be further explored over the Holocene – agreement with the El Junco over the Holcoene would further suggest that Lake Teroto is sensitive to both flavours of El Niño. After ca. 1,100 cal yr BP human impact on Lake Teroto limits the efficacy of Ca/Ti, thus changes inferred solely rely on the Lake Lanoto'o record which is determined to not exhibit human impact (Section 8.3.3.5).

Following ca. 1,200 cal yr BP El Junco indicates an increase in El Niño activity that peaks at ca. 720 cal yr BP and is relatively stable until ca. 350 cal yr BP before declining, in contrast to Lake Lanoto'o where El Niño activity peaks at ca. 500 cal yr BP before declining. The δ^2H_{C26} records from Lake Teroto and Lake Lanoto'o lend further support to El Niño conditions indicating SPCZ contraction and/or migration NW due to reduced precipitation amount (Trenberth, 1976; Folland *et al*., 2002). This difference may relate to a centennial-scale transition from CPE to EPE dominance, beginning at 1,200 cal yr BP with EPE dominance occurring at ca. 700-350 cal yr BP. This would increase mean precipitation, as indicated by the more negative δ^2H_{dino}. An increase in La Niña activity, associated with CPE dominance (Kao and Yu, 2009; Carré *et al*., 2014), has been inferred during the during MCA (ca.1,150-650 cal yr BP) (Dunbar *et al*., 1994; Cobb *et al*., 2003; Conroy *et al*., 2010; Khider *et al*., 2011; Li *et al*., 2011; Restrepo *et al*., 2012; Nelson and Sachs, 2016)

supporting this interpretation. Contrary to this Rustic *et al*. (2015) argued that during peak MCA (AD 900-1150; ca. 1,050-800 cal yr BP) the eastern Pacific was warm, consistent with El Niño conditions. With it being suggested here that a transition to EPE dominance was occurring over the MCA, this may explain the disparity that Rustic *et al*. (2015) highlight. This is because a shift to EPE dominance would cause an increase in SST in the eastern Pacific.

From ca. 700 cal yr BP the SOI_{pr} indicates La Niña-like conditions, whereas El Junco and Lake Lanoto'o indicates prolonged El Niño conditions. This disagreement may relate to the aforesaid effect of strong El Niños, such as EPE, over centennial to millennial timescales resulting in positive precipitation anomalies in the Indo-Pacific, whereas the southwest Pacific will indicate El Niño conditions (Yamoah *et al*., 2016a). Conroy *et al.* (2010) determined a reduced zonal SST gradient from 650 cal yr BP, typical of El Niño conditions, that would cause the SPCZ to take a zonal orientation (van der Wiel *et al*., 2016a). This would cause Lake Lanoto'o to indicate El Niño conditions as the record indicates. Using the El Junco and Lake Lanoto'o records EPE dominance from ca. 700-350 cal yr BP is suggested, which would lead to the SOI_{pr} indicating La Niña-like conditions as is observed. This highlights the need to use a network of records from the Pacific region to fully understand ENSO variability on centennial to millennial timescales.

The LIA (ca. 450-150 cal yr BP) is suggested in various records to be dominated by El Niño conditions (Cobb *et al*., 2003; Conroy *et al*., 2010; Sachs *et al*., 2009; Khider *et al*., 2011; Restropo *et al*. 2012; Rustic *et al*., 2015). The Lake Lanoto'o record, in conjunction with the El Junco record, indicates El Niño conditions at this time. Further, the less negative δ^2H_{C26} values from Lake Teroto suggest decreased precipitation amount consistent with SPCZ contraction and/or migration NW that would occur in El Niño conditions (Trenberth, 1976; Folland *et al*. 2002). A declining trend in El Junco botryococcene concentration and δ^2H and Lake Lanoto'o TOC suggests a reduction in El Niño activity from 350 cal yr BP – it is interpreted here to indicate a transition to CPE dominated conditions.

9.4.1.1 Overview of ENSO over the last 3,000 cal yr BP

The instrumental record, presented in section 6.2 and 6.3, indicated the relationship between precipitation, SPCZ movement, the IPO and ENSO indices that these relationships are consistent with conclusions drawn in the literature. Simply: during El

Niño (La Niña) or positive-phase IPO (negative-phase IPO) the SPCZ contracts and/or migrates NW (expands and/or migrates SE (Trenberth, 1976; Folland *et al*., 2002). When Lake Teroto and Lake Lanoto'o are compared with ENSO records over the past 3,000 cal yr BP (SOI_{pr} and the El Junco record) it suggests that these sites can be used to better understand changes in ENSO over the Holocene – specifically changes in the dominance of ENSO flavours. The Lake Teroto record indicates that it is sensitive to both CPE and EPE and Lake Lanoto'o to EPE only. This is contrary to the instrumental record that suggested only EPE would be recorded in Lake Teroto. With these relationships in mind, changes in the dominant ENSO flavours over the last ca. 9,500 cal yr BP can be explored. In section 9.3.2 it was highlighted that either reduced ENSO activity/negative-phase IPO or increased meridional SST gradients caused the SPCZ to shift to a more southerly position beween ca. 6,000-4,000 cal yr BP (Mantsis *et al*., 2013; Saint-Lu *et al*., 2015), thus meaning that using inferring changes in ENSO from the Lake Teroto and Lake Lanoto'o records alone for this period would be challenging. Comparison with ENSO records from the Pacific, not influenced by the SPCZ, will potentially help disentangle whether the southerly SPCZ position between ca. 6,000-4,000 cal yr BP was due to reduced ENSO activity or increased merdional SST gradients.

9.4.2 ENSO over the last 9,500 cal yr BP

Figure 2.23 has been adapted to include the Lake Teroto and Lake Lanoto'o records (Figure 9.6), showing a remarkable degree of coherence across the Pacific basin – especially when accounting for the lack of isochronous markers in the region. Records from the Pacific basin only are used, rather than those located from the circum-Pacific, due to circum-Pacific records likely representing local responses to deglacial climate forcings rather than ENSO (Liu *et al*., 2014). Dominance of EPE or CPE has been inferred using the relationships outlined in section 9.4.1, but incorporating the results of Carré *et al*. (2014) which ascertained the dominance of EPE or CPE at discrete intervals over the past ca. 9,500 cal yr BP.

9.4.2.1 EPE dominance from 9,500-6,700 cal yr BP and the 8.2 ka event

Between 9,500-6,800 EPE conditions dominate. Increase ENSO variability is inferred throughout this period from proxies in Borneo, the Galápagos, Peru, Easter Island and Samoa (Koutavas and Joanides, 2012; Margalef *et al*., 2013; Zhang *et al*., 2014; Carré *et al*.,

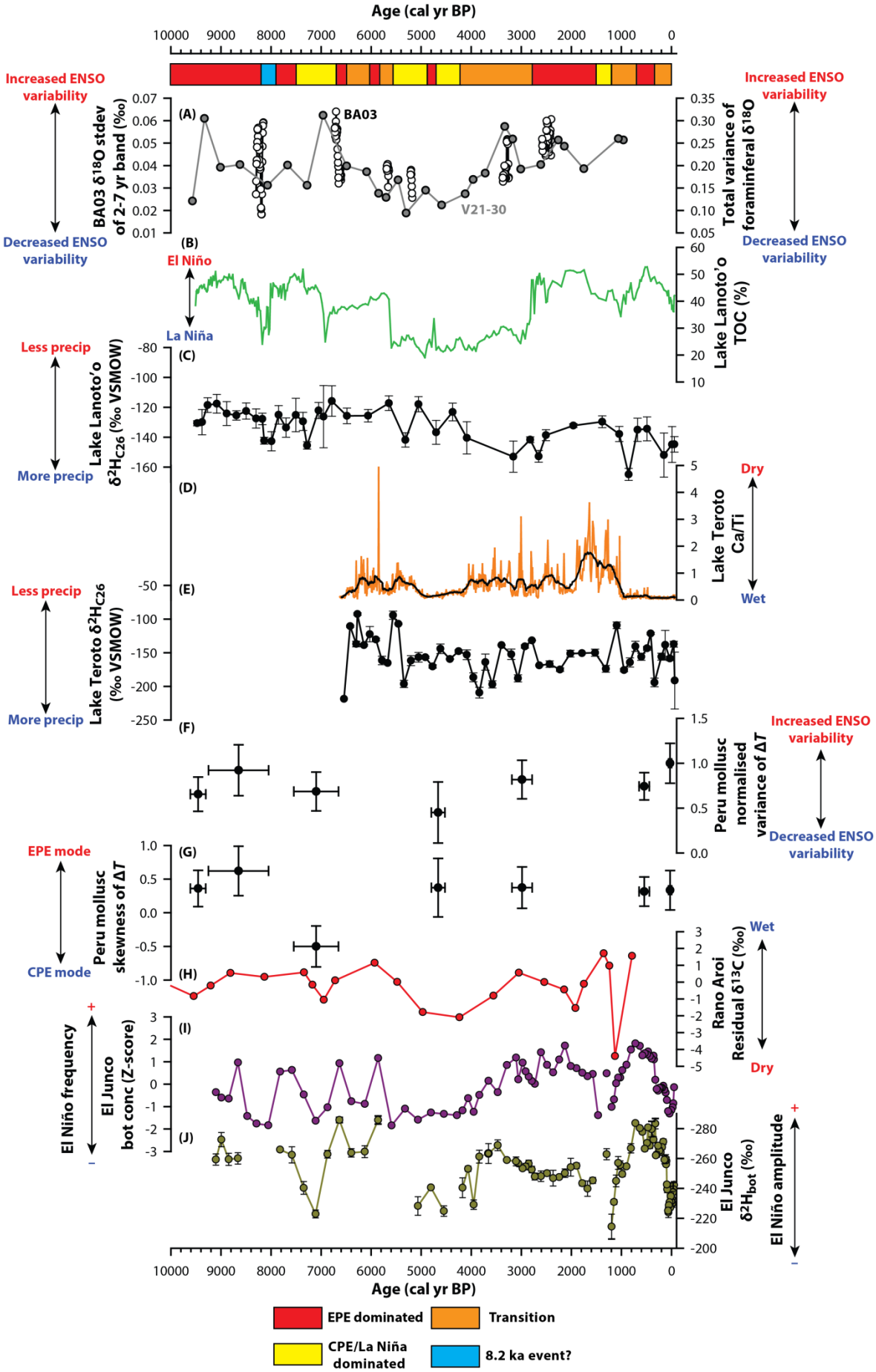
Age (cal yr BP)
10000 9000 8000 7000 6000 5000 4000 3000 2000 1000 0
Increased ENSO variability
Decreased ENSO variability
BA03 δ18O stdev of 2-7 yr band (‰)
(A)
BA03
V21-30
Total variance of foraminferal δ18O
(B)
El Niño
La Niña
Lake Lanoto'o TOC (%)
Less precip
More precip
Lake Lanoto'o δ2HC26 (‰ VSMOW)
(C)
(D)
Dry
Wet
Lake Teroto Ca/Ti
(E)
Lake Teroto δ2HC26 (‰ VSMOW)
(F)
Peru mollusc normalised variance of ΔT
EPE mode
CPE mode
Peru mollusc skewness of ΔT
(G)
(H)
Rano Aroi Residual δ13C (‰)
El Niño frequency
El Junco bot conc (Z-score)
(I)
(J)
El Junco δ2Hbot (‰)
El Niño amplitude
EPE dominated
Transition
CPE/La Niña dominated
8.2 ka event?

Figure 9.6: Comparison of Holocene ENSO records from the Pacific basin. (A) ENSO variability estimates from speleothem BA03, Borneo, (white circles) and foraminifera (grey circles) from V21-30, Galápagos (Koutavas and Joanides, 2012; Chen et al., 2016). BA03 $\delta^{18}O$ estimates are based on the standard deviation (st dev) of the 2-7 year band in overlapping 30-year windows (5-year step) (Chen et al., 2016); foraminferal $\delta^{18}O$ variance is determined using the $\delta^{18}O$ of single tests in each 1-cm stratum (Koutavas and Joanides, 2012). (B) The Lake Lanoto'o TOC record and $\delta^{2}H_{C26}$ record (C), and Lake Teroto Ca/Ti (D) and $\delta^{2}H_{C26}$ record (E) from this study. The black line on (D) indicates LOESS smoothing of the Lake Teroto Ca/Ti values (sampling proportion 0.01, polynomial degree of 1). The seasonal SST range variance (F) (as % difference from modern (0-60 yr BP) and skewness (G) with 1σ uncertainty on the Peruvian coast calculated from monthly molluscan shell $\delta^{18}O$ measurements (Carré et al., 2014). Variance is determined to be ENSO-driven and skewness to indicate the relative contribution of Central Pacific El Niños (CPE) and Eastern Pacific El Niños (Carré et al., 2014). (H) Residual $\delta^{13}C$ values from Rano Aroi, Easter Island, caused by changes in humidity and determined not to relate to long-term C_4-C_3 vegetation changes (Margalef et al., 2013); El Junco, Galápagos, botryococcene concentration (bot conc) (I) and $\delta^{2}H$ ($\delta^{2}H_{bot}$) (J), the former interpreted to indicate El Niño frequency and the latter to indicate the El Niño amplitude (Atwood and Sachs, 2014; Zhang et al., 2014). Added are hypothesised phases of El Niño flavour dominance: EPE (red), CPE (yellow), transition periods from one flavour to another (orange), and the 8.2 ka event (blue). This figure is modified from Chen et al. (2016).

2014). Both El Junco and Lake Lanoto'o indicate increased El Niño frequency and amplitude, which as aforementioned is interpreted to indicate a dominance of EPE conditions in the Pacific. The Peru mollusc record further supports this indicating EPE over this period thus lending credence that the relationships inferred from the El Junco and Lake Lanoto'o records can be relied upon (Carré *et al*., 2014). Moreover, ENSO variance in the east Pacific is similar to present which would be consistent with EPE dominance (Emile-Geay *et al*., 2016).

Prominent during this period is the decrease in ENSO variability between ca. 8,200-7,900 cal yr BP. An increase in precipitation amount in Lake Lanoto'o alongside a decrease in El Niño frequency and amplitude in El Junco (Zhang *et al*., 2104) indicates a shift towards CPE conditions for this period. Additionally Chen *et al*. (2016) found a distinct isotopic excursion towards more positive $\delta^{18}O$ values in Borneo speleothems between ca. 8,230-

8,190 cal yr BP which they suggest may relate to the 8.2 ka event, and low ENSO variance in the west Pacific is concluded for this period (Driscoll *et al*., 2014; Emile-Geay *et al*., 2016) . In section 9.3.1.1 it was concluded that evidence for the 8.2 ka event can be found in Lake Lanoto'o, with Atwood (2015) concluding evidence for it in El Junco. Interestingly Timmermann *et al*. (2007) argued that a weakened AMOC, as occurs during the 8.2 ka event (Alley *et al*., 1997; Barber *et al*., 1999) would lead to an intensification of ENSO using coupled general circulation models, contrary to what is inferred by Atwood (2015) and in this study. Timmermann *et al*. (2007) argued that cooling in the north Atlantic leads to a southward shift in the Pacific ITCZ, leading to a meridional asymmetry that weakens the annual cycle and intensifies ENSO. Atwood (2015) proposed a mechanism – detailed in section 9.3.1.1 – which also invokes a southward shift in the ITCZ; however this lead to a reduction in ENSO activity consistent with observations in the palaeorecords. It is apparent that further research is needed to understand the mechanisms that lead to a reduction in ENSO activity as a result of a weakened AMOC as the Lake Lanoto'o and El Junco (Atwood, 2015) records, and other records in the west Pacific (Driscoll *et al*., 2014; Emile-Geay *et al*., 2016), indicate evidence that contrasts with the findings of Timmermann *et al*. (2007)

The Peru mollusc record indicates that between ca. 7,500-6,700 cal yr BP CPE dominated and reduced ENSO activity, which agrees with the Borneo, Rano Aroi and El Junco record (Margalef *et al*., 2013; Carré *et al*., 2014; Zhang *et al*., 2014; Chen *et al*., 2016). Emile-Geay *et al*. (2016) argued that ENSO variance is low (<1) in the central Pacific over the 7,000 cal yr BP record they present. A fundamental problem with the records used in the central Pacific in this study is that they are not in the centre of action for CPE – this being the Niño4 region (Table 2.2 and Figure 2.2) – and are in the Niño3.4 region where both EPE and CPE have an affect (Kao and Yu, 2009). Thus inferring a change in ENSO variance in the region Emile-Geay *et al*. (2016) use for the central Pacific is arguably flawed. Lake Lanoto'o indicates reduced precipitation amount throughout this period, except at ca. 7,280 cal yr BP, which is consistent with EPE dominate conditions. Closer examination of the Lake Lanoto'o TOC indicates a declining trend, and an increase in precipitation amount at ca. 7,280 cal yr BP, both of which would be consistent with CPE dominated conditions. A return to EPE conditions is suggested to occur at ca. 6,800 cal yr BP from the high TOC in the Lake Lanoto'o record. With the plethora of evidence it is postulated that

the CPE dominated conditions determined by Carré *et al*. (2014) occurred between ca. 7,500-6,800 cal yr BP, a timing refined using the Lake Lanoto'o record and within the chronological error of the Peru mollusc record.

9.4.2.2 CPE dominance 6,800-2,800 cal yr BP

Following the CPE dominant conditions from ca. 7,500-6,800 cal yr BP a transition period is suggested to occur from 6,800-5,600 cal yr BP with a decrease in EPE dominant conditions towards CPE dominant conditions. During this transition EPE punctuates at ca. 6,600 and 5,800 cal yr BP, indicated from the general agreement between the δ^2H_{C26} records from Lake Teroto and Lake Lanoto'o, and the botryococcene record from El Junco that indicates a decrease El Niño frequency and amplitude typical of CPE (Yu *et al*., 2011; Zhang *et al*., 2014).

The mid-Holocene has often been cited as a period of reduced variability (Riedinger *et al*., 2002; McGregor and Gagan, 2004; Rein *et al*., 2005; Conroy *et al*., 2008; Koutavas and Joanides, 2012; McGregor *et al*., 2013a; Carré *et al*., 2014; Zhang *et al*., 2014; Emile-Geay *et al*., 2016; Chen *et al*., 2016). Whilst Emile-Geay *et al*. (2016) concluded that coral records showed a 64% reduction in ENSO variance between ca. 5,000-3,000 cal yr BP this is based on discontinuous, short (ca. 100 yr) coral records – therefore the timing and duration of this reduction is poorly constrained. Using the network of records presented in Figure 9.6 the reduction in ENSO variability is suggested to begin at ca. 5,600 cal yr BP and lasting until ca. 4,200 cal yr BP. The agreement between the Lake Teroto and Lake Lanoto'o records with these other records suggests that SPCZ position was primarily influenced by ENSO during this time rather than increased meridional SST gradients (Mantsis *et al*., 2013; Saint-Lu *et al*., 2015). Nevertheless the influence of increased meridional SST gradients on SPCZ position during this time cannot be completely discounted with the results presented here. The ca. 5,600-4,200 cal yr BP period is inferred to represent CPE dominated conditions, punctuated with EPE dominated conditions with reduced variability at ca. 4,800-4,600 cal yr BP. This is corroborated by the increase in TOC in Lake Lanoto'o, EPE mode and decreased ENSO variability inferred from Peru molluscs, and low El Niño frequency but modest increase in El Niño amplitude indicated in El Junco between ca. 4,800-4,600 cal yr BP (Zhang *et al*., 2014; Carré *et al*.,

2014). This is the first estimate for the duration of this reduction in ENSO variability cited in the literature, and further is the first time the nature of it has been postulated.

As previously mentioned validating this hypothesis that CPE conditions dominated from ca. 5,600-4,200 cal yr BP is difficult both due to the lack of long, continuous records from the central Pacific and that no records are currently available from the centre of action for CPE: this being the Niño4 region (Kao and Yu, 2009). Moreover, a problem with ascribing mechanisms for this change in ENSO is that climate models focus on the ca. 6,000 cal yr BP period. It is apparent, using the network of records presented here, that this time period is actually a period of transition from CPE- to EPE-dominated and that climate models need to focus between ca. 5,600-4,200 cal yr BP, and the periods immediately preceding and following this time, to better understand the mechanisms for changes in ENSO over this period. Emile-Geay *et al*. (2016) argued that the Holocene changes in ENSO do not have a simple relationship with orbital forcing. However, this conclusion was formed from coral records which have the inherent problem of being short (ca. 100 yr). Can inferences on what is causing changes in ENSO flavours throughout the Holocene really be determined from short-term, discontinuous coral records? It is unlikely that valid conclusions on drivers over millennial timescales can be drawn from this type of record. The conclusions made in this study provide testable hypotheses on the driving mechanisms for changes in ENSO over the Holocene.

From ca. 4,200 cal yr BP the records presented indicate a shift to increased ENSO variability and in the case of El Junco an increase in El Niño frequency and amplitude (Zhang *et al*., 2014). Lake Lanoto'o indicates an increase in TOC that peaks at ca. 2,800 cal yr BP, and Lake Teroto an increase in Ca/Ti and more variable δ^2H_{C26} values that become progressively less negative indicating a shift towards less precipitation amount. It is suggested that this period indicates a transition from CPE dominance to EPE dominance at ca. 2,800 cal yr BP when the various records presented are in agreement, further corroborated by the EPE mode indicated from the Peru molluscs (Carré *et al*., 2014). The dominance of El Niño flavours from ca. 2,800 cal yr BP to present has been discussed in detail in section 9.4.1.

9.4.2.3 Overview of Holocene SPCZ movement and ENSO

In Table 2.3 hypotheses were put forward in regards to SPCZ location and IPO phase during the Holocene inferred from a review of the literature. Using the conclusions outlined in this chapter these hypotheses can be compared to determine whether they are supported or rejected by the interpretations from this study (Table 9.2). Overall it can be seen that there are broad similarities that match with hypothesised IPO phase and SPCZ position. A notable difference in SPCZ occurs between ca. 4,200-2,800 when rather than a dominant position SE of average high variability in location is inferred from the Lake Lanoto'o and Lake Teroto records. The proposed dominance in El Niño flavours and SPCZ position from 9,500 cal yr BP to present, as outlined in Figure 9.6, are presented in Figure 9.7.

9.5 Human impact on the Lake Teroto and Lake Lanoto'o records

Chapter 3 outlined the timings of human colonisation to Atiu and Samoa. Specifically the earliest evidence of human colonisation on Samoa is ca. 2,900-2,700 cal yr BP (Rieth and Hunt, 2008), and Atiu at ca. 1,283 cal yr BP (Parkes, 1994). Additionally, Wilmshurst *et al*. (2011) suggested that the Southern Cook Islands were colonised between 700-670 cal yr BP. Whilst there is no distinct evidence of human impact or colonisation in the Lake Lanoto'o record presented in this study, the results presented for Atiu indicate human impact on the Lake Teroto record. The most likely impact relating to human colonisation in the Lake Teroto record occurred at ca. 1,100 cal yr BP, similar to that originally stated by Parkes (1994) within chronological errors (ca. 1,283 cal yr BP). Moreover this is more in agreement with the suggested colonisation of Mangaia at ca. 2,017-1,552 cal yr BP (Kirch and Ellison, 1994; Chagué-Goff *et al*., 2016) than the timing of human colonisation of the Southern Cook Islands proposed by Wilmshurst *et al*. (2011). Considering the colonisation dates for Mangaia and Atiu it lends itself to the idea of a gradual "leakage" of humans from western to eastern Polynesia as suggested by Chagué-Goff *et al*. (2016) in contrast to a singular pulse put forward by Wilmshurst *et al*. (2011).

Having created a framework of changes in ENSO flavours over the last ca. 9,500 cal yr BP it would be remiss not to compare the proposed timings of human colonisation on Samoa, Atiu, and the Southern Cook Islands. Figure 9.8 indicates that proposed timings of

Time (cal yr BP)	Hypothesised IPO phase (Positive/ Negative)	Dominant ENSO flavour and timing (cal yr BP)	Hypothesised SPCZ position (Northwest of average/Southeast of average)	Dominant SPCZ position (cal yr BP)
10,000	Positive	EPE	Northwest of average	
9,000	Positive	EPE	Northwest of average	Northwest of average from 9,600-8,200
?8.2 ka event?	Negative	CPE (8,200-7,900)	Southeast of average	Southeast of average from 8,200-7,900
7,000	Positive	EPE (7,900-7,500) CPE (7,500-6,800)	Northwest of average	Northwest of average from 7,900-7,000
6,000	Negative	EPE (6,800-6,500) Transition from EPE to CPE (6,500-6,000)	Southeast of average	Southeast of average from 7,000-6,800 Northwest of average from 6,800-5,600
5,000	Negative	EPE (6,000-5,800) Transition from EPE to CPE (5,800-5,600) CPE (5,600-4,800) EPE (4,800-4,600) CPE (4,600-4,200)	Southeast of average	Southeast of average from 5,600-4,200
4,000	Negative	Transition (4,200-2,800)	Southeast of average	High variability from 4,200-2,800
3,000	Positive	Transition from CPE to EPE (4,200-2,800) EPE (2,800-1,500)	Northwest of average	Southeast of average from 2,800-2,500 Northwest of average 2,500-1,800
2,000	Positive	CPE (1,500-1,200)	Northwest of average	Southeast of average from 1,800-800
1,150-650 (MCA)	Negative	Transition from CPE to EPE (1,200-700)	Southeast of average	Northwest of average 800 to present
450-150 (LIA)	Positive	EPE (700-350) Transition from EPE to CPE (350 to present)	Northwest of average	

Table 9.2: Hypothesised phases of IPO and SPCZ position in comparison to the dominant ENSO flavours and SPCZ position determined in this study.

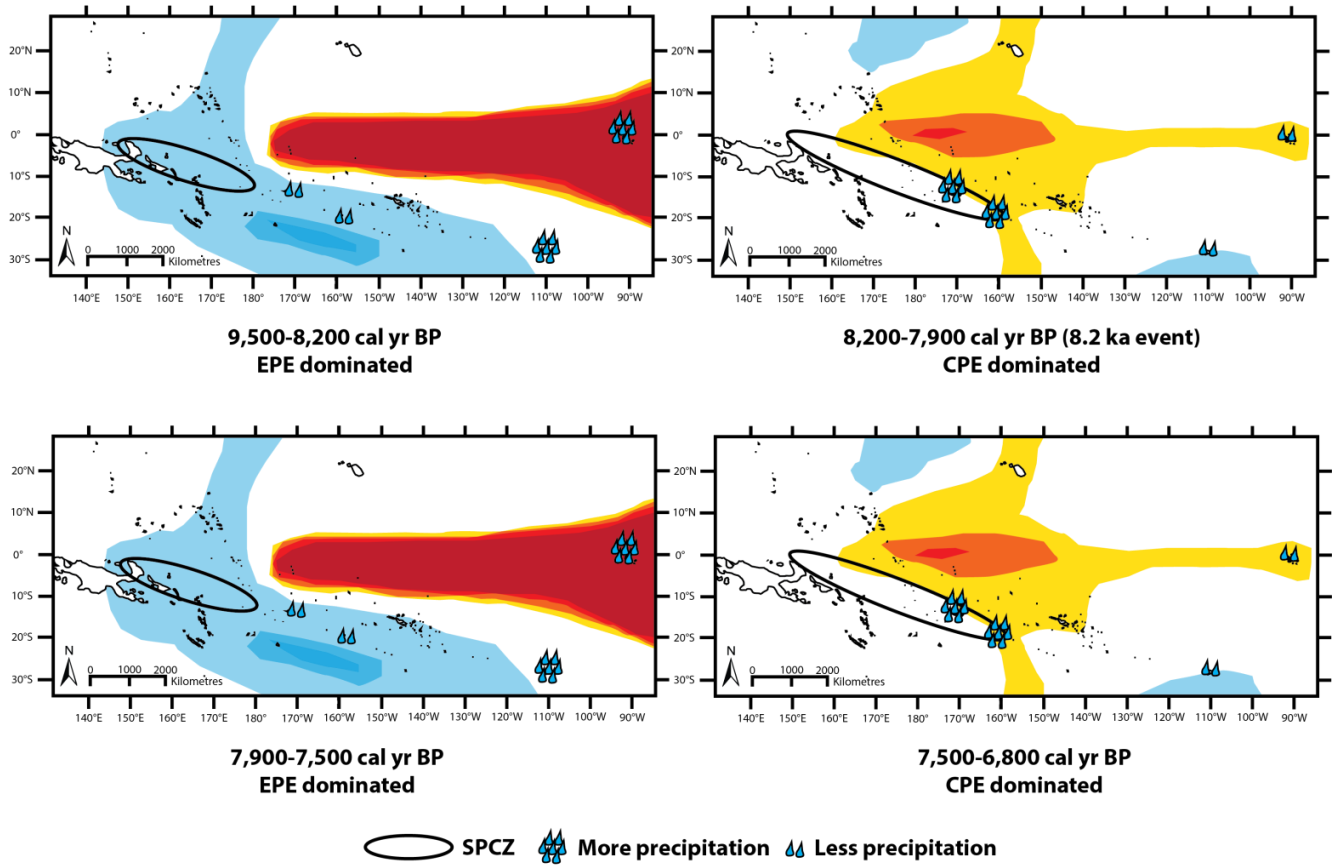

Figure 9.7: The proposed dominance of El Niño flavours (EPE is eastern Pacific El Niño and CPE is central Pacific El Niño) and SPCZ position from 9,500 cal yr BP to present. Red contours indicate warmer sea surface temperatures (SST), blue indicates colder SST, with the SST spatial distribution adapted from Captondi *et al*. (2015). The SST spatial distribution during EPE to CPE transitions and CPE to EPE transitions is conjecture to assist in visualising the transition and should not be viewed as representative of the actual SST spatial distribution.

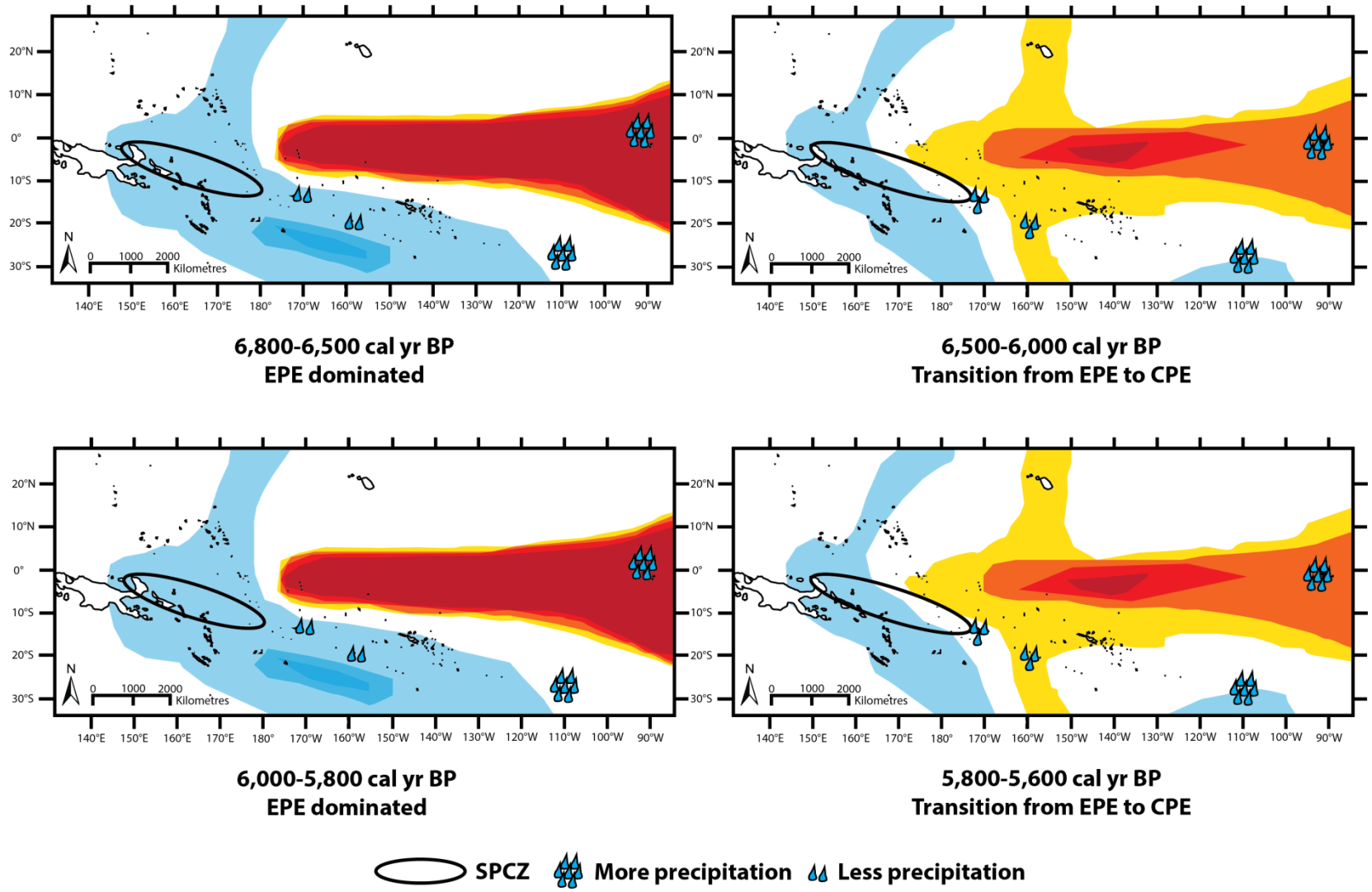

Figure 9.7 continued.

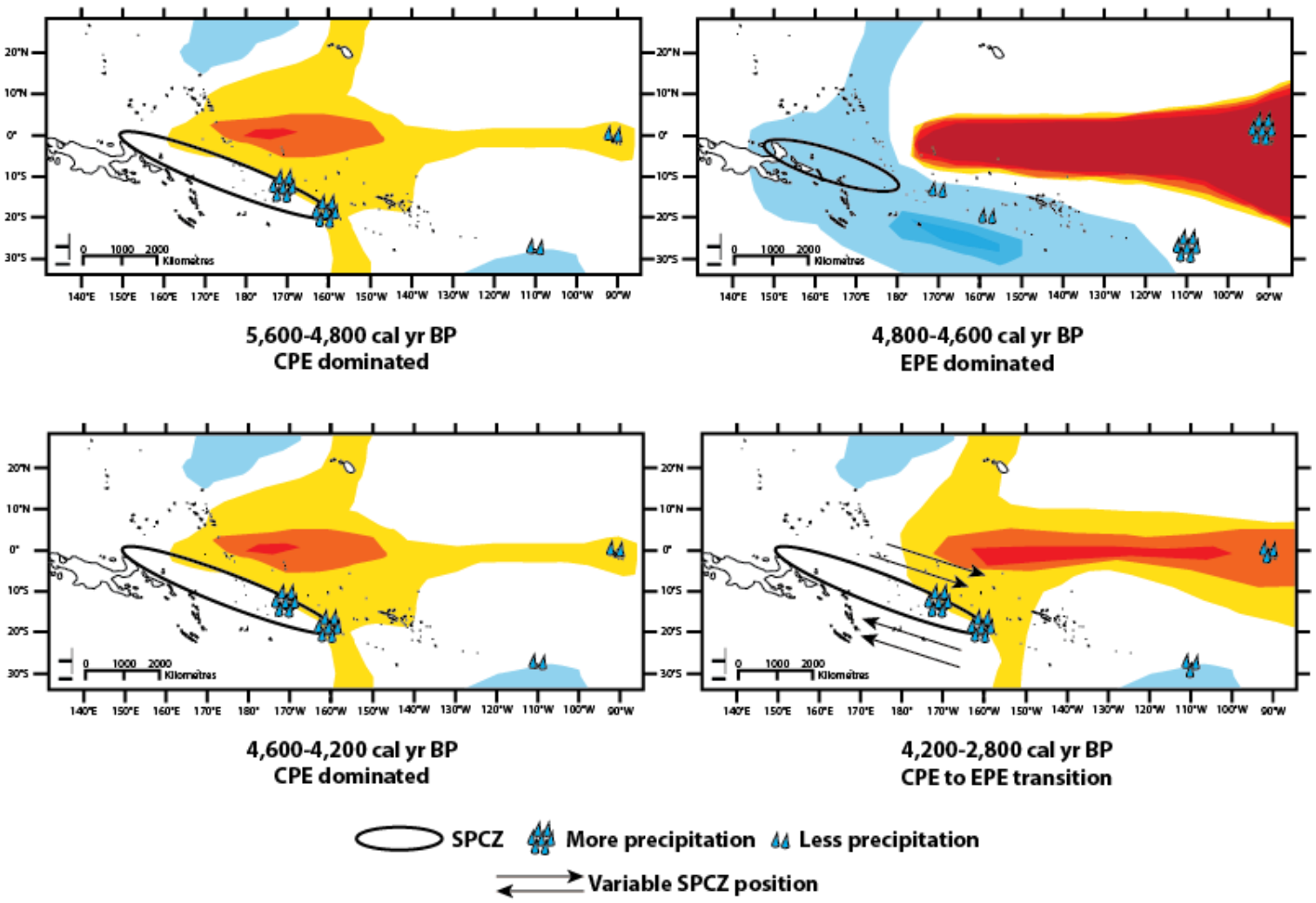

Figure 9.7 continued.

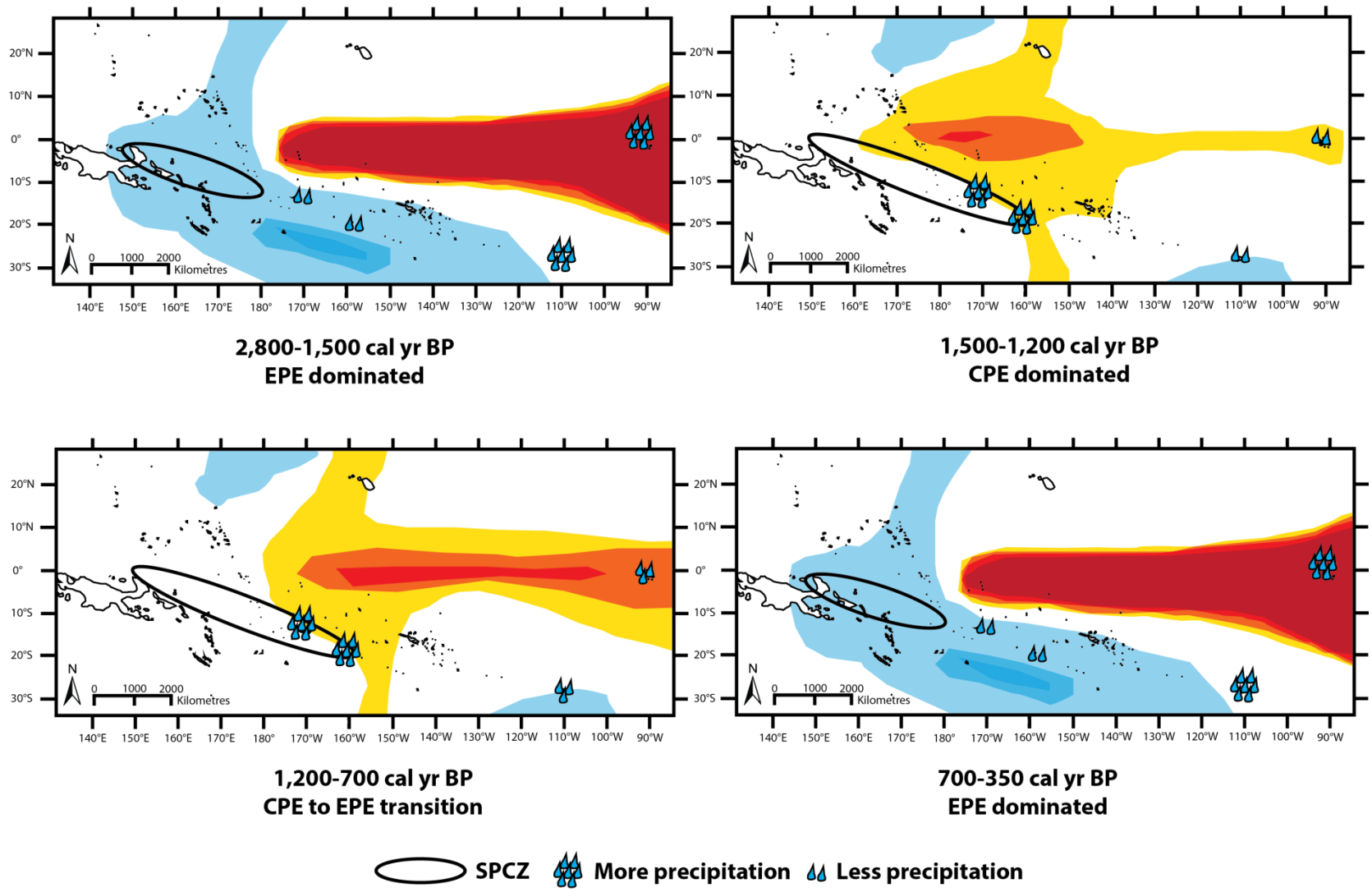

Figure 9.7 continued.

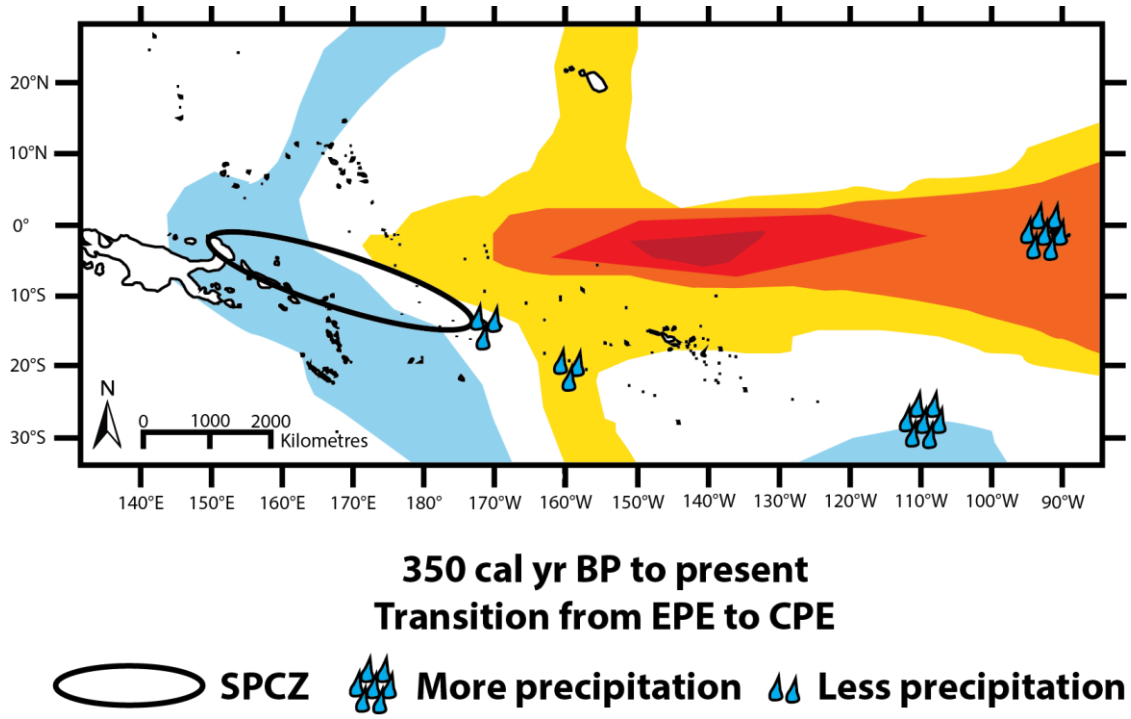

Figure 9.7 continued.

colonisation occurred during either transition periods from CPE to EPE, or EPE dominated conditions. With EPE being the strongest El Niños in the instrumental period (Yu *et al*., 2011), and strong El Niños causing either trade winds to weaken or go from west to east (Bjerknes, 1966), it may be that a shift towards conditions dominated by this flavour encourage Polynesian expansion from west to east. Such a hypothesis has already been postulated by Anderson *et al*. (2006) and Goodwin *et al*. (2014), with the conclusions of this study lending support to it. Moreover transition periods from CPE to EPE and EPE dominated conditions would cause the SPCZ to contract and/or shift NW (Trenberth, 1976; Folland *et al*., 2002) which would lead to a reduction in precipitation amount and potential drought conditions that could encourage humans to migrate to find potable water sources. In addition, Widlansky *et al*. (2014) highlighted that during strong El Niños sea level drops in some western tropical Pacific islands by up to 20-30 cm causing major damage to associated coral ecosystems. This would lead to a reduction in fish and other animals that live within the coral ecosystem, meaning a reduction in a primary food source for people that typically reside along coastlines (Green, 2002; Nunn and Cason 2015). This could provide a driving mechanism to colonise new islands; however this may also encourage peoples to move their settlements inland to locations where agriculture would be more successful (Nunn and Carson, 2015).

A more detailed examination of potential driving mechanisms for human colonisation in Polynesia, and for the cause of the "Dark Ages" in Samoa (Davidson, 1979), is beyond the scope of this study. Nevertheless this study creates a picture of island communities that are encouraged to colonise new islands to survive during EPE dominated conditions due to reduced potable water and food sources. Whilst difficult to test it provides a plausible, if simplistic, framework that implicates ENSO as a forcing mechanism for Polynesian expansion. Moreover, the proposed timing of human colonisation of Atiu from this study implicates a more nuanced colonisation history for eastern Polynesia than that proposed by Wilmshurst *et al*. (2011). This indicates that further research is required to better understand the colonisation history of this region.

9.6 Summary

The Lake Teroto and Lake Lanoto'o records are unique in this region, the former comprising laminae comprised of gypsum not seen in any other laminated Pacific record and the latter having the potential to contain a much longer climate record than that presented in this thesis. Using the two records it can be seen that centennial-scale shifts in SPCZ have occurred over the Holocene – the first time this has been determined. The Lake Lanoto'o record shows evidence for the 8.2 ka event affecting the southwest Pacific, corroborating evidence from El Junco that indicates the effect of the 8.2 ka in the equatorial east Pacific (Atwood, 2015). In addition, the Lake Teroto and Lake Lanoto'o records in comparison with ENSO records from the Pacific indicate periods dominated by a distinct El Niño flavour, and refines the nature and timing of the mid-Holocene reduction in ENSO determined in a variety of Pacific records. Finally, the timing of human colonisation to Atiu is indicated to have occurred at ca. 1,100 cal yr BP from the Lake Teroto record presented in this study. When the timings of human colonisation of Samoa, Atiu and the Southern Cook Islands are compared to the ENSO record presented in this study it suggests that colonisation occurred either during EPE dominated conditions or during transitions from CPE to EPE dominated conditions. It provides a potential climatic forcing mechanism for colonisation of this region that can be explored in future research.

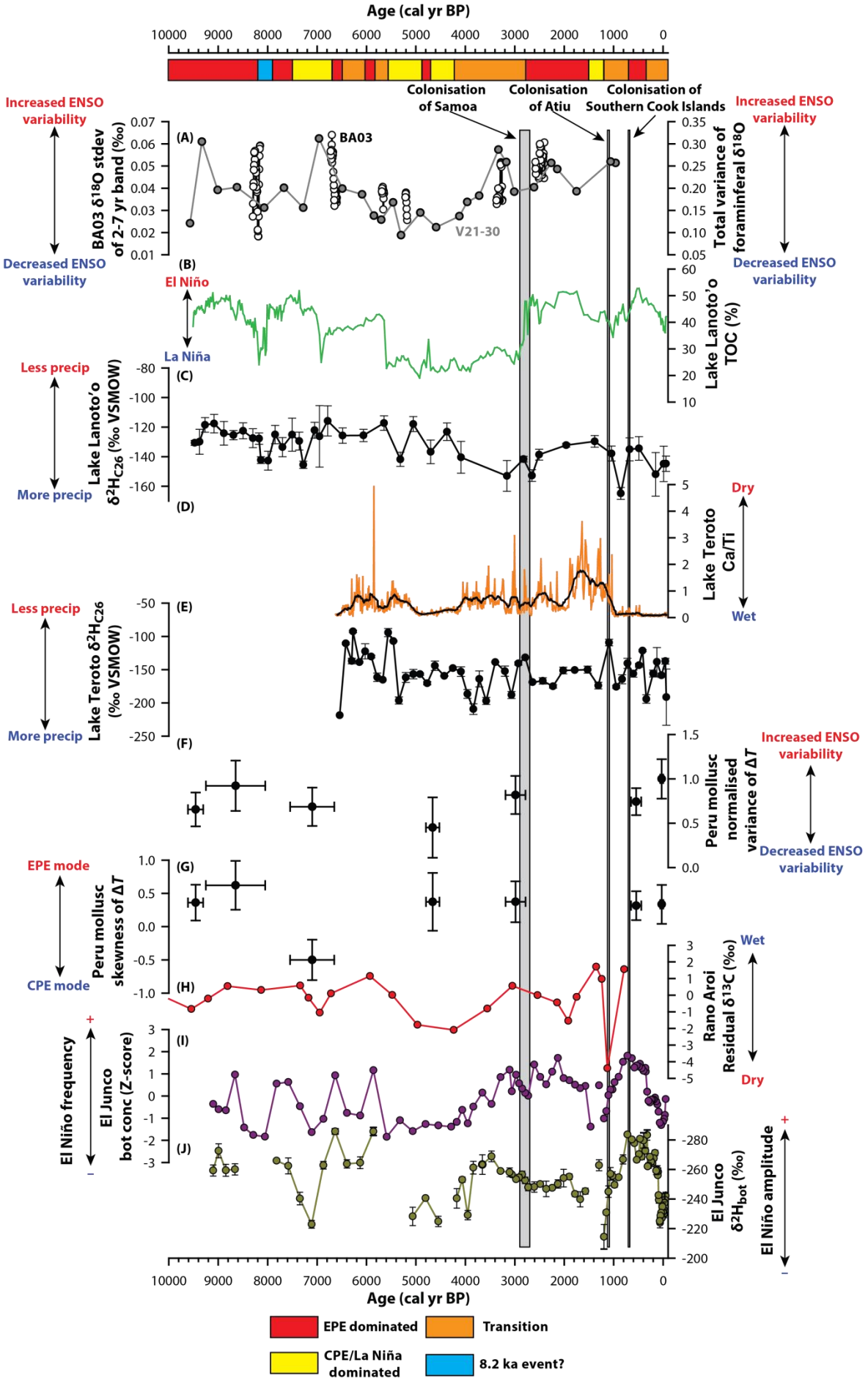
Age (cal yr BP)
10000 9000 8000 7000 6000 5000 4000 3000 2000 1000 0
Colonisation of Samoa
Colonisation of Atiu
Colonisation of Southern Cook Islands
Increased ENSO variability
Decreased ENSO variability
(A)
BA03
V21-30
BA03 δ18O stdev of 2-7 yr band (‰)
Total variance of foraminferal δ18O
(B)
El Niño
La Niña
Lake Lanoto'o TOC (%)
Less precip
More precip
(C)
Lake Lanoto'o δ2HC26 (‰ VSMOW)
(D)
Dry
Wet
Lake Teroto Ca/Ti
(E)
Lake Teroto δ2HC26 (‰ VSMOW)
(F)
Peru mollusc normalised variance of ΔT
EPE mode
CPE mode
(G)
Peru mollusc skewness of ΔT
(H)
Rano Aroi Residual δ13C (‰)
El Niño frequency
(I)
El Junco bot conc (Z-score)
(J)
El Junco δ2Hbot (‰)
El Niño amplitude
EPE dominated
Transition
CPE/La Niña dominated
8.2 ka event?

Figure 9.8: Comparison of Holocene ENSO records from the Pacific basin. (A) ENSO variability estimates from speleothem BA03, Borneo, (white circles) and foraminifera (grey circles) from V21-30, Galápagos (Koutavas and Joanides, 2012; Chen et al., 2016). BA03 $\delta^{18}O$ estimates are based on the standard deviation (st dev) of the 2-7 year band in overlapping 30-year windows (5-year step) (Chen et al., 2016); foraminferal $\delta^{18}O$ variance is determined using the $\delta^{18}O$ of single tests in each 1-cm stratum (Koutavas and Joanides, 2012). (B) The Lake Lanoto'o TOC record and $\delta^{2}H_{C26}$ record (C), and Lake Teroto Ca/Ti (D) and $\delta^{2}H_{C26}$ record (E) from this study. The black line on (D) indicates LOESS smoothing of the Lake Teroto Ca/Ti values (sampling proportion 0.01, polynomial degree of 1). The seasonal SST range variance (F) (as % difference from modern (0-60 yr BP) and skewness (G) with 1σ uncertainty on the Peruvian coast calculated from monthly molluscan shell $\delta^{18}O$ measurements (Carré et al., 2014). Variance is determined to be ENSO-driven and skewness to indicate the relative contribution of Central Pacific El Niños (CPE) and Eastern Pacific El Niños (Carré et al., 2014). (H) Residual $\delta^{13}C$ values from Rano Aroi, Easter Island, caused by changes in humidity and determined not to relate to long-term C_4-C_3 vegetation changes (Margalef et al., 2013); El Junco, Galápagos, botryococcene concentration (bot conc) (I) and $\delta^{2}H$ ($\delta^{2}H_{bot}$) (J), the former interpreted to indicate El Niño frequency and the latter to indicate the El Niño amplitude (Atwood and Sachs, 2014; Zhang et al., 2014). Added are hypothesised phases of El Niño flavour dominance: EPE (red), CPE (yellow), transition periods from one flavour to another (orange), and the 8.2 ka event (blue). The timings of human colonisation are highlighted with grey bars. This figure is modified from Chen et al. (2016).

Chapter 10: Conclusion

This study set out with the aims to:

1. Determine the feasibility of reconstructing long-term climate records from terrestrial/limnic proxies in the southwest Pacific; and
2. Dependent upon 1) assess the precipitation history in light of the SPCZ and broader patterns of internal variability in the Pacific basin over millennial timescales.

The results of this study have shown that the Lake Teroto, Atiu, Cook Islands, and Lake Lanoto'o, Samoa, records provide vital additions not only to the data-poor southwest Pacific but to the tropical Pacific region as a whole. In Lake Teroto the continuous laminations, and the hypothesised genesis of these, suggest that the record may preserve an annual record. Further in comparison to other laminated records from the tropical Pacific the $CaSO_4$ that comprises these laminations is likely unique. The Lake Lanoto'o record is a fairly simple one: increase in precipitation leads to an increase in terrestrial inwash that dilutes the organic component. Both sites have proven to be powerful records for understanding not only past changes in SPCZ location but also for understanding changes in ENSO over the Holocene.

A number of conclusions have been drawn throughout this thesis. With this in mind this chapter will first summarise the main findings obtained from a review of the literature, with this being a first for this region. After this the conclusions drawn from the modern data will be outlined. Following this the principal conclusions relating to this investigation into Pacific palaeoclimate will be delineated. The second section of this chapter will use the main research conclusions to evaluate the limitations of this research and identify future research that could be undertaken.

10.1 Main findings

10.1.1 Regional palaeoclimatic record for the southwest Pacific

- Whilst there are a variety of continuous Holocene-length records from around the Pacific basin, there are only a few from the tropical Pacific. Despite this lack of

continuous records this thesis has undertaken the first comprehensive review of literature from this region. Due to the majority of records having greater-than-decadal chronological resolution the changes in ENSO, typically termed either ENSO variability or ENSO activity in the literature (Cobb *et al*., 2013; Atwood and Sachs, 2014; Zhang *et al*. 2014; Emile-Geay *et al*., 2016), have been framed in the context of the IPO to facilitate comparison at the interdecadal, and greater, timescale. It is suggested that in future unless a record has subdecadal chronological resolution changes should be framed in the context of IPO phase rather than ENSO.

- A generally consistent sequence of changes has occurred in the tropical Pacific according to the literature: an early Holocene (ca. 11,600-6,000 cal yr BP) dominated by positive-phase IPO; a mid-Holocene (ca. 6,000-3,000 cal yr BP) dominated by negative-phase IPO, and a late Holocene (3,000 cal yr BP to present) dominated by positive-phase IPO. This is further refined using the sites in this study and outlined in section 9.4.2**.** The mid-Holocene is often cited as a period with reduced ENSO variability (Conroy *et al*., 2008; Koutavas and Joanides, 2012; McGregor *et al*., 2013; Carré *et al*., 2014; Zhang *et al*., 2014; Emile-Geay *et al*., 2016; Chen *et al*., 2016) – a review of the literature highlighted that the timing and nature of this reduction in ENSO variability has not been properly constrained.

10.1.2 Modern climatic and catchment data

- Reviewing the precipitation data and climatic indices for Samoa and the Cook Islands highlighted the lack of continuous precipitation isotope data for these sites inhibiting a thorough understanding of isotopic precipitation changes in relation to climate indices –specifically the SPCZI (Salinger *et al*., 2014), but also the IPO TPI (Hendy *et al*., 2015) and the Niño indices. In comparison to precipitation amount the precipitation isotopic data indicated that the amount effect is the principal control on precipitation isotope values (Dansgaard, 1964). It is suggested that with the precipitation isotope values reflecting the precipitation amount the δ^2H_{C26} data from Lake Teroto and Lake Lanoto'o can be used to qualitatively investigate past changes in precipitation amount. The precipitation data over the instrumental period indicated that both sites will only conclusively show SPCZ movements when the IPO is in positive phase and El Niño are operating at the

same time. However, the Lake Teroto geochemical record disagrees with this and shows that Lake Teroto is sensitive to both CPE and EPE (section 6.4.2), whereas the Lake Lanoto'o geochemical record shows it is sensitive to EPE.

- Lake Teroto and Lake Lanoto'o respond differently to increases and decreases in precipitation amount. Both sites show an increase (decrease) in Ti as a result of increased (decreased) precipitation amount relating to SPCZ movement, which in turn have been related to El Niño and by extension IPO state (Trenberth, 1976; Folland *et al*., 2002). During drier conditions it is suggested that the evaporative lowering of the lake level in Lake Teroto causes Ca and S to increase in concentration to the extent they precipitate out in the form of gypsum, as indicated by concurrent changes in Ca/Ti and S/Ti. In Lake Lanoto'o drier periods are represented by an increase in TOC and Br concluded to be a result of decreased siliciclastic input.

10.1.3 SPCZ movement over the Holocene

- Comparison of the Lake Teroto and Lake Lanoto'o record indicated that the SPCZ has shifted position over centennial timescales – the first time that this has been shown. It is suggested that the SPCZ has shifted to a different average position over millennial timescales: specifically between ca. 5,600 and 4,000 cal yr BP when it is inferred the SPCZ had expanded and/or migrated SE.
- SPCZ movement is interpreted to be a consequence of changes in IPO state for most of this time; however the high variability in δ^2H_{C26} values between ca. 4,000-2,700 cal yr BP is suggested to relate to either an increased meridional SST gradient and/or ENSO controlling SPCZ position (Mantsis *et al*., 2013; Saint-Lu *et al*., 2015).
- The Ti and δ^2H_{C26} record from Lake Lanoto'o indicates the 8.2 ka event is expressed in the tropical southwest Pacific as SPCZ expansion and/or migration SW. This result corroborates an expression of the 8.2 ka event in the equatorial east Pacific (Atwood, 2015) and a potential expression in Borneo (Chen *et al*., 2016).

10.1.4 Holocene changes in ENSO

- When compared to records of ENSO over the last 3,000 cal yr BP it is determined that there is a strong relationship between Lake Lanoto'o and El Junco, Galápagos (Zhang *et al*., 2014). Moreover Yamoah *et al*. (2016a) suggested that using records from the Indo-Pacific to reconstruct ENSO may be flawed due to strong El Niños potentially resulting in positive precipitation anomalies akin to La Niña. The Lake Lanoto'o record suggests that this is the case and that records from the Indo-Pacific should be used with caution to reconstruct past changes in ENSO. The Lake Teroto record indicated that it is sensitive to both EPE and CPE over millennial timescales akin to its geochemical record over the instrumental period (AD 1899-2012), rather than just EPE in positive-phase IPO as indicated in the instrumental data.
- The Lake Teroto and Lake Lanoto'o records in conjunction with other ENSO records from the tropical Pacific indicate key changes in ENSO over the Holocene: specifically a dominance of certain El Niño flavours. The most salient point is the timing and nature of the reduction in ENSO noted in a number of studies (Conroy *et al*., 2008; Koutavas and Joanides, 2012; McGregor *et al*., 2013; Carré *et al*., 2014; Zhang *et al*., 2014; Emile-Geay *et al*., 2016; Chen *et al*., 2016). This reduction is suggested to have begun with a transition from EPE to CPE conditions at 6,800-5,600 cal yr BP, after which CPE conditions dominated from 5,600-4,200 cal yr BP. This is the first time an estimate for the timing of this reduction in ENSO variability as well as the nature of it has been presented.

10.1.5 Human colonisation of Samoa and Atiu

- The Lake Teroto record indicates that human colonisation occurred at ca. 1,100 cal yr BP due to a range of geochemical proxies showing a coeval pronounced change. This is earlier than the colonisation of the Southern Cook Islands put forward by Wilmshurst *et al*. (2011) and is closer in agreement with the timing of human colonisation of Mangaia suggested by Kirch and Ellison (1994) and Chagué-Goff *et al*. (2016). The timing of human colonisation of Atiu and Mangaia lends itself to the hypothesis that there was a gradual 'leakage' of humans from western to eastern Polynesia.

- The timing of human colonisation on Samoa, Atiu and the Southern Cook Islands occurs during EPE dominated conditions or during transition periods from CPE to EPE dominated conditions. This may suggest a potential climatic driving mechanism for human expansion in Polynesia from west to east.

10.2 Recommendations for future research

- Understanding the changes in carbon source in the two lakes has been restricted by the lack of palaeoecological data obtained in this study. Lake Lanoto'o indicates that shifts in algal communities control the changes in δ^2H_{C16} and δ^2H_{C18} values – is this due to one particular community of algae, or due to changes in species dominance within an algal community? Future studies may wish to undertake palaeoecological investigations into the two sites – be this an examination of diatoms, chironomids, or pigments – to better understand the lacustrine processes. This would provide a more detailed interpretation of how changes in climate influence the lake-catchment system, reducing the potential for erroneous climate interpretations from the lacustrine records.
- The laminations in the Lake Teroto record may be deposited annually. Further work on ascertaining whether these laminations are annually deposited, and if so whether these annually laminations are continuous or discontinuous, would potentially allow for changes in ENSO and the SPCZ over the Holocene to be examined in detail and provide a greater insight into Pacific climate in a data-poor region.
- Whilst this study has provided the first record of SPCZ movement over the last ca. 9,500 cal yr BP it is only a qualitative assessment and interpreted shifts in SPCZ position are not specific. A network of long, continuous records from locales whose precipitation is primarily controlled by the SPCZ is required to better constrain its movement and understand how it has operated over the Holocene. Further the high variability in its position from ca. 4,000-2,700 cal yr BP needs to be explored with records that have an annual chronological resolution to better contextualise how variable the SPCZ was. Key to all of this is drivers of SPCZ movement: it has been interpreted here that changes in ENSO and the IPO are the primary controls; however enhanced meridional SST gradients between ca. 6,000-

4,000 cal yr BP may have influenced the location of the SPCZ (Mantsis *et al*., 2013; Saint-Lu *et al*., 2015). Are these valid interpretations or are they too generalised? Future studies may choose to focus on what drives changes of SPCZ position over the Holocene and how variable its movement actually is.

- Whilst this study has provided estimates for the timing and nature of changes in ENSO over the last ca. 9,500 cal yr BP a conspicuous lack of driving mechanisms have been provided. Emile-Geay *et al*. (2016) argued that changes in ENSO variability do not have a simple relationship with orbital forcing and other factors are at play. Whilst most likely true, determining driving mechanisms for changes in ENSO from coral records is inherently flawed due to their short (ca. 100 yr), discontinuous nature. Long, continuous, high chronological resolution (annual) records from the tropical Pacific are required to better understand the drivers of ENSO changes that can be compared with model outputs.
- Further, it is apparent that the palaeoclimatic modelling community are focussing on the wrong time period when looking at drivers of changes in the mid-Holocene reduction in ENSO. The majority have focussed on the ca. 6,000 cal yr BP period (for example Braconnot *et al*., 2007; Mantsis *et al*., 2013; An and Choi, 2014; Saint-Lu *et al*., 2015) which this study suggests is during a transition period from EPE to CPE conditions. Models need to be run for the ca. 5,000 cal yr BP period, when the majority of records are in agreement that ENSO variability was reduced and suggested in this study to be representative of CPE dominance.
- This study has invoked a dominance of CPE for various times during the Holocene: specifically between ca. 5,600-4,200 cal yr BP. To determine if this is a valid interpretation records are needed from the Niño4 region: the centre of action for CPE (Kao and Yu, 2009). At present none exist, and those records that purport to show shifts in CPE and EPE from the central equatorial Pacific over the Holocene are centred in the Niño3.4 region which is affected by both CPE and EPE (for example Cobb *et al*., 2003; 2013). In addition the network of records presented here indicates that changes in ENSO were broadly coeval. Isochronous markers, i.e. tephra, would allow for examination of leads and lags in ENSO changes across the tropical Pacific.
- With the identification of the 8.2 ka event in Lake Lanoto'o and El Junco it suggests that the Atlantic, at this point, is driving changes in the tropical Pacific.

However it is known that during the instrumental period impacts of ENSO can be observed globally (section 2.1.1). This leads to the question do changes in the tropical Pacific drive global changes in climate or do changes in the Atlantic cause changes in tropical Pacific climate? Are these mutually exclusive, or can the Pacific drive global climate changes at certain periods and the Atlantic drive changes in the Pacific at other times? Further research is required to better understand the relationship between the tropical Pacific and global climate.

The Pacific region as a whole, and more specifically the tropical Pacific, has not received as much attention in palaeoclimatic research in comparison with the Atlantic and northern hemisphere. Whilst efforts are ongoing to improve our understanding of this region, our understanding of past climatic changes in the tropical Pacific is severely lacking. This study has provided a vital contribution to our knowledge on tropical Pacific palaeoclimate, but has highlighted that further research is required to better understand both changes in the SPCZ and ENSO over the Holocene. It provides much needed information on changes in precipitation from the SPCZ that can be used to improve our understanding on changes in precipitation from this region (IPCC, 2014). Although somewhat parochial, simply obtaining more long, continuous records from the tropical Pacific and applying modern proxy techniques as undertaken in this thesis will provide vital palaeoclimatic information. This is necessary to gain a greater insight and understanding into the climate system that is needed for predicting how global warming will affect our planet and impact the small island communities in the Pacific region that are vulnerable not only to sea level rise, but also changes in potable water resources.

Appendix A

Table A1: Site IDs for Figure 2.20, Figure 2.21 and Figure 2.22 with their corresponding name, country and reference.

Site ID	Site	Country	Author
Pa1	Clear Lake	Palau	Richey and Sachs (2016)
Pa2	Ongeim l'Tketau	Palau	Smittenberg *et al*. (2011)
Pa3	Spooky Lake	Palau	Sachs *et al*. (2009)
Pa4	Ulong Channel	Palau	Osbourne *et al*. (2014)
Mi1	Fool Swamp	Yap, Micronesia	Dodson and Itoh (1999)
Mi2	Thool Swamp	Yap, Micronesia	Dodson and Itoh (1999)
P1	Koil Island and Muschu Island	Papua New Guinea	McGregor and Gagan (2004)
P2	Tari Basin	Papua New Guinea	Haberle (1998)
P3	Laing Island	Papua New Guinea	Tudhope *et al*. (1995)
P4	Madang Island	Papua New Guinea	Tudhope *et al*. (1995)
P5	Huon Peninsula	Papua New Guinea	McCulloch *et al*. (1996)
P6	New Ireland	Papua New Guinea	Alibert *et al*. (2008)
P7	Rabual	Papua New Guinea	Quinn *et al*. (2006)
P8	MW91-15	Papua New Guinea	Patrick and Thunnel (1997)
P9	ODP-806	Papua New Guinea	Stott *et al*. (2004)
S1	Lauhutu Swamp	Solomon Islands	Haberle (1996)
S2	Mela Swamp	Solomon Islands	Haberle (1996)
S3	Forestry Cave	Solomon Islands	Maupin *et al*. (2014)
Gu1	Double Reef	Guam, Micronesia	Asami *et al*. (2005)
Ko1	Kosrae	Kosrae, Micronesia	Ward (1988)
Na1	Nauru Island	Nauru	Guilderson and Schrag (1999)
NC1	Grand Lac	New Caledonia	Wirrmann *et al*. (2006)
NC2	Isle of Pines and Lifou Island	New Caledonia	Duprey *et al*. (2014)
NC3	Lac Saint Louis	New Caledonia	Stevenson (2004)
NC4	Plum Swamp	New Caledonia	Stevenson *et al*. (2001)
NC5	Plaine des Lacs	New Caledonia	McCoy *et al*. (1999)
NC6	Plaine des Lacs	New Caledonia	Hope and Pask (1998)
NC7	Lake Xere Wapo	New Caledonia	Stevenson *et al*. (2005, 2010)
NC8	New Caledonia Basin	New Caledonia	Mamo *et al*. (2013)
NC9	Amédée Island	New Caledonia	Crowley *et al*. (1997); Quinn *et al*. (1998); Delong *et al*. (2007, 2012, 2013)
NC10	Bay of Naia	New Caledonia	Lazareth *et al*. (2013)

Appendix A

Site ID	Site	Country	Author
NC11	Gouaro-Déva Sanctuary	New Caledonia	Wirrmann *et al*. (2011)
V1	Sabine Bank	Vanuatu	Gorman *et al*. (2012
V2	Espiritu Santo	Vanuatu	Kilbourne *et al*. (2004)
V3	Shokraon and Makué	Vanuatu	Duprey *et al*. (2014)
V4	Espiritu Santo	Vanuatu	Duprey *et al*. (2012)
V5	Espiritu Santo	Vanuatu	Beck *et al*. (1992, 1997); Corrège *et al*. (2000, 2004); Deng and Wei (2015)
V6	Espiritu Santo	Vanuatu	Partin *et al*. (2013)
V7	Anawau Swamp	Vanuatu	Hope and Sprigs (1982)
F1	Yasawa Island	Fiji	Le Bec *et al*. (2000)
F2	Yasawa Island	Fiji	Julliet-Leclerc *et al*. (2006)
F3	Fiji corals (Suvasavu Bay, Vanua Balavu, Aïwa Island)	Fiji	Bagnato *et al*. (2005); Linsley *et al*. (2004, 2006, 2008); Dassie *et al. (2014)*
F4	Fiji corals (Suvasavu Bay, Vanua Balavu, Aïwa Island)	Fiji	Dassie *et al. (2014)*
F5	Fiji archipelago (Lake Tagamaucia)	Fiji	Hope *et al*. (2009)
F6	Fiji archipelago (Navatu)	Fiji	Hope *et al*. (2009)
F7	Fiji archipelago (Wainisavulevu)	Fiji	Hope *et al*. (2009)
F8	Fiji archipelago (Bonatoa Swamp)	Fiji	Hope *et al*. (2009)
F9	Fiji archipelago (Meli Meli)	Fiji	Hope *et al*. (2009)
F10	Fiji archipelago (Vunimoli)	Fiji	Hope *et al*. (2009)
F11	Fiji archipelago (Doge Doge)	Fiji	Hope *et al*. (2009)
F12	Fiji archipelago (Voli Voli)	Fiji	Hope *et al*. (2009)
F13	Fiji archipelago (Nabuni)	Fiji	Hope *et al*. (2009)
F14	Fiji archipelago (Tagimaucia)	Fiji	Hope *et al*. (2009)
F15	Fiji archipelago (Yacata)	Fiji	Hope *et al*. (2009)
F16	Fiji archipelago (Mudflats)	Fiji	Hope *et al*. (2009)
F17	Fiji archipelago (Cavaure)	Fiji	Hope *et al*. (2009)
F18	Fiji archipelago (Nabuni)	Fiji	Hope *et al*. (2009)
F19	Fiji archipelago (Totoya)	Fiji	Hope *et al*. (2009)
T1	Ha'afera	Tonga	Wu *et al*. (2013)
T2	Tonga corals (Ha'afera, Malinoa, Nomuka Iki)	Tonga	Linsley *et al*. (2008)
Ni1	Avaika Cave	Niue	Rasbury and Aharon (2006)
C1	Rarotonga	Cook Islands	Linsley *et al*. (2000, 2004, 2006)
C2	Rarotonga	Cook Islands	Ren *et al*. (2000)
C3	Karekare Swamp	Cook Islands	Fujiki *et al*. (2014)

Site ID	Site	Country	Author
C4	Mangaia	Cook Islands	Ellison (1994)
C5	Lake Tiriara	Cook Islands	Chagué-Goff *et al*. (2016)
C6	Mangaia	Cook Islands	Kirch and Ellison (1994)
K1	Palmyra Atoll	Kiribati	Cobb *et al*. (2003)
K2	Washington Island	Kiribati	Sachs *et al*. (2009)
K3	Fanning Island	Kiribati	Cobb *et al*. (2013)
K4	Christmas Island	Kiribati	Cobb *et al*. (2013)
K5	Kiritimati	Kiribati	Evans *et al*. (1999)
K6	Kiritimati	Kiribati	McGregor *et al*. (2013)
K7	Palmyra Atoll	Kiribati	Nurhati *et al*. (2009)
K8	Christmas Island	Kiribati	Woodroffe and Beech (2000)
K9	Christmas Island	Kiribati	Sachs *et al*. (2009)
K10	Clipperton Atoll	Kiribati	Wu *et al*. (2014)
K11	Tarawa Atoll	Kiribati	Cole and Fairbanks (1990)
K12	Maiana	Kiribati	Urban *et al*. (2000)
H1	Wai'ānapanapa	Hawai'i	Crausby *et al*. (2014)
H2	Flat Top Bog	Hawai'i	Burney *et al*. (1995)
FP1	Mo'orea Lagoon	French Polynesia	Boiseau *et al*. (1998)
FP2	Apu Bay	French Polynesia	Toomey *et al*. (2003)
FP3	Apu Bay	French Polynesia	Toomey *et al*. (20016)
FP4	Lake Vaihara	French Polynesia	Parkes *et al*. (1992)
FP5	Mo'orea	French Polynesia	Kahn *et al*. (2014)
FP6	Tōvi'i Plateau	French Polynesia	Allen *et al*. (2011)
E1	Rano Aroi	Easter Island	Margalef *et al*. (2013, 2014); Horrocks *et al*. (2015); Rull *et al*. (2015)
E2	Rano Raraku	Easter Island	Dumont *et al*. (1998); Mann *et al*. (2008); Saez *et al.* (2009); Cañellas-Bolta (2012, 2016)
E3	Rano Kao	Easter Island	Flenley *et al*. (1984)
Ga1	Isabella Island	Galápagos Islands	Druffel *et al*. (2015)
Ga2	Genesova Crater Lake	Galápagos Islands	Conroy *et al*. (2014)
Ga3	El Junco	Galápagos Islands	Conroy *et al*. (2008); Conroy *et al*. (2009); Restrepo *et al*. (2012) Atwood and Sachs (2014); Zhang *et al*. (2014)
Ga4	KNR195-5	Galápagos Islands	Rustic *et al*. (2015)
Ga5	V21-30	Galápagos Islands	Koutavas *et al*. (2002, 2006); Koutavas and Joanides (2012)

Appendix A

Site ID	Site	Country	Author
Ga6	CD38-17P	Galápagos Islands	Sadekov *et al*. (2012
Ga7	Bainbridge Crater Lake	Galápagos Islands	Riedenger *et al*. (2002); Bryksina and Last (2005)
Ga8	Poza de las Diablas	Galápagos Islands	Nelson and Sachs (2016)
Ga9	Poza de las Verdes	Galápagos Islands	Nelson and Sachs (2016)
Ga10	Poza de las Escondida	Galápagos Islands	Nelson and Sachs (2016)
Ga11	Urvina Bay	Galápagos Islands	Dunbar *et al*. (1994)

Appendix B

Table B1: XRD results for discrete samples from Lake Teroto. Analyses undertaken at the National Oceanography Centre, Southampton.

	Sample				
Mineral (%)	**T-U2 15-16cm**	**T1-2 18-19cm**	**T1-3 68-69cm**	**T2-7 56-57cm**	**T1-8 74-75cm**
Gypsum	0	7.4±0.4	8.1±0.3	0	13.5±0.4
Halite	5.4±0.2	2.2±0.2	2.5±0.2	14.1±0.3	7.2±0.2
Kaolinite	60.5±0.9	39±0.6	42.4±0.8	27.4±0.8	19.1±1.2
Jarosite	0	4.6±0.2	4.6±0.2	6.4±0.3	4.1±0.3
Pyrite	31.7±0.5	10.4±0.2	12.9±0.2	10±0.2	16.1±0.3
Amorphous content	2.4±2.4	36.3±1.4	29.4±1.7	42±1.5	40±1.9
Chi-squared	8.43	7.51	9.62	7.65	5.9
r-value	0.574	0.57	0.581	0.609	0.585
Sample characteristic	Clay layer; peak in Ti, Si, Sr	Peak in Ca, S and Sr	Peak in Ca and S	Peak in Fe, Mn, Ti, and Sr	Clay layer; peak in Ti, Si, and Al.

Appendix C

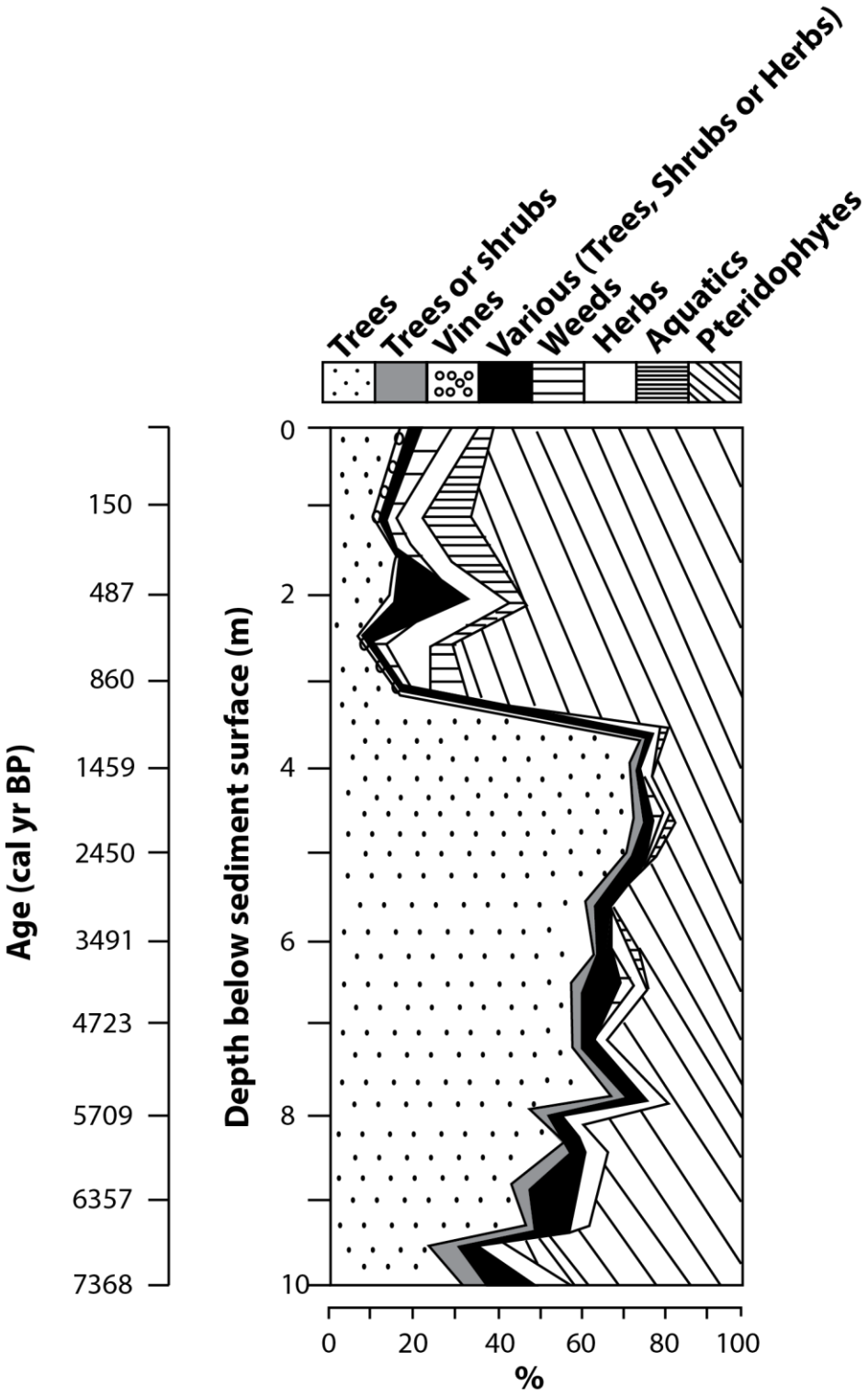

Figure C1: Percentage summary diagram of vegetation types from Lake Teroto. Ages are interpolated from Parkes (1994) and calibrated using BACON v2.2 (Blaauw and Christen, 2011) utilising SHCal13 for southern-hemisphere-specific calibration data (Hogg *et al*., 2013). Figure adapted from Parkes (1994).

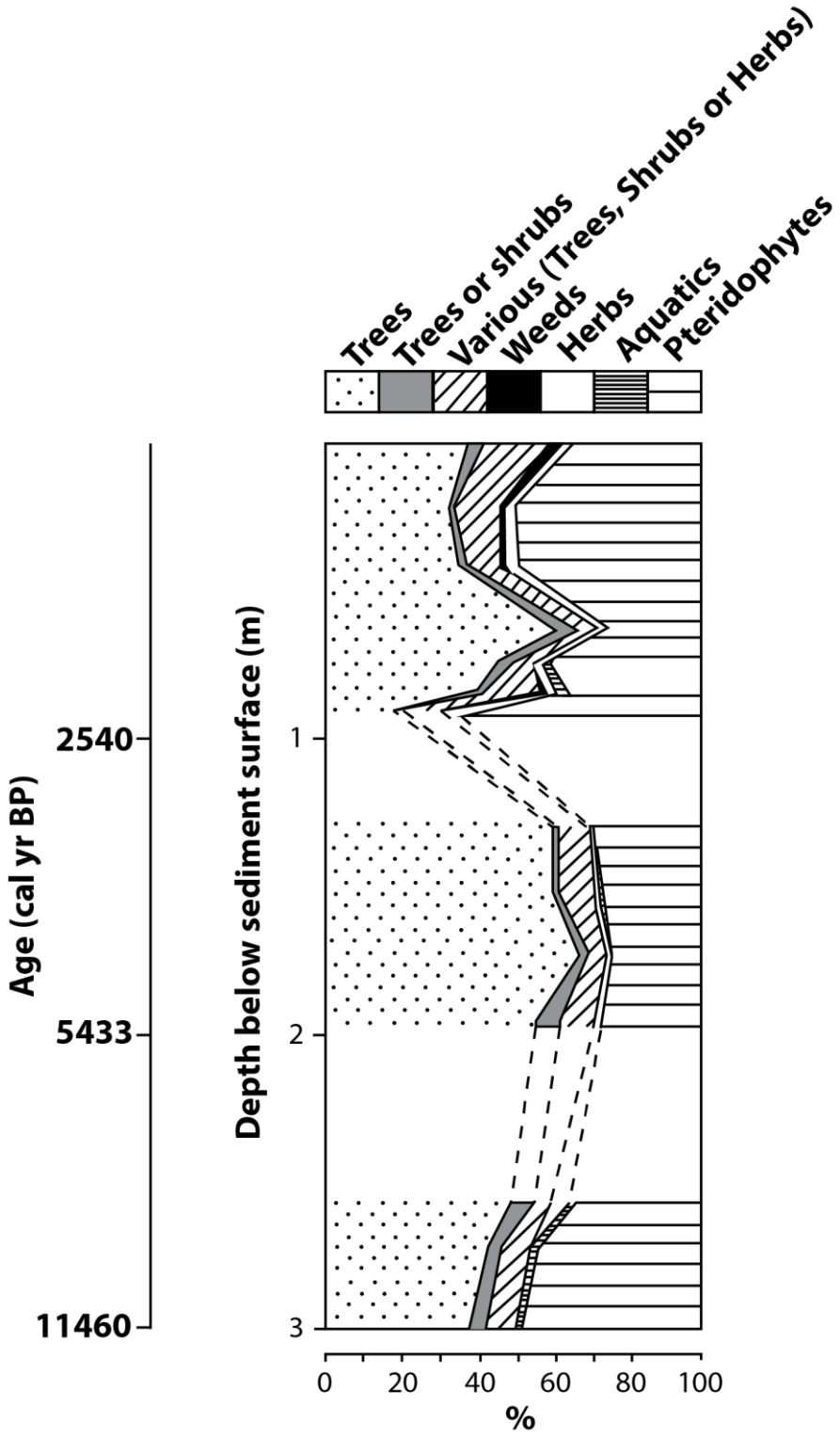

Figure C2: Percentage summary diagram of vegetation types from Lake Lanoto'o. Ages are interpolated from Parkes (1994) and calibrated using BACON v2.2 (Blaauw and Christen, 2011) utilising SHCal13 for southern-hemisphere-specific calibration data (Hogg et al., 2013). Figure adapted from Parkes (1994).

Bibliography

Abril, J. M., Garía-León, M., García-Tenorio, R., Sánchez, C. I., and El-Daoushy, F. (1992) 'Dating of marine sediments by an incomplete mixing model.' *Journal of Environmental Radioactivity*, **15**, 135-151.

Abril, J. M. (2004) 'Constraints on the use of ^{137}Cs as a time-marker to support CRS and SIT chronologies.' *Environmental Pollution*, **129**, 31-37.

Aichner, B., Wilkes, H., Herzschuh, U., Mischke, S. and Zhang, C. (2010) 'Biomarker and compound-specific $\delta^{13}C$ evidence for changing environmental conditions and carbon limitation at Lake Koucha, eastern Tibetan Plateau.' *Journal of Paleolimnology*, **43**, 873-899.

Alexander, M. A. (1992) 'Midlatitude atmosphere-ocean interaction during El Niño. Part I: The North Pacific Ocean.' *Journal of Climate*, **5**, 944-958.

Alexander, M. A. (2010) 'Extratropical air-sea interaction, sea surface temperature variability, and the Pacific Decadal Oscillation.' In: Sun, D. –Z. and Bryan, F. (Eds.) *Climate Dynamics: Why does climate vary?* Washington D.C.: American Geophysical Union, pp.123-148.

Alexander, M. A., Bladé, I., Newman, M., Lanzante, J. R., Lau, N. –C. and Scott, J. D. (2002) 'The atmospheric bridge: the influence of ENSO teleconnections on air-sea interaction over the global oceans.' *Journal of Climate*, **15**, 2205-2231.

Alexander, M. A. and Scott, J. D. (2008) 'The role of Ekman ocean heat transport in the Northern Hemisphere response to ENSO.' *Journal of Climate*, **21**, 5688-5707.

Allen, E.D. and Spence D.H.N. (1981) 'The differential ability of aquatic plants to utilize the inorganic carbon supply in fresh water.' *New Phytologist*, **87**, 269–283.

Allen, M. S., Butler, K., Flenley, J. and Horrocks, M. (2011) 'New pollen, sedimentary and radiocarbon records from Marquesas Islands, East Polynesia: Implications for archaeological and palaeoclimate studies' *The Holocene*, **2**, 473-484.

Allen, M. S. and Wallace, R. (2007) 'New evidence from the east Polynesia Gateway: substantive and methodological results from Aitutaki, Southern Cook Islands.' *Radiocarbon*, **49**, 1163-1179.

Alley, R. B., Mayewski, P. A., Sowers, T., Stuiver, M., Taylor, K., C. and Clark, P. U. (1997) 'Holocene climatic instability: a prominent, widespread event 8200 yr ago.' *Geology*, **25**, 483-486.

An, S. –I. and Choi, J. (2014) 'Mid-Holocene tropical Pacific climate state, annual cycle, and ENSO in PMIP2 and PMIP3.' *Climate Dynamics*, **43**, 957-970.

An, S.-I and Jin, F.-F. (2004) 'Nonlinearity and asymmetry of ENSO.' *Journal of Climate*, **17**, 2399-2412.

Anderson, A. (1995) 'Current approaches in East Polynesian colonisation research.' *The Journal of the Polynesian Society*, **104**, 110-132.

Anderson, A., Chappell, J., Gagan, M. and Grover, R. (2006) 'Prehistoric maritime migration in the Pacific islands: an hypothesis of ENSO forcing.' *The Holocene*, **16**, 1-6.

Appleby, P. G. (2001) 'Chronostratigraphic techniques in recent sediments.' In Last, W. M. and Smol, J. P. (Eds.) *Tracking Environmental Change Using Lake Sediments*, Dordrecht: Kluwer Academic Publishers, pp. 171-203.

Appleby, P. G. and Oldfield, F. (1978) 'The calculation of lead-210 dates assuming a constant rate of supply of unsupported ^{210}Pb to the sediment.' *Catena*, **5**, 1-8.

Asami, R., Yamada, T., Iryu, Y, Quinn, T. M., Meyer, C. P. and Paulay, G. (2005) 'Interannual and decadal variability of the western Pacific sea surface conditions for the years 1787-2000: reconstructions based on stable isotope record from a Guam coral.' *Journal of Geophysical Research: Oceans*, **110**, 1-11.

Ashok, K., Behera, S. K., Rao, S. A., Weng, H. and Yamagata, T. (2007) 'El Niño Modoki and its possible teleconnection.' *Journal of Geophysical Research: Oceans*, **112**, 1-27.

Atwood, A. R. and Sachs, J. P. (2014) 'Separating ITCZ- and ENSO-related rainfall changes in the Galápagos over the last 3 kyr using D/H ratios of multiple lipid biomarkers.' *Earth and Planetary Science Letters*, **404**, 408-419.

Australian Bureau of Meteorology and CSIRO (2011) Climate change in the Pacific: scientific assessment and new research. Volume 1: regional overview. Volume 2: country reports. Hennessy K, Power S and Cambers G (Scientific Editors) from Salinger et al 2014).

Bagnato, S., Linsley, B. K., Howe, S. S., Wellington, G. M. and Salinger, J. (2005) 'Coral oxygen isotope records of interdecadal climate variations in the South Pacific Convergence Zone.' *Geochemistry, Geophysics, Geosystems*, **6**, 1-8.

Baker, J. R. (1929) 'The Northern New Hebrides.' *Geographical Journal*, **73**, 305-325.

Balascio, N. L., Francus, P., Bradley, R. S., Schupack, B. B., Miller, G. H., Kvisvik, B. C., Bakke, J. and Thordarson, T. (2015) 'Investigating the use of scanning X-ray fluorescence to locate cryptotephra in minerogenic lacustrine sediment: experimental results.' In Croudace, I. W. and Rothwell, R. G. (Eds.) *Micro-XRF studies of sediment cores*. London: Springer, pp. 305-324.

Ball, D. (1964) 'Loss-on-ignition as an estimate of organic matter and organic carbon in non-calcareous soils.' *Journal of Soil Science*, **15**, 84-92.

Barber, D. C., Dyke, A., Hillaire-Marcel, C., Jennings, A. E., Andrews, J. T., Kerwin, M. W., Bilodeau, G., McNeely, R., Southon, J., Morehead, M. D. and Gagnon, J. M. (1999) 'Forcing of the cold event of 8,200 years ago by catastrophic drainage of Laurentide lakes.' *Nature*, **400**, 344-348.

Barron, J. A. and Anderson, L. (2011) 'Enhanced Late Holocene ENSO/PDO expression along the margins of the eastern North Pacific.' *Quaternary International*, **235**, 3-12.

Beck, J. W., Edwards, R. L., Ito, E., Taylor, F. W., Récy, J., Rougerie, F., Joannot, P. and Henin, C. (1992) 'Sea-surface temperature from coral skeletal strontium/calcium ratios.' *Science*, **257**, 644-647.

Beck, J. W., Récy, J., Taylor, F., Edwards, R. L and Cabioch, G. (1997) 'Abrupt changes in early Holocene tropical sea surface temperature derived from coral records.' *Nature*, **385**, 705-707.

Bengtsson, L. & M. Enell, 1986. Chemical analysis. In Berglund, B. E. (Ed.) *Handbook of Holocene Palaeoecology and Palaeohydrology.* Chichester: John Wiley & Sons Ltd., pp. 423–451.

Berkeley Earth (2016) *Berkeley Earth Data*. [Online] Available from: http://berkeleyearth.org/data/ [Accessed: 8th December 2016].

Berntsson, A., Rosqvist, G. C. and Velle, G. (2014) 'Late-Holocene temperature and precipitation changes in Vindelfjällen, mid-western Swedish Lapland, inferred from chironomid and geochemical data.' *Holocene*, **24**, 78-92.

Best, E. P. H., Dassen, J. H. A. , Boon, J. J., and Wiegers, G. (1990). 'Studies on decomposition of *Ceratophyllum demersum* litter under laboratory and field conditions: losses of dry mass and nutrients, qualitative changes in organic compounds and consequences for ambient water and sediments.' *Hydrobiologia*, **194**, 91-114.

Bianchi, T. S. and Canuel, E. A. (2011) *Chemical Biomarkers in Aquatic Systems*. Princeton: Princeton University Press, pp. 417.

Biondi, F., Gershunoc, A. and Cayan, D. R. (2001) 'North Pacific Decadal climate variability since 1661.' *Journal of Climate*, **14**. 5-10.

Bird, B. W., Abbott, M. B., Robdell, D. T. and Vuille, M. (2011) 'Holocene tropical South American hydroclimate revealed from a decadal resolved lake sediment $\delta^{18}O$ record.' *Earth and Planetary Science Letters*, **310**, 192-202.

Bishop, T. H. (2015) *A palaeolimnological investigation of central Patagonian climate during the Holocene*. Unpublished PhD thesis. University of Southampton.

Bjerknes, J. (1966) 'A possible response of the atmospheric Hadley circulation to equatorial anomalies of ocean temperature.' *Tellus*, **18**, 820-829.

Bjerknes, J. (1969) 'Atmospheric teleconnections from the equatorial Pacific.' *Monthly Weather Review*, **97**, 163-172.

Blackmon, M. L., Geisler, J. E. and Pitcher, E. J. (1983) 'A general circulation model study of January climate anomaly patterns associated with interannual variation of equatorial Pacific sea surface temperatures.' *Journal of the Atmospheric Sciences*, **40**, 1410-1425.

Blaauw, M. and Christen, J. A. (2011) 'Flexible paleoclimate age-depth models using an autoregressive gamma process.' *Bayesian Analysis*, **6**, 457-474.F

Boiseau, M., Juillet-Leclerc, A., Yiou, P, Salvat, B., Isdale, P. and Guillaume, M. (1998) 'Atmopsheric and oceanic evidences of the El Niño-Southern Oscillation events in the south central Pacific Ocean from coral stable isotope records over the last 137 years.' *Paleoceanography*, **13**, 671-685.

Böning, P., Bard, E. and Rose, J. (2007) 'Toward direct, micro-scale XRF elemental maps and quantitative profles of wet marine sediments.' *Geochemistry, Geophysic, Geosystems*, **8**, doi: 10.1029/2006GC001480.

Borlace, S., Cai, W. J. and Santoso, A. (2013) 'Multidecadal ENSO amplitude variability in a 1000-yr simulation of a coupled global climate model: implications for observed ENSO variability.' *Journal of Climate*, **26**, 9399-9407.

Borlace, S., Santoso, A., Cai, W. J., and Collins, M. (2014) 'Extreme swings of the South Pacific Convergence Zone and the different types of El Niño events.' *Geophysical Research Letters*, **41**, 4695-4703.

Boutton, T. (1991) Stable carbon isotope ratios of natural materials: II. Atmopsheric, terrestrial, marine, and freshwater environments. In Coleman, D. C. and Fry, B. (Eds.) *Carbon Isotope Techniques*. USA: Academic Press, pp. 173-186.

Bowen, G. J. and Revenaugh, J. (2003). 'Interpolating the isotopic composition of modern meteoric precipitation.' *Water Resources Research*, **39**, 9-13.

Bowman, S. (1995) *Radiocarbon Dating*, Great Britain: University of California Press, pp. 64.

Boyle, J. F. Chiverrell, R. C. and Schillereff, D. (2015) 'Approaches to water content correction and calibration for µXRF core scanning: comparing X-ray scattering with simple regression of elemental concentrations.' In Croudace, I. W. and Rothwell, R. G. (Eds.) *Micro-XRF studies of sediment cores*. London: Springer, pp. 373-392.

Braconnot, P., Luan, Y., Brewer, S. and Zheng, W. (2012) 'Impact of Earth's orbit and freshwater fluxes on Holocene climate mean seasonal cycle and ENSO characteristics.' *Climate Dynamics*, **38**, 1081-1092.

Braconnot, P., Otto-Bliesner, B., Harrison, S., Joussaume, S., Peterchmitt, J. Y., Abe-Ouchi, A., Crucifix, M., Driesschaert, E., Fichefet, T., Hewitt, C. D., Kageyama, M., Kitoh, A., Laîné, A., Loutre, M. F., Marti, O., Merkel, U., Ramstein, G., Valdes, G., Weber, S. L., Yu, Y. and Zhao, Y. (2007) 'Results of the PMIP2 coupled simulations of the Mid-Holocene and Last Glacial Maximum – Part 1: experiments and large-scale features.' *Climate of the Past*, **3**, 261-277.

Bradley, R. S., Diaz, H. F., Kiladis, G. N. and Eischeid, J. K. (1987) 'ENSO signal in continental temperature records.' *Nature*, **327**, 497-501.

Bronk Ramsey, C., Staff, R. A., Bryant, C. L., Brock, F., Kitagawa, H., can der Plicht, J., Schlolaut, G., Marshall, M. H., Brauer, A., Lamb, H. F., Payne, R. L., Tarasov, P. E., Haraguchi, T., Gotanda, K., Yonebobu, H., Yokoyama, Y., Tada, R. and Nakagawa, T. (2012) 'A complete terrestrial radiocarbon record for 11.2 to 52.8 kyr B.P.' *Science*, **338**, 370-374.

Brown, J. N., Matear, R. J., Brown, J. R. and Katzfey, J. (2015) 'Precipitation projections in the tropical Pacific are sensitive to different types of SST bias adjustment.' *Geophysical Research Letters*, **42**, 1-11.

Brown, J. R., Moise, A. F. and Colman, R. A. (2013) 'The South Pacific Convergence Zone in CMIP5 model simulations of historical and future climate.' *Climate Dynamics*, **41**, 2179-2197.

Bryksina, N. A. and Last, W. M. (2005) 'Fractal analysis of the gray-scale intensity data of finely laminated sediments from Bainbridge Crater Lake, Galápagos.' *Mathematical Geology*, **37**, 327-336.

Bureau of Meteology (2015) *Pacific Climate Change Data Portal*. [Online] Available from: http://www.bom.gov.au/climate/pccsp/?zoom=7&lat=-13.75905&lon=187.8954&layers=B00TTTTT [Accessed: 6th December 2015]

Burley, D. V. and Clark, J. T. (2003) 'The archaeology of Fiji/Western Polynesia in the post-Lapita era.' In Sand, C. (Ed.) *Pacific Archaeology: Assessments and Prospects*. New Caledonia: New Caledonia Museum, pp.396.

Cai, W. and Cowan, T. (2009) 'La Niña Modoki impacts Australian autumn rainfall variability.' *Geophysical Research Letters*, **36**, 1-4.

Cai, W. J., Borlace, S., Lengaigne, M., van Rensch, P., Collins, M., Vecchi, G., Timmermann, A., Santoso, A., McPhaden, M. J., Wu, L. X., England, M. H., Wang, G. J., Guilyardi, E. and Jin, F. F. (2014) 'Increasing frequency of extreme El Niño events due to greenhouse warming.' *Nature Climate Change*, **4**, 111-116.

Cai, W., Lengaigne, M., Borlace, S., Collins, M., Cowan, T., McPhaden, M. J., Timmermann, A., Power, S., Brown, J., Menkes, C., Ngari, A., Vincent, E. M. and Widlanksy, M. J. (2012) 'More extreme swings of the South Pacific Convergence Zone due to greenhouse wrming.' *Nature*, **488**, 365-369.

Cai, W., Wang, G., Santoso, A., McPhaden, M. J., Wu, L., Jin, F-.F., Timmermann, A., Collins, M., Vecchi, G., Lengaigne, M., England, M. H., Dommenget, D., Takahashi, K. and Guilyardi, E. (2015) 'Increased frequency of extreme La Niña events under greenhouse warming.' *Nature Climate Change*, **5**, 132-137.

Campbell, I. B., Claridge, G. G. C. and Blamkemore, L. C. (1978) 'Pedological study of soils from basaltic parent material on the island of Atiu, Cook Islands.' *New Zealand Journal of Science*, **21**, 229-248.

Campbell, I. B., Wilde, R. H., Wilson, A. D., Frisby, R. H., McCormack, D. D. (1982). *Soils of Atiu, Cook Islands*. New Zealand Soil Bureau, Department of Scientific and Industrial ResearchNew Zealand Soil Bureau, Department of Scientific and Industrial Research.

Cane, M. A. (1998) 'A role for the tropical Pacific.' *Science*, **282**, 59-61.

Cane, M. A. (2005) 'The evolution of El Niño, past and future.' *Easrth and Palnetary Science Letters*, **230**, 227-240.

Cane, M. A. and Zebiak, S. E. (1985) 'A theory for El Niño and the Southern Oscillation.' *Science*, **228**, 1085-1087.

Cañellas-Boltà, N., Rull, V., Sáez, A., Margalef, O., Giralt, S., Pueyo, J. J., Birks, H. H., Birks, H. J. B. and Pla-Rabes, S. (2012) 'Macrofossils in Raraku Lake (Easter Island) integrated with sedimentary and geochemical records: towards a palaeoecological synthesis for the last 34,000 years.' *Quaternary Science Reviews,* **34**, 113-126.

Cañellas-Boltà, N., Rull, V., Sáez, A., Margalef, O., Pla-Rabes, S., Valero-Garcés, B. and Giralt, S. (2016) 'Vegetation dynamics at Raraku Lake catchment (Easter Island) during the past 34,000 years.' *Palaeogeography, Palaeoclimatology, Palaeoecology*, **446**, 55-69.

Capotondi, A., Wittenberg, A. T., Mewman, M., Di Lorenzo, E., Yu, J-. Y., Braconnot, P., Cole, J., Dewitte, B., Giese, B., Guilyardi, E., Jin, F-.F., Karnauskas, K., Kirtman, B., Lee, T., Schneider, N., Xue, Y. and Yeh, S-.W. (2015) 'Understanding ENSO diversity.' *Bulletin of the American Meteorological Society*, **96**, 921-938.

Carré, M., Sachs, J. P., Purca, S., Schauer, A. J., Braconnot, P., Falcón, R. A., Julien, M.and Lavallée, D. (2014) 'Holocene history of ENSO variance and asymmetry in the eastern tropical Pacific.' *Science*, **345**, 1045-1048.

Carroll, J. and Lerche, I. (2003) *Sedimentary Processes: Quantification Using Radionuclides*, London: Elsevier, pp. 282.

Castañeda, I. S. and Shouten, S. (2011) 'A review of molecular organic proxies for examining modern and ancient lacustrine sediment.' *Quaternary Science Reviews*, **30**, 2851-2891.

Castañeda, I. S., Werne, J. P. and Johnson, T. C. (2007) 'Wet and arid phases in the southeast African tropics since the Last Glacial Maximum.' *Geology*, **35**, 823-826.

Castañeda, I. S., Werne, J. P. and Johnson, T. C. (2009a) 'Influence of climate change on algal community and primary productivity of Lake Malawi (East Africa) from the Last Glacial Maximum to present.' *Limnology and Oceanography*, **54**, 2431-2447.

Castañeda, I. S.., Mulitza, S., Schefuβ, E., Lopes dos Santos, R. A., Sinninghe Damsté, J. S. and Schouten, S. (2009b) 'Wet phase in the Sahara/Sahel region and human migration patterns in North Africa.' *Proceedings of the National Academy of Sciences*, **106**, 20159-20163.

Cayan, D. R., Miller, A. J., Barnett, T. P., Graham, N. E., Ritchie, J. N. and Oberhuber, J. M. (1995) *Seasonal-interannual fluctuations in surface temperature over the Pacific: effects of monthly winds and heat fluxes. Natural climate variability on decadal-to-century time scales*. National Academy Press: United States of America, 133-150.

Chagué-Goff, C., Chan, J. C. H., Goff, J. and Gadd, P. (2016) 'Late Holocene record of environmental changes, cyclones and tsunamis in a coastal lake, Mangaia, Cook Islands.' *Island Arc*, **25**, 333-349.

Chawchai, S., Kylander, M. E., Chabangborn, A., Löwemark, L. and Wohlfarth, B. (2016) 'Testing commonly used X-ray fluorescence core scanning-based proxies for organic-rich lake sediments and peat.' *Boreas*, **45**, 180-189.

Chen, J. and Chung, C. (2015) 'Representation of global precipitation anomalies using four major climate patterns.' *Science China*, **58**, 927-934.

Chen, J., Del Genio, A. D., Carlson, B. E. and Bosilovich, M. G. (2008) 'The spatiotemporal structure of twentieth-century climate variations in observations and reanalyses. Part II: Pacific pan-decadal variability.' *Journal of Climate*, **21**, 2634-2650.

Chen, S., Hoffmann, S. S., Lund, D. C., Cobb, K. M., Emile-Geay, J. and Adkins, J. F. (2016) 'A high-resolution speleothem record of western equatorial Pacific rainfall: implications for Holocene ENSO evolution.' *Earth and Planetary Science Letters*, **442**, 61-71.

Chen, X.Y. and Wallace, J. M. (2015) 'ENSO-like variability: 1900-2013' *Journal of Climate*, **28**, 9623-9641.

Chiang, J. H. F., Fang, Y, and Chang, P. (2009) 'Pacific climate change and ENSO activity in the mid-Holocene.' *Journal of Climate*, **22**, 923-939.

Chikaraishi , Y. and Naraoka, H. (2003) 'Compound-specific δD- $\delta^{13}C$ analyses of *n*-alkanes extracted from terrestrial and aquatic plants.' *Phytochemistry*, **63**, 361-371.

Chikaraishi, Y. and Naraoka, H. (2007) $\delta^{13}C$ and δD relationships among three *n*-alkyl compound classes (*n*-alkanoic acid, *n*-alkane and *n*-alkanol) of terrestrial higher plants.' *Organic Geochemistry*, **38**, 198-215.

Chikaraishi, Y., Naraoka, H. and Poulson, S. R. (2004a) 'Hydrogen and carbon isotopic fractionations of lipid biosynthesis among terrestrial (C3, C4 and CAM) and aquatic plants.' *Phytochemistry*, **65**, 1369-1381.

Chikaraishi, Y., Naraoka, H. and Poulson, S. R. (2004b) 'Carbon and hydrogen isotopic fractionation during lipid biosynthesis in a higher plant (*Cryptomeria japonica*).' *Phytochemistry*, **65**, 323-330.

Chung, C. T. Y. and Power, S. B. (2016) 'Modelled impact of global warming on ENSO-driven precipitation changes in the tropical Pacific.' *Climate Dynamics*, **47**, 1303-1323.

Clark, I. and Fritz, P. (1997) *Environmental Isotopes in Hydrogeology*, Boca Raton: Lewis Publishers, pp. 331.

Cobb, K. M., Westphal, N., Sayani, H. R., Watson, J. T., Di Lorenzo, E., Cheng, H., Edwards, R. L. and Charles, C. D. (2013) 'Highly variable El Niño-Southern Oscillation throughout the Holocene.' *Science*, **339**, 67-70.

Cohen, A. S. (2003) *Paleolimnology: The History and Evolution of Lake Systems*. Oxford: Oxford University Press, pp. 500.

Cole, J. E. and Fairbanks, R. G. (1990) 'The Southern Oscillation recorded in the $\delta^{18}O$ of corals from Tarawa Atoll.' *Paleoceanograhy*, **5**, 669-683.

Collins, M. An, S., Cai, W., Ganachaud, A., Guilyardi, E., Jin, F., Jochum, M., Lengaigne, M., Power, S., Timmermann, A., Vecchi, G., and Wittenberg, A. (2010) 'The impact of global warming on the tropical Pacific Ocean and El Niño.' *Nature Geoscience*, **3**, 391-397.

Collister, J. W., Rieley, G., Stern, B., Eglinton, G. and Fry, B. (1994) 'Compound-specific $\delta^{13}C$ analyses of leaf lipids from plants with differing carbon dioxide metabolisms.' *Organic Geochemistry*, **21**, 619-627.

Combettes, C., Sémah, A.-M. and Wirrmann, D. (2015) 'High-resolution pollen record from Efate Island, central Vanuatu: highlighting climatic and human influences on late Holocene vegetation dynamics.' *Comptes Rendus Palevol*, **14**, 251-261.

Conroy, J. L., Cobb, K. M. and Noone, D. (2013) 'Comparison pf precipitation isotope variability across the tropical Pacific in observations and SWING2 model simulations.' *Journal of Geophysical Research: Atmospheres*, **118**, 5867-5892.

Conroy, J. L., Overpeck, J. T. and Cole, J. E. (2010) 'El Niño/Southern Oscillation and changes in the zonal gradient of tropical Pacific sea surface temperature over the last 1.2 ka.' *PAGES News*, **18**, 32-34.

Conroy, J. L., Overpeck, J. T., Cole, J. E., Shanahan, T. M. and Steinitz-Kannan, M. (2008) 'Holocene changes in eastern tropical Pacific climate inferred from a Galápagos lake sediment record.' *Quaternary Science Reviews*, **27**, 1166-1180.

Conroy, J. L., Thompson, D. M., Collins, A., Overpeck, J. T., Bush, M. B. and Cole, J. E. (2014) 'Climate influences on water and sediment properties of Genosva Crate Lake, Galápagos.' *Journal of Paleolimnology*, **52**, 331-347.

Corrège, T., Gagan, M. K., Beck, J. W., Burr, G. S., Cabioch, G. and Le Cornec, F. (2004) 'Interdecadal variation in the extent of South Pacific tropical waters during the Younger Dryas event.; *Nature*, **428**, 927-929.

Craig, H. (1961) 'Isotopic variations in meteoric waters.' *Science*, **133**, 1702-1703.

Cranwell, P. A. (1981) 'Diagenesis of free and bound lipids in terrestrial detritus deposited in a lacustrine sediment.' *Organic Geochemistry,* **3**, 79–89.

Cravatte, S., Delcroix, T., Zhang, D., McPhaden, M. and Leloup, J. (2009) 'Observed freshening and warming of the western Pacific Warm Pool.' *Climate Dynamics*, **33**, 565-589.

Croudace, I. W., Rindby, A. and Rothwell, R. G. (2006) 'ITRAX: description and evaluation of a new multi-function X-ray core scanner.' In Rothwell, R. G. (Ed.) *New techniques in sediment core analysis, vol. 267*. Geological Society Special Publication, pp.51-63.

Cuven, S., Francus, P. and Lamoureux, S. (2011) 'Mid to Late Holocene hydroclimatic and geochemical records from the varved sediments of East Lake, Cape Bounty, Canadian High Arctic.' *Quaternary Science Reviews*, **30**, 2651-2665.

Dansgaard, W. (1964) 'Stable isotopes in precipitation' *Tellus*, **16**, 436-468.

Dai, A., Fyfe, J. C., Xie, S. P. and Dai, X. (2015) 'Decadal modulation of global surface temperature by internal climate variability.' *Nature Climate Change*, **5**, 555-559.

Darling, W. G., Bath, A. H., Gibson, J. J. and Rozanski, K. (2005). 'Isotopes in Water.' In Leng, M. J. (Ed.) *Isotopes in Palaeoenvironmental Research*, Netherlands: Klewer, pp. 1-66.

Dassié, E. P., Linsley, B. K., Corrège, T., Wu, H. C., Lemley, G. M., Howe, S. and Cabioch, G. (2014) 'A Fiji multi-coral $\delta^{18}O$ composite approach to obtaining a more accurate reconstruction of the last two-centuries of the ocean-climate variability in the South Pacific Convergence Zone region.' *Paleooceanography*, **29**, 1196-1213.

Davidson, J. M. (1979) 'Samoa and Tonga.' In Jennings, J. D. (Ed.) *The Prehistory of Polynesia*. Cambridge: Harvard University Press, pp. 82-109.

Davies, S. J., Lamb, H. F. and Roberts, S. J. (2015) 'Micro-XRF core scanning in palaeolimnology: recent developments.' In Croudace, I. W. and Rothwell, R. G. (Eds.) *Micro-XRF studies of sediment cores*. London: Springer, pp. 189-226.

Dean, W. E. (1974) 'Determination of carbonate and organic matter in calcareous sediments and sedimentary rocks by loss on ignition: comparison with other methods.' *Journal of Sedimentary Research*, **44**, 242-248.

Dean, W. E. (1999) 'The carbon cycle and biogeochemical dynamics in lake sediments,' *Journal of Paleolimnology*, **21**, 375-393.

Dearing, J. A. (1994) *Environmental Magnetic Susceptibility: using the Bartington MS2 System*. Kenilworth: Chi Publishing, pp. 111.

Dearing, J. A. (1999) 'Holocene environmental change from magnetic proxies in lake sediments.' In Maher, B. A. and Thompson, R. (Eds.) *Quaternary climates, environments and magnetism*, United Kingdom: Cambridge University Press, pp. 391.

Delcroix, T., Cravatte, S. and McPhaden, M. J. (2007) 'Decadal variations and trends in tropical Pacific sea surface salinity since 1970.' *Journal of Geophysical Research: Oceans*, **112**, 1-15.

DeLong, K. L., Quinn, T. M. and Taylor, F. W. (2007) 'Reconstructing twentieth-century sea surface temperature variability in the southwest Pacific: a replication study using multiple coral Sr/Ca records from New Caledonia.' *Paleoceanography*, **22**, 1-18.

DeLong, K. L., Quinn, T. M., Taylor, F. W., Lin, K. and Shen, C. (2012) 'Sea surface temperature variability in the southwest tropical Pacific since AD 1649.' *Nature Climate Change*, **2**, 799-804.

Deng, W. and Wei, G. (2015) 'Decoupling of seasonal temperature and precipitation over the western Pacific during the early mid-Holocene.' *International Journal of Climatology*, **35**, 794-800.

Deser, C. and Wallace, J. M. (1990) 'Large-scale atmospheric circulation features of warm and cold episodes in the tropical Pacific.' *Journal of Climate*, **3**, 1254-1281.

Diefendorf, A.F., Mueller, K. E., Wing, S. L., Koch, P. L. and Freeman, K. H. (2010) 'Global pattersn in ^{13}C discrimination and implications for studies of past and future climate.' *Proceeding of the National Academy of Sciences*, **107**, 5738-5743.

Dienes, P. (1980) "The isotopic composition of reduced organic carbon. In: P. Fritz and J. C. Fontes (Eds.) *Handbook of Environmental Isotope Geochemistry*, Vol. 1. Elsevier, New York, pp.329-406.

Di Lorenzo, E., Ligouri, G., Schneider, N., Furtado, J. C., Anderson, B. T. and Alexander, M. A. (2015) 'ENSO and meridional modes: a null hypothesis for Pacific climate variability.' *Geophysical Research Letters*, **42**, 9440-9448.

Donachie, S. P., Kinzie III, A., Bidigare, R. R., Sadler, D. W. and Karl, D. M. (1999) 'Lake Kauhakō, Molokai'i, Hawai'i.' *Aquatic Microbial Ecology*, **19**, 93-103.

Donders, T. H., Wagner-Cremer, F. and Visscher, H. (2008) 'Integration of proxy data and model scenarios for the mid-Holocene onset of modern ENSO variability.' *Quaternary Science Reviews*, **27**, 571-579.

Dong, B. and Dai, A. G. (2015) 'The influence of the Interdecadal Pacific Oscillation on temperature and precipitation around the globe.' *Climate Dynamics*, **45**, 2667-2681.

Dong, L., Zhou, T. J. and Chen, X. L. 'Changes of Pacific decadal variability in the twentieth century driven by internal variability, greenhouse gases and aerosols.' *Geophysical Research Letters*, **41**, 8570-8577.

Douglas, P. M., Pagani, M., Brenner, M., Hodell, D. A. and Curtis, J. H. (2012) 'Aridity and vegetation composition are important determinants of leaf-wax δD values in southeastern Mexico and Central America.' *Geochimica et Cosmochimica Acta*, **97**, 24-45.

Douglas, P. M., Pagani, M., Eglinton, T. I., Brenner, M., Hodell, D. A., Curtis, J. H., Ma, K. F. and Breckenridge, A. (2014) 'Pre-aged plant waxes in tropical lake sediments and their influence on the chronology of molecular paleoclimate proxy records.' *Geochimica et Cosmochimica Acta*, **141**, 346-364.

Dowdy, A. J., Qi, L., Jones, D., Ramsay, H., Fawcett, R. and Kuleshov, Y. (2012) 'Tropical cyclone climatology of the South Pacific Ocean and its relationship to El Niño-Southern Oscillation.' *Journal of Climate*, **25**, 6108-6122.

Driscoll, R., Elliot, M., Russon, T., Welsh, K., Yokoyama, Y. and Tudhope, A. (2014) 'ENSO reconstructions over the past 60ka using giant clams (*Tridacna* sp.) from Papua New Guinea.' *Geophysical Research Letters*, **41**, 6819-6825.

Druffel, E. R. M. and Griffin, S. (1993) 'Large variations of surface ocean radiocarbon: evidence of circulation changes in the southwestern Pacific.' *Journal of Geophysical Research: Oceans*, **98**, 20249-20259.

Dunbar, R. B., Wellington, G. M., Colgan, M. W. and Glynn, P. W. (1994) 'Eastern Pacific sea surface temperature since 1600 AD: the $\delta^{18}O$ record of climate variability in Galápagos corals.' *Paleoceanography*, **9**, 291-315.

Eglinton, G. and Hamilton, R. J. (1967) 'Leaf epiticular waxes.' *Science*, **156**, 1322-1335.

Ellison, J. C. (1994) 'Palaeo-lake and swamp stratigraphic records of Holocene vegetation and sea-level changes, Mangaia, Cook Islands.' *Pacific Science*, **48**, 1-15.

Elmqvist, T., Rainey, W. E., Pierson, E. D. and Cox, P. A. 'Effects of tropical cyclones Ofa and Val on the structure of a Samoan lowland rain forest.' *Biotropica*, **26**, 384-391.

Emile-Geay, J., Cobb, K. M., Carré, M., Braconnot, P., Leloup, J., Zhou, Y., Harrison, S. P., Corrège, T., McGregor, H. V., Collins, M., Driscoll, R., Elliot, M., Schneider, B. and Tudhope, A. (2015) 'Links between tropical Pacific seasonal, interannual and orbital variability during the Holocene.' *Nature Geoscience*, **9**, 168-173.

Emile-Geay, J. and Tingley, M. P. (2016) 'Inferring climate variability from nonlinear proxiues: application to paleo-ENSO studies.' *Climate of the Past*, **12**, 31-50.

England., M. H., McGregor, S., Spence, P., Meelh, G. A., Timmermann, A., Cai, W., Sen Gupta, A., McPhaden, M. J., Purich, A. and Sanotoso, A. (2014) 'Recent intensification of wind-driven circulation in the Pacific and the ongoing warming hiatus.' *Nature Climate Change*, **4**, 222-227.

Erb, M. P., Broccoli, A. J. Graham, N. T., Clement, A. C., Wittenberg, A. T. and Vecchi, G. A. (2015) 'Response of the equatorial Pacific seasonal cycle to orbital forcing.' *Journal of Climate*, **28**, 9258-9276.

Evans, M. N., Cane, M. A., Schrag, D. P., Kaplan, A., Linsley, B. K., Vallalba, R. and Wellington, G. M. (2001) 'Support for tropically-driven Pacific decadal variability based on paleoproxy evidence.' *Geophysical Research Letters*, **28**, 3689-3692.

Ficken, K. J., Li, B., Swain, D. L. and Eglinton, G. (2000) 'An *n*-alkane proxy for the sedimentary input of submerged/floating freshwater macrophytes.' *Organic Geochemistry*, **31**, 745-749.

Finney, B. P., Bigelow, N. H., Barber, V. A. and Edwards, M. E. (2012) 'Holocene climate change and carbon cycling in a groundwater-fed, boreal forest lake: Dune Lake, Alaska.' *Journal of Paleolimnology*, **48**, 43054.

Folland, C. K., Renwick, J. A., Salinger, M. J. and Mullan, A. B. (2002) 'Relative influences of the Interdecadal Pacific Oscillation and ENSO on the South Pacific Convergence Zone.' *Geophysical Research Letters*, **29**.

Folland, C. K., Salinger, M. J., Jiang, N. and Rayner, N. A. (2003) 'Trends and variations in South Pacific island and ocean surface temperatures.' *Journal of Climate*, **16**, 2859-2874.

Franklin, J. and Merline, M. (1992) 'Species-environment patterns of forest vegetation on the uplifted reef limestone of Atiu, Mangaia, Ma'uke and Miti'aro, Cook Islands.' *Journal of Vegetation Science*, **3**, 3-14.

Gao, L., Hou, J., Toney, J., MacDonald, D. and Huang, Y. (2011) 'Mathematical modelling of the aquatic macrophyte inputs of mid-chain *n*-alkly lipids to lake sediments: implications

for interpreting compound specific hydrogen isotopc records.' *Geochimica et Cosmochimica Act*, **75**, 157-164.

Garcin, Y., Schwab, V. F., Gleixner, G., Kahmen, A., Todou, G., Séne, O., Onana, J-M., Achoundong, G. and Sachse, D. (2012) 'Hydrogen isotope values of lacustrine sedimentary *n*-alkanes as proxies of tropical African hydrology: Insights from a calibration transect across Cameroon.' *Geochimica et Cosmochimica Acta*, **79**, 106-126.

Garreaud, R. D. and Battisti D. S. (1999) 'Interannual (ENSO) and interdecadal (ENSO-like) variability in the Southern Hemisphere tropospheric circulation.' *Journal of Climate*, **12**, 2113-2123.

Gat, J. R. (1996) 'Oxygen and hydrogen isotopes in the hydrological cycle.' *Annual Review of Earth and Planetary Sciences*, **24**, 225-262.

Ge, L. Q., Lai, W. C. and Lin, Y. C. (2005) 'Influence and correction for moisture in rocks, soils and sediments on in situ XRF analysis.' *X-Ray Spectrometry*, **34**, 28-34.

GeoCore (2016) 'GeoCore sediment coring system.' [Accessed 1 May 2016]. Available from: www.geo-core.com

Gibson, J. J., Prepas, E. E. and Mceachern, P. (2002). 'Quantitative comparison of lake through flow, residency, and catchment runoff using stable isotopes: modelling and results from a regional survey of Boreal lakes. *Journal of Hydrology*, **262**, 128-144.

Gomez, B. Carter, L., Trustrum, N. A., Page, M. J. and Orpin, A. R. (2013) 'Coherent rainfall response to middle- and late-Holocene climate variability across the mid-latitude South Pacific.' *The Holocene*, **23**, 1002-1007.

Gomez, B., Carter, L., Trustrum, N. A., Palmer, A. S. and Roberts, A. P. (2004) 'El Niño-Southern Oscillation signal associated with middle-Holocene climate change in intercorrelated terrestrial and marine sediment cores, North Island, New Zealand.' *Geology*, **32**, 653-656.

Goodwin, I. D., Browning, S. A. and Anderson, A. J. (2014) 'Climate windows for Polynesian voyaging to New Zealand and Easter Island.' *Proceedings of the National Academy of Sciences*, **111**, 14716-14721.

Google Earth (2015) *Google Earth* [Online] Available from: www.google.co.uk [Accessed: 13th September 2016].

Gorman, M. K., Quinn, T. M., Taylor, F. W., Partin, J. W., Cabioch, G., Austin, J. A., Pelletier, B., Ballu, V., Maes, C. and Saustrup S. (2012) 'A coral-based reconstruction of sea surface salinity at Sabine Bank, Vanuatu from 1842 to 2007 CE.' *Paleoceanograph*, **27**, 1-13.

Gouriou, Y. and Delcroix, T. (2002) 'Seasonal and ENSO variation of sea surface salinity and temperature in the South Pacific Convergence Zone during 1976-2000.' *Journal of Geophysical Research*, **107**.

Green, R. C. and Davidson, J. M. (1974) 'A radiocarbon stratigraphic sequence for Samoa.' In Green. R. C. and Davidson, J. M. (Eds.) *Archaeology in Western Samoa*, New Zealand: Bulletin of the Auckland Institute and Museum 7, pp.212-224.

Green, R. C. (2002) 'A retrospective view of settlement pattern studies in Samoa.' In Ladefoged, T. N. and Graves, M. W. (Eds.) *Pacific Landscapes: Archaeological Approaches*, United States of America: Easter Island Foundation, pp. 125-152.

Grimm, E. C., Maher Jr., L. J. and Nelson, D. M. (2009) 'The magnitude of error in conventional bulk-sediment radiocarbon dates from central North America.' *Quatenrary Research*, **72**, 301-308.

Haberle, S. (1996) 'Explanations for palaeoecological changes on the northern plains of Guadalcanal, Solomon Islands: the last 3200 years.' *The Holocene*, **6**, 333-338.

Haberle, S. G. (1998) 'Late Quaternary vegetation change in the Tari Basin, Papua New Guinea.' *Palaeogeography, Palaeoclimatology, Palaeoecology*, **137**, 1-24.

Haberzettl, T., Anselmetti, F., Bowen, S., Fey, M., Mayr, C., Zolitschka, B., Ariztegui, D., Mauz, B., Ohlendorf, C., Kastner, S., Lücke, A., Schäbitz, F. and Wille, M. (2009) 'Late Pleistocene dust deposition in the Patagonian steppe – extending and refining the paleoenvironmental and tephrochronological record from Laguna Potrok Aike back to 55 ka.' *Quaternary Science Review*, **28**, 2927-2939

Haffke, C. and Magnusdottir, G. (2013) 'The South Pacific Convergence Zone in three decades of satellite images.' *Journal of Geophysical Research: Atmosphere*, **118**, 10839-10849.

Ham, Y-.G. and Kug, J-.S. (2016) 'ENSO amplitude changes due to greenhouse warming in CMIP5: role of mean tropical precipitation in the twentieth century.' *Geophysical Research Letters*, **43**, 422-430.

Hamilton, W. M. and Grange, L. I. (1938) *The Soils and Agriculture of Western Samoa*. Wellington: Government Printer.

Hart, S. R., Coetzee, M., Workman, R. K., Blusztajn, J., Johnson, K. T. M., Sinton, J. M., Steinberger, B. and Hawkings, J. W. (2004) 'Genesis of the Western Samoa seamount province: age, geochemical fingerprint and tectonics.' *Earth and Planetary Science Letters*, **227**, 37-56.

Haug, G.H., Hughen, K.A., Sigman, D.M., Peterson, L.C. and Rohl, U. (2001) 'Southward migration of the Intertropical Convergence Zone through the Holocene.' *Science*, **293**, 1304–1308.

Heim, C., Nowaczyk, N. R. and Negendank, J. F. W. (1997) 'Near East desertification: evidence from the Dead Sea.' *Naturwissenschaften*, **84**, 398-401.

Heiri, O., Lotter, A. F. and Lemcke, G. (2001) 'Loss on ignition as a method for estimating organic and carbonate content in sediments: reproducibility and comparability of results.' *Journal of Paleolimnology*, **25**, 101-110.

Henderson, A. K., Nelson, D. M., Hu, F. S., Huang, Y. S., Shuman, B. N. and Williams, J. W. (2010) 'Holocene precipitation seasonality captures by a dual hydrogen and oxygen isotope approach at Steel Lake, Minnesota.' *Earth and Planetary Science Letters*, **300**, 205-214.

Hendy, E. J., Gagan, M. K., Alibert, C. A. McCulloch, M. T., Lough, J. M. and Isdale, P. J. (2002) 'Abrupt decrease in tropical Pacific sea surface salinity at end of Little Ice Age.' *Science*, **295**, 1511-1514.

Henley, B. J., Gergis, J., Karoly, D. J., Power, S., Kennedy, J. and Folland, C. K. (2015) 'A tripole index for the Interdecadal Pacific Oscillation.' *Climate Dynamics*, **45**, 3077-3090.

Henley, B. A., Thyer, M. A. and Kuczera, G. (2013) 'Climate driver informed short-term drought risk evaluation.' *Water Resources Research*, **49**, 2317-2326.

Hennekam, R. and de Lange, G. (2012) 'X-ray fluorescence core scanning of wet marine sediments: methods to improve quality and reproducibility of high-resolution paleoenvironmental records.' *Limnology and Oceanography: Methods*, **10**, 991-1003.

Hogg, A. G., Hua, W., Blackwell, P. G., Nie, M., Buck, C. E., Guilderson, T. P., Heaton, T. J., Palmer, J. G., Reimer, P. J., Reimer, R. W., Turney, C. S. M. and Zimmerman, S. R. H. (2013) 'SHCal13 Southern Hemisphere calibration, 0-50,000 years cal BP.' *Radiocarbon*, **55**, 1889-1903.

Hoerling, M. P., Kumar, A. and Zhong, M. (1997) 'El Niño, La Niña, and the nonlinearity of their teleconnections.' *Journal of Climate*, **10**, 1769-1786.

Hollander, D. J. and Smith, M. A. (2001) 'Microbially mediated carbon cycling as a control on the $\delta^{13}C$ of sedimentary carbon in eutrophic Lake Mendota (USA): new models for interpreting isotopic excursion in the sedimentary record.' *Geochimica et Cosmochimica Acta*, **65**, 4321-4337.

Hope, G. and Pask, J. (1998) 'Tropical vegetational change in the late Pleistocene of New Caledonia.' *Palaeogeogrpahy, Palaeoclimatology, Palaoecology*, **142**, 1-21.

Hou, J., D'Andrea, W. J. and Huang, Y. (2008) 'Can sedimentary leaf waxes record D/H ratios of continental precipitation? Field, model, and experimental assessments.' *Geochimica et Cosmochimica Acta*, **72**, 3502-3517.

Hou, J., Huang, Y. S., Oswald, W. W., Forster, D. R. and Shuman, B. (2007) 'Centennial-scale compound-specific hydrogen isotope record of Pleistocene-Holocene climate transition from southern New England.' *Geophysical Research Letters*, **34**, 1-5.

Hsu, H-. H. and Chen, Y-. L. (2011) 'Decadal to bi-decadal rainfall variation in the western Pacific: a foorprint of South Pacific decadal variability?' *Geophysical Research Letters*, **38**.

Huang, Y., Shuman, B., Wang, Y. and Webb III, T. (2004) 'Hydrogen isotope ratios of individual lipids in lake sediments as novel tracers of climatic and environmental change: a surface sediment test.' *Journal of Paleolimnology*, **31**, 363-375.

IAEA/WMO (2016). Global Network of Isotopes in Precipitation. The GNIP Database. Accessible at: http://www.iaea.org/water

Indermühle, A., Stocker, T. F., Joos, F., Fischer, H., Smith, H. J., Wahlen, M., Deck, B., Mastroianni, D., Tshumi, J., Blunier, T., Meyer, R. and Stauffer, B. (1999) 'Holocene carbon-cycle dynamics based on CO_2 trapped in ice at Taylor Dome, Antarctica.' *Nature*, **398**, 121-126.

IPCC (2014) 'The Physical Science basis. Contribution of Working Gorup 1 to the Fifth assessment Report of the Intergovernmental Panel on Climate Change.' In Stocker, T. F. *et al*. (Eds.) *IPCC: Climate Change*. Cambridge: Cambridge University Press, doi:10.1017/CBO9781107415324.00.

Jansen, J. H. F., van der Gaast, S. J., Koster, B. and Vaars, A. J. (1998) 'CORTEX, a shipboard XRF-scanner for element analyses in split sediment cores.' *Marine Geology*, **151**, 143-153.

Jenkins, R. (1999) *X-Ray Fluorescence Spectrometry*. Chichester: Wiley, pp. 232.

Jenkins, R. and De Vries, J. L. (1970) *Practical X-ray Spectrometry*. London: Macmillian, pp. 189.

Jones, R.I. and Grey, J. (2011) 'Biogenic methane in freshwater food webs.' *Freshwater Biology*, **56**, 213–229.

Jonkman, S. N.(2005) 'Global perspective on loss of human life caused by floods.' *Natural Hazards*, **34**, 151-175.

Jouve, G., Francus, P., Lamoureux, S., Provencher-Nolet, L. and Hanh, A. (2013) 'Microsedimentological characterisation using image analysis and XRF as indicators of sedimentary processes and climate changes during Lateglacial at Laguna Potrok Aike, Santa Cruz, Argentina.' *Quaternary Science Reviews*, **71**, 191-204.

Juillet-Leclerc, A., Thiria, S., Naveau, P., Delcroix, T., Le Bec, N., Blamart, D. and Corrège, T. (2006) 'SPCZ migration and ENSO events during the 20th Century as revealed by climate proxies from a Fiji coral.' *Geophysical Research Letters*, **33**.

Kahman, A., Schefuβ, E. and Sachse, D. (2013a) 'Leaf water deuterium enrichment shapes leaf wax *n*-alkane δD values of angiosperm plants I: experimental evidence and mechanistic insights.' *Geochimica et Cosmochimica Acta*, **111**, 39-49.

Kahman, A., Hoffmann, N., Schefuß, E., Arndt, S. K., Cernusak, L. A., West, J. B. and Sachse, D. (2013b) 'Leaf water deuterium enrichment shapes leaf wax *n*-alkane δD values of angiosperm plants II: observational evidence and global implications.' *Geochimica et Cosmochimica Acta*, **111**, 50-63.

Kao, J. and Yu, J. (2009) 'Contrasting eastern-Pacific and central-Pacific types of ENSO.' *Journal of Climate*, **22**, 615-632.

Karamperidou, C., Di Nezio, P. N., Timmermann, A., Jin, F., Cobb, K. M. (2015) 'The response of ENSO flavors to mid-Holocene climate: implications for proxy interpretation.' *Paleoceanography*, **30**, 527-547.

Kautai'i, N. *et al*. (1984) *Atiu: an island community*. Institute of Pacific Studies. University of the South Pacific. Suva, Fiji.

Kear, D. (1967) 'Geological notes on Western Samoa.' *New Zealand Journal of Geology and Geophysics*, **10**, 1446-1451.

Kear, D. and Wood, B. L. (1959) *The geology and hydrology of Western Samoa*. New Zealand: Department of Scientific and Industrial Research.

Khider, D., Stott, L. D., Emile-Gay, J., Thunell, R. and Hammond, D. E. (2011) 'Assessing El Niño Southern Oscillation variability during the past millennium.' *Paleoceanography*, **26**, 1-20.

Kido, Y., Koshikawa, T. and Tada, R. (2006) 'Rapid and quantitative major element analysis method for wet fine-grained sediments using an XRF microscanner.' *Marine Geology*, **229**, 209-225.

Kidwell, A. Jo, Y. –H., and Yan, X. –H. (2014) 'A closer look at the central Pacific El Niño and warm pool migrations events from 1982-2011.' *Journal of Geophysical Research, Oceans*, **119**, 165-172.

Kidwell, A., Lee, T., Jo, Y.-H. and Yan, X.-H. (2016) 'Characterisation of the variability of the South Pacific Convergence Zone using satellite and reanalysis wind products.' *Journal of Climate*, **29**, 1717-1732.

Kienast, M., Steinke, S., Stattegger, K. and Calvert, S. E. (2001) 'Synchronous tropical South China Sea SST change and Greenland warming during deglaciation.' *Science*, **291**, 2132-2134.

Kiladis, G. N., von Storch, H. and van Loon, H. (1989) 'Origin of the South Pacific Convergence One.' *Journal of Climate*, **2**, 1185-1195.

Kilbourne, K. H., uinn, T. M., Taylor, F. W., Delcroix, T. and Gouriou, Y. (2004) 'El Niño-Southern Oscillation-related salinity variations in the skeletal geochemistry of a *Porites* coral from Espiritu Santo, Vanuatu.' *Paleoceanography*, **19**.

Kirby, M E., Lund, S. P., Anderson, M. A. and Bird, B. W. (2007) 'Insolation forcing of Holocene climate change in southern California: a sediment study from Lake Elsinore.' *Journal of Paleolimnology*, **28**¸395-417.

Kirch, P. V. (1996) 'Late Holocene human-induced modifications to a central Polynesian island ecosystem.' *Proceedings of the National Academy of Sciences of the United States of America*, **93**, 5296-5300.

Kirch, P. V. and Ellison, J. (1994) 'Palaeoenvironmental evidence for human colonisation of remote Oceanic islands.' *Antiquity*, **68**, 310-321.

Kirby, M E., Lund, S. P., Anderson, M. A. and Bird, B. W. (2007) 'Insolation forcing of Holocene climate change in southern California: a sediment study from Lake Elsinore.' *Journal of Paleolimnology*, **28**¸395-417.

Klatt, M. (2013) *PACRAIN*. [ONLINE] Available at: http://pacrain.ou.edu/. [Accessed 2 August 2016].

Koppers, A. P., Russel, J. A., Jacskon, M. G., Konter, J., Staudigel, H. and Hart, S. R. (2008) 'Samoa reinstated as a primary hotspot trail.' *Geology*, **36**, 435-438.

Kosaka, Y. and Xie, S. P. (2013) 'Recent global warming hiatus tied to equatorial Pacific surface cooling.' *Nature*, **501**, 403-407.

Koutavas, A. and Joanides, S. (2012) El Niño-Southern Oscillation extrema in the Holocene and Last Glacial Maximum.' *Paleoceanography*, **27.**

Koutavas, A., Lynch-Stieflitz, J., Marchitton, T. M. and Sachs, J. P. (2002) 'El Niño-like pattern in ice age tropical Pacific sea surface temperature.' *Science*, **297**, 226-230.

Koutavas, A., Olive, G. C. and Lynch-Steiglitz, J. (2006) 'Mid-Holocene El Niño-Southern Oscillation (ENSO) attenuation revealed by individual foraminfera in eastern tropical Pacific sediments.' *Geology*, **34**, 993-996.

Krishnaswamy, S., Lal, D., Martin, J. and Meybeck, M. (1971) 'Geochronology of lake sediments.' *Earth and Planetary Science Letters*, **11**, 407-414.

Kug, J. -S., Choi, J., An, S. -L., Jin, F. -F. and Wittenberg, A. T. (2010) 'Warm pool and cold tongue El Niño events as simulated by the GFDL 2.1 Coupled GCM.' *Journal of Climate*, **23**, 1226-1239.

Kug, J., Jin, F. and An, S. 'Two types of El Niño events: cold tongue El Niño and warm pool El Niño.' *Journal of Climate*, **22**, 1499-1515.

Kylander, M. E., Amplel, L., Wohlfarth, B. and Veres, D. (2011) 'High-resolution X-ray fluorescence core scanning analysis of Les Echets (France) sedimentary sequence: new insights from chemical proxies.' *Journal of Quaternary Science*, **26**, 109-117.

Lamb, A. L. (2004 'Determination of organic and carbonate content in soils and sediments by loss on ignition (LOI).' *NERC Isotope Geosciences Laboratory Report*, **no. 197**.

Lamb, A. L., Leng, M. L., Umer Mohammad, M. and Lamb, F. (2004) 'Holocene climate and vegetation change in the Main Ethiopian Rift Valley, inferred from the composition (C/N and $\delta^{13}C$) of lacustrine organic matter.' *Quaternary Science Reviews*, **23**, 881-891.

Langdon, P. G., Leng, M. L., Holmes, N. and Caseldine, C. J. (2010) 'Lacustrine evidence of early-Holocene environmental change in northern Iceland: a multiproxy palaeoecology and stable isotope study.' *The Holocene*, **20**, 205-214.

Larkin, N. K. and Harrison, D. E. (2002) 'ENSO Warm (El Niño) and cold (La Niña) event life cycles: ocean surface anomaly patterns, their symmetries, asymmetries, and implications.' *Journal of Climate*, **15**, 1118-1140.

Lazareth, C. E., Rosell, M. G. B., Turcq, B., Le Cornexc, F., Mandeng-Yogo, M., Caquineau, S. and Cabioch, G. (2013) 'Mid-Holocene climate in New Caledonia (southwest Pacific): coral and PMIP models monthly resolved results.' *Quaternary Science Reviews*, **69**, 83-97.

Lea, D. W., Pak, D. K and Spero, H. J. (2000) 'Climate impact of late Quaternary equatorial Pacific sea surface temperature variations.' *Science*, **289**, 1719-1724.

Le Bec, N., Juillet-Leclerc, A., Corrège, T., Blamart, D and Decroix, T. (2000) 'A coral $\delta^{18}O$ record of ENO driven by sea surface salinity variability in Fiji (south-western tropical Pacific).' *Geophysical Research Letters*, **27**, 3897-3900.

Lehmann, M. F., Bernasconi, S. M., Barbieri, A. and McKenzie, J. A. (2002). 'Preservation of organic matter and alteration of its carbon and nitrogen isotope composition during simulated and in situ early sedimentary diagenesis.' *Geochimica et Cosmochimica Acta*, **66**, 3573-3584.

Leng, M. L., Lamb, A. L., Heaton, T. H. E., Marshall, J. D., Wolfe, B. B., Jones, M. D., Holmes, J. A. and Arrowsmith, C. (2006) Isotopes in lake sediments. In Leng, M. L. (Ed.) *Isotopes in Palaeoenvironmental Research*. The Netherlands: Springer, pp.147-184.

Leng, M. J. and Marshall, J. D. (2004) 'Palaeoclimate interpretation of stable isotope data from lake sediment archives.' *Quaternary Science Reviews*, **23**, 811-831.

Lewis, C. F. M., Miller, A. A. L., Levac, E., Piper, D. J. W. and Sonnichsen, G. V. (2012) 'Lake Agassiz outburst age and routing by Labrador Current and the 9.2 cal ka cold event.' *Quaternary International*, **260**, 83-97.

Lewis, S. C., LeGrande, A. N., Schmidt, G. A. and Kelley, M. (2014) 'Comparison of forced ENSO-like hydrological expressions in simulations of the preindustrial and mid-Holocene.' *Journal of Geophysical Research: Atmospheres*, **119**, 7064-7082.

Li, J., Xie, S-. P., Cook, E. R., Morales, M. S., Christie, D. A., Johnson, N. C., Chen, F., D'Arrigo, R., Fowler, A. M., Gou, X. and Fang, K. (2013) 'El Niño modulations over the past seven centuries.' *Nature Climate Change*, **3**, 822-826.

Lichtfouse, E., Derenne, S., Mariotti, A. and Largeau, C. (1994) 'Possible algal origin of long chain odd *n*-alkanes in immature sediments as revealed by distributions and carbon isotope ratios.' *Organic Geochemistry*, **22**, 1023–1027.

Lindzen, R. S. and Nigam, S. (1987) 'On the role of sea surface temperature gradients in forcing low-level winds and convergence in the Tropics.' *Journal of the Atmospheric Sciences*, **44**, 2418-2436.

Linsley, B. K., Wllington, G. M., Schrag, D. P., Ren, L., Salinger, M. J. and Tudhope, A. W. (2004) 'Geochemical evidence from corals for changes in the amplitude and spatial patern of the South Pacific interdecadal climate variability over the last 300 yars.' *Climate Dynamics*, **22**, 1-11.

Linsley, B. K., Kaplan, A., Gouriou, Y., Salinger, J., Demenocal, P. B., Wellington, G. M. and Howe, S. S. (2006) 'Tracking the extend of the South Pacific Convergence Zone since the early 1600s.' *Geochemistry, Geophysics, Geosystems*, **7**.

Linsley, B. K., Wellington, G. M. and Schrag, D. P. (2000) 'Decadal sea surface temperature variability in the subtropical South Pacific from 1727 to 1997 AD.' *Science*, **290**, 1145-1148.

Linsley, B. K., Zhang, P., Kaplan, A., Howe, S. S. and Wellington, G. M. (2008) 'Interdecadal-decadal climate variability from multicoral oxygen isotope records in the South Pacific Convergence Zone since 1650 A.D.' *Paleoceanography*, **23**.

Lintner, B. R. and Neelin, J. D. (2008) 'Eastern margin variability of the South Pacific Convergence Zone.' *Geophysical Research Letters*, **35**.

Liu, Z., Lu, Z., Wen, X., Otto-Bliesner, B. L., Timmermann, A. and Cobb, K. M. (2014) 'Evolution and forcing mechanisms of El Niño over the past 21,000 years.' *Nature*, **515**, 550-553.

Liu, W. and Yang, H. (2008) 'Multiple controls for the variability of hydrogen isotopic compositions in higher plant *n*-alkanes from modern ecosystems.' *Global Change Biology*, **14**, 2166-2177.

Liu, W., Yang, H. and Li, L. (2006) 'Hydrogen isotopic compositions of *n*-alkanes from terrestrial plants correlate with their ecological life forms.' *Oecologia*, **150**, 330-338.

Lorrey, A., Dalu, G., Renwick, J., Diamond, H. and Gaetani, M. (2012) 'Reconstructing the South Pacific Convergence one position during the presatellite era: a La Niña case study.' *Monthly Weather Review*, **140**, 3653-3668.

Löwemark. L., Chen, H. –F, Yang, T. –N., Kylander, M., Yu, E. –F., Hsu, Y. –W., Lee, T. –Q., Song, S. –R. and Jarvis, S. (2011) 'Normalising XRF-scanner data: a cautionary note on the interpretation of high-resolution records from organic-rich lakes.' *Journal of Asian Earth Sciences*, **40**, 1250-1256.

Lowe, J. J. and Walker, M. J. C. (2015) *Reconstructing Quaternary Environments*. United Kingdom: Routledge, pp. 538.

Luan, Y., Braconnot, P., Yu, Y., Zheng, W. and Marti, O. (2012) 'Early and mid-Holocene climate in the tropical Pacific: seasonal cycle and interannual variability induced by insolation changes.' *Climate of the Past*, **8**, 1093-1108.

Lucas, W. J. (1983) 'Photosynthetic assimilation of exogenous HCO_3^- by aquatic plants.' *Annual Review of Plant Physiology*, **34**, 71-104.

Maciolek, J. and Yamada, R. (1981) 'Vai Lahi and other lakes of Tonga.' V*erhandlungen - Internationale Vereinigung für Theoretische und Angewandte Limnologie*, **21**, 693-698.

Mann, D., Edwards, J., Chase, J., Beck, W., Reanier, R., Mass, M., Finney, B. and Loret, J. (2008) 'Drought, vegetation change, and human history on Rapa Nui (Idea de Pascua, Easter Island).' *Quaternary Research*, **69**, 16-28.

Mantsis, D. F., Lintner, B. R., Broccoli, A. J. and Khodri, M. (2013) 'Mechanisms of mid-Holocene precipitation change in the South Pacific Convergence Zone.' *Journal of Climate*, **26**, 6937-3953.

Mantua, N. J. and Hare, S. R. (2002) 'The Pacific decadal oscillation.' *Journal of Oceanography*, **58**, 35-44.

Mantua, N. J., Hare, S. R., Zhang, Y., Wallace, J. M., and Francis, R. C. (1997) 'A Pacific interdecadal climate oscillation with impacts on salmon production.' *Bulletin of the American Meteorological Society*, **78**, 1069-1079.

Margalef, O., Cañellas-Boltà, N., Pal-Rabes, S., Firalt, S., Pueyo, J. J., Joosten, H., Rull, V., Buchaca, T., Valero-Garces, B. L., Moreno, A., Saez, A. (2013) 'A 70,000 year multiproxy record of climatic and environmental change from Rano Aroi peatland (Easter Island).' *Global and Planetary Change*, **108**, 72-84.

Margalef, O., Martínez Cortizas, A., Kylander, M., Pla-Rabes, S., Cañellas-Boltà, N., Pueyo, J. J. and Sáez, A. (2014) 'Environmental processes in Rano Aroi (Easter Island) peat geochemistry forced by climate variability during the last 70 kyr.' *Paleogeography, Palaeoclimatology, Palaeoecology*, **414**, 438-450.

Marriner, N., Flaux, C., Kaniewski, D., Morhange, C., Leduc, G., Moron, V., Chen, Z., Gasse, F., Empereur, J-.Y. and Stanley, J-., D. (2012). 'ITCZ and ENSO-like pacing of Nile delta hydro-geomorphology during the Holocene' *Quaternary Science Reviews*, **45**, 73-84.

Marshall, M. H., Lamb, H. F., Huws, D., Davies, S. J., Bates, R., Bloemendal, J., Boyle, J., Leng, M. J., Umer, M. and Bryant, C. (2011) 'Late Pleistocene and Holocene drought events at Lake Tana, the source of the Blue Nile.' *Global and Planetary Change*, **78**, 147-161.

Marshall, P. (1930) 'Geology of Rarotonga and Atiu.' *Bull. Bernie P. Bishop Mus*., **36**, 1-48.

Matthews, A. J. (2012) 'A multiscale framework for the origin and variability of the South Pacific Convergence Zone.' *Quarterly Journal of the Royal Meteorological Society*, **138**, 1165-1178.

Matthews, A. J. and Li, H. Y. Y. (2005) 'Modulation of station rainfall over the western Pacific by the Madden-Julian oscillation.' *Atmospheric Science*, **32**.

Maupin, C. R., Partin, J. W., Shen, C.-C., Quinn, T. M., Lin, K., Taylor, F. W., Banner, J. L., Thirmalai, K. and Sinclair, D. J. (2014) 'Persistent decadal-scale rainfall variability in the tropical South Pacific Convergence Zone through the past six centuries.' *Climate of the Past*., **10**, 1319-1332.

McAfee, S. A. (2014) 'Consistency or lack thereof in Pacific Decadal Oscillation impacts on North American winter climate.' *Journal of Climate*, **19**, 7410-7431.

McCulloch, M., Mortimer, G., Esat, T., Xianhua, K., Pillans, B. and Chappell, J. (1996) 'High resolution windows into early Holocene climate: Sr/Ca coral records form the Huon Peninsula.' *Earth and Planetary Science Letters*, **138**, 169-178.

McGregor, H. V., Fischer, M. J., Gagan, M. K., Fink, D., Phipps, S. J., Wong, H. and Woodroffe, C. D. (2013a) 'A weak El Niño/Southern Oscillation with delayed seasonal growth around 4,300 years ago.' *Nature Geoscience*, **6**, 949-953.

McGregor, H. V. and Gagan, M. K. (2004) 'Western Pacific coral $\delta^{18}O$ records of anomalous Holocene variability in the El Niño-Southern Oscillation.' *Geophysical Research Letters*, **31**, 1-4.

McGregor, S., Timmermann, A., England, M. H., Timm, O. E. and Wittenberg, A. T. (2013b) 'Inferred changes in El Niño-Southern Oscillaton variance over the past six centuries.' *Climate of the Past Discussions*, **9**, 2929-2966.

McGregor, S., Timmermann, A., Stuecker, M. F., England, M. H., Merrifield, M., Jin, F-.F. and Chikamoto, Y. (2014) 'Recent Walker circulation strengthening and Pacific cooling amplified by Atlantic Warming.' *Nature Climate Change*, **4**, 888-892.

McGregor, S., Timmermann, A. and Timm, O. (2010) 'A unified proxy for ENSO and PDO variability since 1650.' *Climate of the Past*, **6**, 1-17.

McInerney, F. A., Hellicker, B. R. and Freeman, K. H. (2011) 'Hydrogen isotope ratios of leaf wax *n*-alkanes in grasses are insensitive to transpiration.' *Geochimica et Cosmochimica Acta*, **75**, 541-554.

McPhaden, M. J. (1999) 'Genesis and evolution of the 1997-98 El Niño.' *Science*, **283**, 950-954

McPhaden, M. J., Lee, T., and McClurg, D. (2011)'El Niño and its relationship to changing background conditions in the tropical Pacific Ocean.' *Geophysical Research Letters*, **38**, L15709.

McPhaden, M. J., Zebiak, S. E., and Glantz, M. H. (2006) 'ENSO as an integrating concept in Earth Science.' *Science*, **314**, 1740-1745.

Meehl, G. A. and Hu, A. (2006) 'Megadroughts in the Indian monsoon region and southwest North America and a mechanism for associated multidecadal Pacific sea surface temperature anomalies.' *Journal of Climate*, **19**, 1605-1623.

Méon, H. and Pannetier, W. (1994) 'Palynological study of the late Quaternary of Loyalty Basin (SW Pacific).' *Palaeogeography, Palaeoclimatology, Palaeoecology*, **111**, 135-147.

Metcalfe, S. E., Jones, M. D., Davies, S. J., Noren, A. and MacKenzie, A. (2010) 'Climate variability over the last two millennia in the North American monsoon region, recorded in

laminated lake sediments from Laguna de Juanacatlán, Mexico.' *The Holocene*, **8**, 1195-1206.

Meyers, P. A. (1994) 'Preservation of elemental and isotopic source identification of sedimentary organic matter.' *Chemical Geology*, **144**, 289-302.

Meyers, P. A. and Teranes, J. L. (2001) 'Sediment organic matter.' In Last, W. M. and Smol, J. P. (Eds.) *Tracking Environmental Change using lake sediments*. Netherlands: Springer, pp. 239-269.

Miller, A. J. and Schneider, N. (2000) 'Interdecadal climate regime dynamics in the North Pacific Ocean: theories, observations and ecosystem impacts.' *Progress in Oceanography*, **47**, 355-379.

Ministry of Finance and Economic Management (2012) *Cook Islands Census 2011* [Online] Available from: http://www.mfem.gov.ck/docs/Stats/2012/Census/2011%20Cook%20Islands%20Population%20Census%20Report.pdf [Accessed: 6th December 2015]

Ministry of Natural Resources and Environment (2015) *Climate Summary August 2015*. [Online] Available from: http://www.samet.gov.ws/CS/Climate%20Summary%20August%202015.pdf [Accessed: 6th December 2015]

Minobe, S. (1997) 'A 50-70 year climatic oscillation over the North Pacific and North America.' *Geophysical Research Letters*, **24**, 683-686.

Minobe, S. (1999) 'Resonance in bidecadal and pentadecadal climate oscillaitons over the North Pacific: role in climatic regime shifts.' *Geophysical Research Letters*, **26**, 855-858.

Minobe, S. (2000) 'Spatio-temporal structure of the pentadecadal variability over the North Pacific.' *Progress in Oceanography*, **47**, 381-408.

Minobe, S., Manabe, T. and Shouji, A. (2002) 'Maximal wavelet filter and its application to bidecadal oscillation over then Northern Hemisphere through the twentieth century.' *Journal of Climatology*, **15**, 1064-1075.

Monnin, E., Indermühle, A., Dällenbach, A., Flückiger, J., Stauffer, B., Stocker, T. F., Raynaud, D. and Barnola, J-. M. (2001) 'Atmospheric CO_2 concentrations over the Last Glacial Termination.' *Science*, **291**, 112-114.

Moy, C. M., Seltzer, G. O., Robdell, D. T., and Anderson, D. M. (2002) 'Variability of El Niño/Southern Oscillation activity at millennial timescales during the Holocene epoch.' *Nature,* **420**, 162-165.

Murphy, B. F., Power, S. B. and McGree, S. (2014) 'The varied impacts of El Niño-Southern Oscillation on Pacific island climates.' *Journal of Climate*, **27**, 4015-4036.

Naeher, S., Gilli, A., North, R. P., Hamann, Y. and Schubert, C. J. (2013) 'Tracing bottom water oxygenation with sedimentary Mn/Fe ratios in lake Zurich, Switzerland.' *Chemical Geology*, **352**, 125-133.

Nakagawa, T., Gotranda, K., Haraguchi, T., Danhara, T., Yonenobu, H., Baryer, A., Yokoyama, Y., Tada, R., Takemura, K., Staff, R. A., Payne, R., Bronk Ramsey, C., Bryant, C., Brock, F., Schlolaut, G., Marshall, M., Tarasov, P., Lamb, H. F. and Suigetsu 2006 Project Members (2012) 'SG06, a fully continuous and varved sediment core form Lake Suigetsu, Japan: stratigraphy and potential for improving the radiocarbon calibration model and understanding of late Quaternary climate changes.' *Quanternary Science Reviews*, **36**, 164-176.

Nakamura, Y. and Tatsumoto, M. (1988) 'Pb, Nd, and Sr isotopic evidence for a multicomponent source for rocks of Cook-Austral Islands and heterogeneities of mantle plumes.' *Geochimica et Cosmochimica Acta*, **52**, 2909-2924.

Neelin, J. D., Battisti, D. S., Hirst, A. C., Jin, F-. F., Wakata, Y., Yamagata, T., and Zebiak, S. E. (1998) 'ENSO theory.' *Journal of Geophysical Research*., **103**, 14261-14290.

Nelson, D. B. and Sachs, J. P. (2016) 'Galápagos hydroclimate of the Common Era paired from microalgal and mangrove biomarker $^{2}H/^{1}H$ values.' *Proceedings of the National Academy of Sciences*, **113**, 3476-3481.

Newman, M., Alexander, M. A., Ault, T. R., Cobb, K. M., Deser, C., Di Lorenzo, E., Mantua, N. J., Miller, A. J., Minobe, S., Nakamura, H., Schneider, N., Vimont, D. J., Phillips, A. S.,

Scott, J. D. and Smith, C. A. (2016) 'The Pacific Decadal Oscillation, revisited.' *Journal of Climate*, **29**, 4399-4427.

Newman, M., Compo, G. P. and Alexander, M. A. (2003) 'ENSO-forced varaiblity of the Pacific Decadal Oscillation.' *Journal of Climate*, **16**, 3853-3857.

Nitta, T. and Yamada, S. (1989) 'Recent warming of tropical sea surface temperature and its relation to the Northern Hemisphere circulation.' *Journal of the Meteorological Society of Japan*, **67**, 375-383.

NOAA (2016) *Working Group on Surface Pressure*. [ONLINE] Available at: http://www.esrl.noaa.gov/psd/gcos_wgsp/Timeseries/. [Accessed 2 August 2016].

Nunn, P. D. and Carson, M. T. (2015) 'Sea-level fall implicated in profound societal change about 2570 cal yr BP (620 BC) in western Pacific island groups.' *Geo: Geography and Environment*, **2**, 17-32.

O'Leary, M. H. (1988) 'Carbon isotopes in photosynthesis.' *Bioscience*, **38**, 328-336.

Ollier, C., Whistler, W. A. and Amerson, A. B. (1979) *O Le Pupū-Pu'e National Park*. Fiji: United Nations Development team, pp. 163.

Osborne . M .C., Dunbar, R. B., Mucciarone, D. A., Druffel, E., Sanchez-Cabeza, J. –A. (2014) 'A 215-yr coral $\delta^{18}O$ time series from Palau records dynamics of the West Pacific Warm Pool following the end of the Little Ice Age.' *Coral Reefs*, **33**, 719-731.

Papadimitrou, S., Kennedy, H., Kennedy, D. P. and Borum, J. (2005) 'Seasonal and spatial variation in the organic carbon and nitrogen concentration and their stable isotopic composition in Zostera marina (Denmark).' *Limnology and Oceanography*, **50**, 1084-1095.

Parker, D., Folland, C. K., Scaife, A., Knight, J., Colman, A., Baines, P and Dong, B. (2007) 'Decadal to multidecadal variability and the climate change background.' *Journal of Geophyscial Research*, **112**, 10.1029/2007JD008411

Parkes, A. (1994) 'Holocene environment and vegetational change on four Polynesian islands.' Ph.D. thesis, University of Hull.

Partin, J. W., Quinn, T. M., Shen, C. C., Emile-Geay, J., Taylor, F. W., Maupin, C. R., Lin, K., Jackson, C. S., Banner, J. L. and Sinclair, D. J. (2013) 'Multidecadal rainfall variability in

South Pacific Convergence Zone as revealed by stalagmite geochemistry.' *Geology*, doi:10.1130/H34718.1

Patrick, A. and Thunnell, R. C. (1997) 'Tropical Pacific sea surface temperatures and upper water column thermal structure during the last glacial maximum.' *Paleoceanography*, **12**, 648-657.

Pearson, E. J., Farrimond, P., and Juggins, S. (2007) 'Lipid geochemistry of lake sediments from semi-arid Spain: relationships with source inputs and environmental factors.' *Organic Geochemistry*, **38**, 1169-1195.

Peinerud, E. K. (2000) 'Interpretation of Si concentrations in lake sediments: three case studies.' *Environmental Geology*, **40**, 64-72.

Peters, K. E., Walters, C. C. and Moldowan, J. M. (2005) *The Biomarker Guide. Volume 1: Biomarkers and isotopes in the environment and human history*. Cambridge: Cambridge University Press, pp. 471.

Philander, S. G. H. (1985) 'El Niño and La Niña.' *Journal of the Atmospheric Sciences*, **42**, 2652-2662.

Picaut, J., Ioualalen, M., Menkès, C., Delcroix, T. and McPhaden, M. J. (1996) 'Mechanism of the zonal displacement of the Pacific warm pool: implications for ENSO.' *Science*, **274**, 1486-1489.

Polissar, P. J. and Freeman, K. H. (2010) 'Effects of aridity and vegetation on plant-wax δD in modern lake sediments.' *Geochimica et Cosmochimica Acta*, **74**, 5785-5797.

Polissar, P. J., Freeman, K. H., Rowley, D. B., McInerney, F. A. and Currie, B. S. (2009) 'Paleoaltimetry of the Tibetan Plateau from D/H ratios of lipid biomarkers.' *Earth Planetary Science Letters*, **287**, 64-76.

Potts, P. J. (1987) *A handbook of silicate rock analysis*. Glasgow: Blackie, pp. 636.

Power, S., Casey. T., Folland, C., Colman, A. and Mehta V. (1999) 'Inter-decadal modulation of the impact of ENSO on Australia.' *Climate Dynamics*, **15**, 319-324.

Power, S. B., Schiller, A., Cambers, G., Jones, D. and Hennessy, K. (2011) 'The Pacific climate change science program.' *Bulletin of the American Meterological Society*, **92**, 1409-1411.

Prins, H. B. A. and Elzenga, J. T.M. (1989) 'Bicarbonate utilization: function and mechanism.*'* *Aquatic Botany*, **34,** 59-83.

Qiu, B. (2003) 'Kuroshio Extension variability and forcing of the Pacific decadal oscillations: responses and potential feedback.' *Journal of Physical Oceanography*, **33**, 2465-2482.

Quinn, T. M., Crowley, T. J. and Taylor, F. W. (1996) 'New stable isotope results from a 173-year coral rom Espiritu Santo, Vanuatu.' *Geophysical Research Letters*, **23**, 3413-3416.

Quinn, T. M. Taylor, F. W. and Crowley, T. J. (1993) 'A 173 year stable isotope record from a tropical South Pacific coral.' *Quaternary Science Reviews*, **12**, 407-418. 1-11.

Quinn, T. M. Taylor, F. W. and Crowley, T. J. (2006) 'Coral-based climate variability in the Western Pacific Warm Pool since 1867.' *Journal of Geophysical Research: Oceans*, **111**, 1-11.

Ramsey, M. H., Potts, P. J., Webb, C., Watkins, P., Watkins, J. S. and Coles, B. J. (1995) 'An objective assessment of analytical method precision: comnparison of ICP-AES and XRF for the analysis of silicate rocks.' *Chemical Geology*, **124**, 1-19.

Rao, S. M., Jain, S. K., Navada, S. V., Nair, A. R., and Shivanna, K. (1987) 'Isotopic studies on sea water intrusion and interrelations between water bodies: some field experiments.' In IAEA (Eds.) *Isotope Techniques in Water Resources Development*, Austria: IAEA, pp. 836.

Rasmussen, S. O., Andersen, K. K. Svensson, A. M., Steffensen, J. O., Vinther, B. M., Clausen, H. B., Siggaard-Andersern, M. –L., Johnsen, S. J., Larsen, L. B., Dahl-Jensen, D., Bigler, M., Röthlisberger, R., Fischer, H., Goto-Azuma, K., Hansson, M. E. and Ruth, U. (2006) 'A new Greenland ice core chronology for the last glacial termination.' *Journal of Geophysical Research: Atmospheres*, **111**, 1-16.

Reason, C. J. C. and Rouault, M. (2002) 'ENSO like decadal variability and South African rainfall.' *Geophysical Research Letters*, **29**, doi:10.1029/2002GL014663

Reimer, P. J., Bard, E., Bayliss, A., Beck, J. W., Blackwell, P. G., Bronk Ramsey, C., Buck, C. E., Cheng, H., Edwards, R. L., Friedrich, M., Grootes, P. M., Guiilderson, T. P., Haflidason, H., Hajdas, I., Hatté, C., Heaton, T. J., Hoffmann, D. L., Hogg, A. G., Hughen, K. A., Kaiser, K. F., Kromer, B., Manning, S. W., Niu, M., Reimer, R. W., Richards, D. A., Scott, E. M., Southon, J. R., Staff, R. A., Turney, C. S. and can der Plicht, J. (2013) 'IntCal13 and Marine13 radiocarbon age calibration curves 0-50,000 years cal BP.' *Radiocarbon*, **55**, 1869-1887.

Rein. B., Lückge, A., Reinhardt, L., Sirocko, F., Wolf, A. and Dullo, W-.C. (2005) 'El Niño variability off Peru during the last 20,000 years.' *Paleoceanography*, **20**, 1-18.

Restrepo, A., Colinvaux, P., Bush, M., Correa-Metrio, A., Conroy, J., Gardener, M. R., Jaramillo, P., Steinitz-Kannan, M. and Overpeck, J. (2012) 'Impacts of climate variability and human colonization on the vegetation of the Galápagos Islands' *Ecology*, **93**, 1853-1866.

Revell, C. G. and Goulter, W. (1986) 'South Pacific tropical cyclones and the Southern Oscillation.' *Monthly Weather Reviews*, **114**, 1138-1145.

Richter, T. O., Van der Gaast, S., Koster, B., Vaars, A., Gieles, R., de Stigter, H. C., de Haas, H. and van Weering, T. C. E. (2006) 'The Avaatech XRF Core Scanner: technical description and applications to NE Atlantic sediments.' In Rothwell, R. G. (Ed.) *New techniques in sediment core analysis, vol. 267*. Geological Society Special Publication, pp.39-50.

Riedinger, M. A., Steinitz-Kannan, M., Last, W. M. and Brenner, M. (2002) 'A ~6100 ^{14}C yr record of El Niño activity from the Galápagos Islands.' *Journal of Paleolimnology*, **27**, 1-7.

Rieth, T. M. and Hunt, T. L. (2008) 'A radiocarbon chronology for Sāmoan prehistory.' *Journal of Archaeological Science*, **35**, 1901-1927.

Riley, W. J., Still, C. J., Torn, M. S. and Berry, J. A. (2002) 'A mechanistic model of $H_2{}^{18}O$ and $C^{18}OO$ fluxes between ecosystems and the atmosphere: model description and sensitivity analyses.' *Global Biogeochemistry Cycles*, **16**, 1-14.

Risi, C., Bony, S. and Vimeux, F. (2008) 'Influence of convective processes on the isotopic composition ($\delta^{18}O$ and δD) of precipitation and water vapour in the tropics: 2. Physical interpretation of the amount effect.' *Journal of Geophysical Research*, **113**, 1-12.

Robbins, J. A. (1978) 'Geochemical and geophysical applications of radioactive lead.' In Nriagu, J. O. (Ed.) *The Biogeochemistry of Lead in the Environment*. Netherlands: Elsevier, pp. 285-393.

Robdell, D. T., Seltzer, G. O., Anderson, D. M., Abbott, M. B., Enfield, D. B. and Newman, J. H. (1999) 'An ~15,000-year record of El Niño-driven alluviation in southwestern Ecuador.' *Science*, **283**, 516-520.

Robdell, D. T., Seltzer, G. O., Mark, B. G., Smith, J. A. and Abbott, M. B. (2008) 'Clastic sediment flux to tropical Andean lakes: reocrds of glaciation and soil erosion.' *Quaternary Science Reviews*, **27**, 1612-1626.

Rodgers, K. B., Mikaloff-Feltcher, S. E., Bianchi, D., Beaulieu, C., Galbraith, E. D., Gnanadesikan, A., Hogg, A. G., Iudicone, D., Lintner, B. R., Naegler, T., Reimer, P. J., Rustic , G. T., Koutavas, A., Marchitto, T. M. and Linsley, B. K. (2015) 'Dynamical excitation of the tropical Pacific Ocean and ENSO variability by Little Ice Age cooling.' *Science*, **350,** 1537-1541.

Rodgers, K. B., Mikaloff-Feltcher, S. E., Bianchi, D., Beaulieu, C., Galbraith, E. D., Gnanadesikan, A., Hogg, A. G., Iudicone, D., Lintner, B. R., Naegler, T., Reimer, P. J., Sarmiento, J. L. and Slater, R. D. (2011) 'Interhemispheric gradient of atmospheric radiocarbon reveals natural variability of Southern Ocean winds.' *Climate of the Past*, **7**, 1123-1138.

Rodriguez-Ramirez, A., Grove, C. A., Zinke, J., Pandolfi, J. M. and Zhao, J. X. (2014) 'Coral luminescence identifies the Pacific Decadal Oscillation as a primary driver of river runoff variability impacting the Southern Great Barrier Reef.' *PLOS One*, **9**, 1-11.

Rollinson, H. R. (1993) *Using geochemical data: evaluation, presentation, interpretation.* London: Routledge, pp. 384.

Ropelewski, C. F. and Halpert, M. S. (1987) 'Global and Regional Scale Precipitation Patterns Associated with the El Niño/Southern Oscillation.' *Monthly Weather Review*, **115**, 1606-1626.

Rothwell, R. G. and Croudace, I. W. (2015) 'Micro-XRF studies of sediment cores: a perspective on capability and application in the environmental sciences.' In Croudace, I.

W. and Rothwell, R. G. (Eds.) *Micro-XRF studies of sediment cores*. London: Springer, pp. 1-24.

Rothwell, R. G., Hoogakker, B., Thomson, J., Croudace, I. W. and Frenz, M. (2006) 'Turbidite emplacement on the sourthern Balaearic Abyssal Plain (western Mediterranean Sea) during Marine Isotope Stages 1-3: an application of ITRAX XRF-scanning of sediment cores to lithostratigraphic analysis.' In Rothwell, R. G. (Ed.) *New techniques in sediment core analysis*, *vol. 267*. Geological Society Special Publication, pp.79-80.

Rozanski, K., Araguás-Araguás, L and Gonfiantini, R. (1993) 'Isotopic patterns in modern global precipitation.' In Swart, P. K., Lohmann, K. C., McKenzie, J. and Savin, S. (Eds.*) Climate Change in Continental Isotopic Records*, California: American Geophysical Union, pp. 374.

Rull, V., Cañellas-Bolta, N., Margalef, O., Sáez, A., Pla-Rabes, S. and Giralt, S. (2015) 'Late Holocene vegetation dynamics and deforestation in Rano Aroi: implications for Easter Island's ecological and cultural history.' *Quaternary Science Reviews*, **126**, 219-226.

Rustic, G. T., Koutavas, A., Marchitto, T. M. and Linsley, B. K. (2015) 'Dynamical excitation of the tropical Pacific Ocean and ENSO variability by Little Ice Age cooling.' *Science*, **350**, 1537-1541.

Sachs, J. P., Sachse, D., Smittenberg, R. H., Zhang, Z., Battisti, D. S. and Golubic, S. (2009) 'Southward movement of the Pacific intertropical convergence zone AD 1400-1850.' *Nature Geoscience*, **2**, 519-525.

Sachs, J. P. and Schwab, V. F. (2011) 'Hydrogen isotopes in dinosterol from the Chesapeake Bay estuary.' *Geochimica et Cosmochimica Acta*, **75**, 444-459.

Sachse, D., Billault, I., Bowen, G. J., Chikaraishi, Y., Dawson, T. E., FEakin, S. J., Freeman, K. H., Magill, C. R., McInerney, F. A., van der Meer, M. T. J., Polissar, P., Robins, R. J., Sachs, J. P., Schmidt, H-.L., Session, A. L., White, J. W. C., West, J. B. and Kahman, A. (2012) 'Molecular paleohydrology: interpreting the hydrogen-isotopic composition of lipid biomarkers from photosynthesising organisms.' *Annual Review of Earth and Planetary Sciences*, **40**, 221-249.

Sachse, D., Radke, J. and Gleixnir, G. (2004) 'Hydrogen isotope ratios of recent lacustrine sedimentary *n*-alkanes record modern climate variability.' *Geochimica et Cosmochimica Acta*, **68**, 4877-4889.

Sachse, D., Radke, J., Gleixnir, G. (2006) 'δD values of individual n-alkanes from terrestrial plants along a climatic gradient – implications for the sedimentary biomarker record.' *Organic Geochemistry*, **37**, 469-483.

Sachse, D. and Sachs, J. P. (2008) 'Inverse relationship between D/H fractionation in cyanobacterial lipids and salinity in Christmas Island saline ponds.' *Geochimica et Cosmochimica Acta*, **72**, 793-806.

Sadekov, A. Y., Ganeshram, R., Pichevin, L., BErdin, R., McClymont, E., Elderfield, H. and Tudhope, A. W. (2013) 'Palaeoclimate reconstructions reveal a strong link between El Niño-Southern Oscillation and tropical Pacific mean state.' *Nature Communications*, **4**, 1-8.

Sáez, A., Valero-Garcés, B. L., Giralt, S., Moreno, A., Bao, R., Pueyo, J. J., Hernández, A. and Casa, D. (2009) 'Glacial to Holocene climate changes in the SE Pacific. The Raraku lake sedimentary record (Easter Island, 27°S).' *Quaternary Science Reviews*, **28**, 2743-2759.

Saint-Lu, M., Braconnot, P., Leloup, J., Lengaigne, M. and Marti, O. (2015) 'Changes in the ENSO/SPCZ relationship from past to future climates.' *Earth and Planetary Science Letters*, **412**, 18-24.

Salinger, M. J., McGree, S., Beucher, F., Power, S. B. an Delage, F. (2014) 'A new index for variations in the position of the South Pacific Convergence Zone 1910/11-2011-12.' *Climate Dynamics*, **43**, 881-892.

Salinger, M. J., Renwick, J. A. and Mullan, A. B. (2001) 'Interdecadal Pacific oscillation and south Pacific climate.' *International Journal of Climatology*, **21**, 1705-1721.

Sandweiss, D. H, Richardson, J. B. Reitz, E. J., Rollins, H. B. and Maasch, K. A. (1996) 'Geoarchaeological evidence from Peru for a 5000 years BP onset of El Niño.' *Science*, **273**, 1531-1533.

Sauer, P. E., Eglinton, T. I., Hayes, J. M., Schimmelmann, A. and Sessions, A. L. (2001) 'Compound-specific D/H ratios of lipid biomarkers from sediments as a proxy for environmental and climatic conditions.' *Geochimica et Cosmochimica Acta*, **65**, 2113-222.

Schabetsberger, R., Drozdowski, G., ROtt, E., Lenzenweger, R., Jersabek, C. D., Fiers, F., Traunspurger, W., Reiff, N., Stoch, F., Kotov, A. A., Martens, K., Schatz, H and Kaiser, R. (2009) 'Losing the bounty? Investigating species richness in isolated freshwater ecosystems of Oceania.' *Pacific Science*, **63**, 153-179.

Schouten, S., Ossebaar, J., Schreiber, K., Kienhis, M. V. M., Langer, G., Benthien, A. and Bijma, J. (2006) 'The effect of temperature, salinity and growth rate on the stable hydrogen isotopic composition of long chain alkenones produced by *Emiliania huxleyi* and *Gephyrocapsa oceanica*.' *Biogeosciences*, **3**, 113-119.

Sessions, A. L., Burgoyne, T. W. and Hayes, J. M. (2001) 'Determination of the H3 factor in hydrogen isotope ratio mass spectrometry.' *Analytical Chemistry*, **73**, 200-207.

Sessions, A. L., Sylva, S. P., Summons, R. E. and Hayes, J. M. (2004) 'Isotopic exchange of carbon-bound hydrogen over geologic timescales.' *Geochimica et Cosmochimica Acta*, **68**, 1545-1559.

Shakun, J. D. and Shaman, J. (2009) 'Tropical origins of North and South Pacific decadal variability.' *Geophysical Research Letters*, **36**, 1-5.

Sichrowsky, U., Schabetsberger, R., Sonntag, B., Stoyneva, M., Maloney, A. E., Nelson, D. B., Richey, J. N. and Sachs, J. P. (2014) 'Limnological characterisation of volcanic crater lakes on Uvea Island (Wallis and Futuna, South Pacific.' *Pacific Science*, **68**, 333-343.

Smith, J. N. (2001) 'Why should we believe ^{210}Pb sediment geochronologies?' *Journal of Environmental Radioactivity*, **55**, 121-123.

Smith, D. M., Booth, B. B. B., Dunstone, N. J., Eade, R., Hermanson, L., Jones, G. S., Scaife, A. A., Sheen, K. L. and Thompson, V. (2016) 'Role of volcanic and anthropogenic aerosols in the recent global surface warming slowdown.' *Nature Climate Change*, **6**, 936-940.

Smith, F. A. and Freeman, K. H. (2006) 'Influence of physiology and climate on δD of leaf wax n-alkanes from C3 and C4 grasses.' *Geochimica et Cosmochimica Acta*, **70**, 1172-1187.

Smith, F. A. and Walker, N. A. (1980) 'Photosynthesis by aquatic plants: effect of unstirred layers in relation to assimilation of CO_2 and HCO_3^- and to carbon isotopic discrimination.' *New Phytologist*, **86**, 245-259.

Smittenberg, R. H., Saenger, C., Dawson, M. N. and Sachs, J. P. (2011) 'Compound-specific D/H ratios of the marine lakes of Palau as proxies for West Pacific Warm Pool hydrologic variability.' *Quaternary Science Reviews*, **30**, 921-933.

Southern, W. J., Ash, J., Brodie, J. and Ryan, P. (1986) 'The flora, fauna and water chemistry of Tagimaucia crater, a tropical highland lake and swamp in Fiji.' *Freshwater Biology*, **16**, 509-520.

Sponberg, K. (1999) *Compendium of Climatological Impacts, University Corporation for Atmospheric Research, Vol. 1.* National Oceanoic and Atmospheric Administration, Office of Global Programs.

Stevenson, J. (2004) 'A late-Holocene record of human impact from the southeast coast of New Caledonia.' *The Holocene*, **14**, 888-898.

Stevenson, J., Dodson, J. R. and Prosser, I. P. (2001) 'A late Quaternary record of environmental change and human impact form New Caledonia.' *Palaeogeography, Palaeoclimatology, Palaeoecology*, **168**, 97-123.

Stevenson, J., Gillespie, R., Jacobsen, G., Fallon, S. and Levchenco, V. (2010) 'The archaic and puzzling record of Lake Xere Wapo, New Caledonia.' *Terra Australis*, **32**, 381-394.

Stevenson, J. and Hope, G. (2005) 'A comparison of late Quaternary forest changes in New Caledonia and northeastern Australia.' *Quaternary Research*, **64**, 373-383.

Stoddart, D. R., Wodroffe, C. D. and Spencer, T. (1990) 'Mauke, Mitiaro and Atiu: geomorphology of makatea islands in the Southern Cooks.' *Atoll Research Bulletin*, **341**, 1-71.

Stott, L., Cannariato, K., Thunell, R., Haug, G. H., Koutavas, A. and Lund, S. (2004) 'Decline of surface temperature and salinity in the western tropical Pacific Ocean in the Holocene epoch.' *Nature*, **431**, 56-59.

Street-Perrot, F. A., Ficken, K. J., Huang, Y. and Eglinton, G. (2004) 'Late Quaternary changes in carbon crycling on Mt. Kenya, East Africa: an overview of the $\delta^{13}C$ record in lacustrine organic matter.' *Quaternary Science Reviews*, **23**, 861-879.

Street-Perrott, F. A., Huang, Y., Perrott, R. A. and Eglinton, G. (1998) 'Carbon isotopes in lake sediments and peats of last glacial age: implications for the global carbon cycle.' In: Griffiths, H. (Ed.) *Stable Isotopes: Integration of Biological, Ecological and Geochemical Processes*. BIOS Scientific Publishers, Oxford, pp. 381–396.

Stuiver, M. and Polach, H. A. (1977) 'Discussion: reporting of ^{14}C data.' *Radiocarbon*, **19**, 355-363.

Sun, Q., Miao, C., AghaKouchak, A. and Duan, Q. (2016) 'Century-scale causal relationships between global dry/wet conditions and the state of the Pacific and Atlantic Oceans.' *Geophysical Research Letters*, **43**, 6528-6537.

Sykes, W. R. (1976) *Vegetation of Atiu*. Unpublished Report, N. Z. Department of Science and Industrial Research, Botany Division, Christchurch, New Zealand.

Takahashi, K. and Battisti, D. S. (2007) 'Processes controlling the mean tropical Pacific precipitation pattern. Part II: The SPCZ and the southeast Pacific Dry Zone.' *Journal of Climate*, **20**, 5696-5706.

Takahashi, T., Nakagawa, H., Satofuka, Y. and Kawaike, K. (1999) 'Flood and sediment disaster triggered by 1999 rainfall in Venezuela; a river restoration plan for an alluvial fan.' *Journal of Natural Disaster Science*, **23**, 65-82.

Takhtajan, A. L. (1969) *Flowering Plants: Origin and dispersal*. Edinburgh: Oliver & Boyd, pp. 310.

Talbot, M. R. and Lærdal, T. (2000) 'The Late Pleistocene-Holocene palaeolimnology of Lake Victoria, East Africa, based upon elemental and isotopic analyses of sedimentary organic matter.'*Journal of Paleolimnology*, **23**, 141-164.

Terry, J. P., Kostaschuk, R. A. and Garimella, S. (2006) 'Sediment deposition rate in the Falefa River basin, Upolu island, Samoa.' *Journal of Environmental Radioactivity*, **86**, 45-63.

Thirumalai, K., Partin, J. W., Jackson, C. S. and Quinn, T. M. (2013) 'Statistical constraints on El Niño Southern Oscillation reconstructions using individual foraminfera: a sensitivity analysis.' *Paleoceanography*, **28**, 401-412.

Thomas, E. R., Wolff, E. W., Mulvaney, R., Steffensen, J. P., Johnsen, S. J., Arrowsmith, C., White, J. W. C., Vaughn, B. and Popp, T. (2007) 'The 8.2 ka event from Greenland ice cores.' *Quaternary Science Reviews*, **26**, 70-81.

Thomson, J. A. (1921) 'The Geology of Western Samoa.' *New Zealand Journal of Science and Technology*, **4**.

Thompson, C. S. (1986) *The climate and weather of the Southern Cook Islands*. New Zealand Meteorological Service.

Timmermann, A., Okumura, Y., An, S-.I., Clement, A., Dong, B., Guilyardi, E., Hu, A., Jungclaus, J. H., Renold, M., Stocker, T. F., Stouffer, R. J., Sutton, R., Xie, S-.P. and Yin, J. (2007) 'The influence of a weakening of the Atlantic Meridional Overturning on ENSO. *Journal of Climate*, **20**, 4899-4919.

Tjallingii, R., Röhl, U., Kölling, M. and Bickert, T. (2007) 'Influence of the water content on X-ray fluorescence core-canning measurements in soft marine sediments.' *Geochemistry, Geophysics, Geosystems*, **8**, 1-12.

Toomey, M. R., Donnelly, J. P. and Tierney, J. E. (2016) 'South Pacific hydrological and cyclone variability during the last 3000 years.' *Paleoceanography*, **31**, 491-504.

Tourre, Y. M., Rajagopalan, B., Kushnir, Y., Barlow, M. and White, W. B. (2001) 'Patterns of coherent decadal and interdecadal climate signals in the Pacific Basin during the 20th century.' *Geophysical Research Letters*, **28**, 2069-2072.

Trabucco, A., and Zomer, R.J. (2009) 'Global Potential Evapo-Transpiration (Global-PET) and Global Aridity Index (Global-Aridity) Geo-Database. CGIAR Consortium for Spatial Information.' [Accessed 11 September 2016]. Available from: http://www.csi.cgiar.org

Trenberth, K. E. (1976) 'Spatial and temporal variations of the Southern Oscillation.' *Quarterly Journal of the Royal Meteorological Society*, **102**, 639-653.

Trenberth, K. E. (1990) 'Recent observed interdecadal climate changes in the Northern Hemisphere.' *Bulletin of the American Meteorological Society*, **71**, 988-993.

Trenberth, K. E. (1997) 'The definition of El Niño.' *Bulletin of the American Meteorological Society*, **78**, 2771-2777.

Trenberth, K. E. and Hurrell, J. W. (1994) 'Decadal atmosphere-ocean variations in the Pacific.' *Climate Dynamics*, **9**, 303-319.

Tudhope, A. W., Chilcott, C. P., McCulloch, M. T., Cook, E. R., Chappell, J., Ellam, R. M., Lea, D. W., Lough, J. M and Shimmield, G. B. (2001) 'Variability in the El Niño-Southern Oscillation through a glacial-interglacial cycle.' *Science*, **291**, 1511-1517.

Tudhope, A. W., Shimmield, G. B., Chilcott, C. P., Jebb, M., Fallick A. E. and Dalgleish, A. N. (1995) 'Recent changes in climate in the far western equatorial Pacific and their relationship to the Southern Oscillation; oxygen isotope records from massive corals, Papua New Guinea.' *Earth and Planetary Science Letters*, **136**, 575-590.

Turner, D. L. and Jarrard, R. D. (1982) 'K-Ar dating of the Cook-Austral island chain: a test of the hot-spot hypothesis.' *Journal of Volcanology and Geothermal Research*, **12**, 187-220.

United Nations (2014) *Demographic Yearbook* [Online] Available from: http://unstats.un.org/unsd/demographic/products/dyb/dyb2013/Table03.pdf [Accessed: 6th December 2015].

Urban, F. E. Cole, J. E. and Overpeck, J. T. (2000) 'Influence of mean climate change on climate variability from a 155-year tropical Pacific coral record.' *Nature*, **407**, 989-993.

USGS (2012) *Shuttle Radar Topography Mission* [Online] Available from: http://earthexplorer.usgs.gov/ [Accessed 13th September 2016].

UWITEC (2016) 'UWITEC Sampler.' [Accessed 1 May 2016]. Available from: http://www.uwitec.at/

Vance, T. R., Roberts, J. L., Plummer, C. T., Kiem, A. S. and van Ommen, T. D. (2015) 'Interdecadal Pacific variability and eastern Australian megadroughts over the last millennium.' *Geophysical Research Letters*, **42**, 129-137.

van der Wiel, K., Matthews, A. J., Joshi, M. M. and Stevens, D. P. (2016a) 'Why the South Pacific Convergence Zone is diagonal.' *Climate Dynamics*, **46**, 1683-1698.

van der Wiel, K., Matthews, A. J., Joshi, M. M. and Stevens, D. P. (2016b) 'The influence of diabatic heating in the South pacific Convergence Zone on Rossby wave propagation and the mean flow.' *Quarterly Journal of the Royal Meteorological Society*, **142**, 901-910.

van der Wiel, K., Matthews, A. J., Stevens, D. P. and Joshi, M. M. (2015) 'A dynamical framework for the origin of the South Pacific and South Atlantic Convergence Zones.' *Quarterly Journal of the Royal Meteorological Society*, **141**, 1997-2010.

Verdon, D. C. and Franks, S. W. (2006) 'Long-term behaviour of ENSO: interactions with the PDO over the past 400 years inferred from paleoclimate records.' *Geophysical Research Letters*, **33**, doi: 10.1029/2005GL025052.

Vincent, D. G. (1994) 'The South Pacific Convergence Zone (SPCZ): a review.' *Monthly Weather Review*, **122**, 1949-1970.

Vincent, E. M., Lenaigne, M., Menkes, C. E., Jourdain, N. C., Marchesiello, P. and Madec, G. (2011) 'Interannual variability of the South Pacific Convergence Zone and implications for tropical cyclone genesis.' *Climate Dynamics*, **36**, 1881-1896.

Volkman, J. K., Barrett, S. M., Blackburn, S. I., Mansour, M. P., Sikes, E. L. and Gelin, F. (1998) 'Microalgal biomarkers: a review of recent research developments.' *Organic Geochemistry*, **29**, 1163-1179.

Wahlberg, J. S., Baker, J. H., Vernon, R. W. and Dewar, R. S. (1965) 'Exchange adsorption of strontium on clay minerals.' *Geological Survey Bulletin 1140-C*, Washington D.C.: USGS, pp. 36.

Walker, M. J. C., Berkelhammer, M., Björck, S., Cwynar, L. C., Fisher, D. A., Long, A. J., Lowe, J. J., Newnham, R. M. and Rasmussen, S. O. and Weiss, H. (2012) 'Formal subdivision of the Holcoene series/epoch: a discussion paper by a working group of INTIMATE (Integration of ice-core, marine and terrestrial records) and the Subcommision of Quaternary Stratigraphy (International Commission on Stratigraphy).' *Journal of Quaternary Science*m **27**, 649-659.

Ward, P. J., Jongman, B., Kummu, M., Dettinger, M. D., Weiland, F. C. S. and Winsemius, H. C. (2014) 'Strong influence of El Niño Southern Oscillation on flood risk around the world.' *Proceedings of the Natinoal Academy of Sciences*, **111**, 15659-15664.

Weltje, G. J. and Tjallingii, R. (2008) 'Calibration of XRF core scanners for quantitative geochemical logging of sediment cores: theory and application.' *Earth and Planetary Science Letters*, **274**, 423-438.

Weltje, P. J., Bloemsma, M. R., Tjallingii, R., Heslop, D., Röhl, U and Croudace, I. W. (2015) 'Prediction of geochemical composition from XRF core scanner data: a new multivariate approach including automatic selection of calibration samples and quantification uncertainties.' In Croudace, I. W. and Rothwell, R. G. (Eds.) *Micro-XRF studies of sediment cores*. London: Springer, pp. 507-534.

Wetzel, R. G. (2001) *Limnology*. London: Elsevier, pp. 1006.

Whistler, W. A. (1980) 'The vegetation of eastern Samoa.' *Allertonia*, **2**, 159-190.

Whistler, W. A. (1992) 'Vegetation of Samoa and Tonga.' *Pacific Science*, **46**, 159-178.

Widlansky, M. J., Timmermann, A., McGregor, S., Suecker, M. F. and Cai, W. (2014) 'An interhemispheric tropical sea level seesaw due to El Niño Taimasa.' *Journal of Climate*, **27**, 1070-1081.

Widlanksy, M. J., Timmermann, A., Stein, K., McGregor, S., Schneider, N., England, M. H., Lengaigne, M and Cai, W. (2013) 'Changes in South Pacific rainfall bands in a warming climate.' *Natura Climate Change*, **3**, 417-423.

Widlansky, M. J., Webster, P. J. and Hoyos, C. D. (2011) 'On the location and orientation of the South Pacific Convergence Zone.' *Climate Dynamics*, **36**, 561-578.

Wilmshurst, J. M., Hunt, T. L., Lipo, C. P. and Anderson, A. J. (2011) 'High-precision radiocarbon dating shows recent and rapid initial human colonization of East Polynesia.' *PNAS*, **108**, 1815-1820.

Wirrmann, D., Sémah, A. and Chacornac-Rault, M. (2006) 'Late Holocene paleoenvironment in northern New Caledonia, southwestern Pacific, from a multiproxy analysis of lake sediments.' *Quaternary Research*, **66**, 213-232.

Wirrmann, D., Eagar, S. H., Harper, M. A., Leroy, É. And Sémah, A. (2011a) 'First insights into mid-Holocene environmental change in central Vanuatu inferred from a terrestrial record from Emaotfer Swamp, Efaté Island.' *Quaternary Science Reviews*, **30**, 3908-3924.

Wirrmann, D., Sémah, A., Debenay, J. and Chacornac-Rault, M. (2011b) 'Mid- to late Holocene environmental and climatic changes in New Caledonia, southwest tropical Pacific, inferred from the littoral plain Gouaro-Déva.' *Quaternary Research*, **76**, 229-242.

Wise, E. K. (2015) 'Tropical Pacific and Northern Hemisphere influences on the coherence of the Pacific Decadal Oscillation reconstructions.' *International Journal of Climatology*, **35**, 154-160.

Wolff, C., Haug, G. H., Timmermann, A., Damsté, J. S. S., Brauer, A., Sigman, D. M., Cane, M. A. and Vershuren, D. (2011) 'Reduced interannual rainfall variability in East Africa during the last ice age.' *Science*, **333**, 743-747.

Wood, B. L. (1967) 'Geology of the Cook Islands.' *New Zealand Journal of Geology and Geophysics*, **10**, 1429-1445.

Wood, C. P. (1978) 'Petrology of Atiu and Mangaia, Cook Islands (Note)' *New Zealand Journal of Geology and Geophysics*, **21**, 767-771.

Wood, B. L. and Hay, R. F. (1970) 'Geology of the Cook Islands.' *New Zealand Geological Survery Bulletin*, **82**, 1-103.

Wright, A. C. S. (1963) 'Soil and Land use of Western Samoa.' *New Zealand Soil Bureau Bulletin*, **22**, 1-191.

Wu, H. C., Linsley, B. K., Dassie, E. P., Schiraldi, B. and deMenocal, P. B. (2013) 'Oceanographic variability in the South Pacific Convergence Zone region over the last 210 years from multi-site coral Sr/Ca records.' *Geochemistry, Geophysics, Geosystems,* **14**, 1435-1453.

Yamoah, K. K. A., Chabangborn, A., Chawchai, S., Schenk, F., Smittenberg, R. and Wohlfarth, B. (2016a) 'A 2000-year leaf wax-based hydrogen isotope record from Southeast Asia suggests low frequency ENSO-like teleconnections on a sub-millennial timescale.' *Quaternary Science Reviews*, **148**, 44-53.

Yamoah, K. K. A., Chabangborn, A., Chawchai, S., Väliranta, M., Wohlfarth, B. and Smitthenberg, R. J. (2016b) 'Large variability in *n*-alkane $\delta^{13}C$ values in Lake Pa Kho (Thailand) driven by wetland wetness and aquatic productivity.' *Organic Geochemistry*, **97**, 53-60.

Yan, H., Sun, L., Wang, Y., Hang, W., Qui, S. and Yang, C. (2011) 'A record of the Southern Oscillation Index for the past 2,000 years from precipitation proxies.' *Nature Geoscience*, **4**, 611-614.

Yim, B. Y., Kwon, M., Min, H. S. and Kug, J. S. (2015) 'Pacific Decadal Oscillation and its relation to the extratropical atmospheric variation in CMIP5.' *Climate Dynamics*, **44**, 1521-1540

Yu, J. -Y., Kao, H. -Y., Lee, T. and Kim, S. T. (2011) 'Subsurface ocean temperature indices for central-Pacific and Eastern-Pacific types of El Niño and La Niña events.' *Theoretical and Applied Climatology*, **103**, 337-344.

Yuan, Y and Yan, H. (2013) 'Different types of La Niña events and different responses of the tropical atmosphere.' *Chinese Science Bulletin*, **58**, 406-415.

Zhang, L. P. and Delworth, T. L. (2015) 'Analysis of the characteristics and mechanisms of the Pacific Decadal Oscillation in a suite of coupled models from the Geophysical Fluids Laboratory.' *Journal of Climate*, **28**, 7678-7701.

Zhang, Z. H., Leduc, G. and Sachs, J. P. (2014) 'El Niño evolution during the Holocene revealed by a biomarker rain gauge in the Galápagos Islands.' *Earth and Planetary Science Letters*, **404**, 420-434.

Zhang, Z. H. and Sachs J. P. (2007) 'Hydrogen isotope fractionation in freshwater algae: I. Variations among lipids and species.' *Organic Geochemistry*, **38**, 582-608.

Zhang, Z. H., Sachs, J. P. and Marchetti, A. (2009) 'Hydrogen isotope fractionation in freshwater and marine algae: II. Temperature and nitrogen limited growth rate effects.' *Organic Geochemistry*, **40**, 428-439.